SOME INVESTIGATIONS ON POWER SYSTEM STABILIZERS FOR SMALL-SIGNAL STABILITY ENHANCEMENT

Submitted in

fulfilment of the requirements for the degree of

Doctor of Philosophy

by

Dhanraj Chitara
ID: 2010REE508

Under the Supervision of

Prof. K. R. Niazi and Dr. Anil Swarnkar

DEPARTMENT OF ELECTRICAL ENGINEERING

MALAVIYA NATIONAL INSTITUTE OF TECHNOLOGY, JAIPUR

APRIL, 2018

CERTIFICATE

This is to certify that the thesis entitled, "**Some Investigations on Power System Stabilizers for Small-Signal Stability Enhancement**" being submitted by **Dhanraj Chitara (ID: 2010REE508)** is a bonafide research work carried out under my supervision and guidance in fulfilment of the requirement for the award of the degree of **Doctor of Philosophy** in the Department of Electrical Engineering and Power System Engineering, Malaviya National Institute of Technology, Jaipur, India. The matter embodied in the thesis is original and has not been submitted to another University or Institute for the award of any other degree.

Place: Jaipur
Date:

(Dr. Anil Swarnkar)
Supervisor & Assistant Professor
Dept. of Electrical Engineering
M. N. I. T., Jaipur

(Dr. K. R. Niazi)
Supervisor & Professor
Dept. of Electrical Engineering
M. N. I. T., Jaipur

DECLARATION

I, **Dhanraj Chitara,** declare that this thesis titled, "**Some Investigations on Power System Stabilizers for Small-Signal Stability Enhancement"** and the work presented in it are my own. I confirm that:

- The work done wholly or mainly while in candidature for a research degree at this university.
- Where any part of this thesis has previously been submitted for a degree or any other qualification at this university or any other Institution, this has been clearly stated.
- Where I have consulted the published work of others, this is always clearly attributed.
- Where I have quoted from the work of others, the source is always given. With the exception of such quotations, this thesis is entirely my own work.
- I have acknowledged all main sources of help.
- Where the thesis is based on work done by myself, jointly with others, I have made clear exactly what was done by others and what I have contributed myself.

Date:

Dhanraj Chitara
(ID: 2010REE508)

ACKNOWLEDGEMENT

This doctoral thesis would not have been possible without wonderful people who helped and inspired me during my doctoral study. I sincerely acknowledge and thank, from the core of my heart, to a number of individuals who have supported me during my Ph.D. work.

First, I would like to express my sincere gratitude and thanks to my supervisor, **Prof. *K. R. Niazi*** for his valuable guidance, help, and suggestions during the years of my thesis work. This feat was possible only because of the unconditional support provided by him. A man with an amicable and positive disposition, he has always made himself available to clarify my doubts despite his busy schedule and it was a great opportunity to do Ph.D. under his supervision and to learn from him. I thank him again for all his help and support.

I am deeply grateful to my joint supervisor, **Dr. Anil Swarnkar**, Electrical Engineering Department, MNIT Jaipur for his constant support, inspiration and motivation to carry out this challenging work to its logical end. His valuable guidance and thoughtful advices were the vital factors in the successful completion of this research work.

I owe my most sincere gratitude to ***Prof. Udaykumar Yaragatti***, Director, MNIT, Jaipur for extending all kinds of infrastructural facilities required for pursuing my Ph.D. I would like to thank ***Dr. Vikas Gupta***, Head of the Department and ***Dr. H. P. Tiwari***, Conveners, DPGC for encouraging me in all possible manners during the course of my Ph.D. I would like to extend my special gratitude towards ***Prof. Manoj Fozdar***, ***Dr. Nikhil Gupta, Dr. Rajiv Tiwari*** and ***Dr. Kusum Verma*** the members of DREC committee for their help and cooperation during my Ph.D. work.

My special thanks to my wonderful friends **Nand Kishore Meena, Saurabh Ratra, Ajeet Singh, Prasanta Pranda, Pradeep Singh, Abhilash Gupta, Rayesh, Jaiprakash, Pankaj Kumar, Satyendra Singh, Manoj Kumawat** and other fellow researchers. I cherish the prayers and support extended by them during low phases. I treasure the shared precious moments. I am also very grateful to other faculty and staff members of the Electrical Engineering Department for their constant moral support which enabled me to complete this work.

My family has always been supportive and encouraging. I will be forever indebted to my wife ***Mrs. Manisha Chitara***, for being a pillar of support and whose prayer has showered the blessings of the Almighty God.

My special thanks to my children ***Khyati*** and ***Aradhya***, and my other family members for their patience, cooperation and understanding during the course of my Ph.D. work.

For any glitches or inadequacies that may remain in this work, the responsibility is entirely my own.

(Dhanraj Chitara)

ABSTRACT

The increasing demand of energy and simultaneously cost of fossil fuels along with global warming has transformed the interest in interconnected power system for transmitting large amount of power during peak times of load demand. Moreover, for the power systems operating under stressed and complex operating conditions, maintaining systems stability is a challenging task. A major root cause of large-scale power system blackouts is poorly-damped and/or unstable electromechanical oscillations which are inherent to interconnected power systems. Therefore, reliable planning and operation of power systems to ensure satisfactory damping performance is of considerable practical interest. Indeed, due to a number of factors including the increasing size, dynamic complexity and utilization of power systems, provision of adequate damping remains an important research challenge. This thesis attempts to investigate the application of meta-heuristic optimization techniques for designing Power System Stabilizer (PSS) by optimizing its parameters for multi-machine power system. In Chapter 1, a brief introduction of the small-signal stability enhancement strategy has been discussed. In Chapter 2, detailed literature survey and modelling of power system components is presented. On the basis of the literature survey, the critical issues are identified and research objectives are framed in this chapter.

In Chapter 3 and 4, well established meta-heuristic technique Genetic Algorithm (GA) and Particle Swarm Optimization (PSO) are reinvestigated for optimal designing of PSS parameters of standard IEEE test systems under wide range of operating conditions. For guaranteed stability and assured the relative stability of the MMPS, an eigenvalue based multi-objective function is defined for simultaneous control of damping factor and damping ratio to transfer unstable and/or poorly damped mode eigenvalues to a specified D-shape zone in the left half of the *s*-plane and optimized using GA and PSO. Moreover, the efficacy of designed GA-based PSS (GAPSS) and PSO-based PSS (PSOPSS) controllers is evaluated by eigenvalue analysis, eigenvalue maps, and time-domain simulations and performances indices. Furthermore, the robustness of designed GAPSS controllers are tested on wide range of unseen operating conditions for severe disturbance scenarios. In Chapter 5 and 6, new meta-heuristic techniques Harmony Search Optimization (HSO) and Cuckoo Search Optimization (CSO) is explored and investigated for optimal designing of PSS parameters of four IEEE test systems using mentioned eigenvalue based multi-objective function for same operating conditions and application results are presented. Chapter 7 summarizes the thesis work. A comparative analysis of all designed PSS controllers has been carried out. Various optimization techniques applied are also analyzed and compared.

TABLE OF CONTENTS

TABLE OF CONTENTS

TABLE OF CONTENTS

TABLE OF CONTENTS

TABLE OF CONTENTS

LIST OF TABLES

Cont…

LIST OF TABLES (Cont…)

Cont…

LIST OF TABLES (Cont…)

LIST OF FIGURES

Cont…

LIST OF FIGURES (Cont…)

Cont…

LIST OF FIGURES (Cont…)

Cont…

LIST OF FIGURES (Cont…)

Cont…

LIST OF FIGURES (Cont…)

Cont…

LIST OF FIGURES (Cont…)

LIST OF SYMBOLS

b_{range}	Pitch bandwidth
c_1 , c_2	Acceleration coefficients
D	Damping constant
e	Random number
E'_{qi}	Internal voltage behind X'_{di} of ith generator
E_{fd}	Equivalent excitation voltage (pu)
E_{fdi}	Equivalent excitation voltage (pu) of ith generator
E'_{di}	Internal voltage behind X'_{qi} of ith generator
$gbest_i^k$	Best particle position based on overall swarm experience
I_{di}	d-axis component of armature current of ith generator
I_{qi}	q-axis component of armature current of ith generator
J	Multi-objective function
K_a	Regulator gain
K	Damping gain of power system stabilizer
k_{max}	Maximum number of iterations
K_i	Damping gain of ith power system stabilizer
p_a	Probability index
$pbest_i^k$	Each particle j best position at kth iteration
P_i^{load}	Active power of ith load bus
Q_i^{load}	Reactive power of ith load bus
r_1 , r_2	Radom numbers between 0 and 1
$stepsize_i$	Required step size
T_w	Wash-out time constant (sec)
T_1, T_2, T_3, T_4	Power system stabilizer tuning parameters (sec)
T_{1i}, T_{3i}	Desired tuning parameters of ith power system stabilizer (sec)
T_a	Regulator time constant (sec)
T_m	Mechanical torque (pu)
T_{mi}	Mechanical torque (pu) of ith generator
T_e	Electrical torque (pu)
T_{ei}	Electrical torque (pu) of ith generator
T_r	Terminal voltage transducer time constant (sec)
T'_{d0i}	d-axis open circuit transient time constant (sec) of ith generator
T'_{q0i}	q-axis open circuit transient time constant (sec) of ith generator
V_i^k	Existing speed of each particle
V_i^{k+1}	New speed of each particle
V_t	Terminal voltage of generator (pu)
V_{tr}	Output voltage of terminal voltage transducer (pu)

Cont…

LIST OF SYMBOLS (Cont…)

V_{PSS}	Output of power system stabilizer
V_i	Voltage of *i*th load bus
w	Inertia weight
w	Rotor speed (pu)
w_i	Rotor speed of *i*th generator (pu)
w_{min}	Minimum inertia weight
w_{max}	Maximum inertia weight
w_0	Synchronous speed (pu)
X_i^k	Each particle position
X_{di}	Steady state reactance of *d*-axis (pu) of *i*th generator
X'_{di}	Transient reactance of *d*-axis (pu) of *i*th generator
X_{qi}	Steady state reactance of *q*-axis (pu) of *i*th generator
X'_{qi}	Transient reactance of *q*-axis (pu) of *i*th generator
x_{old}	Existing pitch
x_{new}	New pitch
x_{best}	Best fitness
$x_i^{(t)}$	Existing solution
$x_i^{(t+1)}$	New solution
Y_i^{load}	Shunt admittance of *i*th load bus
Δt	Time step
Δw_i	Rotor speed deviation (pu) of *i*th generator (pu)
Δw	Rotor speed deviation (pu)
Δw_{ij}	Rotor speed deviation (pu) between *i*th generator and *j*th generator
ε	Step size
Φ	Detection step
β	Scale factor
δ	Rotor angle
δ_i	Rotor angle of *i*th generator
σ_0	Desired damping factor
$\sigma_{i,j}$	Damping factor of the *i*th eigenvalue of the *j*th operating point
ξ_0	Desired damping ratio
$\xi_{i,j}$	Damping ratio of the *i*th eigenvalue of the *j*th operating point

LIST OF ABBREVATIONS

AI	Artificial Intelligence
ANN	Artificial Neural Network
AVR	Automatic Voltage Regulator
BA	BAT Algorithm
BF	Bacteria Foraging
BW	Bandwidth
CA	Cultural Algorithm
CPCE	Culture-PSO-Co Evolutionary
CPSS	Conventional Power System Stabilizer
CSO	Cuckoo Search Optimization
CSOPSS	CSO-based PSS
DC	Direct Current
DFIG	Doubly Fed Induction Generator
FL	Fuzzy Logic
FLC	Fuzzy Logic Control
FLPSS	FL-based PSS
FNN	Feed-Forward Neural Network
FNNPSS	FNN-based PSS
GA	Genetic Algorithm
GAPSS	GA-based PSS
HMCR	Harmony Memory Considering Rate
HSO	Harmony Search Optimization
HSOPSS	HSO-based PSS
IAE	Integral of Absolute Error
IEEE	Institute of Electrical and Electronics Engineers
ITAE	Integral of Time Multiplied Absolute Value of Error
LFO	Low Frequency Oscillations
MMPS	Multi-Machine Power Systems
NEEPS	New England Extended Power System
NEPS	New England Power System
NETS	New England Test System

LIST OF ABBREVATIONS (Cont…)

NF	Neuro-Fuzzy
NYPS	New York Power System
PAR	Pitch Adjusting Rate
PSAT	Power System Analysis Toolbox
PSO	Particle Swarm Optimization
PSOPSS	PSO-based PSS
PSS	Power System Stabilizer
RNNPSS	RNN-based PSS
SA	Simulated Annealing
SMIB	Single-Machine Infinite Bus
SSS	Small-Signal Stability
TFAM	Two-Area, Four-Machine
TS	Tabu Search
WSCC	Western System Coordinating Council

CHAPTER-1
INTRODUCTION

Rapid changes are taking place around the world in the electrical power systems. Issues such as limited investment in new generation and transmission facilities, new regulatory requirements for transmission access, environmental concerns and deregulated competitive business environment are forcing utilities to maximize the utilization of existing transmission, distribution and generation resources. This has resulted in stressed operating conditions. Moreover, the complexity of power systems is also growing on account of rapid growth in interconnections, use of new technologies, renewable energy sources integration and new system loading patterns. Under such stressed and complex operating conditions, maintaining systems stability is a challenging task.

In power system parlance, the term stability is essentially related to the ability of power systems to respond to disturbances. Although power system stability is one phenomenon, it has been classified into various categories for the ease of analysis and for planning the control action. It can be broadly classified as Small-Signal Stability (SSS) and large signal stability. The SSS is usually a slow occurring phenomenon which is characterized by low frequency electromechanical oscillations. The SSS mainly depends on the initial operating state of the system and type of small disturbance such as small changes in load. Small disturbances occur due to variation of load changes continuously and the system adjusts to the changing conditions. The system must be capable to operate satisfactorily under these conditions and effectively meet the load requirement. It depends on the ability to maintain equilibrium between mechanical torque and electromagnetic torque of synchronous generators. Instability results in the form of increasing rotor angular swings of some generators leading to their loss of synchronism with other generators. Due to disturbances, the change in electrical torque of a synchronous machine can be divided into two components: first synchronizing torque component, which is in phase with a rotor angle deviation and second damping torque component, which is in phase with the speed deviation [2]. The time span in SSS analysis is in the order of 10 to 20 sec after a disturbance [3]. For the analysis of SSS, the disturbance is assumed to be sufficiently small so that linearization of system equations is possible.

In recent years, power system low frequency electromechanical oscillations is one of the most frequently encountered problems in SSS analysis of interconnected systems [1]. A small disturbance irrespective of its origin can significantly affect the characteristic of electromechanical oscillations of generators in the power system. Such poorly damped oscillations are extremely undesirable for the operation of power system because they threaten

the security and integrity of the power grid and limit the power transfer between interconnected generating areas, which may become even more serious now-a-days when power system interconnections are growing very large [1]-[3]. Furthermore, these oscillations can also decrease the life of the power system machines. These small magnitude Low Frequency Oscillations (LFO) named as local mode (1.0-2.5 Hz) when one of the generator is swinging against rest of the others or as inter-area mode (0.2-0.8 Hz) when swinging of one area generators with respect to other areas or sometimes both [2]. These oscillations produce oscillatory instability and causing system separation if sufficient damping is not provided to system. In the context of modern power system, The SSS has assumed significant importance. This concern emerges from the fact that the trend towards competitive business environment has forced modern utilities to operate their system under stressed operating conditions. Under such fragile conditions, even a small disturbance, if not taken care of, could endanger system security and may lead to system collapse with consequent loss of economy, besides interruption in power supply. Therefore, power system SSS problem must be reinvestigated in the present scenario.

The damping of power system plays an important role in enhancement of power transfer capability and stabilizes the system. Generally, the electromechanical oscillations in power system have been controlled through Power System Stabilizer (PSS) controllers [1]. To improve the damping performance and SSS enhancement of Single Machine Infinite Bus (SMIB) system and Multi-Machine Power Systems (MMPS), the generators are equipped with PSS which is most common and economical device. The PSSs are feedback controllers which are injecting an additional stabilizing signal to fast acting static Automatic Voltage Regulator (AVR) in the excitation system. It modulates the generator excitation in such a way that damping torque component of electrical torque comes in phase with rotor speed that reduces LFO. Earlier lead-lag based Conventional Power System Stabilizer (CPSS) with fixed parameters were generally used due to its simple concept and structure [3]. The dynamic behaviour of modern power system is quite different at different operating conditions. Now, CPSS which were designed for specific operating condition may no longer produce satisfactory results when operating conditions are varied under wide ranges [3]. This phenomenon is called as non-coordination among CPSSs. Therefore, coordination of PSSs is very significant problem in MMPS. Due to this non-coordination of CPSSs, a lot of conventional and modern control techniques have been proposed in the literature to design most robust stabilizers against wide range of operating conditions under different scenarios of severe disturbances.

The problem of designing of PSS parameters has been solved using numerical, analytical, exhaustive search, meta-heuristic techniques, etc. Analytical methods are simple to implement and rapid to execute, but their solutions are sub-optimal. Numerical methods are

competent, but some of them need linearized modelling whereas exhaustive search techniques suffer from the curse of dimensionality, so are not suitable for large-scale systems. Recently, due to fast computational facilities, a large number of heuristic and meta-heuristic soft computing techniques, e.g., Genetic Algorithm (GA), Tabu Search (TS), Simulated Annealing (SA), evolutionary programming, Particle Swarm Optimization (PSO), Bacteria Foraging (BF), BAT Algorithm (BA), strength pareto approach, chaotic algorithm, honey bee mating optimization, ant colony optimization, Harmony Search Optimization (HSO) and Cuckoo Search Optimization (CSO) etc. have proposed to solve diverse optimization problems of power systems. The main advantage of these meta-heuristic techniques is that they do not require any mathematical modelling of power system and are able to explore the optimal or near-optimal solution of the optimization problem. From the literature survey, it is observed that GA and PSO have successfully used for the design of PSS parameters. However, their performances have not been investigated on wider and stressed operating conditions of modern power systems. Moreover, some recently developed techniques, e.g., HSO and CSO are not yet explored for designing PSS parameters.

Therefore, the focus of the present thesis work is to reinvestigate the applicability of GA and PSO for the design of PSS parameters for wider and more stressed operating conditions of modern power systems and to explore the applicability HSO and CSO for robust designing of PSS parameters of MMPS. The thesis also aims to carry out comparative studies of developed methods.

1.1 Organization of Thesis

The organization of the thesis is as follows:

In Chapter 1 a brief introduction of the thesis work is presented. Chapter 2 presents the basic modelling and operation of power system components like synchronous generator, interconnected transmission line network, loads, excitation system and PSS are illustrated. A comprehensive literature survey of PSS parameters design has been carried out. On the basis of critical reviews of the literature survey, the objectives of the thesis are framed.

In Chapter 3, well established meta-heuristic technique GA is reinvestigated for optimal designing of PSS parameters of standard Institute of Electrical and Electronics Engineers (IEEE) test systems: 3-machine, 9-bus Western System Coordinating Council (WSCC) power system; Two-Area, Four-Machine (TAFM) power system; 10-machine, 39-bus New England Power System (NEPS) and 16-machine, 68-bus New England Extended Power System (NEEPS) under wide range of operating conditions. The participation factor method [50] is used for evaluating the optimum locations of PSS to be installed on the generators in MMPS. For guaranteed stability and assured the relative stability of the MMPS, an eigenvalue based multi-objective

function is defined for simultaneous control of damping factor and damping ratio to transfer unstable and/or poorly damped mode eigenvalues to a specified D-shape zone in left half of the *s*-plane and optimized using GA. Moreover, the effectiveness of designed GA-based PSS (GAPSS) controllers is analysed by eigenvalue analysis, eigenvalue maps, time-domain simulations and performances indices, i.e. Integral of Absolute Error (*IAE*) and Integral of Time Multiplied Absolute Value of Error (*ITAE*). Furthermore, the robustness of designed GAPSS controllers are tested on wide range of unseen operating conditions for severe disturbance scenarios.

In Chapter 4, another well establish algorithm PSO is reinvestigated for optimal designing of PSS parameters of four IEEE test systems using above mentioned eigenvalue based multi-objective function for similar operating conditions and application results are presented.

In Chapter 5, HSO is explored and investigated for optimal designing of PSS parameters of four IEEE test systems using mentioned eigenvalue based multi-objective function for same the operating conditions and application results are presented.

In Chapter 6, another new meta-heuristic technique CSO is investigated for optimal designing of PSS parameters of four IEEE test systems using mentioned eigenvalue based multi-objective function for same operating conditions and application results are presented.

Chapter 7 summarizes the research work. A comparative analysis of all investigated techniques has been carried out. The conclusions drawn from the thesis work are presented. The contributions and future research scope of the work are also presented.

CHAPTER-2
LITERATURE SURVEY

The complex power system is a combination of multiple electrical and mechanical components. Generally, these components are nonlinear and their parameters vary with wide range of operating conditions, and unpredictable disturbances. Such disturbances exhibit poorly damped LFO problem due to insufficient damping. These LFO may interrupt the power transfer between different areas and sometime generators may go to out of synchronism. Therefore, the SSS plays an important role in damping enhancement of the power system. In the present era, modern power systems require fast static excitation system for providing sufficient synchronizing torque, but the presence of AVR with high gain in the synchronous generators and long transmission network establish weak link between different areas of power system. Hence, for providing fast damping performance, the PSS is commonly used to mitigate these LFO by injecting additional control signal in the excitation system [2] [3].

The main objective of this chapter is to discuss the preliminaries associated with the design of PSS such as modelling of different power system components like synchronous generator, transmission line network, loads, static exciter and PSS. A thoroughly literature survey on designing PSS parameters for SMIB and MMPS under wide range of operating conditions have been presented. On the basis of critical reviews, the objectives of the thesis are framed.

2.1 Modelling of Power System Components

Modern power systems exhibit on-linear complex behaviour and it becomes very tedious and challenging to analyze dynamic process as the size and complexity of system increases. The first and important step during analysis and simulation studies of system is precise modelling of nonlinear and time-varying power system components. The power system components are: synchronous machine, transformer, interconnected transmission line network, loads, excitation system, AVR and PSS. Each electrical component has its own characteristic that may require modelling for a stability analysis. These components are described by a set of nonlinear differential equations for evaluating their dynamic behaviour. The power flow in the network is represented by a set of differential-algebraic equations describing the behaviour of a power system.

2.1.1 Modelling of Synchronous Machine

A synchronous machine is one of the most essential power system components. It can generate active and reactive power independently and has a key role in rotor angle stability. The role of synchronizing torques between generators in large power systems to makes

all generators rotate at synchronous speed. A synchronous machine can be modelled for both transient and SSS analysis.

The synchronous machines are modelled using two to six order differential equations depending on the type of stability analysis problem and are developed from the basic equation using Park's transformation [1]. The synchronous machine is represented by model 1.1 in which field circuit has one equivalent damper winding on q-axis. In this thesis, the standard machine equations of forth order are used and given by:

$$\dot{\delta}_i = w_i - w_0 \tag{2.1}$$

$$\dot{w}_i = \frac{1}{2H}\left[-D_i(\mathrm{w}_i - w_0) + w_0(T_{mi} - T_{ei})\right] \tag{2.2}$$

$$\dot{E}'_{qi} = \frac{1}{T'_{d0i}}\left[E_{fdi} - E'_{qi} + (X_{di} - X'_{di})\,\mathrm{I}_{di}\right] \tag{2.3}$$

$$\dot{E}'_{di} = \frac{1}{T'_{q0i}}\left[-E'_{di} - (X_{qi} - X'_{qi})\,\mathrm{I}_{qi}\right] \tag{2.4}$$

2.1.2 Modelling of Interconnected Transmission Line Network

For power system stability analysis, it is assumed that transmission line network is collection of lumped parameters like series resistance, series inductance, shunt conductance and shunt capacitance. The line series resistance and inductance are very important. In this thesis, the transmission lines are modelled as lumped parameter using common π-representation [3].

2.1.3 Modelling of Loads

Electromechanical oscillations can affect both voltage magnitude and frequency across the network and loads which are sensitive to these changes may require more detailed models to ensure accurate results. In this thesis, a constant impedance load model is used and represented as a shunt admittance Y_i^{load} connected to the i^{th} load bus as in (2.5).

$$Y_i^{load} = \frac{P_i^{load} - Q_i^{load}}{V_i} \tag{2.5}$$

The modelling of system loads is not critical for the methodologies developed within this work and the use of a constant impedance representation is sufficient for SSS analysis.

2.1.4 Modelling of Excitation Systems

The main function of an excitation system is to provide Direct Current (DC) to field winding of synchronous machine. Moreover, the excitation system performs control and protective functions for the satisfactory performance of power system by controlling the field

voltage via field current [2]. The main components of excitation systems are: exciter, AVR, terminal voltage transducer & load compensator, PSS, limiters & protective circuits. The main function of AVR is to process and amplifies input control signal to an appropriate level for control of the exciter. The terminal voltage transducer senses generator terminal voltage, rectifies and filters it to DC quantity and compared with reference or desired terminal voltage. In addition, load compensation may be provided, if it is desired to hold constant voltage at some point electrically remote from the generator terminal. The PSS provides an additional input signal to the AVR to damp out low frequency power system oscillations. The limiters and protective circuits includes a wide array of control and protective functions to ensure the capabilities limits of the exciter and synchronous generators are not exceeded. Excitation systems are broadly classified in to two types: DC exciter and static exciter [4].

All components in static exciter are static or stationary. Static controlled or uncontrolled rectifiers supply the excitation current to the field winding of main synchronous generator through slip rings. A simplified version of IEEE Type ST1A static exciter is as shown in Fig. 2.1.

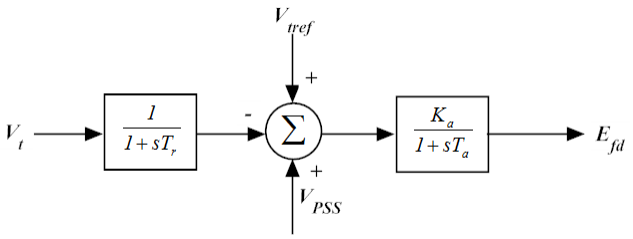

Fig. 2.1 Block diagram of IEEE type ST1A static exciter

Modern large machines are equipped with fast acting thyristor based excitation systems. The exciter power is drawn from the generator bus through an exciter transformer. The error signal is used as input and E_{fd} as output. Normally, T_a is neglected. When T_a is ignored, the dynamics are described by the following two equations:

$$\frac{dV_{tr}}{dt} = -\frac{1}{T_r}[V_{tr} - V_t] \tag{2.6}$$

$$E_{fd} = K_a(V_{ref} - V_{tr}) \tag{2.7}$$

In the case where the voltage regulators gain K_a is too large for better transient stability performance, the damping torque introduced by the exciter becomes negative.

2.1.5 Modelling of Power System Stabilizer

The main function of PSS is to add sufficient damping to generator rotor oscillations by injecting auxiliary stabilizing signals to its excitation system. The auxiliary stabilizing signals

are rotor speed, terminal frequency or power. Moreover, the PSS is to compensate the phase lag error between the exciter input and the electrical torque and generate torque component on the rotor. The block diagram of PSS as speed input is shown in Fig. 2.2.

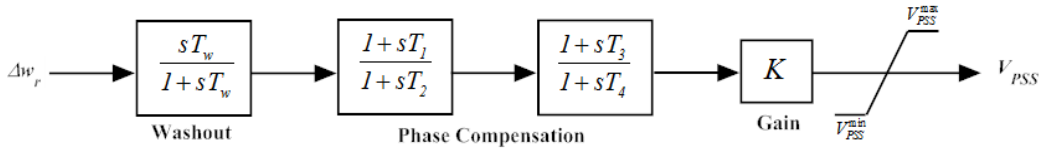

Fig. 2.2 Block diagram of power system stabilizer

This structure consists of a dynamic gain, washout filter and a lag-lead phase compensator. The input signal Δw_r is the rotor speed deviation from synchronous speed of machine in pu. The output signal V_{PSS} is fed an auxiliary signal to the excitation system. The dynamic gain is used for controlling the damping, washout block work as high-pass filter to reduce the terminal voltage error in steady state and the phase compensator block consist of two lead-lag blocks for reducing error between excitation and electrical torque. The value of time constant T_w, T_2, and T_4 are chosen as specific value while dynamic gain K, and other time constants T_1 and T_3 values are to be determined.

2.2 Literature Survey

A lot of research work has been carried out in the field of design of PSSs. These research efforts have led to the development of various techniques to design of PSS such as conventional control techniques, Artificial Neural Network (ANN) and/or Fuzzy Logic (FL) Techniques, meta-heuristic optimization techniques, other techniques.

2.2.1 Conventional Control Techniques

Initially conventional control techniques were used to solve SSS problems. DeMello and Concordia [4] have proposed the phenomena of stability of synchronous machines under small disturbances by investigating the frequency response of a SMIB system. They have explained the LFO by the concept of synchronizing and damping torque analysis. Classical control techniques are based on transfer function approach and they have analyzed by root locus [5], frequency domain techniques [6] [7] for designing speed based CPSS. However, these techniques are applicable for linear system only, therefore modern control techniques such as digital control techniques [8]-[10], pole placement methods [11] [12] and eigenvalue analysis [13] [14] have proposed for improving damping performance of power system. Moreover, in these methods the system is linearized for a specific operating condition and PSS parameters have been designed for that condition only. The performance of PSS has exploited when the system operating conditions varied under wide range. In earlier years, a PSS sensing

synchronous machine terminal frequency deviation as input [15], speed and electrical power as inputs [16] have been successfully developed for designing PSS parameters to remove some of the limitation in other PSS designs. Larsen and Swann [17]-[19] have explained the general concept, tuning concepts and practical applications with applying PSS utilizing speed, frequency and electrical power as inputs.

Demello et al. [20] have proposed the first method for effective selection of generator for PSS installation in MMPS. The sequential algorithm [21] has proposed for determining the speed based PSS parameters of MMPS. Lefebvre [22] has proposed an eigenvalue analysis method for evaluating sequentially effective PSS site locations in MMPS. However, this algorithm has not produce overall optimal PSS parameters because sequential addition have disturbed the previously assigned eigenvalues. In order to remove the undesirable effect of eigenvalues drift, a lot of approaches for simultaneously designing of PSS parameters have been proposed for MMPS [23]-[26]. Moreover, the PSS designed for one electromechanical mode produces adversely effect on the other modes. Therefore, the sequential designing of PSS parameter has been eliminated in [27] [28]. The other types of controllers such as analog and digital proportional-integral stabilizers [29] and self-tuning proportional-integral-derivative [30]-[32] have also been proposed for better system dynamic performance than that obtained by using the CPSS. The coordinated PSS application was effective not only for the local modes but also for low frequency inter-area modes of oscillations. It was very difficult to identify natural mode characteristics by examination of swing curves resulting from specific disturbances, because there were many modes of oscillations and only some of these inadequately damped in MMPS. Therefore, the new methods like participation factor method [33] and eigenvalue sensitivity analysis [34] have been proposed to identify the most suitable location for installing PSS in MMPS.

The synchronous machine parameter changes with different operating conditions and load, therefore CPSS designed for specific operating condition produces satisfactory results. For optimum performance of controller, it is desirable to track and compute the system operating conditions. Therefore, adaptive control [35] methods like self-tuning adaptive control [36]-[39], model reference adaptive control [40], decentralized control method [41] and other methods [42] have described for designing PSS in MMPS for wide range of operating conditions. The main limitations of self-tuning PSS was that it requires model identification in real time which is very time consuming. Kundur [43] has explained the detailed of PSS control designing for MMPS to increase the transient and steady state limits of local and inter-area modes and to check the robustness of controller performance during islanding condition.

Due to higher capability of damped out local and inter-area modes, the linear optimal control techniques like Riccati equations [44] [45], linear matrix inequalities [46] [47], output feedback control [48] [49],decentralized output feedback [50] have been described for designing of optimal multivariable stabilizer using output feedback of PSS in SMIB system and MMPS. To provide better damping performance for oscillatory modes of the MMPS than the CPSS, robust control methods [51]-[57] have been developed for designing PSS parameters. The other robust control techniques such as H_∞ based PSS [58]-[60], H_2 based PSS [61] and Wavelet-based PSS [62] have been presented to design PSS parameters under wide range of operation conditions of MMPS. The main advantage of these methods was that they presented normal tool for effectively modelling of system uncertainties.

Several interesting approaches like Prony analysis [63], μ-synthesis [64], mathematical programming [65] [66], probabilistic sensitivity indexes [67], probabilistic eigenvalue sensitivity analysis [68] [69] and conic programming approach [70] have been addressed in the literature for simultaneous tuning PSS parameters under different operating conditions of MMPS. The modern power system is practically a non-linear system and its operating conditions are varied continuously. Therefore, Gurrala and Sen [71]-[73] have proposed replacing a conventional AVR and PSS with a nonlinear voltage regulator using the concepts of synchronizing and damping torque components in SMIB and MMPS. Recently other non-linear control techniques such as variable structure control [74]-[76], sliding-mode control [77], synergetic control [78], back-steeping control [79] and Lyapunov functions [80], optimal predictive excitation control [81] have been described for designing robust PSS parameters in MMPS. The different types of PSS like PSS2B and PSS4B [82] [83], switching PSS [84] [85] 2-channel PSS [86] and classification of PSS [87] have been discussed for designing parameters of multi-machine PSS for enhancement of damping performance. Recently new control approaches such as phase compensation method [88], model decomposition [89] and point-wise min-norm control law [90] have been addressed for PSS designing to mitigate inter-area modes of oscillations in power system.

2.2.2 Artificial Intelligence Techniques

A set of PSS parameters which provide good dynamic performance under a certain operating condition may no longer yield satisfactory results when there is a drastic change in the operating point. To maintain good damping characteristic over a wide range of operating conditions, it is desirable to adapt PSS parameters in real-time based on on-line measurements. However, it is very difficult to apply both the frequency domain approach and the time-domain simulation method to on-line stability assessment in system operation because they have required large computational time either in computing eigenvalues or in solving differential

equations. Therefore, Artificial Intelligence (AI) techniques such as ANN, FL and NF were developed for designing of PSS for wide range of operating condition of SMIB system and MMPS.

It has been observed that the ANN have many advantages such as the capability of synthesizing complex and transparent mappings, rapidity, robustness, fault tolerance, quick response, high speed processing, adaptivity, interpolation, on-line & off-line applications, software simulation, hardware implementation and less memory required as compared to fixed parameter designed CPSS for one operating condition. A lot of literature work has been available using ANN techniques. Zhang and Chen [91] have presented ANN based off-line steady-state stability analysis using PSS. The ANN based PSS parameters have been designed using multilayer Feed-Forward Neural Network (FNN) [92] [93], multi-layer error back-propagation training method [94]-[96] to provide good damping performance over a wider range of operating conditions. A major disadvantage of the multilayer FNN employed is that there still exists no efficient learning technique for this kind of neural network though back-propagation momentum learning method. This learning method has slow convergence and it is suitable for problems with continuous output. Also, a set of rules is not available to help in the selection of an optimal structure of the ANN for a particular problem.

A new approach NN based PSS has been designed using Neuro-Identifier and Neuro-Controller [97] [98] for MMPS for a wider range of operating conditions. Shamsollahi and Malik [99] [100] have proposed neural adaptive PSS design using back propagation algorithm and observed implementation and experimental results to damp out LFO. Moreover, a new approach for real time tuning the PSS parameters using Radial Basis function network [101]-[103] has been implemented on SMIB system and MMPS for different operating conditions. However, the earlier ANN based PSS designing methods require large training time and large number of neurons to deal with complex problem. Therefore, to overcome these drawbacks a generalized neuron concept has been proposed by Chaturvedi and Malik [104]-[106] for SMIB system and MMPS over a wide range of operating conditions. A new recurrent neural network [107] [108] based adaptive PSS based has been discussed for tuning their parameters. In [109] [100] an intelligent system centric controller approach has been developed for designing of PSS using feed forward neural network to damp out inter-area modes of oscillations. To deal with dynamical problems, a FNNPSS requires a large number of neurons to represent dynamical responses in the time-domain. Moreover, the internal information of a FNNPSS cannot be utilized for weight updates and the function approximation is sensitive to the training data, on the other hand a Recurrent Neural Networks (RNN) is a dynamic mapping. A RNN bases PSS (RNNPSS) can capture the dynamic response of a system without delays caused by external

feedback because the recurrent neuron has an internal feedback loop. The configuration of the multilayer ANN has to be determined by experience since there are no definite rules to select the number of hidden layers and number of neurons in each hidden layer.

Therefore, the FL incorporates an alternative way which allows one to design a controller using a higher level of abstraction without knowing the plant model and no numerical training data is required. This makes fuzzy logic controllers very attractive for ill-defined systems or systems with uncertain parameters. With the help of fuzzy logic concepts, expert's knowledge can be used directly to design a controller. Due to its lower computation burden and its ability to accommodate uncertainties in the plant model, Fuzzy Logic PSS (FPSS) appear to be suitable for implementing PSSs. The FPSSs can be implemented through simple microcomputers with A/D and D/A converters. The performance of FPSSs depends on the operating conditions of the system, although it is less sensitive than conventional linear PSSs. The Fuzzy Logic Control (FLC) algorithm can be implemented using heuristic strategies, defined by linguistically described statements. The main FLC processes are fuzzification, rules definition, inference mechanism and defuzzification.

A lot of literature work is available using FL techniques. In [111] a new type of PSS has been designed which does not require real-time model identification using fuzzy set theory. Application of fuzzy controller as PSS has been described in [112] [113] for wide range of operating conditions. The robustness of FL-based PSS (FLPSS) applied to multi-machine PSS has been illustrated in [114]. Furthermore, the fuzzy polar PSS [115], augmented FLPSS [116] have been developed for wide range of operating conditions of power system. A self-organizing PSS design using fuzzy auto regressive moving average [117] and adaptive fuzzy PSS [118]-[122] design have been presented for SMIB system and MMPS respectively. A new robust adaptive fuzzy PSS have been designed using nonlinear control techniques like sliding mode [123] [124], synergetic control [125] [126] for MMPS under wide range of operating conditions.

It is observed that unlike other classical control methods, FLC and ANN are model-free controllers, i.e. they do not require an exact mathematical model of the controlled system. Moreover, rapidity and robustness are the most profound and interesting properties in comparison to the classical schemes. Although, FLC introduces a good tool to deal with complicated, nonlinear and ill-defined systems, it suffers from a drawback the parameter tuning for the controller. ANN has the powerful capability of learning and adaptation, such advantages that cannot be found in the FLC. However, one of the drawbacks of using conventional ANN is its black-box characteristic. Therefore, NF based PSS design are addressed in [127]-[133] for SMIB system and MMPS under wide range of operating conditions in order to incorporate the advantages of both ANN and FL techniques.

2.2.3 Meta-Heuristic Optimization Techniques

It is important to note that synchronous machine parameter changes with load and disturbances which make the dynamic behaviour of machine at different operating conditions. Such parameters varies in a complex manner, therefore a set of PSS parameters which stabilize the system for a particular operating point may produce unsatisfactory results when power system operating conditions changes.

Now, with the advancement of fast computational facilities, a large number of heuristic and meta-heuristic soft computing techniques are presented for off-line designing of PSS parameters. However, the main attribute of these meta-heuristic techniques is that they do not require any mathematical modelling of power system but they have definite merits and demerits. GA is very simple, independent of the complexity of problem and robust, but it suffers from the problem of premature convergence and high computation time. The simultaneous designing of PSSs using GA [134]-[147] is addressed for SMIB system and MMPS over a wide range of operating conditions. The TS [148] [149] and SA [150] [151] have been illustrated as another heuristic algorithms for robust designing of PSS parameters at different operating conditions for SMIB system and MMPS. The main advantage of TS and SA has independent of complexity of problem and ability to escape local minima. A new evolutionary algorithm like evolutionary programming [152] and based on swarm intelligence like PSO [153]-[155] has been addressed for optimal setting of PSS parameters under different disturbances, loading conditions and system configurations of MMPS. The main advantage of PSO is stable convergence, shorter evaluation time and high quality solutions.

To eliminate the problems in GA, a relatively to newer evolutionary algorithm called BF [156] has been presented for robust PSS design using eigenvalue based function over wide range of operating cases of MMPS. The advantage of BF is global convergence, less computational burden, less computational time requirement. The BF algorithm depends on random search directions which may lead to delay in reaching the global solution. Therefore, to overcome these drawbacks several new interesting optimization algorithm like BA [157] [158], strength pareto approach [159], chaotic algorithm [160], Cultural Algorithm (CA) [161], Culture-PSO-Co Evolutionary (CPCE) algorithm [162], vector evaluated improved honey bee mating optimization [163], GA, BA, and ant colony [164], chaotic teaching-learning [165], HSO [166] and CSO [167]-[169], back-tracking search algorithm [170], gradient based hybrid meta-heuristic technique [171] have been presented for optimization of eigenvalue-based multi-objective function to simultaneous control of damping factor and damping ratio of SMIB system and MMPS under wide range of operating conditions. The main feature of BA is simple, robust, significantly faster than other algorithms and easy to implement. Chaotic Algorithm has features

of less execution time, easy implementation, and robust mechanisms of escaping from the local optimum. The CA is robust and computationally efficient as compared to other meta-heuristic algorithms. The CPCE is a hybrid algorithm, i.e., the combination of CA, PSO and co-evolutionary algorithm.

Combinatorial discrete and continuous action reinforcement learning automata method [172], small population based PSO and BF algorithm [173], and hybrid algorithms like mixed-integer ant direction hybrid differential evolution algorithm [174], bacterial swarm optimization [175], artificial bee colony algorithm [176] have been used for robust designing of PSS using speed based objective function for mitigate local and inter-area modes of oscillations of MMPS.

2.2.4 Other Techniques

The FLCs have many advantages such as simple structure, easy implementation, and mathematical model not required. However, the following disadvantages limit its applications. First, FL controllers are designed mainly from the knowledge of human expertise. This sort of knowledge is sometimes difficult to acquire and represent in the required form. Second, FL controller parameters are usually determined by trial and error method. This method is time consuming and does not guarantee an optimal controller. To overcome such types of limitations, new methods like heuristics algorithms, i.e., GA [177]-[181], differential evolutions [182], global optimization [183], PSO [184] [185], seeker optimization [186], chaotic ant swarm optimization [187], gravitational search [188], have been used for designing FL controllers. The NF based PSS parameters using meta-heuristic techniques like GA [189] [190] are illustrated in literature for damping enhancement of MMPS. Recently some other techniques such as Hybrid differential evolutions [191], variable neighbourhood search algorithm [192] and GA & rough set theory [193] are presented for designing PSS parameters with FACTS devices under different operating conditions of MMPS. The wide area control system technology is also used for SSS analysis of MMPS with Doubly Fed Induction Generator (DFIG) [194] [195]. For SSS enhancement, the co-ordinated control of DFIG and PSS for wide range of operating conditions of MMPS is illustrated in [196]-[201].

2.3 Critical Review

Initially used conventional analytical techniques have requirement of mathematical modelling of MMPS either in transfer function form or in state-space form. Moreover, these limitations are overcome by use of ANN and FL techniques but ANN is suffered from selection of number of neurons and hidden-layer and FL has demerits of trial-and-error based fuzzy rules for parameters designing. Therefore, with the advancement of fast computational facilities, a large number of heuristic and meta-heuristic soft computing techniques are developed. The main advantages of meta-heuristic techniques discussed earlier are derivation free and are able to explore the optimal or near-optimal solution of the optimization problem. Out of these meta-heuristic techniques, GA and PSO have most widely used for designing PSS parameters under wide range of operating conditions. However, their applicability and performance under unseen operating conditions have not been fully investigated. Very recently, new optimization techniques namely; HSO [166] and CSO [167] have been used in diverse power system optimization problems. The HSO is basically a music-based meta-heuristic optimization algorithm developed by Geem et al. [202] [203] and it was influenced by observing that the objective of music is to discover for a perfect state of harmony which is determined by an aesthetic standard. The main advantage of CSO algorithm over other meta-heuristic algorithms is that there are only two parameters, the population size n, and the probability index p_a. Once n is fixed, p_a essentially controls the elitism and the balance of the randomization and local search [204]-[206].

From the literature survey, it is observed that recently developed HSO [166] and CSO [167] have not been fully explored for designing PSS parameters under wide range of operating conditions.

2.4 Research Objectives

Based on the critical review, following broad research objectives are framed for the thesis work:

1. A lot of research work has been carried out in the field of design of PSSs. These research efforts have led to the development of various techniques to design of PSS. One of the objectives is to carry out thorough literature survey pertaining to PSSs designs to lay down the foundation of the thesis.
2. To re-investigate the applicability of GA for designing PSS parameters under wide range of operating conditions and to evaluate their performance under wide range of unseen operating conditions on standard IEEE test systems. The effectiveness of all designed

PSS controllers is to be evaluated using eigenvalue analysis, eigenvalue maps, time-domain simulation results and using performance indices such as *IAE* and *ITAE*.

3. To re-investigate the applicability of PSO for designing PSS parameters under wide range of operating conditions and to evaluate their performance under wide range of unseen operating conditions on standard test systems. The effectiveness of all designed PSS controllers is to be evaluated by eigenvalue analysis, eigenvalue maps, time-domain simulation results and performance indices: *IAE* and *ITAE*.
4. To explore the applicability of recently developed HSO algorithm and to investigate the performance of developed HSO-based PSS (HSOPSS) on four different standard test systems under wide range of operating conditions.
5. To explore the applicability of recently developed CSO algorithm for designing PSS parameters and to investigate the performance of developed CSO-based PSS (CSOPSS) on four different standard test systems under wide range of operating conditions.
6. To carry out a comparative analysis of the proposed CSO, HSO, PSO and GA for optimal designing of PSSs on standard test system under wide range of operating conditions and to bring out the relative features of the proposed CSO, HSO, PSO and GA.

CHAPTER–3

MULTI-MACHINE POWER SYSTEM STABILIZERS DESIGN USING GENETIC ALGORITHM

Genetic Algorithm (GA) is one of the most popular population-based search algorithms, which has the capability to optimize the complex combinatorial problems [207] [208]. As already discussed, GA has been successfully implemented in different optimization problems of power systems [209]-[212]. In [134]-[147], it has been used particularly to solve the power system SSS problem. The main objective of this chapter is to explore GA for robust designing of PSS parameters of four standard power transmission systems, e.g., 3-machine, 9-bus WSCC power system [2], TAFM power system [1], 10-machine, 39-bus NEPS [213] and 16-machine, 68-bus NEEPS [214]. An eigenvalue-based multi-objective function is used for simultaneous control of damping factor and damping ratio to mitigate low frequency electromechanical oscillations of MMPS. The parameters of PSS are so designed that unstable and/or poorly damped open-loop (without PSS) eigenvalues are shifted to a specified D-shape zone in the left-half of the *s*-plane for wide range of operating conditions and tested under different scenarios of severe disturbances. The effectiveness of all designed controllers is evaluated by eigenvalue analysis, eigenvalue maps, time-domain simulation results and performance indices: *IAE* and *ITAE* [134] and their comparative analysis with open-loop are performed. The robustness of all designed controllers is also checked by testing them on unseen operating conditions under different scenarios of severe disturbances and compared.

3.1 Genetic Algorithm

The GA is one of the most widely used derivative free meta-heuristic techniques for solving constrained and unconstrained optimization problem based on evolutionary ideas of natural selection and genetics. The concept and development of GA is credited to the work of Holland [207] and Goldberg [208]. The GA is inspired by Darwin's theory development that is survival of fitness. It is a promising tool for solving single and multi-objective optimization problem. It represents an intelligent exploitation of a random search used to solve the optimization problem.

GA is started with a set of solutions of chromosomes called the populations than repeatedly modifies a population of individual solutions. The GA selects individuals at each step from the existing population to be parents based on their fitness values and uses them to produce the children for the next generation using crossover and mutation operator. Over consecutive generations, the population evolves toward an optimal solution. The different terms associated with GA are as follows:

3.1.1 Chromosome

A chromosome represents a set of parameters that encodes a candidate solution problem which is solved by GA. Generally, a chromosome is represented by a simple string that includes real or binary numbers.

3.1.2 Fitness

A fitness function is particular type of objective function which is defined according to optimization problem. It measures the quality of the represented solution. The fitness is determined using a specified range of parameters defined in the chromosome string of an individual using the single or multi-objective function of the problem.

3.1.3 Initialization

Initially pre-determined numbers of individual's solutions are randomly generated to form initial population which covering entire range of possible solutions in the search space. The size of populations depends upon the nature of problem and the search space.

3.1.4 Selection

In the evolutionary operation of GA the operator selects the chromosome parents in the population for reproduction or next generation. The more fitness of the chromosome indicates the higher probability of selection for reproduction. Thus, selection is based on the survival of-the-fittest strategy. There are lots of methods available in literature like roulette wheel, tournament selection, etc. are used for selection procedure. After selection of the pairs of parent strings, the crossover operator is applied to each of these pairs to produce offspring.

3.1.5 Crossover

In crossover, two parent strings are combined to produce better offspring strings. Two parents exchange their genetic properties in the offspring strings. Generally, all parents are not selected in mating process for crossover operation. This is completed by selecting a fixed percentage of parents for mating, known as crossover probability. Many crossover operators like single-point crossover, double-point crossover, uniform crossover etc. are available in GA literature.

3.1.6 Mutation

Mutation operator randomly flips or alters one or more bit values at randomly selected locations in a chromosome. Mutation is applied to very small percentage of the population (usually 2-10%) and it is used to come out of local minima.

3.1.7 Elitism

Elitism is the process of carrying forward a small proportion of best fitness candidates to the next generation so as to preserve the best solution. This small proportion is known as *Elite Count*. The children so created are known as elite children.

3.1.8 Termination

The GA iterative process is terminated naturally when all individuals reach to the solution with same fitness. But, sometimes it can be terminated earlier depending on the nature of problem and the choice of the user. This termination condition includes the generation limit, time limit, fitness limit, stall generations etc. The flow chart of GA is shown in Fig. 3.1:

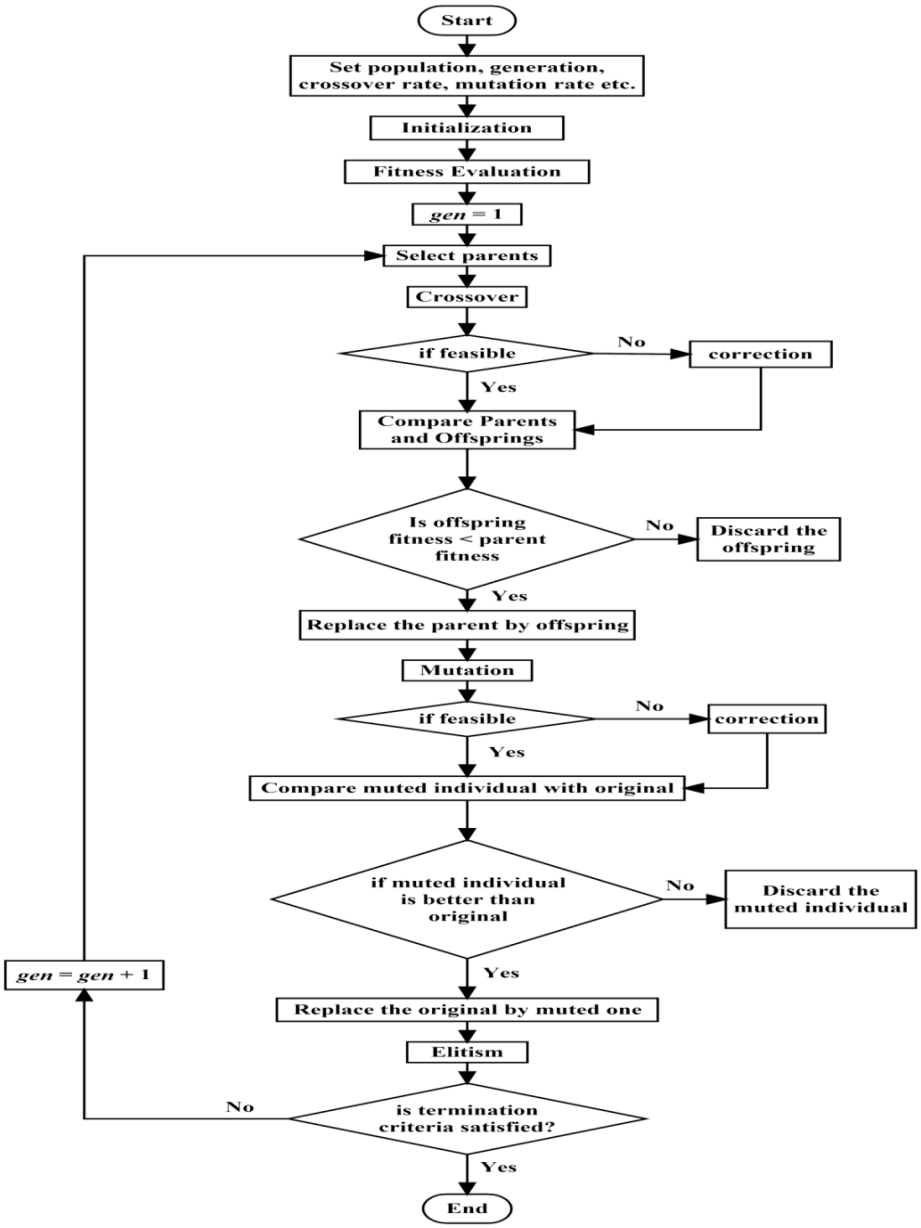

Fig. 3.1 Flow chart of genetic algorithm

3.2 Objective Function

For guaranteed stability and to assure the relative stability of the MMPSs to damp out LFO, the parameters of the PSS are designed so as to minimize the following eigenvalue-based multi-objective function that simultaneous control the damping factor and damping ratio [142]:

$$J = \sum_{j=1}^{np} \sum_{\sigma_{i,j} \geq \sigma_0} (\sigma_0 - \sigma_{i,j})^2 + \sum_{j=1}^{np} \sum_{\xi_{i,j} \leq \xi_0} (\xi_0 - \xi_{i,j})^2 \tag{3.1}$$

This will place the unstable and/or poorly damped eigenvalues of all operating conditions to a D-shape zone characterized by $\sigma_{i,j} \leq \sigma_0$ and $\xi_{i,j} > \xi_0$ [142] in the left-half of the *s*-plane as shown in Fig. 3.2.

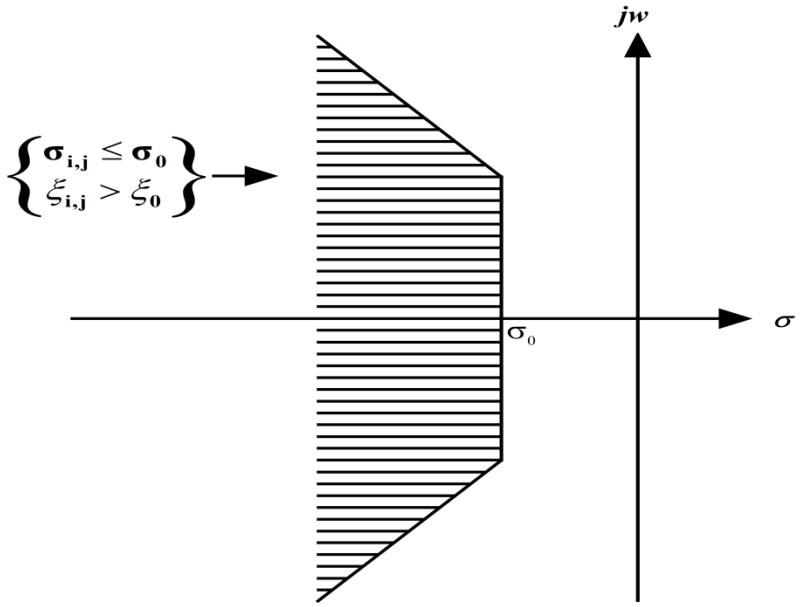

Fig. 3.2 A D-shape zone in the left half of the *s*-plane where $\sigma_{i,j} \leq \sigma_0$ and $\xi_{i,j} > \xi_0$

where *np* is the number of operating points considered in the design problem, $\sigma_{i,j}$ and $\xi_{i,j}$ is the damping factor (real part) and the damping ratio of the *i*th eigenvalue of the *j*th operating point. The value of desired damping factor σ_0 and damping ratio ξ_0 are selected according the requirement of problem. The multi-objective function is formulated with the following constrained of PSS parameters bounds: Minimize *J* subject to:

$$K_i^{\min} \leq K_i \leq K_i^{\max} \tag{3.2}$$

$$T_{1i}^{\min} \leq T_{1i} \leq T_{1i}^{\max} \tag{3.3}$$

$$T_{3i}^{\min} \leq T_{3i} \leq T_{3i}^{\max} \tag{3.4}$$

The objective of the optimization is to search for the optimal set of PSSs parameters setting so that the minimum settling time and overshoots of the system is achieved. Furthermore,

the targets are enhancing the damping performance for wide range of operating conditions to mitigate LFO and finally design a low order controller for easy implementation [137] [150].

3.3 Performance Indices

The performance index is a single measure value of the system performance which emphasis those characteristics of the response that are deemed to be important. The essential function of closed-loop or feedback control system in PSS designing is to reduce the error in speed deviations. Therefore, the effectiveness and robustness of the designed controllers are evaluated through some performance indices. The two performance indices are: Integral of Absolute Error (*IAE*) and Integral of Time Multiplied Absolute Value of Error (*ITAE*) which reflects the settling time and overshoot are evaluated and presented to see the improvement of the system with PSS as compared to without PSS. The values of *IAE* and *ITAE* are given by:

$$IAE = \int_0^t |\Delta w| dt \tag{3.5}$$

$$ITAE = \int_0^t t\,|\Delta w| dt \tag{3.6}$$

It is to be noted that lower the values of these indices, better the system response in terms of speed deviations characteristics. The *ITAE* index is better indicator than *IAE* index to estimate overshoots and oscillations of the system.

3.4 Simulation and Results

The GA is applied on four standard test systems e.g., 3-machine, 9-bus WSCC power system, TAFM power system, 10-machine, 39-bus NEPS and 16-machine, 68-bus NEEPS to obtain the optimal parameters of PSS for wide range of operating conditions. A conventional speed-based lead-lag PSS is used with IEEE type-I ST1A static excitation system. An eigenvalue-based multi-objective function is used for simultaneous control of damping factor and damping ratio to mitigate low frequency electromechanical oscillations of MMPS. The parameters of PSS are so designed that unstable and/or poorly damped open-loop eigenvalues are shifted to a specified D-shape zone in the left-half of the *s*-plane for wide range of operating conditions under different scenarios of severe disturbances. This is obtained by minimizing the objective function (3.1) using GA. The effectiveness of all designed controllers are evaluated by eigenvalue analysis, eigenvalue maps, time-domain simulation results and performance indices *IAE, ITAE* and the system performance with GAPSSs is compared with that of without PSS. The robustness of all designed controllers is also checked by testing them on unseen operating conditions under different scenarios of severe disturbances and compared with that of without PSS.

3.4.1 Example 1: Three-Machine, Nine-Bus WSCC Power System

The 3-machine, 9-bus WSCC power system and its data are referred from [2]. It consists of three-generators, nine-buses, six-lines, three two-winding transformers and three-loads. A local load is also connected at the generator G_1. Here, the three generators G_1, G_2 and G_3 are represented by fourth order nonlinear model with fast static excitation systems. The three loads A, B and C are situated near to the buses 5, 6 and 7 respectively. Other details and the single-line diagram of the system are given in Appendix. Three different operating conditions of generators and loads are shown in Table 3.1 and are considered for SSS analysis [167].

Table 3.1: Three operating conditions of generators and loads for WSCC power system

Generator	Case-1		Case-2		Case-3	
	P	***Q***	***P***	***Q***	***P***	***Q***
	(p. u.)					
G_1	0.71	0.62	0.96	0.22	3.57	1.81
G_2	1.63	0.06	1.00	− 0.19	2.20	0.71
G_3	0.85	–0.10	0.45	− 0.26	1.35	0.43
Load						
A	1.25	0.50	0.70	0.35	2.00	0.90
B	0.90	0.30	0.50	0.30	1.80	0.60
C	1.00	0.35	0.60	0.20	1.60	0.65
Load at G_1	1.00	0.35	0.60	0.20	1.60	0.65

A. Eigenvalue Analysis of WSCC Power System without PSS and with GAPSSs

The participation factor method [33] is used to identify the optimum locations of installation of PSS in this system. Power System Analysis Toolbox (PSAT) [215] is used for eigenvalue analysis of the system for the three cases. Generally, it is observed that damping ratio of 0.10 is required for damping out unstable and/or lightly damped modes oscillations of power systems. Hence, open-loop eigenvalues, damping ratio, frequency, participation modes and participation factor associated with electromechanical modes of the system having damping ratios below 0.10 only are shown in Table 3.2.

Table 3.2: Open-loop eigenvalues, damping ratio, frequency, participation modes and participation factor for operating cases 1-3 of WSCC power system

Cases	Eigenvalues &Damping Ratio	Frequency (p. u.)	Participation Modes	Participation Factor
Case-1	− 0.110 ± j 8.588, 0.012	1.366	w_2, δ_2	0.290
	− 0.653 ± j 13.023, 0.050	2.072	w_3, δ_3	0.374
Case-2	− 0.637 ± j 8.515, 0.074	1.355	w_2, δ_2	0.278
	− 1.274 ± j 12.752, 0.099	2.029	w_3, δ_3	0.355
Case-3	**0.158 ± j 8.372, − 0.018**	1.332	w_2, δ_2	0.288
	− 0.308 ± j 12.896, 0.024	2.052	w_3, δ_3	0.384

The table reveals that for open-loop system, the WSCC system becomes unstable as well as poorly damped for Case-3 through two local modes of oscillations. These modes primarily associated with rotor angles δ_2, δ_3 and speed w_2, w_3 with high participation in their respective modes. Therefore, the corresponding generators G_2 and G_3 are the optimum locations for installing PSSs.

For guaranteed stability of unstable local modes and to assured the relative stability of poorly damped local modes, LFO are to be damped out by increasing the damping performance of WSCC power system. An eigenvalue-based multi-objective function J presented in (3.1) is minimized using GA by tuning the six parameters of PSSs. In this case, the value of desired damping factor σ_0 and damping ratio ξ_0 are selected as –0.5 and 0.1 respectively [167]. The value of washout time constant is chosen as 5 sec, T_2 and T_4 are kept constant at numerical values of 0.05 sec. The range of design parameters K, T_1 and T_3 are set as [1-100], [0.06-1] and [0.06-1] respectively [171]. The PSSs designed using GA is named as GAPSS. The GA is applied with population size 100, maximum generation 100, crossover rate 0.75 and mutation rate 0.01.

The GA is able to find the desired solution for which fitness function J is zero. The final value of J equal to zero indicates that two unstable and/or poorly damped eigenvalues are shifted to a specified D-shape zone in the left-half of the s-plane. The optimal six parameters obtained by GAPSSs for two generators are shown in Table 3.3.

Table 3.3: Optimal designed parameters of GAPSSs

Generators	K	T_1	T_3
G_2	1	0.464	0.06
G_3	1	0.610	0.679

The closed-loop eigenvalues and their damping ratio with GAPSSs for three operating cases are evaluated using PSAT [215] and are shown in Table 3.4. Fig. 3.3 (a)-(c) and (d)-(f) show the eigenvalue maps for without PSS and with GAPSSs for operating cases 1-3 respectively.

Table 3.4: Eigenvalues and damping ratio with GAPSSs for operating cases 1-3

Case-1	**Case-2**	**Case-3**
− 1.778 ± j 8.323, 0.209	− 1.659 ± j 7.724, 0.210	– 0.961 ± j 7.148, 0.133
− 1.887 ± j 7.160, 0.254	− 2.811 ± j 7.480, 0.351	– 1.930 ± j 8.508, 0.221

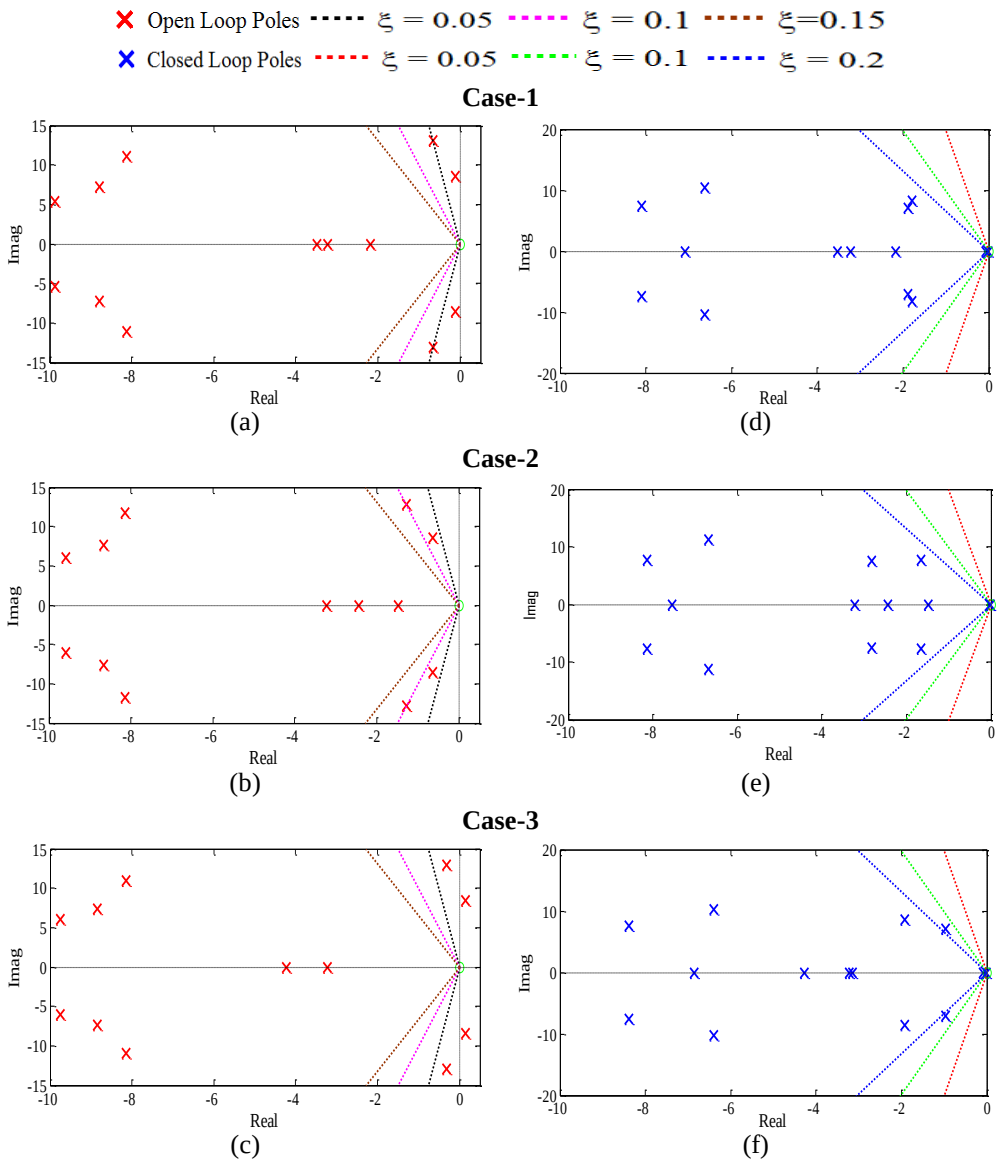

Fig. 3.3 Eigenvalue maps (a)-(c) without PSS (d)-(f) with GAPSSs for operating cases 1-3 of WSCC power system

From Figure 3.3 (a)-(c), it is observed that for Case-3, one pair of open-loop eigenvalues lie in right-half of the s-plane and $\xi < 0$. Similarly for Case-1 one pair of open-loop eigenvalues has $0 < \xi < 0.05$ and other has $\xi = 0.05$, for Case-2 two pairs of open-loop eigenvalues have $0.05 < \xi < 0.10$, lie nearest to left-half of the imaginary axis in the *s*-plane. Moreover, it is observed that unstable modes and poorly damped modes as shown in the Table 3.2 have high participation as compared to other frequency modes.

Table 3.4 and Fig. 3.3 (d)-(f) show that the GAPSSs shift the eigenvalues to a specified D-shape zone in the left half of the *s*-plane with desired damping factor and damping ratio as compared to that of without PSS. Hence, designed GAPSS controllers provide improved stability and damping performance of the WSCC power system as compared to same obtained using without PSS.

B. Time-Domain Simulation Results and Discussions with GAPSSs and without PSS of WSCC Power System

In order to examine the performance of designed GAPSS controllers in previous section, in terms of speed deviations, various scenarios of disturbances on WSCC power system without PSS are considered as shown in Table 3.5. Established index *i.e. ITAE* is evaluated for each scenario of disturbances for operating cases 1-3 and presented as bar charts in the Fig. 3.4 (a)-(c) respectively.

Table 3.5: Various scenarios of disturbances at t = 1 sec on WSCC power system

Scenarios	Scenarios of Disturbances
S-1	A 6-cycle 3-phase fault at bus 1
S-2	A 6-cycle 3-phase fault at bus 2
S-3	A 6-cycle 3-phase fault at bus 3
S-4	A 6-cycle 3-phase fault at bus 4
S-5	A 6-cycle 3-phase fault at bus 5
S-6	A 6-cycle 3-phase fault at bus 6
S-7	A 6-cycle 3-phase fault at bus 7
S-8	A 6-cycle 3-phase fault at bus 8
S-9	A 6-cycle 3-phase fault at bus 9

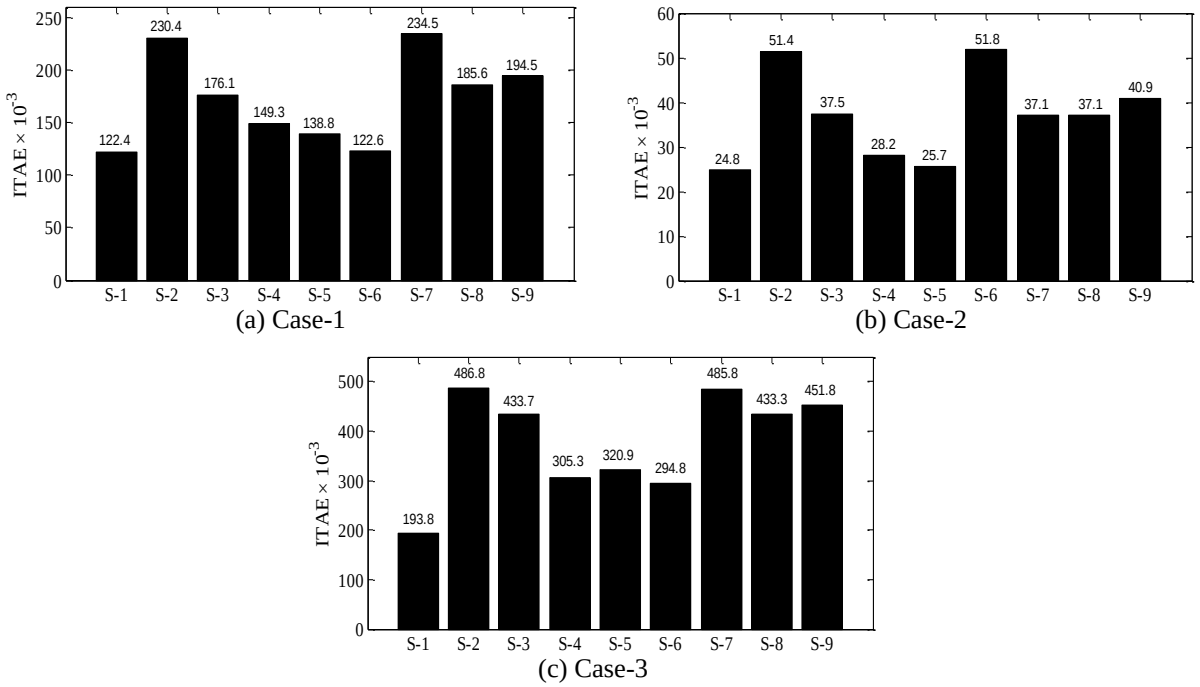

Fig. 3.4 (a)-(c) Value of *ITAE* without PSS for scenarios S-1 to S-9 of operating cases 1-3 respectively

From the figure it may be noticed that the values of *ITAE* for each scenario are maximum for operating Case-3 as compared to other operating cases values. Therefore, Case-3 is most severe operating case. Moreover, it is observed that for Case-3 the values of *ITAE* for scenarios of severe disturbances, i.e. S-2 and S-7 are higher as compared to other scenarios of the cases.

Therefore, these two most severe scenarios of disturbances are chosen for testing the performance of the designed GAPSS controllers and are renamed in Table 3.6.

Table 3.6: Scenarios of disturbances for testing the performance of GAPSSs on WSCC power system

Scenarios	Most Severe Scenarios of Disturbances
Scenario-1 (S2)	A 6-cycle, 3-phase fault occur at t = 1 sec on bus 2
Scenario-2 (S7)	A 6-cycle, 3-phase fault occur at t = 1 sec on bus 7

The time-domain simulation of WSCC power system is performed with GAPSSs for observed severe scenarios of disturbances for severe operating Case-3 only. The generator speed deviations Δw_{12}, Δw_{23} and Δw_{31} for selected severe scenarios of Case-3 for the system without PSS and with GAPSSs are shown in Fig. 3.5 (a)-(b) and (c)-(d), respectively.

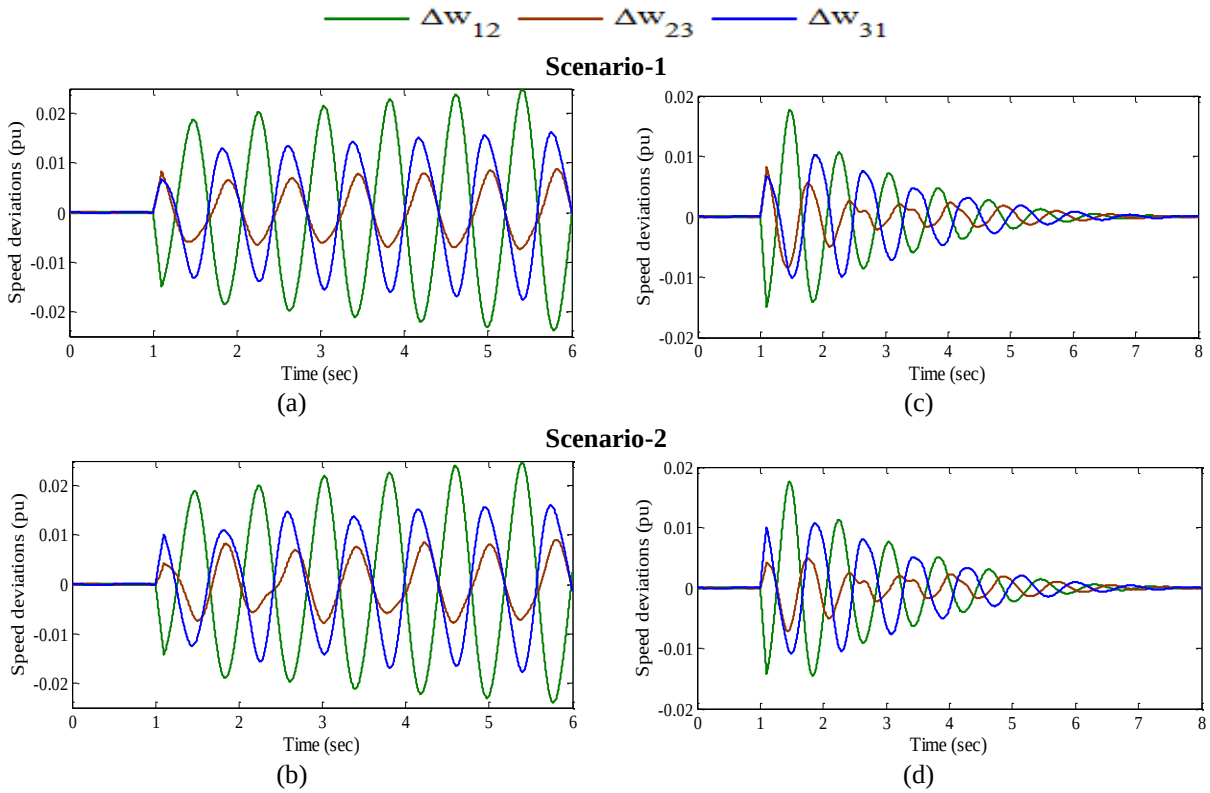

Fig. 3.5 Speed deviations (a)-(b) without PSS and (c)-(d) with GAPSSs for scenarios 1-2 of operating case-3

From Fig. 3.5 (a)-(b), it is observed that in all these response plots, the system without PSS is not capable to damp out LFO because these oscillations are continuously increasing in amplitude with time and therefore, all generators may go out of synchronism. Moreover, the speed deviation Δw_{12} is most severe due to large amplitude of oscillations. Furthermore, it may be clearly observed from Fig. 3.5 (c)-(d) that with GAPSSs system performance is improved and all oscillations for both scenarios are well damped out. This illustrates the potential of GA to obtain a desired set of PSS parameters for WSCC power system and the designed GAPSSs are

capable to damp out LFO for wide range of operating cases under severe scenarios of disturbances.

C. Performance Indices Results and Discussions with GAPSSs of WSCC Power System

In addition to time-domain simulation results, the effectiveness of designed GAPSS controllers is also observed by evaluating two performance indices: *IAE* and *ITAE* to indicate the overshoot and settling time for two observed severe scenarios of disturbances. Established both indices are evaluated for each scenario of disturbances for operating cases 1-3 and presented as bar charts in the Fig. 3.6 (a)-(b) and (c)-(d) respectively.

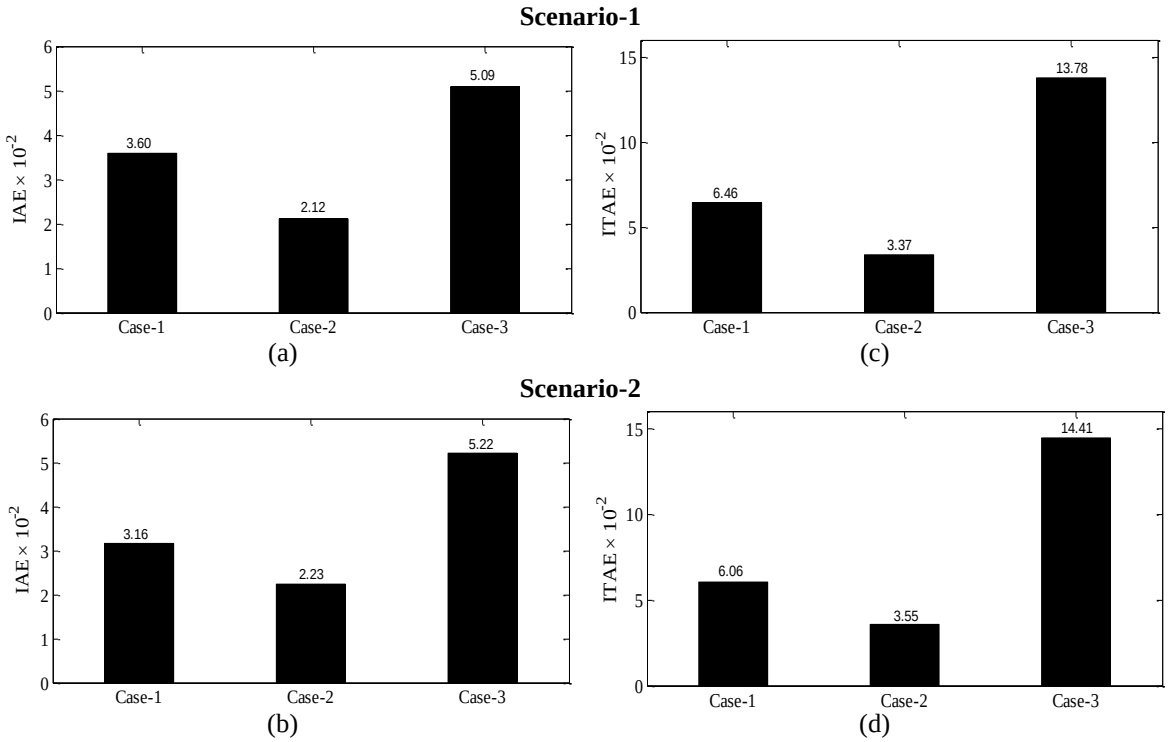

Fig. 3.6 Values of (a)-(b) *IAE* and (c)-(d) *ITAE* with GAPSSs for scenarios1-2 of operating cases 1-3

The figure reveals that the values of both indices for the GAPSSs are minimum for each scenario of Case-2 and maximum for each scenario of Case-3, which indicates that Case-3 is the most severe whereas Case-2 is the least severe. Moreover, for operating Case-1, Scenario-1 is more severe but for cases 2-3, Scenario-2 is more severe. Comparing Fig. 3.6 with Fig. 3.4, it may be observed that the designed GAPSS controllers of WSCC power system provide sufficient damping to damp out low frequency local modes of oscillations with less overshoot and settling time than that of without PSS.

D. Robustness Test of Designed GAPSS Controllers of WSCC Power System

To test the robustness of earlier designed GAPSS controllers for WSCC power system, unseen operating conditions of generators and loads as cases 4-6 are considered as shown in Table 3.7.

Table 3.7: Three unseen generator's operating conditions and loads of WSCC power system

Generator	Case-4		Case-5		Case-6	
	P	***Q***	***P***	***Q***	***P***	***Q***
	(p. u.)					
G_1	0.33	1.12	1.09	0.79	1.41	0.59
G_2	2.00	0.57	2.45	0.57	2.60	0.38
G_3	1.50	0.38	1.27	0.21	1.2	0.02
Load						
A	1.50	0.90	1.90	0.75	2.00	0.60
B	1.20	0.80	1.30	0.45	1.50	0.30
C	1.00	0.50	1.50	0.50	1.60	0.20

In this section, the effectiveness of GAPSS controllers for three unseen cases is evaluated by eigenvalue analysis, time-domain simulation results, performance indices and compared with that of without PSS. Open-loop eigenvalues, damping ratio, frequency, participation modes, participation factor for unstable and poorly damped modes of unseen operating cases 4-6 of WSCC power system without PSS and closed-loop eigenvalues &damping ratio with earlier designed GAPSSs for the same cases are obtained using PSAT [215] and shown in Table 3.8.

Table 3.8 Open-loop eigenvalues, damping ratio, frequency, participation modes, participation factor and closed-loop eigenvalues, damping ratio with GAPSSs for unseen operating cases 4-6

Case	Open-loop				Closed-loop
	Eigenvalues & Damping Ratio	**Frequency (p. u.)**	**Participation Modes**	**Participation Factor**	**Eigenvalues & Damping Ratio**
Case-4	**0.341 ± j 8.339, – 0.040**	1.327	w_2, δ_2	0.269	– 0.766 ± j 7.225, 0.105
	– 0.109 ± j 12.803, 0.0085	2.037	w_3, δ_3	0.363	– 1.829 ± j 8.273, 0.215
Case-5	**0.465 ± j 8.357, – 0.055**	1.330	w_2, δ_2	0.272	– 1.228 ± j 8.052, 0.150
	– 0.250 ± j 12.931, 0.019	2.058	w_3, δ_3	0.382	– 1.327 ± j 7.440, 0.175
Case-6	**0.604 ± j 8.375, – 0.072**	1.333	w_2, δ_2	0.270	– 0.746 ± j 8.283, **0.089**
	– 0.233 ± j 12.981, 0.018	2.065	w_3, δ_3	0.383	– 1.692 ± j 7.092, 0.232

The table reveals that for open-loop, the WSCC power system becomes unstable as well as poorly damped with two local modes of oscillations for unseen operating cases 4-6. The Case-6 is highly unstable due to more negative damping than other unseen operating cases and cases 1-3 considered earlier. The table also shows that for cases 4-6 one pair of open-loop eigenvalues lie in right-half of the *s*-plane and $\xi < 0$ and other one pair eigenvalues has $0 < \xi < 0.05$. These modes primarily associated with rotor angles δ_2, δ_3 and speed w_2, w_3 with high

participation in their respective modes which also show that the optimal locations to install the PSS are at G_2 and G_3 as also concluded in Section 3.4.1 (A).

The table shows that the GAPSSs shift the eigenvalues in the left half of the *s*-plane with improved damping factor and damping ratio as compared to without PSS for unseen cases. This ensures that the system will be stable for all considered unseen cases also. It is also observed that designed GAPSS controllers satisfy the earlier selected criterion for the value of desired damping factor and damping ratio for PSS design except in unseen Case-6 where slightly more overshoot may occur. Hence, the designed GAPSS controllers are robust as it works with satisfactory damping performance for unseen operating cases 4-6 of the WSCC power system also.

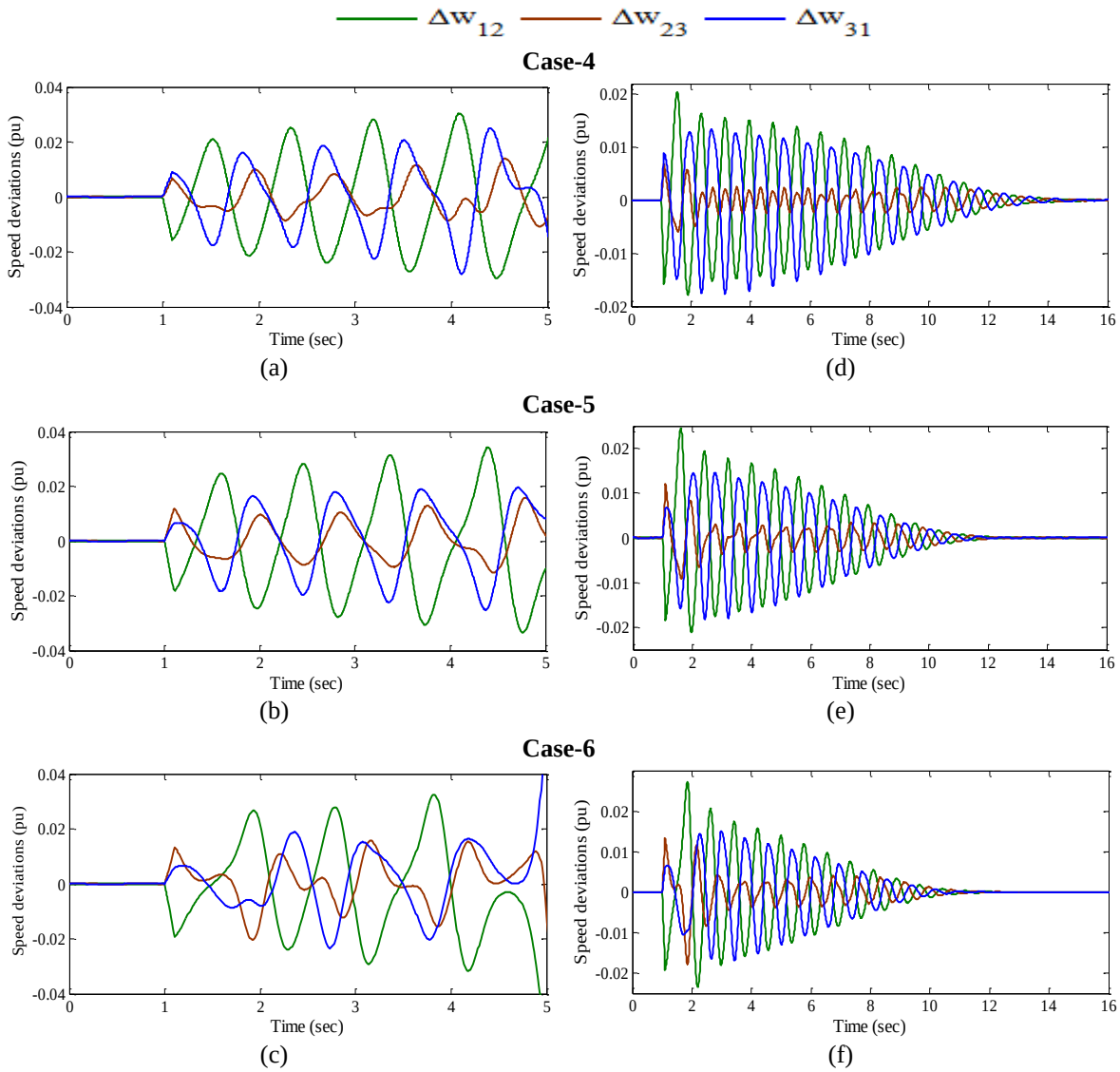

Fig. 3.7 Speed deviations (a)-(c) without PSS and (d)-(f) with GAPSSs for scenario-1 of operating cases 4-6

In order to further examine the robustness performance of the GAPSSs in terms of speed deviations, the time-domain simulations are performed using PSAT [215] for two earlier observed severe scenarios of disturbances shown in Table 3.6, on unseen operating cases 4-6 of

WSCC power system. The speed deviations Δw_{12}, Δw_{23} and Δw_{31} without PSS for scenarios 1 and 2 of cases 4-6 are shown in Fig. 3.7 (a)-(c) and Fig. 3.8 (a)-(c) respectively whereas the Δw_{12}, Δw_{23} and Δw_{31} with GAPSSs are shown in Fig. 3.7 (d)-(f) and Fig. 3.8 (d)-(f) respectively. The response plots in Fig. 3.7 (a)-(c) and 3.8 (a)-(c) show that the system without PSS is not capable to damp out LFO due to high deviations in speed response and all generators loose the synchronism. Moreover, the speed deviation Δw_{12} is most severe due to large amplitude oscillations. Furthermore, it is also observed that the Case-6 is most severe operating case as generators quickly go out of synchronism than other unseen cases.

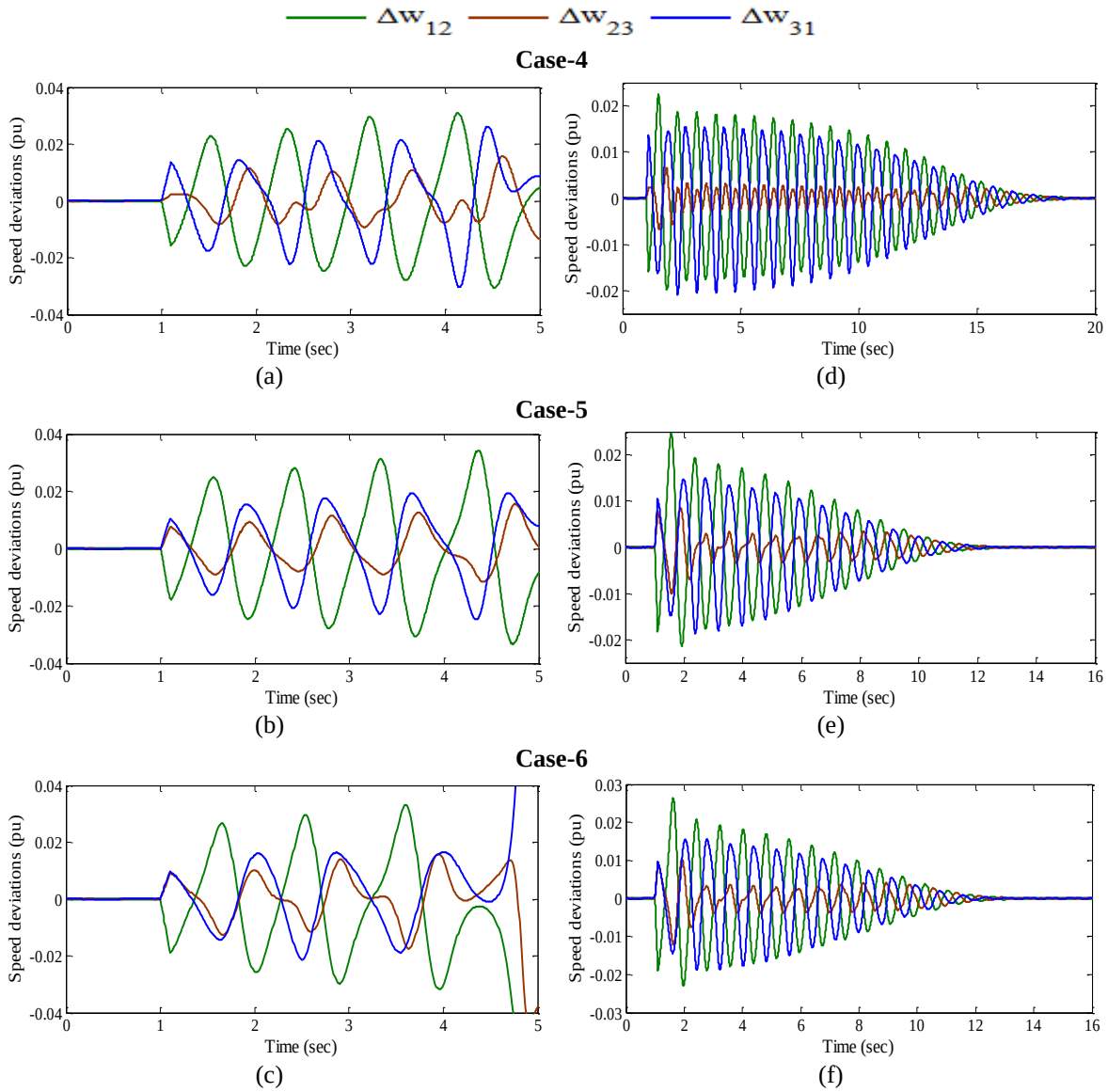

Fig. 3.8 Speed deviations (a)-(c) without PSS and (d)-(f) with GAPSSs for scenario-2 of operating cases 4-6

From the response plots in Fig. 3.7 (d)-(f) and Fig. 3.8 (d)-(f), the speed deviation responses with GAPSSs for scenarios 1-2 of Case-4 produce more oscillations as compared to other cases. Moreover, peak overshoot in speed deviation responses for scenarios 1-2 of Case-6 is more as compared to other cases. Furthermore, the speed deviations with GAPSSs for scenarios 1-2 of unseen operating cases 4-6 take more time to damp out LFO as compared to earlier cases 1-3. This may be concluded that the designed GAPSSs work satisfactorily for all the scenarios of severe disturbances of unseen operating cases of WSCC power system.

In addition to time-domain simulation results, the effectiveness and robustness of designed GAPSS controllers is also observed by calculating predefined indices: *IAE* and *ITAE* for observed scenarios of unseen operating cases. Established both indices with GAPSSs are determined for each scenario of disturbances for operating cases 4-6 and presented as bar charts in the Fig. 3.9 (a)-(b) and (c)-(d) respectively.

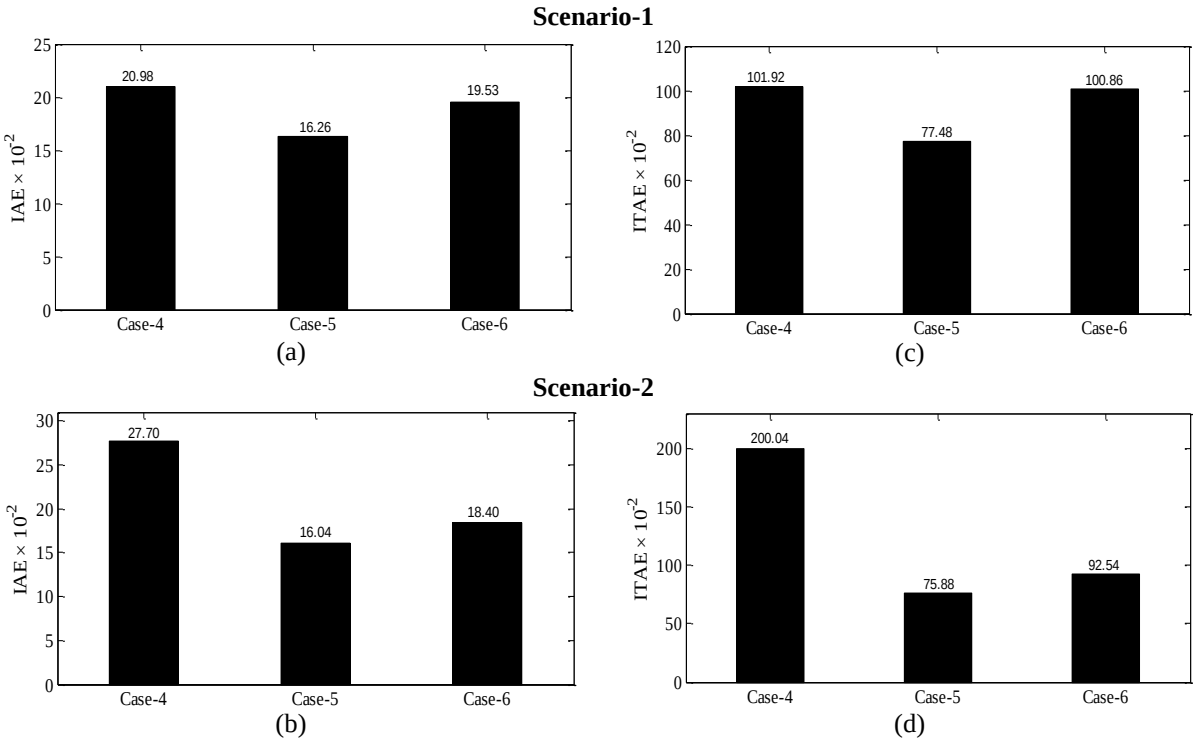

Fig. 3.9: Values of (a)-(b) *IAE* and (c)-(d) *ITAE* with GAPSSs for scenarios 1-2 of operating cases 4-6

The figure reveals that the values of both indices for the GAPSSs are minimum for each scenario of Case-5 and maximum for each scenario of Case-4, which indicates that Case-4 is the most severe whereas Case-5 is the least severe. Moreover, for operating Case-4, Scenario-2 is more severe but for cases 5-6, Scenario-1 is more severe.

Hence, the designed GAPSS controllers for WSCC power system is able to damp out LFO with improved stability and damping performances for wide range of operating cases under scenarios of severe disturbances and also for unseen operating cases under same scenarios of disturbances.

3.4.2 Example 2: Two-Area, Four-Machine (TAFM) Power System

This system comprising of two generating areas connected by 220-Km, 230-KV double circuit tie-line. The two areas 1 and 2 consist of two generators G_1, G_2 and G_3, G_4 respectively [1]. All generators mechanical and electrical parameters are same, except their inertia constants. These generators are represented by fourth order nonlinear model with fast static excitation system. The single-line diagram and other details of the system are given in Appendix. Three cases of different loading conditions are considered for tuning the PSS parameters for SSS analysis, i.e., Case-1 as normal loading, Case-2 as light loading and Case-3 as high loading [161], shown in Table 3.9.

Table 3.9: Three operating conditions of TAFM power system

Case-1	Case-2	Case-3
Nominal active power	Total active power decreasing by 20%	Total active power increasing by 20%
Nominal reactive power	Total reactive power decreasing by 15%	Total reactive power increasing by 15%

A. Eigenvalue Analysis of TAFM Power System without PSS and with GAPSSs

The PSAT [215] is used for eigenvalue analysis of the system for three different loading cases. Normally, the PSS is not required for the swing generator [161]. Therefore, all generators are equipped with PSS except swing generator $G_3$and the PSS parameters of only three generators G_1, G_2, G_4 are to be optimized. The open-loop eigenvalues, damping ratio, frequency, participation modes and participation factor are calculated for only unstable and/or poorly damped electromechanical modes of the system are shown in Table 3.10.

Table 3.10: Open-loop eigenvalues, damping ratio, frequency, participation modes and participation factor for operating cases 1-3 of TAFM power system

Cases	Eigenvalues &Damping Ratio	Frequency (p. u.)	Participation Modes	Participation Factor
Case-1	**0.026 ± j 3.803, – 0.070**	**0.605**	w_3, δ_3	0.16492
	– 0.541 ± j 7.027, 0.076	1.118	w_4, δ_4	0.23660
	– 0.543 ± j 6.810, 0.079	1.083	w_2, δ_2	0.23336
Case-2	– 0.068 ± j 3.279, 0.021	**0.521**	w_3, δ_3	0.19819
	– 1.010 ± j 6.380, 0.156	1.015	w_4, δ_4	0.23344
	– 0.535 ± j 6.786, 0.078	1.080	w_2, δ_2	0.23546
Case-3	**0.160 ± j 3.751, – 0.042**	**0.596**	w_3, δ_3	0.13831
	0.042 ± j 7.129, – 0.005	1.134	w_4, δ_4	0.23691
	– 0.545 ± j 6.803, 0.079	1.082	w_2, δ_2	0.23904

The table reveals that for open-loop system, the TAFM system becomes unstable as well as lightly damped for Case-1, Case-3 and only lightly damped for Case-2. Also, the system has one inter-area mode and two local area modes for all loading cases. These inter-area modes are associated with rotor angles $\delta_3$and speed w_3 whereas local modes are associated with δ_4, $\delta_2$and w_4, w_2 with high participation in their respective modes.

To assure the relative stability of lightly damped local modes and for guaranteed stability of unstable inter-area modes, LFO are to be damped out by increasing the damping of TAFM power system. An eigenvalue-based multi-objective function J presented in (3.1) is minimized using GA by tuning the nine parameters of PSSs. In this case, the desired value of damping factor σ_0 and damping ratio ξ_0 are chosen as –1.0 and 0.2 respectively. The value of washout time constant is selected as 10 sec; T_2 and T_4 are held constant at numerical values of 0.01 sec. The values of design parameters K, T_1 and T_3 are set in the range of [1-100], [0.01–1] and [0.01–1] respectively [161]. The GA is applied with population size 50, maximum generation 50, crossover rate 0.75 and mutation rate 0.01.

The GA is able to find the desired solution for which fitness function J is zero. The final value of J equal to zero indicates that three unstable and/or poorly damped eigenvalues are shifted to a specified D-shape zone in the left-half of the *s*-plane. The optimum designed nine parameters of GAPSSs for three generators are shown in Table 3.11.

Table 3.11: Optimal designed parameters of GAPSSs

Generators	K	T_1	T_3
G_1	21.315	0.079	0.634
G_2	26.026	0.239	0.056
G_4	32.569	0.044	0.046

The closed-loop eigenvalues and their damping ratio with GAPSSs for loading cases 1-3 are determined using PSAT [215] and shown in Table 3.12. The Fig. 3.10 (a)-(c) and (d)-(f) show the eigenvalue maps for without PSS and with GAPSSs for three cases of loading respectively.

Table 3.12: Eigenvalues and damping ratio with GAPSSs for loading cases 1-3

Case-1	**Case-2**	**Case-3**
– 1.109 ± j 4.044, 0.26	– 1.098 ± j 3.354, 0.31	– 1.433 ± j 5.434, 0.25
– 2.240 ± j 1.175, 0.88	– 2.058 ± j 0.841, 0.92	– 1.231 ± j 2.490, 0.44
– 1.493 ± j 2.582, 0.50	– 1.426 ± j 2.758, 0.45	– 2.393 ± j 3.439, 0.57

Figure 3.10 (a)-(c) show that for Case-1 and Case-3, one and two pairs of open-loop eigenvalues lie in right-half of the *s*-plane respectively and $\xi < 0$ (see also Table 3.10).

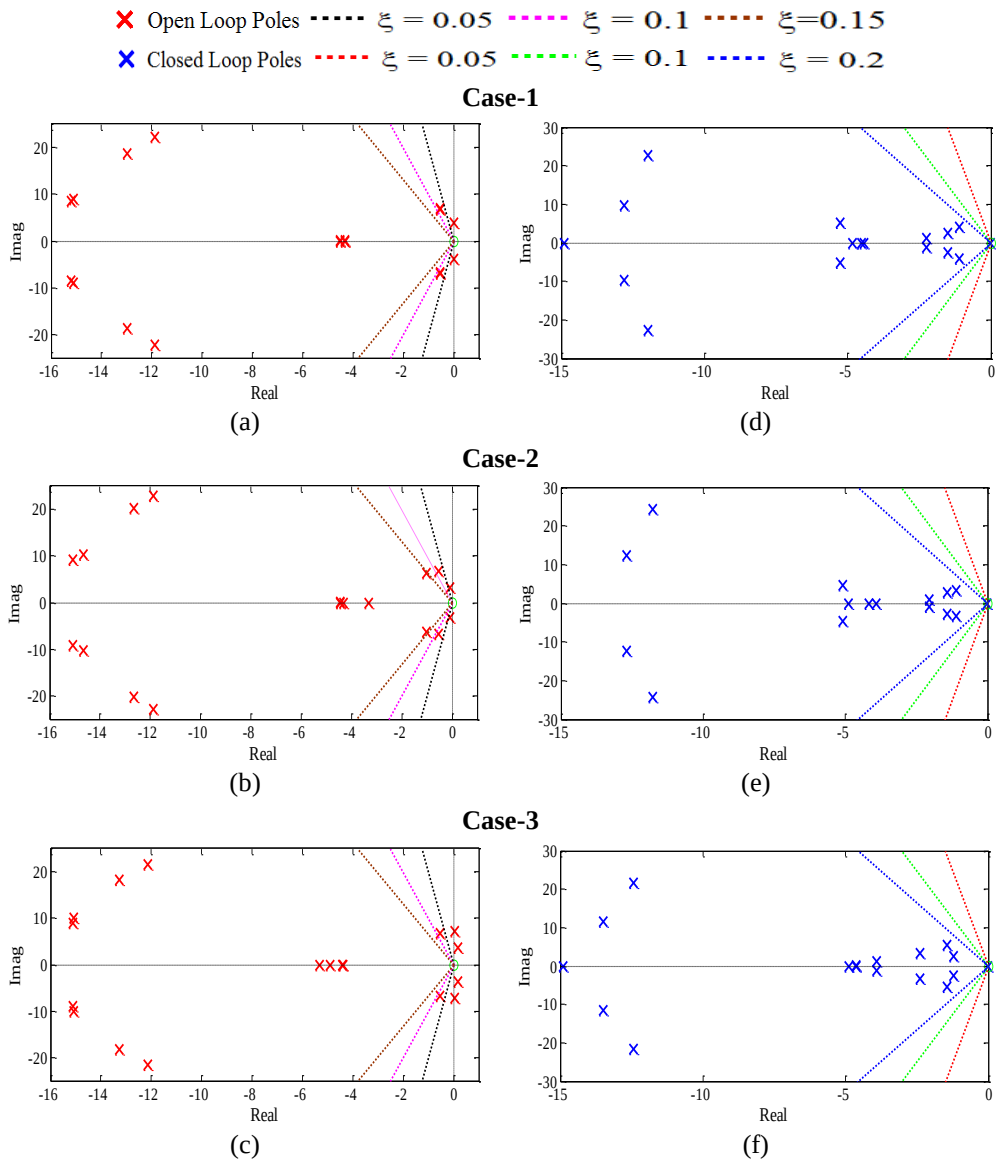

Fig. 3.10 Eigenvalue maps (a)-(c) without PSS (d)-(f) with GAPSSs for loading cases 1-3 of TAFM power system

Similarly for Case-1, two pairs of open-loop eigenvalues have $0.05 < \xi < 0.10$, for Case-2 three pairs of open-loop eigenvalues have $0 < \xi < 0.05$, $0.05 < \xi < 0.10$ and $\xi > 0.15$ and for Case-3 one pair of open-loop eigenvalues has $0.05 < \xi < 0.10$, lie close to imaginary axis in left-half of the *s*-plane. Moreover, it is observed that one inter-area mode eigenvalue of Case-3 is highly unstable with most negative damping and high participation of the mode shown in Table 3.10 as compared to other frequency modes.

Table 3.12 and Fig. 3.10 (d)-(f) show that the GAPSSs shift the eigenvalues to a specified D-shape zone in the left half of the *s*-plane with improved damping factor and damping ratio as compared to that of without PSS for all loading cases. Hence, designed GAPSS controllers provide enhanced stability and damping performance of the TAFM power system as compared to same obtained using without PSS.

B. Time-Domain Simulation Results and Discussion with GAPSSs and without PSS of TAFM Power System

In order to examine the performance of previously designed GAPSS controllers in terms of speed deviations under different scenarios of severe disturbances on TAFM power system without PSS are considered as shown in Table 3.13. Established index *i.e. ITAE* is evaluated for each scenario of disturbances for loading cases 1-3 and presented as bar charts in the Fig. 3.11 (a)-(c) respectively.

Table 3.13: Various scenarios of disturbances at t = 1 sec on TAFM power system

Scenarios	Scenarios of Disturbances
S-1	A 6-cycle 3-phase fault at bus 7 without tripping the line 7-8
S-2	A 6-cycle 3-phase fault at bus 8 without tripping the line 7-8
S-3	A 6-cycle 3-phase fault at bus 8 without tripping the line 8-9
S-4	A 6-cycle 3-phase fault at bus 9 without tripping the line 8-9
S-5	A 6-cycle 3-phase fault at bus 1
S-6	A 6-cycle 3-phase fault at bus 2
S-7	A 6-cycle 3-phase fault at bus 3
S-8	A 6-cycle 3-phase fault at bus 4

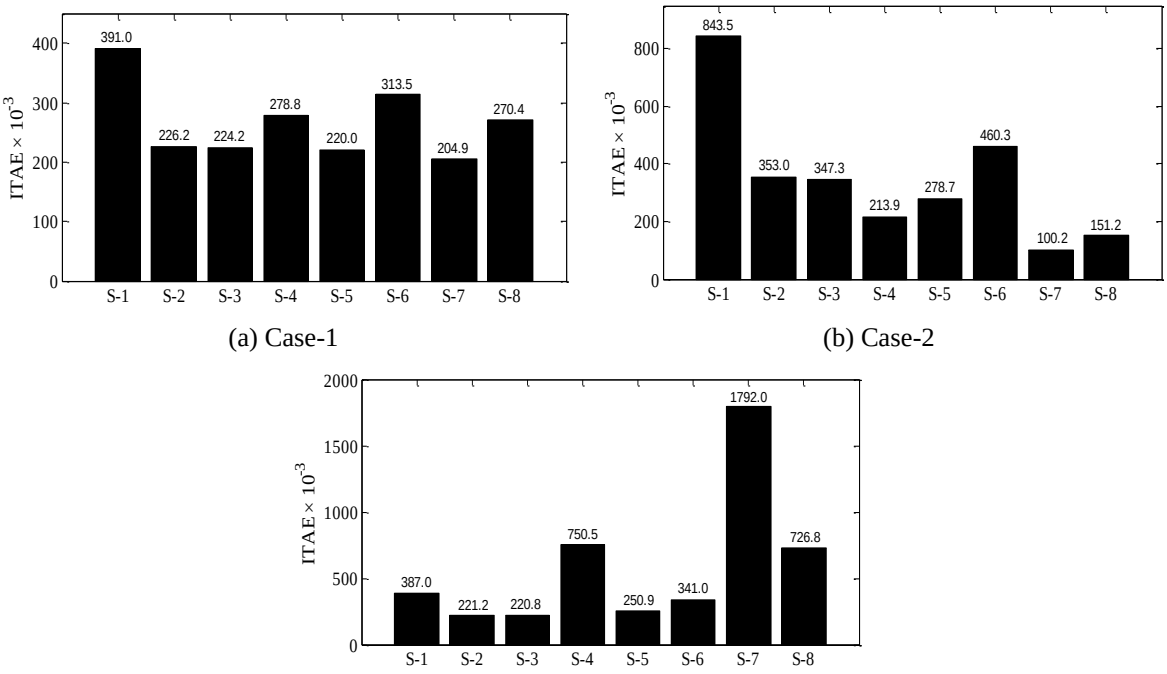

Fig. 3.11(a)-(c) Value of *ITAE* without PSS for scenarios S-1 to S-8 of loading cases 1-3

Figure reveals that the values of *ITAE* are higher for S-1 of Case 2 and S-4, S-7 and S-8 of Case-3 as compared to other scenarios. Therefore, these four most severe disturbances scenarios are selected for testing the performance of the designed GAPSS controllers for three loading cases of TAFM power system.

Normally, 5-6 cycles (0.083 or 0.1 sec) of operation are required for controlling and protection of 60-Hz operated power system. For the sake of robustness, the number of cycles of operation increases with three-phase faults until designed controllers for the system fails. Therefore, the above selected scenarios with increased duration of disturbances are renamed and shown in Table 3.14.

Table 3.14: Scenarios of disturbances for testing the performance of GAPSSs on TAFM power system

Scenarios	Most Severe Scenarios of Disturbances
Scenario-1	A 9-cycle, 3-phase fault occur at t = 1 sec on bus 7 without tripping the line 7-8 for Case-2
Scenario-2	A 12-cycle, 3-phase fault occur at t = 1 sec on bus 9 without tripping the line 8-9 for Case-3
Scenario-3	A 6-cycle 3-phase fault at t = 1 sec on bus 3 for Case-3
Scenario-4	A 12-cycle 3-phase fault at t = 1 sec on bus 4 for Case-3

The time-domain simulations of TAFM power system is performed with GAPSSs for above scenarios and speed deviations $\Delta w_1, \Delta w_2$, Δw_3 and Δw_4 without PSS and with GAPSSs are shown in Fig. 3.12 (a)-(d) and (e)-(h) respectively.

From Fig. 3.12 (a)-(d), it may be observed that in all these response plots, the LFO are rapidly growing with time for the system without PSS and is not capable to damp out theses oscillations. Moreover, the oscillations are continuously increasing in amplitude with time in one direction in scenarios 2-4 whereas in Scenario-1 the oscillations of $\Delta w_1, \Delta w_2$ and $\Delta w_3, \Delta w_4$ move in opposite directions and in all scenarios generators may go out of synchronism. Furthermore, the Scenario-1 is most severe disturbance scenario as compared to other scenarios of loading cases.

From Fig. 3.12 (e)-(h), it is observed that with GAPSSs oscillations for all generators are well damped with less overshoot and settling time for all scenarios of severe loading cases. Moreover, it is clear that the system performance with GAPSSs is much improved than that of without PSS for all severe disturbance scenarios of loading cases and oscillations die out smoothly. Furthermore, on the basis of number of cycles of operation, it may be observed that the speed response with GAPSSs for Scaneraio-4 consumed more time to damp out oscillations as compared to Scenario-2 of loading Case-3. This demonstrates the potential of GA to obtain a desired set of PSS parameters for TAFM power system and the designed GAPSSs are capable to improve the damping performance of the system than that of without PSS for wide range of loading cases under severe scenarios of disturbances.

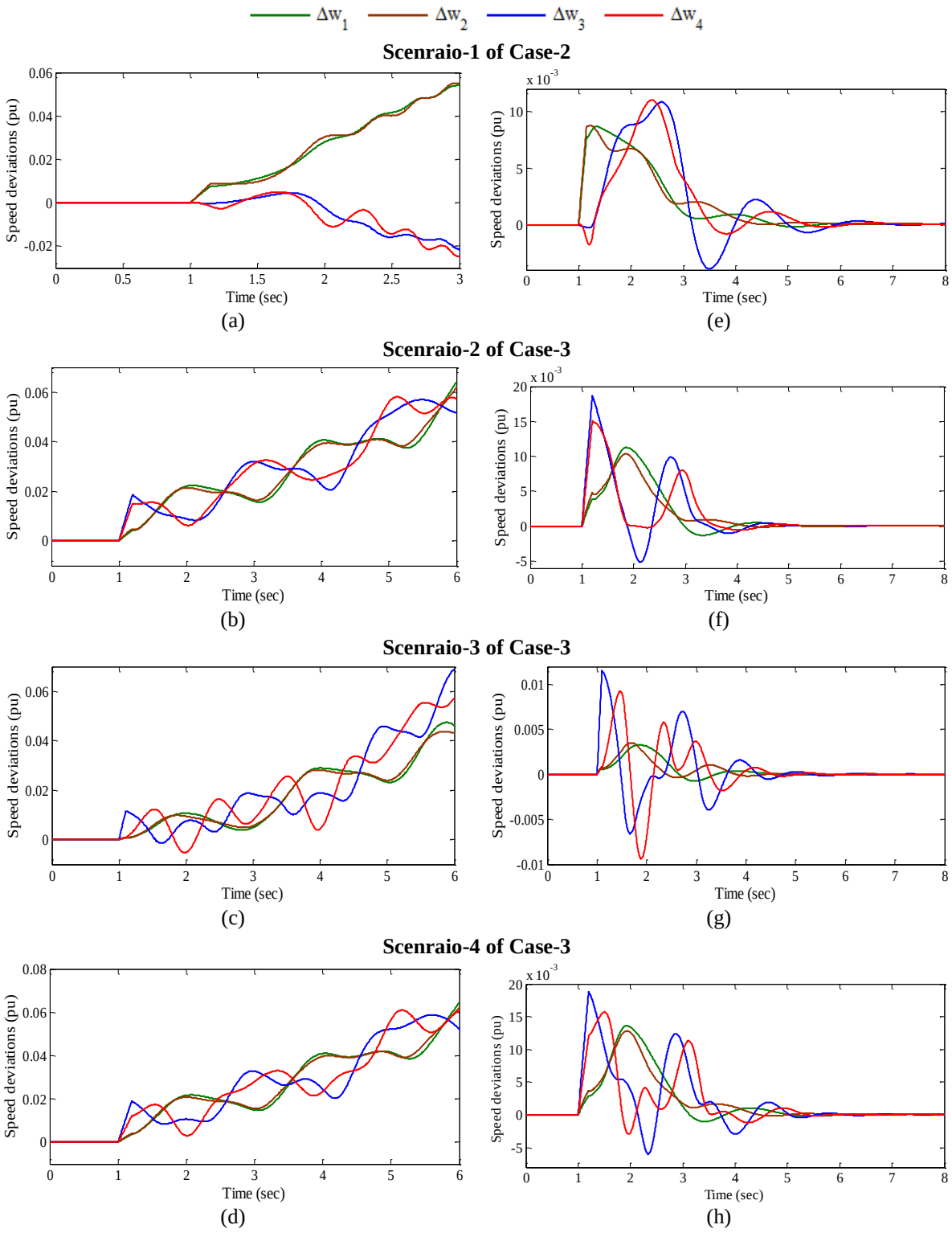

Fig. 3.12 Speed deviations (a)-(d) without PSS and (e)-(h) with GAPSSs for scenarios 1-4 of severe loading cases

C. Performance Indices Results and Discussions with GAPSSs of TAFM Power System

In addition to time-domain simulation results, the effectiveness of designed GAPSS controllers is also analysed by determining two indices *IAE* and *ITAE* for four observed scenarios of different disturbances. Established both indices with GAPSSs is evaluated for each scenario of disturbances for loading cases 1-3 and presented as bar charts in the Fig. 3.13 (a)-(d) and (e)-(h) respectively.

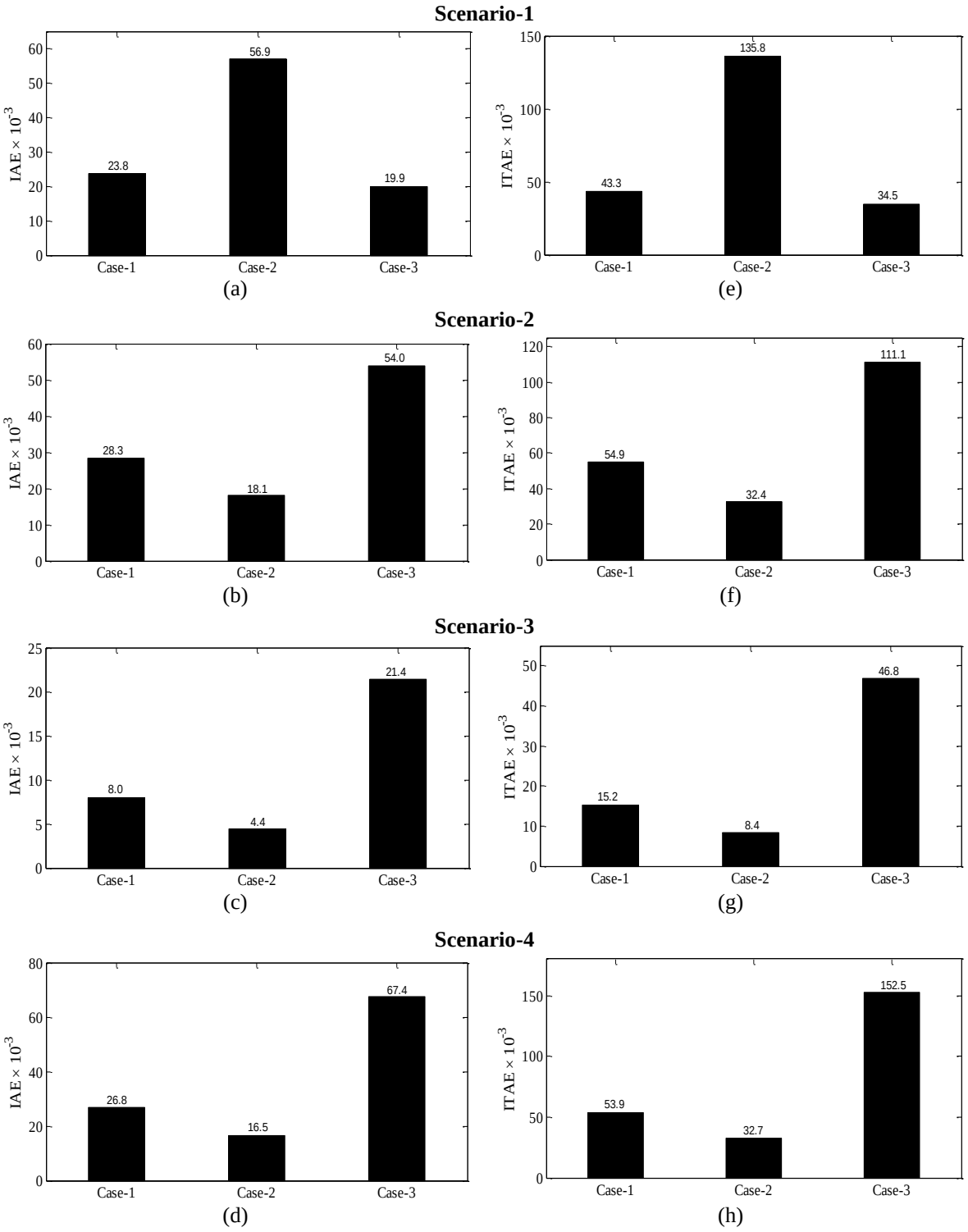

Fig. 3.13 Values of (a)-(d) *IAE* and (e)-(h) *ITAE* with GAPSSs for scenarios 1-4 of loading cases 1-3

The figure reveals that the values of both indices for the GAPSSs are lower for scenarios 2-4 of Case-2 loading and higher for same scenarios of Case-3 loading. Similarly, both indices are lower for Scenario-1 of Case-3 and higher for Case-2 loading, which indicates that Case-3 is the most severe for scenarios 2-4 whereas Case-2 is the least severe. Comparing Fig. 3.13 with Fig. 3.11, it may be observed that the designed GAPSS controllers provide sufficient damping to damp out low frequency local and inter-area modes of oscillations with less overshoot and

settling time than that of without PSS, although the disturbances are simulated for more number of cycles on the system with GAPSSs.

D. Robustness Test of Designed GAPSS Controllers of TAFM Power System

To test the robustness of previously designed GAPSSs for TAFM power system, nine unseen operating cases 4-12 are considered as shown in Table 3.15. In this section, the effectiveness of all GAPSSs is checked by eigenvalue analysis, time-domain simulation results and performance indices for unseen cases and compared with that of without PSS.

Table 3.15: Nine unseen operating cases 4-12 of TAFM power system

Case-4	Normal active and reactive power through single line between 7 and 8 while other is out of service
Case-5	Total active power increasing by 20% and reactive power increasing by 15% through single line between 7 and 8 while other is out of service
Case-6	Normal active and reactive power through single line between 8 and 9 while other is out of service
Case-7	Total active power increasing by 20% and reactive power increasing by 15% through single line between 8 and 9 while other is out of service
Case-8	Total active power decreasing by 25% and reactive power decreasing by 20%
Case-9	Total active power increasing by 25% and reactive power increasing by 20%
Case-10	Total active power increasing by 25% and reactive power increasing by 20% through single line between 7 and 8 while other is out of service
Case-11	Total active power increasing by 25% and reactive power increasing by 20% through single line between 8 and 9 while other is out of service
Case-12	Total active power and reactive power decreasing by 30%

Open-loop eigenvalues, damping ratio, frequency, participation modes and participation factor for only unstable and poorly damped modes of unseen operating cases 4-12 of TAFM power system without PSS and closed-loop eigenvalues and damping ratio with earlier designed GAPSSs for the same unseen cases of system are obtained using PSAT [215] and shown in Table 3.16.

The table reveals that for open-loop system, the TAFM power system becomes highly unstable for Case-9 due to more negative damping than other unseen cases and cases 1-3 considered earlier. Moreover, it is concluded that one inter-area and two-local mode are present in cases 4-12. Also, the table shows that for cases 5, 7 and 9-11 two pairs of open-loop eigenvalues lie in right-half of the *s*-plane and $\xi < 0$ and other has $0.05 < \xi < 0.10$ and for cases 4, 6 one pair of open-loop eigenvalues lie in right-half of the *s*-plane and $\xi < 0$ and others have $0.05 < \xi < 0.10$. All unseen operating cases have one or two unstable modes except cases 8 and 12 with three lightly damped mode eigenvalues are present.

Table 3.16: Open-loop eigenvalues, damping ratio, frequency, participation modes, participation factor and closed-loop eigenvalues, damping ratio for unseen operating cases 4-12 of TAFM power system

Cases	Open-loop				Closed-loop
	Eigenvalues &Damping Ratio	**Frequency (p.u.)**	**Participation Modes**	**Participation Factor**	**Eigenvalues &Damping Ratio**
Case-4	**0.023 ± j 2.969, – 0.0079**	**0.472**	w_3, δ_3	0.188	– 1.528 ± j 2.511, 0.519
	– 0.518 ± j 7.000, 0.0738	1.114	w_4, δ_4	0.232	– 1.601 ± j 3.600, 0.406
	– 0.534 ± j 6.770, 0.0786	1.077	w_2, δ_2	0.231	– 4.460 ± j 5.011, 0.664
Case-5	**0.129 ± j 3.173, – 0.0400**	**0.505**	w_3, δ_3	0.152	– 1.189 ± j 2.169, 0.480
	0.061 ± j 7.128, – 0.0085	1.134	w_4, δ_4	0.236	– 1.469 ± j 5.736, 0.248
	– 0.544 ± j 6.787, 0.0799	1.080	w_2, δ_2	0.234	– 2.058 ± j 2.873, 0.582
Case-6	**0.025 ± j 2.984, – 0.0086**	**0.474**	w_3, δ_3	0.187	– 1.522 ± j 2.495, 0.520
	– 0.518 ± j 6.998, 0.0738	1.113	w_4, δ_4	0.232	– 1.597 ± j 3.602, 0.405
	– 0.536 ± j 6.775, 0.0789	1.078	w_2, δ_2	0.231	– 4.443 ± j 5.013, 0.663
Case-7	**0.131 ± j 3.180, – 0.0410**	**0.506**	w_3, δ_3	0.152	– 1.181 ± j 2.172, 0.477
	0.062 ± j 7.127, – 0.0087	1.134	w_4, δ_4	0.236	– 1.466 ± j 5.742, 0.247
	– 0.545 ± j 6.792, 0.0080	1.081	w_2, δ_2	0.234	– 2.068 ± j 2.868, 0.584
Case-8	– 0.048 ± j 3.098, 0.0156	**0.493**	w_3, δ_3	0.200	– 1.163 ± j 3.358, 0.327
	– 0.530 ± j 6.773, 0.0780	1.078	w_2, δ_2	0.234	– 1.370 ± j 2.743, 0.446
	– 1.047 ± j 6.275, 0.1646	0.998	w_4, δ_4	0.229	– 4.678 ± j 4.262, 0.739
Case-9	**0.191 ± j 3.515, – 0.0544**	**0.559**	w_1, δ_1	0.142	– 1.035 ± j 2.446, 0.389
	0.199 ± j 7.048, – 0.0282	1.121	w_4, δ_4	0.250	– 1.066 ± j 5.864, **0.178**
	– 0.543 ± j 6.787, 0.0798	1.080	w_2, δ_2	0.238	– 1.988 ± j 3.117, 0.537
Case-10	**0.157 ± j 2.965, – 0.0529**	**0.471**	w_3, δ_3	0.142	– 0.993 ± j 2.042, 0.437
	0.225 ± j 7.039, – 0.0391	1.120	w_4, δ_4	0.250	– 1.004 ± j 6.012, **0.164**
	– 0.542 ± j 6.777, 0.0798	1.078	w_2, δ_2	0.234	– 1.876 ± j 2.840, 0.551
Case-11	**0.158 ± j 2.969, – 0.0533**	**0.472**	w_3, δ_3	0.141	**– 0.987** ± j 2.045, 0.434
	0.226 ± j 7.038, – 0.0321	1.120	w_4, δ_4	0.250	– 1.000 ± j 6.015, **0.164**
	– 0.544 ± j 6.782, 0.0799	1.079	w_2, δ_2	0.233	– 1.884 ± j 2.828, 0.554
Case-12	– 0.002 ± j 2.841, 0.0009	**0.452**	w_3, δ_3	0.233	– 1.291 ± j 3.475, 0.348
	– 0.521 ± j 6.756, 0.0769	1.075	w_2, δ_2	0.220	– 1.319 ± j 2.645, 0.446
	– 1.045 ± j 6.279, 0.1641	0.999	w_4, δ_4	0.200	– 3.971 ± j 4.007, 0.703

The table reveals that the designed GAPSSs shift the eigenvalues in the left half of the *s*-plane with improved damping factor and damping ratio as compared to without PSS for unseen cases 4-12. This ensures that the TAFM power system will be stable for all considered unseen cases also. It is also observed that designed GAPSS controllers satisfy the earlier selected criterion for the value of desired damping factor and damping ratio for PSS design except in unseen cases 9, 10 and 11 where slightly more overshoot and settling time may occur. Hence, the GA provides robustness with improved stability and grater damping performance for unseen operating cases 4-12 of the TAFM power system as compared to that of without PSS.

In order to check the robustness performance of the designed GAPSS controllers in terms of speed deviations, only five scenarios of disturbances i.e., S-1, S-4, and S-6 to S-8 mentioned in Table 3.13 are considered for unseen operating cases 4-12 of TAFM power system without PSS. Established index *ITAE* is evaluated for each considered scenario of unseen cases 4-12 and presented using bar charts as shown in Fig. 3.14.

From the figures it is observed that the values of *ITAE* are higher for scenarios S-1 of cases 4, 6, 8 and 12 and S-7 of cases 5, 7, 9-11 as compared to other scenarios. When time-domain simulations are performed for scenarios S-7 of cases 9-11, S-1 of Case-12 and S-1 of Case-4, it is observed that the oscillations are not damped out by GAPSS controllers. Therefore, next severe scenarios S-8 of cases 9, 11 and S-6 of cases 10, 12 for 6-cycle of operation whereas Scenario S-1 of Case-4 for 5-cycle of operation are considered for time-domain analysis with GAPSSs.

For the sake of robustness, number of cycle of operation is increased with three-phase faults in other scenarios of unseen cases 4-12 till generators may go out of synchronism. Therefore, nine severe modified scenarios 5-13 are considered and shown in Table 3.17 for testing the performance of earlier designed GAPSSs for unseen operating cases 4-12.

Table 3.17: Nine severe scenarios 5-13 of disturbances for testing performance of GAPSSs on TAFM power system

Scenarios	Most Severe Scenarios of Disturbances
Scenario-5	A 5-cycle 3-phase fault occurs on bus 7 at t = 1 sec on one end of the line 7-8 without tripping it for Case-4.
Scenario-6	A 6-cycle 3-phase fault occurs at t = 1 sec on bus 3 for Case-5.
Scenario-7	A 9-cycle 3-phase fault occurs at t = 1 sec on bus 7 at one end of the line 7-8 without tripping it for Case-6.
Scenario-8	A 6-cycle 3-phase fault occurs at t = 1 sec on bus 3 for Case-7.
Scenario-9	A 6-cycle 3-phase fault occurs at t = 1 sec on bus 7 at one end of the line 7-8 without tripping it Case-8.
Scenario-10	A 6-cycle 3-phase fault occurs at t = 1 sec on bus 4 for Case-9.
Scenario-11	A 6-cycle 3-phase fault occurs at t = 1 sec on bus 2 for Case-10.
Scenario-12	A 6-cycle 3-phase fault occurs at t = 1 sec on bus 4 for Case-11.
Scenario-13	A 6-cycle 3-phase fault occurs at t = 1 sec on bus 2 for Case-12.

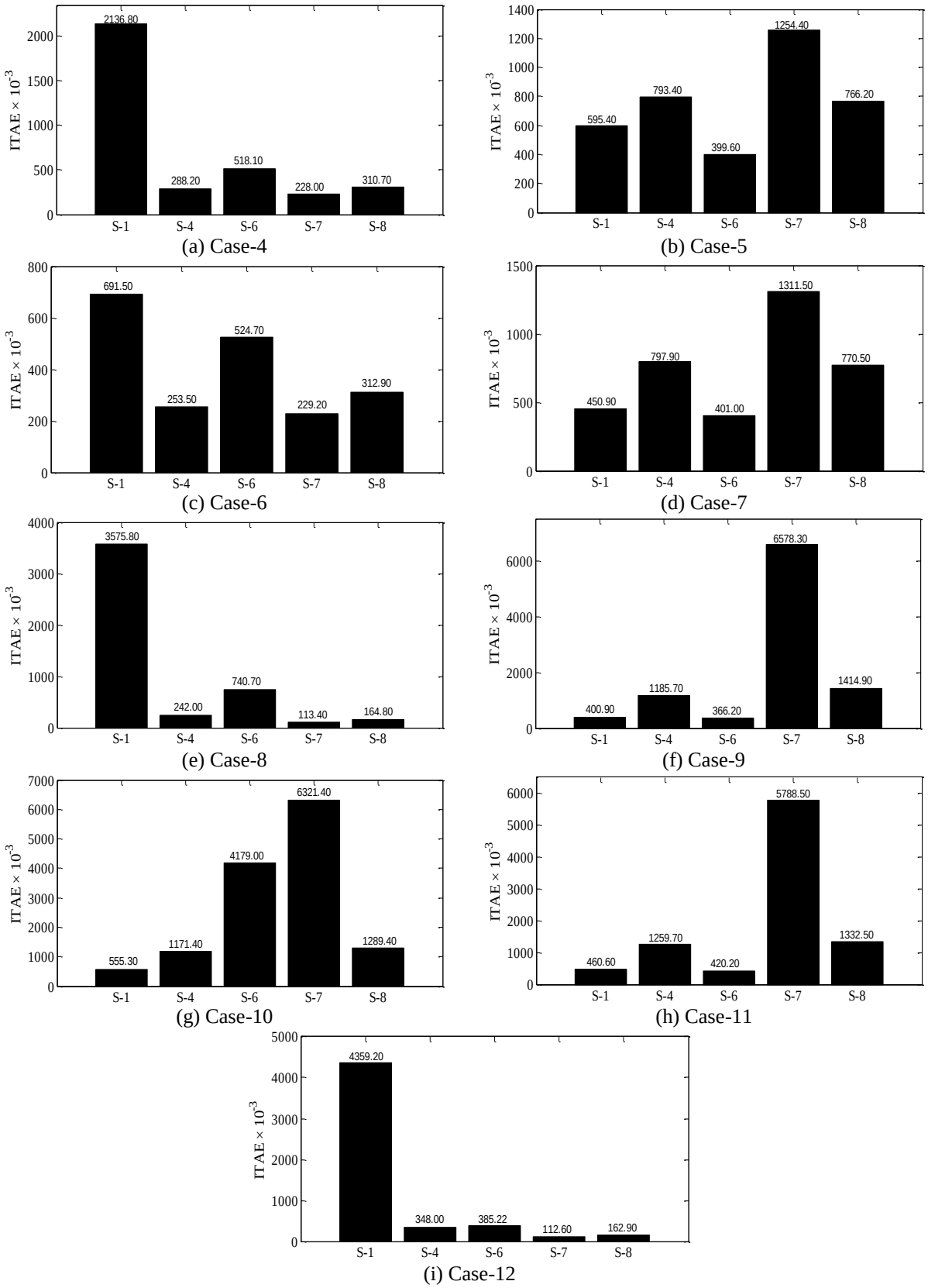

Fig. 3.14 Value of (a)-(i) *ITAE* without PSS for scenarios S-1, S-4 and S-6 to S-8 of unseen cases 4-12 of TAFM power system

The speed deviations Δw_1, Δw_2, Δw_3 and Δw_4 for the system without PSS and with GAPSSs for nine modified severe disturbances scenarios 5-13 of unseen cases 4-12 of TAFM power system are shown in Fig. 3.15 (a)-(i) and (j)-(r) respectively.

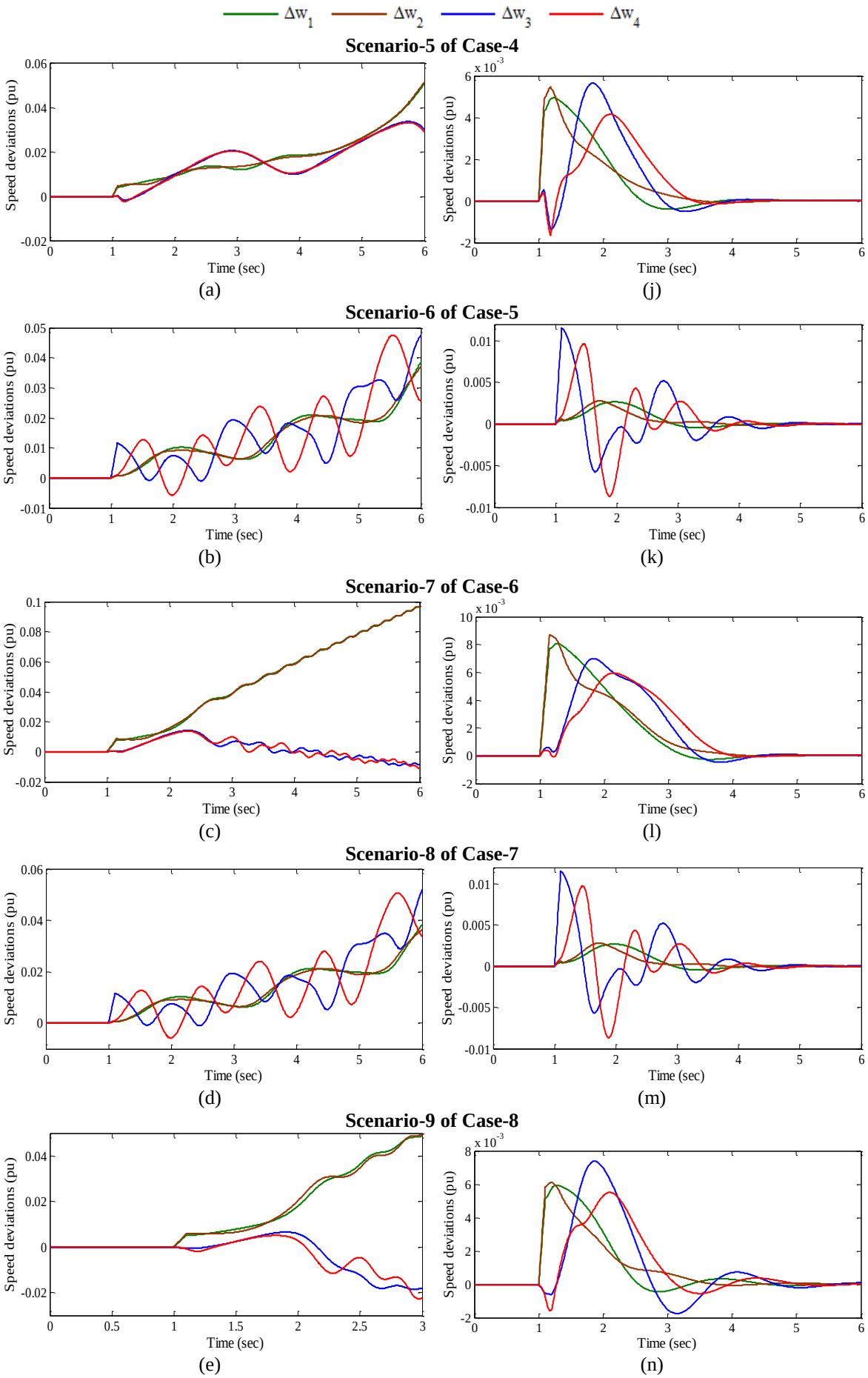
Δw1 Δw2 Δw3 Δw4
Scenario-5 of Case-4
Speed deviations (pu)
Time (sec)
x 10-3
(a)
(j)
Scenario-6 of Case-5
(b)
(k)
Scenario-7 of Case-6
(c)
(l)
Scenario-8 of Case-7
(d)
(m)
Scenario-9 of Case-8
(e)
(n)

Cont.

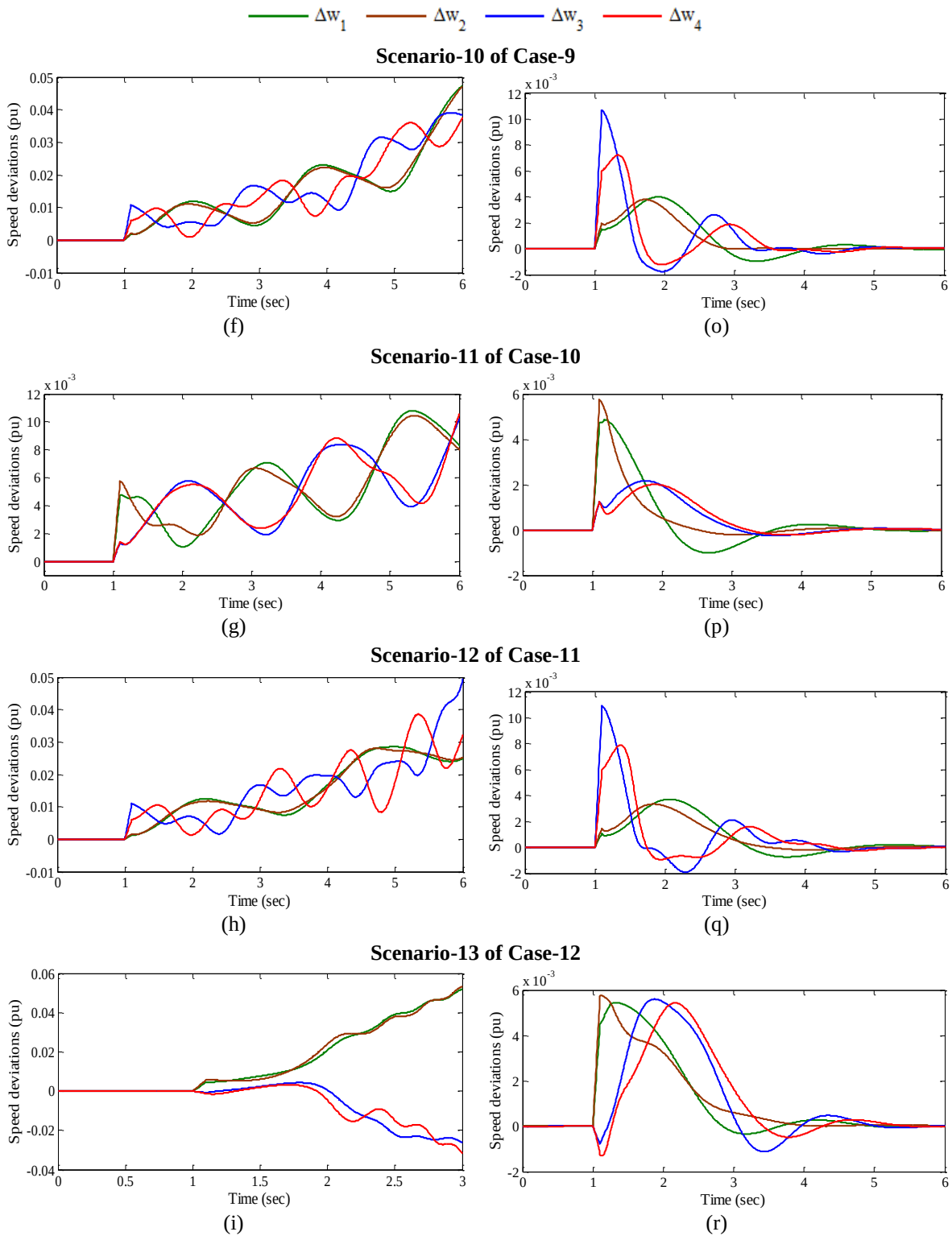

Fig. 3.15 Speed deviations (a)-(i) without PSS and (j)-(r) with GAPSSs for scenarios 5-13 of unseen operating cases 4-12

From Fig. 3.15 (a)-(i), it is observed that in all these response plots, the system without PSS is not capable to damp out LFO because these oscillations are rapidly growing up with time for unseen cases 5, 7, 9-11 and for unseen cases 4, 6, 8, 12 these are in non-oscillatory mode. Moreover, for unseen cases 6, 8 and 12 the Δw_1, Δw_2, and Δw_3, Δw_4 oscillate in opposite directions. Furthermore, in all scenarios generators may go out of synchronism.

From Fig. 3.15 (j)-(r), it is analyzed that the system performance with designed GAPSSs is improved for nine severe disturbance scenarios 5-13 of unseen cases 4-12 and all oscillations are well damped out. Moreover, the comparison of speed deviations with GAPSSs basis on number of cycle operation, the Scenario-13 of Case-12 for 6-cycle of operation is consumed more time to damp out oscillations than all other scenarios. This may be concluded that the designed GAPSSs work satisfactorily for most of the scenarios of severe disturbances of unseen operating cases of TAFM power system.

In addition to time-domain simulation results, the robustness and effectiveness of designed GAPSS controllers is also observed by evaluating two indices *IAE* and *ITAE* for observed scenarios 5-13 of unseen operating cases 4-12. The bar charts of both indices values obtained with GAPSSs, for defined scenarios are shown in Fig. 3.16 (a) and (b) respectively.

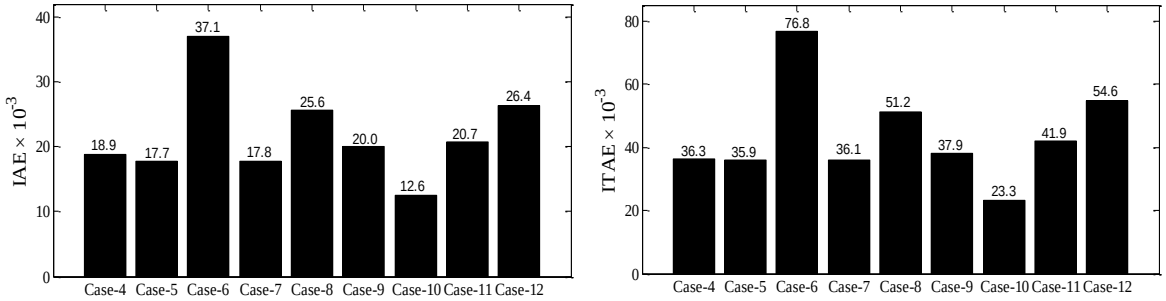

Fig. 3.16 Value of (a) *IAE* and (b) *ITAE* with GAPSSs for scenarios 5-13 of unseen operating cases 4-12

In above figure, both indices with GAPSSs for corresponding scenarios of Case-4 and Case-6 are evaluated for 5 and 9-cycle of operation respectively whereas remaining cases are determined for 6-cycle of operation. Both indices values with GAPSSs are minimum and maximum for 6-cycle operation of unseen cases 10 and 12 respectively. Therefore, it is concluded that with GAPSSs, Scenario-11 of Case-10 and Scenario-13 of Case-12 are least and most severe scenario of disturbance respectively.

Hence, the designed GAPSS controllers for TAFM power system is able to damp out low frequency local and inter-area modes of oscillations with improved stability and damping performances for wide range of loading cases under different scenarios of severe disturbances and also for unseen operating cases under severe scenarios of disturbances.

3.4.3 Example 3: Ten-Machine, Thirty-Nine Bus New England Power System

This system has ten-generators, thirty-six transmission lines, nineteen-loads and twelve power transformers [213]. All generators are represented by the fourth order non-linear model equipped with IEEE type-1 static excitation systems. Loads are simulated as constant impedances. The single-line diagram and other details of the system are given in Appendix. The tuning procedure is carried out for three pre-specified operating conditions [164] viz. Case-1 as normal loading, Case-2 as high loading and Case-3 as light loading, as presented in Table 3.18 for enhancement of SSS.

Table 3.18: Three operating cases of NEPS

Case-1	Nominal active and reactive power
Case-2	Total active and reactive power increasing by 30%
Case-3	Total active and reactive power decreasing by 30%

A. Eigenvalue Analysis of NEPS without PSS and with GAPSSs

The generator G_1 is part of an equivalent power source representing parts of the U.S.-Canadian interconnection system [164]. Therefore, it is considered as swing generator and only nine generators G_2-G_{10} PSS parameters are to be optimized. The open-loop eigenvalues, damping ratio, frequency, participation modes and participation factor are evaluated using PSAT [215] for only unstable and/or poorly damped electromechanical modes of the system and are shown in Table 3.19.

The table reveals that for open-loop system, the NEPS becomes unstable for all three different loading cases through one inter-area and eight local modes of LFO. Moreover, These inter-area modes associated with rotor angles δ_1, speed w_1, whereas local modes are associated with and δ_2, δ_3, δ_4, δ_5, δ_6, δ_7, δ_8, δ_9, δ_{10} and w_2, w_3, w_4, w_5, w_6, w_7, w_8, w_9, w_{10} with high participation in their respective modes respectively.

To assured the relative stability of poorly damped local modes and for guaranteed stability of unstable local and inter-area modes, LFO are damped out by increasing the damping of NEPS. An eigenvalue-based multi-objective function J (equation 3.1) presented in Section 3.2 is minimized using GA for designing twenty-seven PSS parameters of nine generators. In this case, the desired value of damping factor σ_0 and damping ratio ξ_0 are selected as –0.75 and 0.1 respectively. The value of washout time constant is chosen as 10 sec; T_2 and T_4 are held constant at numerical values of 0.01 sec. The values of designed parameters K, T_1 and T_3 are set in the range of [1-100], [0.01-1] and [0.01-1] respectively. The GA is applied with population size 100, maximum generation 100, crossover rate 0.75 and mutation rate 0.01.

Table 3.19: Open-loop eigenvalues, damping ratio, frequency, participation modes and participation factor for operating cases 1-3 of NEPS

Cases	Eigenvalues &Damping Ratio	Frequency (p. u.)	Participation Modes	Participation Factor
Case-1	**0.121 ± j 6.069, – 0.0199**	0.966	w_9, δ_9	0.255
	0.014 ± j 3.879, – 0.0036	**0.617**	w_1, δ_1	0.189
	– 0.016 ± j 6.472, 0.0025	1.030	w_5, δ_5	0.138
	– 0.160 ± j 7.187, 0.0223	1.144	w_6, δ_6	0.167
	– 0.202 ± j 8.019, 0.0252	1.276	w_{10}, δ_{10}	0.206
	– 0.214 ± j 8.285, 0.0258	1.318	w_2, δ_2	0.272
	– 0.396 ± j 9.238, 0.0429	1.470	w_4, δ_4	0.367
	– 0.415 ± j 9.530, 0.0435	1.516	w_8, δ_8	0.253
	– 0.597 ± j 9.546, 0.0624	1.519	w_7, δ_7	0.257
Case-2	**0.074 ± j 6.063, – 0.0122**	0.965	w_9, δ_9	0.253
	– 0.045 ± j 6.446, 0.0071	1.025	w_3, δ_3	0.136
	– 0.037 ± j 3.952, 0.0094	**0.629**	w_1, δ_1	0.119
	– 0.192 ± j 8.451, 0.0227	1.345	w_2, δ_2	0.274
	– 0.198 ± j 7.118, 0.0279	1.132	w_6, δ_6	0.174
	– 0.232 ± j 7.927, 0.0292	1.261	w_{10}, δ_{10}	0.202
	– 0.442 ± j 9.324, 0.0474	1.484	w_4, δ_4	0.365
	– 0.542 ± j 9.571, 0.0565	1.523	w_8, δ_8	0.255
	– 0.653 ± j 9.603, 0.0679	1.528	w_7, δ_7	0.249
Case-3	**0.397 ± j 3.063, – 0.1286**	**0.487**	w_1, δ_1	0.210
	0.133 ± j 6.012, – 0.022	0.956	w_9, δ_9	0.219
	0.070 ± j 6.365, – 0.111	1.013	w_9, δ_9	0.136
	– 0.143 ± j 7.161, 0.020	1.139	w_6, δ_6	0.169
	– 0.169 ± j 7.930, 0.0213	1.262	w_{10}, δ_{10}	0.209
	– 0.212 ± j 8.251, 0.0257	1.313	w_2, δ_2	0.268
	– 0.385 ± j 9.204, 0.0418	1.465	w_4, δ_4	0.364
	– 0.413 ± j 9.530, 0.0433	1.516	w_8, δ_8	0.261
	– 0.583 ± j 9.535, 0.0610	1.517	w_7, δ_7	0.258

The GA is able to find the desired solution for which fitness function *J* is zero. The final value of *J* equal to zero indicates that nine unstable and/or poorly damped eigenvalues are shifted to a specified D-shape zone in the left-half of the *s*-plane. The optimum designed parameters for GAPSSs are shown in Table 3.20. The closed-loop eigenvalues and their damping ratio with GAPSSs for loading cases 1-3 are determined using PSAT [215] and shown in Table 3.21. The eigenvalue maps for without PSS and with GAPSSs for loading cases 1-3 of NEPS are shown in Fig. 3.17 (a)-(c) and (d)-(f) respectively.

Table 3.20: Optimal designed parameters of GAPSSs

Optimized Parameters	Generators								
	G_2	G_3	G_4	G_5	G_6	G_7	G_8	G_9	G_{10}
K_1	53.552	5.049	0.938	91.802	35.821	44.248	98.527	4.296	5.321
T_1	0.725	0.307	0.779	0.695	0.201	0.082	0.100	0.599	0.823
T_3	0.079	0.382	0.360	0.387	0.115	0.336	0.765	0.154	0.829

Table 3.21: Eigenvalues and damping ratio with GAPSSs for loading cases 1-3

Case-1	Case-2	Case-3
– 1.136 ± j 8.283, 0.135	– 1.240 ± j 8.427, 0.145	– 1.032 ± j 8.191, 0.125
– 1.195 ± j 7.568, 0.155	– 1.249 ± j 6.369, 0.192	– 1.180 ± j 7.502, 0.155
– 1.030 ± j 6.289, 0.161	– 1.101 ± j 7.700, 0.141	–0.864 ± j 6.184, 0.138

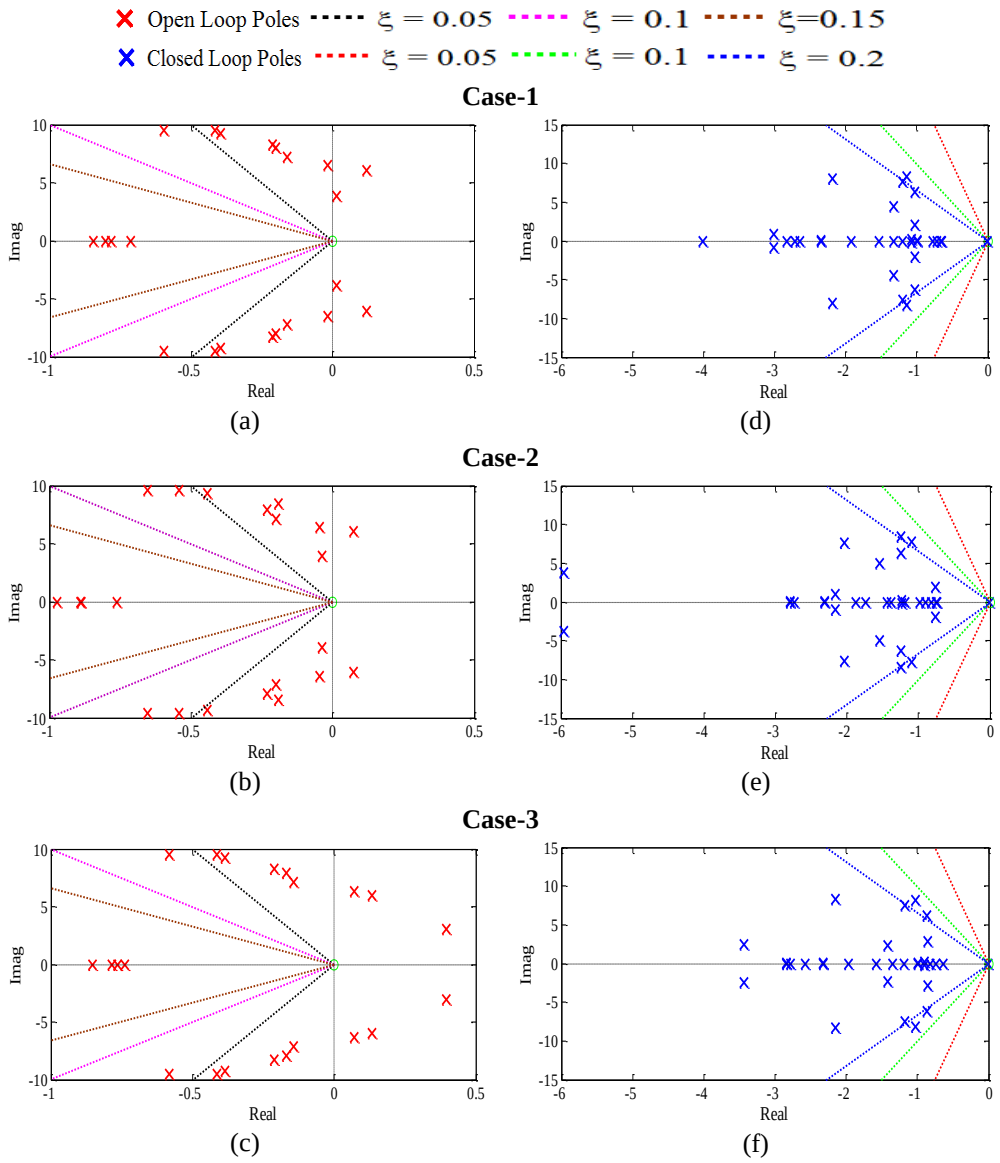

Fig. 3.17 Eigenvalue maps (a)-(c) without PSS and (d)-(f) with GAPSSs for loading cases 1-3 of NEPS

Figure 3.17 (a)-(c) shows that for Case-1, Case-2 and Case-3: two, one and three pairs of open-loop eigenvalues lie in right-half of the *s*-plane respectively and $\xi < 0$. Similarly for Case-1 six and one pair of open-loop eigenvalues have $0 < \xi < 0.05$ and $0.05 < \xi < 0.10$ respectively, for Case-2 six and two pairs of open-loop eigenvalues have $0 < \xi < 0.05$ and $0.05 < \xi < 0.10$ respectively and for Case-3 five and one pair of open-loop eigenvalues have $0 < \xi < 0.05$ and $0.05 < \xi < 0.10$ respectively, lie close to imaginary axis in left-half of the *s*-plane. Moreover, it is noticed that Case-3 is highly unstable with most negative damping than other cases. Furthermore, it is observed that unstable and poorly damped modes are as shown in the Table 3.19 with high participation as compared to other frequency modes.

Table 3.21 and Fig. 3.17 (d)-(f) show that the designed GAPSSs shift the eigenvalues to a specified D-shape zone in the left half of the *s*-plane with enhanced damping factor and damping ratio as compared to without PSS for three loading cases. Hence, GAPSS controllers provide improved stability and damping characteristics of the NEPS as compared to same obtained using without PSS.

B. Time-Domain Simulation Results and Discussions with GAPSSs and without PSS of NEPS

In order to examine the performance of the designed GAPSS controllers in previous section in terms of speed deviations, twenty-eight different scenarios of disturbances on severe loading Case-3 of NEPS without PSS are considered as shown in Table 3.22.

Established index *ITAE* is evaluated for twenty-eight scenarios of Case-3 loading and is presented using bar charts as shown in Fig. 3.18. Figure reveals that the values of *ITAE* are higher for ten scenarios, i.e. S-28, S-26, S-24, S-25, S-27, S-14, S-13, S-5, S-15 and S-4 as compared to other disturbances scenarios.

Moreover, the effectiveness of GAPSSs is also observedby conducting ten different scenarios of three-phase faults at generator terminals of NEPS without PSS for Case-3 loading and is shown in Table 3.23. Established index *ITAE* is evaluated for ten scenarios of Case-3 loading and is presented using bar charts as shown in Fig. 3.19.

Figure reveals that the value of *ITAE* is maximum for scenarios B-9 as compared to other disturbances scenarios. Now, five severe disturbances scenarios, i.e., S-28, S-14, S-13, S-15 and B-9 are selected for testing the performance of designed GAPSS controllers for three loading cases. Therefore, observed five scenarios of disturbances of NEPS are renamed and shown in Table 3.24.

Table 3.22: Different scenarios of disturbances for loading case-3 at t = 1 sec on NEPS

Scenarios	Scenarios of disturbances
S-1	A 6-cycle 3-phase fault at bus 1 without tripping the line 1-2
S-2	A 6-cycle 3-phase fault at bus 1 without tripping the line 1-39
S-3	A 6-cycle 3-phase fault at bus 2 without tripping the line 2-3
S-4	A 6-cycle 3-phase fault at bus 4 without tripping the line 3-4
S-5	A 6-cycle 3-phase fault at bus 4 without tripping the line 4-5
S-6	A 6-cycle 3-phase fault at bus 5 without tripping the line 5-6
S-7	A 6-cycle 3-phase fault at bus 7 without tripping the line 6-7
S-8	A 6-cycle 3-phase fault at bus 8 without tripping the line 5-8
S-9	A 6-cycle 3-phase fault at bus 8 without tripping the line 7-8
S-10	A 6-cycle 3-phase fault at bus 9 without tripping the line 8-9
S-11	A 6-cycle 3-phase fault at bus 11 without tripping the line 6-11
S-12	A 6-cycle 3-phase fault at bus 11 without tripping the line 10-11
S-13	A 6-cycle 3-phase fault at bus 13 without tripping the line 10-13
S-14	A 6-cycle 3-phase fault at bus 14 without tripping the line 13-14
S-15	A 6-cycle 3-phase fault at bus 14 without tripping the line 14-15
S-16	A 6-cycle 3-phase fault at bus 18 without tripping the line 3-18
S-17	A 6-cycle 3-phase fault at bus 18 without tripping the line 17-18
S-18	A 6-cycle 3-phase fault at bus 19 without tripping the line 19-20
S-19	A 6-cycle 3-phase fault at bus 21 without tripping the line 16-21
S-20	A 6-cycle 3-phase fault at bus 22 without tripping the line 21-22
S-21	A 6-cycle 3-phase fault at bus 22 without tripping the line 22-23
S-22	A 6-cycle 3-phase fault at bus 23 without tripping the line 23-24
S-23	A 6-cycle 3-phase fault at bus 24 without tripping the line 16-24
S-24	A 6-cycle 3-phase fault at bus 26 without tripping the line 25-26
S-25	A 6-cycle 3-phase fault at bus 26 without tripping the line 26-27
S-26	A 6-cycle 3-phase fault at bus 26 without tripping the line 26-28
S-27	A 6-cycle 3-phase fault at bus 27 without tripping the line 17-27
S-28	A 6-cycle 3-phase fault at bus 29 without tripping the line 26-29

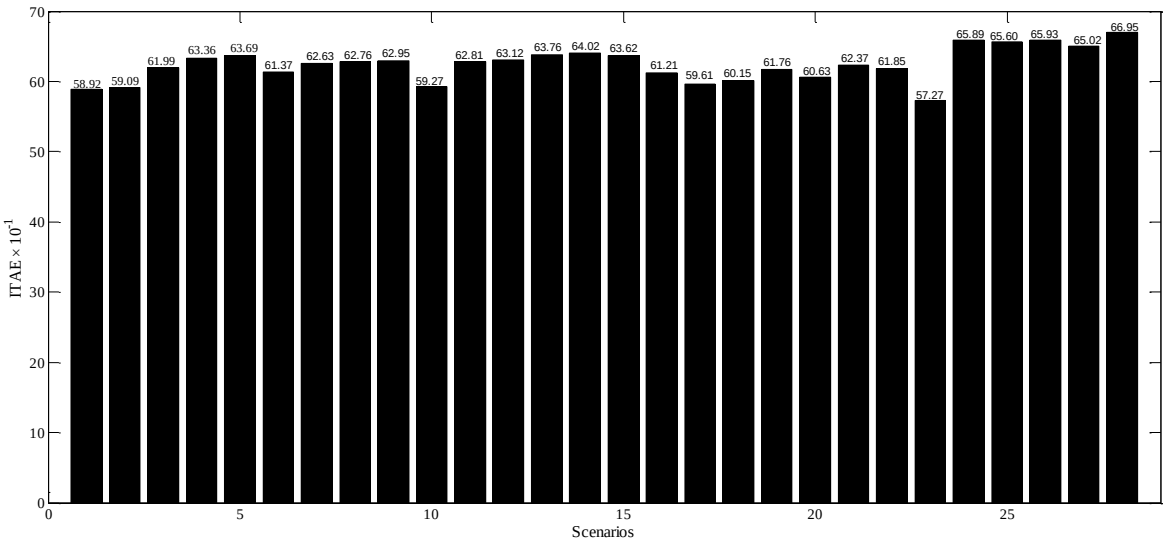

Fig. 3.18 Value of *ITAE* for different scenarios of disturbances for loadingcase-3

Table 3.23: Different severe disturbances at generator terminals for case-3 loading at t = 1 sec on NEPS

Scenarios	Scenarios of Disturbances
B-1	A 6-cycle 3-phase fault at bus 30
B-2	A 6-cycle 3-phase fault at bus 31
B-3	A 6-cycle 3-phase fault at bus 32
B-4	A 6-cycle 3-phase fault at bus 33
B-5	A 6-cycle 3-phase fault at bus 34
B-6	A 6-cycle 3-phase fault at bus 35
B-7	A 6-cycle 3-phase fault at bus 36
B-8	A 6-cycle 3-phase fault at bus 37
B-9	A 6-cycle 3-phase fault at bus 38
B-10	A 6-cycle 3-phase fault at bus 39

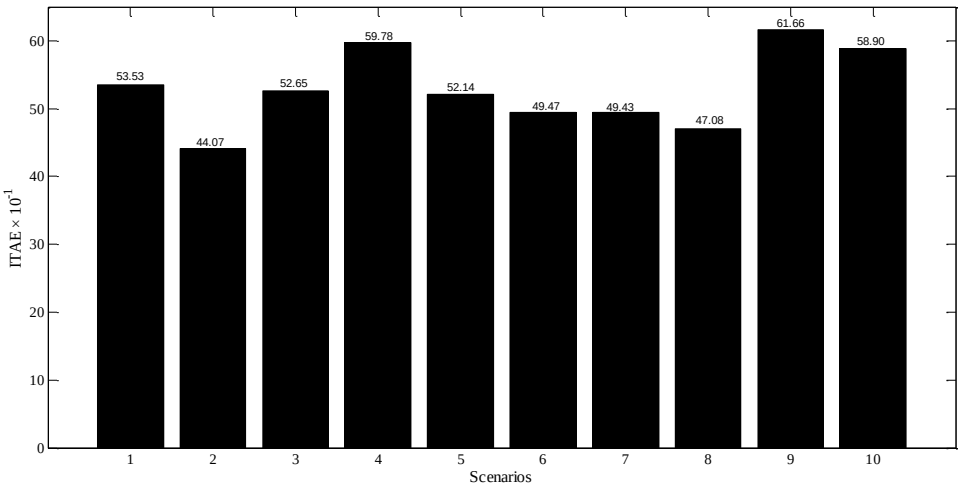

Fig. 3.19 Value of *ITAE* for severe disturbances on generator terminals for case-3 loading

Table 3.24: Five observed scenarios of disturbances for testing performance of GAPSSs on NEPS

Scenarios	Scenarios
Scenario-1	A 6-cycle 3-phase fault at t = 1 sec on bus 29 without tripping the line 26-29
Scenario-2	A 6-cycle 3-phase fault at t = 1 sec on bus 14 without tripping the line 13-14
Scenario-3	A 6-cycle 3-phase fault at t = 1 sec on bus 13 without tripping the line 10-13
Scenario-4	A 6-cycle 3-phase fault at t = 1 sec on bus 14 without tripping the line 14-15
Scenario-5	A 6-cycle 3-phase fault at t = 1 sec on bus 38

The time-domain simulations of NEPS are performed with PSSs for observed scenarios of three loadings cases. The speed deviations $\Delta w_1, \Delta w_2, \Delta w_3, \Delta w_4, \Delta w_5, \Delta w_6, \Delta w_7, \Delta w_8, \Delta w_9$ and Δw_{10} for without PSS and with GAPSSs for scenarios 1-5 of Case-3 loading are shown in Fig. 3.20 (a)-(e) and (f)-(j) respectively.

From Fig. 3.20 (a)-(e), it is observed that in all these response plots, the system without PSS is not capable to die out low frequency electromechanical oscillations because these oscillations are continuously growing in amplitude in same direction except Δw_1 and in five scenarios all generators may go out of synchronism. Moreover, it is also noticed that speed deviations Δw_9 is most severe than other speed deviations. Furthermore, the Scenario-4 is most severe scenario due to large magnitude oscillatory instability than other scenarios responses.

Figure 3.20 (f)-(j) reveals that the speed response with GAPSSs for Scenario-1 of Case-3 loading has large peak overshoot as compared to others. Moreover, the Scenario-4 of Case-3 loading consumed more time to die out oscillations as compared to other. Therefore, it is concluded that with GAPSSs Scenario-4 is most severe scenario due more oscillations sustain for long time than others. This demonstrates the potential of GA technique to obtain the desired set of PSS parameters for NEPS and the designed GAPSSs are capable to damp out LFO for wide range of operating cases under severe scenarios of disturbances.

C. Performance Indices Results and Discussions with GAPSSs of NEPS

In addition to time-domain simulation results, the effectiveness of designed GAPSS controllers is also observed by determining indices *IAE* and *ITAE* for five observed scenarios of disturbances. The bar charts of both indices values with GAPSSs for scenarios 1-5 of three loading cases are shown in Fig. 3.21 (a)-(e) and (f)-(j) respectively.

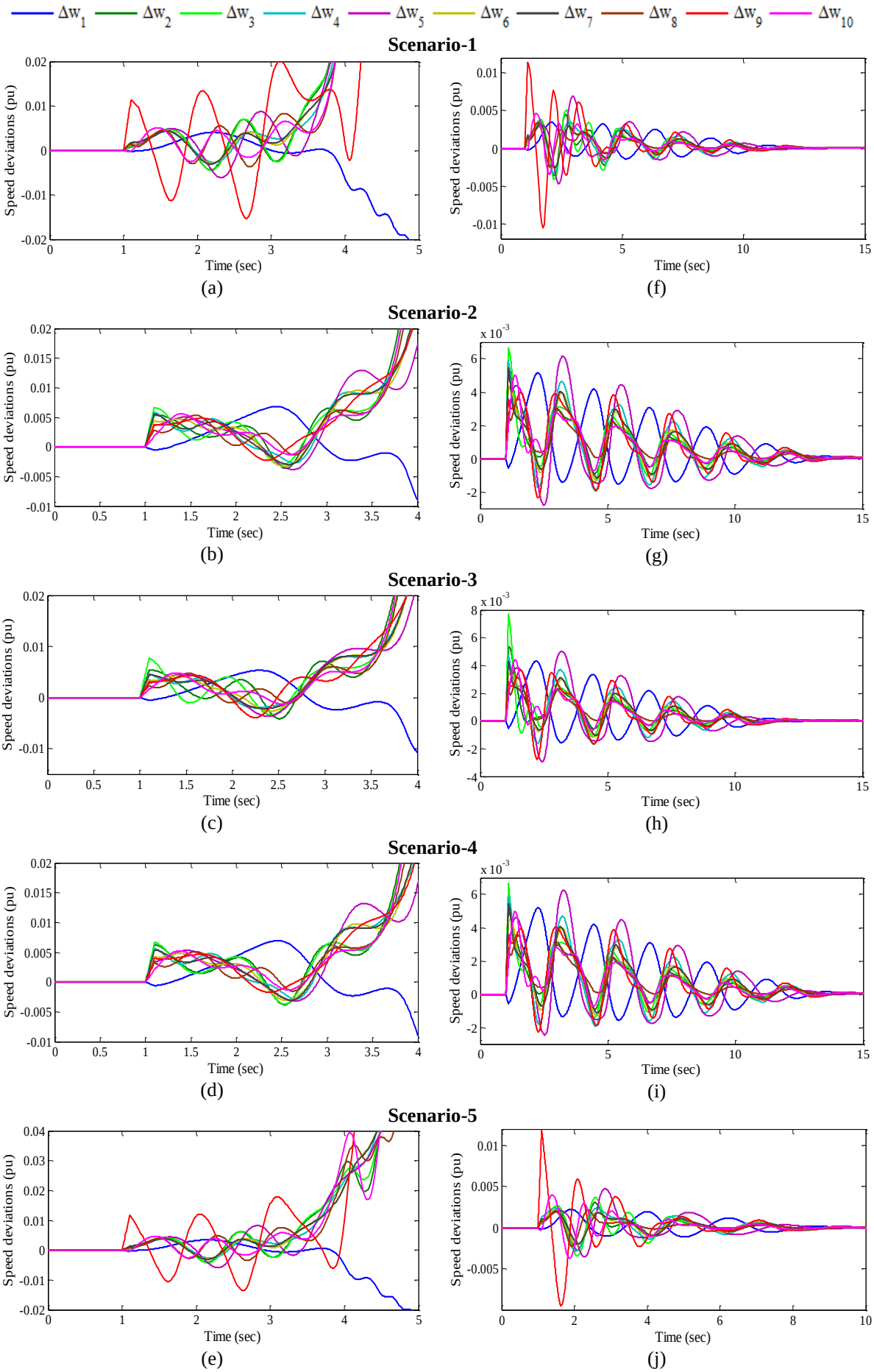

Fig. 3.20 Speed deviations (a)-(e) without PSS and (f)-(j) with GAPSSs for scenarios 1-5 ofloadingcase-3

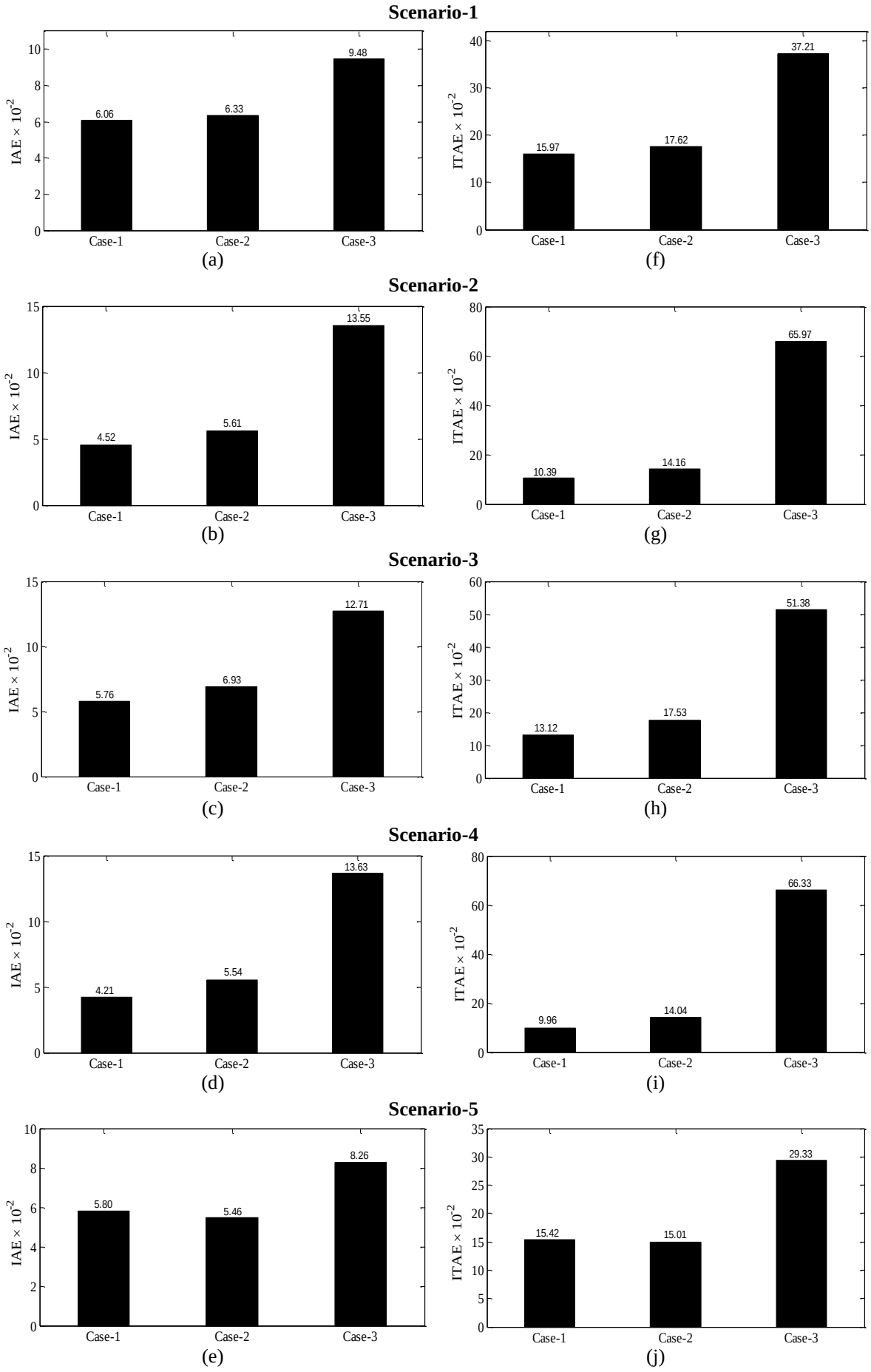

Fig. 3.21 Values of (a)-(e) *IAE* and (f)-(j) *ITAE* with GAPSSs for scenarios 1-5 of loading cases 1-3

The values of both indices with GAPSSs for five scenarios of loading Case-1 and Case-3 are minimum and maximum respectively except Scenario-5. Moreover, the Scenario-4 of Case-3 loading is most severe whereas the Scenario-5 of Case-3 loading is least severe than others. Comparing Fig. 3.21 with Figs. 3.18 and 3.19, it may be observed that the designed GAPSS controllers of NEPS provide sufficient damping to damp out low frequency local and inter-area modes oscillation with less overshoot and settling time than that of without PSS.

D. Robustness Test of Designed GAPSS Controllersof NEPS

To test the robustness of previously designed GAPSS controllers, fifteen unseen operating cases 4-18 are considered as shown in Table 3.25. In this section, the effectiveness of GAPSS controllers is checked by eigenvalue analysis, time-domain simulation results and performance indices for four observed earlier scenarios of cases 4-18 and compared with that of without PSS.

Table 3.25: Fifteen unseen operating cases 4-18 of NEPS

Cases	**Operating Conditions**
Case-4	Outage of line 3-18 and 25-26
Case-5	Outage of line 4-14 and16-17
Case-6	Outage of line 6-11
Case-7	360 MW load increase
Case-8	Outage of line 4-14, 16-17 and 25-26
Case-9	Outage of line 4-14, 16-17, 25-26 and 1-39
Case-10	Outage of line 21-22
Case-11	Outage of line 9-39
Case-12	Outage of line 21-22 with load increase 50% at bus-16 and 21
Case-13	Outage of line 16-21 and 28-29
Case-14	Outage of line 17-27 and 28-29
Case-15	Outage of line 16-17 and 28-29
Case-16	Outage of line 16-21, 26-27 and 28-29
Case-17	Outage of line 16-17, 26-27 and 28-29
Case-18	Outage of line 2-25, 16-17, 16-21 and 28-29

Open-loop eigenvalues, damping ratio, frequency, participation modes and participation factor for only unstable modes and some critical poorly damped modes of unseen cases 4-18 of NEPS without PSS and closed-loop eigenvalues and damping ratio with earlier designed GAPSSs for the same unseen cases are obtained using PSAT [215] and shown in Table 3.26.

Table 3.26: Open-loop eigenvalues, damping ratio, frequency, participation modes, participation factor and closed-loop eigenvalues, damping ratio for unseen operating cases 4-18 of NEPS

Cases	Open-loop				Closed-loop
	Eigenvalues &Damping Ratio	**Frequency (p.u.)**	**Participation Modes**	**Participation Factor**	**Eigenvalues &Damping Ratio**
Case-4	**0.221 ± j 5.759, – 0.0384**	0.916	w_9, δ_9	0.300	– 1.059 ± j 7.378, 0.142
	0.103 ± j 3.282, – 0.0316	**0.522**	w_1, δ_1	0.159	– 1.132 ± j 5.861, 0.189
	– 0.093 ± j 6.083, 0.0152	0.968	w_5, δ_5	0.153	– 1.681 ± j 8.275, 0.199
Case-5	**0.156 ± j 3.035, – 0.0516**	**0.483**	w_1, δ_1	0.157	**– 0.747** ± j 4.840, 0.142
	0.168 ± j 4.994, – 0.0336	**0.794**	w_9, δ_9	0.289	– 1.051 ± j 7.615, 0.136
	– 0.075 ± j 6.478, 0.0116	1.031	w_5, δ_5	0.192	– 1.254 ± j 7.135, 0.170
Case-6	**0.127 ± j 6.074, – 0.0209**	0.966	w_9, δ_9	0.259	– 0.750 ± j 6.112, 0.121
	0.039 ± j 3.729, – 0.0106	**0.593**	w_1, δ_1	0.193	– 1.017 ± j 2.034, 0.447
	– 0.006 ± j 6.400, 0.0009	1.018	w_3, δ_3	0.160	– 1.132 ± j 8.279, 0.135
Case-7	**0.114 ± j 6.075, – 0.0189**	0.967	w_9, δ_9	0.255	– 1.147 ± j 8.295, 0.136
	– 0.022 ± j 6.483, 0.0034	1.031	w_5, δ_5	0.137	– 1.195 ± j 7.578, 0.155
	– 0.014 ± j 3.967, 0.0036	**0.631**	w_1, δ_1	0.181	– 1.005 ± j 1.992 0.450
Case-8	**0.286 ± j 4.621, – 0.0619**	**0.735**	w_9, δ_9	0.364	**– 0.448** ± j 4.329, 0.102
	0.154 ± j 3.029, – 0.0509	**0.482**	w_1, δ_1	0.159	**– 0.736** ± j 1.840, 0.371
	– 0.059 ± j 6.340, 0.0093	1.009	w_5, δ_5	0.143	– 1.074 ± j 7.388, 0.143
Case-9	**0.238 ± j 4.004, – 0.0594**	**0.637**	w_9, δ_9	0.229	**– 0.416** ± j 1.721, 0.235
	0.114 ± j 2.581, – 0.0442	**0.410**	w_1, δ_1	0.207	– 1.067 ± j 6.290, 0.167
	0.113 ± j 6.030, – 0.0188	0.959	w_9, δ_9	0.170	– 1.157 ± j 7.284, 0.156
Case-10	**0.180 ± j 5.853, – 0.0307**	0.931	w_9, δ_9	0.251	– 0.996 ± j 8.389, 0.117
	0.079 ± j 3.650, – 0.0216	**0.581**	w_1, δ_1	0.192	– 1.007 ± j 2.115, 0.429
	0.003 ± j 6.555, – 0.0005	1.043	w_3, δ_3	0.186	– 1.097 ± j 7.747, 0.140
Case-11	**0.105 ± j 6.140, – 0.0171**	0.977	w_9, δ_9	0.223	**– 0.617** ± j 1.867, 0.313
	0.025 ± j 3.087, – 0.0080	**0.491**	w_1, δ_1	0.189	– 0.972 ± j 6.128, 0.156
	0.038 ± j 6.185, – 0.0060	0.984	w_5, δ_5	0.171	– 1.139 ± j 8.290, 0.136

Cont.

Cases	Open-loop				Closed-loop
	Eigenvalues &Damping Ratio	**Frequency (p.u.)**	**Participation Modes**	**Participation Factor**	**Eigenvalues &Damping Ratio**
Case-12	**0.176 ± j 5.836, – 0.0300**	0.928	w_9, δ_9	0.250	– 0.971 ± j 2.078, 0.423
	0.045 ± j 3.738, – 0.0120	**0.595**	w_1, δ_1	0.181	– 0.997 ± j 8.406, 0.117
	– 0.004 ± j 6.555, 0.0007	1.043	w_3, δ_3	0.188	– 1.089 ± j 7.755, 0.139
Case-13	**0.390 ± j 5.196, – 0.0750**	0.827	w_9, δ_9	0.332	**– 0.604** ± j 4.498, 0.133
	0.085 ± j 3.682, – 0.0230	**0.586**	w_1, δ_1	0.190	– 1.100 ± j 7.640, 0.142
	– 0.049 ± j 6.477, 0.0075	1.030	w_3, δ_3	0.182	–0.998 ± j 8.369, 0.118
Case-14	**0.406 ± j 4.607, – 0.0878**	**0.733**	w_9, δ_9	0.310	**– 0.283** ± j 4.078, **0.069**
	0.070 ± j 3.815, – 0.0185	**0.607**	w_1, δ_1	0.183	– 1.174 ± j 7.501, 0.154
	– 0.115 ± j 6.393, 0.0181	1.017	w_5, δ_5	0.245	–1.236 ± j 8.138, 0.150
Case-15	**0.422 ± j 4.560, – 0.0922**	**0.725**	w_9, δ_9	0.352	**– 0.320** ± j 4.280, **0.074**
	0.087 ± j 3.424, – 0.0256	**0.544**	w_1, δ_1	0.173	– 1.038 ± j 7.545, 0.136
	– 0.060 ± j 6.362, 0.0095	1.012	w_5, δ_5	0.145	–1.308 ± j 6.999, 0.183
Case-16	**0.479 ± j 4.489, – 0.1062**	**0.714**	w_9, δ_9	0.325	**– 0.208** ± j 4.054, **0.051**
	0.076 ± j 3.701, – 0.0207	**0.589**	w_1, δ_1	0.183	– 1.016 ± j 8.302, 0.121
	– 0.082 ± j 6.115, 0.0134	0.973	w_5, δ_5	0.250	–1.065 ± j 7.640, 0.138
Case-17	**0.495 ± j 4.233, – 0.1163**	**0.673**	w_9, δ_9	0.357	**– 0.179** ± j 3.996, **0.044**
	0.085 ± j 3.408, – 0.0251	**0.542**	w_1, δ_1	0.170	– 1.015 ± j 7.534, 0.133
	– 0.065 ± j 6.310, 0.0103	1.004	w_5, δ_5	0.151	–1.309 ± j 6.975, 0.184
Case-18	**0.501 ± j 3.670, – 0.1350**	**0.584**	w_9, δ_9	0.273	**– 0.511** ± j 3.993, 0.127
	0.145 ± j 3.186, – 0.0456	**0.507**	w_1, δ_1	0.189	– 0.928 ± j 7.471, 0.123
	0.029 ± j 6.373, – 0.0046	1.014	w_3, δ_3	0.179	– 1.139 ± j 8.029, 0.140

The table reveals that for open-loop system, the NEPS becomes highly unstable for unseen Case-18 due to more negative damping than other unseen cases and cases 1-3 considered earlier. Moreover, it is concluded that for NEPS two and one inter-area modes are present in unseen cases 5, 8, 9, 14-19 and cases 4, 6, 7, 10-13 respectively. These two inter-area modes are associated with rotor angles δ_1, δ_9 and speed w_1, w_9 due to high participation in their respective modes. Furthermore, the table shows that for Case-7, cases 4-6, 8, 12-18 and cases 9-11 have

one, two and three pairs of open-loop eigenvalues lie in right-half of the *s*-plane respectively and $\xi < 0$.

The table reveals that with GAPSSs eigenvalues are shifted in the left half of the *s*-plane with enhance damping factor and damping ratio as compared to without PSS for all unseen operating cases. This ensures that the NEPS will be stable for all considered unseen cases also. It is also found that designed GAPSS controllers satisfy the earlier selected criterion for the value of desired damping factor and damping ratio for all unseen cases except cases 5, 8, 9, 11, 13-18 where slightly more overshoot and settling time may occur. Hence, the GA provides robustness with improved stability and damping performance for unseen operating cases 4-18 of the NEPS as compared to that of without PSS.

In order to check the robustness performance of the designed GAPSS controllers in terms of speed deviations, earlier scenarios 1-4 are considered for unseen operating cases 4-18 of NEPS without PSS. The speed deviations $\Delta w_1, \Delta w_2, \Delta w_3, \Delta w_4, \Delta w_5, \Delta w_6, \Delta w_7, \Delta w_8, \Delta w_9$ and Δw_{10} for NEPS without PSS and with GAPSSs for Scenario-1 of unseen cases 4-12 [164] of the system are shown in Fig. 3.22 (a)-(i) and (j)-(r) respectively. Moreover, the Scenario-1 is applicable for unseen cases 4-12 only.

From Fig. 3.22 (a)-(i), it is observed that in all these response plots, the system without PSS is not capable to damp out LFO quickly because these oscillations are continuously growing up with time and all generators may go out of synchronism. Moreover, it is also noticed that Δw_9 is most severe speed deviation than others. Furthermore, the Case-8 is most severe operating cases due to Δw_9 quickly go to out of synchronism and large magnitude oscillatory instability than others.

From Fig. 3.22 (j)-(r), it is noticed that with GAPSSs, the oscillations in speed response are well damped out. Moreover, it is observed that the unseen Case-8 deliver more oscillations as compared to others. The Δw_9 is most severe speed deviations in unseen cases 4-12. Furthermore, peak overshoot of the Δw_9 is almost similar in all considered unseen cases.

To check the robustness of designed GAPSS controllers on other unseen cases, the Scenario-4 is performed on other unseen operating cases 13-18. The speed deviations of NEPS without PSS and with GAPSSs for Scenario-4 of cases 13-18 are shown in Fig. 3.23 (a)-(f) and (g)-(l) respectively.

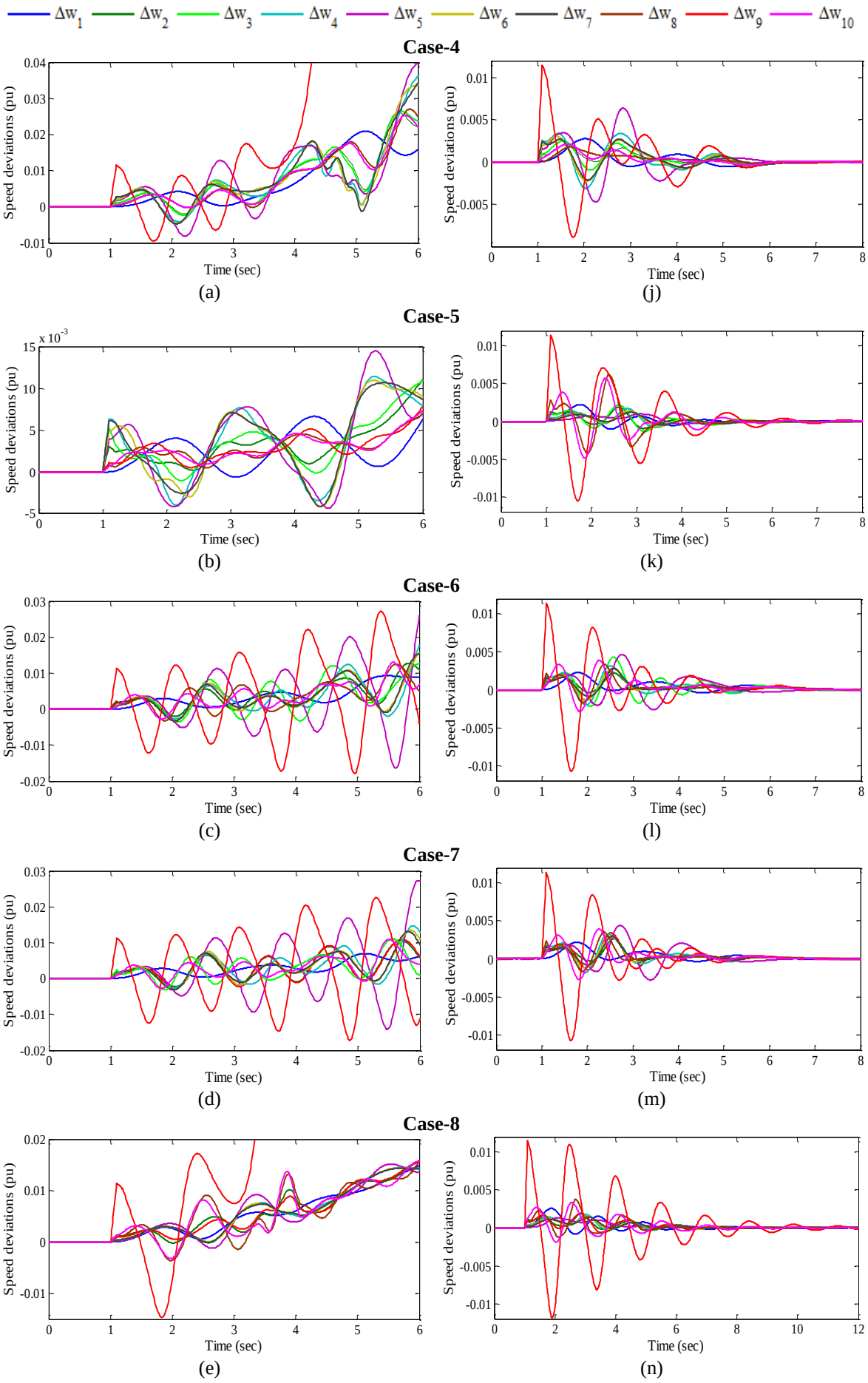
Δw1 Δw2 Δw3 Δw4 Δw5 Δw6 Δw7 Δw8 Δw9 Δw10
Case-4
Speed deviations (pu)
Time (sec)
(a)
(j)
Case-5
x 10-3
(b)
(k)
Case-6
(c)
(l)
Case-7
(d)
(m)
Case-8
(e)
(n)

Cont.

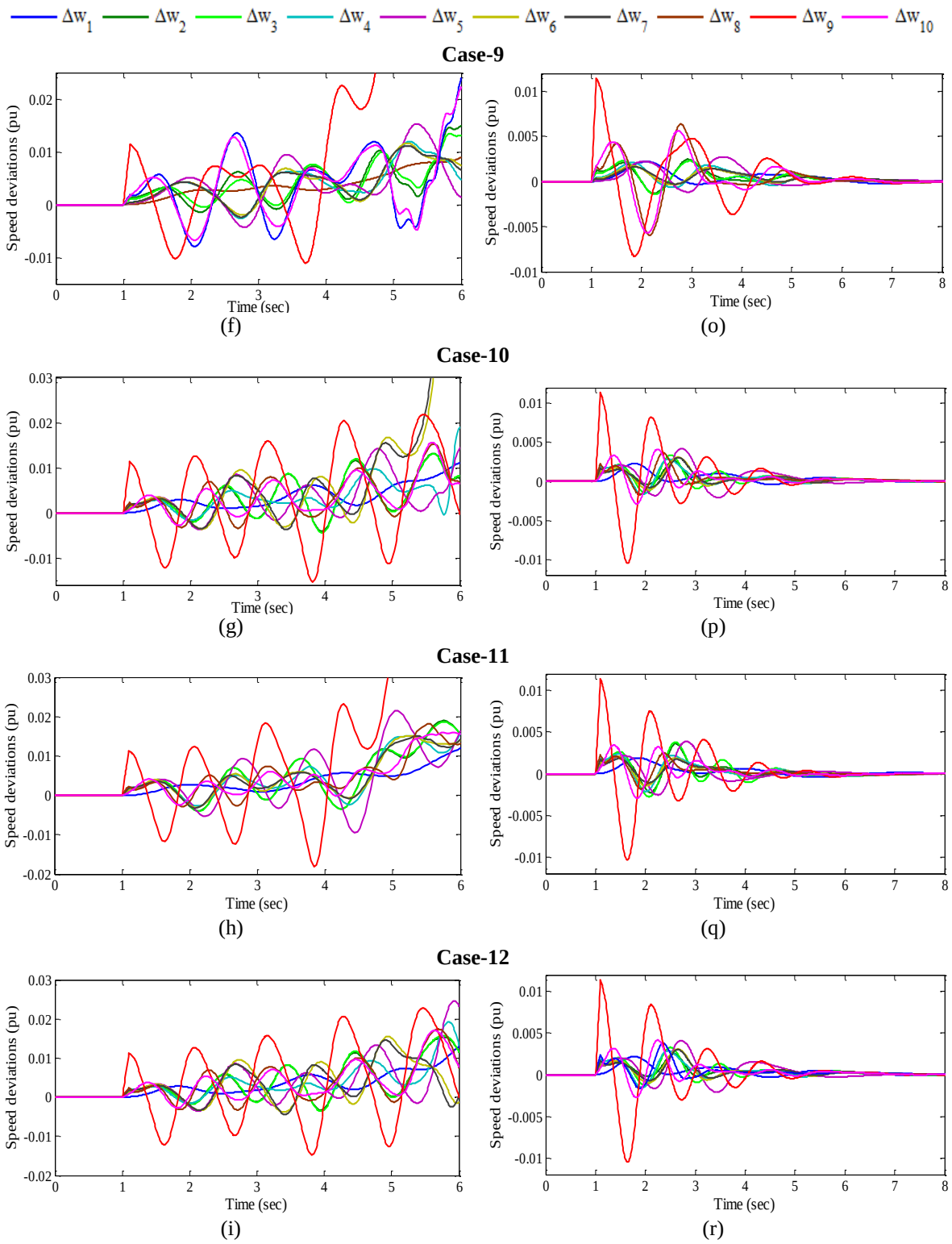

Fig. 3.22 Speed deviations (a)-(i) without PSS and (j)-(r) with GAPSSs for scenario-1 of unseen operating cases 4-12

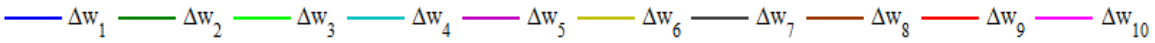

Case-13

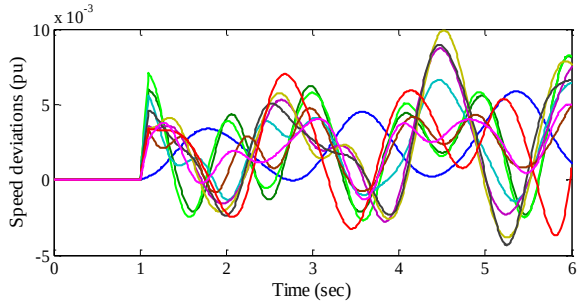

(a)

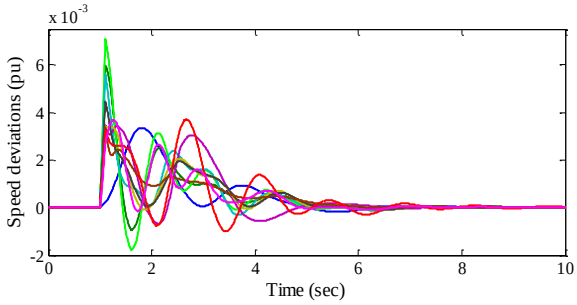

(g)

Case-14

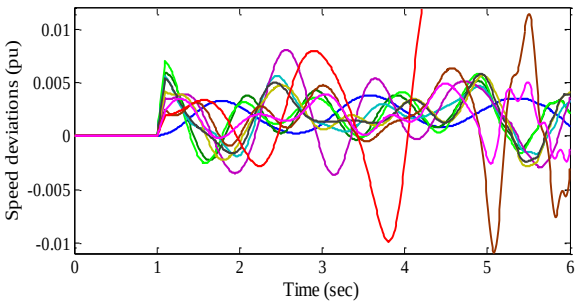

(b)

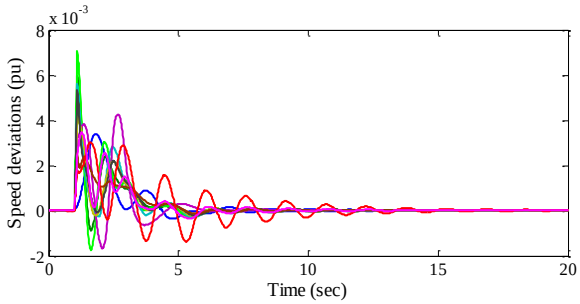

(h)

Case-15

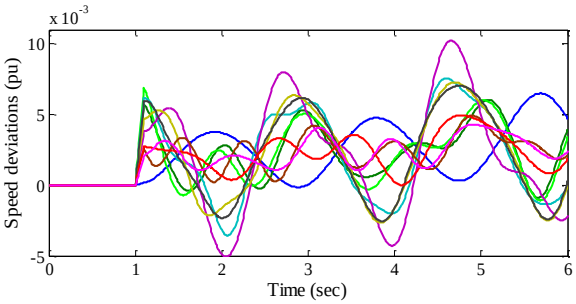

(c)

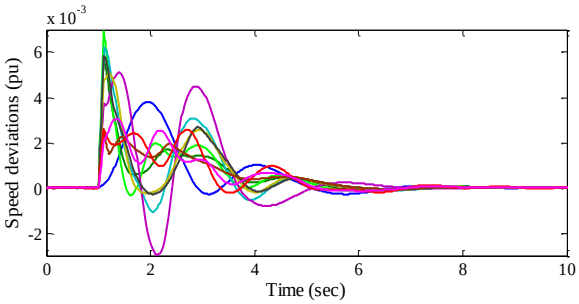

(i)

Case-16

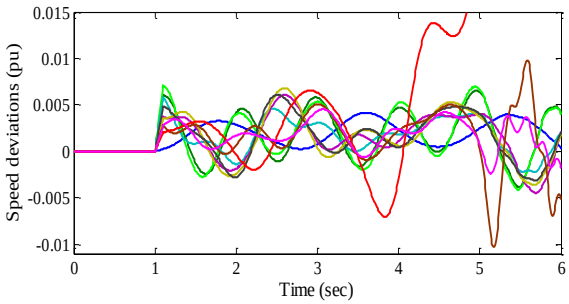

(d)

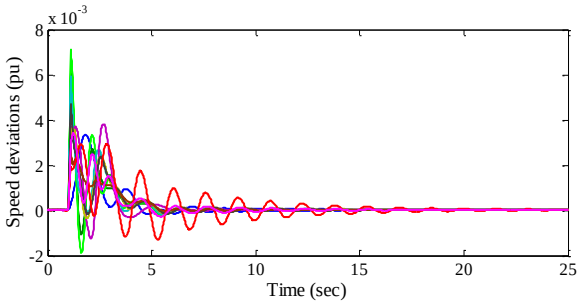

(j)

Case-17

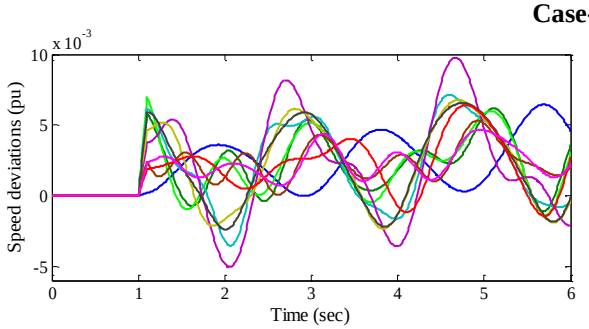

(e)

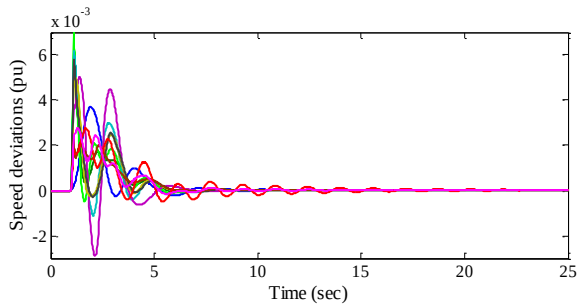

(k)

Cont.

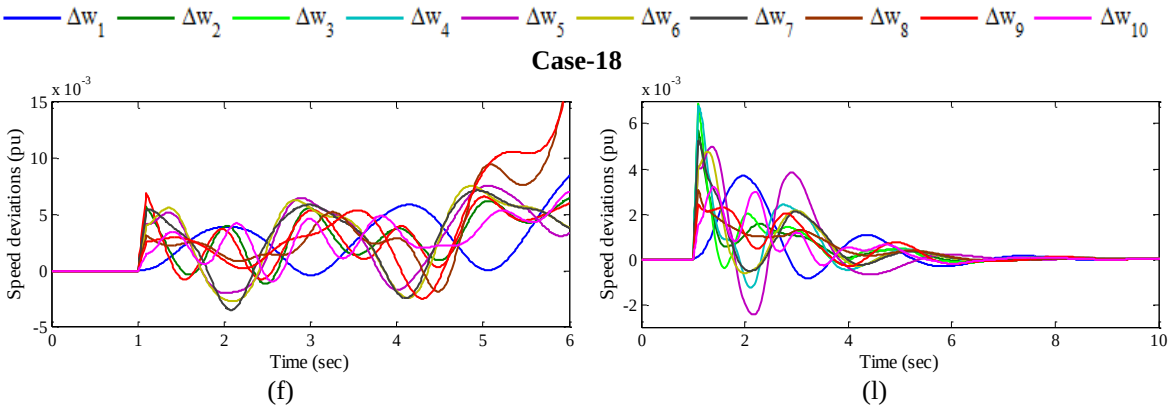

Fig. 3.23 Speed deviations (a)-(f) without PSS and (g)-(l) with GAPSSs for scenario-4 of unseen operating cases 13-18

From Fig. 3.23 (a)-(f), it is observed that in all these response plots, the system without PSS is not capable to damp out LFO quickly because these oscillations are growing up smoothly with time. Moreover, it is also observed that the Δw_9 is most severe speed deviations than others. Furthermore, in unseen cases 14, 16 and 18 the Δw_9 quickly go out of synchronism than others.

From Fig. 3.23 (g)-(l), it is noticed that LFO in speed response with GAPSSs are well damped out. Moreover, it is observed that in unseen Case-16, speed responses have high peak overshoot and consumed more time to die out oscillations as compared to others. Furthermore, the Δw_9 is most severe speed deviations in unseen cases 13-18 and takes more time to reach in steady state as compared to others. It is clear that the system performance with GAPSSs is improved to that of without PSS for severe disturbance scenarios 1 and 4 of unseen operating cases. This may be concluded that the designed GAPSSs work satisfactorily for most of the scenarios of severe disturbances of unseen operating cases of NEPS.

In addition to time-domain simulation results, the effectiveness of GAPSS controllers is observed by calculating two indices: *IAE* and *ITAE* for observed scenarios 1-4 of all unseen operating cases. The bar charts of both indices with designed GAPSS controllers for Scenario-1 of unseen cases 4-12 are shown in Fig. 3.24 (a) and (b) respectively.

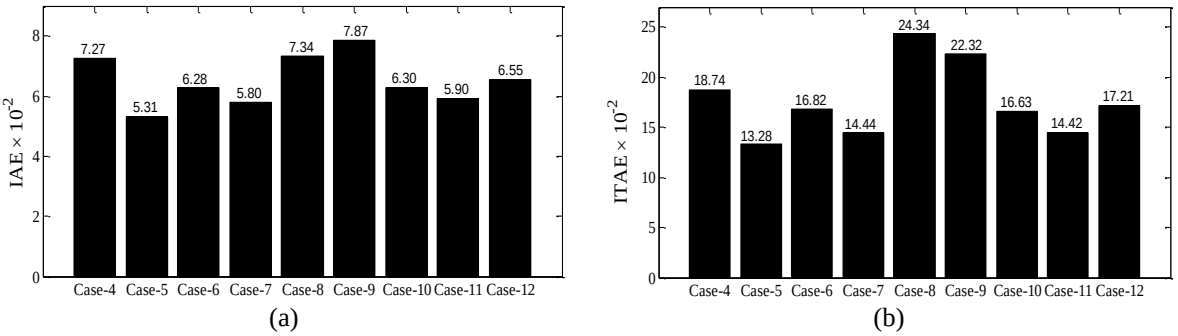

Fig. 3.24 Values of (a) *IAE* and (b) *ITAE* for scenario-1 of unseen operating cases 4-12

From Fig. 3.24 (a)-(b), it is observed that values of *IAE* with GAPSSs for unseen cases 5 and 9 of Scenario-1 are minimum and maximum respectively whereas values of *ITAE* for cases 5 and 8 are minimum and maximum respectively. Therefore, it is concluded that Case-8 under Scenario-1 is severe than others.

Similarly, both indices with designed GAPSSs for Scenario-2 of unseen cases 4-18 except Case-6, for Scenario-3 of cases 4-18 except cases 6, 9 and for Scenario-4 of cases 4-18 are shown in Fig. 3.25 (a)-(c) and (d)-(f) respectively.

From Fig. 3.25 (a)-(c), it is noticed that values of *IAE* with GAPSSs for cases 5 and 11 of Scenario-2 are minimum and maximum respectively whereas for cases 7 and 5 of Scenario-3 are minimum and maximum respectively and for cases 6 and 17 of Scenario-4, are minimum and maximum respectively. Similarly, from Fig. 3.25 (d)-(f), it is observed that values of *ITAE* with GAPSSs for Case-7 of scenarios 2-4 is minimum and for Case-16 of scenarios 2-3 and for Case-9 of Scenario-4 is maximum respectively. Moreover, the Scenario-2 of Case-16 is most severe than others scenarios 1, 3-4 for other unseen cases.

Hence, the designed GAPSS controllers for NEPS is capable to damp out low frequency local and inter-area modes of oscillations with enhanced stability and damping performances for wide range of loading cases under different scenarios of severe disturbances and also for unseen operating cases under severe scenarios of disturbances.

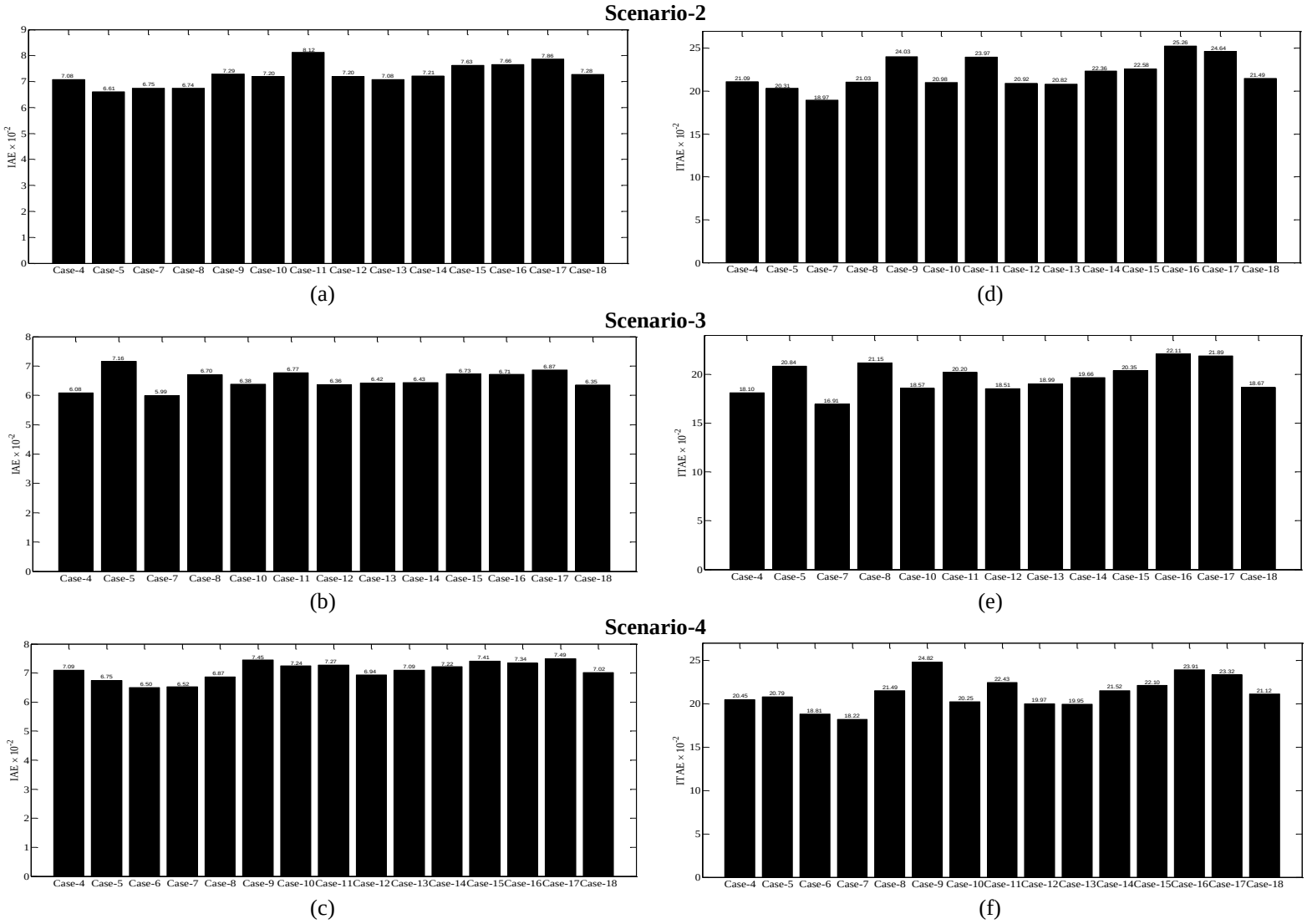

Fig. 3.25 Values of (a)-(c) *IAE* and (d)-(f) *ITAE* for scenarios 2-4 of unseen operating cases 4-18

3.4.4 Example 4: Sixteen-Machine, Sixty-Eight Bus New England Extended Power System

A single line diagram of IEEE 16-machine, 68-bus New England Extended Power System (NEEPS) is reduced order equivalent of interconnected New England Test System (NETS)-New York Power System (NYPS) [214]. In this system there are sixteen-generators and sixty-eight buses. Generators G_1-G_9 is in NETS, generators G_{10}-G_{13} are in NYPS and G_{14}-G_{16} are equivalent generators in the neighbourhood of New York system. The entire system can be divided into five areas.

1. New England (G_1-G_9)
2. New York (G_{10}-G_{13})
3. Generator G_{14}
4. Generator G_{15}
5. Generator G_{16}

Fourth order model with fast static excitation (ST1A) is considered for all the synchronous generators G_1 to G_{16} in the system. The other details of NEEPS and single-diagram are shown in Appendix. The Table 3.27 shows the six different operating cases for SSS analysis as in [163].

Table 3.27: Six operating cases of NEEPS [163]

Cases	Operating Conditions
Case-1	Base case
Case-2	Outage of line 1-2
Case-3	Outage of line 1-27
Case-4	Outage of line 8-9
Case-5	Increase 20% load to bus-17
Case-6	Outage of line 46-49, load increase 25% at bus-20,21 and generation increase 20% at G_9

A. Eigenvalue Analysis of NEEPS without PSS and with GAPSSs

The participation factor method [33] is used to identify the optimum locations of installation of PSS in this system. The PSAT [215] is used for eigenvalue analysis of the system for six different operating cases. Generally, it is observed that damping of 0.10 is required for damping out unstable and/or lightly damped modes oscillations of MMPSs. Hence, open-loop eigenvalues, damping ratio, frequency, participation modes and participation factor associated with unstable and/or lightly damped modes of operating cases 1-6 of NEEPS are shown in Tables 3.28.

Table 3.28: Open-loop eigenvalues, damping ratio, frequency, participation modes and participation factor for operating cases 1-6 of NEEPS

S. No.	Case-1				Case-2			
	Eigenvalues & Damping Ratio	**Frequency (p. u.)**	**Participation Modes**	**Participation Factor**	**Eigenvalues & Damping Ratio**	**Frequency (p. u.)**	**Participation Modes**	**Participation Factor**
1.	**0.388 ± j 6.439,– 0.0602**	1.024	w_9, δ_9	0.350	**0.358 ± j 6.411, - 0.0558**	1.020	w_9, δ_9	0.325
2.	**0.030 ± j 6.662,– 0.0045**	1.060	w_2, δ_2	0.189	**0.032 ± j 6.658, - 0.0048**	1.059	w_2, δ_2	0.195
3.	**0.009 ± j 11.306,– 0.00085**	1.799	w_{11}, δ_{11}	0.440	**0.023 ± j 11.248, - 0.0020**	1.790	w_{11}, δ_{11}	0.442
4.	– 0.069 ± j 7.845, 0.0088	1.248	w_3, δ_3	0.259	- 0.052 ± j 7.926, 0.0065	1.261	w_{10}, δ_{10}	0.422
5.	– 0.074 ± j 7.983, 0.0093	1.270	w_{10}, δ_{10}	0.373	- 0.071 ± j 7.848, 0.0090	1.249	w_3, δ_3	0.261
6.	– 0.123 ± j 7.191, 0.0172	1.144	w_{12}, δ_{12}	0.366	- 0.119 ± j 7.160, 0.0166	1.139	w_{12}, δ_{12}	0.358
7.	– 0.164 ± j 4.139, 0.0397	**0.658**	w_{13}, δ_{13}	0.177	- 0.388 ± j 8.072, 0.0481	1.284	w_8, δ_8	0.361
8.	– 0.349 ± j 7.221, 0.0493	1.149	w_5, δ_5	0.218	- 0.350 ± j 7.218, 0.0484	1.148	w_5, δ_5	0.219
9.	– 0.464 ± j 9.378, 0.0494	1.492	w_4, δ_4	0.312	- 0.466 ± j 9.380, 0.0497	1.492	w_4, δ_4	0.311
10.	– 0.464 ± j 8.335, 0.0556	1.326	w_8, δ_8	0.359	- 0.643 ± j 10.882, 0.0590	1.731	w_1, δ_1	0.430
11.	– 0.640 ± j 10.867, 0.0588	1.729	w_1, δ_1	0.437	- 0.575 ± j 9.077, 0.0632	1.444	w_7, δ_7	0.252
12.	- 0.574 ± j 9.077, 0.0631	1.444	w_7, δ_7	0.252	- 0.257 ± j 3.601, 0.0713	**0.573**	w_{13}, δ_{13}	0.213
13.	- 0.597 ± j 4.957, 0.1197	**0.789**	w_{15}, δ_{15}	0.305	- 0.206 ± j 2.362, 0.0868	**0.375**	w_{13}, δ_{13}	0.089
14.	- 0.368 ± j 3.208, 0.1139	**0.510**	w_{16}, δ_{16}	0.247	- 0.362 ± j 3.187, 0.1129	**0.507**	w_{16}, δ_{16}	0.413

Cont.

S. No.	Case-3				Case-4			
	Eigenvalues & Damping Ratio	**Frequency (p. u.)**	**Participation Modes**	**Participation Factor**	**Eigenvalues & Damping Ratio**	**Frequency (p. u.)**	**Participation Modes**	**Participation Factor**
1.	**0.382 ± j 6.428, – 0.0594**	1.023	w_9, δ_9	0.348	**0.410 ± j 6.400, – 0.0639**	1.018	w_9, δ_9	0.363
2.	**0.030 ± j 6.661, – 0.0045**	1.060	w_2, δ_2	0.195	**0.016 ± j 6.450, – 0.0026**	1.026	w_2, δ_2	0.192
3.	**0.012 ± j 11.306, – 0.0011**	1.799	w_{11}, δ_{11}	0.440	**0.017 ± j 11.285, – 0.0015**	1.796	w_{11}, δ_{11}	0.439
4.	– 0.069 ± j 7.845, 0.0088	1.248	w_3, δ_3	0.258	– 0.073 ± j 7.949, 0.0092	1.265	w_{10}, δ_{10}	0.366
5.	– 0.073 ± j 7.971, 0.0091	1.268	w_{10}, δ_{10}	0.376	– 0.087 ± j 7.875, 0.0111	1.253	w_3, δ_3	0.250
6.	– 0.115 ± j 7.172, 0.0016	1.141	w_{12}, δ_{12}	0.367	– 0.116 ± j 7.135, 0.0163	1.135	w_{12}, δ_{12}	0.359
7.	– 0.350 ± j 7.219, 0.0484	1.148	w_5, δ_5	0.218	– 0.351 ± j 7.216, 0.0486	1.148	w_5, δ_5	0.218
8.	– 0.466 ± j 9.379, 0.0496	1.492	w_4, δ_4	0.311	– 0.468 ± j 9.381, 0.0499	1.326	w_4, δ_4	0.312
9.	– 0.171 ± j 4.079, 0.0419	**0.649**	w_{13}, δ_{13}	0.177	– 0.468 ± j 8.333, 0.0561	1.493	w_8, δ_8	0.361
10.	– 0.469 ± j 9.379, 0.0562	1.325	w_8, δ_8	0.361	– 0.639 ± j 10.889, 0.0586	1.733	w_1, δ_1	0.438
11.	– 0.640 ± j 10.881, 0.0587	1.731	w_1, δ_1	0.437	– 0.577 ± j 9.077, 0.0635	1.444	w_7, δ_7	0.252
12.	– 0.575 ± j 9.077, 0.0633	1.444	w_7, δ_7	0.252	– 0.293 ± j 3.488, 0.0837	**0.555**	w_{13}, δ_{13}	0.189
13.	– 0.367 ± j 3.210, 0.1137	**0.510**	w_{16}, δ_{16}	0.246	– 0.233 ± j 2.443, 0.0952	**0.388**	w_{13}, δ_{13}	0.104
14.	– 0.597 ± j 4.957, 0.1197	**0.789**	w_{15}, δ_{15}	0.305	– 0.347 ± j 3.149, 0.1096	**0.501**	w_{14}, δ_{14}	0.169

Cont.

S. No.	Case-5				Case-6			
	Eigenvalues & Damping Ratio	**Frequency (p.u.)**	**Participation Modes**	**Participation Factor**	**Eigenvalues & Damping Ratio**	**Frequency (p.u.)**	**Participation Modes**	**Participation Factor**
1.	**0.387 ± j 6.437, –0.0600**	1.024	w_9, δ_9	0.350	**0.585 ± j 6.312, – 0.0923**	1.004	w_9, δ_9	0.342
2.	**0.031 ± j 6.663, – 0.0047**	1.060	w_2, δ_2	0.196	**0.017 ± j 6.666, – 0.0026**	1.061	w_2, δ_2	0.192
3.	**0.014 ± j 11.315, – 0.0012**	1.800	w_{11}, δ_{11}	0.441	**0.010 ± j 11.284, – 0.0008**	1.795	w_{11}, δ_{11}	0.437
4.	– 0.068 ± j 7.844, 0.0087	1.248	w_3, δ_3	0.259	– 0.064 ± j 7.920, 0.0081	1.260	w_{10}, δ_{10}	0.350
5.	– 0.074 ± j 7.982, 0.0093	1.270	w_{10}, δ_{10}	0.376	– 0.072 ± j 7.845, 0.0091	1.248	w_3, δ_3	0.239
6.	– 0.114 ± j 7.171, 0.0159	1.141	w_{12}, δ_{12}	0.369	– 0.118 ± j 7.174, 0.0165	1.141	w_{12}, δ_{12}	0.361
7.	– 0.164 ± j 4.152, 0.0396	**0.660**	w_{13}, δ_{13}	0.173	– 0.148 ± j 4.170, 0.0356	**0.663**	w_{13}, δ_{13}	0.157
8.	– 0.350 ± j 7.219, 0.0484	1.149	w_5, δ_5	0.218	– 0.476 ± j 9.387, 0.0507	1.494	w_4, δ_4	0.313
9.	– 0.465 ± j 9.379, 0.0496	1.492	w_4, δ_4	0.312	– 0.379 ± j 7.212, 0.0525	1.147	w_5, δ_5	0.224
10.	– 0.465 ± j 8.334, 0.0557	1.326	w_8, δ_8	0.359	– 0.465 ± j 8.325, 0.0557	1.325	w_8, δ_8	0.360
11.	– 0.641 ± j 10.867, 0.0588	1.729	w_1, δ_1	0.437	– 0.635 ± j 10.915, 0.0581	1.737	w_1, δ_1	0.436
12.	– 0.575 ± j 9.077, 0.0632	1.444	w_7, δ_7	0.252	– 0.579 ± j 9.078, 0.0637	1.444	w_7, δ_7	0.253
13.	– 0.367 ± j 3.212, 0.1137	**0.511**	w_{16}, δ_{16}	0.248	– 0.598 ± j 4.942, 0.1201	**0.786**	w_{15}, δ_{15}	0.311
14.	– 0.597 ± j 4.958, 0.1196	**0.789**	w_{15}, δ_{15}	0.305	– 0.378 ± j 3.035, 0.1235	**0.483**	w_{14}, δ_{14}	0.247

The table reveals that for open-loop system, the NEEPS becomes unstable as well as poorly damped for operating case 1-6 through three inter-areas and eleven local modes of oscillations. These unstable modes primarily associated with rotor angles δ_9, δ_2, δ_{11} and speed w_9, w_2, w_{11} and lightly damped associated with δ_1, δ_3-δ_5, δ_7, δ_8, δ_{10}, δ_{12}-δ_{13}, δ_{15}, δ_{16} and w_1, w_3-w_5, w_7, w_8, w_{10}, w_{12}-w_{13}, w_{15}, w_{16} with high participation in their respective modes. Therefore, the corresponding fourteen generators out of sixteen generators except G_6 and G_{14} are the optimum locations for installing PSSs.

For guaranteed stability of unstable local modes and to assure the relative stability of poorly damped local and inter-area modes, LFO are to be damped out by increasing the damping performance of NEEPS. An eigenvalue-based multi-objective function J (equation 3.1) is used in Section 3.2 and minimized using GA for tuning the forty-two parameters of PSSs. In this case, the particular value of σ_0 and ξ_0 are selected as –0.5 and 0.1 respectively. The value of washout time constant is chosen as 10 sec, T_2 and T_4 are kept constant at numerical values of 0.1 sec. The values of designed parameters K, T_1 and T_3 are set in the range of [1-100], [0.01–1] and [0.01–1] respectively. The GA is applied with population size 100, maximum generation 100, crossover rate 0.80 and mutation rate 0.01.

The GA is able to find the desired solution for which fitness function J is zero. The final value of J equal to zero indicates that fourteen unstable and/or poorly damped eigenvalues are shifted to a specified D-shape zone in the left-half of the s-plane. The optimum designed forty-two parameters of GAPSSs for fourteen generators are shown in Table 3.29.

Table 3.29: Optimal designed parameters of GAPSSs

Generators	K_1	T_1	T_3
G_1	76.425	0.162	0.888
G_2	26.315	0.551	0.510
G_3	47.143	0.323	0.572
G_4	17.558	0.994	0.509
G_5	59.035	0.281	0.329
G_7	10.756	0.814	0.677
G_8	52.683	0.431	0.109
G_9	26.648	0.520	0.489
G_{10}	75.727	0.549	0.245
G_{11}	15.281	0.310	0.249
G_{12}	4.496	0.766	0.687
G_{13}	37.969	0.512	0.235
G_{15}	38.367	0.388	0.263
G_{16}	42.826	0.478	0.878

The closed-loop eigenvalues and their damping ratio for only unstable modes with designed GAPSS controllers for operating cases 1-6 are evaluated using PSAT [215] and are shown in Table 3.30.

Table 3.30: Eigenvalues and damping ratio with GAPSSs for operating cases 1-6 of NEEPS

Cases	With GAPSSs		
Case-1	– 0.601 ± j 2.214, 0.262	– 0.609 ± j 1.265, 0.434	– 0.744 ± j 3.996, 0.183
Case-2	– 0.643 ± j 1.138, 0.492	– 0.655 ± j 2.214, 0.283	– 0.750 ± j 3.987, 0.184
Case-3	– 0.638 ± j 1.251, 0.454	– 0.645 ± j 2.218, 0.279	– 0.746 ± j 3.992, 0.183
Case-4	– 0.633 ± j 1.181, 0.472	– 0.652 ± j 2.225, 0.281	– 0.743 ± j 2.436, 0.291
Case-5	– 0.601 ± j 2.215, 0.262	– 0.608 ± j 1.269, 0.472	– 0.744 ± j 3.997, 0.183
Case-6	– 0.623 ± j 2.186, 0.274	– 0.651 ± j 0.984, 0.552	– 0.688 ± j 2.391, 0.276

The eigenvalue maps of NEEPS without PSS for operating cases 1-3 and 4-6 are shown in Fig. 3.26 (a)-(c) and (g)-(i) whereas with GAPSSs for same cases are shown in Fig. 3.26 (d)-(f) and (j)-(l) respectively.

Fig. 3.26 (a)-(c) and (g)-(i) reveals that for cases 1-6, three pairs of open-loop eigenvalues lie in right-half of the *s*-plane and $\xi < 0$, and also for Case-6, four, five and two pairs of open-loop eigenvalues have $0 < \xi < 0.05$, $0.05 < \xi < 0.10$ and $\xi > 0.1$ respectively. Similarly for cases 1-3, 5 and for Case-4, six and five pairs of open-loop eigenvalues have $0 < \xi < 0.05$ respectively and for cases 1, 3, 5, Case-2 and Case-4 three, four and five pairs of open-loop eigenvalues have $0.05 < \xi < 0.10$ respectively and remaining two and one pair of open-loop eigenvalues for cases 1, 3, 5 and Case-4 have $\xi > 0.10$ respectively. Moreover, it is also observed that operating Case-6 is highly unstable and provide more negative damping than others.

Table 3.30 and Fig. 3.26 (d)-(f) and (j)-(l) show that the GAPSSs shift the eigenvalues to the particular D-shape zone in the left half of the *s*-plane with better damping factor and damping ratio as compared to without PSS for all operating cases. Hence, GAPSS controllers provide improved stability and damping characteristics of the NEEPS as compared to same obtained using without PSS.

B. Time-Domain Simulation Results and Discussions with GAPSSs and without PSS of NEEPS

In order to examine the performance of designed GAPSS controllers in previous section in terms of speed deviations, fifty-eight scenarios of severe disturbances on NEEPS without PSS are considered as shown in Table 3.31. Established index *ITAE* is evaluated for all considered scenarios of operating Case-1 and is presented using bar charts as shown in Fig 3.30.

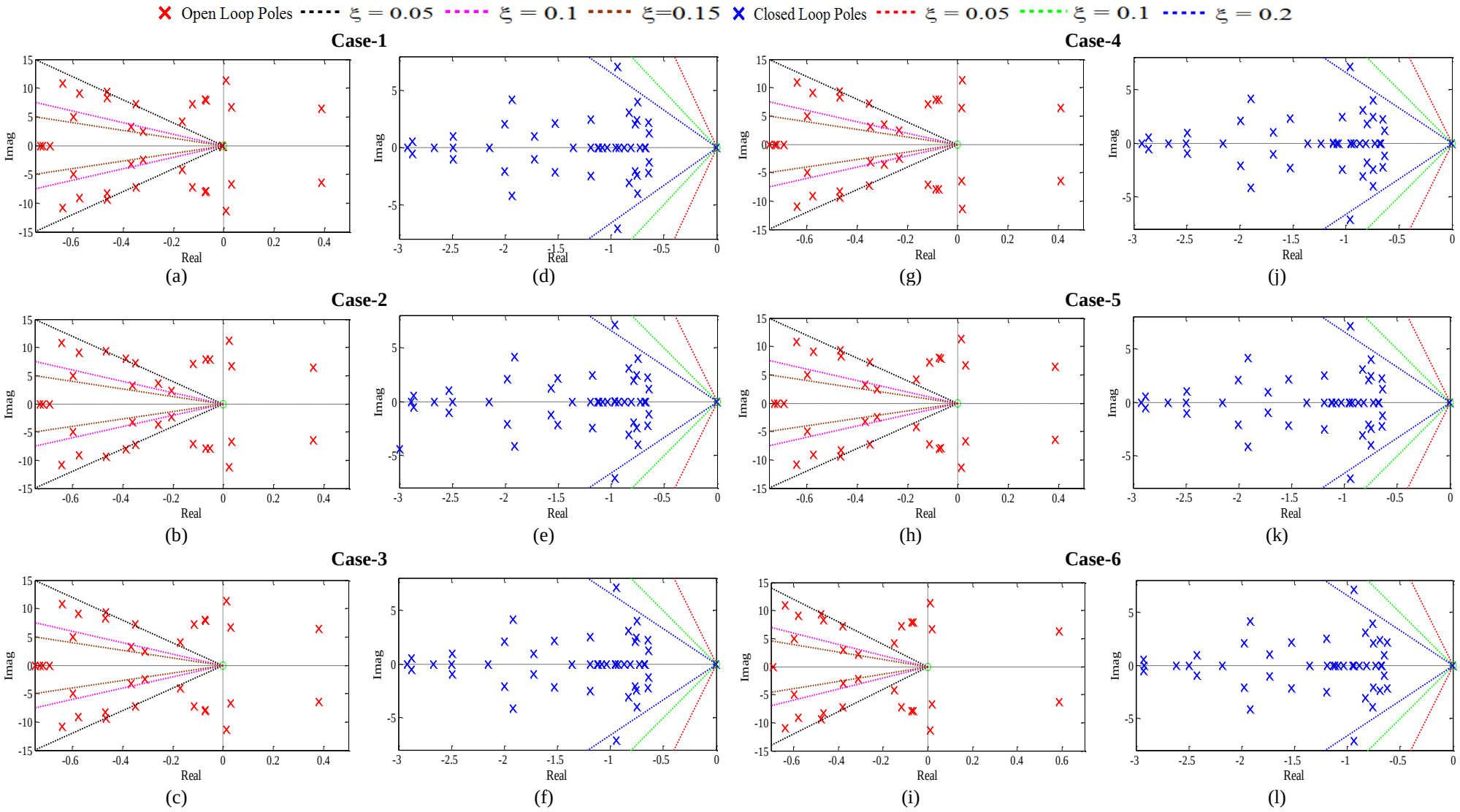

Fig. 3.26 Eigenvalue maps (a)-(c)& (g)-(i) without PSS and (d)-(f) & (j)-(l) with GAPSSs for operating cases 1-6 of NEEPS

Table 3.31: Various scenarios of disturbances at t = 1 sec on NEEPS

	Scenarios of Disturbances		Scenarios of Disturbances
S-1	A 6-cycle 3-phase fault at bus 1 without tripping the line 1-31	S-30	A 6-cycle 3-phase fault at bus 23 without tripping the line 23-24
S-2	A 6-cycle 3-phase fault at bus 1 without tripping the line 1-47	S-31	A 6-cycle 3-phase fault at bus 25 without tripping the line 2-25
S-3	A 6-cycle 3-phase fault at bus 2 without tripping the line 1-2	S-32	A 6-cycle 3-phase fault at bus 26 without tripping the line 25-26
S-4	A 6-cycle 3-phase fault at bus 2 without tripping the line 2-3	S-33	A 6-cycle 3-phase fault at bus 26 without tripping the line 26-27
S-5	A 6-cycle 3-phase fault at bus 3 without tripping the line 3-18	S-34	A 6-cycle 3-phase fault at bus 27 without tripping the line 1-27
S-6	A 6-cycle 3-phase fault at bus 4 without tripping the line 3-4	S-35	A 6-cycle 3-phase fault at bus 27 without tripping the line 17-27
S-7	A 6-cycle 3-phase fault at bus 5 without tripping the line 4-5	S-36	A 6-cycle 3-phase fault at bus 28 without tripping the line 26-28
S-8	A 6-cycle 3-phase fault at bus 5 without tripping the line 5-8	S-37	A 6-cycle 3-phase fault at bus 29 without tripping the line 26-29
S-9	A 6-cycle 3-phase fault at bus 6 without tripping the line 5-6	S-38	A 6-cycle 3-phase fault at bus 30 without tripping the line 1-30
S-10	A 6-cycle 3-phase fault at bus 6 without tripping the line 6-7	S-39	A 6-cycle 3-phase fault at bus 30 without tripping the line 9-30
S-11	A 6-cycle 3-phase fault at bus 6 without tripping the line 6-11	S-40	A 6-cycle 3-phase fault at bus 30 without tripping the line 30-31
S-12	A 6-cycle 3-phase fault at bus 8 without tripping the line 7-8	S-41	A 6-cycle 3-phase fault at bus 31 without tripping the line 31-38
S-13	A 6-cycle 3-phase fault at bus 8 without tripping the line 8-9	S-42	A 6-cycle 3-phase fault at bus 32 without tripping the line 30-32
S-14	A 6-cycle 3-phase fault at bus 10 without tripping the line 10-11	S-43	A 6-cycle 3-phase fault at bus 33 without tripping the line 33-34
S-15	A 6-cycle 3-phase fault at bus 10 without tripping the line 10-13	S-44	A 6-cycle 3-phase fault at bus 33 without tripping the line 33-38
S-16	A 6-cycle 3-phase fault at bus 11 without tripping the line 11-12	S-45	A 6-cycle 3-phase fault at bus 34 without tripping the line 34-35
S-17	A 6-cycle 3-phase fault at bus 13 without tripping the line 12-13	S-46	A 6-cycle 3-phase fault at bus 35 without tripping the line 35-45
S-18	A 6-cycle 3-phase fault at bus 13 without tripping the line 13-14	S-47	A 6-cycle 3-phase fault at bus 36 without tripping the line 9-36
S-19	A 6-cycle 3-phase fault at bus 14 without tripping the line 4-14	S-48	A 6-cycle 3-phase fault at bus 36 without tripping the line 34-36
S-20	A 6-cycle 3-phase fault at bus 14 without tripping the line 14-15	S-49	A 6-cycle 3-phase fault at bus 37 without tripping the line 37-43
S-21	A 6-cycle 3-phase fault at bus 16 without tripping the line 15-16	S-50	A 6-cycle 3-phase fault at bus 38 without tripping the line 38-46
S-22	A 6-cycle 3-phase fault at bus 16 without tripping the line 16-17	S-51	A 6-cycle 3-phase fault at bus 41 without tripping the line 40-41
S-23	A 6-cycle 3-phase fault at bus 16 without tripping the line 16-21	S-52	A 6-cycle 3-phase fault at bus 41 without tripping the line 41-42
S-24	A 6-cycle 3-phase fault at bus 16 without tripping the line 16-24	S-53	A 6-cycle 3-phase fault at bus 42 without tripping the line 42-52
S-25	A 6-cycle 3-phase fault at bus 17 without tripping the line 17-18	S-54	A 6-cycle 3-phase fault at bus 43 without tripping the line 43-44
S-26	A 6-cycle 3-phase fault at bus 19 without tripping the line 16-19	S-55	A 6-cycle 3-phase fault at bus 45 without tripping the line 39-45
S-27	A 6-cycle 3-phase fault at bus 19 without tripping the line 19-20	S-56	A 6-cycle 3-phase fault at bus 46 without tripping the line 46-49
S-28	A 6-cycle 3-phase fault at bus 21 without tripping the line 21-22	S-57	A 6-cycle 3-phase fault at bus 47 without tripping the line 47-48
S-29	A 6-cycle 3-phase fault at bus 22 without tripping the line 22-23	S-58	A 6-cycle 3-phase fault at bus 52 without tripping the line 42-52

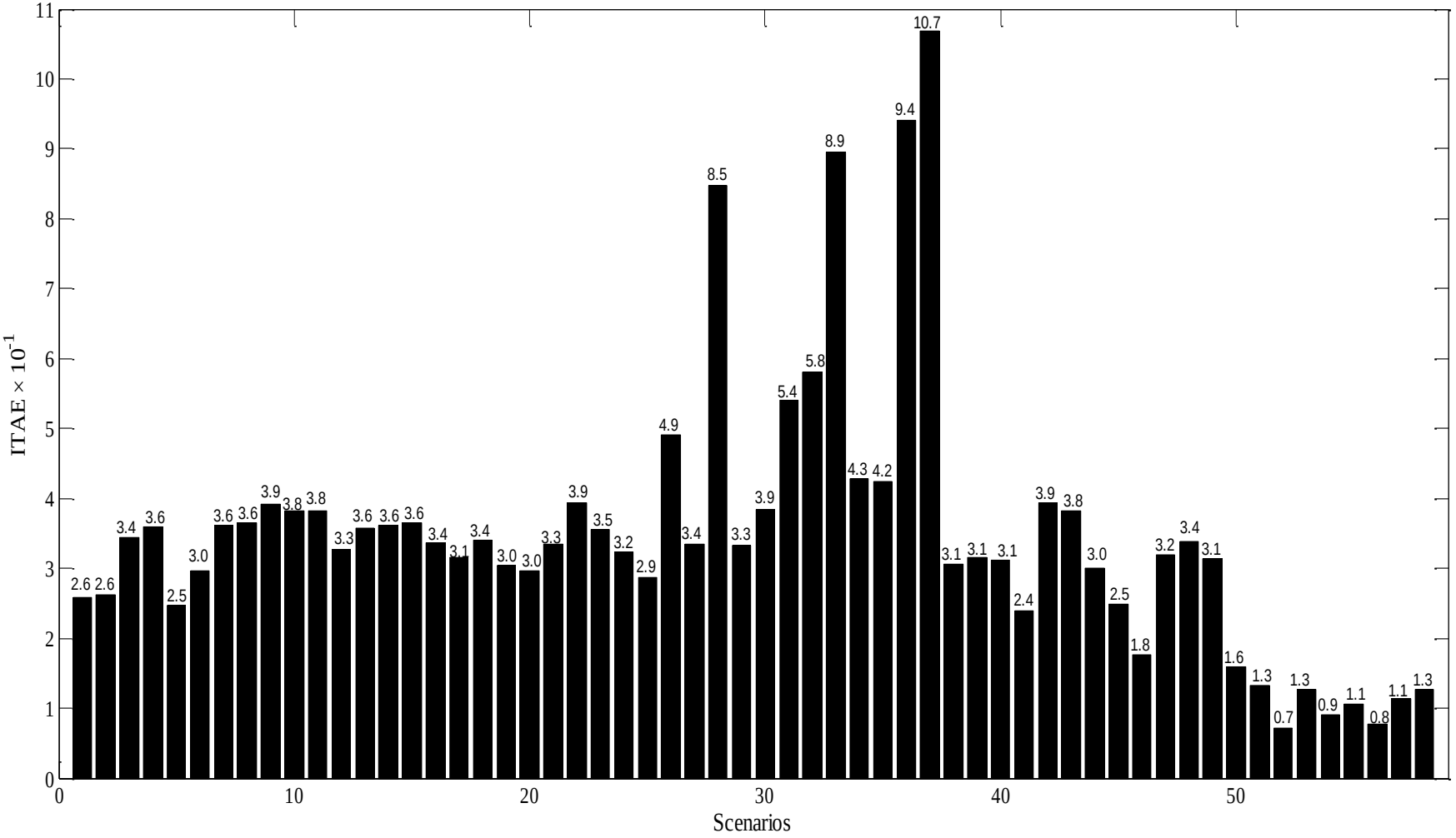

Fig. 3.27 Value of *ITAE* without PSS for scenarios S-1 to S-58 of operating case-1 of NEEPS

From the figure it may be observed that the values of *ITAE* are higher for eight severe scenarios of disturbances, i.e., S-26, S-28, S-31 to S-34, S-36 and S-37 respectively. The selected scenarios, i.e. S-37, S-28, S-31 and S-26 of severe disturbance at different locations are chosen for testing the performance of the designed GAPSS controllers on NEEPS are renamed and as shown in Table 3.32.

Table 3.32: Observed scenarios of disturbances for testing performance of GAPSSs for NEEPS

Scenarios	Most Severe Scenarios of Disturbances
Scenario-1 (S-37)	A 6-cycle 3-phase fault at t = 1 sec on bus 29 without tripping the line 26-29
Scenario-2 (S-28)	A 6-cycle 3-phase fault at t = 1 sec on bus 21 without tripping the line 21-22
Scenario-3 (S-31)	A 6-cycle 3-phase fault at t = 1 sec on bus 25 without tripping the line 2-25
Scenario-4 (S-26)	A 6-cycle 3-phase fault at t = 1 sec on bus 19 without tripping the line 16-19

Now, the time-domain simulation of NEEPS is performed for without PSS and with GAPSSs for observed four scenarios of severe operating Case-6 only. The speed deviations Δw_1, Δw_2, Δw_3, Δw_4, Δw_5, Δw_6, Δw_7, Δw_8, Δw_9, Δw_{10}, Δw_{11}, Δw_{12}, Δw_{13}, Δw_{14}, Δw_{15} and Δw_{16} for without PSS and with GAPSSs for scenarios 1-4 of operating Case-6 are shown in Fig. 3.28 (a)-(d) and (e)-(h) respectively.

From Fig. 3.28 (a)-(d), it is observed that in all these response plots, the system without PSS is not capable to die out LFO because these oscillations are growing up smoothly except the Δw_9. Moreover, it also found that Δw_9 is most severe speed deviations than others. Furthermore, the Scenario-1 is most severe disturbance scenario than others because the Δw_9 quickly go to out of synchronism.

From Fig. 3.28 (e)-(h), it is noticed that that with GAPSSs, LFO are well damped out for all scenarios. Moreover, the Δw_9 has larger peak overshoot and generates more oscillations in Scenario-1 than others. It is clear that the system performance with GAPSSs is much improved to that of without PSS for all scenarios of operating Case-6.

This demonstrates the potential of GA technique to obtain the desired set of PSS parameters for NEEPS and the designed GAPSSs are capable to damp out LFO for wide range of operating cases under severe scenarios of disturbances.

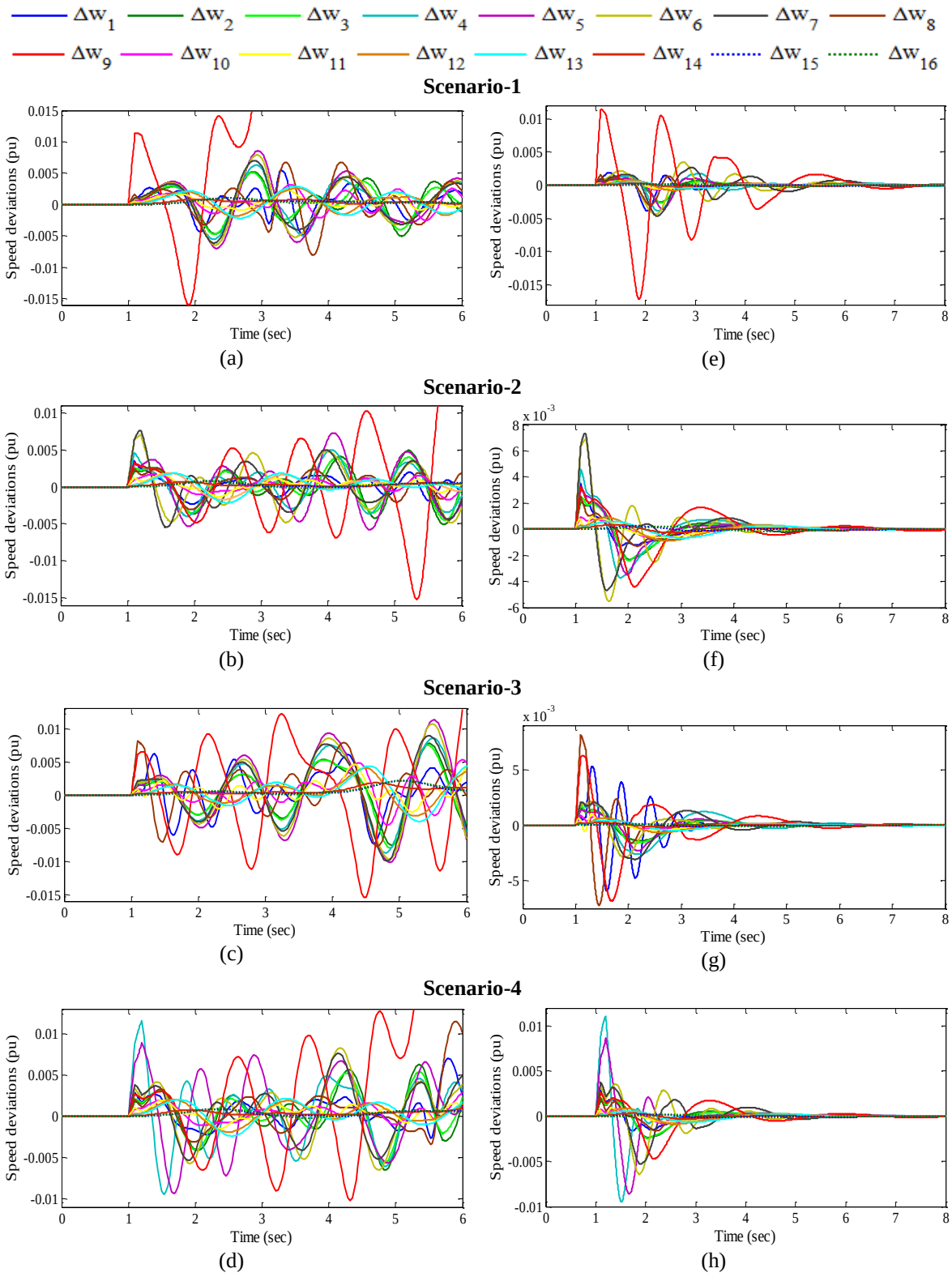

Fig. 3.28 Speed deviations (a)-(d) without PSS and (e)-(h) with GAPSSs for scenarios 1-4 of operating case-6

C. Performance Indices Results and Discussions with GAPSSs of NEEPS

In addition to time-domain simulation results, the effectiveness of designed GAPSS controllers is observed by evaluating two indices: *IAE* and *ITAE* for observed four scenarios of

different disturbances. The bar charts of both indices values with GAPSSs for scenarios 1-4 of cases 1-6 are shown in Fig. 3.29 (a)-(d) and (e)-(h) respectively.

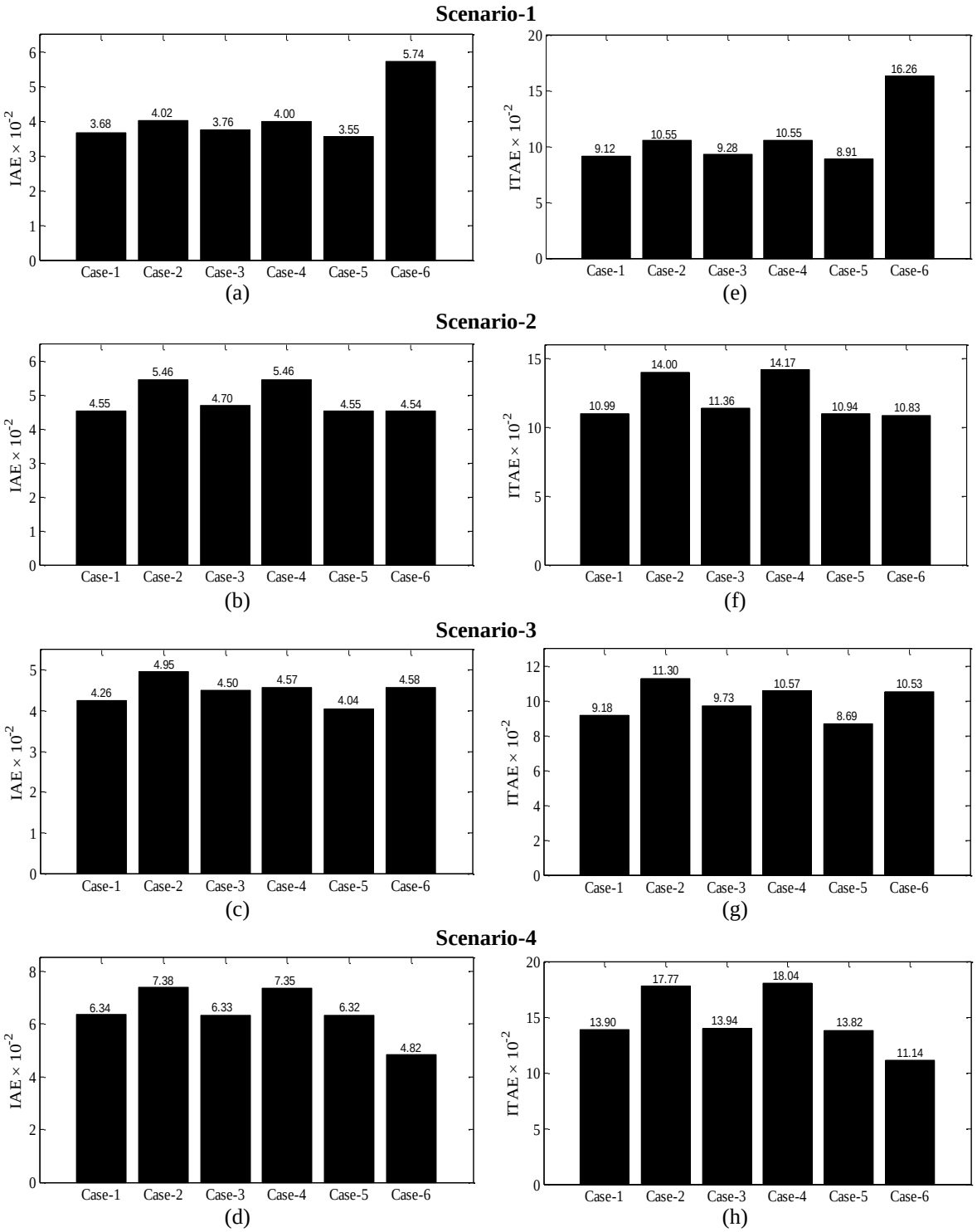

Fig. 3.29 Values of (a)-(d) *IAE* and (e)-(h) *ITAE* with GAPSSs for scenarios 1-4 of operating cases 1-6

From the Fig. 3.29 (a)-(d), it is observed that both indices for Scenario-1, Case-5 and Case-6, for Scenario-2, Case-6 and Case-4, for Scenario-3, Case-5 and Case-2 are lower and higher values respectively whereas for Scenario-4, the *ITAE* is higher for Case-4 and lower for Case-6 respectively. Moreover, it is concluded that for scenarios 1 to 4 operating cases 6, 4, 2

and 4 are most severe than others respectively. Furthermore, it is also noticed that for all cases the Scenario-4 is most severe others scenarios whereas for Case-6, the Scenario-1 is most severe than others. Comparing Fig. 3.29 with Fig. 3.27, it may be observed that the designed GAPSS controllers of NEEPS provide sufficient damping to damp out low frequency local and inter-area modes oscillation with less overshoot and settling time than that of without PSS.

D. Robustness Test of Designed GAPSS Controllers of NEEPS

To test the robustness of earlier designed GAPSS controllers for NEEPS, nine unseen operating cases 7-15 are considered as shown in Table 3.33. In this section, the effectiveness of GAPSSs is evaluated by eigenvalue analysis, time-domain simulation results and performance indices for earlier observed four scenarios of all unseen operating cases and compared with that of without PSS.

Table 3.33: Nine unseen operating conditions of NEEPS

Cases	Operating Conditions
Case-7	Total active and reactive power increased by 25%
Case-8	Outage of line 1-31,30-32 and 33-34
Case-9	Outage of line 1-31,10-11, 30-32 and 33-34
Case-10	Outage of line 10-11, 30-32 and 33-34
Case-11	Total active and reactive power decreased by 15%
Case-12	Outage of line 1-31, 10-11, 26-29 , and 33-34,
Case-13	Outage of line 26-27 and 28-29
Case-14	Outage of line 2-3,26-27 and 28-29
Case-15	Total active and power decreased by 15% with outage of line 2-3, 26-27 and 28-29

Open-loop eigenvalues, damping ratio, frequency, participation modes and participation factor for only unstable modes of unseen operating cases 7-15 of NEEPS without PSS and closed-loop eigenvalues and damping ratio with designed GAPSSs for the same unseen cases of system are obtained using PSAT [215] and shown in Table 3.34.

The table reveals that the NEEPS becomes unstable with two, three, four and five pairs of open-loop eigenvalues for cases 7, 11, 14; cases 13, 15; cases 8, 10, 12 and Case-9 respectively and they lie in the right half of the s-plane with $\xi < 0$. Moreover, it is noticed that the Case-9 has highest five unstable modes than others. Furthermore, the Case-15 is highly unstable due to more negative damping than other unseen cases and cases 1-6 considered earlier. These unstable modes primarily associated with rotor angles δ_9, δ_2, δ_8 and speed w_9, w_2, w_8 with high participation in their respective modes.

Table 3.34: Open-loop eigenvalues, damping ratio, frequency, participation modes, participation factor and closed-loop eigenvalues, damping ratio for unseen operating cases 7-15 of NEEPS

Cases	Open-loop				Closed-loop
	Eigenvalues &Damping Ratio	**Frequency (p.u.)**	**Participation Modes**	**Participation Factor**	**Eigenvalues &Damping Ratio**
Case-7	**0.310 ± j 6.418, - 0.0483**	1.021	w_9, δ_9	0.345	- 0.756 ± j 2.440, 0.295
	0.0005 ± j 6.628, - 0.00008	1.055	w_2, δ_2	0.185	- 0.705 ± j 4.039, 0.171
Case-8	**0.381 ± j 6.427, - 0.0591**	1.022	w_9, δ_9	0.351	- 0.949 ± j 7.084, 0.132
	0.328 ± j 5.499, - 0.0597	0.875	w_{11}, δ_{11}	0.350	- 0.754 ± j 3.966, 0.186
	0.032 ± j 6.667, - 0.0048	1.061	w_2, δ_2	0.197	- 0.829 ± j 3.083, 0.259
	0.004 ± j 8.094, - 0.0005	1.288	w_{10}, δ_{10}	0.375	- 0.584 ± j 2.184, 0.258
Case-9	**0.386 ± j 6.420, - 0.0599**	1.021	w_9, δ_9	0.352	- 0.956 ± j 7.077, 0.133
	0.329 ± j 5.485, - 0.0599	0.873	w_{11}, δ_{11}	0.350	- 0.754 ± j 7.084, 0.186
	0.038 ± j 6.661, - 0.0057	1.060	w_2, δ_2	0.235	- 0.831 ± j 3.084, 0.260
	0.013 ± j 7.368, - 0.0018	1.172	w_2, δ_2	0.165	- 0.750 ± j 2.434, 0.294
	0.003 ± j 8.090, - 0.0003	1.287	w_{10}, δ_{10}	0.374	- 0.584 ± j 2.183, 0.258
Case-10	**0.395 ± j 6.426, - 0.0614**	1.022	w_9, δ_9	0.356	- 0.953 ± j 7.078, 0.133
	0.294 ± j 5.998, - 0.0490	0.954	w_{11}, δ_{11}	0.357	- 0.751 ± j 3.988, 0.185
	0.047 ± j 6.671, - 0.0070	1.061	w_2, δ_2	0.164	- 0.832 ± j 3.084, 0.260
	0.015 ± j 7.367, - 0.0021	1.172	w_2, δ_2	0.237	- 0.750 ± j 2.433, 0.294
Case-11	**0.406 ± j 6.425, - 0.0631**	1.022	w_9, δ_9	0.347	- 0.953 ± j 7.048, 0.134
	0.035 ± j 6.610, - 0.0054	1.052	w_2, δ_2	0.188	- 0.810 ± j 3.862, 0.205
Case-12	**0.417 ± j 5.744, - 0.0724**	0.914	w_9, δ_9	0.354	- 0.958 ± j 7.073, 0.134
	0.057 ± j 10.263, - 0.0055	1.633	w_{11}, δ_{11}	0.396	- 0.748 ± j 3.990, 0.184
	0.023 ± j 6.629, - 0.0035	1.055	w_2, δ_2	0.162	- 0.830 ± j 3.076, 0.260
	0.007 ± j 7.339, - 0.0009	1.168	w_3, δ_3	0.164	- 0.636 ± j 2.385, 0.257
Case-13	**0.438 ± j 5.034, - 0.0866**	0.801	w_9, δ_9	0.330	- 0.971 ± j 7.038, 0.133
	0.031 ± j 6.653, - 0.0047	1.059	w_2, δ_2	0.204	- 0.745 ± j 3.995, 0.183
	0.001 ± j 11.305, - 0.0001	1.798	w_{11}, δ_{11}	0.436	- 0.516 ± j 2.229, 0.225

Cont.

Cases	Open-loop				Closed-loop
	Eigenvalues &Damping Ratio	**Frequency (p.u.)**	**Participation Modes**	**Participation Factor**	**Eigenvalues &Damping Ratio**
Case-14	**0.404 ± j 4.154, - 0.0969**	**0.661**	w_9, δ_9	0.324	- 0.596 ± j 2.196, 0.261
	0.014 ± j 6.620, - 0.0021	1.053	w_2, δ_2	0.200	- 0.532 ± j 1.991, 0.258
Case-15	**0.455 ± j 3.919, - 0.1153**	**0.623**	w_9, δ_9	0.319	**- 0.488** ± j 2.018, 0.235
	0.036 ± j 6.592, - 0.0055	1.049	w_2, δ_2	0.200	- 0.820 ± j 3.840, 0.208
	0.013 ± j 7.060, - 0.0019	1.123	w_8, δ_8	0.101	- 1.045 ± j 6.920, 0.149

The table shows that the GAPSSs shift the eigenvalues to the left half of the *s*-plane with improved damping factor and damping ratio as compared to without PSS for all unseen operating cases. This ensures that the NEEPS will be stable for all considered unseen cases also. It is also observed that designed GAPSS controllers satisfy the earlier selected criterion for the value of desired damping factor and damping ratio for all unseen cases except Case-15 where slightly more settling time may occur. Hence, the GA provides robustness with enhanced stability and improved damping performance for unseen operating cases 7-15 of NEEPS as compared to that of without PSS.

In order to examine the robustness performance of the designed GAPSSs in terms of speed deviations, the simulations are performed using PSAT [215] for four earlier observed scenarios on unseen cases 7-15 of NEEPS. The speed deviations $\Delta w_1, \Delta w_2, \Delta w_3, \Delta w_4, \Delta w_5, \Delta w_6, \Delta w_7, \Delta w_8, \Delta w_9, \Delta w_{10}, \Delta w_{11}, \Delta w_{12}, \Delta w_{13}, \Delta w_{14}, \Delta w_{15}$ and Δw_{16} without PSS and with GAPSSs for severe test Scenario-1 of cases 7-11 are shown in Fig. 3.30 (a)-(e) and (f)-(j) respectively whereas for Scenario-2 of cases 12-15 are shown in Fig. 3.31 (a)-(d) and (e)-(h) respectively.

From Figs. 3.30 (a)-(e) and 3.31 (a)-(d), it is observed that in all these response plots, the system without PSS is not capable to die out LFO because these oscillations are growing up and generator G_9 quickly go to out of synchronism than others.

From Figs. 3.30 (f)-(j) and 3.31 (e)-(h), it is observed that with GAPSSs all oscillations of speed deviations are well damped out for Sceanrio-1 of cases 7-11 and Scenario-2 of cases 12-15. Moreover, the peak overshoot of speed responses in Scenario-1 and Scenario-2 are almost same in all considered operating cases. Furthermore, oscillations in response of cases 13-15 in Scenario-2 take more time to reach in steady state as compared to others.

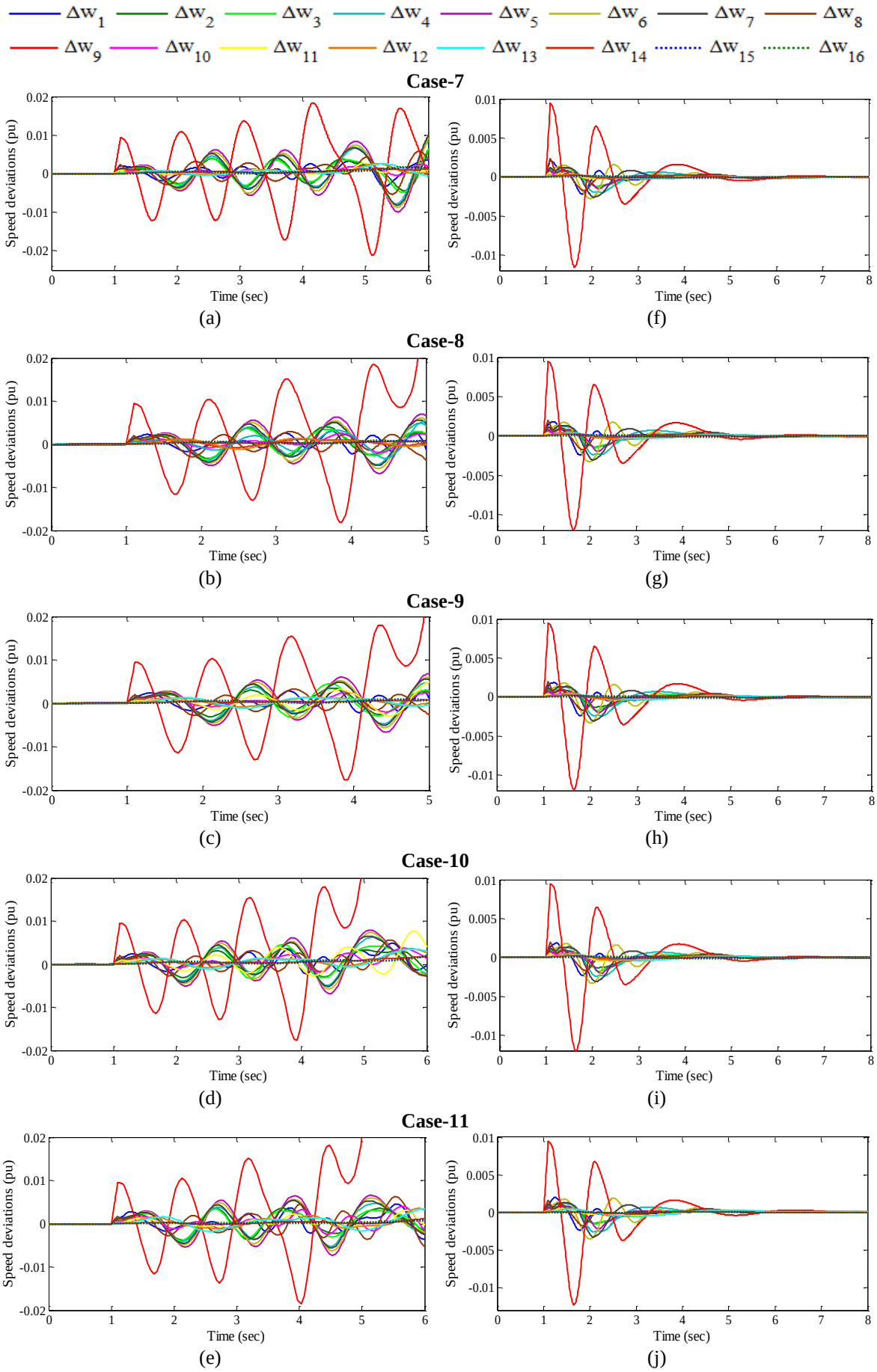

Fig. 3.30 Speed deviations (a)-(e) without PSS and (f)-(j) with GAPSSs for scenario-1 of unseen operating cases 7-11

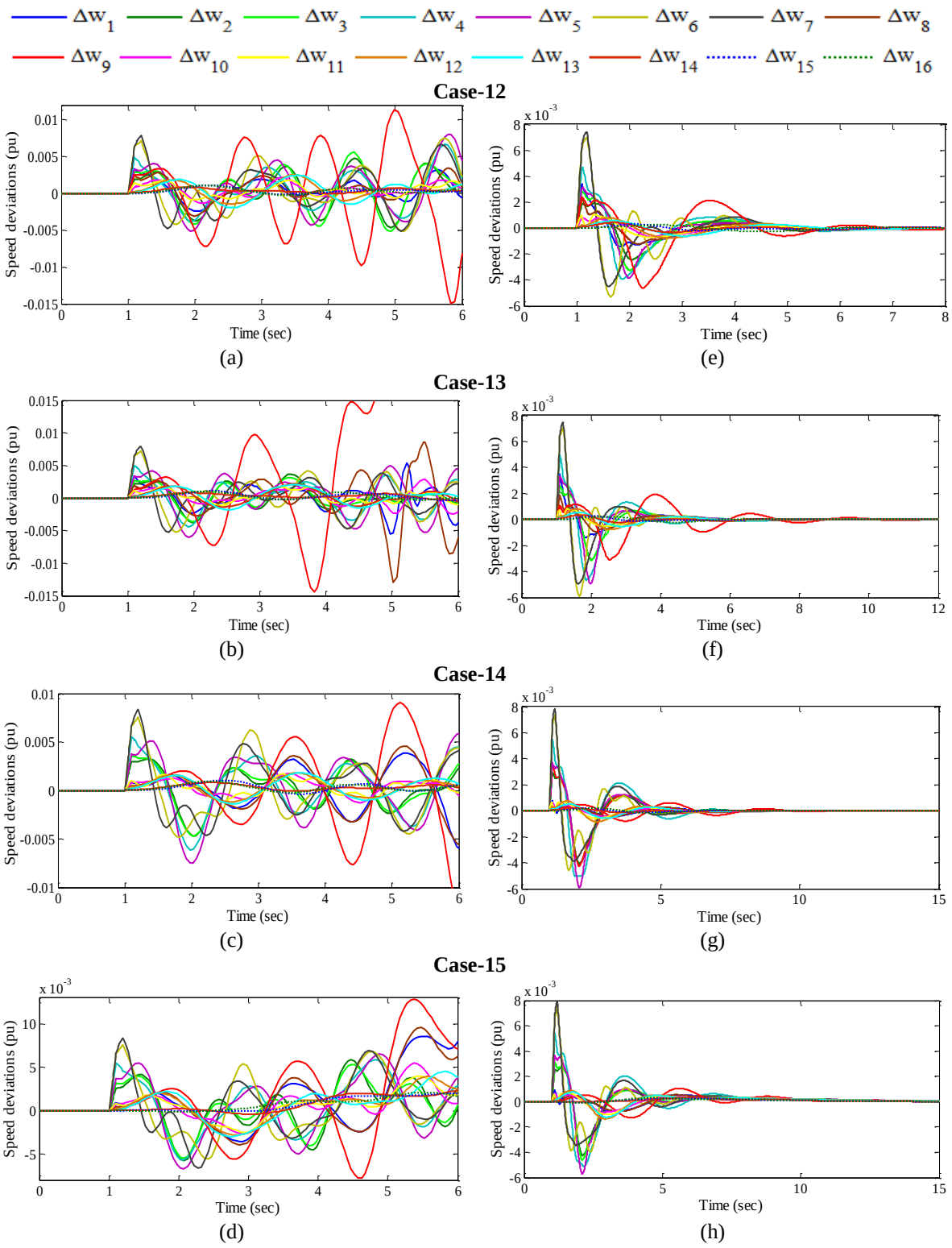

Fig. 3.31 Speed deviations (a)-(d) without PSS and (e)-(h) with GAPSSs for scenario-2 of unseen operating cases 12-15

It is clear that the system performance with GAPSSs is improved to that of without PSS for considered scenarios of unseen operating cases. This may be concluded that the designed GAPSSs work satisfactorily for observed scenarios of severe disturbances of unseen operating cases of NEEPS.

In addition to time-domain simulation results, the effectiveness of designed GAPSS controllers is observed by evaluating *IAE* and *ITAE* for observed four scenarios of unseen cases 7-15. The bar charts of both indices with GAPSSs for Scenario-1 of cases 7-11, Scenario-2 of cases 7-15, Scenario-3 of cases 7-12 and Scenario-4 of cases 7-10 & 12-14 are shown in Fig. 3.32 (a)-(d) and (e)-(h) respectively.

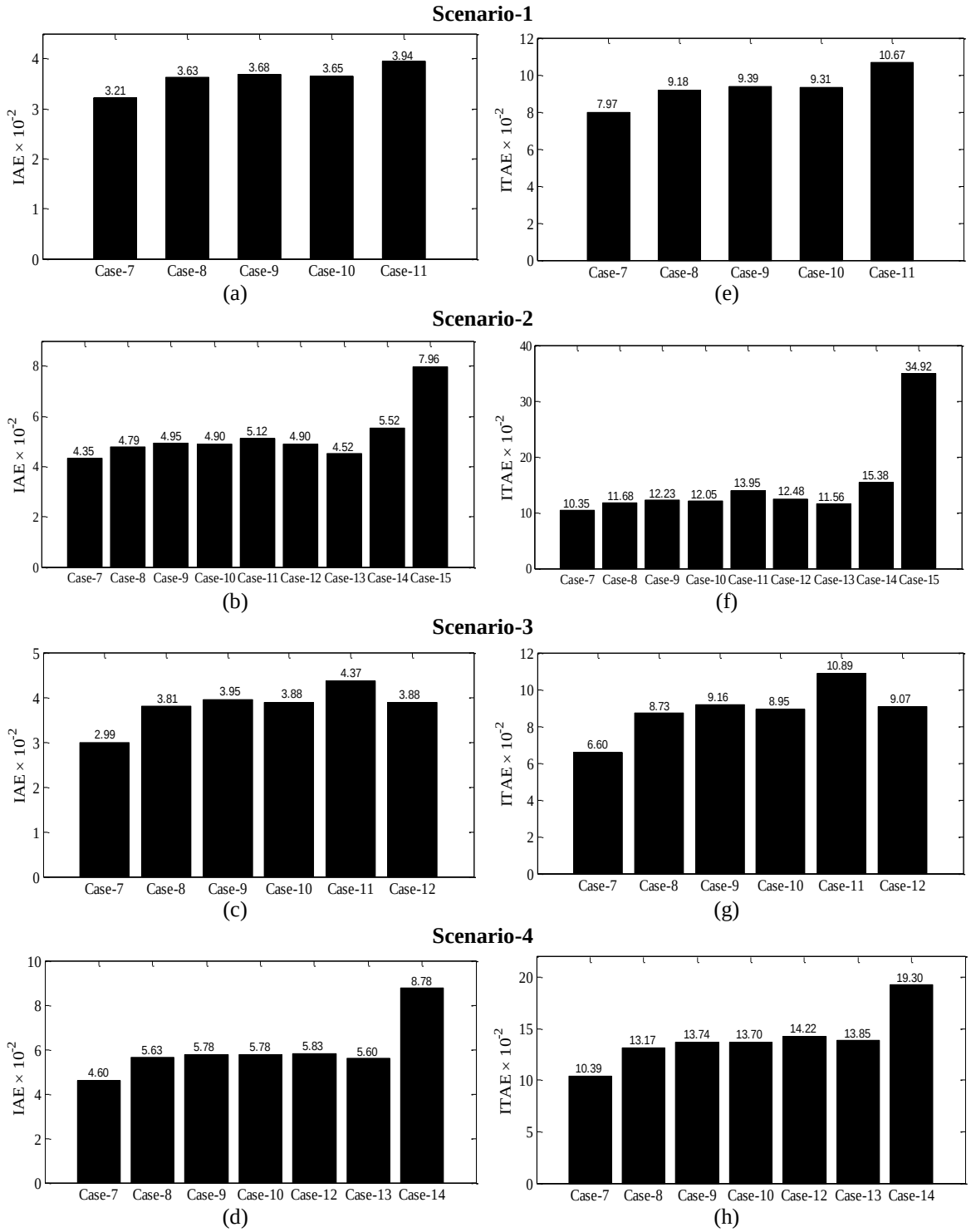

Fig. 3.32 Values of (a)-(d) *IAE* and (e)-(h) *ITAE* with GAPSSs for scenarios 1-4 of unseen operating cases 7-15

From the figure, it is noticed that the values of both indices for Case-11 of Scenario-1, Case-15 of Scenario-2, Case-11 of Scanerio-3 and Case-14 of Scenario-4 are higher than others. Moreover, it is concluded that the unseen Case-15 of Scenario-2 and Case-7 of Scenario-3 are most and least severe than others.

Hence, the designed GAPSS controllers for NEEPS is capable to damp out low frequency local and inter-area modes of oscillations with enhanced stability and damping performance for wide range of operating cases under different scenarios of severe disturbances and also for unseen operating cases under severe scenarios of disturbances.

3.5 Summery

In this chapter, a meta-heuristic technique GA is explored for effectively designing of PSS under wide range of operating conditions of WSCC power system, TFAM power system, NEPS and NEEPS for SSS enhancement. The GA is capable of shifting all unstable and/or poorly damped eigenvalues of MMPS to a specified D-shape zone in the left half of the *s*-plane. Moreover, the effectiveness of designed GAPSS controllers has been evaluated by eigenvalue analysis, eigenvalue maps, time-domain simulation results and performance indices namely*IAE* and *ITAE*. Furthermore, the robustness of designed GAPSSs is observed by testing them on under wide range of unseen operating cases of MMPS. It is found that the design GAPSSs have shifted unstable and/or poorly damped eigenvalues of all unseen cases of MMPS to the left half of the *s*-plane for mitigating low frequency local and inter-area modes of oscillations.

CHAPTER-4

MULTI-MACHINE POWER SYSTEM STABILIZERS DESIGN USING PARTICLE SWARM OPTIMIZATION

The Particle Swarm Optimization (PSO) is another popular meta-heuristic technique which is capable to solve complex combinatorial optimization problems. It has been successfully implemented to solve various optimization problems of power system [216]-[219] and also applied to designing of PSS parameters of SMIB and MMPS under wide range of operating conditions [153]-[155].

The main objective of this chapter is to explore the brief insight in the meta-heuristic technique: PSO and reinvestigate it for robust designing of PSS parameters of WSCC power system, TAFM power system, NEPS and NEEPS. An eigenvalue-based multi-objective function is used for simultaneous control of damping factor and damping ratio. The parameters of PSS are so designed that unstable and/or poorly damped open-loop eigenvalues are shifted to a specified D-shape zone in the left-half of the *s*-plane. The PSS designed using PSO is named PSOPSS. The effectiveness of PSOPSS controllers are evaluated by eigenvalue analysis, eigenvalue maps, time-domain simulation results and performance indices for wide range of operating conditions and tested under different scenarios of severe disturbances and their comparative analysis with PSOPSSs and without PSS is performed. The robustness of PSOPSSs is also checked by testing them on unseen operating conditions and compared.

4.1 Particle Swarm Optimization

The PSO is a population based meta-heuristic technique, developed by Eberhart and Kennedy in 1995 [220] and inspired by social behaviour of bird flocking or fish schooling. Different variants of the PSO algorithm were proposed but the most standard one is introduced by Shi and Eberhart in [221]. In PSO, initial population is created with random solutions within the search space. These solutions represent particle which search for the optimal solution by updating their position based on cognitive and social behavior of the swarm.

Each particle in populations has a position (X_i^k) in the search space and a fitness. In each iteration based on the fitness of particles, the best position of each particle ($pbest_i^k$) and the best position among all particles ($gbest_i^k$) are stored. Each particle's new speed (V_i^{k+1}) and new position is updated based on its own best exploration; best swarm overall experience, and its previous velocity vector according to the following model:

$$V_i^{k+1} = w \times V_i^k + c_1 \times r_1 \times (pbest_i^k - X_i^k) + c_2 \times r_2 \times (gbest_i^k - X_i^k) \tag{4.1}$$

$$X_i^{k+1} = X_i^k + V_i^{k+1} \times \Delta t \tag{4.2}$$

where c_1 and c_2 are positive numbers representing the weight of the acceleration of each term which guiding each particle reaches the best individual (*pbest*) and the best swarm (*gbest*) positions, r_1 and r_2 are two random number in the range [0-1], Δt is the time step, usually set to1sec and w is the inertia calculated by the following equation [221]:

$$w = w_{\max} - \left(\frac{w_{\max} - w_{\min}}{k_{\max}} \right) \times k \tag{4.3}$$

where w_{min} and w_{max} are the minimum and maximum values of w, k_{max} is the maximum number of iterations and k is the current iteration number.

In equation (4.1), first term represents the inertia of the particle whereas second term represents the personal influence and the last term represents the social influence of the particle. Equation (4.2) finds the new position of the particle according to the new velocity evaluated by (4.1). A large inertia weight facilitates a global search while a small inertia weight facilitates a local search. By linearly decreasing the inertia weight from a relatively large value to a small value through the course of the PSO run, the PSO tends to have more global search ability at the beginning of the run while having more local search ability near the end of the run. The flow chart of PSO algorithm is shown in Fig. 4.1:

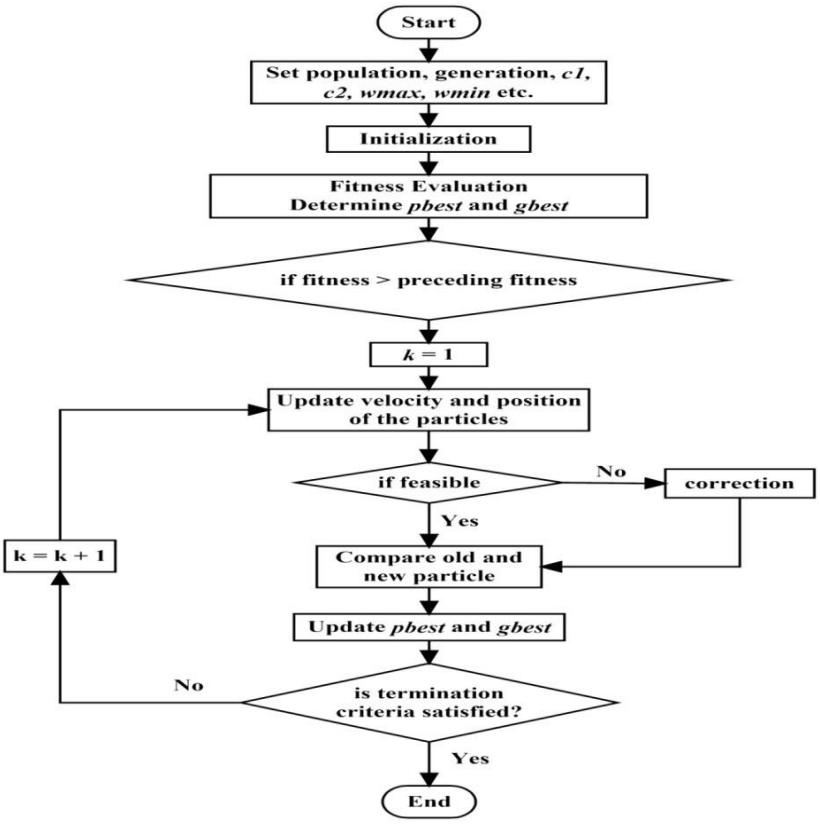

Fig. 4.1 Flow chart of particle swarm optimization algorithm

4.2 Simulation and Results

The PSO is applied on four standard test systems e.g., WSCC power system, TAFM power system, NEPS and NEEPS, to obtain the optimal parameters of PSS for wide range of operating conditions. An eigenvalue-based multi-objective function is used for simultaneous control of damping factor and damping ratio to mitigate low frequency electromechanical oscillations of MMPS. The parameters of PSS are so designed that unstable and/or poorly damped open-loop eigenvalues are shifted to a specified D-shape zone in the left-half of the *s*-plane for wide range of operating conditions under different scenarios of severe disturbances. This is obtained by minimizing the objective function (3.1) using PSO. The effectiveness of all designed PSOPSS controllers are evaluated by eigenvalue analysis, eigenvalue maps, time-domain simulation results and performance indices *IAE* and *ITAE*and the system performance with PSOPSSs is compared with that of without PSS. The robustness of all designed controllers is also checked by testing them on unseen operating conditions under different scenarios of severe disturbances and compared with that of without PSS.

4.2.1 Example 1: Three-Machine, Nine-Bus WSCC Power System

The operating condition details and single-line diagram of WSCC power system is described in Section 3.4.1 and Appendix respectively.

A. Eigenvalue Analysis of WSCC Power System without PSS and with PSOPSSs

The open-loop eigenvalues, damping ratio, frequency, participation modes and participation factor associated with electromechanical modes of the system are illustrated in Table 3.2 and discussed in Section 3.4.1 (A). An eigenvalue-based multi-objective function *J* presented in (3.1) is minimized using PSO by tuning the six parameters of PSSs. The PSO is applied with population size 100, maximum generation 100 and $c_1 = c_2 = 2$, $w_{min} = 0.4$, $w_{max} = 0.9$.

The PSO is able to find the desired solution for which fitness function *J* is zero. The final value of *J* equal to zero indicates that two unstable and/or poorly damped eigenvalues using PSO are shifted to a specified D-shape zone in the left-half of the *s*-plane. The optimal six parameters obtained by PSOPSSs for two generators are shown in Table 4.1. The closed-loop eigenvalues and their damping ratio with PSOPSSs for three operating cases are evaluated using PSAT [215] and are shown in Table 4.2.

Table 4.1: Optimal designed parameters of PSOPSSs for WSCC power system

Generators	***K***	T_1	T_3
G_2	1	1	0.156
G_3	1	0.400	0.06

Table 4.2: Eigenvalues and damping ratio with PSOPSSs for operating cases 1-3 of WSCC power system

Case-1	Case-2	Case-3
– 1.212 ± j 7.549, 0.158	– 1.614 ± j 7.563, 0.208	– 0.768 ± j 7.381, 0.103
– 2.007 ± j 14.393, 0.138	– 2.669 ± j 14.041, 0.351	– 1.570 ± j 14.157, 0.110

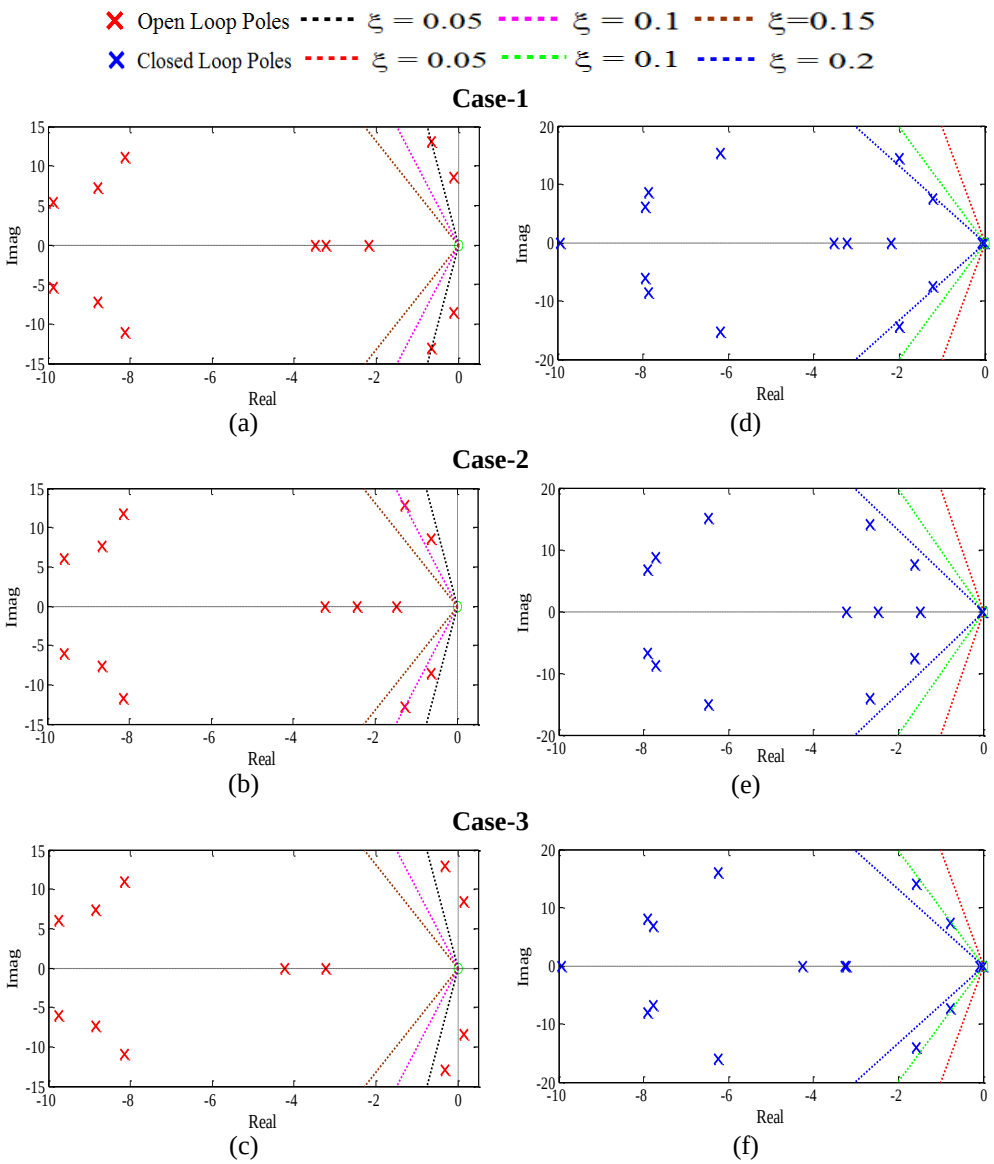

Fig. 4.2 Eigenvalue maps (a)-(c) without PSS and (d)-(f) with PSOPSSs for operating cases 1-3 of WSCC power system

Fig. 4.2 (a)-(c) and (d)-(f) show the eigenvalue maps for without PSS and with PSOPSSs for operating cases 1-3 respectively. The analysis of eigenvalue maps without PSS for unstable and poorly damped modes of cases 1-3 of WSCC power system is discussed in Section 3.4.1 (A). Table 4.2 and Fig. 4.2 (d)-(f) show that the PSOPSSs shift the eigenvalues to a specified D-shape zone in the left half of the *s*-plane with desired damping factor and damping ratio as compared to that of without PSS for all operating cases. Hence, designed PSOPSS controllers provide improved stability and damping characteristics of the WSCC power system as compared to same obtained using without PSS.

B. Time-Domain Simulation Results and Discussions with PSOPSSs and without PSS of WSCC Power System

The time-domain simulations of WSCC power system is performed with PSOPSS controllers, designed in previous section for observed severe scenarios of operating Case-3 mentioned earlier in Table 3.6. The speed deviations Δw_{12}, Δw_{23} and Δw_{31} for selected severe scenarios of Case-3 for the system without PSS and with PSOPSSs are shown in Fig. 4.3 (a)-(b) and (c)-(d) respectively. The time-domain performance analysis of the system without PSS is already discussed in Section 3.4.1 (B).

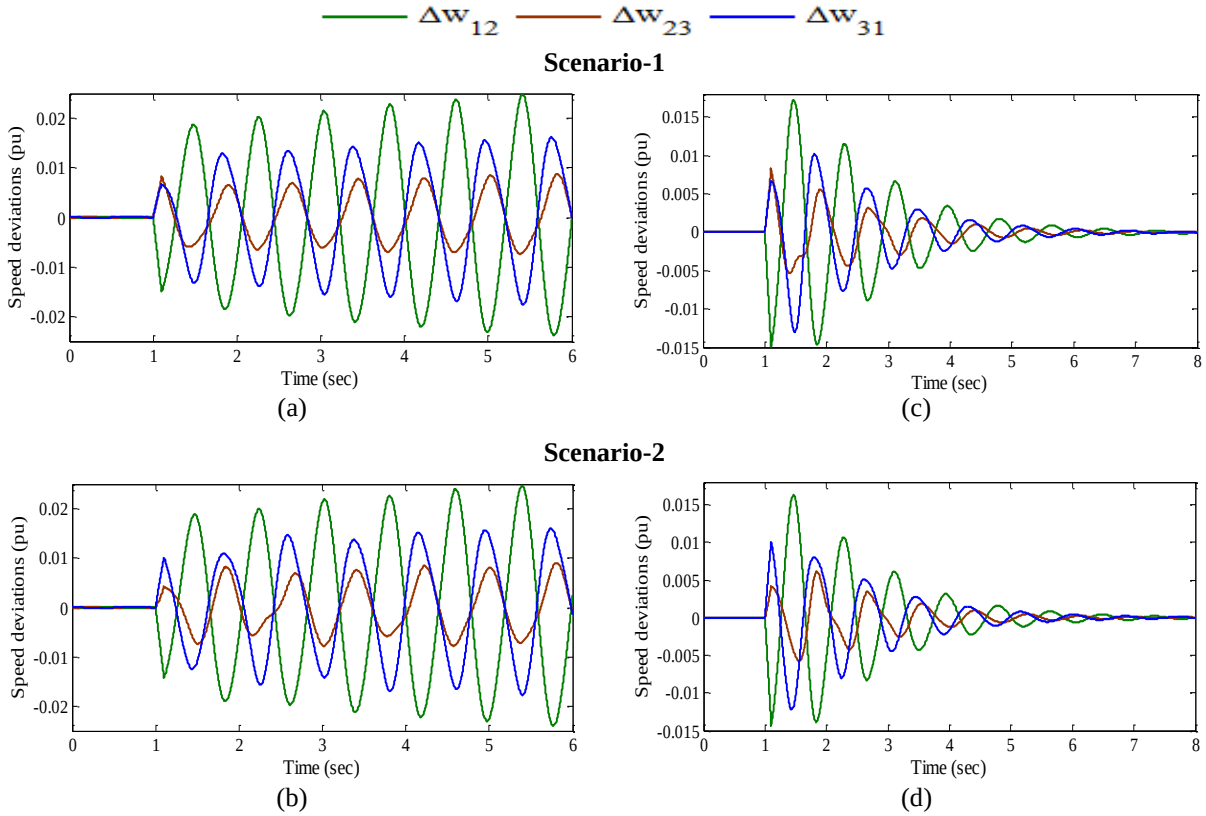

Fig. 4.3 Speed deviations (a)-(b) without PSS and (c)-(d) with PSOPSSs for scenarios 1-2 of operating case-3

It may be clearly observed from Fig. 4.3 (c)-(d) that with PSOPSSs system performance is improved and all oscillations for both scenarios are well damped out. Moreover, the Δw_{12} is most severe due to large peak overshoot and consumed more time to reach in steady state. This illustrates the potential of PSO to obtain a desired set of PSS parameters and the designed PSOPSSs are capable to damp out the LFO for wide range of operating conditions under variety of severe disturbances.

C. Performance Indices Results and Discussions with PSOPSSs of WSCC Power System

In addition to simulation results, the effectiveness of designed PSOPSS controllers is also observed by determining two indices *IAE* and *ITAE* for two observed severe scenarios of disturbances. Established both indices are calculated for each scenario of disturbances for operating cases 1-3 and presented as bar charts in the Fig. 4.4 (a)-(b) and (c)-(d) respectively.

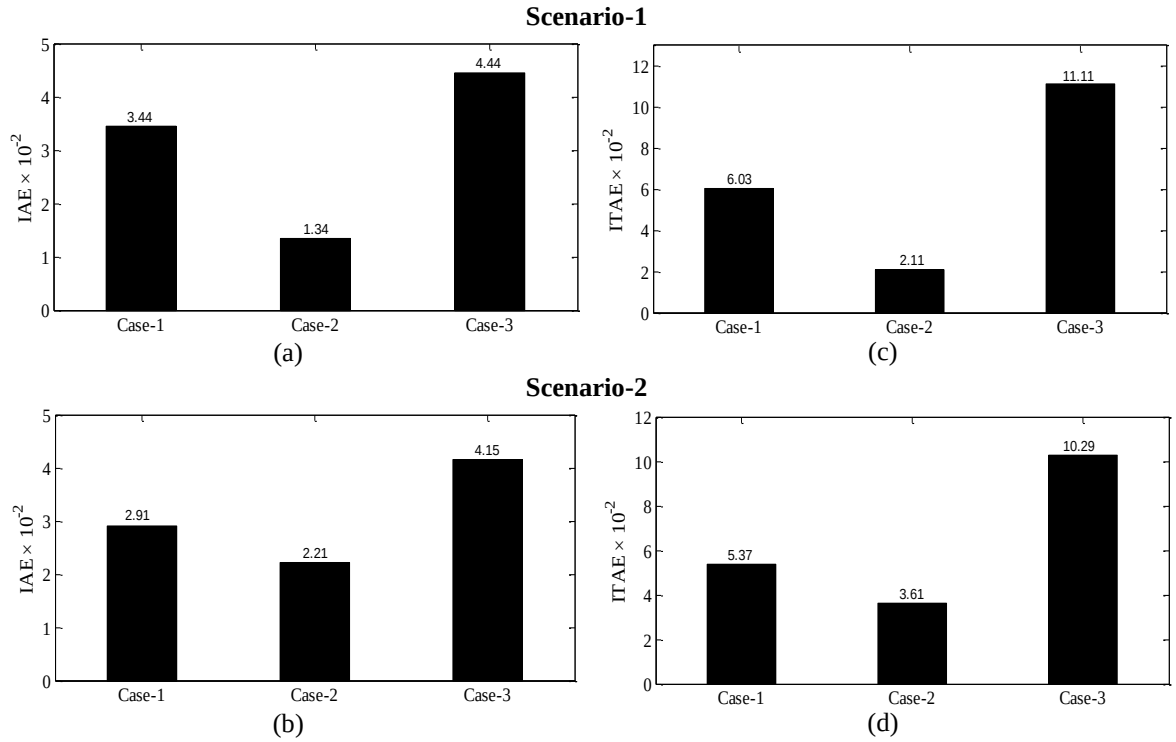

Fig. 4.4 Values of (a)-(b) *IAE* and (c)-(d) *ITAE* with PSOPSSs for scenarios 1-2 of operating cases 1-3

The figure depicts that the values of both indices for the PSOPSSs are minimum for each scenario of Case-2 and maximum for each scenario of Case-3, which indicates that Case-3 is the most severe whereas Case-2 is the least severe. Moreover, for operating cases 1 & 3, Scenario-1 is more severe but for Case-2, Scenario-2 is more severe. Comparing Fig. 4.4 with Fig. 3.4, it may be noticed that the designed PSOPSS controllers provide improved damping to damp out low frequency local modes of oscillations with less overshoot and settling time than that of without PSS.

D. Robustness Test of Designed PSOPSS Controllers of WSCC Power System

To test the robustness of earlier designed PSOPSS controllers for WSCC power system, three unseen operating cases 4-6 mentioned in Table 3.7 are considered. In this section, the effectiveness of PSOPSS controllers for these unseen cases is evaluated by eigenvalue analysis, time-domain simulation results, performance indices and compared with that of without PSS.

Open-loop eigenvalues, damping ratio, frequency, participation modes and participation factor for unseen cases 4-6 of WSCC power system without PSS are illustrated in Table 3.8 and discussed in Section 3.4.1 (D). Now, the designed PSOPSSs parameters are used to obtain

closed-loop eigenvalues and damping ratio using PSAT [215]. Table 4.3 shows the closed-loop eigenvalues and damping ratio for unseen cases 4-6 of WSCC power system with PSOPSS controllers for only unstable and poorly damped modes.

Table 4.3: Closed-loop eigenvalues and damping ratio with PSOPSSs for unseen operating cases 4-6 of WSCC power system

Case-4	**Case-5**	**Case-6**
– 0.664 ± j 7.530, **0.087**	– 0.557 ± j 7.442, **0.074**	– 0.465 ± j 7.442, **0.062**
– 1.565 ± j 13.977, 0.111	– 1.587 ± j 14.234, 0.110	– 1.495 ± j 14.387, 0.103

The table reveals that the PSOPSSs shift the eigenvalues in the left half of the *s*-plane with improved damping factor and damping ratio as compared to without PSS for unseen cases. This ensures that the system will be stable for all considered unseen cases also. It is also observed that designed PSOPSS controllers satisfy the earlier selected criterion for the value of desired damping factor and damping ratio for PSS design except one mode of unseen case 4-6 where slightly more overshoot may occur. Hence, the designed PSOPSSs are robust as it works with acceptable damping performance for unseen operating cases 4-6 of the WSCC power system also.

In order to further examine the robustness performance of the PSOPSSs in terms of speed deviations, the time-domain simulations are performed using PSAT [215] for two earlier observed severe scenarios of disturbances on unseen operating cases 4-6 of WSCC power system. The speed deviations Δw_{12}, Δw_{23} and Δw_{31} without PSS for scenarios 1 and 2 of cases 4-6 are shown in Fig. 4.5 (a)-(c) and Fig. 4.6 (a)-(c) respectively whereas the Δw_{12}, Δw_{23} and Δw_{31} with PSOPSSs are shown in Fig. 4.5 (d)-(f) and Fig. 4.6 (d)-(f) respectively.

The analysis of response plots without PSS is already discussed in Section 3.4.2 (D). From Fig. 4.5 (d)-(f) and 4.6 (d)-(f), it may be clearly observed that with PSOPSSs, the speed deviation responses for scenarios 1-2 of Case-6 produce more oscillations as compared to other cases. Moreover, peak overshoot in speed deviation responses for scenarios 1-2 of Case-6 is more as compared to other cases. Furthermore, the speed deviations with PSOPSSs for scenarios 1-2 of unseen operating cases 4-6 take more time to damp out LFO as compared to earlier cases 1-3. This may be concluded that the designed PSOPSSs work acceptably for all the scenarios of severe disturbances of unseen operating cases of WSCC power system.

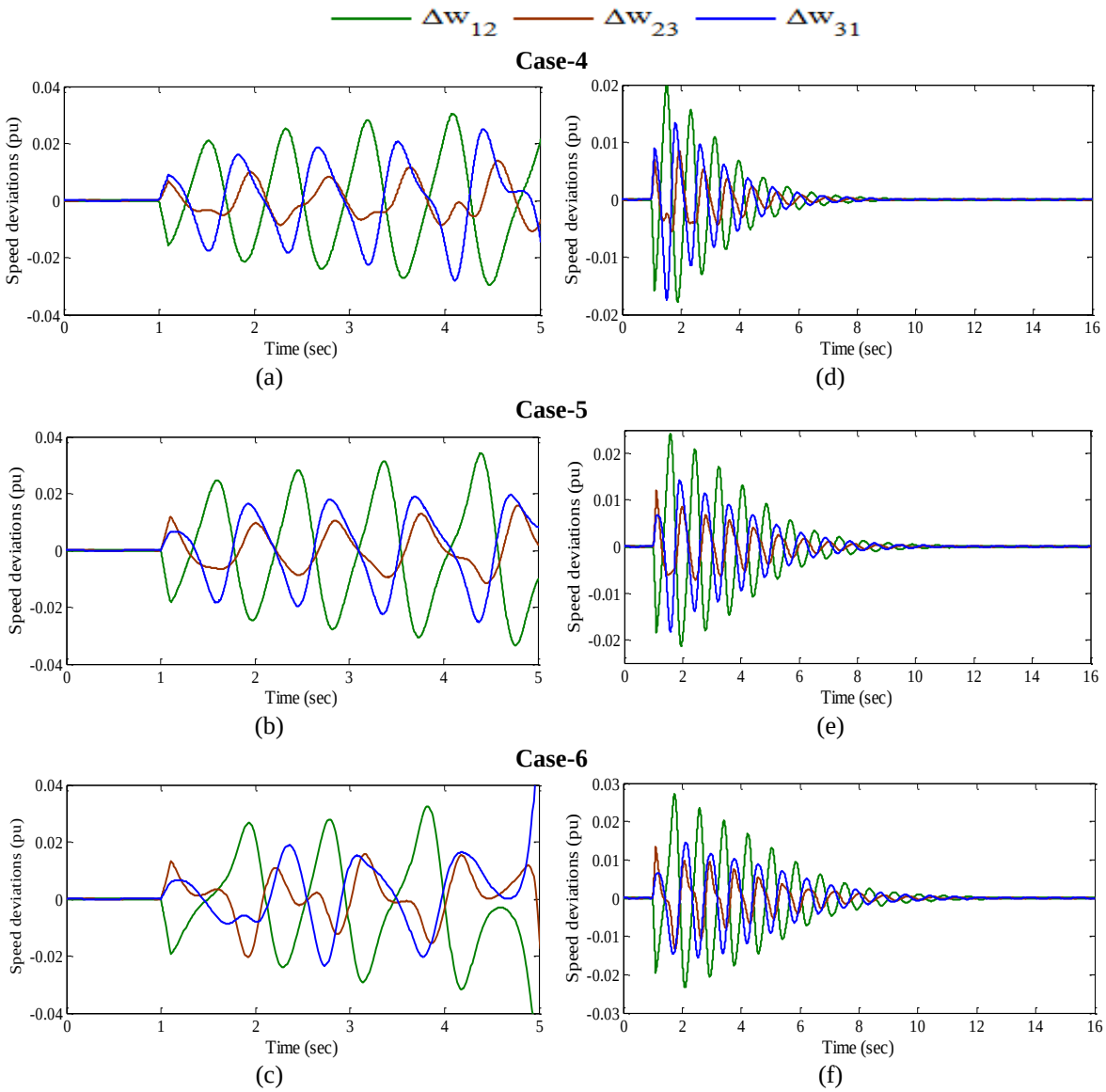

Fig. 4.5 Speed deviations (a)-(c) without PSS and (d)-(f) with PSOPSSs for scenario-1 of unseen operating cases 4-6

In addition to time-domain simulation results, the effectiveness and robustness of PSOPSS controllers is also noticed by evaluating indices *IAE* and *ITAE* for observed scenarios of unseen operating cases. Established both indices with PSOPSSs are determined for each scenario of disturbances for operating cases 4-6 and presented as bar charts in the Fig. 4.7 (a)-(b) and (c)-(d) respectively.

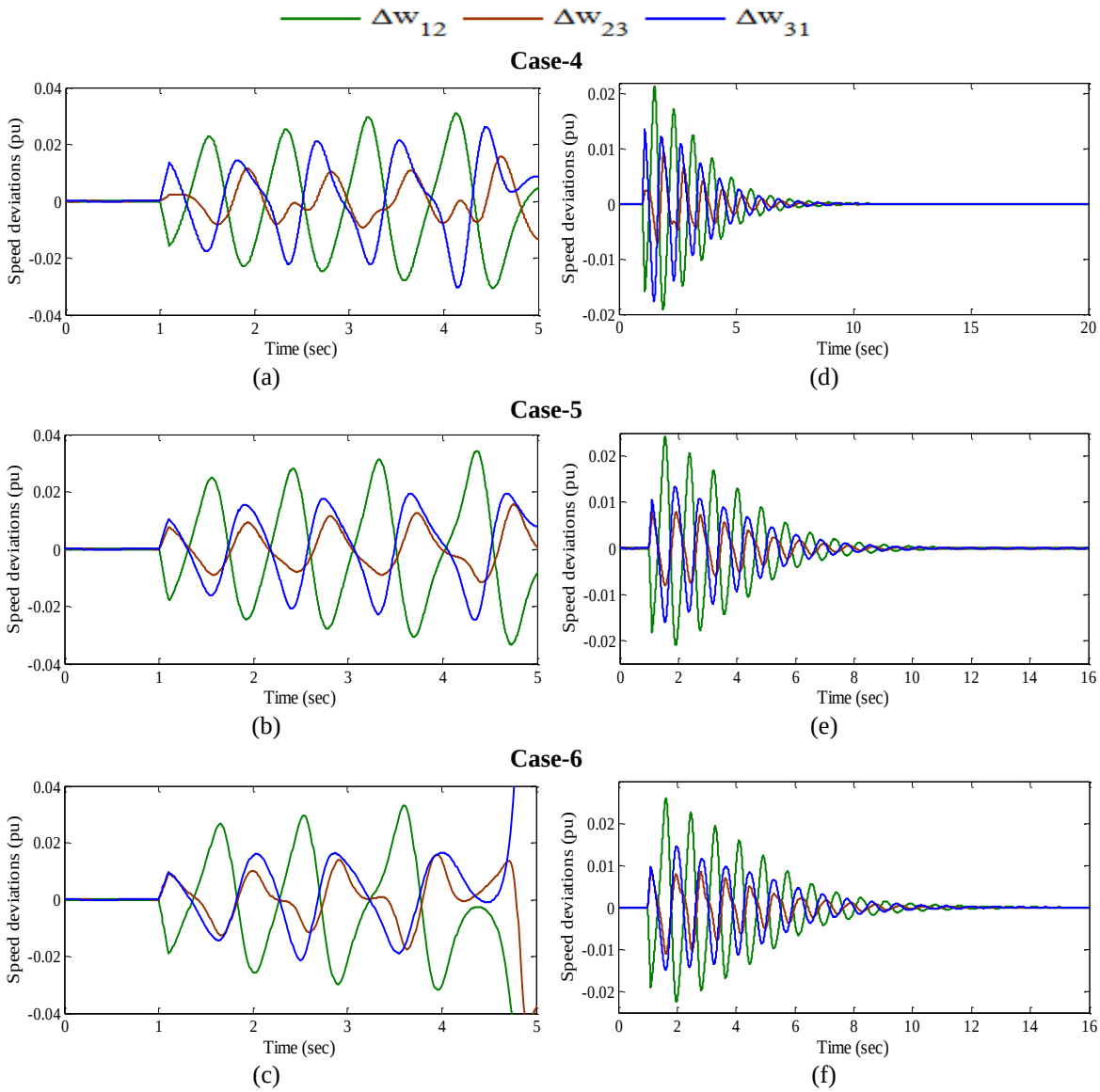

Fig. 4.6 Speed deviations (a)-(c) without PSS and (d)-(f) with PSOPSSs for scenario-2 of unseen operating cases 4-6

The figure reveals that the values of both indices for the PSOPSSs are minimum for each scenario of Case-4 and maximum for each scenario of Case-6, which indicates that Case-6 is the most severe whereas Case-4 is the least severe. Moreover, for operating Case-4, Scenario-2 is more severe but for cases 5-6, Scenario-1 is more severe.

Hence, the designed PSOPSS controllers for WSCC power system is capable to damp out LFO with enhanced stability and damping performance for wide range of operating cases under different scenarios of severe disturbances and also for unseen operating cases under same scenarios of disturbances.

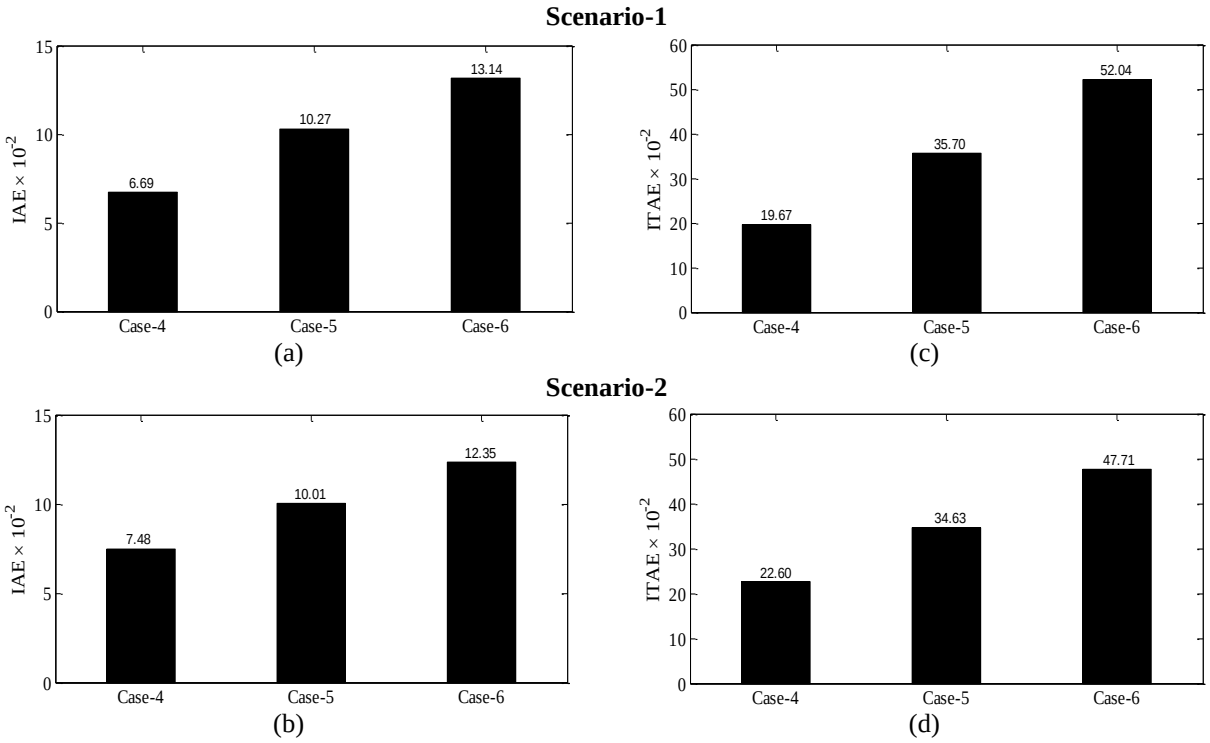

Fig. 4.7: Values of (a)-(b) *IAE* and (c)-(d) *ITAE* with PSOPSSs for scenarios1-2 of unseen operating cases 4-6

4.2.2 Example 2: Two-Area, Four-Machine (TAFM) Power System

The operating condition details and single-line diagram of TAFM power system is described in Section 3.4.2 and Appendix respectively.

A. Eigenvalue Analysis of TAFM Power System without PSS and with PSOPSSs

The open-loop eigenvalues, damping ratio, frequency, participation modes and participation factor associated with electromechanical modes of the system are depicted in Table 3.10 and discussed in Section 3.4.2 (A). An eigenvalue-based multi-objective function *J* presented in (3.1) is minimized using PSO by tuning the nine parameters of PSSs. The PSO is applied with population size 50, maximum generation 50, $c_1 = c_2 = 2$, $w_{min} = 0.4$, $w_{max} = 0.9$.

The PSO is able to find the desired solution for which fitness function *J* is zero. The final value of *J* equal to zero indicates that three unstable and/or poorly damped eigenvalues are shifted to a specified D-shape zone in the left-half of the *s*-plane. The optimum designed nine parameters of PSOPSSs for three generators are shown in Table 4.4. The closed-loop eigenvalues and their damping ratio using PSOPSSs for three loading cases are determined using PSAT [215] and shown in Table 4.5.

Table 4.4: Optimal designed parameters of PSOPSSs for TAFM power system

Generators	***K***	T_1	T_3
G_1	39.000	0.010	0.010
G_2	19.840	0.010	0.454
G_4	29.717	0.103	0.010

Fig. 4.8 (a)-(c) and (d)-(f) show the eigenvalue maps for without PSS and with PSOPSSs for cases 1-3 respectively.

Table 4.5: Eigenvalues and damping ratio with PSOPSSs for loading cases 1-3 of TAFM power system

Case-1	Case-2	Case-3
– 1.188 ± j 4.045, 0.28	– 1.000 ± j 3.362, 0.28	– 1.174 ± j 5.643, 0.20
– 3.707 ± j 4.290, 0.65	– 2.276 ± j 0.673, 0.95	– 1.637 ± j 3.019, 0.47
– 2.378 ± j 0.945, 0.92	– 3.841 ± j 3.968, 0.69	–2.732 ± j 0.721, 0.96

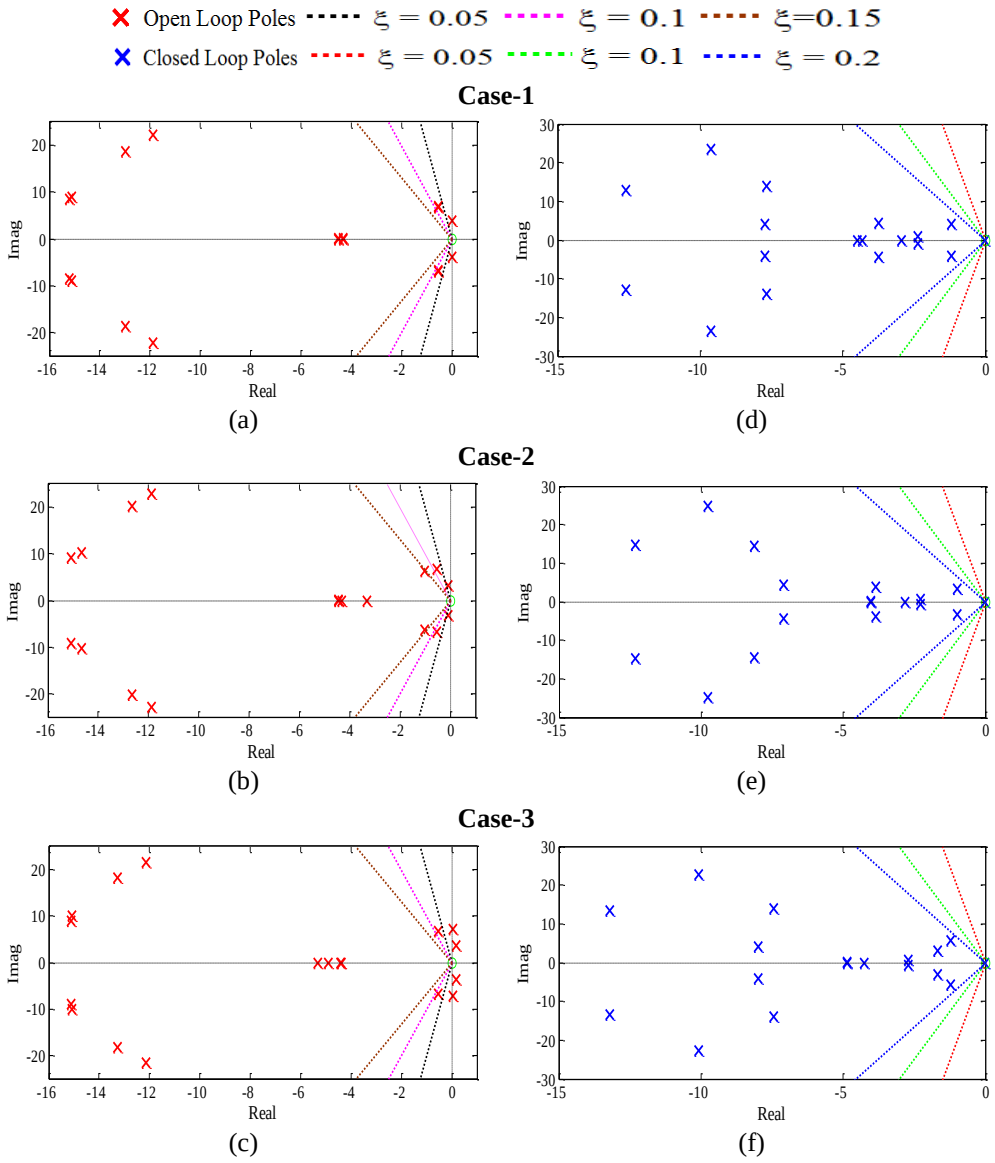

Fig. 4.8 Eigenvalue maps (a)-(c) without PSS and (d)-(f) with PSOPSSs for loading cases 1-3 of TAFM power system

The eigenvalue maps of without PSS for unstable and lightly damped modes with TAFM system are discussed in Section 3.4.2 (A). Table 4.5 and Fig. 4.8 (d)-(f) show that the PSOPSSs shift the eigenvalues to a specified D-shape zone in the left half of the *s*-plane with desired damping factor and damping ratio as compared to that of without PSS for three loading cases.

Hence, designed PSOPSS controllers provide improved stability and damping performance of the TAFM power system as compared to same obtained using without PSS.

B. Time-Domain Simulation Results and Discussions with PSOPSSs and without PSS of TAFM Power System

The time-domain simulations of TAFM power system is performed with designed PSOPSSs for different test scenarios mentioned earlier in Table 3.14 of severe operating cases. The speed deviations $\Delta w_1, \Delta w_2, \Delta w_3$ and Δw_4 for the system without PSS and with PSOPSSs are shown in Fig. 4.9 (a)-(d) and (e)-(h) respectively.

The analysis of response plots without PSS already discussed in Section 3.4.2 (B). From Fig. 4.9 (e)-(h), it is observed that with PSOPSSs, oscillations for all generators are well damp out with less overshoot and settling time for all scenarios of severe loading cases. Moreover, it is clear that the system performance with PSOPSSs is much improved than that of without PSS for all severe scenarios of disturbance of loading cases and oscillations are die out smoothly. Furthermore, on the basis of number of cycles of operation, it may be observed that the speed response with PSOPSSs for Scaneraio-4 consumed more time to damp out oscillations as compared to Scenario-2 of loading Case-3.

This demonstrates the potential of PSO to obtain a desired set of PSS parameters for TAFM power system and the designed PSOPSSs are able to improve the damping performance of the system than that of without PSS for wide range of loading cases under severe scenarios of disturbances.

C. Performance Indices Results and Discussions with PSOPSSs of TAFM Power System

In addition to simulation results, the effectiveness of PSOPSS controllers is also observed by determining indices *IAE* and *ITAE* values for considered scenarios of different disturbances mentioned in Table 3.14. The bar charts of both indices obtained by PSOPSSs for scenarios 1-4 of loading cases 1-3 are shown in Fig. 4.10 (a)-(d) and (e)-(h) respectively.

The figure reveals that both indices values for the PSOPSSs are higher for Scenario-1 of Case-2 loading and lower for Case-3 loading. Similarly, both indices are lower for scenarios 2-4 of Case-2 and higher for Case-3 loading, which indicates that Case-3 is the most severe for scenarios 2-4 whereas Case-2 is the least severe. Comparing Fig. 4.10 with Fig. 3.11, it may be observed that the designed PSOPSS controllers provide sufficient damping to damp out low frequency local and inter-area modes of oscillations with less overshoot and settling time than that of without PSS, although the disturbances are simulated for more number of cycles on the system with PSOPSSs.

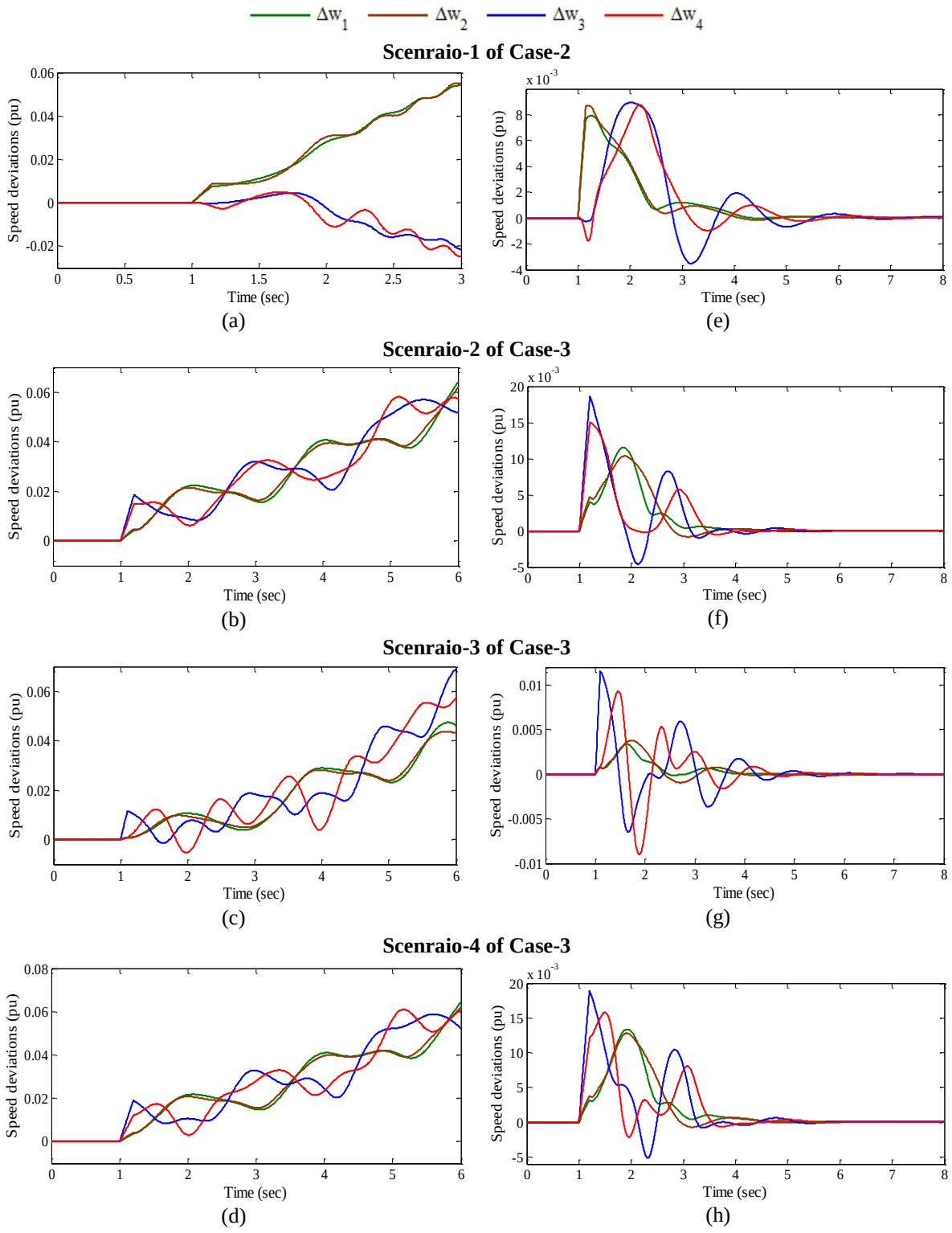

Fig. 4.9 Speed deviations (a)-(d) without PSS and (e)-(h) with PSOPSSs for scenarios 1-4 of severe loading cases

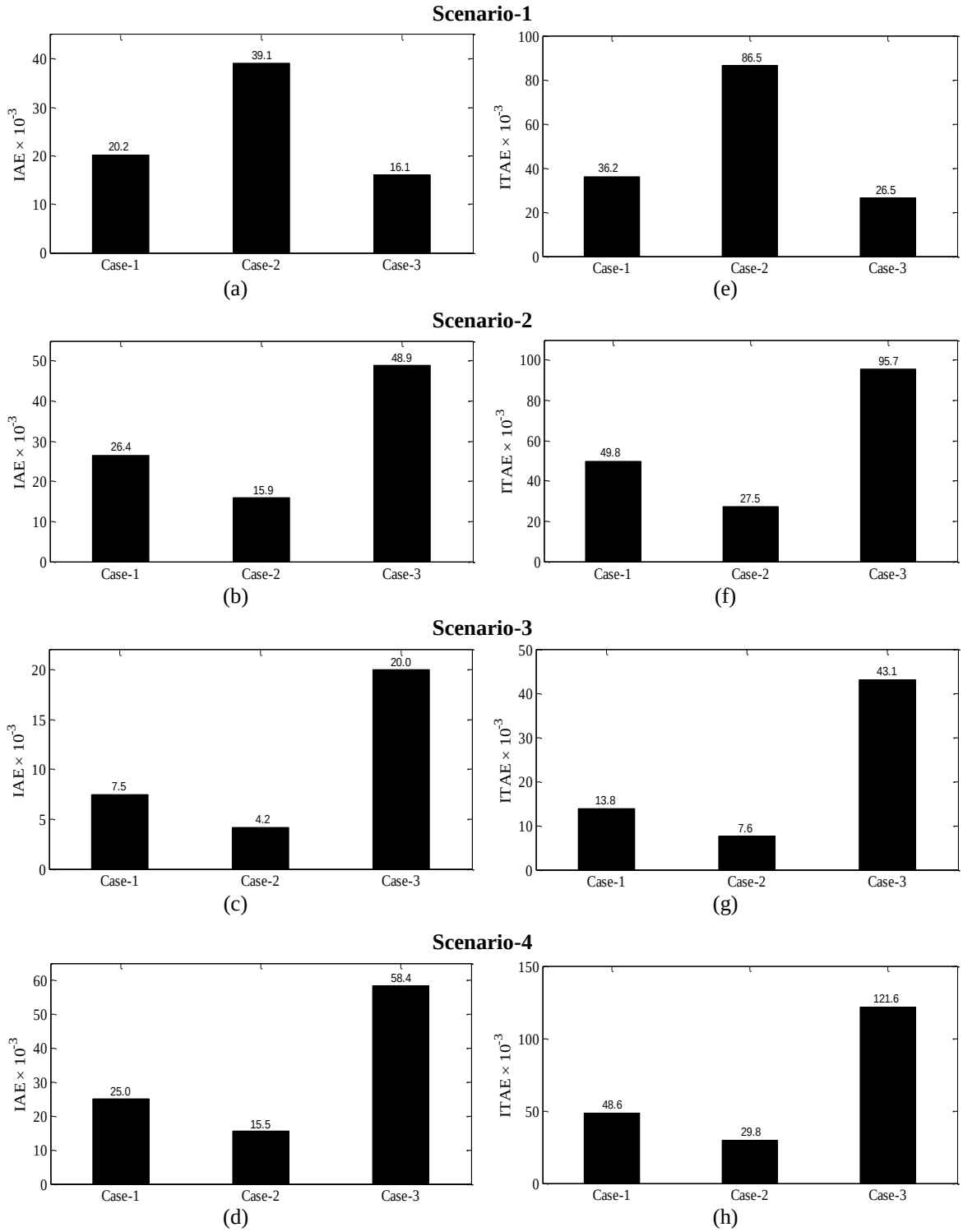

Fig. 4.10 Values of (a)-(d) *IAE* and (e)-(h) *ITAE* with PSOPSSs for scenarios 1-4 of loading cases 1-3

D. Robustness Test of PSOPSS Controllers of TAFM Power System

To test the robustness of previously design PSOPSS controllers for TAFM power system, nine unseen operating cases 4-12 are depicted in Table 3.15. In this section, the effectiveness of designed PSOPSSs is checked by eigenvalue analysis, time-domain simulation results and performance indices for unseen cases and compared with that of without PSS.

Open-loop eigenvalues, damping ratio, frequency, participation modes and participation factor for unseen operating cases 4-12 of TAFM power system without PSS are illustrated in Table 3.16 and explained in Section 3.4.2 (D). Now, previously designed PSOPSSs parameters are used to obtain closed-loop eigenvalues and damping ratio for only unstable and poorly damped modes using PSAT [215] for unseen cases 4-12 of TAFM power system and are shown in Table 4.6.

Table 4.6: Eigenvalues and damping ratio with PSOPSSs for unseen operating cases 4-12 of TAFM power system

Cases	**With PSOPSSs**		
Case-4	– 2.928 ± j 4.650, 0.532	– 1.667 ± j 3.064, 0.477	– 7.335 ± j 4.306, 0.862
Case-5	– 1.438 ± j 2.435, 0.508	– 1.245 ± j 5.825, 0.209	– 7.560 ± j 14.156, 0.471
Case-6	– 2.923± j 4.656, 0.531	– 1.655 ± j 3.076, 0.473	– 7.920 ± j 14.435, 0.481
Case-7	– 1.436 ± j 2.442, 0.506	– 1.242 ± j 5.829, 0.208	– 7.521 ± j 14.150, 0.469
Case-8	– 1.026 ± j 3.305, 0.296	– 3.483 ± j 3.821, 0.673	– 6.918 ± j 4.464, 0.840
Case-9	– 1.315 ± j 2.822, 0.422	**– 0.889** ± j 5.908, **0.148**	– 7.922 ± j 4.131, 0.886
Case-10	– 1.191 ± j 2.227, 0.471	**– 0.856** ± j 6.031, **0.140**	– 7.542 ± j 14.138, 0.470
Case-11	– 1.188 ± j 2.230, 0.470	**– 0.853** ± j 6.033, **0.139**	– 7.504 ± j 14.133, 0.468
Case-12	– 1.173 ± j 3.219, 0.342	– 2.830 ± j 3.827, 0.594	– 6.691 ± j 4.518, 0.828

The table reveals that the PSOPSSs shift the eigenvalues in the left half of the *s*-plane with improved damping factor and damping ratio as compared to without PSS for unseen cases 4-12. This ensures that the TAFM power system will be stable for all considered unseen cases also. It is also observed that PSOPSS controllers satisfy the earlier selected criterion for the value of desired damping factor and damping ratio for PSS design except in unseen cases 9, 10 and 11 where slightly more overshoot and settling time may occur. Hence, the PSO provides robustness with improved stability and grater damping performance for unseen operating cases 4-12 of the TAFM power system as compared to that of without PSS.

In order to check the robustness performance of designed PSOPSS controllers in terms of speed deviations, earlier severe scenarios 5-13 of unseen operating cases 4-12 of TAFM power system mentioned in Table 3.17 are considered. The speed deviations $\Delta w_1, \Delta w_2$, Δw_3 and Δw_4 for the system without PSS and with PSOPSSs for scenarios 5-13 of unseen cases 4-12 are shown in Fig. 4.11 (a)-(i) and (j)-(r) respectively. The analysis of response plots without PSS already discussed in Section 3.4.2 (D). From Fig. 4.11 (j)-(r) it is noticed that the system performance with PSOPSSs is improved for severe disturbance scenarios 5-13 of unseen operating cases 4-12 and oscillations are well damped out. Furthermore, the comparison of speed deviations with PSOPSSs basis on number of cycle operation, the Scenario-13 of Case-12 takes more time to reach in steady state than all other scenarios.

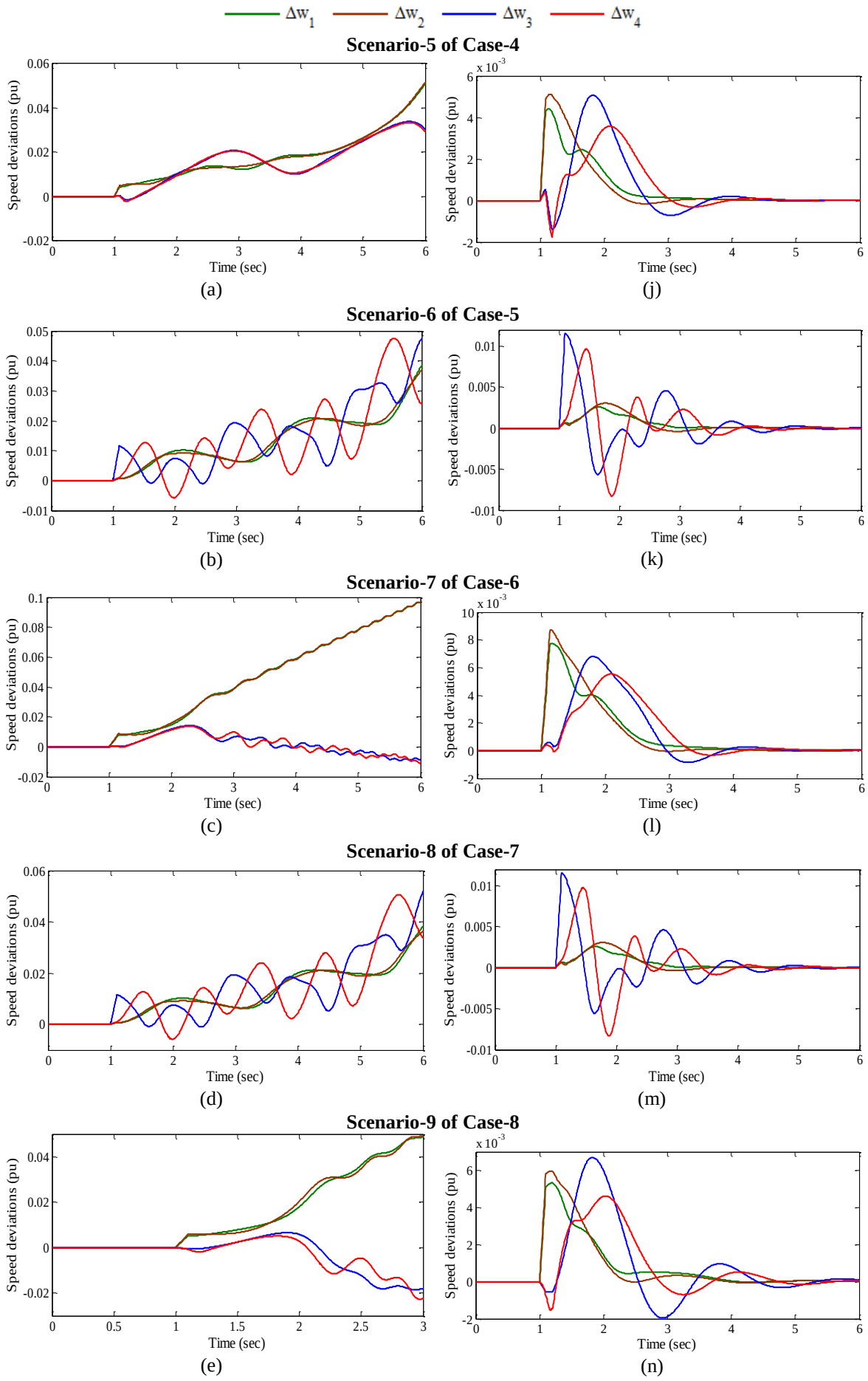
Δw1 Δw2 Δw3 Δw4
Scenario-5 of Case-4
Speed deviations (pu)
Time (sec)
(a)
x 10-3
Speed deviations (pu)
Time (sec)
(j)
Scenario-6 of Case-5
Speed deviations (pu)
Time (sec)
(b)
Speed deviations (pu)
Time (sec)
(k)
Scenario-7 of Case-6
Speed deviations (pu)
Time (sec)
(c)
x 10-3
Speed deviations (pu)
Time (sec)
(l)
Scenario-8 of Case-7
Speed deviations (pu)
Time (sec)
(d)
Speed deviations (pu)
Time (sec)
(m)
Scenario-9 of Case-8
Speed deviations (pu)
Time (sec)
(e)
x 10-3
Speed deviations (pu)
Time (sec)
(n)

Cont.

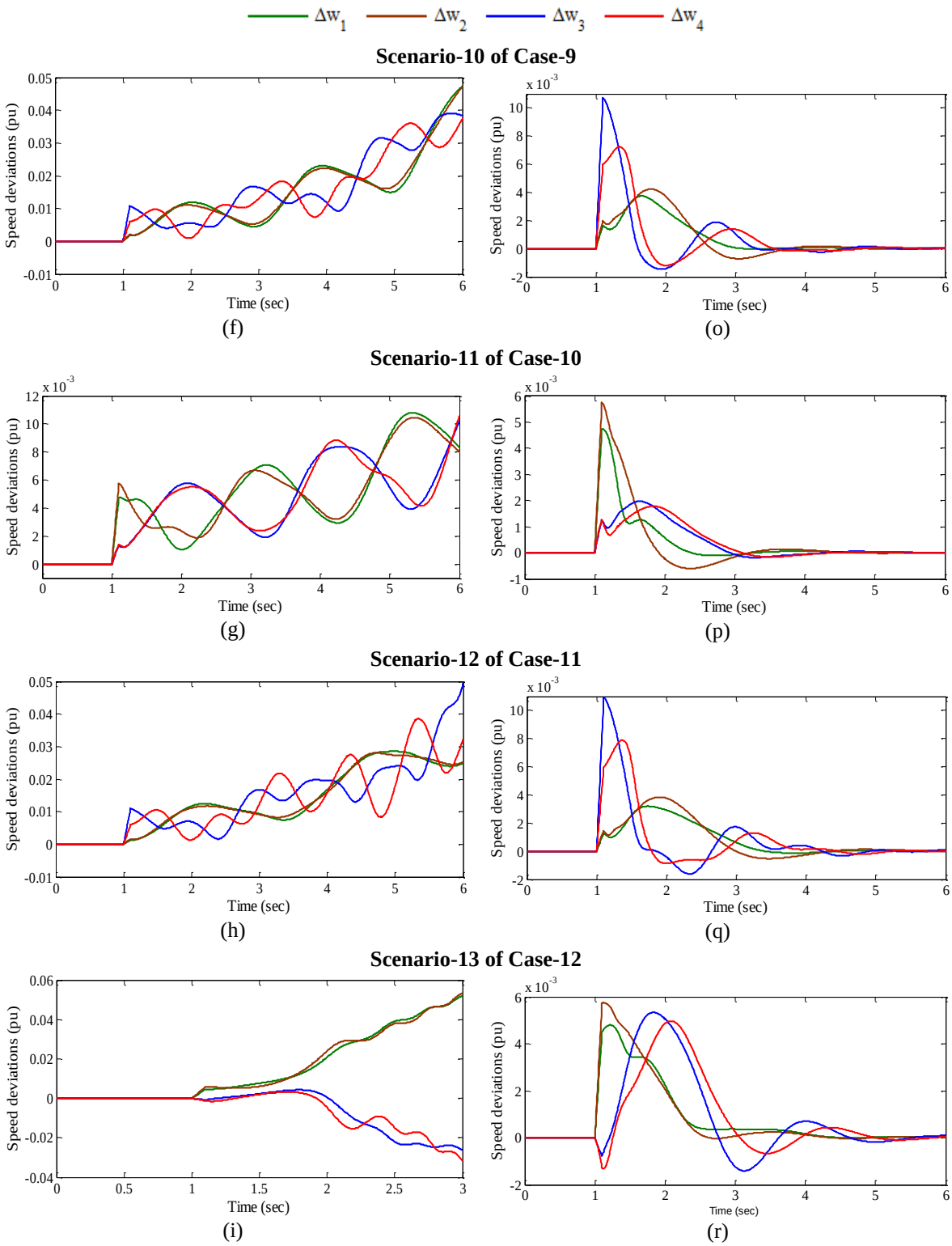

Fig. 4.11 Speed deviations (a)-(i) without PSS and (j)-(r) with PSOPSSs for scenarios 5-13 of unseen operating cases 4-12

This may be concluded that the designed PSOPSSs work satisfactorily for most of the scenarios of severe disturbances of unseen operating cases of TAFM power system.

In addition to time-domain simulation results, the robustness and effectiveness of PSOPSS controllers is also noticed by calculating indices *IAE* and *ITAE* for observed scenarios

5-13 of unseen operating cases 4-12. The bar charts of both indices values obtained with PSOPSSs, for defined scenarios are shown in Fig. 4.12 (a) and (b) respectively.

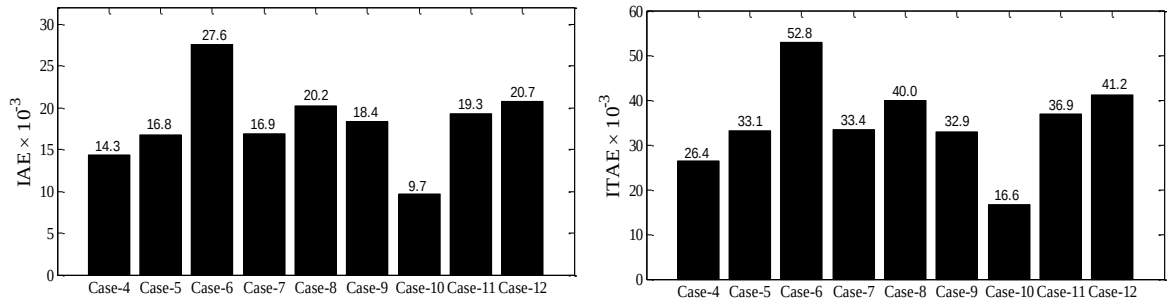

Fig. 4.12 Value of (a) *IAE* and (b) *ITAE* with PSOPSSs for scenarios 5-13 of unseen operating cases 4-12

In above figure, both indices with PSOPSSs for corresponding scenarios of Case-4 and Case-6 are evaluated for 5 and 9-cycle of operation respectively whereas remaining cases are determined for 6-cycle of operation. Both indices values with PSOPSSs are minimum and maximum for 6-cycle operation of unseen cases 10 and 12 respectively. Therefore, it is concluded that with PSOPSSs, Scenario-11 of Case-10 and Scenario-13 of Case-12 are least and most severe scenario of disturbance respectively.

Hence, the designed PSOPSS controllers for TAFM power system is capable to damp out low frequency local and inter-area modes of oscillations with improved stability and damping performances for wide range of loading cases under different scenarios of severe disturbances and also for unseen operating cases under severe scenarios of disturbances.

4.2.3 Example 3: Ten-Machine, Thirty-Nine Bus New England Power System (NEPS)

The operating condition details and single-line diagram of NEPS is described in Section 3.4.3 and Appendix respectively.

A. Eigenvalue Analysis of NEPS without PSS and with PSOPSSs

Open-loop eigenvalues, damping ratio, frequency, participation modes and participation factor associated with electromechanical modes of the system are illustrated in Table 3.19 and discussed in Section 3.4.3 (A). An eigenvalue-based multi-objective function J (equation 3.1) presented in Section 3.2 is minimized using PSO for designing twenty-seven PSS parameters of nine generators. The PSO is applied with population size 100, maximum generation 100, $c_1 = c_2 = 2$, $w_{min} = 0.4$, $w_{max} = 0.9$.

The PSO is able to find the desired solution for which fitness function J is zero. The final value of J equal to zero indicates that nine unstable and/or poorly damped eigenvalues are shifted to a specified D-shape zone in the left-half of the *s*-plane. The optimum designed parameters for PSOPSSs are shown in Table 4.7.

Table 4.7: Optimal designed parameters of PSOPSSs for NEPS

Optimized Parameters	Generators								
	G_2	G_3	G_4	G_5	G_6	G_7	G_8	G_9	G_{10}
K_1	7.839	16.011	22.541	97.207	83.293	0.187	10.681	71.82	26.397
T_1	0.473	0.704	0.041	0.052	0.118	0.841	0.319	0.381	0.912
T_3	0.125	0.102	0.178	0.976	0.076	0.878	0.647	0.168	0.236

The closed-loop eigenvalues and their damping ratio with PSOPSSs for loading cases 1-3 are determined using PSAT [215] and are shown in Table 4.8. Figure 4.14 (a)-(c) and (d)-(f) present the eigenvalue maps for without PSS and with PSOPSSs of NEPS for loading cases 1-3 respectively.

Table 4.8: Eigenvalues and damping ratio with PSOPSSs for loading cases 1-3 of NEPS

Case-1	Case-2	Case-3
– 1.439 ± j 7.822, 0.181	– 1.248 ± j 9.976, 0.124	– 1.180 ± j 9.910, 0.118
– 1.231 ± j 9.971, 0.122	– 1.329 ± j 8.106, 0.161	– 1.442 ± j 7.800, 0.181
– 0.818 ± j 7.691, 0.105	– 0.848 ± j 7.619, 0.110	– 0.789 ± j 7.644, 0.102

The eigenvalue maps of without PSS for unstable and lightly damped modes of NEPS are discussed in Section 3.4.3 (A). Table 4.8 and Fig. 4.13 (d)-(f) show that the PSOPSSs shift the eigenvalues to a specified D-shape zone in the left half of the *s*-plane with desired damping factor and damping ratio as compared to without PSS for three loading cases. Hence, PSOPSS controllers provide improved stability and damping characteristics of the NEPS as compared to same obtained using without PSS.

B. Time-Domain Simulation Results and Discussions with PSOPSSs and without PSS of NEPS

The simulations of NEPS are performed with PSSs for five different scenarios of disturbances mentioned in Table 3.24 for three loadings cases. The speed deviations $\Delta w_1, \Delta w_2, \Delta w_3, \Delta w_4, \Delta w_5, \Delta w_6, \Delta w_7, \Delta w_8, \Delta w_9$ and Δw_{10} for without PSS and with PSOPSSs for scenarios 1-5 of severe Case-3 loading are shown in Fig. 4.14 (a)-(e) and (f)-(j) respectively. The analysis of response plots without PSS already discussed in Section 3.4.3 (B).

Figure 4.14 (f)-(j) reveals that the speed response with PSOPSSs for Scenario-1 of Case-3 loading have large peak overshoot and consumed more time to die out oscillations as compared to others. Therefore, it is concluded that with PSOPSSs Scenario-1 is most severe scenario than others. This demonstrates the potential of PSO technique to obtain the desired set of PSS parameters for NEPS and the designed PSOPSSs are capable to damp out LFO for wide range of operating cases under severe scenarios of disturbances.

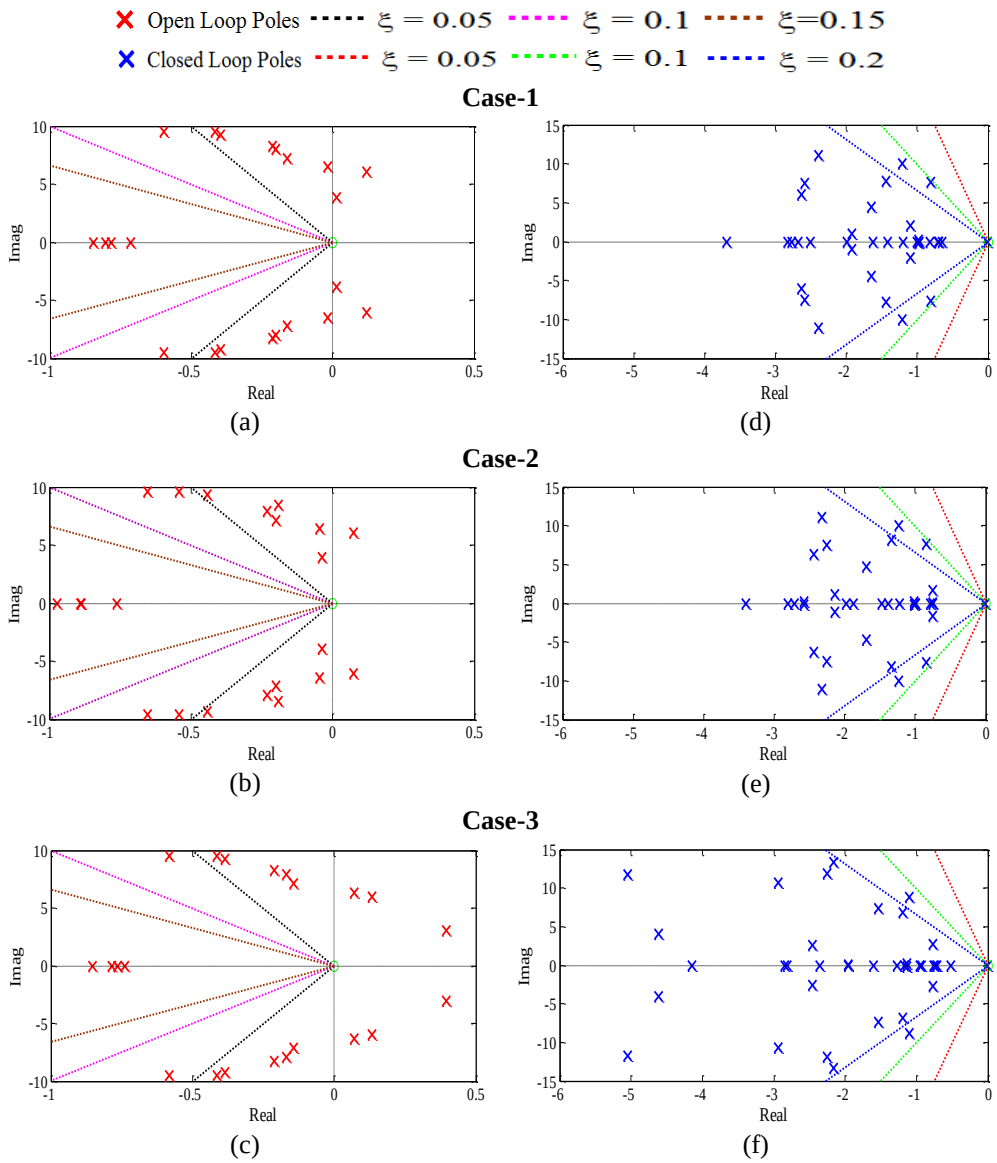

Fig. 4.13 Eigenvalue maps (a)-(c) without PSS and (d)-(f) with PSOPSSs for loading cases 1-3 of NEPS

C. Performance Indices Results and Discussions with PSOPSSs of NEPS

In addition to simulation results, the effectiveness of designed PSOPSS controllers is also observed by determining indices *IAE* and *ITAE* for earlier five observed scenarios of different disturbances. The bar charts of both indices values obtained by PSOPSS controllers for scenarios 1-5 of three loading cases are shown in Fig. 4.15 (a)-(e) and (f)-(j) respectively.

The values of both indices with PSOPSSs for scenarios 1 & 5 of loading Case-1 and Case-3 are minimum and maximum respectively whereas for scenarios 2-4 of loading Case-2 and Case-3 are minimum and maximum respectively. Moreover, the scenarios 1 and 5 for Case-3 loading are most and least severe scenario than others.

Comparing Fig. 4.15 with Figs. 3.18 and 3.19, it may be observed that the designed PSOPSS controllers of NEPS provide sufficient damping to damp out low frequency local and inter-area modes of oscillation with less overshoot and settling time than that of without PSS.

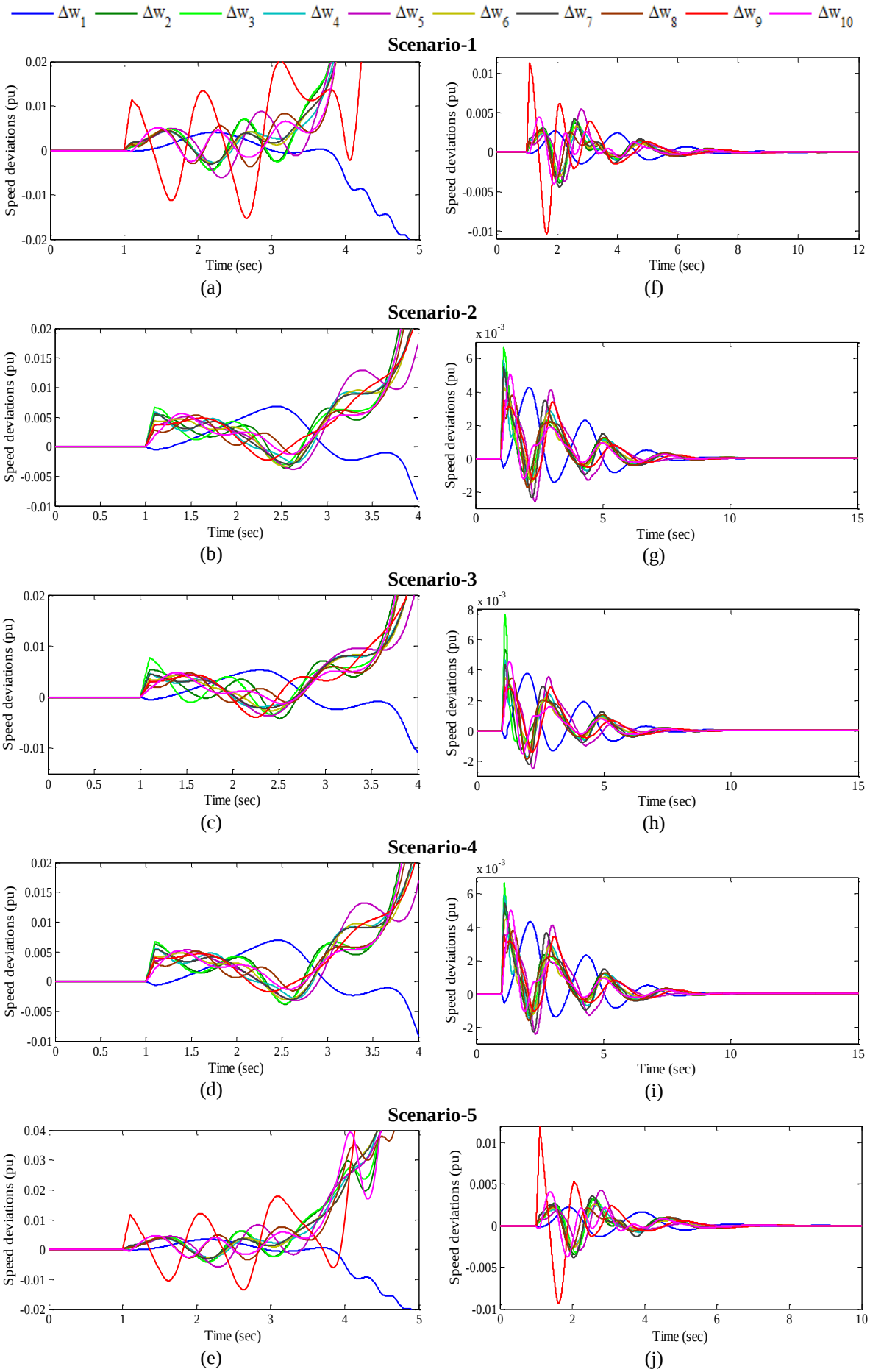

Fig. 4.14 Speed deviations (a)-(e) without PSS and (f)-(j) with PSOPSSs for scenarios 1-5 of loading case-3

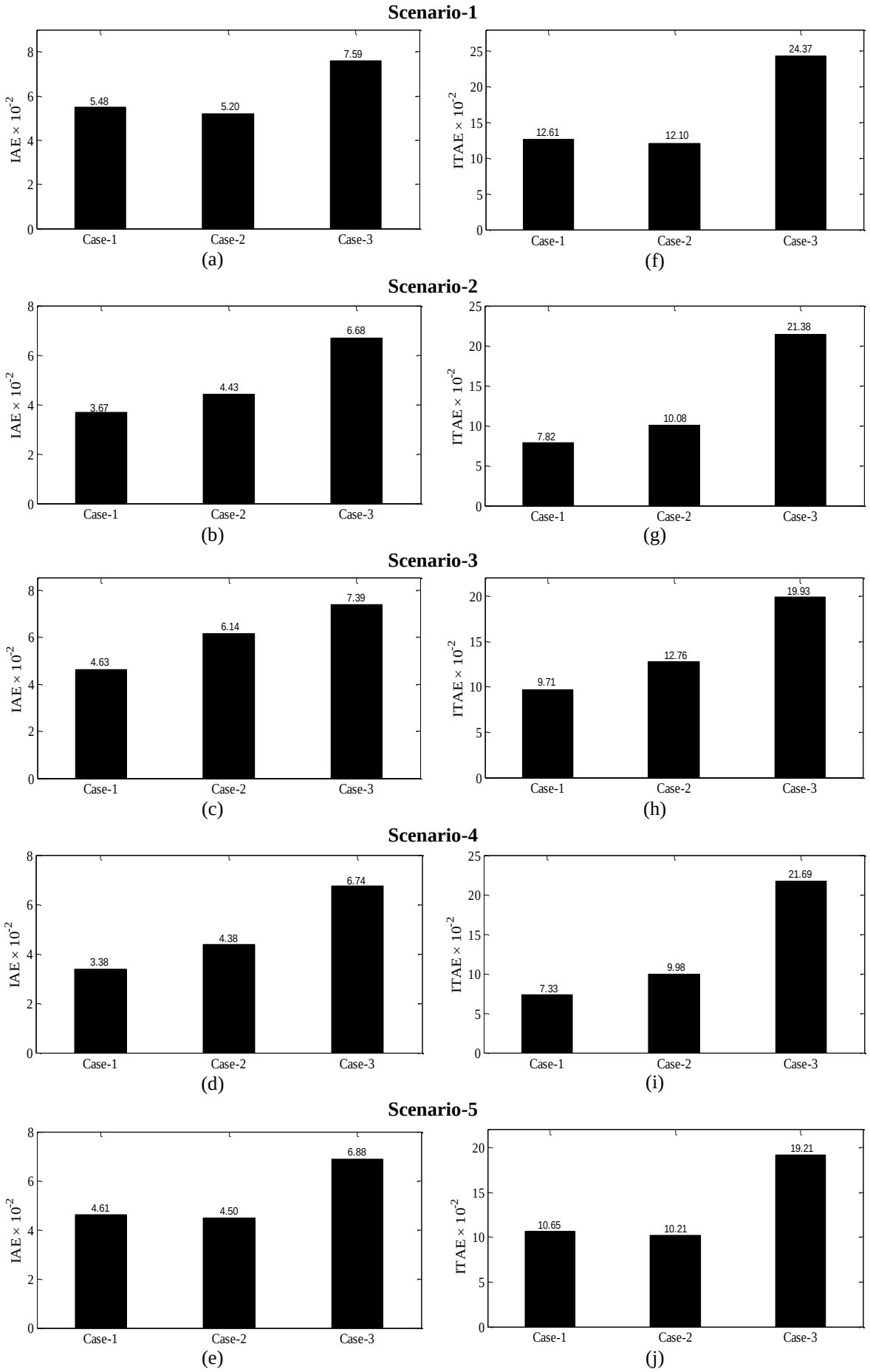

Fig. 4.15 Values of (a)-(e) *IAE* and (f)-(j) *ITAE* with PSOPSSs for scenarios 1-5 of loading cases 1-3

D. Robustness Test of Designed PSOPSS Controllers of NEPS

To test the robustness of previously designed PSOPSS controllers, fifteen unseen operating cases 4-18 mentioned in Table 3.25 are considered. In this section, the effectiveness of PSOPSS controllers is checked by eigenvalue analysis, time-domain simulation results and performance indices for four observed scenarios of cases 4-18 and compared with to that of without PSS.

Open-loop eigenvalues, damping ratio, frequency, participation modes and participation factor for only unstable and critical poorly damped modes of unseen cases 4-18 of NEPS without PSS illustrated in Table 3.26 and discussed in Section 3.4.3 (D). Table 4.9 shows the closed-loop eigenvalues and damping ratio for unseen cases 4-18 of NEPS with PSOPSS controllers for only unstable and critical poorly damped modes respectively.

Table 4.9: Eigenvalues and damping ratio with PSOPSSs for unseen operating cases 4-18 of NEPS

Cases	With PSOPSSs		
Case-4	– 1.189 ± j 7.153, 0.164	– 1.320 ± j 7.628, 0.170	– 2.398 ± j 11.136, 0.210
Case-5	– 1.271 ± j 7.615, 0.164	– 1.157 ± j 9.781, 0.117	– 1.806 ± j 7.232, 0.242
Case-6	– 1.167 ± j 7.607, 0.151	– 1.039 ± j 2.082, 0.448	– 1.232 ± j 9.969, 0.122
Case-7	– 1.240 ± j 9.988, 0.123	– 1.435 ± j 7.821, 0.180	– 1.063 ± j 1.997 0.470
Case-8	– 1.157 ± j 9.781, 0.117	– 0.800 ± j 1.951, 0.379	– 1.271 ± j 7.613, 0.164
Case-9	**– 0.469** ± j 1.764, 0.256	– 1.214 ± j 7.600, 0.157	– 1.555 ± j 5.203, 0.286
Case-10	– 0.889 ± j 6.393, 0.137	– 1.066 ± j 2.138, 0.446	– 1.375 ± j 7.817, 0.173
Case-11	**– 0.663** ± j 1.831, 0.340	– 1.501 ± j 7.908, 0.186	– 1.230 ± j 9.968, 0.122
Case-12	– 1.045 ± j 2.065, 0.450	– 1.282 ± j 9.817, 0.129	– 1.374 ± j 7.829, 0.172
Case-13	– 0.907 ± j 6.657, 0.135	– 1.374 ± j 7.805, 0.173	– 1.274 ± j 9.835, 0.128
Case-14	– 0.876 ± j 7.581, 0.114	– 1.539 ± j 7.761, 0.194	– 1.215 ± j 9.910, 0.121
Case-15	– 1.161 ± j 9.793, 0.117	– 1.295 ± j 7.636, 0.167	– 1.647 ± j 6.850, 0.233
Case-16	– 1.000 ± j 6.561, 0.150	– 1.283 ± j 9.734, 0.130	– 1.420 ± j 7.811, 0.178
Case-17	– 1.160 ± j 9.789, 0.117	– 1.318 ± j 7.847, 0.165	– 1.580 ± j 6.943, 0.222
Case-18	– 1.216 ± j 6.313, 0.189	– 1.259 ± j 9.477, 0.131	– 1.301 ± j 7.805, 0.164

The table reveals that with PSOPSSs eigenvalues are shifted in the left half of the *s*-plane with improved damping factor and damping ratio as compared to without PSS for all unseen operating cases. This ensures that the NEPS will be stable for all considered unseen cases also. It is also found that designed PSOPSS controllers satisfy the earlier selected criterion for the value of desired damping factor and damping ratio for all unseen operating cases except cases 9 and 11 where slightly more settling time may occur. Hence, the PSO provides robustness with improved stability and damping performance for unseen operating cases 4-18 of the NEPS as compared to that of without PSS.

In order to check the robustness performance of the designed PSOPSS controllers in terms of speed deviations, earlier four scenarios of disturbances mentioned in Table 3.24 are considered for unseen cases 4-18 of NEPS without PSS. The speed deviations Δw_1, Δw_2, Δw_3, Δw_4, Δw_5, Δw_6, Δw_7, Δw_8, Δw_9 and Δw_{10} for the system without PSS and with PSOPSSs for severe disturbances Scenario-1 of various unseen cases 4-12 of NEPS are shown in Fig. 4.16 (a)-(i) and (j)-(r) respectively.

The analysis of response plots without PSS already discussed in Section 3.4.3 (D). From Fig. 4.16 (j)-(r), it is observed that the speed deviations with PSOPSSs, the oscillations are well damped out. Moreover, it is observed that the Case-9 delivers more oscillations and consumed more time to reach in steady state as compared to others. In unseen cases 4-12, the Δw_9 is most severe speed deviations than others. Furthermore, peak overshoot of Δw_9 is almost similar in all considered operating cases.

To check the robustness of designed PSOPSS controllers on other unseen cases, the Scenario-4 is performed on other unseen operating cases 13-18. The speed deviations of NEPS without PSS and with PSOPSSs for Scenario-4 of cases 13-18 are shown in Fig. 4.17 (a)-(f) and (g)-(l) respectively.

The analysis of response plots without PSS already discussed in Section 3.4.3 (D). From Fig. 4.17 (g)-(l), it is noticed that LFO in speed response with PSOPSSs are well damped out. Moreover, it is observed that speed responses in unseen Case-16 have high peak overshoot and Case-18 consumed more time to die out oscillations as compared to others. It is clear that the system performance with PSOPSSs is improved to that of without PSS for severe disturbance scenarios 1 and 4 of all unseen operating cases. This may be concluded that the designed PSOPSSs work satisfactorily for most of the scenarios of severe disturbances of unseen operating cases of NEPS.

In addition to time-domain simulation results, the effectiveness of PSOPSS controllers is observed by evaluating two indices: *IAE* and *ITAE* for observed scenarios 1-4 of all unseen operating cases. The bar charts of both indices values with designed PSOPSS controllers for Scenario-1 of unseen cases 4-12 are shown in Fig. 4.18 (a) and (b) respectively. Similarly, both indices with designed PSOPSSs for Scenario-2 of unseen cases 4-18 except Case-6, for Scenario-3 of cases 4-18 except cases 6, 9 and for Scenario-4 of cases 4-18 are shown in Fig. 4.19 (a)-(c) and (d)-(f) respectively.

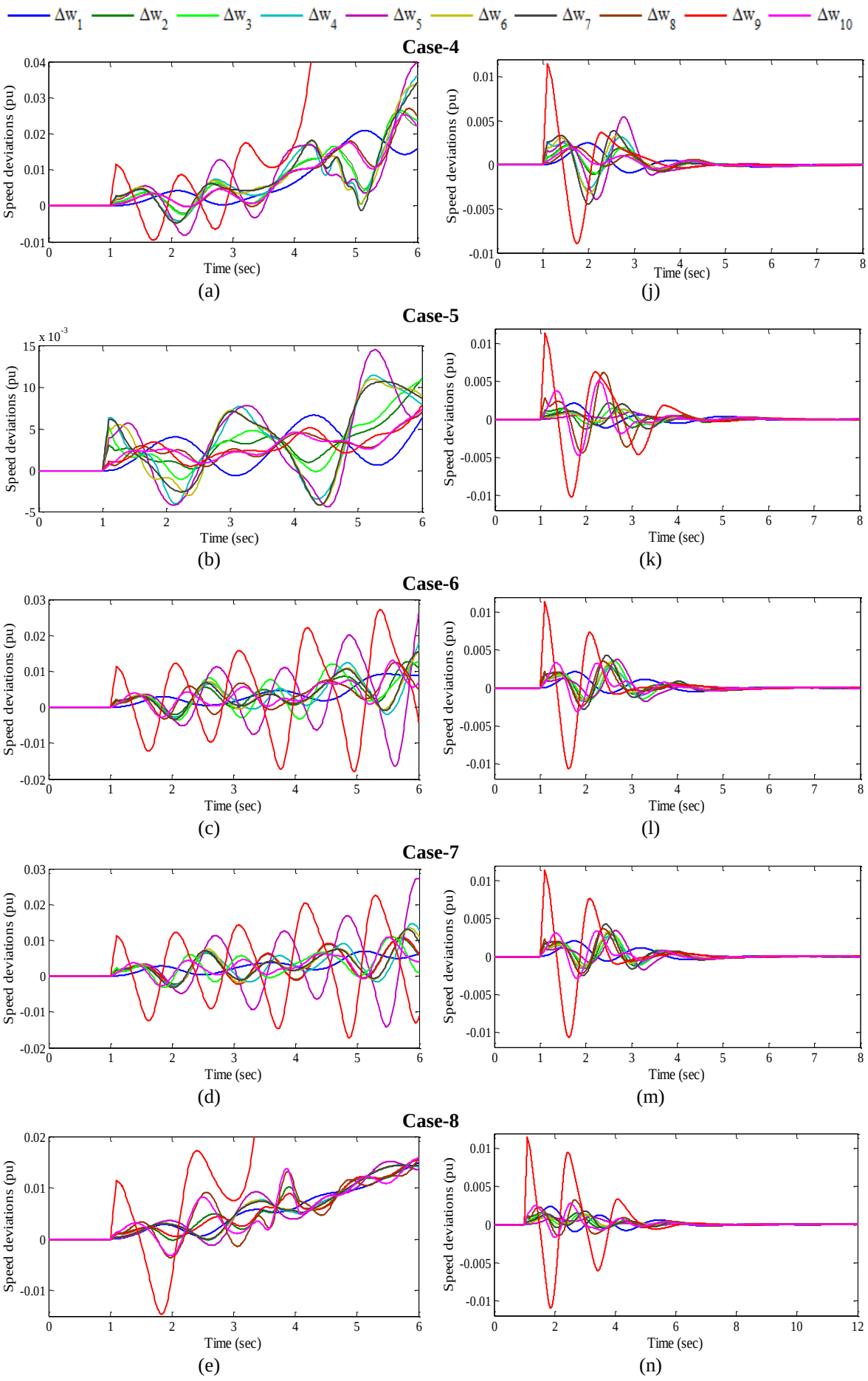
Δw1 Δw2 Δw3 Δw4 Δw5 Δw6 Δw7 Δw8 Δw9 Δw10
Case-4
Speed deviations (pu)
Time (sec)
(a)
(j)
Case-5
x 10-3
(b)
(k)
Case-6
(c)
(l)
Case-7
(d)
(m)
Case-8
(e)
(n)

Cont.

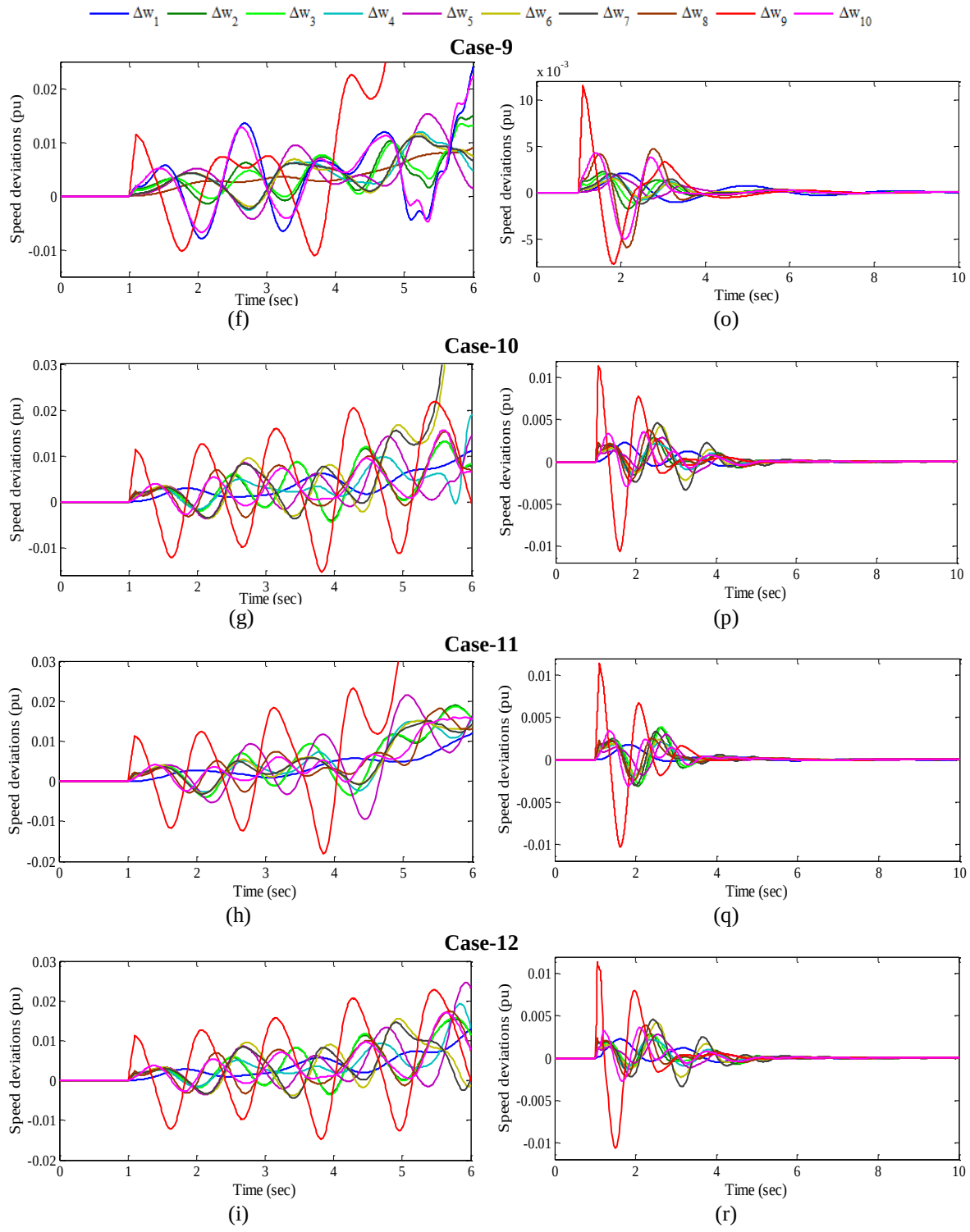

Fig. 4.16 Speed deviations (a)-(i) without PSS and (j)-(r) with PSOPSSs for scenario-1 of unseen operating cases 4-12

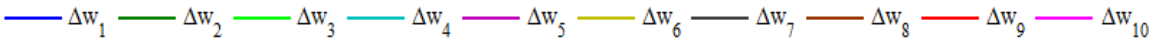

Case-13

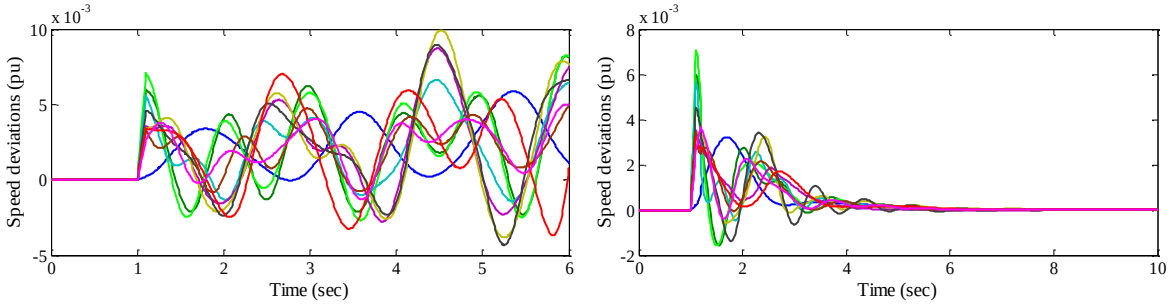

(a) (g)

Case-14

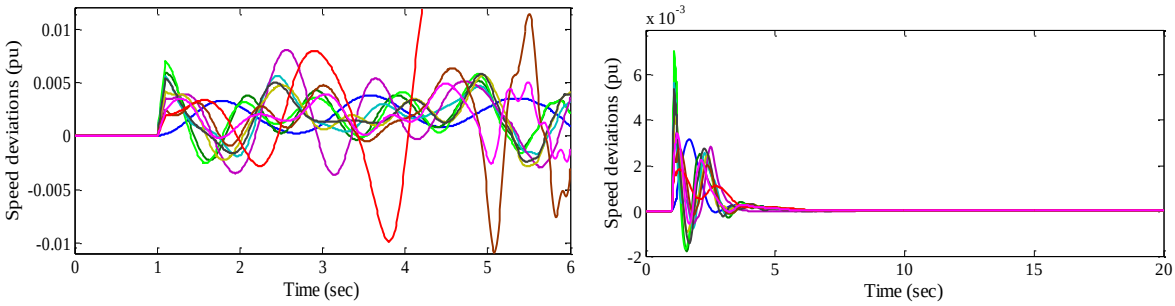

(b) (h)

Case-15

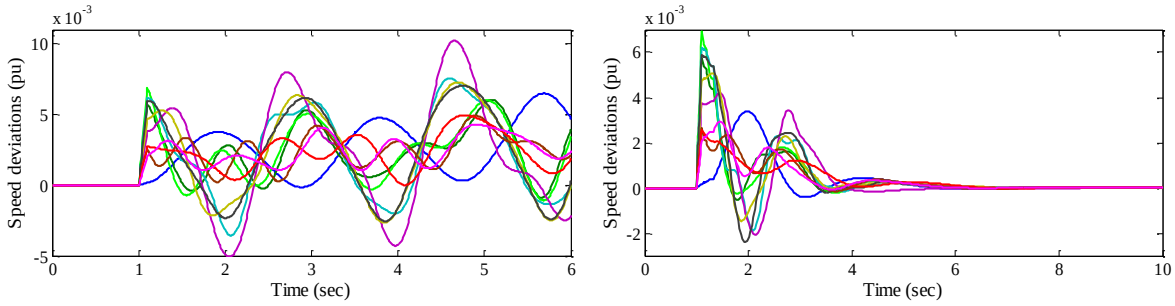

(c) (i)

Case-16

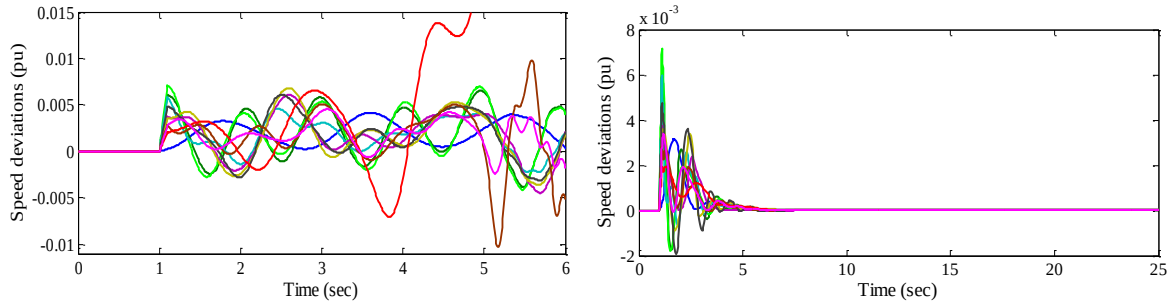

(d) (j)

Case-17

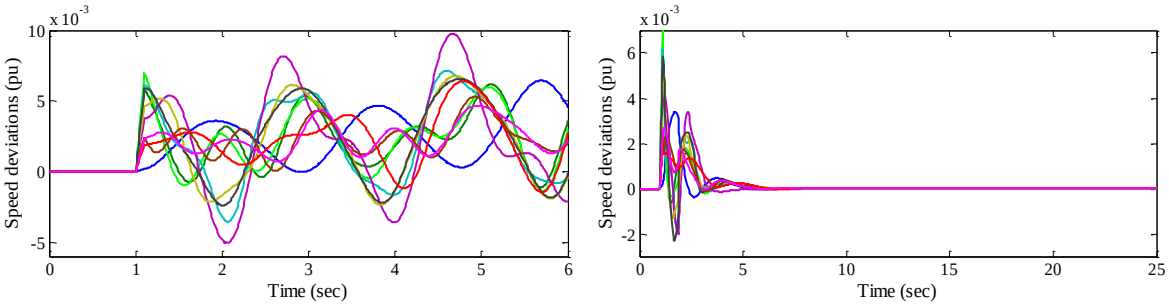

(e) (k)

Cont.

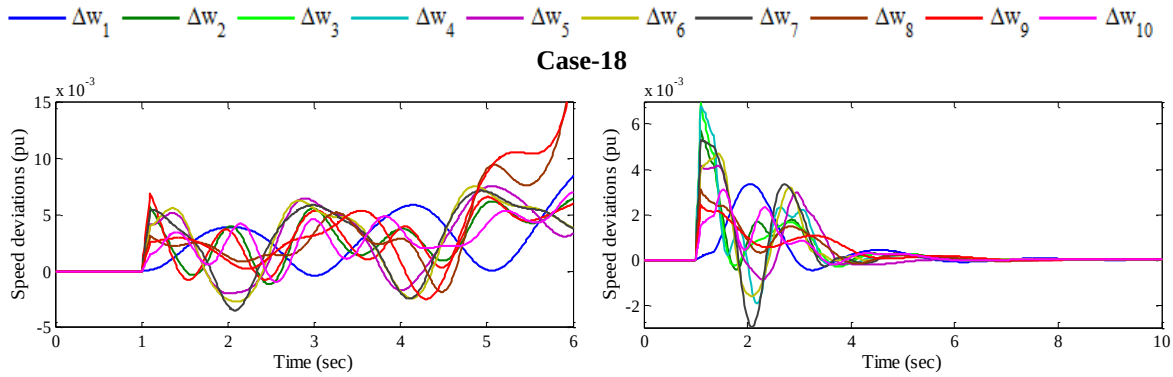

Fig. 4.17 Speed deviations (a)-(f) without PSS and (g)-(l) with PSOPSSs for scenario-4 of unseen operating cases 13-18

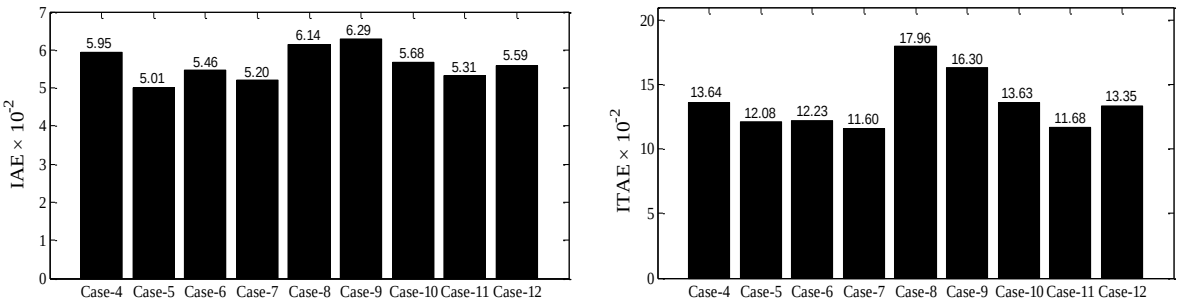

Fig. 4.18 Values of (a) *IAE* and (b) *ITAE* with PSOPSSs for scenario-1 of unseen operating cases 4-12

From Fig. 4.18 (a)-(b), it is observed that values of *IAE* with PSOPSSs for unseen cases 5 and 9 of Scenario-1 are minimum and maximum respectively whereas values of *ITAE* for cases 7 and 8 are minimum and maximum respectively. Therefore, it is concluded that Case-8 under Scenario-1 is severe than others.

From Fig. 4.19 (a)-(c) and (d)-(f), it is noticed that values of both indices with PSOPSSs for cases 5 and 11 of scenarios 2 & 4 are minimum and maximum respectively. Similarly, values of *IAE* with PSOPSSs for unseen cases 5 and 11 of Scenario-3 are minimum and maximum respectively whereas values of *ITAE* for cases 14 and 11 of Scenario-3 are minimum and maximum respectively. Moreover, the Scenario-2 of Case-11 is most severe than other scenarios 1, 3-4 of unseen cases.

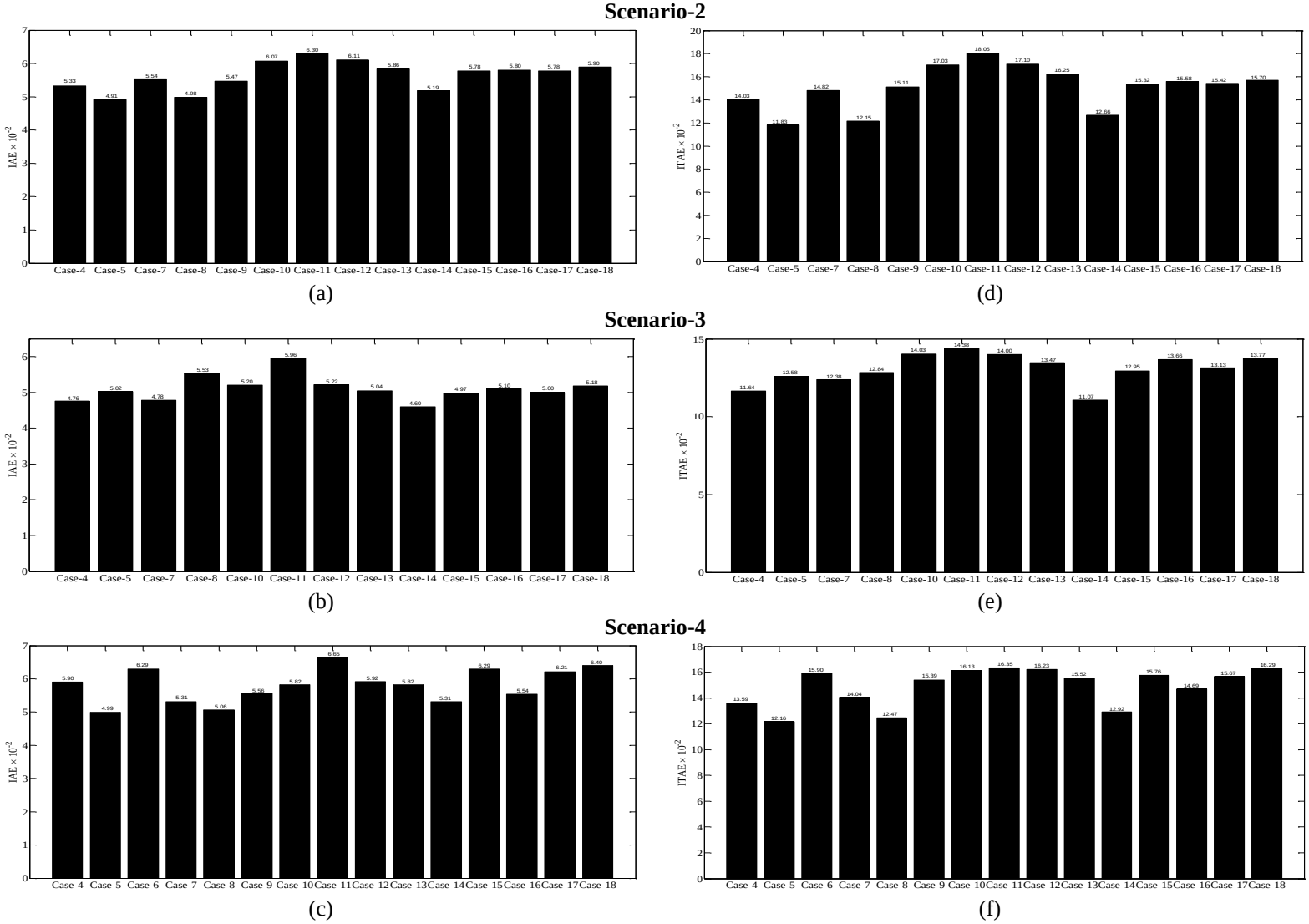

Fig. 4.19 Values of (a)-(c) *IAE* and (d)-(f) *ITAE* with PSOPSSs for scenarios 2-4 of unseen operating cases 4-18

Hence, the designed PSOPSS controllers for NEPS is capable to damp out low frequency local and inter-area modes of oscillations with improved stability and damping performances for wide range of loading cases under different scenarios of severe disturbances and also for unseen operating cases under severe scenarios of disturbances.

4.2.4 Example 4: Sixteen-Machine, Sixty-Eight Bus New England Extended Power System (NEEPS)

The operating condition details and single-line diagram of NEEPS is described in Section 3.4.4 and Appendix respectively.

A. Eigenvalue Analysis of NEEPS without PSS and with PSOPSSs

Open-loop eigenvalues, damping ratio, frequency, participation modes and participation factor associated with electromechanical modes of the system are illustrated in Table 3.28 and discussed in Section 3.4.4 (A). An eigenvalue-based multi-objective function J (equation 3.1) is used in Section 3.2 and minimized using PSO for tuning the forty-two parameters of PSSs. The PSO is applied with population size 100, maximum generation 100, $c_1 = c_2 = 2$, $w_{min} = 0.4$, $w_{max} = 0.9$.

The PSO is able to find the desired solution for which fitness function J is zero. The final value of J equal to zero indicates that fourteen unstable and/or poorly damped eigenvalues are shifted to a specified D-shape zone in the left-half of the s-plane. The optimum designed forty-two parameters of PSOPSSs for fourteen generators are shown in Table 4.10.

Table 4.10: Optimal designed parameters of PSOPSSs for NEEPS

Generators	K_1	T_1	T_3
G_1	17.023	0.275	0.306
G_2	41.948	0.916	0.185
G_3	4.988	0.929	0.401
G_4	14.840	0.566	0.632
G_5	31.782	0.652	0.155
G_7	32.704	0.270	0.895
G_8	15.694	0.461	0.294
G_9	49.067	0.217	0.412
G_{10}	24.965	0.858	0.813
G_{11}	20.833	0.276	0.144
G_{12}	90.180	0.335	0.500
G_{13}	4.632	0.887	0.817
G_{15}	71.071	0.203	0.848
G_{16}	92.741	0.226	0.344

The closed-loop eigenvalues and their damping ratio with designed PSOPSSs for operating cases 1-6 are determined using PSAT [215] and are shown in Table 4.11.

Table 4.11: Eigenvalues and damping ratio with PSOPSSs for operating cases 1-6 of NEEPS

Cases	With PSOPSSs		
Case-1	- 0.755 ± j 2.426, 0.297	- 0.914 ± j 1.707, 0.472	- 0.847 ± j 1.341, 0.534
Case-2	- 0.972 ± j 1.642, 0.509	- 0.698 ± j 2.776, 0.243	- 0.790 ± j 1.195, 0.551
Case-3	- 0.945 ± j 1.616, 0.504	- 0.742 ± j 2.409, 0.294	- 0.883 ± j 1.350, 0.547
Case-4	- 0.959 ± j 1.654, 0.501	- 0.683 ± j 2.266, 0.288	- 0.709 ± j 2.717, 0.252
Case-5	- 0.676 ± j 2.806, 0.234	- 0.915 ± j 1.707, 0.473	- 0.755 ± j 2.423, 0.297
Case-6	- 0.751 ± j 2.387, 0.300	- 0.688 ± j 2.799, 0.238	- 0.899 ± j 1.659, 0.476

The eigenvalue maps of NEEPS without PSS for operating cases 1-3 and 4-6 are shown in Fig. 4.20 (a)-(c) and (g)-(i) whereas with PSOPSSs for same cases are shown in Fig. 4.20 (d)-(f) and (j)-(l) respectively.

The eigenvalue maps of without PSS for unstable and lightly damped modes of NEEPS system are discussed in Section 3.4.4 (A). Table 4.11 and 4.20 (d)-(f) & (j)-(l) show that the PSOPSSs shift the eigenvalues to a specified D-shape zone in the left half of the *s*-plane with desired damping factor and damping ratio as compared to without PSS for all operating cases. Hence, PSOPSS controllers provide improved stability and damping characteristics of the NEEPS as compared to same obtained using without PSS.

B. Time-Domain Simulation Results and Discussions with PSOPSSs and without PSS of NEEPS

In order to examine the performance of designed PSOPSS controllers in previous section in terms of speed deviations, the time-domain simulation of NEEPS is performed for without PSS and with PSOPSSs for observed four scenarios of severe operating Case-6 only. The speed deviations $\Delta w_1, \Delta w_2, \Delta w_3, \Delta w_4, \Delta w_5, \Delta w_6, \Delta w_7, \Delta w_8, \Delta w_9, \Delta w_{10}, \Delta w_{11}, \Delta w_{12}, \Delta w_{13}, \Delta w_{14}, \Delta w_{15}$ and Δw_{16} for without PSS and with PSOPSSs for scenarios 1-4 of operating Case-6 are shown in Fig. 4.21 (a)-(d) and (e)-(h) respectively.

The analysis of response plots without PSS already discussed in Section 3.4.4 (B). From Fig. 4.21 (e)-(h), it is noticed that that with PSOPSSs, LFO are well damped out for all scenarios. Moreover, the Δw_9 has larger peak overshoot and generates more oscillations in Scenario-1 than others. It is clear that the system performance with PSOPSSs is much improved to that of without PSS for all scenarios of operating Case-6.

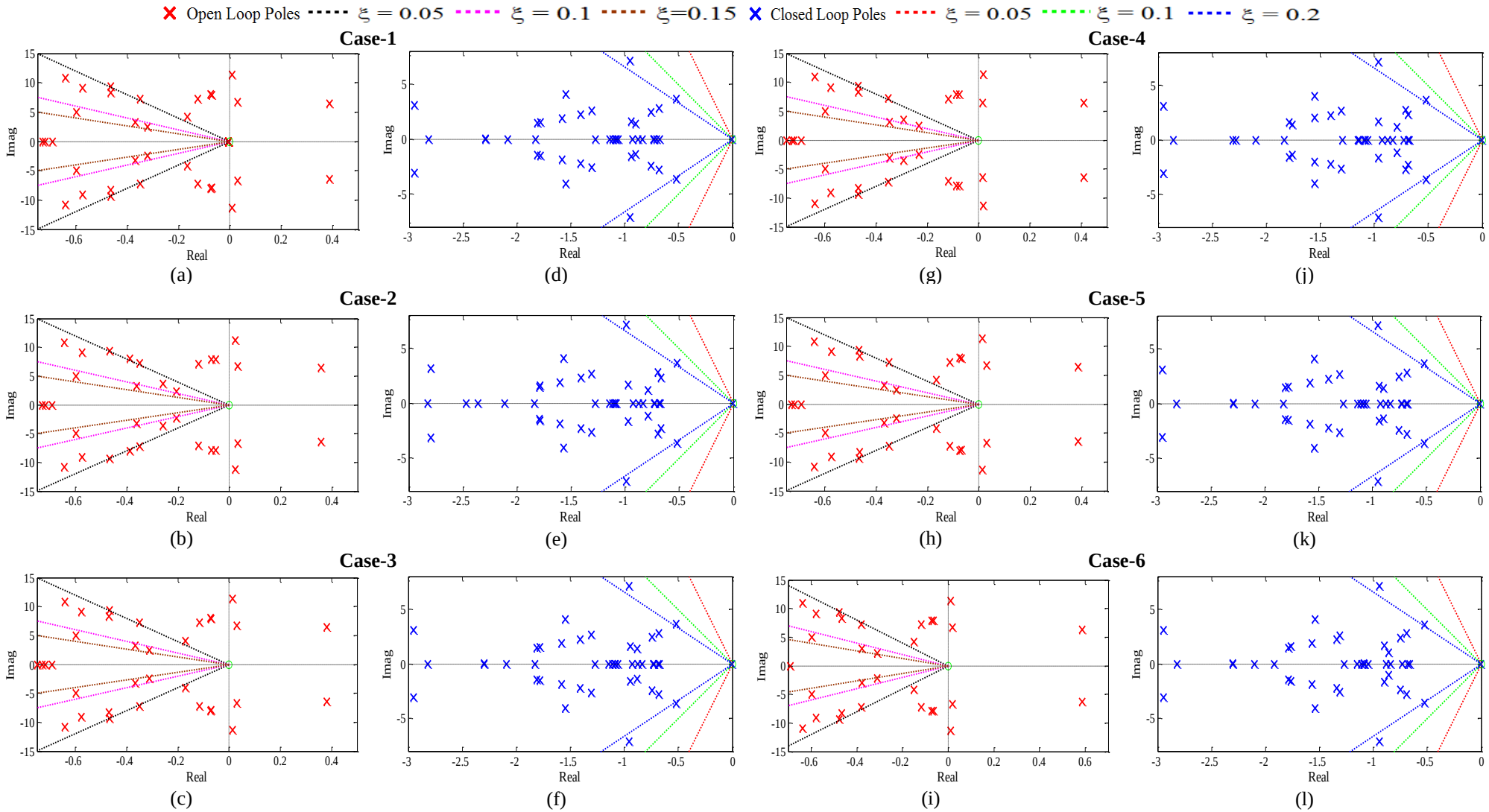

Fig. 4.20 Eigenvalue maps (a)-(c) & (g)-(i) without PSS and (d)-(f) & (j)-(l) with PSOPSSs for operating cases 1-6 of NEEPS

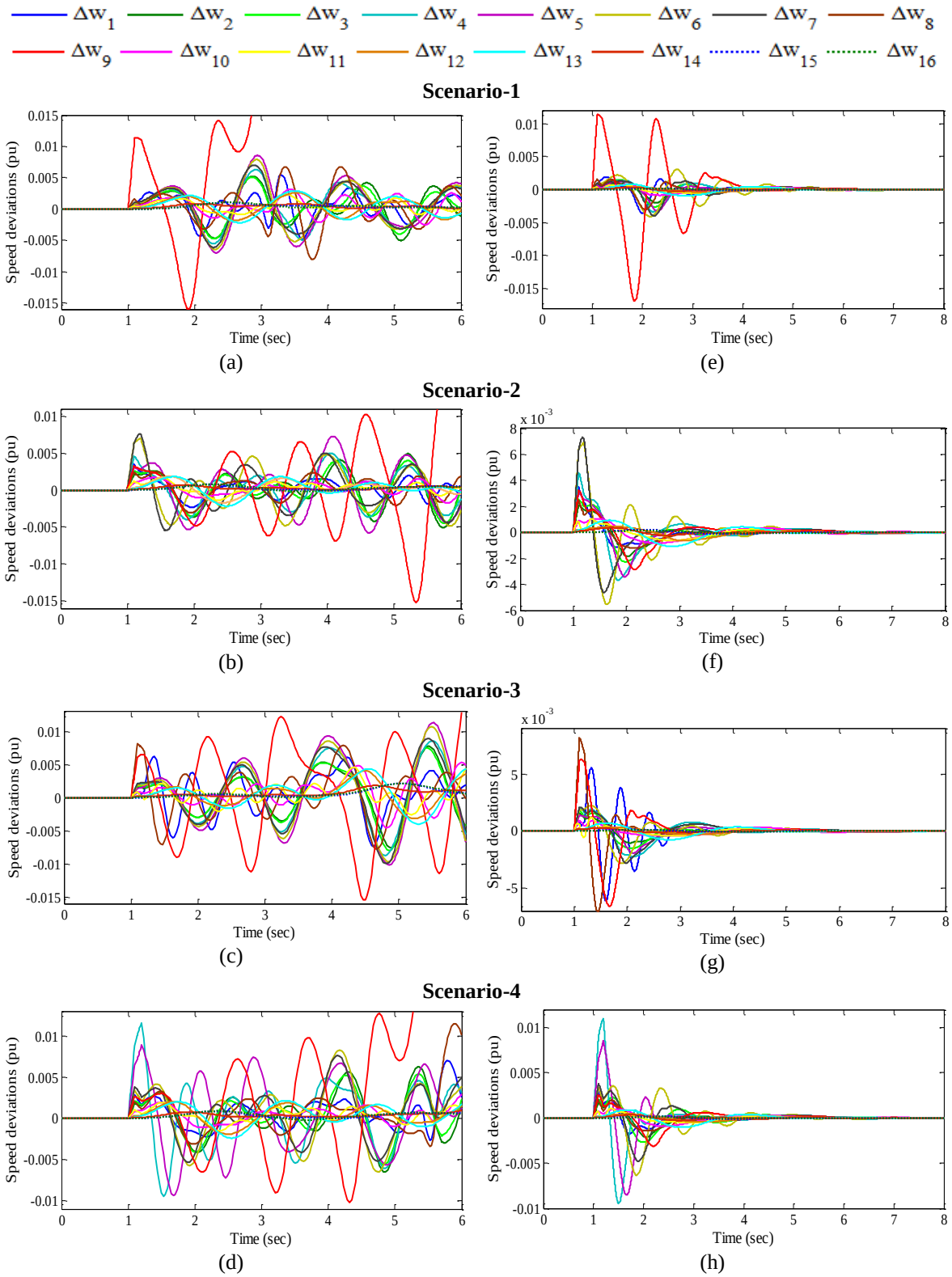

Fig. 4.21 Speed deviations (a)-(d) without PSS and (e)-(h) with PSOPSSs for scenarios 1-4 of operating case-6

This demonstrates the potential of PSO technique to obtain the desired set of PSS parameters for NEEPS and the designed PSOPSSs are capable to damp out LFO for wide range of operating cases under severe scenarios of disturbances.

C. Performance Indices Results and Discussions with PSOPSSs of NEEPS

In addition to time-domain simulation results, the effectiveness of designed PSOPSS controllers is noticed by evaluating *IAE* and *ITAE* for observed four scenarios of different disturbances. The bar charts of both indices values with PSOPSSs for scenarios 1-4 of cases 1-6 are shown in Fig. 4.22 (a)-(d) and (e)-(h) respectively.

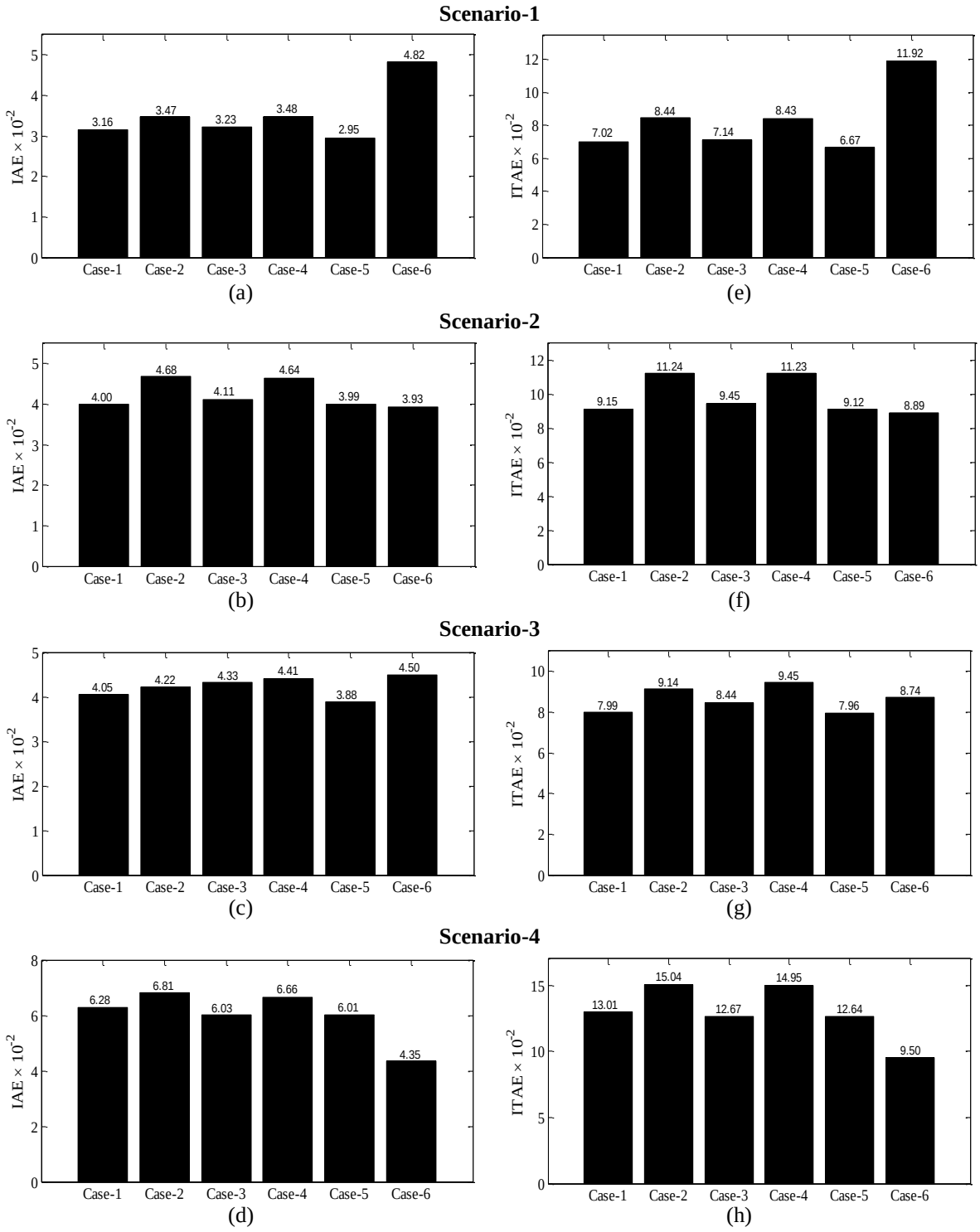

Fig. 4.22 Values of (a)-(d) *IAE* and (e)-(h) *ITAE* with PSOPSSs for scenarios 1-4 of operating cases 1-6

From the Fig. 4.22 (a)-(d), it is observed that both indices for Case-5 and Case-6 of Scenario-1, for Case-6 and Case-5 of Scenario-2, for Case-6 and Case-2 of Scenario-4, are lower and higher values respectively whereas for Scenario-3, the *ITAE* is higher for Case-4 and lower for Case-5 respectively. Moreover, it is concluded that for scenarios 1 to 4 operating cases 6, 2, 4 and 2 are most severe than others respectively. Furthermore, it is also noticed that for all cases the Scenario-4 is most severe than other scenarios whereas for Case-6, the Scenario-1 is most severe than others.

Comparing Fig. 4.22 with Fig. 3.27, it may be observed that the designed PSOPSS controllers of NEEPS provide sufficient damping to damp out low frequency local and inter-area modes of oscillation with less overshoot and settling time than that of without PSS.

D. Robustness Test of Designed PSOPSS Controllers of NEEPS

To test the robustness of earlier designed PSOPSS controllers for NEEPS, nine unseen operating cases 7-15 mentioned in Table 3.33 are considered. In this section, the effectiveness of designed PSOPSSs is evaluated by eigenvalue analysis, time-domain simulation results and performance indices for earlier observed four scenarios of all unseen operating cases and compared with that of without PSS. Open-loop eigenvalues, damping ratio, frequency, participation modes and participation factor for only unstable modes of unseen operating cases 7-15 of NEEPS without PSS and closed-loop eigenvalues and damping ratio with designed PSOPSSs for the same unseen cases of system are obtained using PSAT [215] and shown in Table 4.12.

The table shows that the designed PSOPSSs shift the eigenvalues to the left half of the *s*-plane with improved damping factor and damping ratio as compared to without PSS for all unseen operating cases. This ensures that the NEEPS will be stable for all considered unseen cases also. It is also observed that designed PSOPSS controllers satisfy the earlier selected criterion for the value of desired damping factor and damping ratio for all unseen cases. Hence, the PSO provides robustness with enhanced stability and improved damping performance for unseen operating cases 7-15 of NEEPS as compared to that of without PSS.

Table 4.12: Eigenvalues and damping ratio with PSOPSSs for unseen operating cases 7-15 of NEEPS

Cases	With PSOPSSs
Case-7	– 0.765 ± j 2.238, 0.323
	– 0.821 ± j 4.178, 0.192
Case-8	– 0.781 ± j 7.420, 0.104
	– 0.874 ± j 4.129, 0.207
	– 0.979 ± j 3.429, 0.274
	– 0.719 ± j 2.173, 0.314
Case-9	– 0.784 ± j 7.417, 0.105
	– 0.875 ± j 4.129, 0.207
	– 0.979 ± j 3.397, 0.276
	– 0.514 ± j 2.631, 0.192
	– 0.720 ± j 2.172, 0.314
Case-10	– 0.783 ± j 7.418, 0.105
	– 0.867 ± j 4.146, 0.204
	– 0.987 ± j 3.462, 0.274
	– 0.723 ± j 2.184, 0.314
Case-11	– 0.762 ± j 7.419, 0.102
	– 0.929 ± j 4.052, 0.223
Case-12	– 0.785 ± j 7.417, 0.105
	– 0.865 ± j 4.151, 0.204
	– 1.005 ± j 3.414, 0.282
	– 0.729 ± j 2.203, 0.314
Case-13	– 0.787 ± j 7.409, 0.105
	– 0.864 ± j 4.153, 0.203
	– 0.729 ± j 2.220, 0.312
Case-14	– 0.659 ± j 2.778, 0.231
	– 0.726 ± j 2.208, 0.312
Case-15	– 0.671 ± j 2.886, 0.226
	– 0.939 ± j 4.037, 0.226
	– 0.783 ± j 7.385, 0.105

In order to examine the robustness performance of the designed PSOPSSs in terms of speed deviations, the simulations are performed using PSAT [215] for four earlier observed scenarios on unseen cases 7-15 of NEEPS. The speed deviations $\Delta w_1, \Delta w_2, \Delta w_3, \Delta w_4, \Delta w_5, \Delta w_6, \Delta w_7, \Delta w_8, \Delta w_9, \Delta w_{10}, \Delta w_{11}, \Delta w_{12}, \Delta w_{13}, \Delta w_{14}, \Delta w_{15}$ and Δw_{16} without PSS and with PSOPSSs for severe test Scenario-1 of cases 7-11 are shown in Fig. 4.23 (a)-(e) and (f)-(j) respectively whereas for Scenario-2 of cases 12-15 are shown in Fig. 4.24 (a)-(d) and (e)-(h) respectively.

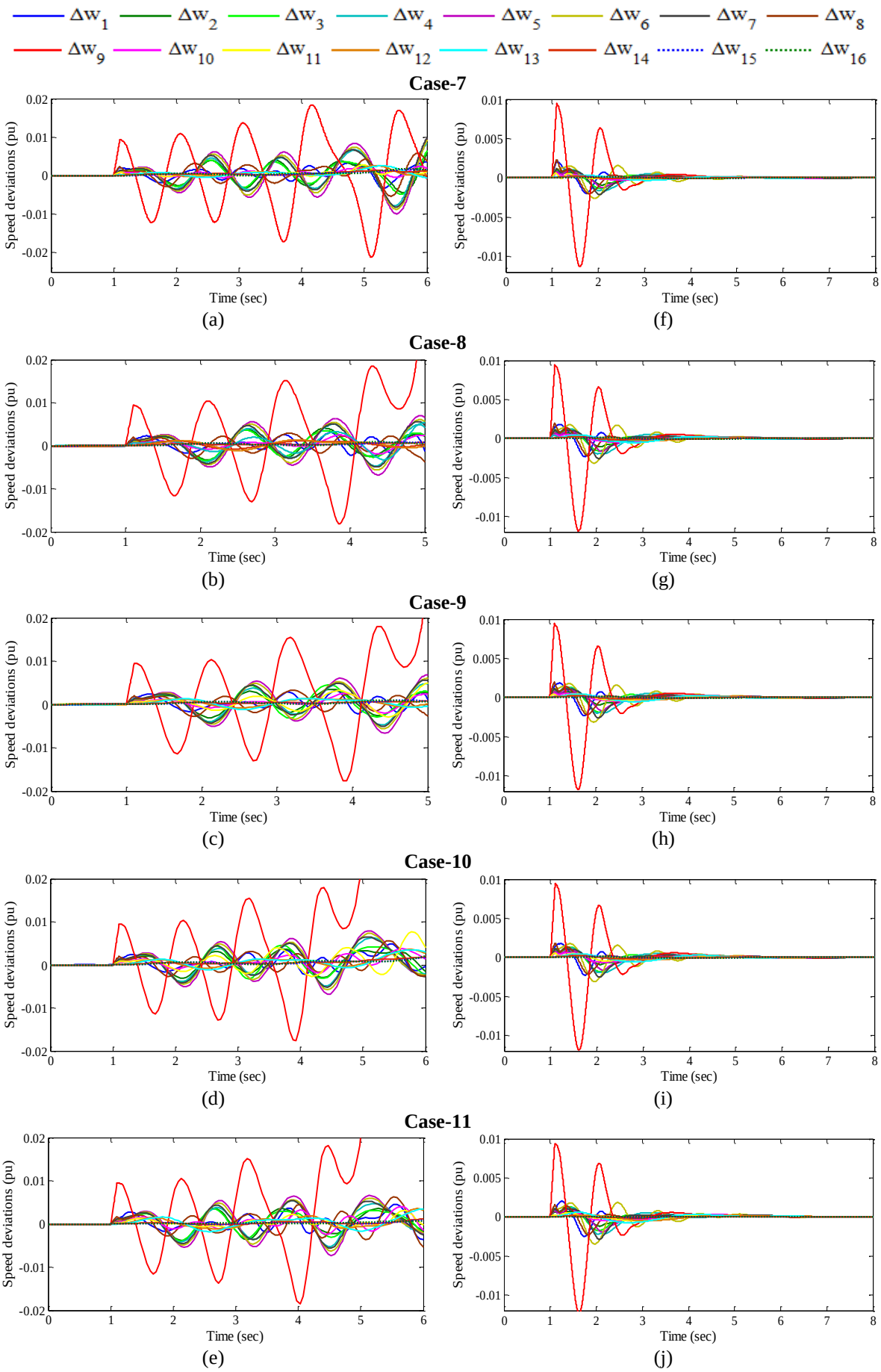

Fig. 4.23 Speed deviations (a)-(e) without PSS and (f)-(j) with PSOPSSs for scenario-1 of unseen operating cases 7-11

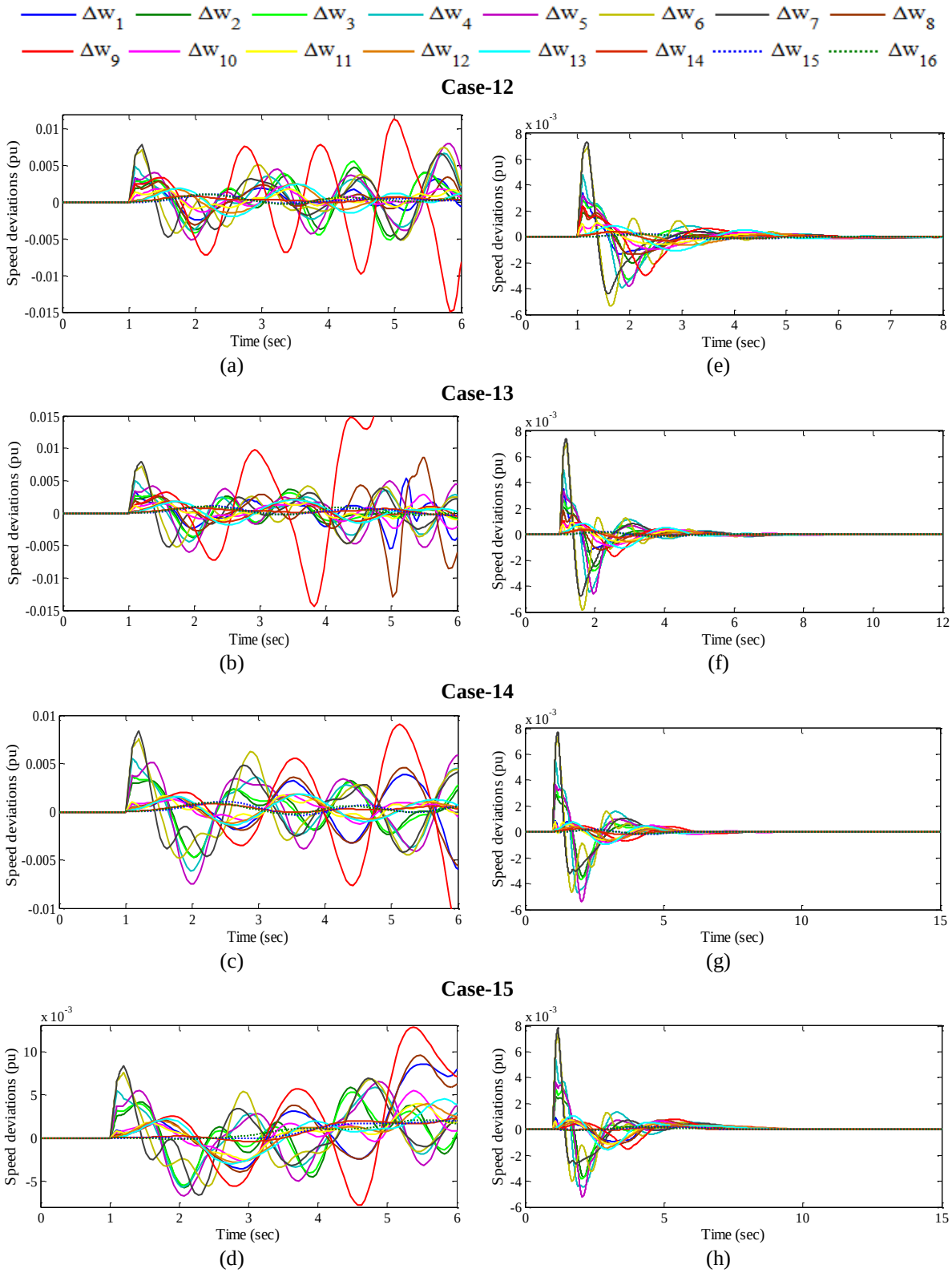

Fig. 4.24 Speed deviations (a)-(d) without PSS and (e)-(h) with PSOPSSs for scenario-2 of unseen operating cases 12-18

The analysis of response plots without PSS already discussed in Section 3.4.4 (D). From Figs. 4.23 (f)-(j) and 4.24 (e)-(h), it is observed that with PSOPSSs all oscillations of speed deviations are well damped out for Sceanrio-1 of cases 7-11 and Scenario-2 of cases 12-15.

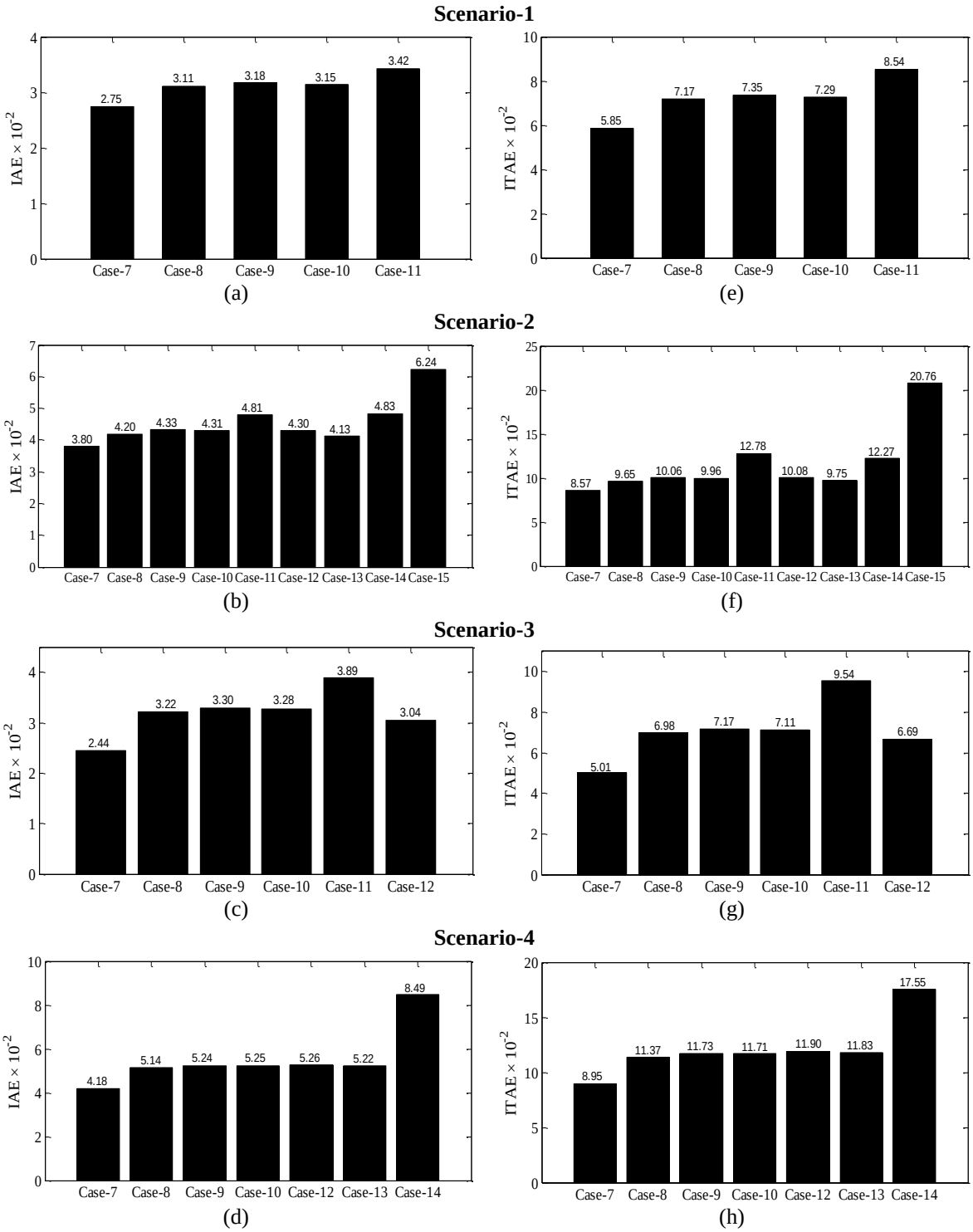

Fig. 4.25 Values of (a)-(d) *IAE* and (e)-(h) *ITAE* with PSOPSSs for scenarios 1-4 of unseen operating cases 7-15

Moreover, the peak overshoot of speed responses in scenarios 1 and 2 are almost same in all considered operating cases. Furthermore, oscillations in response of cases 13-15 in Scenario-2 take more time to reach in steady state as compared to others. It is clear that the system performance with PSOPSSs is improved to that of without PSS for considered scenarios of unseen operating cases. This may be concluded that the designed PSOPSSs work satisfactorily for observed scenarios of severe disturbances of unseen operating cases of NEEPS.

In addition to time-domain simulation results, the effectiveness of designed PSOPSS controllers is observed by evaluating *IAE* and *ITAE* for observed four scenarios of unseen cases 7-15. The bar charts of both indices with PSOPSSs for Scenario-1 of cases 7-11, Scenario-2 of cases 7-15, Scenario-3 of cases 7-12 and Scenario-4 of cases 7-14 are shown in Fig. 4.25 (a)-(d) and (e)-(h) respectively.

From the figure, it is noticed that the values of both indices with PSOPSSs for Case-11 of Scenario-1, Case-15 of Scenario-2, Case-11 of Scanerio-3 and Case-14 of Scenario-4 are higher than others. Moreover, it is concluded that the unseen Case-15 of Scenario-2 of and Case-7 of Scenario-3 are most and least severe than others.

Hence, the designed PSOPSS controllers for NEEPS is capable to damp out low frequency local and inter-area modes of oscillations with enhanced stability and damping performances for wide range of operating cases under different scenarios of severe disturbances and also for unseen operating cases under severe scenarios of disturbances.

4.3 Summery

In this chapter, a meta-heuristic technique PSO is implemented for effectively designing of PSS under wide range of operating conditions of WSCC power system, TFAM power system, NEPS and NEEPS for SSS enhancement. The PSO is capable of shifting all unstable and/or poorly damped eigenvalues of MMPS to a specified D-shape zone in the left half of the *s*-plane. Moreover, the effectiveness of designed PSOPSS controllers has been evaluated by eigenvalue analysis, eigenvalue maps, time-domain simulation results and performance indices namely *IAE* and *ITAE*. Furthermore, the robustness of designed PSOPSSs is observed by testing them on under wide range of unseen operating cases of MMPS. It is found that the design PSOPSSs have shifted unstable and/or poorly damped eigenvalues of all unseen cases of MMPS to the left half of the *s*-plane for mitigating low frequency local and inter-area modes of oscillation.

CHAPTER-5

MULTI-MACHINE POWER SYSTEM STABILIZERS DESIGN USING HARMONY SEARCH OPTIMIZATION

As modern electrical power systems become more complex and control of such systems using traditional methods face lot of difficulties. Many new meta-heuristic techniques have been introduced recently to solve such complex optimization problems. The Harmony Search Optimization (HSO), inspired by the improvisation process of music, is one of such meta-heuristic technique which has received a considerable attention to solve most complex power system optimization problems [222]-[225] but not yet explored much to solve PSS optimization problem in MMPS. Therefore, in this chapter HSO is explored to optimize the parameters of PSS for stabilize the LFO of MMPS. The HSO is applied on four standard power transmission systems, e.g., WSCC power system, TAFM power system, NEPS and NEEPS.An eigenvalue-based multi-objective function mentioned in Section 3.2 is minimized using HSO for designing PSS parameters of MMPS. The PSS designed using HSO is named as HSOPSS. The effectiveness of all designed HSOPSS controllers are evaluated by eigenvalue analysis, eigenvalue maps, time-domain simulation results and specified performance indices and the system performance with HSOPSS is compared with that of without PSS. The robustness of all designed HSOPSS controllers is also checked by testing them on unseen operating conditions under different scenarios of severe disturbances.

5.1 Harmony Search Optimization

A Harmony Search (HS) is basically a music-based new meta-heuristic technique developed by Geem etal. [203]. The HS is based on the concept of the musical process of searching for a perfect state of harmony. It was influenced by observing that the objective of music is to discover for a perfect state of harmony which is determined by an aesthetic standard. This harmony in music is similarly to obtain the optimal solution in optimization process. The aesthetic qualities indicate the pitch of every musical instrument that same as the objective function value is evaluated by the set of values assigned to every decision variable. When a musician is correcting himself or herself, there three possible choices: (i) play any popular tune of music exactly from his or her memory; (ii) play something similar to a known tune; or (iii) compose new or random notes. Geem et al. [202] [203] developed these three options into the three corresponding components: Harmony Memory Considering Rate (HMCR), Pitch Adjusting Rate (PAR), and Randomization.

The use of harmony memory is similar to the choice of best fitness in the GA. This will ensure that best fitness solutions or harmonics are carry forward to New Harmony memory. In

order to use this memory more effectively, it is desired to assign a parameter called HMCR [0-1]. The low values of this parameter indicate that only few best harmonies are selected and it may converge too slowly whereas higher value (near 1) shows that almost all the harmonies are used in the harmony memory, then other harmonies are not explored well, leading to potentially wrong solutions. Therefore, generally HMCR is considered in the range [0.7-0.95].

The second component, the pitch adjustment is evaluated by a pitch Band-Width (BW) b_{range} and a PAR [202]. The meaning of pitch adjustment is to change the frequencies in music which corresponds to producing a slightly different solution in the HSO algorithm. The pitch can be changed linearly or nonlinearly but normally linear adjustment is used as

$$x_{new} = x_{old} + b_{range}.e \tag{5.1}$$

where x_{old} is the existing pitch or solution from the harmony memory, and x_{new} is the new pitch after the implementation of PAR. This essentially generates a new solution around the existing quality solution by varying the pitch slightly by a small random amount. Here e is a random number generated in the range $[-1, 1]$. The PAR is similar to the mutation rate in the GA. The degree of the adjustment is controlled by the PAR. A low value of PAR with a narrow BW can slow down the convergence of HS due to the limitation in the exploration of only a small subspace of the whole search space whereas a very high value of PAR with a wide BW may cause the solution to spread out around some potential optima as in a random search. Thus, PAR is considered in the range [0.1-0.5] in most applications.

The third component is the randomization which increases the diversity of the solutions. Although role of pitch adjustment is also similar but it is limited to certain local pitch adjustment and thus corresponds to a local search. The use of randomization is to further diversify the search to explore the global optima [166].The flow chart of HSO algorithm is shown in Fig. 5.1:

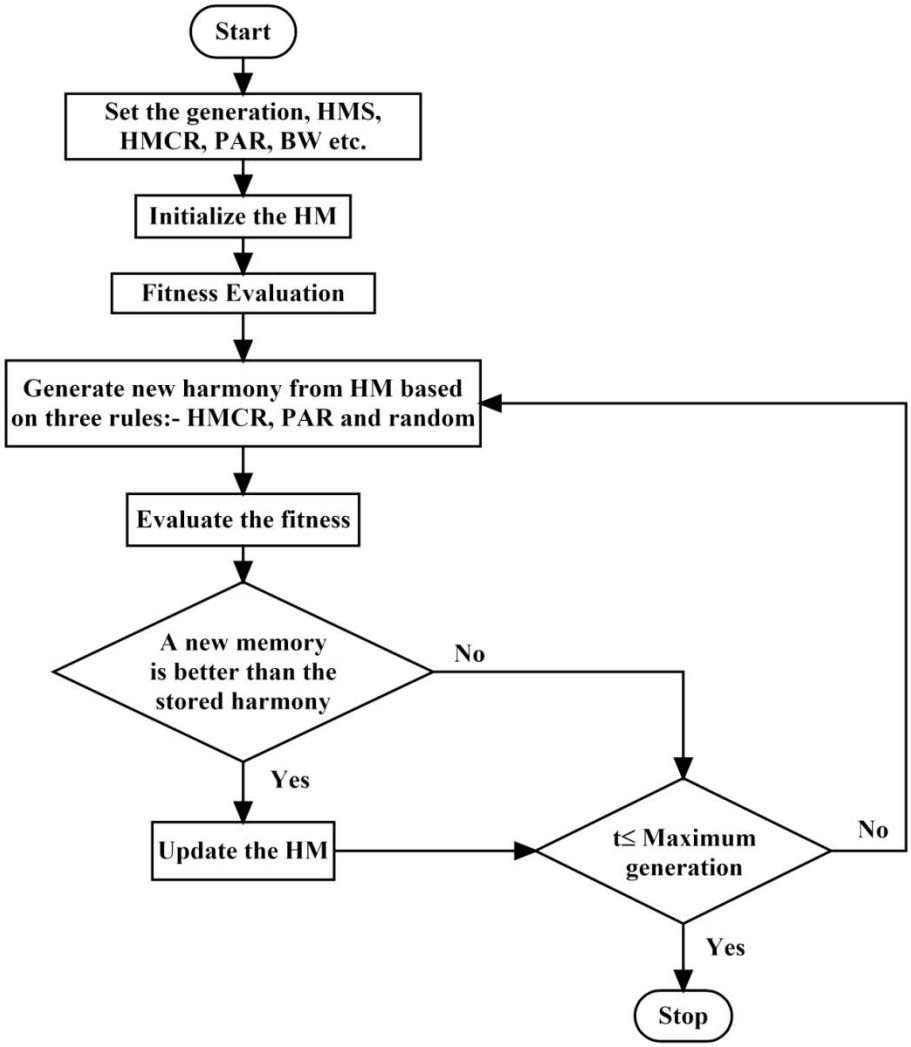

Fig. 5.1 Flow chart of harmony search optimization algorithm

5.2 Simulation and Results

The HSO is applied on four standard test systems e.g., WSCC power system, TAFM power system, NEPS and NEEPS, to obtain the optimal parameters of PSS for wide range of operating conditions. An eigenvalue-based multi-objective function is used for simultaneous control of damping factor and damping ratio to mitigate low frequency electromechanical oscillations of MMPS. The parameters of PSS are so designed that unstable and/or poorly damped open-loop eigenvalues are shifted to a specified D-shape zone in the left-half of the *s*-plane for wide range of operating conditions under different scenarios of severe disturbances. This is obtained by minimizing the objective function (3.1) using HSO. The effectiveness of all designed controllers are evaluated by eigenvalue analysis, eigenvalue maps, time-domain simulation results and performance indices *IAE* and *ITAE*and the system performance with HSOPSSs is compared with that of without PSS. The robustness of all designed controllers is also checked by testing them on unseen operating conditions under different scenarios of severe disturbances and compared with that of without PSS.

5.2.1 Example 1: Three-Machine, Nine-Bus WSCC Power System

The operating condition details and single-line diagram of WSCC power system is described in Section 3.4.1 and Appendix respectively.

A. Eigenvalue Analysis of WSCC Power System without PSS and with HSOPSSs

The open-loop eigenvalues, damping ratio, frequency, participation modes and participation factor associated with electromechanical modes of the system are illustrated in Table 3.2 and discussed in Section 3.4.1 (A). An eigenvalue-based multi-objective function *J* presented in (3.1) is minimized using HSO by tuning the six parameters of PSSs. The HSO is applied with population size 100, maximum generation 100, *HMCR* = 0.75, *PAR* = 0.30, *BW* = 0.01.

The HSO is able to find the desired solution for which fitness function *J* is zero. The final value of *J* equal to zero indicates that two unstable and/or poorly damped eigenvalues using HSO are shifted to a specified D-shape zone in the left-half of the *s*-plane. The optimal six parameters obtained by HSOPSSs for two generators are shown in Table 5.1. The closed-loop eigenvalues and their damping ratio with HSOPSSs for operating cases 1-3 are evaluated using PSAT [215] and are shown in Table 5.2.

Table 5.1: Optimal designed parameters of HSOPSSs for WSCC power system

Generators	K	T_1	T_3
G_2	1.770	1	0.133
G_3	1.810	0.06	0.714

Table 5.2: Eigenvalues and damping ratio with HSOPSSs for operating cases 1-3 of WSCC power system

Case-1	**Case-2**	**Case-3**
– 1.466 ± j 6.856, 0.209	– 1.876 ± j 6.935, 0.261	– 0.982 ± j 6.791, 0.143
– 2.278 ± j 17.457, 0.129	– 2.918 ± j 16.950, 0.169	– 1.956 ± j 17.143, 0.113

Fig. 5.2 (a)-(c) and (d)-(f) show the eigenvalue maps for without PSS and with HSOPSSs for operating cases 1-3 respectively. The analysis of eigenvalue maps without PSS for unstable and poorly damped modes of cases 1-3 of WSCC power system is discussed in Section 3.4.1 (A). Table 5.2 and Fig. 5.2 (d)-(f) show that the HSOPSSs shift the eigenvalues to a specified D-shape zone in the left half of the *s*-plane with desired damping factor and damping ratio as compared to that of without PSS for all operating cases. Hence, designed HSOPSS controllers provide improved stability and damping characteristics of the WSCC power system as compared to same obtained using without PSS.

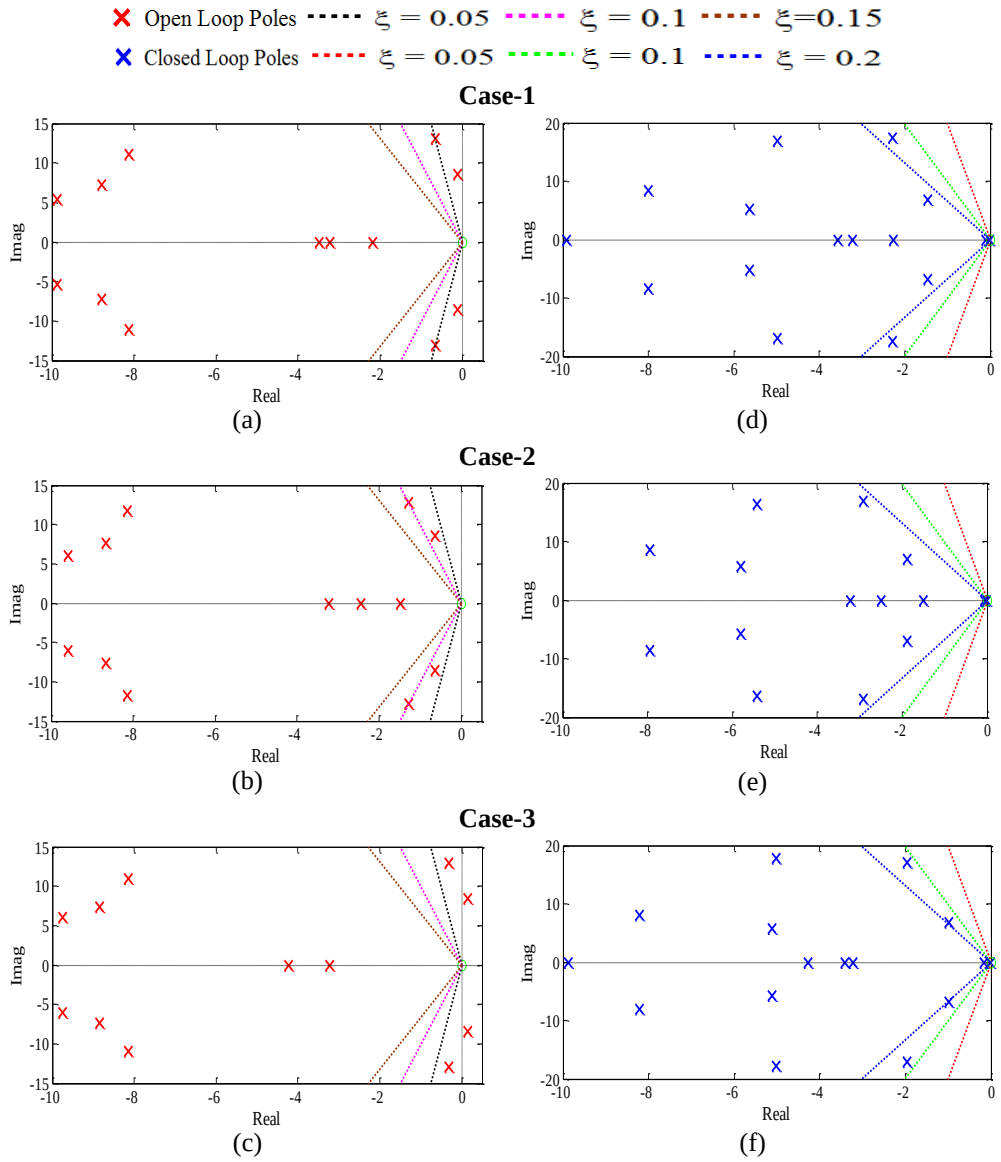

Fig. 5.2 Eigenvalue maps (a)-(c) without PSS and (d)-(f) with HSOPSSs for operating cases 1-3 of WSCC power system

B. Time-Domain Simulation Results and Discussions with HSOPSSs and without PSS of WSCC Power System

The time-domain simulations of WSCC power system is performed with HSOPSS controllers, designed in previous section for observed severe scenarios of operating Case-3 mentioned earlier in Table 3.6. The speed deviations Δw_{12}, Δw_{23} and Δw_{31} for selected severe scenarios of Case-3 for the system without PSS and with HSOPSSs are shown in Fig. 5.3 (a)-(b) and (c)-(d) respectively. The time-domain performance analysis of the system without PSS is already discussed in Section 3.4.1 (B).

It may be clearly observed from Fig. 5.3 (c)-(d) that with HSOPSSs system performance is improved and all oscillations for both scenarios are well damped out. Moreover, the Δw_{12} is most severe due to large peak overshoot and consumed more time to reach in steady state. This illustrates the potential of HSO to obtain a desired set of PSS parameters and the designed

HSOPSSs are capable to damp out oscillations for wide range of operating conditions under variety of severe disturbances.

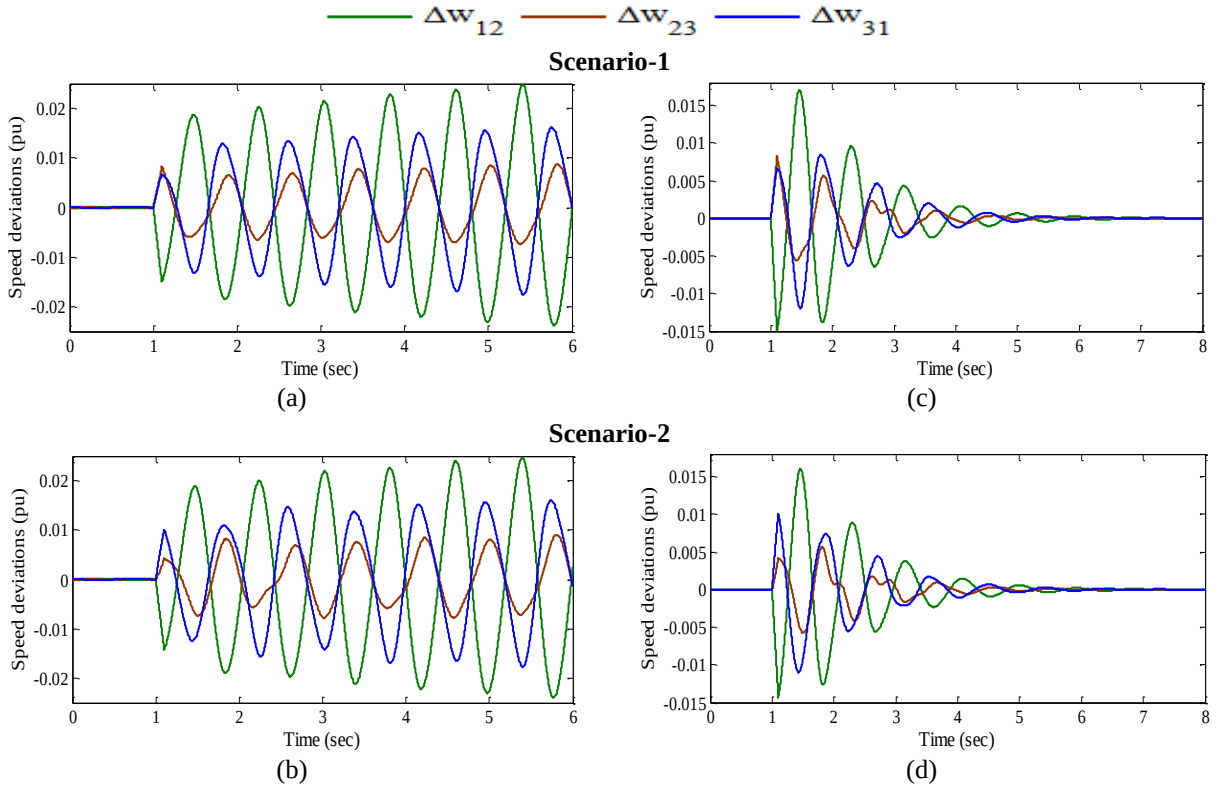

Fig. 5.3 Speed deviations (a)-(b) without PSS and (c)-(d) with HSOPSSs for scenarios 1-2 of operating case-3

C. Performance Indices Results and Discussions with HSOPSSs of WSCC Power System

In addition to simulation results, the effectiveness of designed HSOPSS controllers is also observed by determining two indices *IAE* and *ITAE* for two observed severe scenarios of disturbances. Established both indices are calculated for each scenario of disturbances for operating cases 1-3 and presented as bar charts in the Fig. 5.4 (a)-(b) and (c)-(d) respectively.

The figure depicts that the values of both indices for the HSOPSSs are minimum for each scenario of Case-2 and maximum for each scenario of Case-3, which indicates that Case-3 is the most severe whereas Case-2 is the least severe. Moreover, for operating cases 1 & 3, Scenario-1 is more severe but for Case-2, Scenario-2 is more severe. Comparing Fig. 5.4 with Fig. 3.4, it may be noticed that the designed HSOPSS controllers provide improved damping to damp out low frequency local modes of oscillations with less overshoot and settling time than that of without PSS.

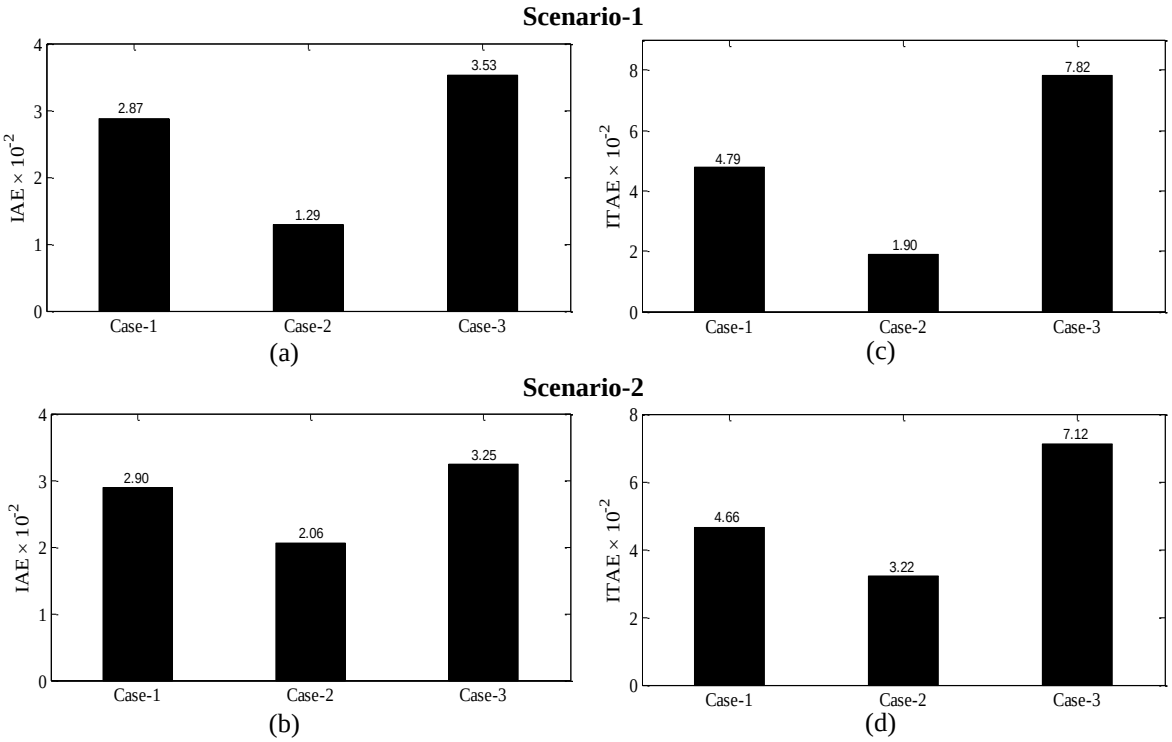

Fig. 5.4 Values of (a)-(b) *IAE* and (c)-(d) *ITAE* with HSOPSSs for scenarios 1-2 of operating cases 1-3

D. Robustness Test of HSOPSSs Controllers of WSCC Power System

To test the robustness of earlier designed HSOPSS controllers for WSCC power system, three unseen operating cases 4-6 mentioned in Table 3.7 are considered. In this section, the effectiveness of HSOPSS controllers for these unseen cases is evaluated by eigenvalue analysis, time-domain simulation results, and performance indices and compared with that of without PSS.

Open-loop eigenvalues, damping ratio, frequency, participation modes and participation factor for unseen cases 4-6 of WSCC power system without PSS are illustrated in Table 3.8 and discussed in Section 3.4.1 (D). Now, the designed HSOPSSs parameters are used to obtain closed-loop eigenvalues and damping ratio using PSAT [215]. Table 5.3 shows the closed-loop eigenvalues and damping ratio for unseen cases 4-6 of WSCC power system with HSOPSS controllers for only unstable and poorly damped modes.

Table 5.3: Eigenvalues and damping ratio with HSOPSSs for unseen operating cases 4-6 of WSCC power system

Case-4	**Case-5**	**Case-6**
– 0.939 ± j 6.922, 0.134	– 0.828 ± j 6.835, 0.120	– 0.746 ± j 6.827, 0.108
– 2.038 ± j 17.156, 0.118	– 1.974 ± j 17.283, 0.113	– 1.816 ± j 17.429, 0.103

The table reveals that the HSOPSSs shift the eigenvalues in the left half of the *s*-plane with improved damping factor and damping ratio as compared to without PSS for all unseen cases. This ensures that the system will be stable for all considered unseen cases also. It is also observed that designed HSOPSS controllers satisfy the earlier selected criterion for the value of

desired damping factor and damping ratio for PSS design. Hence, the designed HSOPSSs are robust as it works with acceptable damping performance for unseen operating cases 4-6 of the WSCC power system also.

In order to further examine the robustness performance of the HSOPSSs in terms of speed deviations, the time-domain simulations are performed using PSAT [215] for two earlier observed severe scenarios of disturbances on unseen operating cases 4-6 of WSCC power system. The speed deviations Δw_{12}, Δw_{23} and Δw_{31} without PSS for scenarios 1 and 2 of cases 4-6 are shown in Fig. 5.5 (a)-(c) and Fig. 5.6 (a)-(c) respectively whereas the Δw_{12}, Δw_{23} and Δw_{31} with HSOPSSs are shown in Fig. 5.5 (d)-(f) and Fig. 5.6 (d)-(f) respectively.

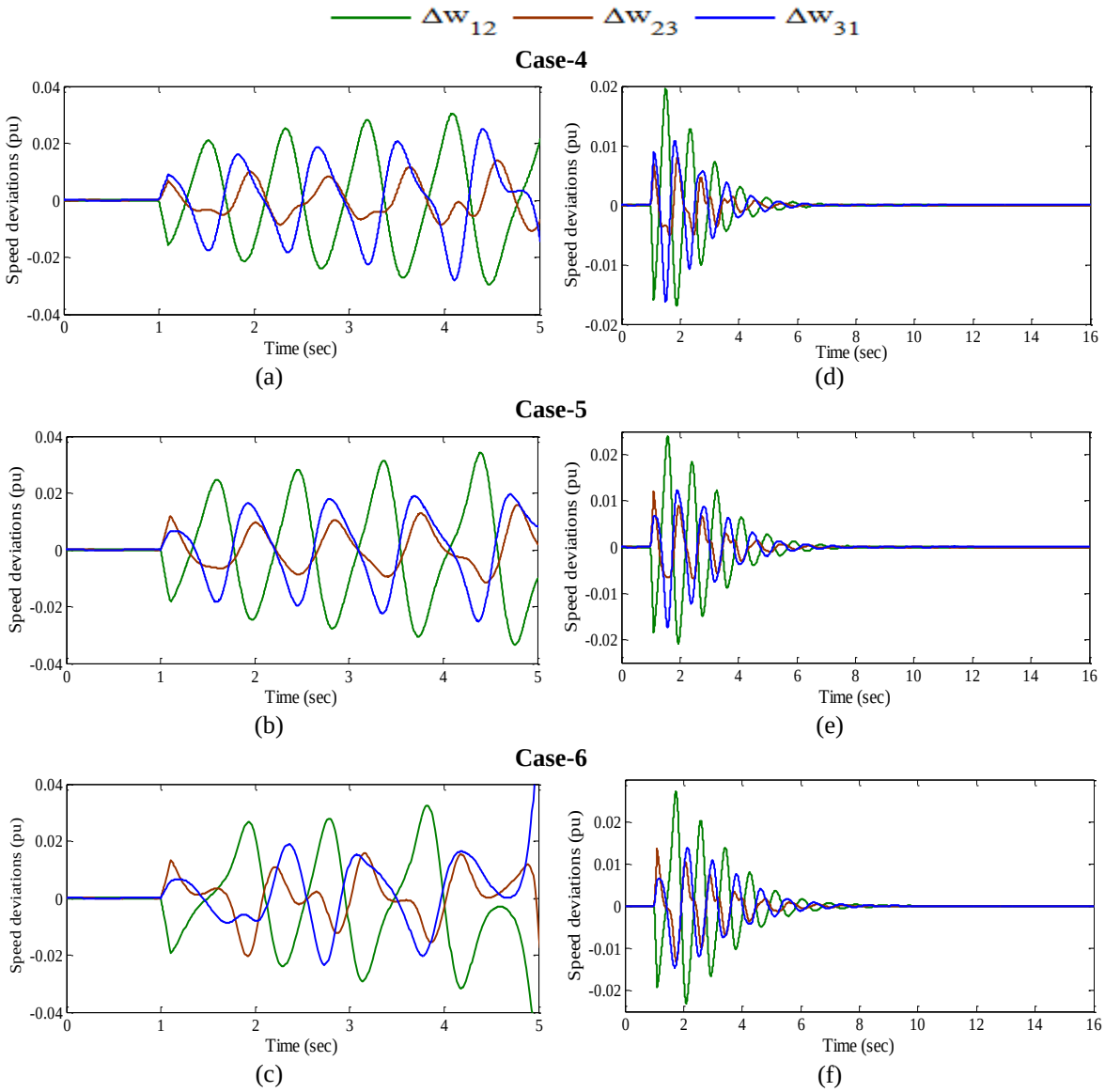

Fig. 5.5 Speed deviations (a)-(c) without PSS and (d)-(f) with HSOPSSs for scenario-1 of operating cases 4-6

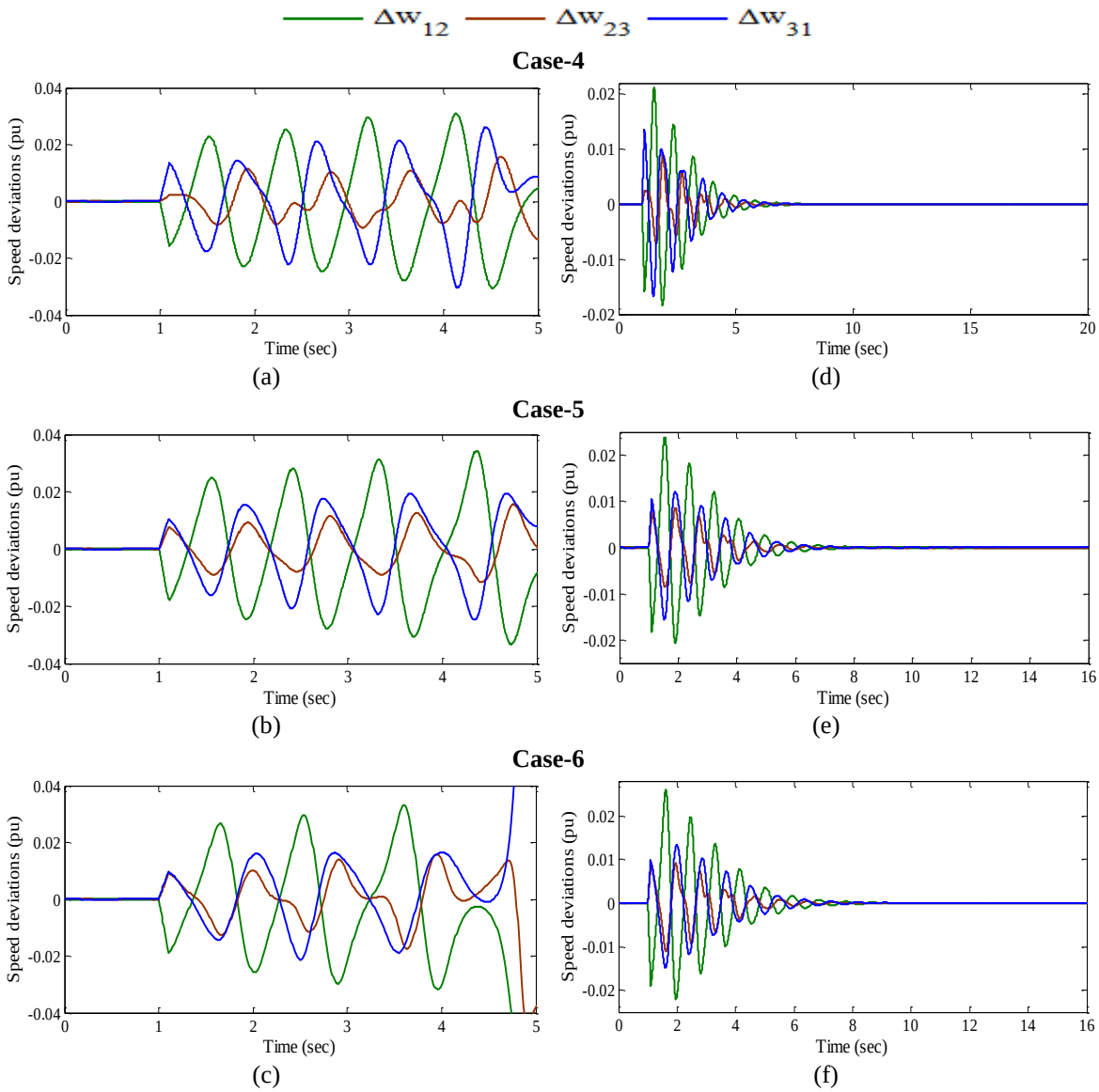

Fig. 5.6 Speed deviations (a)-(c) without PSS (d)-(f) with HSOPSSs for scenario-2 of operating cases 4-6

The analysis of response plots without PSS is already discussed in Section 3.4.2 (D). From Fig. 5.5 (d)-(f) and 5.6 (d)-(f), it may be clearly observed that with HSOPSSs, the speed deviation responses for scenarios 1-2 of Case-6 produce more oscillations as compared to other cases. Moreover, peak overshoot in speed deviation responses for scenarios 1-2 of Case-6 is more as compared to other cases. Furthermore, the speed deviations with HSOPSSs for scenarios 1-2 of unseen operating cases 4-6 take more time to damp out LFO as compared to earlier cases 1-3. This may be concluded that the designed HSOPSSs work acceptably for all the scenarios of severe disturbances of unseen operating cases of WSCC power system.

In addition to time-domain simulation results, the effectiveness and robustness of HSOPSS controllers is also noticed by evaluating indices *IAE* and *ITAE* for observed scenarios of unseen operating cases. Established both indices with HSOPSSs are determined for each

scenario of disturbances for operating cases 4-6 and presented as bar charts in the Fig. 5.7 (a)-(b) and (c)-(d) respectively.

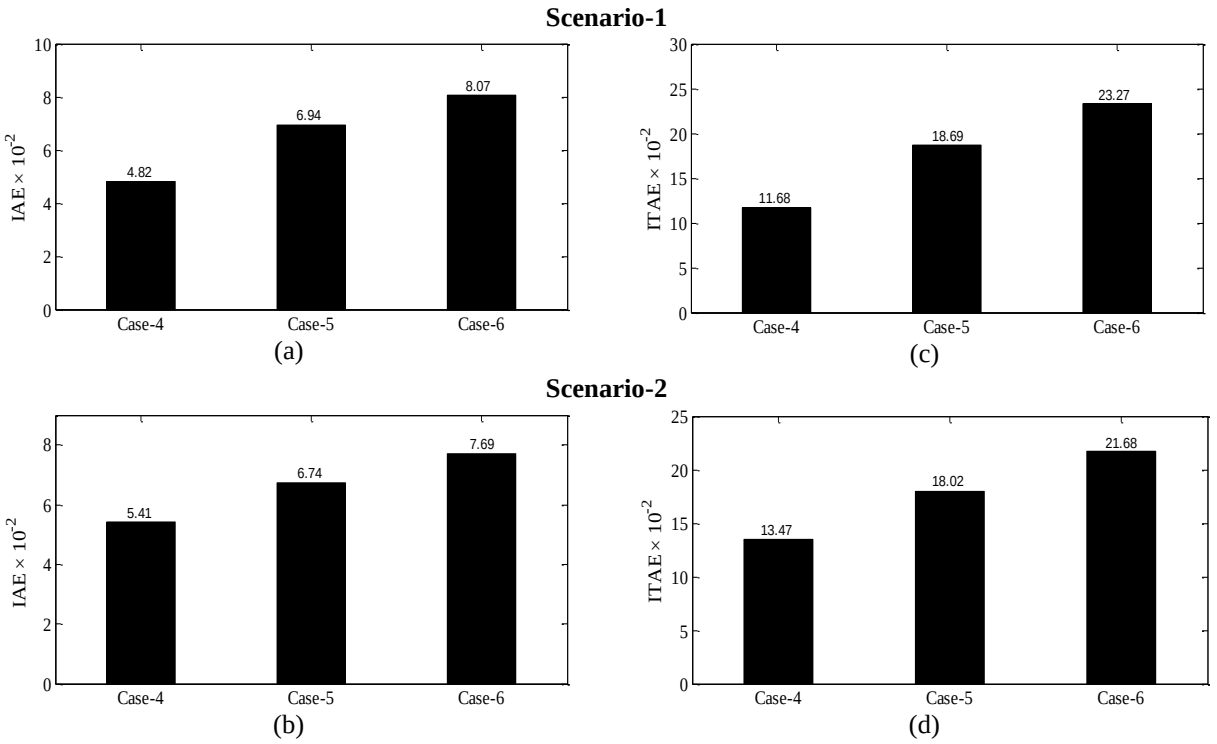

Fig. 5.7: Values of (a)-(b) *IAE* and (c)-(d) *ITAE* with HSOPSSs for scenarios1-2 of operating cases 4-6

The figure reveals that the values of both indices for the HSOPSSs are minimum for each scenario of Case-4 and maximum for each scenario of Case-6, which indicates that Case-6 is the most severe whereas Case-4 is the least severe. Moreover, for operating Case-4, Scenario-2 is more severe but for cases 5-6, Scenario-1 is more severe.

Hence, the designed HSOPSS controllers for WSCC power system is capable to damp out LFO with enhanced stability and damping performance for wide range of operating cases under different scenarios of severe disturbances and also for unseen operating cases under same scenarios of disturbances.

5.2.2 Example 2: Two-Area, Four-Machine (TAFM) Power System

The operating condition details and single line diagram of TAFM power system is described in Section 3.4.2 and Appendix respectively.

A. Eigenvalue Analysis of TAFM Power System without PSS and with HSOPSSs

The open-loop eigenvalues, damping ratio, frequency, participation modes and participation factor associated with electromechanical modes of the system are depicted in Table 3.10 and discussed in Section 3.4.2 (A). An eigenvalue-based multi-objective function *J* presented in (3.1) is minimized using HSO by tuning the nine parameters of PSSs. The HSO is

applied with population size 50, maximum generation 50, *HMCR* = 0.75, *PAR* = 0.30, *BW* = 0.01. The HSO is able to find the desired solution for which fitness function *J* is zero. The final value of *J* equal to zero indicates that three unstable and/or poorly damped eigenvalues are shifted to a specified D-shape zone in the left-half of the *s*-plane. The optimum designed nine parameters of GAPSSs for three generators are shown in Table 5.4. The closed-loop eigenvalues and their damping ratio with unstable and lightly damped modes using HSOPSSs for three loading cases are determined using PSAT [215] and shown in Table 5.5.

Table 5.4: Optimal designed parameters of HSOPSSs for TAFM power system

Generators	***K***	T_1	T_3
G_1	22.600	0.044	0.013
G_2	84.786	0.034	0.064
G_4	34.392	0.072	0.025

Table 5.5: Eigenvalues and damping ratio with HSOPSSs for loading cases 1-3 of TAFM power system

Case-1	**Case-2**	**Case-3**
– 1.085 ± j 4.318, 0.24	– 1.000 ± j 3.602, 0.26	– 1.127 ± j 5.401, 0.20
– 4.920 ± j 4.658, 0.72	– 2.996 ± j 1.555, 0.88	– 2.623 ± j 3.873, 0.56
– 3.228 ± j 1.803, 0.87	– 4.741 ± j 4.268, 0.74	– 4.964 ± j 1.080, 0.97

Fig. 5.8 (a)-(c) and (d)-(f) show the eigenvalue maps for without PSS and with HSOPSSs for cases 1-3 respectively. The eigenvalue maps of without PSS for unstable and lightly damped modes with TAFM system are discussed in Section 3.4.2 (A). Table 5.5 and Fig. 5.8 (d)-(f) show that the HSOPSSs shift the eigenvalues to a specified D-shape zone in the left half of the *s*-plane with desired damping factor and damping ratio as compared to that of without PSS for all loading cases. Hence, designed HSOPSS controllers provide improved stability and damping performance of the TAFM power system as compared to same obtained using without PSS.

B. Time-Domain Simulation Results and Discussions with HSOPSSs and without PSS of TAFM Power System

The time-domain simulations of TAFM power system is performed with designed HSOPSSs for different test scenarios mentioned earlier in Table 3.14 of severe loading cases. The speed deviations $\Delta w_1, \Delta w_2, \Delta w_3$ and Δw_4 for the system without PSS and with HSOPSSs are shown in Fig. 5.9 (a)-(d) and (e)-(h) respectively. The analysis of response plots without PSS already discussed in Section 3.4.2 (B).

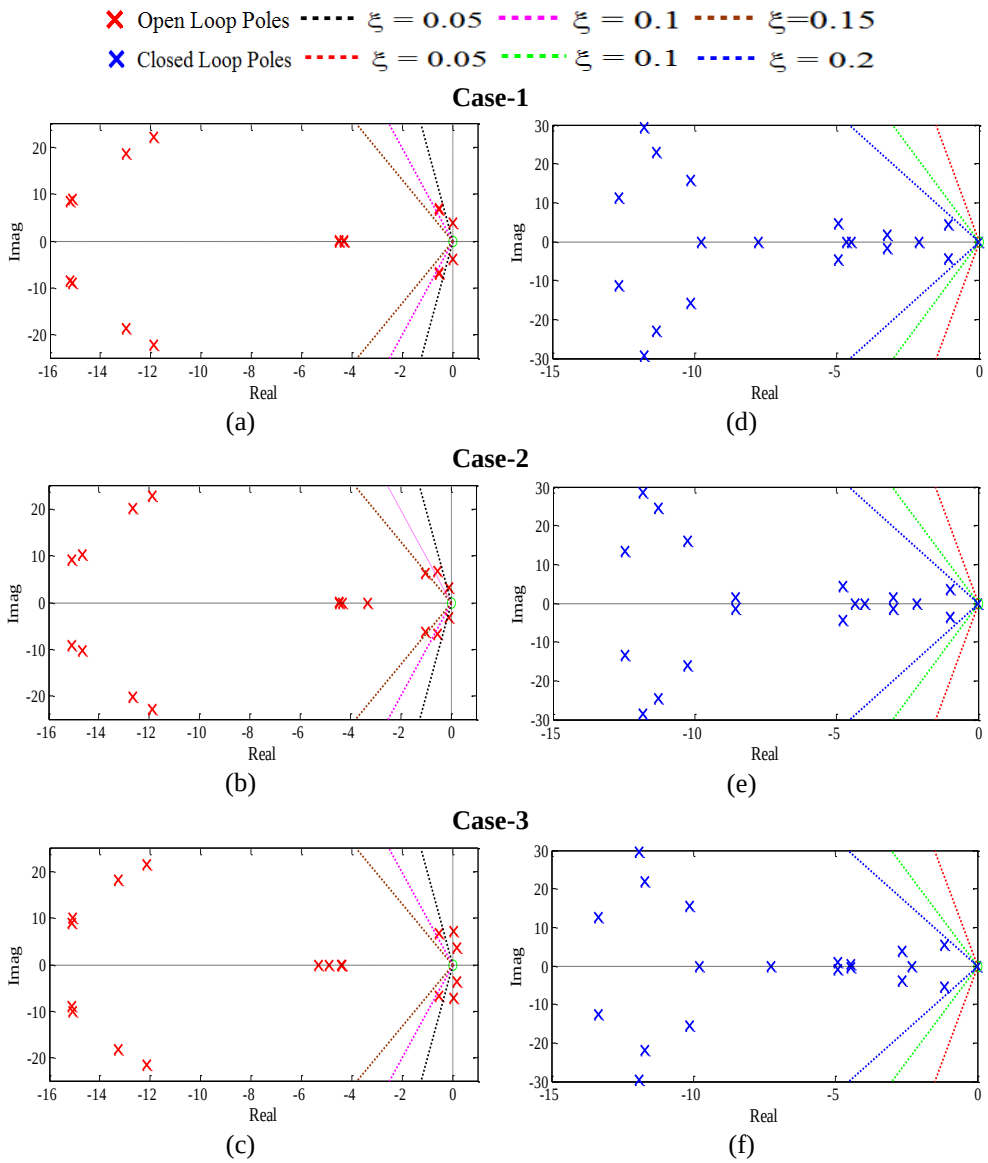

Fig. 5.8 Eigenvalue maps (a)-(c) without PSS (d)-(f) with HSOPSSs for loading cases 1-3 of TAFM power system

From Fig. 5.9 (e)-(h), it is observed that with HSOPSSs, oscillations for all generators are well damped out with less overshoot and settling time for all scenarios of severe loading cases. Moreover, it is clear that the system performance with HSOPSSs is improved than that of without PSS for all severe disturbance scenarios of loading cases and oscillations are die out smoothly. Furthermore, on the basis of number of cycles of operation, it may be observed that that the speed response with HSOPSSs for Scaneraio-4 consumed more time to damp out oscillations as compared to Scenario-2 of loading Case-3.

This demonstrates the potential of HSO to obtain a desired set of PSS parameters for TAFM power system and the designed HSOPSSs are able to improve the damping performance of the system than that of without PSS for wide range of loading cases under severe scenarios of disturbances.

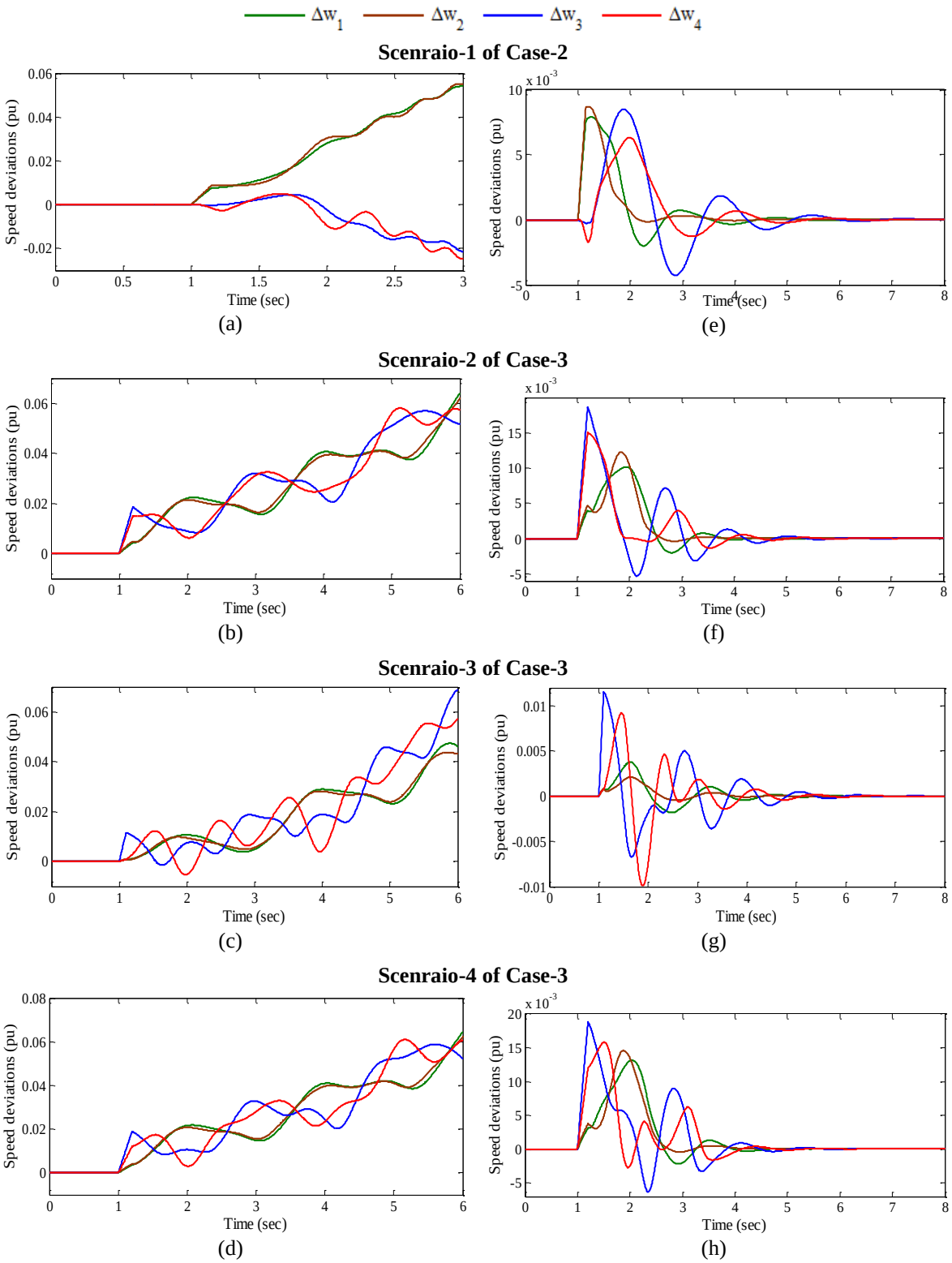

Fig. 5.9 Speed deviations (a)-(d) without PSS (e)-(h) with HSOPSSs for scenarios 1-4 of severe loading cases

C. Performance Indices Results and Discussions with HSOPSSs of TAFM Power System

In addition to simulation results, the effectiveness of HSOPSS controllers is also observed by determining indices *IAE* and *ITAE* values for considered scenarios of different disturbances mentioned in Table 3.14. The bar charts of both indices obtained by HSOPSSs for scenarios 1-4 of loading cases 1-3 are shown in Fig. 5.10 (a)-(d) and (e)-(h) respectively.

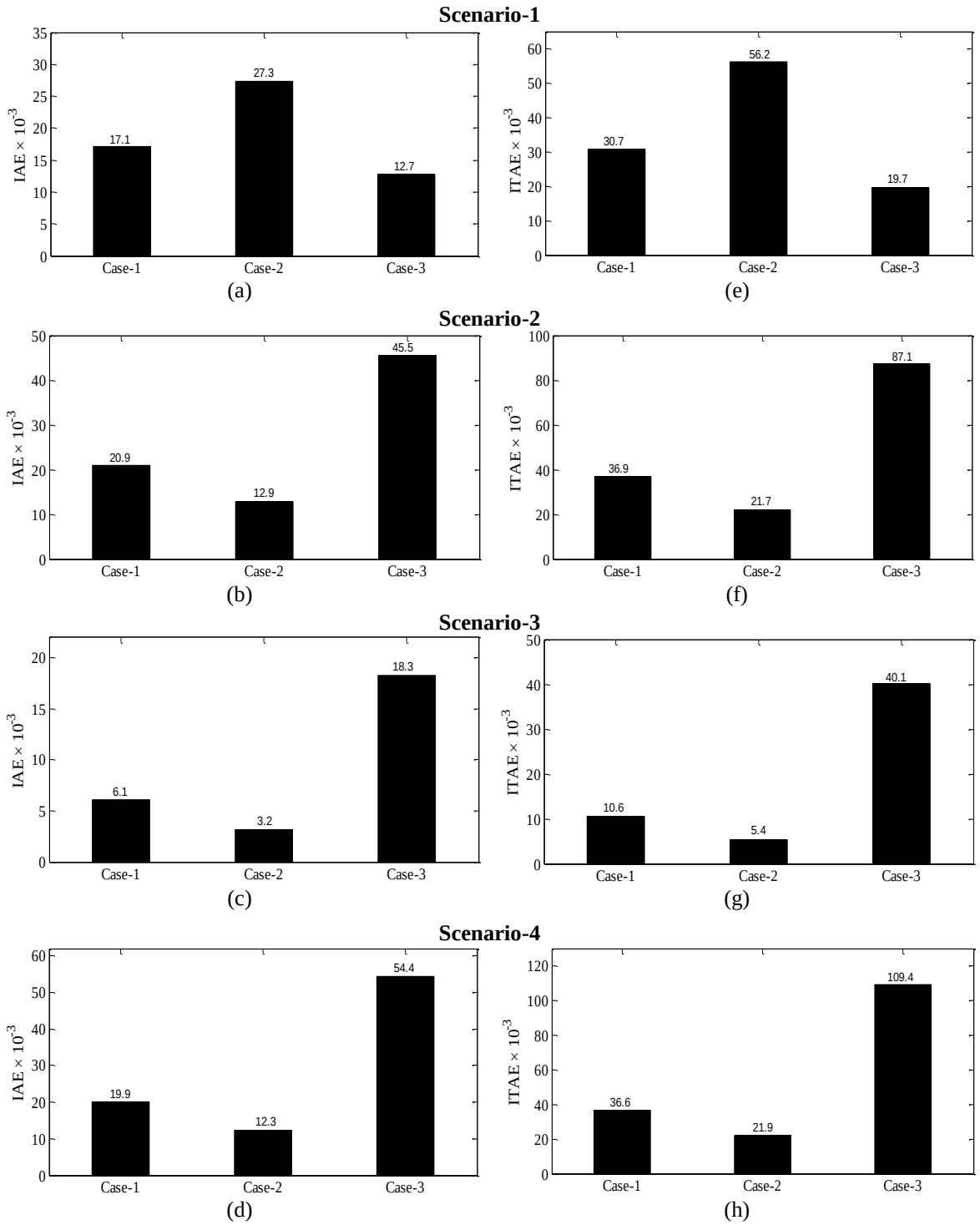

Fig. 5.10 Values of (a)-(d) *IAE* and (e)-(h) *ITAE* with HSOPSSs for scenarios 1-4 of loading cases 1-3

The figure reveals that both indices values for the HSOPSSs are higher for Scenario-1 of Case-2 loading and lower for Case-3 loading. Similarly, both indices are lower for scenarios 2-4 of Case-2 and higher for Case-3 loading, which indicates that Case-3 is the most severe for scenarios 2-4 whereas Case-2 is the least severe. Comparing Fig. 5.10 with Fig. 3.11, it may be observed that the designed HSOPSS controllers provide sufficient damping to damp out low frequency local and inter-area modes of oscillations with less overshoot and settling time than

that of without PSS, although the disturbances are simulated for more number of cycles on the system with HSOPSSs.

D. Robustness Test of HSOPSS Controllers of TAFM Power System

To test the robustness of previously design HSOPSS controllers for TAFM power system, nine unseen operating cases 4-12 are depicted in Table 3.15. In this section, the effectiveness of designed HSOPSSs is checked by eigenvalue analysis, time-domain simulation results and performance indices for unseen cases and compared with that of without PSS.

Open-loop eigenvalues, damping ratio, frequency, participation modes and participation factor for unseen operating cases 4-12 of TAFM power system without PSS are illustrated in Table 3.16 and explained in Section 3.4.2 (D). Now, previously designed HSOPSSs parameters are used to obtain closed-loop eigenvalues and damping ratio using PSAT [215] for unseen cases 4-12 of TAFM power system for only unstable and poorly damped modes are shown in Table 5.6.

Table 5.6: Eigenvalues and damping ratio with HSOPSSs for unseen operating cases 4-12 of TAFM power system

Cases	**With HSOPSSs**		
Case-4	– 4.249 ± j 4.479, 0.688	– 1.473 ± j 3.759, 0.365	– 3.323 ± j 1.819, 0.877
Case-5	– 2.451 ± j 3.108, 0.619	– 1.311 ± j 5.617, 0.227	– 10.119 ± j 15.675, 0.542
Case-6	– 4.237 ± j 4.485, 0.686	– 1.467 ± j 3.765, 0.363	– 12.806 ± j 11.598, 0.741
Case-7	– 2.440 ± j 3.111, 0.617	– 1.309 ± j 5.622, 0.226	– 10.095 ± j 15.663, 0.541
Case-8	– 0.961 ± j 3.568, 0.260	– 4.337 ± j 4.125, 0.724	– 8.387 ± j 1.778, 0.978
Case-9	– 2.228 ± j 3.571, 0.529	**– 0.938** ± j 5.745, **0.161**	– 13.520 ± j 13.591, 0.705
Case-10	– 2.321 ± j 2.812, 0.636	**– 0.924** ± j 5.907, **0.154**	– 10.143 ± j 15.653, 0.543
Case-11	– 2.308 ± j 2.812, 0.634	**– 0.921** ± j 5.910, **0.154**	– 10.120 ± j 15.642, 0.543
Case-12	– 0.955 ± j 3.583, 0.257	– 3.731 ± j 4.082, 0.674	– 8.301 ± j 1.978, 0.972

The table reveals that the HSOPSSs shift the eigenvalues in the left half of the *s*-plane with improved damping factor and damping ratio as compared to without PSS for unseen cases 4-12. This ensures that the TAFM power system will be stable for all considered unseen cases also. It is also observed that HSOPSS controllers satisfy the earlier selected criterion for the value of desired damping factor and damping ratio for PSS design except in unseen cases 9-11 where slightly more overshoot and settling time may occur. Hence, the HSO provides robustness with improved stability and grater damping performance for unseen operating cases 4-12 of the TAFM power system as compared to that of without PSS.

In order to check the robustness performance of designed HSOPSS controllers in terms of speed deviations, earlier severe scenarios 5-13 of unseen operating cases 4-12 of TAFM power system mentioned in Table 3.17 are considered.

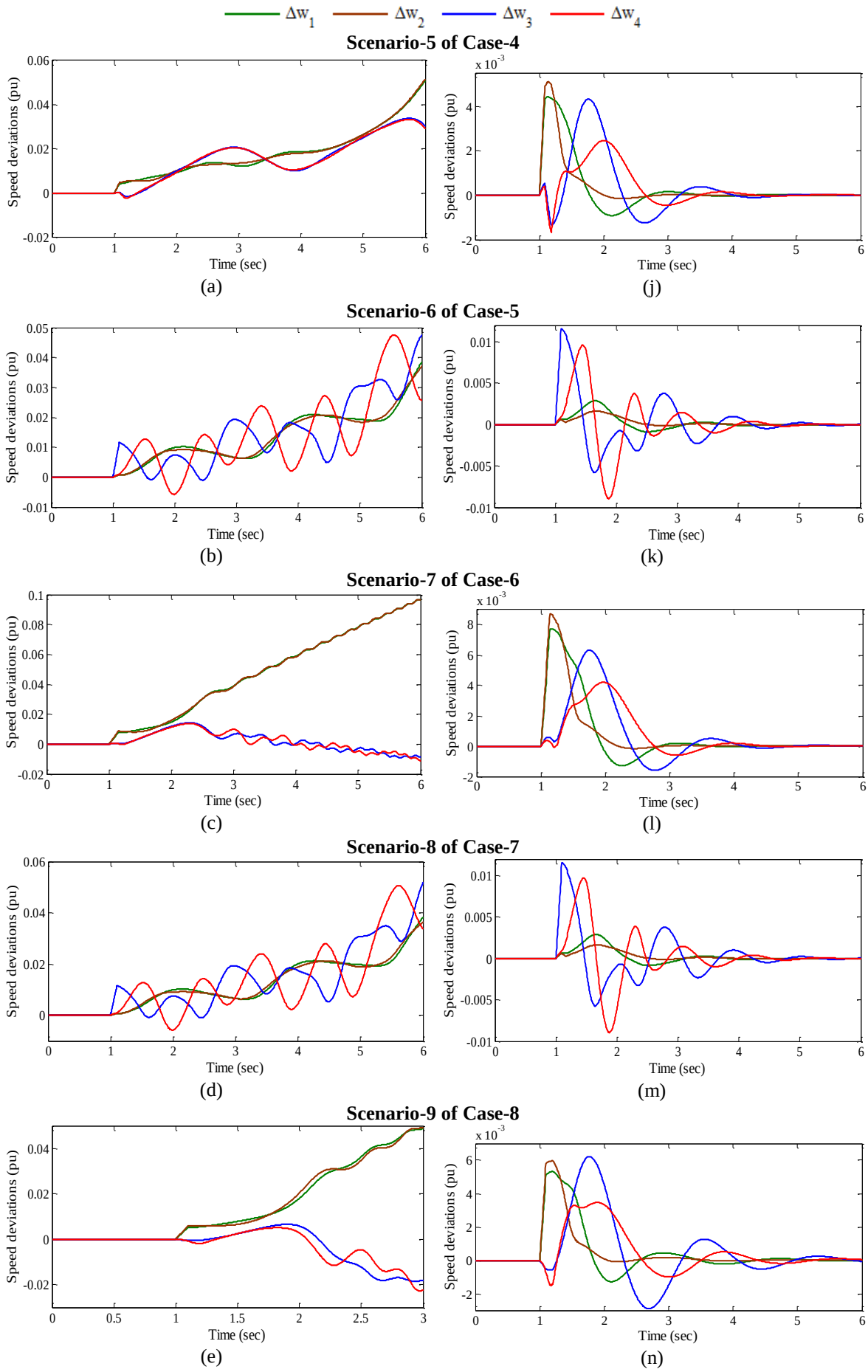
Δw1 Δw2 Δw3 Δw4
Scenario-5 of Case-4
Speed deviations (pu)
Time (sec)
x 10-3
(a)
(j)
Scenario-6 of Case-5
(b)
(k)
Scenario-7 of Case-6
(c)
(l)
Scenario-8 of Case-7
(d)
(m)
Scenario-9 of Case-8
(e)
(n)

Cont-

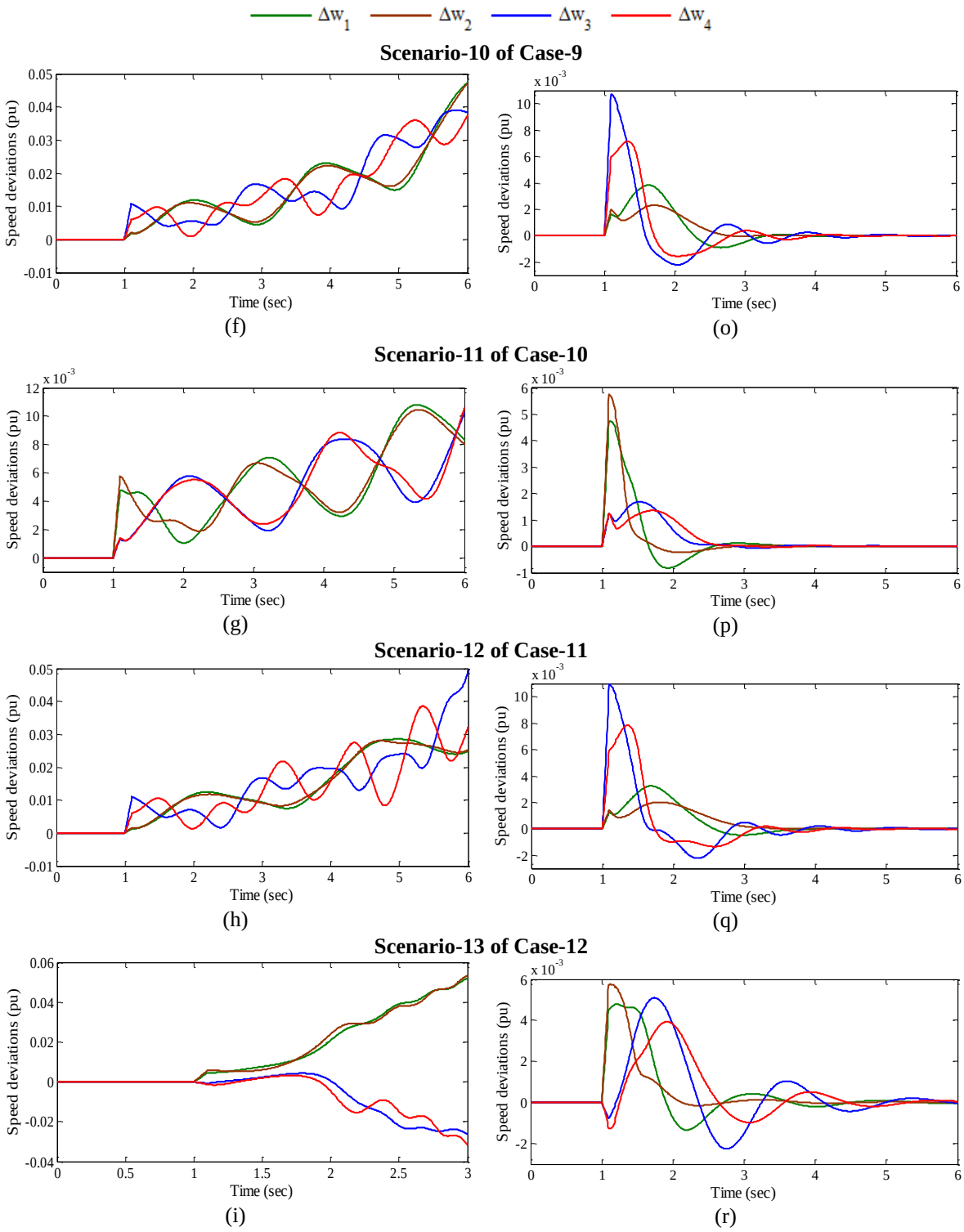

Fig. 5.11 Speed deviations (a)-(i) without PSS and (j)-(r) with HSOPSSs for scenarios 5-13 of unseen operating cases 4-12

The speed deviations Δw_1, Δw_2, Δw_3 and Δw_4 for the system without PSS and with HSOPSSs for scenarios 5-13 of unseen cases 4-12 are shown in Fig. 5.11 (a)-(i) and (j)-(r).

The analysis of response plots without PSS already discussed in Section 3.4.2 (B). From Fig. 5.11 (j)-(r), it is noticed that the system performance with HSOPSSs is improved for severe disturbance scenarios 6-13 of unseen operating cases 4-12 and oscillations are well damped out. Furthermore, the comparison of speed deviations with HSOPSSs basis on number of cycle

operation, the Scenario-9 of Case-8 takes more time to reach in steady state than other scenarios. This may be concluded that the designed HSOPSSs work satisfactorily for most of the scenarios of severe disturbances of unseen operating cases of TAFM power system.

In addition to time-domain simulation results, the robustness and effectiveness of HSOPSS controllers is also noticed by calculating indices *IAE* and *ITAE* for observed scenarios 5-13 of unseen operating cases 4-12. The bar charts of both indices values obtained with HSOPSSs, for defined scenarios are shown in Fig. 5.12 (a) and (b) respectively.

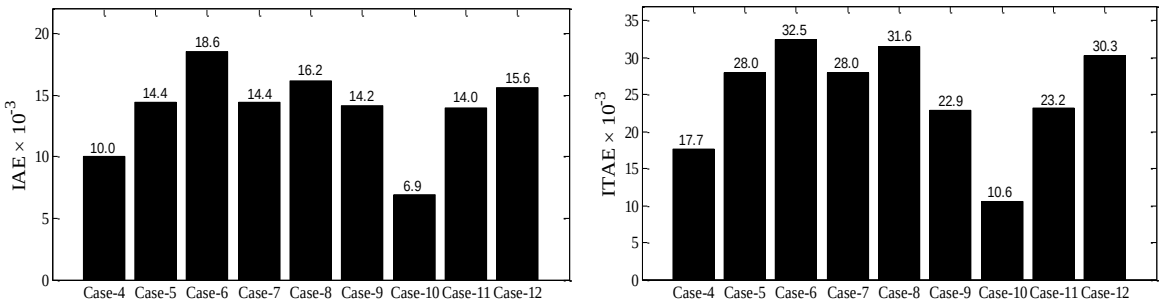

(a) (b)

Fig. 5.12 Value of (a) *IAE* (b) *ITAE* with HSOPSSs for nine observed scenarios 5-13 of unseen operating cases 4-12

In above figure, both indices with HSOPSSs for corresponding scenarios of Case-4 and Case-6 are evaluated for 5 and 9-cycle of operation respectively whereas remaining cases are determined for 6-cycle of operation. Both indices values with HSOPSSs are minimum and maximum for 6-cycle operation of unseen cases 10 and 8 respectively. Therefore, it is concluded that with HSOPSSs, Scenario-11 of Case-10 and Scenario-9 of Case-8 are least and most severe scenarios of disturbance respectively.

Hence, the designed HSOPSS controllers for TAFM power system is capable to damp out low frequency local and inter-area modes of oscillations with improved stability and damping performance for wide range of loading cases under different scenarios of severe disturbances and also for unseen operating cases under severe scenarios of disturbances.

5.2.3 Example 3: Ten-Machine, Thirty-Nine Bus New England Power System (NEPS)

The operating condition details and single-line diagram of NEPS is described in Section 3.4.3 and Appendix respectively.

A. Eigenvalue Analysis of NEPS without PSS and with HSOPSSs

Open-loop eigenvalues, damping ratio, frequency, participation modes and participation factor associated with electromechanical modes of the system are illustrated in Table 3.19 and discussed in Section 3.4.3 (A). An eigenvalue-based multi-objective function *J* (equation 3.1) presented in Section 3.2 is minimized using HSO for designing twenty-seven PSS parameters of

nine generators. The HSO is applied with population size 100, maximum generation 100, *HMCR* = 0.75, *PAR* = 0.30, *BW* = 0.01.

The HSO is able to find the desired solution for which fitness function *J* is zero. The final value of *J* equal to zero indicates that nine unstable and/or poorly damped eigenvalues are shifted to a specified D-shape zone in the left-half of the *s*-plane. The optimum designed parameters for PSOPSSs are shown in Table 5.7.The closed-loop eigenvalues and their damping ratio with HSOPSSs for loading cases 1-3 are determined using PSAT [215] and are shown in Table 5.8.

Table 5.7: Optimal designed parameters of HSOPSSs for NEPS

Optimized Parameters	**Generators**								
	G_2	G_3	G_4	G_5	G_6	G_7	G_8	G_9	G_{10}
K_1	13.282	1.851	100	51.298	9.589	77.368	8.677	38.04 o	6.004
T_1	0.012	1.000	0.153	0.018	0.263	0.010	0.557	0.010	1.000
T_3	0.997	1.000	0.073	0.207	0.010	0.368	0.644	0.603	0.327

Table 5.8: Eigenvalues and damping ratio with HSOPSSs for loading cases 1-3 of NEPS

Case-1	**Case-2**	**Case-3**
– 1.812 ± j 9.262, 0.192	– 1.490 ± j 9.092, 0.161	– 1.719 ± j 16.765, 0.102
– 1.351 ± j 8.337, 0.160	– 1.390 ± j 8.283, 0.165	– 1.306 ± j 8.308, 0.155
– 0.948 ± j 8.420, 0.111	– 0.999 ± j 8.362, 0.118	– 0.897 ± j 8.384, 0.106

Figure 5.14 (a)-(c) and (d)-(f) present the eigenvalue maps for without PSS and with HSOPSSs of NEPS for loading cases 1-3 respectively. The eigenvalue maps of without PSS for unstable and lightly damped modes of NEPS are discussed in Section 3.4.3 (A). Table 5.8 and Fig. 5.13 (d)-(f) show that the HSOPSSs shift the eigenvalues to a specified D-shape zone in the left half of the *s*-plane with desired damping factor and damping ratio as compared to without PSS for three loading cases. Hence, HSOPSS controllers provide improved stability and damping characteristics of the NEPS as compared to same obtained using without PSS.

B. Time-Domain Simulation Results and Discussions with HSOPSSs and without PSS of NEPS

The simulations of NEPS are performed with PSSs for five different scenarios of disturbances mentioned in Table 3.24 for three loadings cases. The speed deviations $\Delta w_1, \Delta w_2$, Δw_3, Δw_4, Δw_5, $\Delta w_6, \Delta w_7$, $\Delta w_8, \Delta w_9$ and Δw_{10} for without PSS and with HSOPSSs for scenarios 1-5 of severe Case-3 loading are shown in Fig. 5.14 (a)-(e) and (f)-(i) respectively. The analysis of response plots without PSS already discussed in Section 3.4.3 (B). Figure 5.14 (f)-(j) reveals that the speed response with HSOPSSs for Scenario-1 of Case-3 loading have large peak overshoot and consumed more time to die out oscillations as compared to others.

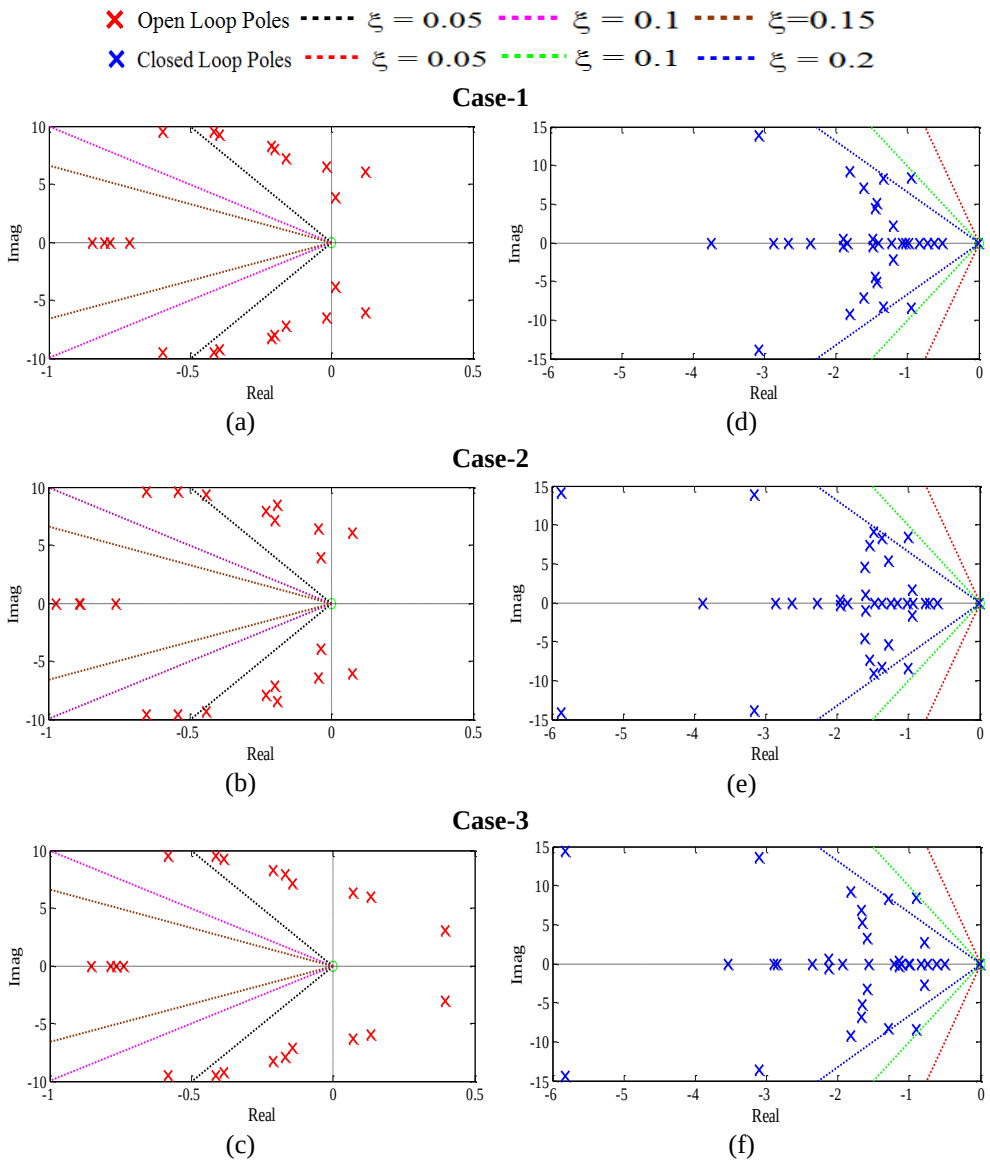

Fig. 5.13 Eigenvalue maps (a)-(c) without PSS (d)-(f) with HSOPSSs for loading cases 1-3 of NEPS

Therefore, it is concluded that with HSOPSSs Scenario-1 is most severe scenario than others. This demonstrates the potential of HSO technique to obtain the desired set of PSS parameters for NEPS and the designed HSOPSSs are capable to damp out LFO for wide range of operating cases under severe scenarios of disturbances.

C. Performance Indices Results and Discussions with HSOPSSs of NEPS

In addition to simulation results, the effectiveness of designed HSOPSS controller is also observed by determining indices *IAE* and *ITAE* for earlier five observed scenarios of different disturbances. The bar charts of both indices values obtained by HSOPSS controllers for scenarios 1-5 of three loading cases are shown in Fig. 5.15 (a)-(e) and (f)-(j) respectively.

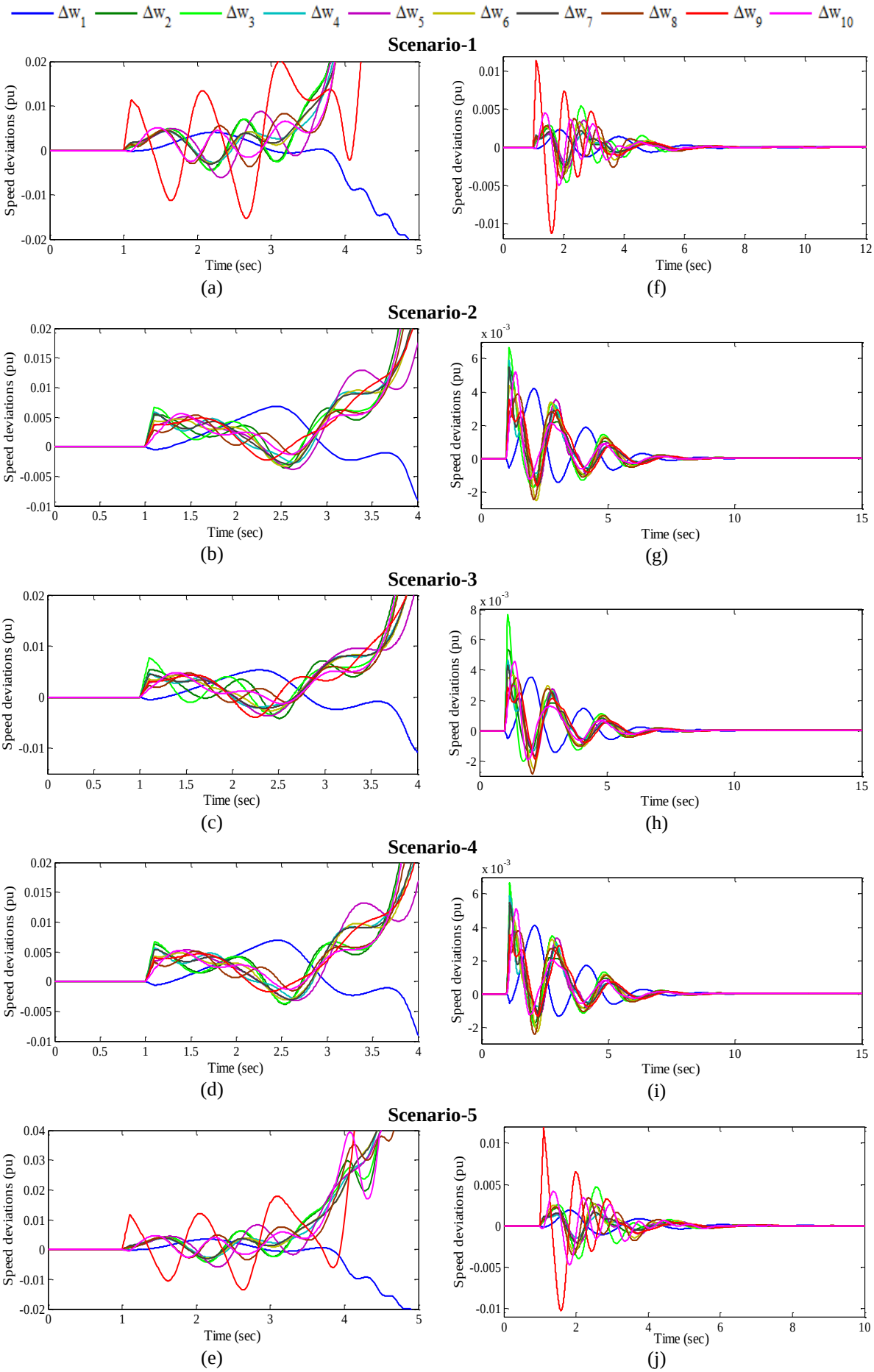

Fig. 5.14 Speed deviations (a)-(e) without PSS and (i)-(j) with HSOPSSs for scenarios 1-5 of loading case-3

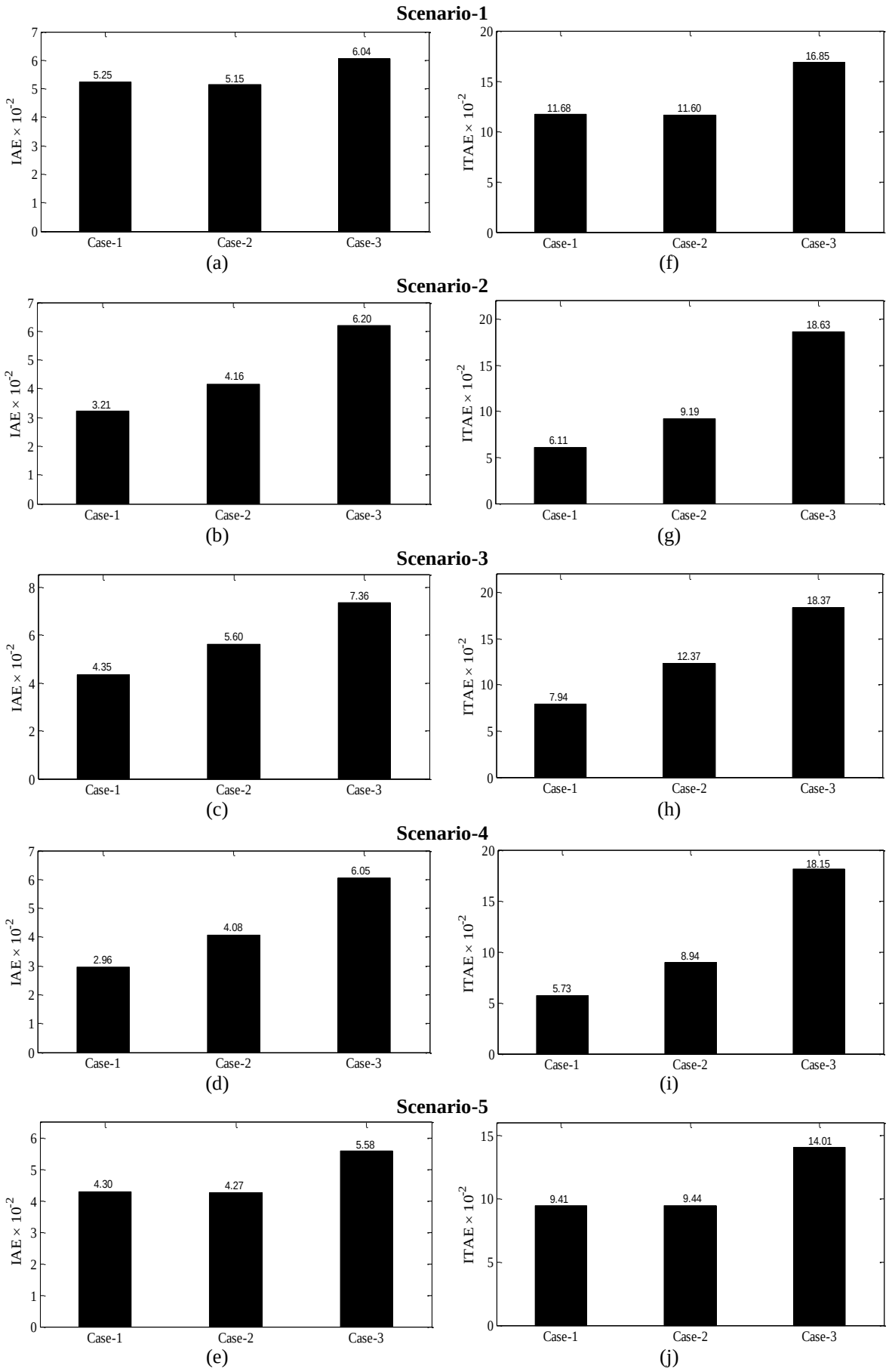

Fig. 5.15 Values of (a)-(e) *IAE* and (f)-(j) *ITAE* with HSOPSSs for scenarios 1-5 of loading cases 1-3

The values of both indices with HSOPSSs for scenarios 1 & 5 of loading Case-1 and Case-3 are minimum and maximum respectively whereas for scenarios 2-4 of loading Case-2 and Case-3 are minimum and maximum respectively. Moreover, the Scenario-2 and Scenario-5 for Case-3 loading is most and least severe scenario than others. Comparing Fig. 5.15 with Figs. 3.18 and 3.19, it may be observed that the designed HSOPSSs controllers of NEPS provide sufficient damping to damp out low frequency local and inter-area modes of oscillation with less overshoot and settling time than that of without PSS.

D. Robustness Test of Designed HSOPSS Controllers of NEPS

To test the robustness of previously designed HSOPSS controllers, fifteen unseen operating cases 4-18 mentioned in Table 3.25 are considered. In this section, the effectiveness of HSOPSS controllers is checked by eigenvalue analysis, time-domain simulation results and performance indices for four observed scenarios of cases 4-18 and compared with to that of without PSS. Open-loop eigenvalues, damping ratio, frequency, participation modes and participation factor for only unstable and critical lightly damped modes of unseen cases 4-18 of NEPS without PSS illustrated in Table 3.26 and discussed in Section 3.4.3 (D). Table 5.9 shows the closed-loop eigenvalues and damping ratio for unseen cases 4-19 of NEPS with HSOPSS controllers for only unstable and critical poorly damped modes respectively.

Table 5.9: Eigenvalues and damping ratio with HSOPSSs for unseen operating cases 4-18 of NEPS

Cases	**With HSOPSSs**		
Case-4	– 1.207 ± j 7.664, 0.155	– 1.411 ± j 5.125, 0.265	– 3.536 ± j 13.616, 0.251
Case-5	– 1.292 ± j 8.389, 0.152	– 1.466 ± j 7.671, 0.187	– 3.128 ± j 13.735, 0.222
Case-6	– 1.196 ± j 4.409, 0.261	– 1.152 ± j 2.216, 0.469	– 1.377 ± j 8.342, 0.162
Case-7	– 1.359 ± j 8.342, 0.160	– 1.608 ± j 7.207, 0.217	– 1.176 ± j 2.093 0.489
Case-8	– 1.292 ± j 8.388, 0.152	– 0.848 ± j 1.978, 0.394	– 1.354 ± j 7.641, 0.174
Case-9	**– 0.476** ± j 1.740, 0.264	– 1.577 ± j 6.848, 0.224	– 1.324 ± j 3.657, 0.340
Case-10	– 1.091 ± j 6.478, 0.168	– 1.093 ± j 2.239, 0.438	– 1.506 ± j 7.854, 0.188
Case-11	**– 0.737** ± j 1.814, 0.376	– 1.598 ± j 7.390, 0.211	– 1.723 ± j 9.076, 0.186
Case-12	– 1.089 ± j 2.159, 0.451	– 1.773 ± j 9.227, 0.188	– 1.542 ± j 7.891, 0.191
Case-13	– 1.236 ± j 8.220, 0.148	– 1.468 ± j 7.869, 0.173	– 1.792 ± j 9.236, 0.190
Case-14	– 1.039 ± j 8.349, 0.122	– 1.583 ± j 7.089, 0.218	– 1.347 ± j 8.322, 0.159
Case-15	– 1.288 ± j 8.377, 0.152	– 1.339 ± j 7.852, 0.168	– 1.615 ± j 6.837, 0.229
Case-16	– 1.153 ± j 6.619, 0.171	– 1.081 ± j 8.805, 0.121	– 1.494 ± j 7.878, 0.186
Case-17	– 1.291 ± j 8.373, 0.152	– 1.344 ± j 7.655, 0.172	– 1.610 ± j 6.836, 0.229
Case-18	– 1.210 ± j 6.067, 0.195	– 1.778 ± j 9.227, 0.189	– 1.585 ± j 7.914, 0.196

The table reveals that with HSOPSSs eigenvalues are shifted in the left half of the *s*-plane with improved damping factor and damping ratio as compared to without PSS for all

unseen operating cases. This ensures that the NEPS will be stable for all considered unseen cases also. It is also found that designed HSOPSS controllers satisfy the earlier selected criterion for the value of desired damping factor and damping ratio for all unseen operating cases except cases 9 and 11 where slightly more overshoot and settling time may occur. Hence, the HSO provides robustness with improved stability and damping performance for unseen operating cases 4-18 of the NEPS as compared to that of without PSS.

In order to check the robustness performance of the designed HSOPSS controllers in terms of speed deviations, earlier four scenarios of disturbances mentioned in Table 3.24 are considered for unseen cases 4-18 of NEPS without PSS. The speed deviations Δw_1, Δw_2, Δw_3, Δw_4, Δw_5, Δw_6, Δw_7, Δw_8, Δw_9 and Δw_{10} for the system without PSS and with HSOPSSs for severe disturbances Scenario-1 of various unseen cases 4-12 of NEPS are shown in Fig. 5.16 (a)-(i) and (j)-(r) respectively.

The analysis of response plots without PSS already discussed in Section 3.4.3 (D). From Fig. 5.16 (j)-(r), it is observed that the speed deviations with HSOPSSs, the oscillations are well damped out. Moreover, it is observed that the Case-9 delivers more oscillations and consumed more time to reach in steady state as compared to others. In unseen cases 4-12, the Δw_9 is most severe speed deviations than others. Furthermore, peak overshoot of Δw_9 is almost similar in all considered operating cases.

To check the robustness of designed HSOPSS controllers on other unseen cases, the Scenario-4 is performed on other unseen operating cases 13-18. The speed deviations of NEPS without PSS and with HSOPSSs for Scenario-4 of cases 13-18 are shown in Fig. 5.17 (a)-(f) and (g)-(l) respectively. The analysis of response plots without PSS already discussed in Section 3.4.3 (D). From Fig. 5.17 (g)-(l), it is noticed that LFO in speed response with HSOPSSs are well damped out.

Moreover, it is observed that speed responses in unseen Case-16 have high peak overshoot and Case-18 consumed more time to die out oscillations as compared to others. It is clear that the system performance with HSOPSSs is improved to that of without PSS for severe disturbance scenarios 1 and 4 of unseen operating cases. This may be concluded that the designed HSOPSSs work satisfactorily for most of the scenarios of severe disturbances of unseen operating cases of NEPS.

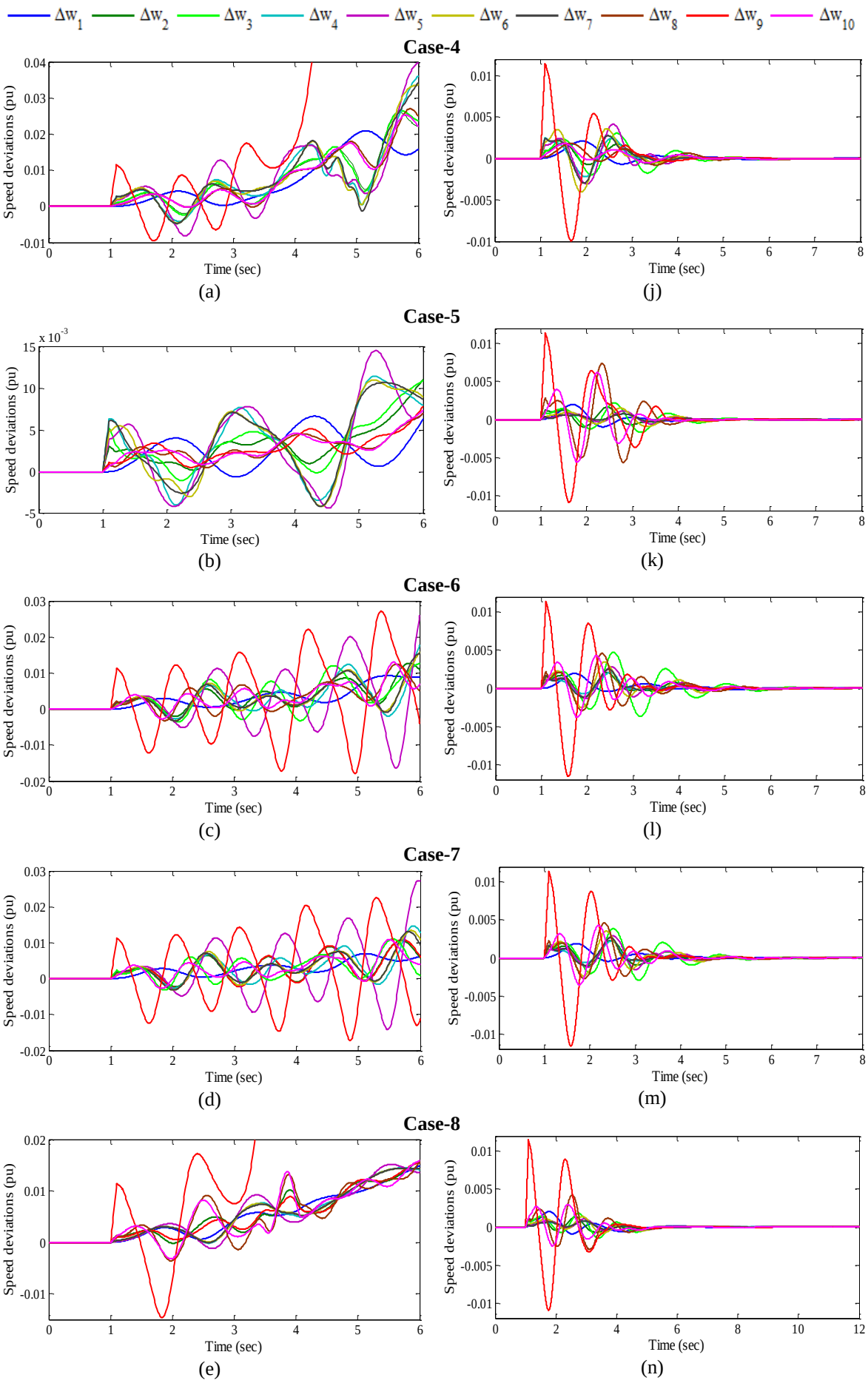
Δw1 Δw2 Δw3 Δw4 Δw5 Δw6 Δw7 Δw8 Δw9 Δw10
Case-4
Speed deviations (pu)
Time (sec)
(a)
(j)
Case-5
x 10-3
(b)
(k)
Case-6
(c)
(l)
Case-7
(d)
(m)
Case-8
(e)
(n)

Cont.

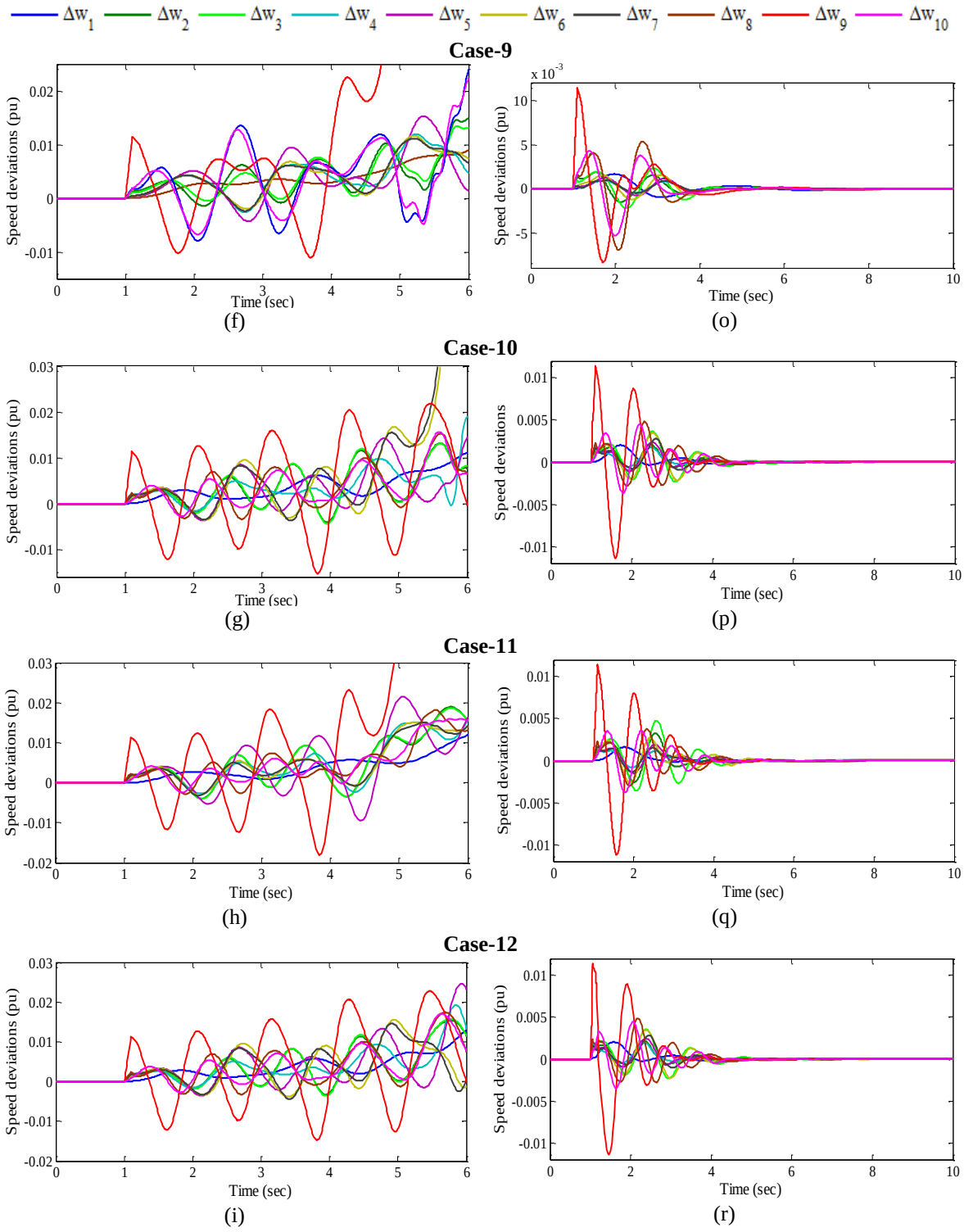

Fig. 5.16 Speed deviations (a)–(i) without PSS and (j)-(r) with HSOPSSs for scenario-1 of unseen operating cases 4-12

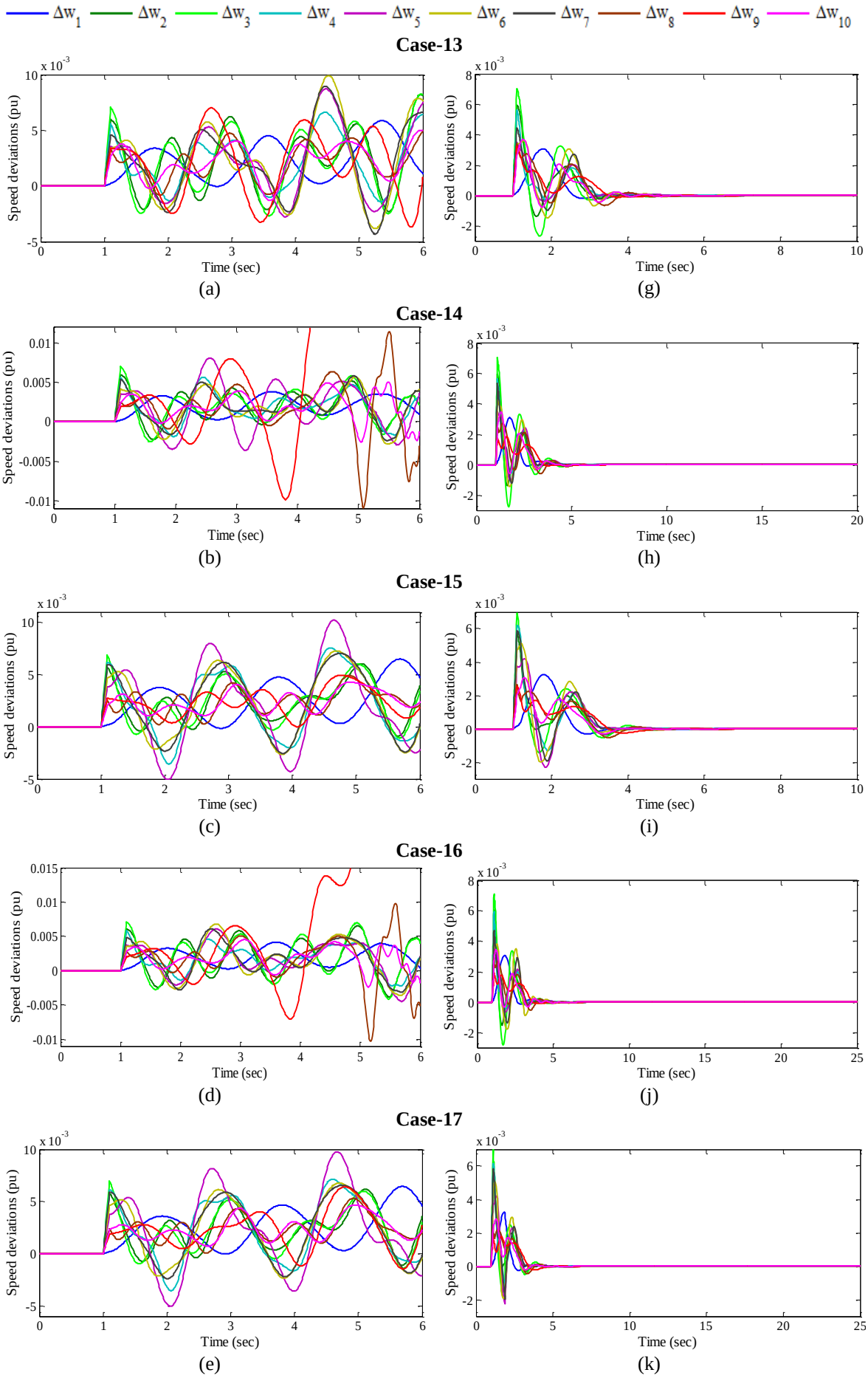
Δw1 Δw2 Δw3 Δw4 Δw5 Δw6 Δw7 Δw8 Δw9 Δw10
Case-13
Speed deviations (pu)
Time (sec)
(a)
(g)
Case-14
(b)
(h)
Case-15
(c)
(i)
Case-16
(d)
(j)
Case-17
(e)
(k)

Cont.

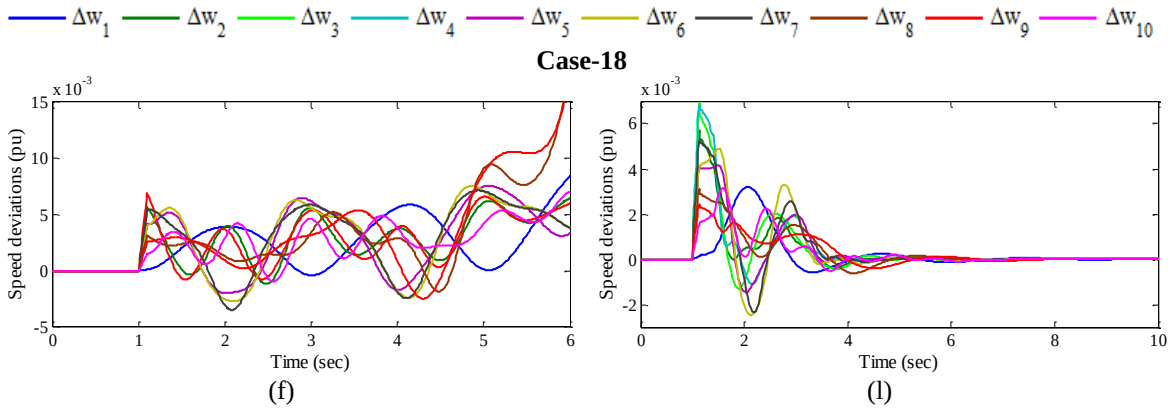

Fig. 5.17 Speed deviations (a)-(f) without PSS and (g)-(l) with HSOPSS for scenario-4 of unseen operating cases 13-18

In addition to time-domain simulation results, the effectiveness of HSOPSS controllers is observed by evaluating two indices: *IAE* and *ITAE* for observed scenarios 1-4 of all unseen operating cases. The bar charts of both indices values for designed HSOPSS controllers for Scenario-1 of unseen cases 4-12 are shown in Fig. 5.18 (a) and (b) respectively. Similarly, both indices with designed HSOPSSs for Scenario-2 of unseen cases 4-18 except Case-6, for Scenario-3 of cases 4-18 except cases 6, 9 and for Scenario-4 of cases 4-18 are shown in Fig. 5.19 (a)-(c) and (d)-(f) respectively.

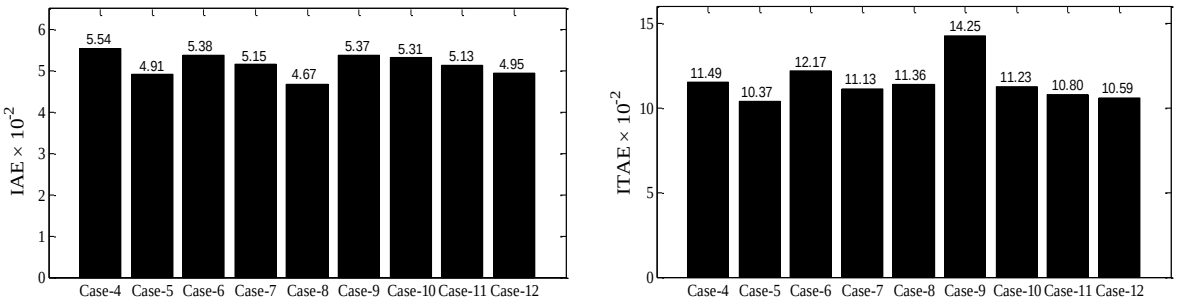

Fig. 5.18 Values of (a) *IAE* and (b) *ITAE* with HSOPSSs for scenario-1 of unseen operating cases 4-12

From Fig. 5.18 (a)-(b), it is observed that values of *IAE* with HSOPSSs for unseen cases 8 and 4 of Scenario-1 are minimum and maximum respectively whereas values of *ITAE* for cases 5 and 9 are minimum and maximum respectively. Therefore, it is concluded that Case-9 under Scenario-1 is severe than others.

From Fig. 5.19 (a)-(c) and (d)-(f), it is noticed that values of *IAE* with HSOPSSs for cases 5 and 18 of Scenario-2, for cases 7 and 11 of Scenario-3 and for cases 5 and 18 of Scenario-4 are minimum and maximum respectively. Similarly, values of *ITAE* with HSOPSSs for unseen cases 5 and 9 of Scenario-2, for cases 7 and 11 of Scenario-3 and for cases 7 and 9 of Scenario-4 are minimum and maximum respectively. Moreover, the Scenario-4 of Case-9 is most severe than other scenarios of unseen cases.

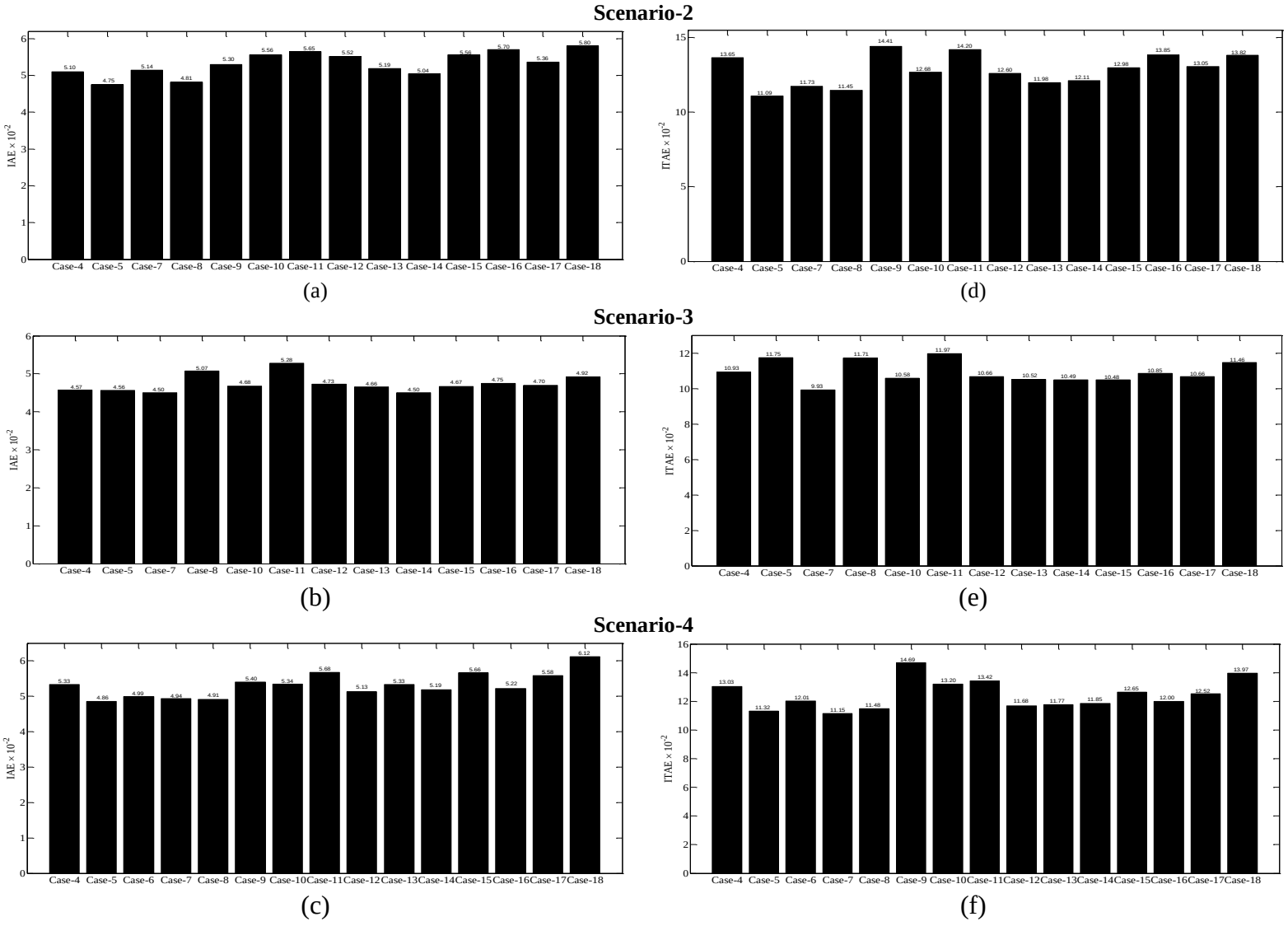

Fig. 5.19 Values of (a)-(c) *IAE* and (d)-(f) *ITAE* with HSOPSSs for scenarios 2-4 of unseen operating cases 4-18

Hence, the designed HSOPSS controllers for NEPS is capable to damp out low frequency local and inter-area modes of oscillations with improved stability and damping performances for wide range of loading cases under different scenarios of severe disturbances and also for unseen operating cases under severe scenarios of disturbances.

5.2.4 Example 4: Sixteen-Machine, Sixty-Eight Bus New England Extended Power System (NEPS)

The operating condition details and single-line diagram of NEEPS is described in Section 3.4.4 and Appendix respectively.

A. Eigenvalue Analysis of NEEPS without PSS and with HSOPSSs

Open-loop eigenvalues, damping ratio, frequency, participation modes and participation factor associated with electromechanical modes of the system are illustrated in Table 3.28 and discussed in Section 3.4.4 (A). An eigenvalue-based multi-objective function J (equation 3.1) is used in Section 3.2 and minimized using HSO for tuning the forty-two parameters of PSSs. The HSO is applied with population size 100, maximum generation 100, $HMCR$ = 0.75, PAR = 0.30, BW = 0.01.

The HSO is able to find the desired solution for which fitness function J is zero. The final value of J equal to zero indicates that fourteen unstable and/or poorly damped eigenvalues are shifted to a specified D-shape zone in the left-half of the s-plane. The optimum designed forty-two parameters of HSOPSSs for fourteen generators are shown in Table 5.10.

Table 5.10: Optimal designed parameters of HSOPSSs for NEEPS

Generators	K_1	T_1	T_3
G_1	76.425	0.162	0.888
G_2	26.315	0.551	0.510
G_3	47.143	0.323	0.572
G_4	17.558	0.994	0.509
G_5	59.035	0.281	0.329
G_7	10.756	0.814	0.677
G_8	52.683	0.431	0.109
G_9	26.648	0.520	0.489
G_{10}	75.727	0.549	0.245
G_{11}	15.281	0.310	0.249
G_{12}	4.496	0.766	0.687
G_{13}	37.969	0.512	0.235
G_{15}	38.367	0.388	0.263
G_{16}	42.826	0.478	0.878

The closed-loop eigenvalues and their damping ratio of only unstable modes with designed HSOPSSs for operating cases 1-6 are determined using PSAT [215] and are shown in Table 5.11. The eigenvalue maps of NEEPS without PSS for operating cases 1-3 and 4-6 are shown in Fig. 5.20 (a)-(c) and (g)-(i) whereas with HSOPSSs for same cases are shown in Fig. 5.20 (d)-(f) and (j)-(l) respectively.

Table 5.11: Eigenvalues and damping ratio with HSOPSSs for operating cases 1-6 of NEEPS

Cases	With HSOPSSs		
Case-1	– 0.601 ± j 2.214, 0.262	– 0.609 ± j 1.265, 0.434	– 0.744 ± j 3.996, 0.183
Case-2	– 0.643 ± j 1.138, 0.492	– 0.655 ± j 2.214, 0.283	– 0.750 ± j 3.987, 0.184
Case-3	– 0.638 ± j 1.251, 0.454	– 0.645 ± j 2.218, 0.279	– 0.746 ± j 3.992, 0.183
Case-4	– 0.633 ± j 1.181, 0.472	– 0.652 ± j 2.225, 0.281	– 0.743 ± j 2.436, 0.291
Case-5	– 0.601 ± j 2.215, 0.262	– 0.608 ± j 1.269, 0.472	– 0.744 ± j 3.997, 0.183
Case-6	– 0.623 ± j 2.186, 0.274	– 0.651 ± j 0.984, 0.552	– 0.688 ± j 2.391, 0.276

The eigenvalue maps of without PSS for unstable and lightly damped modes of NEEPS system are discussed in Section 3.4.4 (A). Table 5.15 and 5.20 (d)-(f) & (j)-(l) show that the HSOPSSs shift the eigenvalues to a specified D-shape zone in the left half of the *s*-plane with desired damping factor and damping ratio as compared to without PSS for all operating cases. Hence, HSOPSS controllers provide improved stability and damping characteristics of the NEEPS as compared to same obtained using without PSS.

B. Time-Domain Simulation Results and Discussions with HSOPSSs and without PSS of NEEPS

In order to examine the performance of designed HSOPSS controllers in previous section in terms of speed deviations, the time-domain simulation of NEEPS is performed for without PSS and with HSOPSSs for observed four scenarios of severe operating Case-6 only. The speed deviations $\Delta w_1, \Delta w_2, \Delta w_3, \Delta w_4, \Delta w_5, \Delta w_6, \Delta w_7, \Delta w_8, \Delta w_9, \Delta w_{10}, \Delta w_{11}, \Delta w_{12}, \Delta w_{13}, \Delta w_{14}, \Delta w_{15}$ and Δw_{16} for without PSS and with HSOPSSs for scenarios 1-4 of operating Case-6 are shown in Fig. 5.21 (a)-(d) and (e)-(h) respectively.

The analysis of response plots without PSS already discussed in Section 3.4.4 (D). From Fig. 5.21 (e)-(h), it is noticed that that with HSOPSSs, LFO are well damped out for all scenarios. Moreover, the Δw_9 has larger peak overshoot and generates more oscillations in Scenario-1 than others. It is clear that the system performance with HSOPSSs is much improved to that of without PSS for all scenarios of operating Case-6.

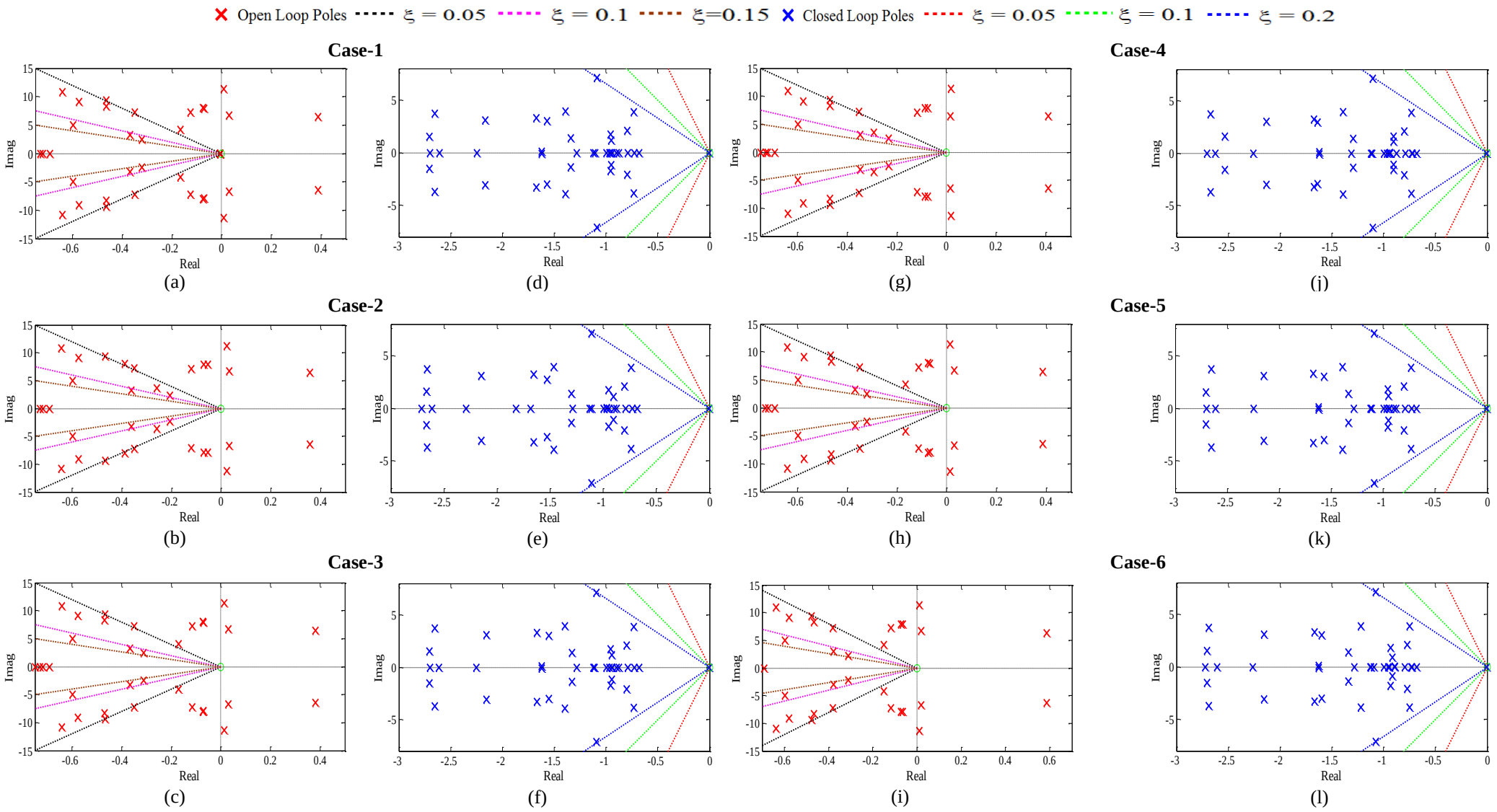

Fig. 5.20 Eigenvalue maps (a)-(c) & (g)-(i) without PSS and (d)-(f) & (j)-(l) with HSOPSSs for operating cases 1-6 of NEPS

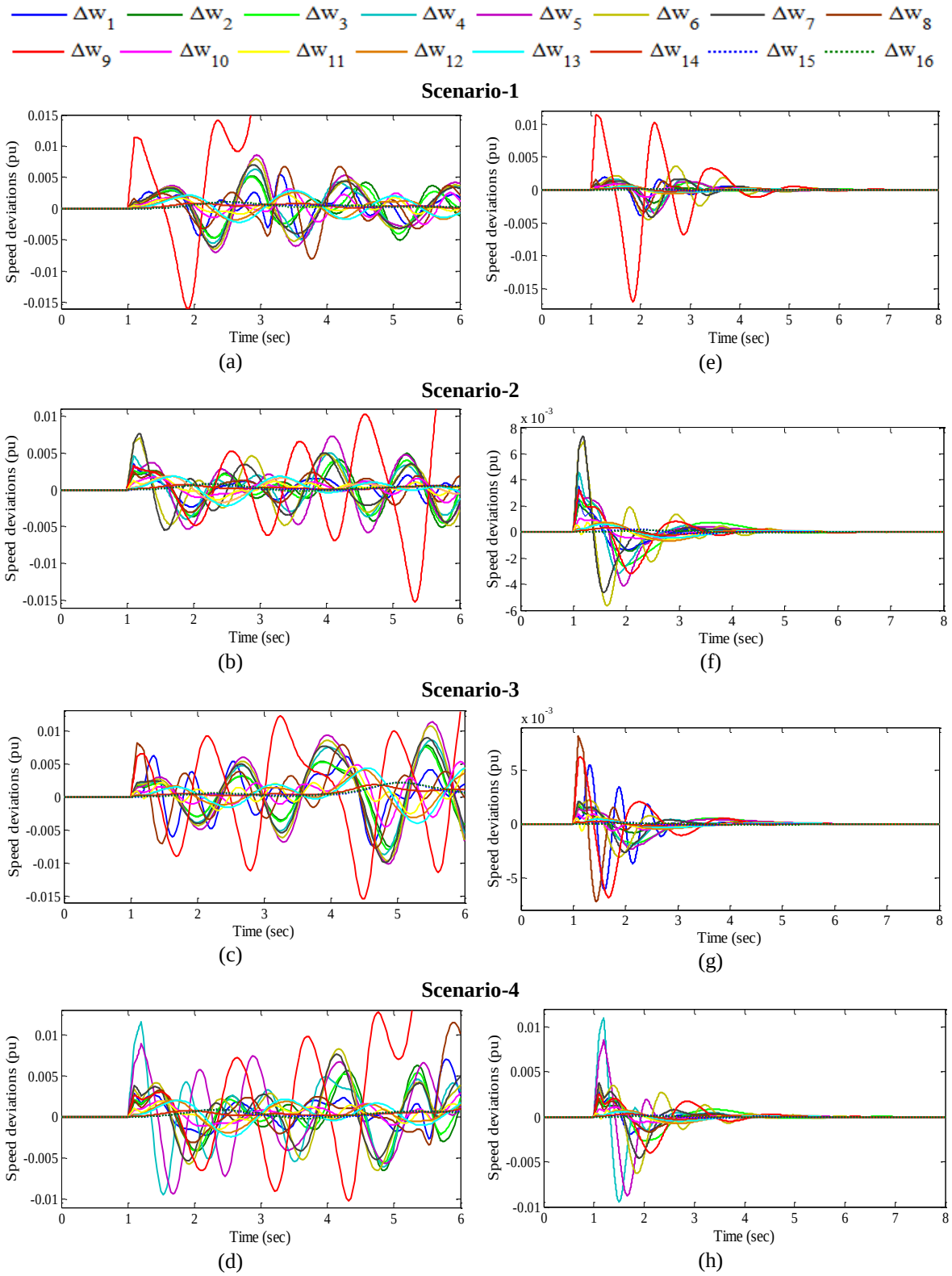

Fig. 5.21 Speed deviations (a)-(d) without PSS and (e)-(h) with HSOPSSs for scenarios 1-4 of operating case-6

This demonstrates the potential of HSO technique to obtain the desired set of PSS parameters for NEEPS and the designed HSOPSSs are capable to damp out LFO for wide range of operating cases under severe scenarios of disturbances.

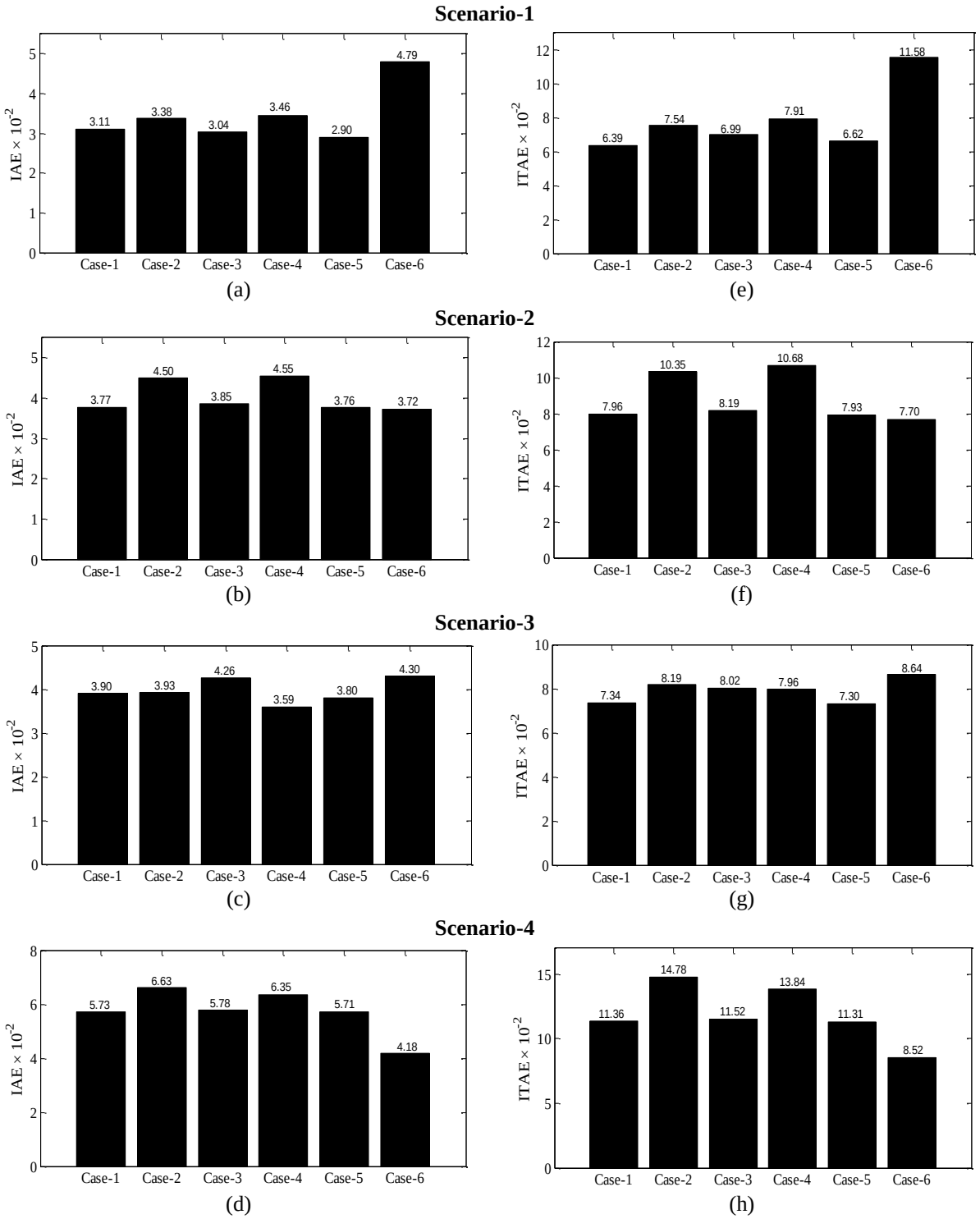

Fig. 5.22 Values of (a)-(d) *IAE* and (e)-(h) *ITAE* with HSOPSSs for scenarios 1-4 of operating cases 1-6

C. Performance Indices Results and Discussions with HSOPSSs of NEEPS

In addition to time-domain simulation results, the effectiveness of designed HSOPSS controller is noticed by evaluating *IAE* and *ITAE* for observed four scenarios of different disturbances. The bar charts of both indices values with HSOPSSs for scenarios 1-4 of cases 1-6 are shown in Fig. 5.22 (a)-(d) and (e)-(h) respectively.

From the Fig. 5.22 (a)-(d), it is observed that both indices for Case-6 and Case-4 of scenarios 2 and 4, are lower and higher values respectively whereas for Scenario-1, the *ITAE* is higher for Case-6 and lower for Case-1 and for Scenario-3, the *ITAE* is higher for Case-6 and lower for Case-5 respectively. Moreover, it is concluded that for scenarios 1 to 4, operating cases 6, 4, 6 and 2 are most severe case than others respectively. Furthermore, it is also noticed that for all cases the Scenario-4 is most severe than other scenarios whereas for Case-6, the Scenario-1 is most severe than others. Comparing Fig. 5.22 with Fig. 3.27, it may be observed that the designed HSOPSS controllers of NEEPS provide sufficient damping to damp out low frequency local and inter-area modes of oscillations with less overshoot and settling time than that of without PSS.

D. Robustness Test of Designed HSOPSS Controllers of NEEPS

To test the robustness of earlier designed HSOPSS controllers for NEEPS, nine unseen operating cases 7-15 mentioned in Table 3.33 are considered. In this section, the effectiveness of designed HSOPSSs is evaluated by eigenvalue analysis, time-domain simulation results and performance indices for earlier observed four scenarios of all unseen operating cases and compared with that of without PSS.

Open-loop eigenvalues, damping ratio, frequency, participation modes and participation factor for only unstable modes of unseen operating cases 7-15 of NEEPS without PSS and closed-loop eigenvalues and damping ratio with designed HSOPSSs for the same unseen cases of system are obtained using PSAT [215] and shown in Table 5.12.

The table shows that the designed HSOPSSs shift the eigenvalues to the left half of the *s*-plane with improved damping factor and damping ratio as compared to without PSS for all unseen operating cases. This ensures that the NEEPS will be stable for all considered unseen cases also.

It is also observed that designed HSOPSS controllers satisfy the earlier selected criterion for the value of desired damping factor and damping ratio for all unseen cases. Hence, the HSO provides robustness with enhanced stability and improved damping performance for unseen operating cases 7-15 of NEEPS as compared to that of without PSS.

In order to examine the robustness performance of the designed HSOPSSs in terms of speed deviations, the simulations are performed using PSAT [215] for four earlier observed scenarios on unseen cases 7-15 of NEEPS. The speed deviations $\Delta w_1, \Delta w_2, \Delta w_3, \Delta w_4, \Delta w_5, \Delta w_6, \Delta w_7, \Delta w_8, \Delta w_9, \Delta w_{10}, \Delta w_{11}, \Delta w_{12}, \Delta w_{13}, \Delta w_{14}, \Delta w_{15}$ and Δw_{16} without PSS and with HSOPSSs for severe test Scenario-1 of cases 7-11 are shown in Fig. 5.23 (a)-(e) and (f)-(j) respectively whereas for Scenario-2 of cases 12-15 are shown in Fig. 5.24 (a)-(d) and (e)-(h) respectively.

Table 5.12: Eigenvalues and damping ratio with HSOPSSs for unseen operating cases 7-15 of NEEPS

Cases	With HSOPSSs
Case-7	– 0.790 ± j 2.113, 0.350
	– 0.689 ± j 3.942, 0.172
Case-8	– 1.095 ± j 7.090, 0.152
	– 0.744 ± j 3.844, 0.190
	– 1.403 ± j 3.909, 0.337
	– 0.737 ± j 2.728, 0.260
Case-9	– 1.103 ± j 7.084, 0.153
	– 0.744 ± j 3.843, 0.190
	– 1.405 ± j 3.913, 0.338
	– 0.735 ± j 2.724, 0.260
	– 0.819 ± j 1.770, 0.420
Case-10	– 1.104 ± j 7.084, 0.154
	– 0.737 ± j 3.865, 0.187
	– 1.403 ± j 3.913, 0.337
	– 0.812 ± j 2.828, 0.276
Case-11	– 1.118 ± j 7.055, 0.156
	– 0.811 ± j 3.7133, 0.213
Case-12	– 1.114 ± j 7.064, 0.155
	– 0.735 ± j 3.877, 0.186
	– 0.997 ± j 3.750, 0.256
	– 0.750 ± j 2.113, 0.334
Case-13	– 1.155 ± j 7.022, 0.162
	– 0.732 ± j 3.876, 0.185
	– 0.754 ± j 2.126, 0.334
Case-14	– 0.603 ± j 3.076, 0.192
	– 0.757 ± j 2.112, 0.337
Case-15	– 0.550 ± j 2.986, 0.181
	– 0.820 ± j 3.683, 0.217
	– 1.280 ± j 6.932, 0.181

The analysis of response plots without PSS already discussed in Section 3.4.4 (D). From Figs. 5.23 (f)-(j) and 5.24 (e)-(h), it is observed that with HSOPSSs all oscillations of speed deviations are well damped out for Sceanrio-1 of cases 7-11 and Scenario-2 of cases 13-15. Moreover, the peak overshoot of speed responses in Scenario-1 and Scenario-2 are almost same in all considered operating cases. Furthermore, oscillations in response of cases 13-15 in Scenario-2 take more time to reach in steady state as compared to others.

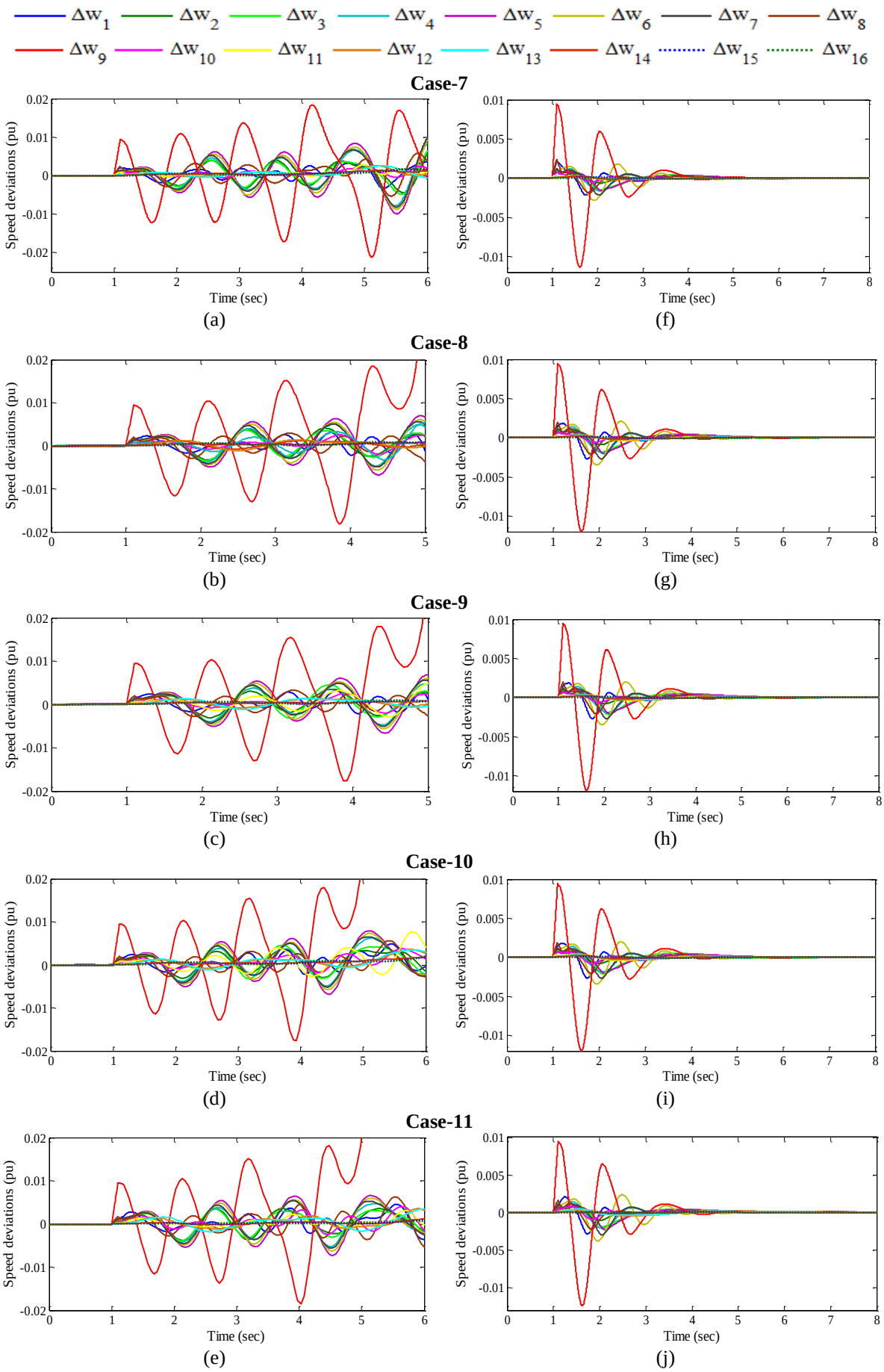

Fig. 5.23 Speed deviations (a)-(e) without PSS and (e)-(j) with HSOPSSs for scenario-1 of unseen cases 7-11

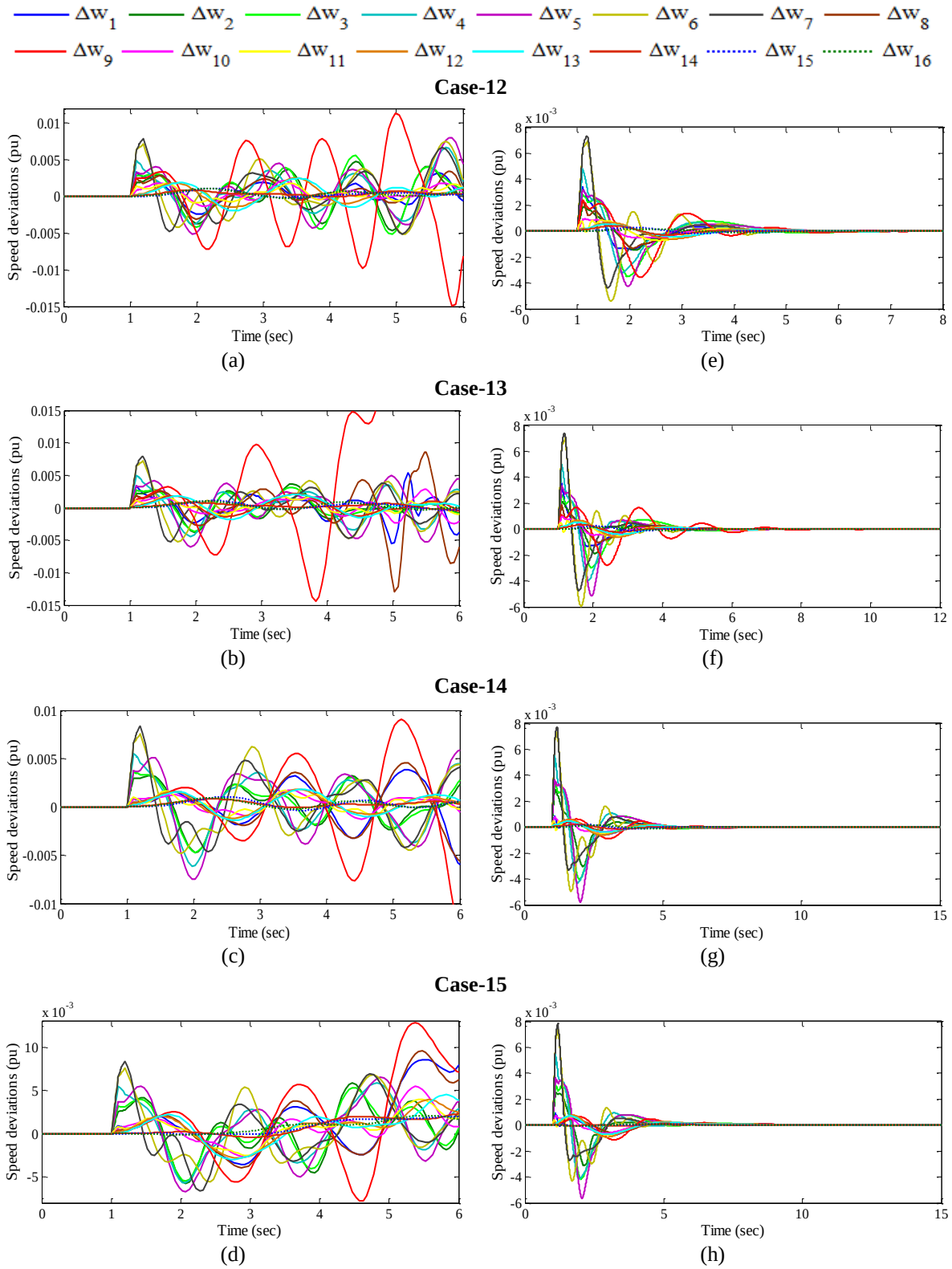

Fig. 5.24 Speed deviations (a)-(d) without PSS and (e)-(h) with HSOPSSs for scenario-2 of unseen cases 12-15

It is clear that the system performance with HSOPSSs is improved to that of without PSS for considered scenarios of unseen operating cases. This may be concluded that the designed HSOPSSs work satisfactorily for observed scenarios of severe disturbances of unseen operating cases of NEEPS.

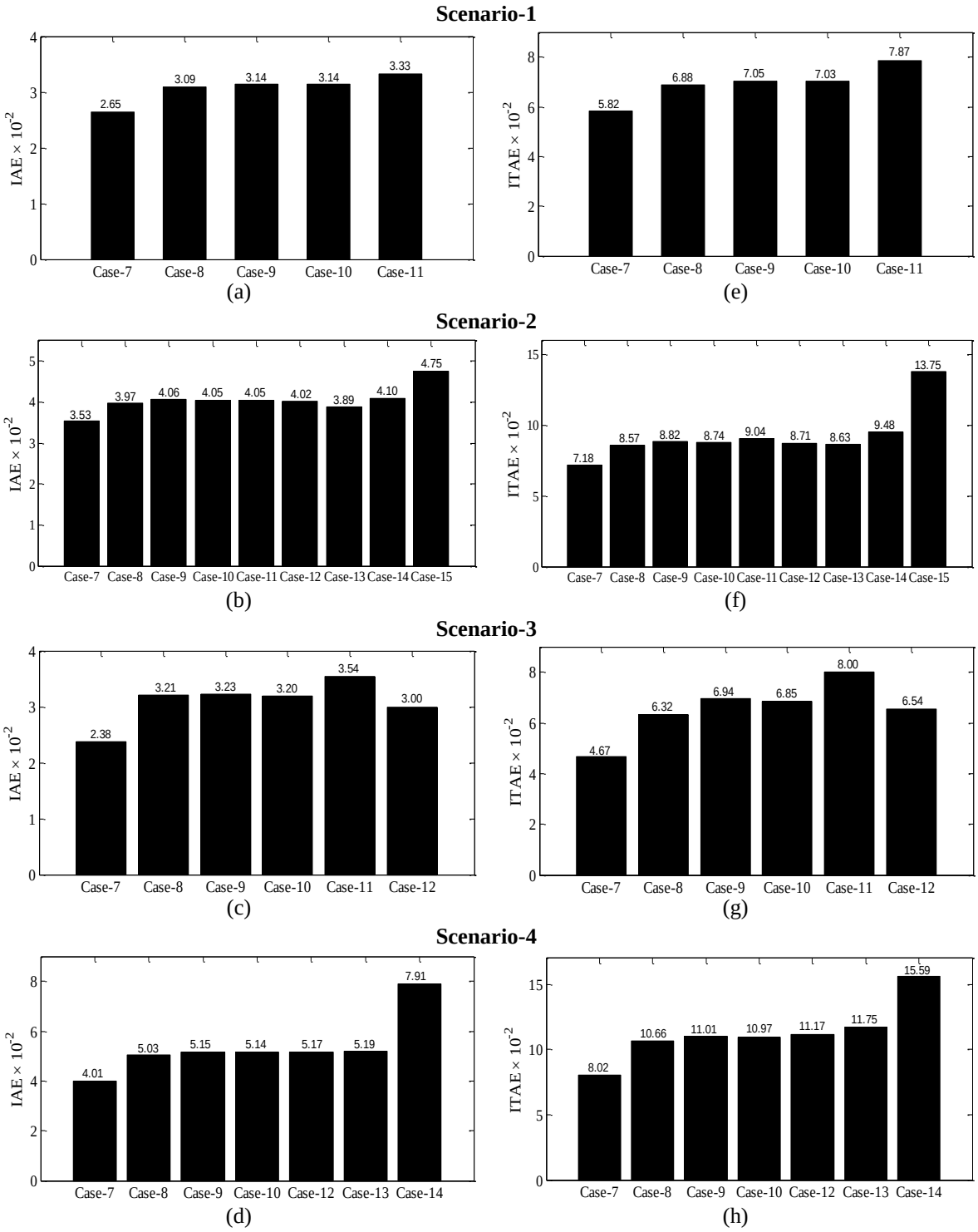

Fig. 5.25 Values of (a)-(d) *IAE* and (e)-(h) *ITAE* with HSOPSSs for scenarios 1-4 of unseen cases 7-15

In addition to time-domain simulation results, the effectiveness of designed HSOPSS controllers is observed by evaluating *IAE* and *ITAE* for observed four scenarios of unseen cases 7-15. The bar charts of both indices with HSOPSSs for Scenario-1 of cases 7-11, Scenario-2 of cases 7-15, Scenario-3 of cases 7-12 and Scenario-4 of cases 7-14 are shown in Fig. 5.25 (a)-(d) and (e)-(h) respectively.

From the figure, it is noticed that the values of both indices for Case-11 of Scenario-1, Case-15 of Scenario-2, Case-11 of Scanerio-3 of and Case-14 of Scenario-4 are higher than

others. Moreover, it is concluded that the unseen Case-14 of Scenario-4 of and Case-7 of Scenario-3 are most and least severe than others.

Hence, the designed HSOPSS controllers for NEEPS is capable to damp out low frequency local and inter-area modes of oscillations with enhanced stability and damping performance for wide range of operating cases under different scenarios of severe disturbances and also for unseen operating cases under severe scenarios of disturbances.

5.3 Summery

In this chapter, a meta-heuristic technique HSO is implemented for effectively designing of PSS under wide range of operating conditions of WSCC power system, TFAM power system, NEPS and NEEPS for SSS enhancement. The HSO is capable of shifting all unstable and/or poorly damped eigenvalues of MMPS to a specified D-shape zone in the left half of the *s*-plane. Moreover, the effectiveness of designed HSOPSS controllers has been evaluated by eigenvalue analysis, eigenvalue maps, time-domain simulation results and performance indices namely *IAE* and *ITAE*. Furthermore, the robustness of designed HSOPSSs is observed by testing them on under wide range of unseen operating cases of MMPS. It is found that the design HSOPSSs have shifted unstable and/or poorly damped eigenvalues of all unseen cases of MMPS to the left half of the *s*-plane for mitigating low frequency local and inter-area modes of oscillations.

CHAPTER–6

MULTI-MACHINE POWER SYSTEM STABILIZERS DESIGN USING CUCKOO SEARCH OPTIMIZATION

The Cuckoo Search Optimization (CSO) algorithm is one of the recently developed bio-inspired meta-heuristic algorithms which are capable to solve complex combinatorial optimization problems. The CSO describes cuckoos foraging behaviour based on parasitized breeding mechanism of cuckoos egg and Levy flight search principle. It has been successfully implemented to solve various optimization problems of power system [226]-[227] but not yet explored much to solve PSS optimization problem. In [167], the designing of PSS using CSO is implemented only for WSCC power system. The main objective of this chapter is to explore CSO for robust designing of PSS parameters of four standard power transmission systems, e.g., WSCC power system, TAFM power system, NEPS and NEEPS.An eigenvalue-based multi-objective function mentioned in Section 3.2 is minimized using CSO for designing PSS parameters of MMPS. The PSS designed using CSO is named CSOPSS. The effectiveness of all designed CSOPSS controllers are evaluated by eigenvalue analysis, eigenvalue maps, time-domain simulation results and specified performance indices and the system performance with CSOPSS is compared with that of without PSS. The robustness of all designed CSOPSS controllers is also checked by testing them on unseen operating conditions under different scenarios of severe disturbances.

6.1 Cuckoo Search Optimization

The CSO is a new evolutionary meta-heuristic optimization technique proposed by Yang and Deb recently [204] which is inspired by the obligate brood parasitism of some cuckoo species. The cuckoo is pretty bird, not only due to attractive sounds they can create but also due to forceful reproduction strategy by which adult cuckoos lay their eggs in the nests of other host birds or species. In this section, first the breeding behaviour of cuckoos and the characteristics of Levy flights of some birds and fruit flies are introduced, and then the CSO algorithm [205] is described.

6.1.1 Cuckoo Breeding Behaviour

Cuckoos are fascinating birds not only due to their beautiful sounds but also because of their aggressive reproduction strategy. Some cuckoo species like the *ani* and *Guira* lay their eggs in common nests, though they may remove other eggs to increase the hatching probability of their own eggs. There are large numbers of cuckoo species that engage the obligate brood parasitism by laying their eggs in the nests of other host birds (often other species).

In cuckoo search, there are three main types of brood parasitism: intra-specific brood parasitism, cooperative breeding, and nest takeover. A little host birds can engage direct conflict with the interfering cuckoos. If a host bird discovers the eggs are not their own, they will either throw these unknown eggs away or simply leave its nest or build a new nest somewhere else. Some cuckoo species such as the New World brood-parasitic *Tapera* have evolved in such a way that female parasitic cuckoos are often very specialized in the mimicry in colour and pattern of the eggs of a few chosen host species [204] [205]. This reduces the probability of their eggs being abandoned and thus increases their reproductively.

6.1.2 Levy Flights

A Levy Flight named for French mathematician Paul Pierre Levy and is a random walk where the step size has a Levy tailed probability distribution. The term Levy Flight was coined by Benoit Mandelbrot who used specific definition of the distribution of the step sizes. Ultimately Levy Flight term has been used to refer discrete grid rather than continuous space. It is basically a Markov Process and exponential property of Levy Flight gives it a scale invariant property and they are used to model data for exhibiting/ showing clusters. In nature many animals and insects follow the properties of Levy Flight. Recent studies of Reynolds and Frye demonstrate that behaviour of fruit flies or *Drosophila Melanogaster* which covers the skies by using numerous series of straight flight paths/ routes followed by a sudden right angle turn which is a Levy-flight-style intermittent scale free [204]-[206].

6.1.3 Cuckoo Search Optimization Algorithm

Initially, each egg in the nest represents a solution and a cuckoo egg represents a new solution. The algorithm is described by breeding strategy of some cuckoo species in conjunction with Lévy flight behaviour of a few birds. In this study, if a host bird searches the eggs are not its own, they either throw these foreign eggs away or just abandon its nest and construct a new nest at other places [204].

- Each cuckoo lays one egg at a time and dumps its egg in arbitrarily selected nest.
- The best nest with excellence fitness or egg will be carried forward to the next generation.
- The number of present host nest is fixed and the egg laid by a cuckoo is searched by the host bird with a probability index $p_a \in (0, 1)$.

The new solution (cuckoo) $x_i^{(t+1)}$ is generated by application of Lévy flight as:

$$x_i^{(t+1)} = x_i^{(t)} + \varepsilon \oplus Levy(\lambda) \tag{6.1}$$

where $\varepsilon > 0$ is the step size that should be related to scale problem of interest. Mostly, the value of step size ε=1 is chosen. The product $\oplus$ means entry wise walk during multiplication. A Lévy flight is an arbitrary walk in which the steps are defined in terms of step-length, which have a definite probability distribution with the directions of the steps being isotropic and random, may be defined as:

$$\text{Lévy} \sim u = t^{-\lambda}, (1 < \lambda \leq 3) \tag{6.2}$$

Here the steps essentially form a random walk process with a power law step-length distribution with a heavy tail. Some of the new solutions should be generated by Levy walk around the best solution obtained so far, this will speed up the local search.

Before starting the iteration process, the CSO identify the best fitness $x_{best.}$ This equation (6.2) has infinite mean with infinite variance. The detection step Φ is given by

$$\Phi = \left(\frac{\Gamma(1+\beta).\sin\left(\pi \frac{\beta}{2}\right)}{\Gamma\left(\left(\frac{1+\beta}{2}\right).\beta.2^{\frac{\beta-2}{2}}\right)} \right)^{\frac{1}{\beta}} \tag{6.3}$$

where Ґ denotes the gamma function. In CSO algorithm β is taken as 1.5. Evolution phase of the x_i begins by defining v, where $v = x_i$ [205]. After this step, the required step is evaluated using

$$stepsize_i = 0.01\left(\frac{u_i}{v_i}\right)^{\frac{1}{\beta}}.(v - X_{best}) \tag{6.4}$$

However, a substantial fraction of the new solutions should be generated by far field randomization and whose locations should be far enough from the current best solution, this will make sure the system will not be trapped in a local optimum. The CSO algorithm control parameters are the scale factor (β) and index (p_a). The flow chart of CSO algorithm is shown in Fig. 6.1:

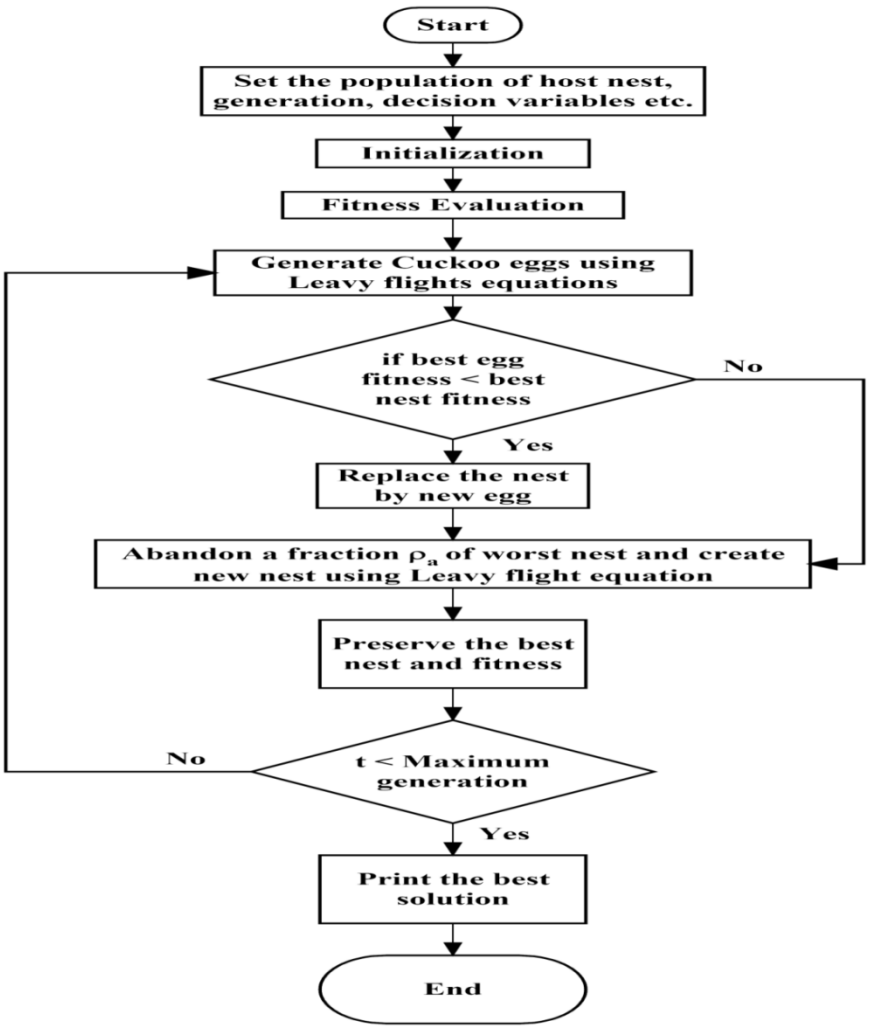

Fig. 6.1 Flow chart of cuckoo search optimization algorithm

6.2 Simulation and Results

The CSO is applied on four standard test systems e.g., WSCC power system, TAFM power system, NEPS and NEEPS, to obtain the optimal parameters of PSS for wide range of operating conditions. An eigenvalue-based multi-objective function is used for simultaneous control of damping factor and damping ratio to mitigate low frequency electromechanical oscillations of MMPS. The parameters of PSS are so designed that unstable and/or poorly damped open-loop eigenvalues are shifted to a specified D-shape zone in the left-half of the *s*-plane for wide range of operating conditions under different scenarios of severe disturbances. This is obtained by minimizing the objective function (3.1) using CSO. The effectiveness of all designed PSS controllers are evaluated by eigenvalue analysis, eigenvalue maps, time-domain simulation results and performance indices *IAE*, *ITAE* and the system performance with CSOPSSs is compared with that of without PSS. The robustness of all designed CSOPSS controllers is also checked by testing them on unseen operating conditions under different scenarios of severe disturbances and compared with that of without PSS.

6.2.1 Example 1: Three-Machine, Nine-Bus WSCC Power System

The operating condition details and single-line diagram of WSCC power system is described in Section 3.4.1 and Appendix respectively.

A. Eigenvalue Analysis of WSCC Power System without PSS and with CSOPSSs

The open-loop eigenvalues, damping ratio, frequency, participation modes and participation factor associated with electromechanical modes of the system are illustrated in Table 3.2 and discussed in Section 3.4.1 (A). An eigenvalue-based multi-objective function *J* presented in (3.1) is minimized using CSO by tuning the six parameters of PSSs. The CSO is applied with population size 100, maximum generation 100, probability index (p_a) = 0.25.

The CSO is able to find the desired solution for which fitness function *J* is zero. The final value of *J* equal to zero indicates that two unstable and/or poorly damped eigenvalues using CSO are shifted to a specified D-shape zone in the left-half of the *s*-plane. The optimal six parameters obtained by CSOPSSs for two generators are shown in Table 6.1. The closed-loop eigenvalues and their damping ratio with CSOPSSs for three operating cases are evaluated using PSAT [215] and are shown in Table 6.2. The Fig. 6.2 (a)-(c) and (d)-(f) show the eigenvalue maps for without PSS and with CSOPSSs for operating cases 1-3 respectively.

Table 6.1: Optimal designed parameters of CSOPSSs for WSCC power system

Generators	***K***	T_1	T_3
G_2	10.198	0.329	0.06
G_3	1.857	0.287	0.314

Table 6.2: Eigenvalues and damping ratio with CSOPSSs for operating cases 1-3 of WSCC power system

Case-1	**Case-2**	**Case-3**
– 2.982 ± j 19.103, 0.154	– 2.563 ± j 7.596, 0.319	– 1.852 ± j 7.060, 0.253
– 3.526 ± j 17.245, 0.200	– 3.133 ± j 18.265, 0.169	– 2.332 ± j 17.774, 0.130

The analysis of eigenvalue maps without PSS for unstable and poorly damped modes of cases 1-3 of WSCC power system is discussed in Section 3.4.1 (A). Table 6.2 and Fig. 6.2 (d)-(f) show that the CSOPSSs shift the eigenvalues to a specified D-shape zone in the left half of the *s*-plane with desired damping factor and damping ratio as compared to that of without PSS for all operating cases. Hence, designed CSOPSS controllers provide improved stability and damping characteristics of the WSCC power system as compared to same obtained using without PSS.

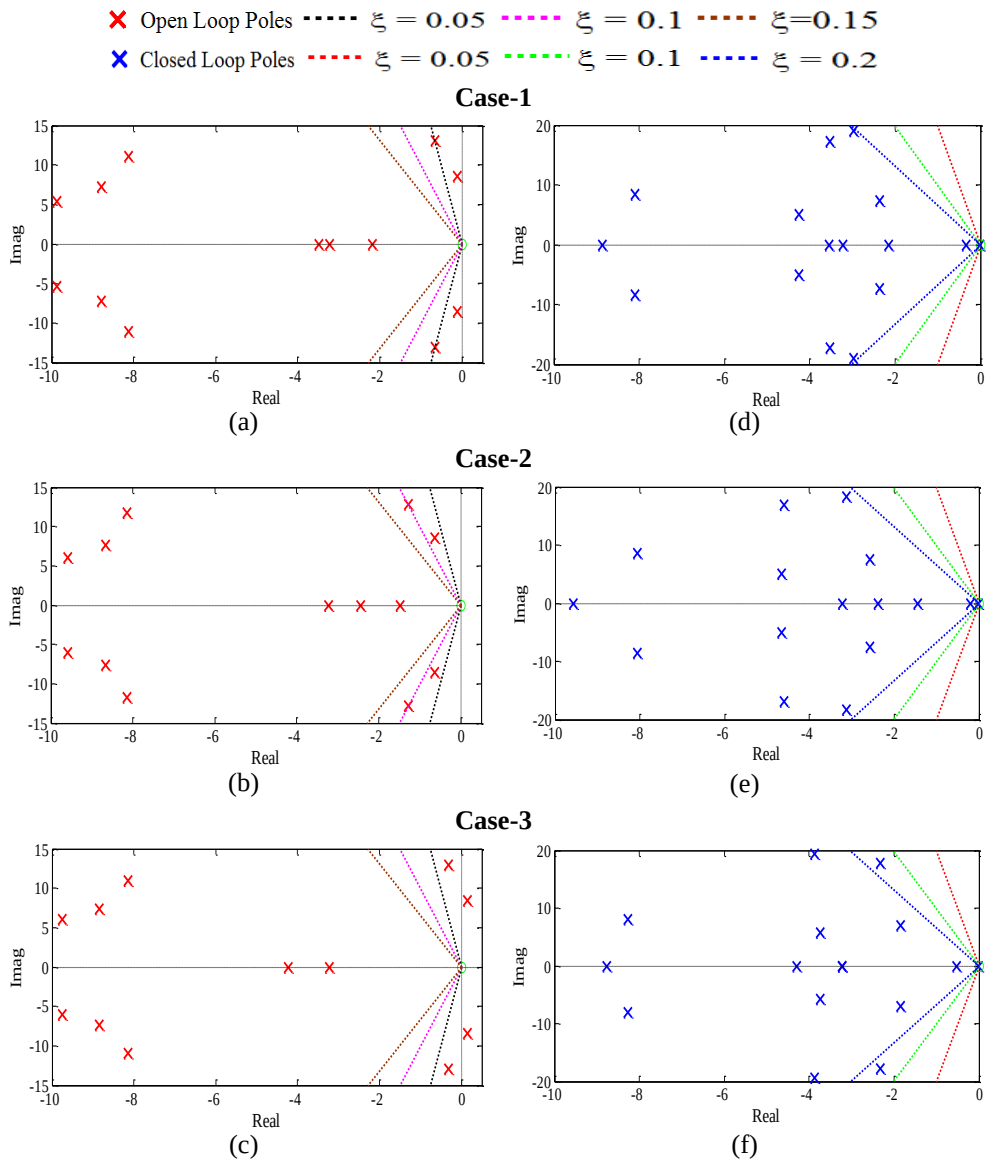

Fig. 6.2 Eigenvalue maps (a)-(c) without PSS and (d)-(f) with CSOPSSs for operating cases 1-3 of WSCC power system

B. Time-Domain Simulation Results and Discussions with CSOPSSs and without PSS of WSCC Power System

The time-domain simulation of WSCC power system is performed with designed CSOPSS controllers in previous section for observed severe scenarios of operating Case-3 mentioned earlier in Table 3.6. The speed deviations Δw_{12}, Δw_{23} and Δw_{31} for selected severe scenarios of Case-3 for the system without PSS and with CSOPSSs are shown in Fig. 6.3 (a)-(b) and (c)-(d) respectively. The time-domain performance analysis of the system without PSS is already discussed in Section 3.4.1 (B).

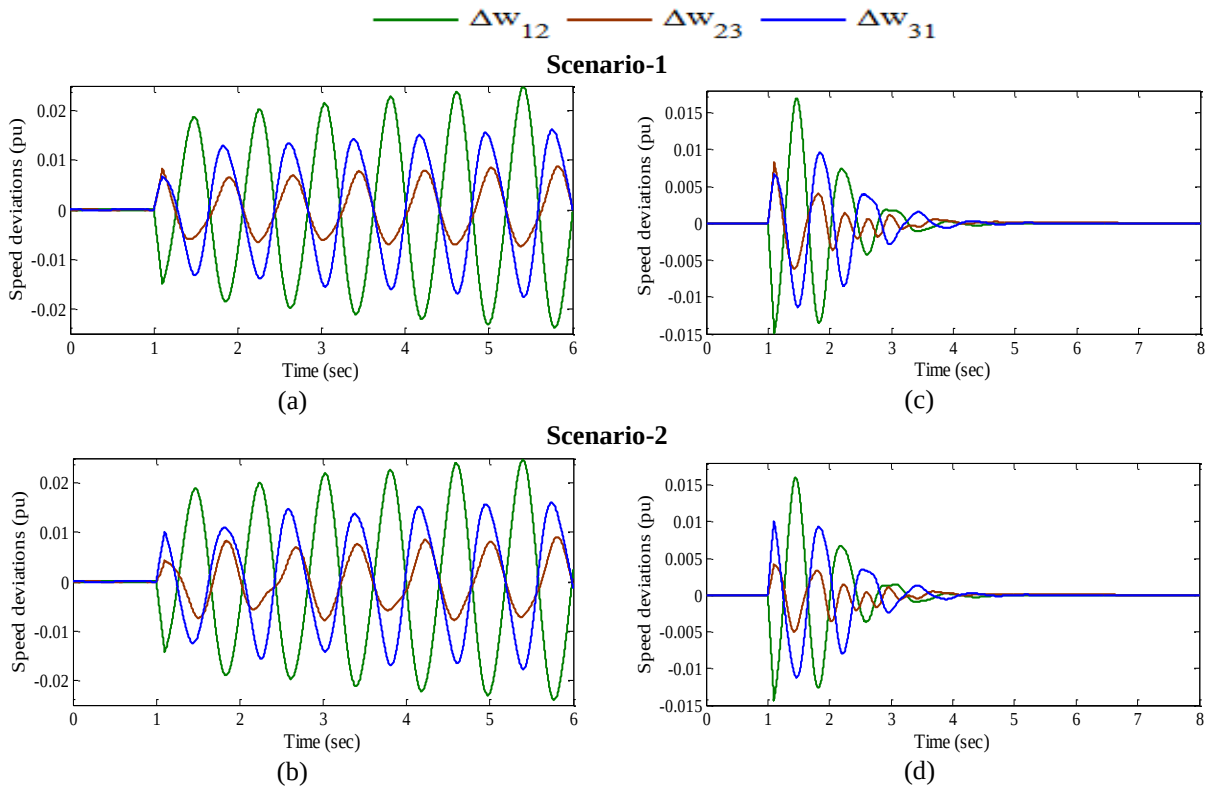

Fig. 6.3 Speed deviations (a)-(b) without PSS and (c)-(d) with CSOPSSs for scenarios 1-2 of operating case-3

It may be clearly observed from Fig. 6.3 (c)-(d) that with CSOPSSs system performance is improved and all oscillations for both scenarios are well damped out. Moreover, the Δw_{12} is most severe due to large peak overshoot and consumed more time to reach in steady state. This illustrates the potential of CSO to obtain a desired set of PSS parameters and the designed CSOPSSs are capable to damp out oscillations for wide range of operating conditions under variety of severe disturbances.

C. Performance Indices Results and Discussions with CSOPSSs of WSCC Power System

In addition to simulation results, the effectiveness of designed CSOPSS controllers is also observed by determining two indices *IAE* and *ITAE* for two observed severe scenarios of disturbances. Established both indices are calculated for each scenario of disturbances for operating cases 1-3 and presented as bar charts in the Fig. 6.4 (a)-(b) and (c)-(d) respectively.

The figure inform that the values of both indices for the CSOPSSs are minimum for each scenario of Case-2 and maximum for each scenario of Case-3, which indicates that Case-3 is the most severe whereas Case-2 is the least severe. Moreover, for operating cases 1 & 3, Scenario-1 is more severe but for Case-2, Scenario-2 is more severe. Comparing Fig. 6.4 with Fig. 3.4, it may be noticed that the designed CSOPSS controllers provide improved damping to damp out low frequency local modes of oscillations with less overshoot and settling time than that of without PSS.

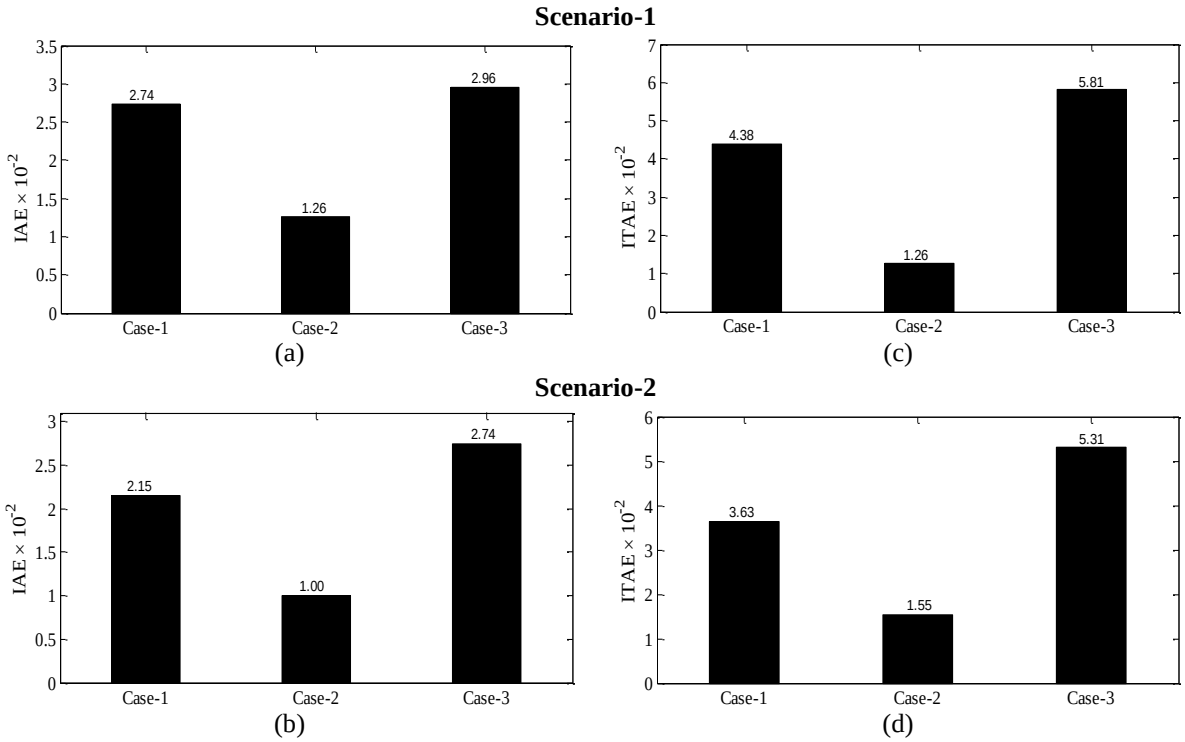

Fig. 6.4 Values of (a)-(b) *IAE* and (c)-(d) *ITAE* with CSOPSSs for scenarios 1-2 of operating cases 1-3

D. Robustness Test of Designed CSOPSS Controllers of WSCC Power System

To test the robustness of earlier designed CSOPSS controllers for WSCC power system; unseen operating cases 4-6 mentioned in Table 3.7 are considered. In this section, the effectiveness of CSOPSS controllers for these unseen cases is evaluated by eigenvalue analysis, time-domain simulation results, and performance indices and compared with that of without PSS.

Open-loop eigenvalues, damping ratio, frequency, participation modes and participation factor for unseen cases 4-6 of WSCC power system without PSS are illustrated in Table 3.8 and discussed in Section 3.4.1 (D). Now, the designed CSOPSSs parameters are used to obtain closed-loop eigenvalues and damping ratio using PSAT [215]. Table 6.3 shows the closed-loop eigenvalues and damping ratio for unseen cases 4-6 of WSCC power system with CSOPSS controllers for only unstable and poorly damped modes.

Table 6.3: Eigenvalues and damping ratio with CSOPSSs for unseen operating cases 4-6 of WSCC power system

Case-4	Case-5	Case-6
– 1.619 ± j 7.332, 0.215	– 1.781 ± j 7.056, 0.244	– 1.761 ± j 6.908, 0.247
– 3.119 ± j 18.920, 0.162	– 2.587 ± j 17.855, 0.143	– 2.390 ± j 17.777, 0.133

The table reveals that the CSOPSSs shift the eigenvalues in the left half of the *s*-plane with improved damping factor and damping ratio as compared to without PSS for all unseen cases. This ensures that the system will be stable for all considered unseen cases also. It is also observed that designed CSOPSS controllers satisfy the earlier selected criterion for the value of

desired damping factor and damping ratio for PSS design. Hence, the designed CSOPSSs are robust as it works with acceptable damping performance for unseen operating cases 4-6 of the WSCC power system also.

In order to further examine the robustness performance of the CSOPSSs in terms of speed deviations, the time-domain simulations are performed using PSAT [215] for two earlier observed severe scenarios of disturbances on unseen operating cases 4-6 of WSCC power system. The speed deviations Δw_{12}, Δw_{23} and Δw_{31} without PSS for scenarios 1 and 2 of cases 4-6 are shown in Fig. 6.5 (a)-(c) and Fig. 6.6 (a)-(c) respectively whereas the Δw_{12}, Δw_{23} and Δw_{31} with CSOPSSs are shown in Fig. 6.5 (d)-(f) and Fig. 6.6 (d)-(f) respectively.

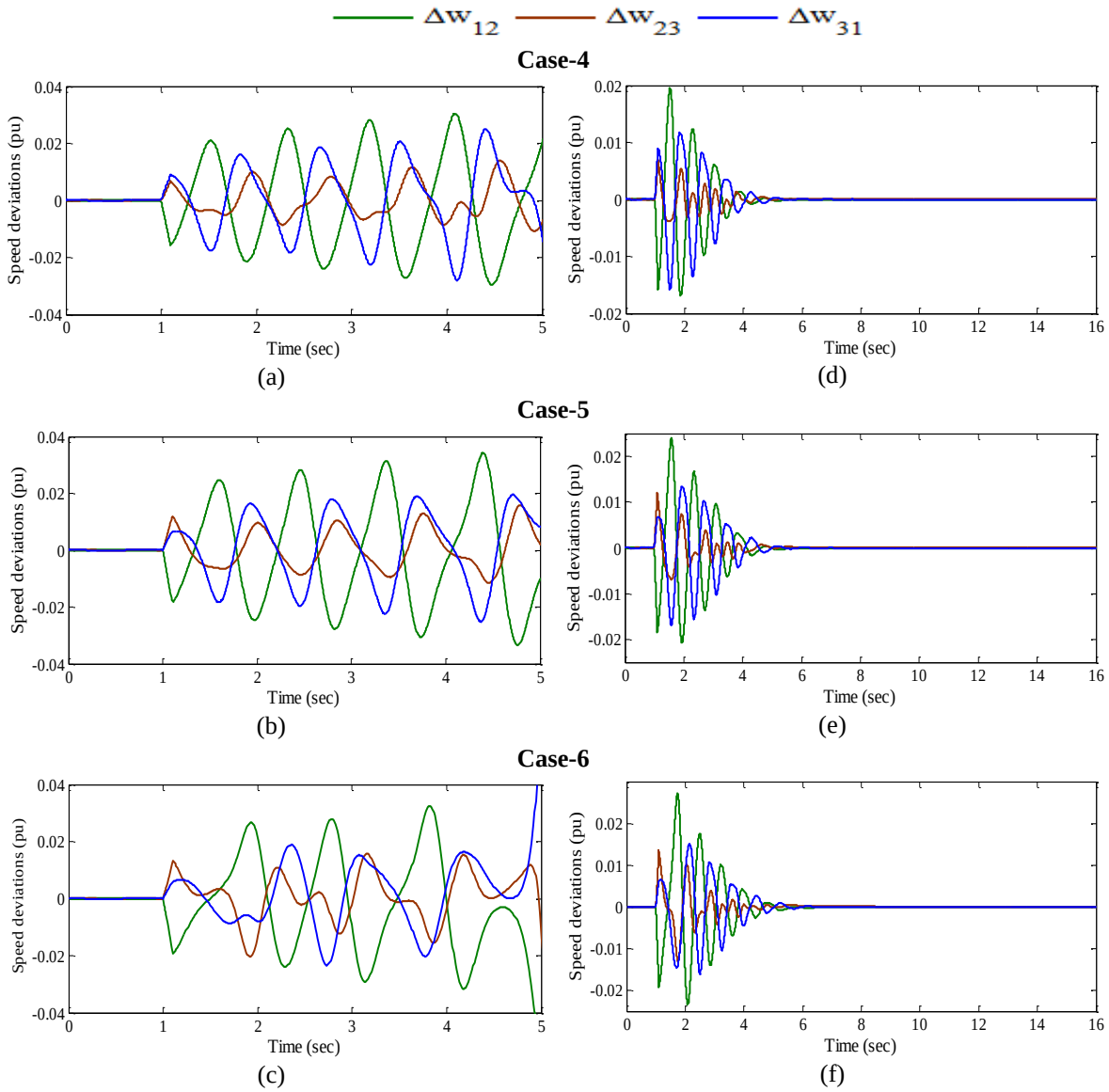

Fig. 6.5 Speed deviations (a)-(c) without PSS and (d)-(f) with CSOPSSs for scenario-1 of unseen operating cases 4-6

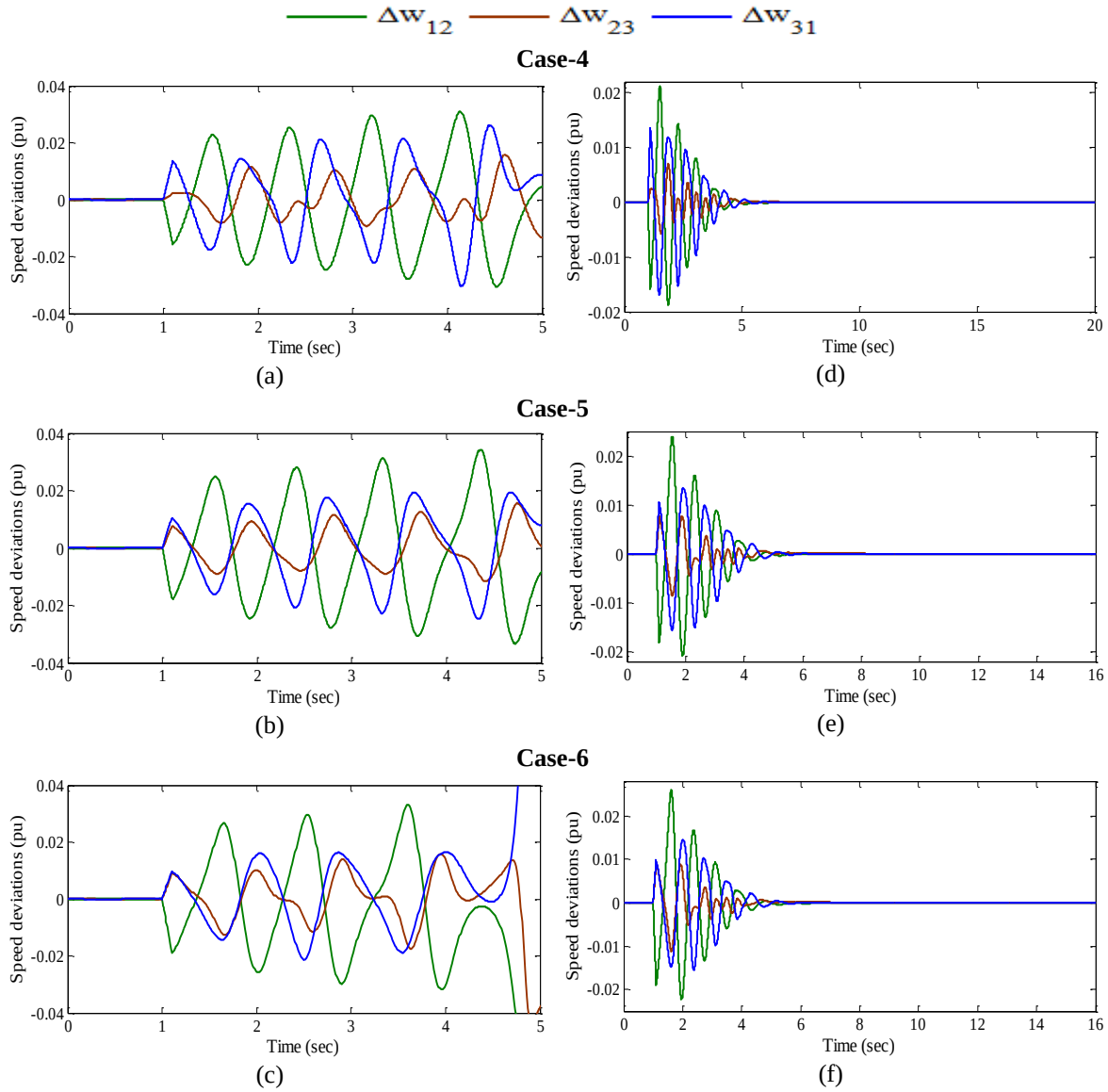

Fig. 6.6 Speed deviations (a)-(c) without PSS and (d)-(f) with CSOPSSs for scenario-2 of unseen operating cases 4-6

The analysis of response plots without PSS is already discussed in Section 3.4.2 (D). From Figs. 6.5 (d)-(f) and 6.6 (d)-(f), it may be clearly observed that with CSOPSSs, the speed deviation responses for scenarios 1-2 of Case-6 produce more oscillations as compared to other cases. Moreover, peak overshoot in speed deviation responses for scenarios 1-2 of Case-6 is more as compared to other cases. Furthermore, the speed deviations with CSOPSSs for scenarios 1-2 of unseen operating cases 4-6 take more time to damp out LFO as compared to earlier cases 1-3. This may be concluded that the designed CSOPSSs work acceptably for all the scenarios of severe disturbances of unseen operating cases of WSCC power system.

In addition to time-domain simulation results, the effectiveness and robustness of CSOPSS controllers is also noticed by evaluating indices *IAE* and *ITAE* for observed scenarios of unseen operating cases. Established both indices with CSOPSSs are determined for each

scenario of disturbances for operating cases 4-6 and presented as bar charts in the Fig. 6.7 (a)-(b) and (c)-(d) respectively.

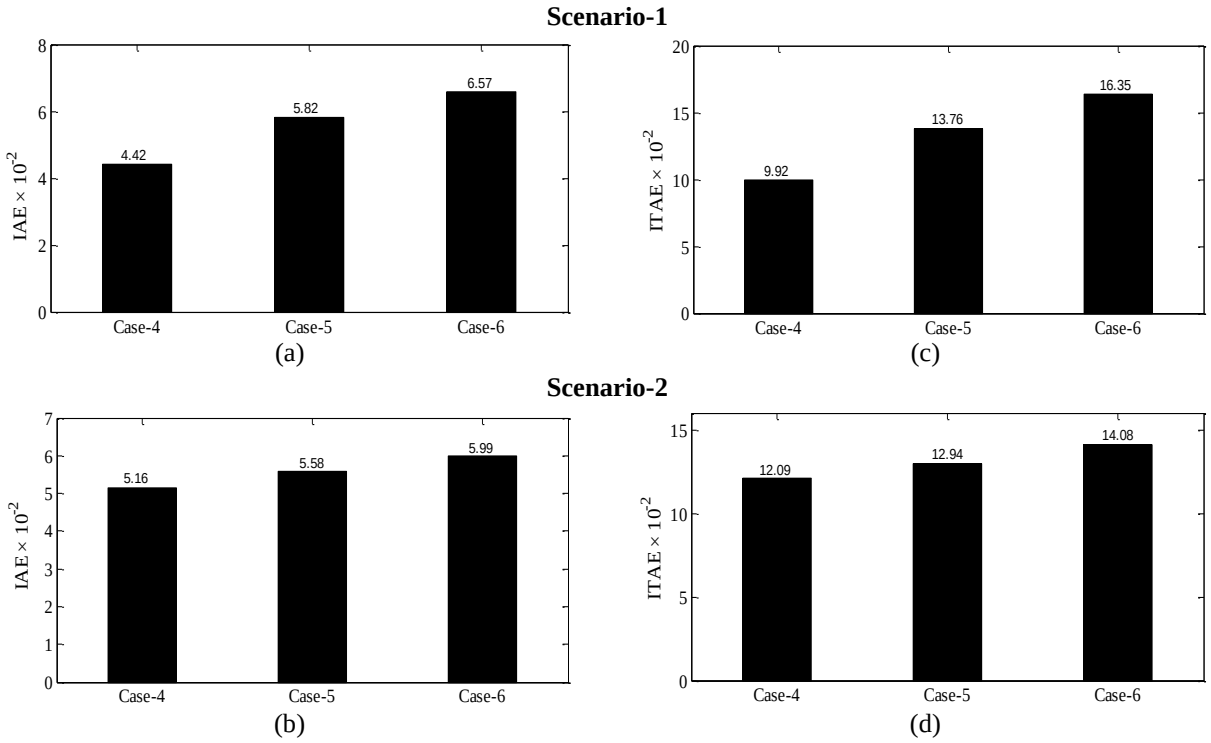

Fig. 6.7: Values of (a)-(b) *IAE* and (c)-(d) *ITAE* with CSOPSSs for scenarios1-2 of unseen operating cases 4-6

The figure reveals that the values of both indices for the CSOPSSs are minimum for each scenario of Case-4 and maximum for each scenario of Case-6, which indicates that Case-6 is the most severe whereas Case-4 is the least severe. Moreover, for operating Case-4, Scenario-2 is more severe but for cases 5-6, Scenario-1 is more severe.

Hence, the designed CSOPSS controllers for WSCC power system is capable to damp out LFO with enhanced stability and damping performances for wide range of operating cases under different scenarios of severe disturbances and also for unseen operating cases under same scenarios of disturbances.

6.2.2 Example 2: Two-Area, Four-Machine (TAFM) Power System

The operating condition details and single-line diagram of TAFM power system is described in Section 3.4.2 and Appendix respectively.

A. Eigenvalue Analysis of TAFM Power System without PSS and with CSOPSSs

The open-loop eigenvalues, damping ratio, frequency, participation modes and participation factor associated with electromechanical modes of the system are depicted in Table 3.10 and discussed in Section 3.4.2 (A). An eigenvalue-based multi-objective function *J* presented in (3.1) is minimized using CSO by tuning the nine parameters of PSSs. The CSO is applied with population size 50, maximum generation 50, probability index (p_a) = 0.25.

The CSO is able to find the desired solution for which fitness function *J* is zero. The final value of *J* equal to zero indicates that three unstable and/or poorly damped eigenvalues are shifted to a specified D-shape zone in the left-half of the *s*-plane. The optimum designed nine parameters of CSOPSSs for three generators are shown in Table 6.4. The closed-loop eigenvalues and their damping ratio using CSOPSSs for three loading cases are determined using PSAT [215] and shown in Table 6.5. The Fig. 6.8 (a)-(c) and (d)-(f) show the eigenvalue maps for without PSS and with CSOPSSs for loading cases 1-3 respectively.

Table 6.4: Optimal designed parameters of CSOPSSs for TAFM power system

Generators	K	T_1	T_3
G_1	99.421	0.014	0.116
G_2	41.590	0.059	0.010
G_4	36.781	0.049	0.035

Table 6.5: Eigenvalues and damping ratio with CSOPSSs for loading cases 1-3 of TAFM power system

Case-1	**Case-2**	**Case-3**
– 1.157 ± j 4.275, 0.26	– 1.090 ± j 3.595, 0.29	– 1.119 ± j 5.322, 0.20
– 6.742 ± j 4.788, 0.81	– 7.472 ± j 2.563, 0.94	– 4.343 ± j 2.917, 0.83
– 7.733 ± j 2.332, 0.95	– 6.237 ± j 4.167, 0.83	– 5.049 ± j 0.353, 0.99

The eigenvalue maps of without PSS for unstable and lightly damped modes with TAFM system are discussed in Section 3.4.2 (A). Table 6.5 and Fig. 6.8 (d)-(f) show that the CSOPSSs shift the eigenvalues to a specified D-shape zone in the left half of the *s*-plane with desired damping factor and damping ratio as compared to that of without PSS for all loading cases. Hence, designed CSOPSS controllers provide improved stability and damping performance of the TAFM power system as compared to same obtained using without PSS.

B. Time-Domain Simulation Results and Discussions with CSOPSSs and without PSS of TAFM Power System

The time-domain simulation of TAFM power system is performed with designed CSOPSSs for different test scenarios mentioned earlier in Table 3.14 of severe loading cases. The speed deviations $\Delta w_1, \Delta w_2$, $\Delta w_3$and $\Delta w_4$for the system without PSS and with CSOPSSs are shown in Fig. 6.9 (a)-(d) and (e)-(h) respectively.

The analysis of response plots without PSS already discussed in Section 3.4.2 (B). From Fig. 6.9 (e)-(h), it is observed that with CSOPSSs, oscillations for all generators are well damp out with less overshoot and settling time for all scenarios of severe loading cases. Moreover, it is clear that the system performance with CSOPSSs is much improved than that of without PSS for all severe disturbance scenarios of loading cases and oscillations are die out smoothly. Furthermore, on the basis of number of cycles of operation, it may be observed that the speed

response with CSOPSSs for Scaneraio-4 consumed more time to damp out oscillations as compared to Scenario-2 of loading Case-3.

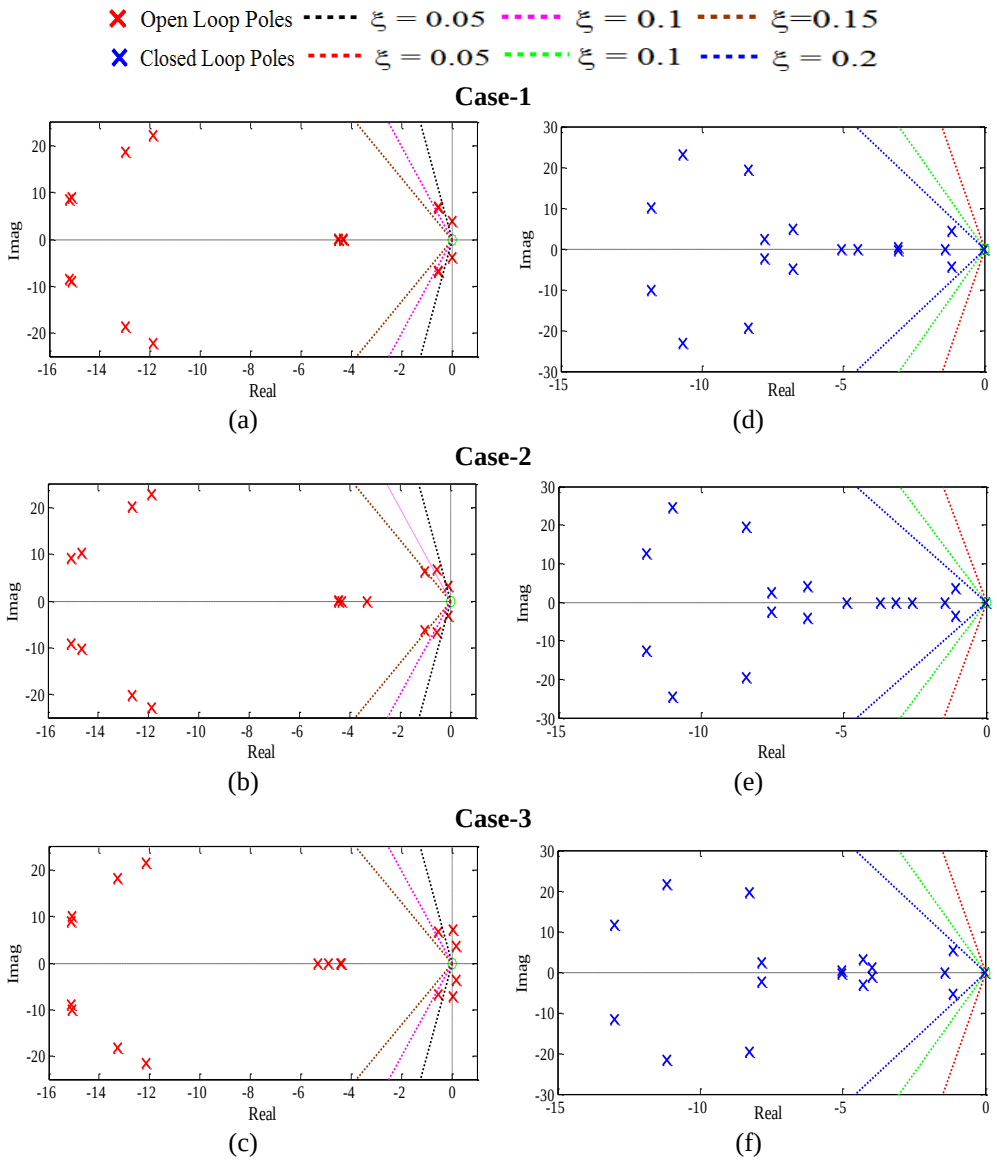

Fig. 6.8 Eigenvalue maps (a)-(c) without PSS and (d)-(f) with CSOPSSs for loading cases 1-3 of TAFM power system

This demonstrates the potential of CSO to obtain a desired set of PSS parameters for TAFM power system and the designed CSOPSSs are able to improve the damping performance of the system than that of without PSS for wide range of loading cases under severe scenarios of disturbances.

C. Performance Indices Results and Discussions with CSOPSSs of TAFM Power System

In addition to simulation results, the effectiveness of CSOPSS controllers is also observed by determining indices *IAE* and *ITAE* values for considered scenarios of different disturbances mentioned in Table 3.14. The bar charts of both indices obtained by CSOPSSs for scenarios 1-4 of loading cases 1-3 are shown in Fig. 6.10 (a)-(d) and (e)-(h) respectively.

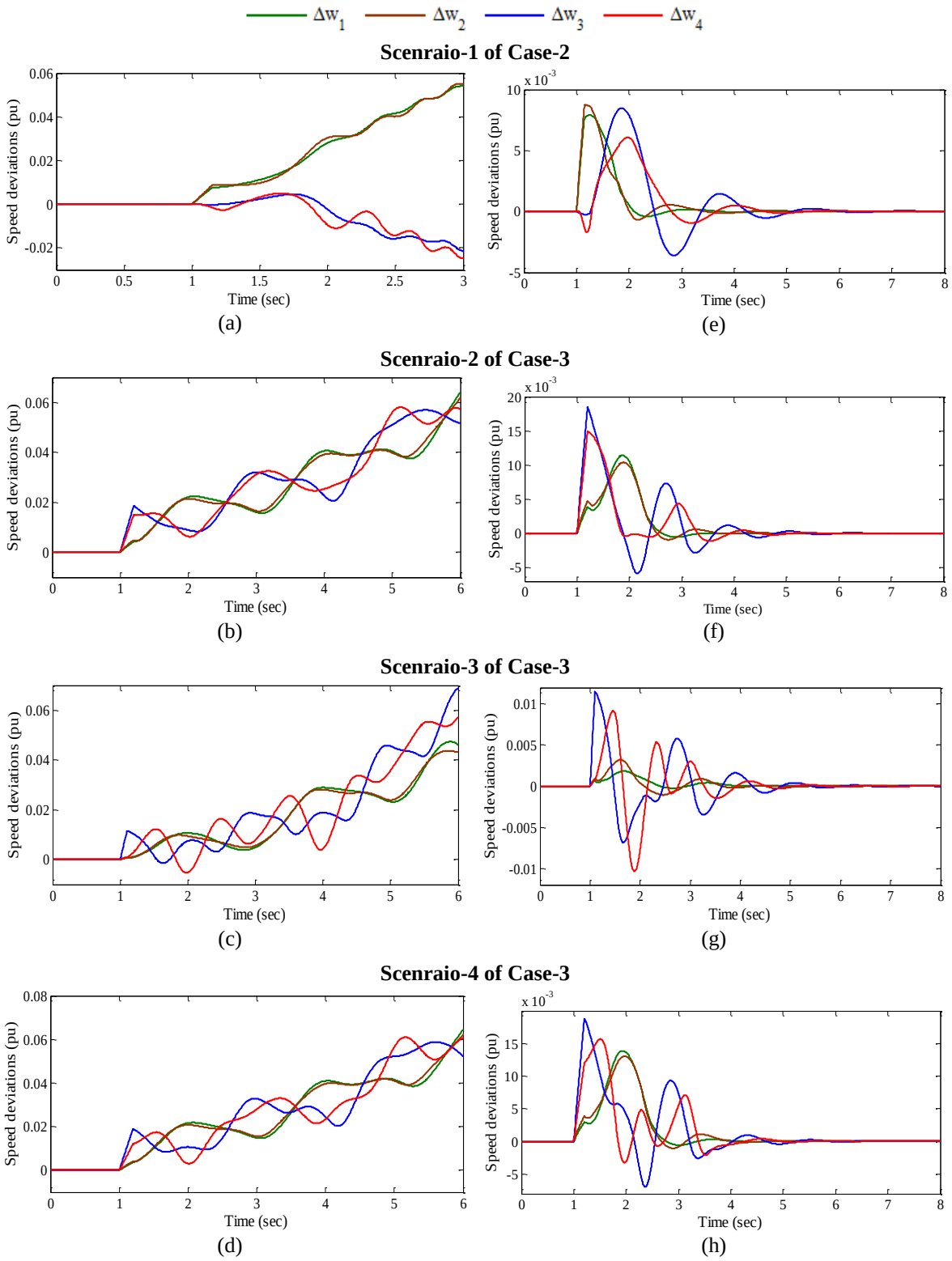

Fig. 6.9 Speed deviations (a)-(d) without PSS and (e)-(h) with CSOPSSs for scenarios 1-4 of severe loading case

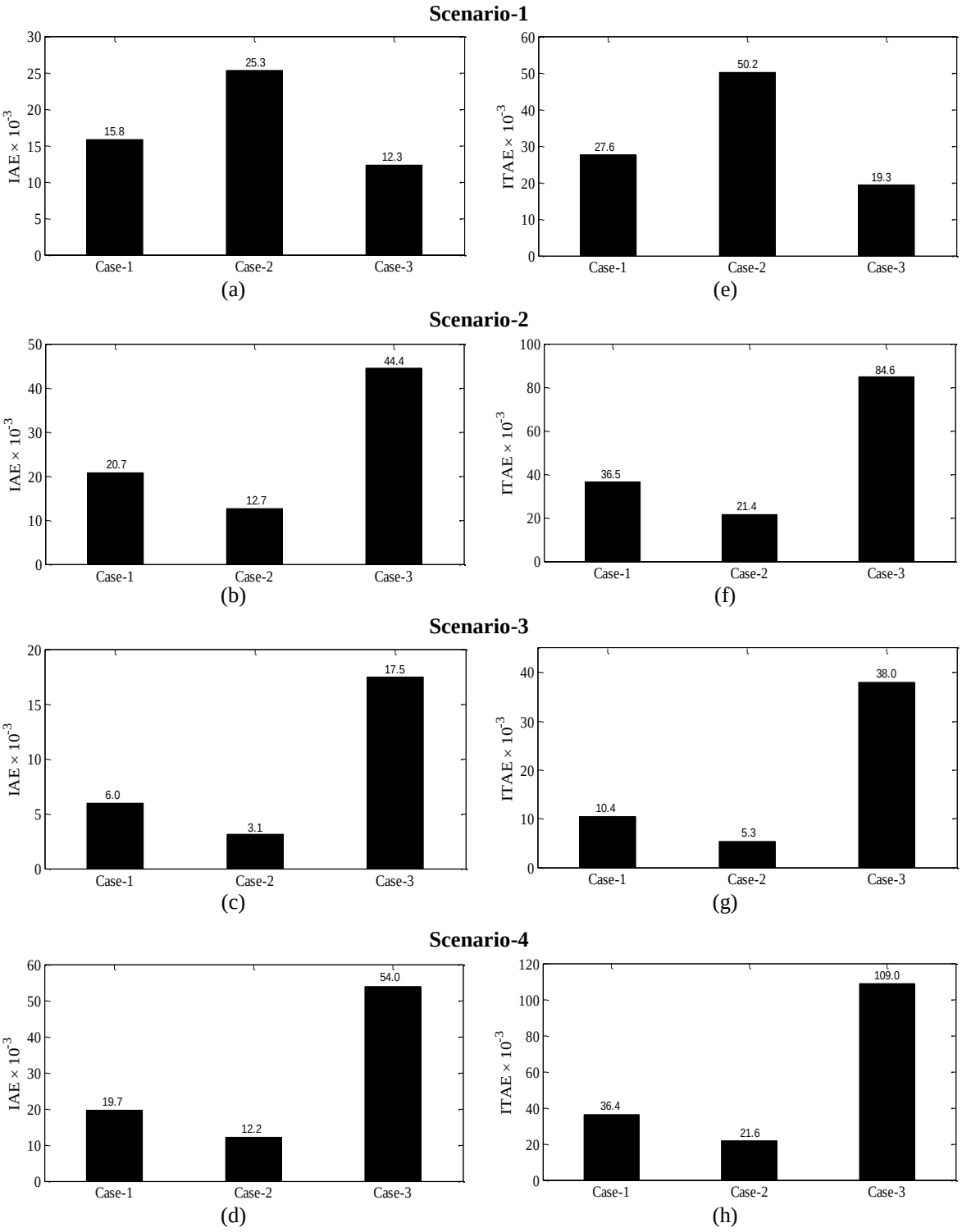

Fig. 6.10 Values of (a)-(d) *IAE* and (e)-(h) *ITAE* with CSOPSSs for scenarios 1-4 of loading cases 1-3

The figure reveals that both indices values for the CSOPSSs are higher for Scenario-1 of Case-2 loading and lower for Case-3 loading. Similarly, both indices are lower for scenarios 2-4 of Case-2 and higher for Case-3 loading, which indicates that Case-3 is the most severe for scenarios 2-4 whereas Case-2 is the least severe. Comparing Fig. 6.10 with Fig. 3.11, it may be observed that the designed CSOPSS controllers provide sufficient damping to damp out low frequency local and inter-area modes of oscillations with less overshoot and settling time than

that of without PSS, although the disturbances are simulated for more number of cycles on the system with CSOPSSs.

D. Robustness Test of CSOPSS Controllers of TAFM Power System

To test the robustness of previously design CSOPSS controllers for TAFM power system, nine unseen operating cases 4-12 are depicted in Table 3.15. In this section, the effectiveness of designed CSOPSSs is checked by eigenvalue analysis, time-domain simulation results and performance indices for unseen cases and compared with that of without PSS.

Open-loop eigenvalues, damping ratio, frequency, participation modes and participation factor for unseen operating cases 4-12 of TAFM power system without PSS are illustrated in Table 3.16 and explained in Section 3.4.2 (D). Now, previously designed CSOPSS parameters are used to obtain closed-loop eigenvalues and damping ratio using PSAT [215] for unseen cases 4-12 of TAFM power system for only unstable and poorly damped modes and are shown in Table 6.6.

Table 6.6: Eigenvalues and damping ratio with CSOPSSs for unseen operating cases 4-12 of TAFM power system

Cases	**With CSOPSSs**		
Case-4	– 5.878 ± j 4.573, 0.789	– 1.454 ± j 3.902, 0.349	– 7.597 ± j 2.453, 0.951
Case-5	– 4.720 ± j 1.945, 0.924	– 1.339 ± j 5.466, 0.237	– 13.058 ± j 11.902, 0.739
Case-6	– 5.856 ± j 4.573, 0788	– 1.451 ± j 3.907, 0.348	– 12.198 ± j 10.415, 0.760
Case-7	– 4.707 ± j 1.922, 0.925	– 1.337 ± j 5.471, 0.237	– 13.062 ± j 11.920, 0.738
Case-8	– 1.064 ± j 3.604, 0.283	– 5.796 ± j 3.977, 0.824	– 7.391 ± j 2.632, 0.942
Case-9	– 2.988 ± j 2.547, 0.760	**– 0.968** ± j 5.650, **0.168**	– 13.262 ± j 12.968, 0.715
Case-10	– 2.597 ± j 1.572, 0.855	**– 0.987** ± j 5.815, **0.167**	– 13.273 ± j 13.125, 0.711
Case-11	– 2.587 ± j 1.583, 0.852	**– 0.984** ± j 5.818, **0.166**	– 13.275 ± j 13.142, 0.710
Case-12	– 1.060 ± j 3.701, 0.275	– 5.161 ± j 3.783, 0.806	– 7.338 ± j 2.685, 0.939

The table reveals that the CSOPSSs shift the eigenvalues in the left half of the *s*-plane with improved damping factor and damping ratio as compared to without PSS for unseen cases 4-12. This ensures that the TAFM power system will be stable for all considered unseen cases also. It is also observed that CSOPSS controllers satisfy the earlier selected criterion for the value of desired damping factor and damping ratio for PSS design except in unseen cases 9, 10 and 11 where slightly more overshoot and settling time may occur. Hence, the CSO provides robustness with improved stability and grater damping performance for unseen operating cases 4-12 of the TAFM power system as compared to that of without PSS.

In order to check the robustness performance of designed CSOPSS controllers in terms of speed deviations, earlier severe scenarios 5-13 of unseen operating cases 4-12 of TAFM power system mentioned in Table 3.17 are considered.

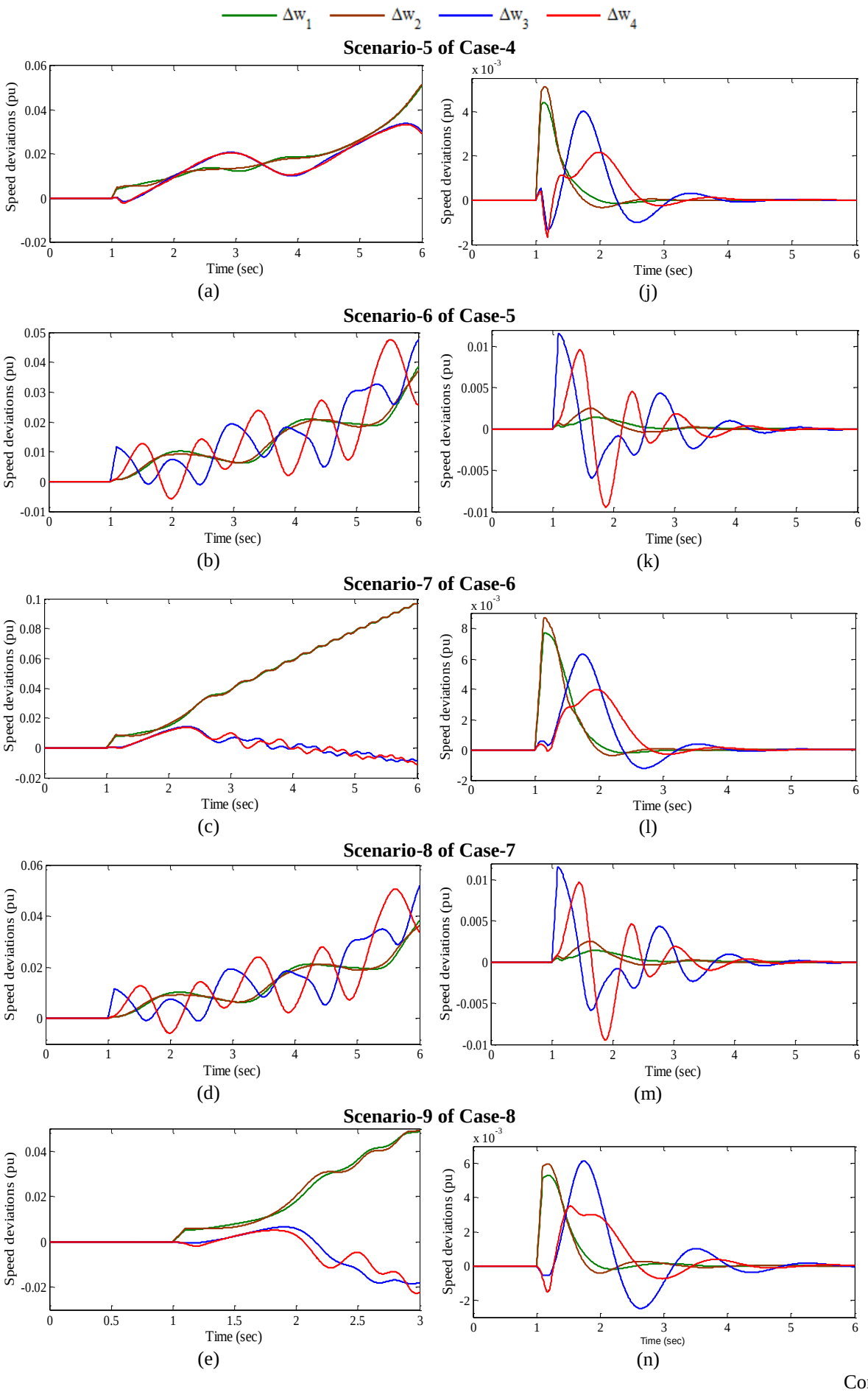
Δw1 Δw2 Δw3 Δw4
Scenario-5 of Case-4
Speed deviations (pu)
Time (sec)
x 10-3
(a)
(j)
Scenario-6 of Case-5
(b)
(k)
Scenario-7 of Case-6
(c)
(l)
Scenario-8 of Case-7
(d)
(m)
Scenario-9 of Case-8
(e)
(n)

Cont.

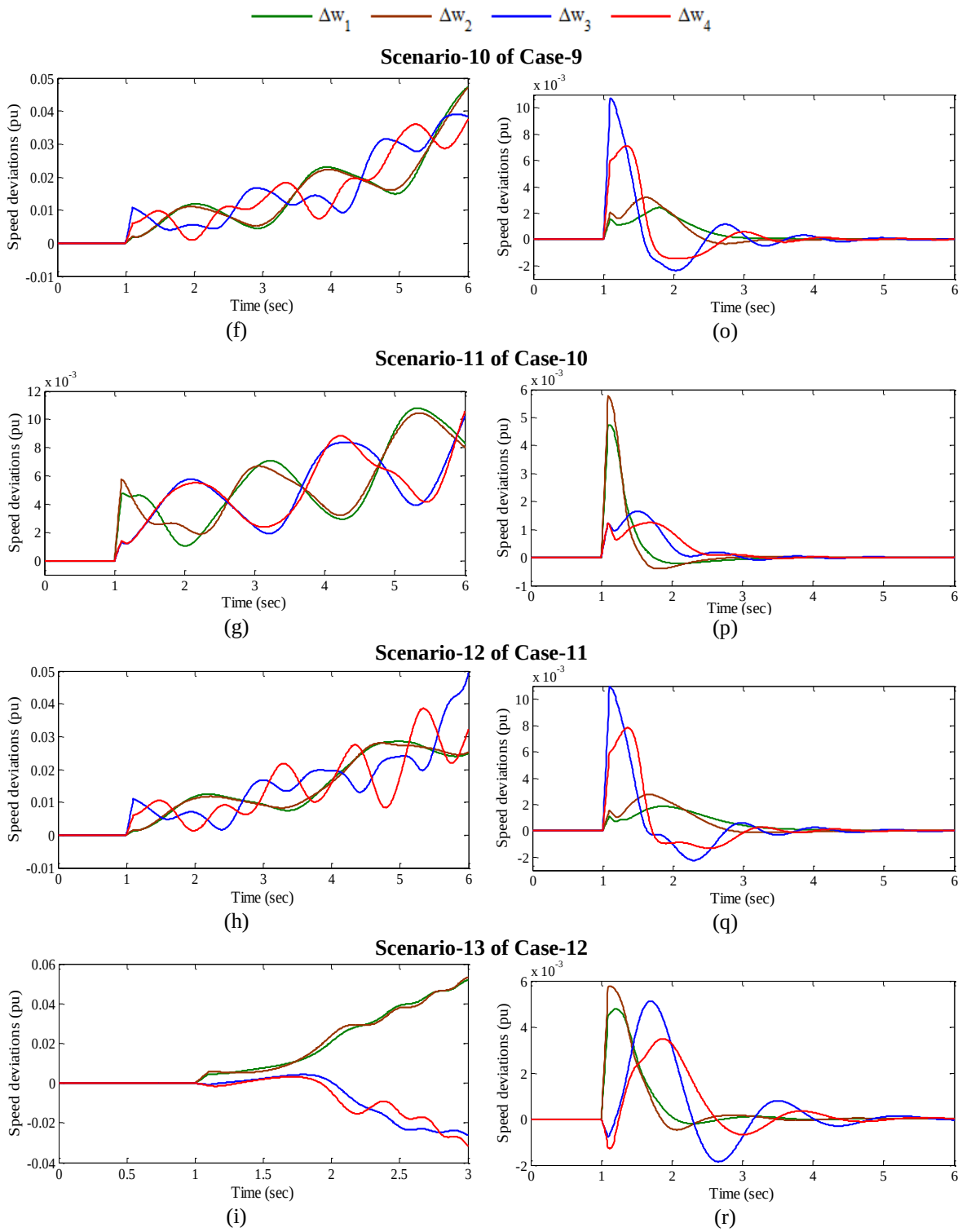

Fig. 6.11 Speed deviations (a)-(i) without PSS and (j)-(r) with CSOPSSs for scenarios 5-13 of unseen operating cases 4-12

The speed deviations Δw_1, Δw_2, Δw_3 and Δw_4 for the system without PSS and with CSOPSSs for scenarios 5-13 of unseen cases 4-12 are shown in Fig. 6.11 (a)-(i) and (j)-(r) respectively.

The analysis of response plots without PSS already discussed in Section 3.4.2 (D). From Fig. 6.11 (j)-(r) it is noticed that the system performance with CSOPSSs is improved for severe

disturbance scenarios 6-13 of unseen operating cases 4-12 and oscillations are well damped out. Furthermore, the comparison of speed deviations with CSOPSSs basis on number of cycle operation, the Scenario-8 of Case-7 takes more time to reach in steady state than other scenarios. This may be concluded that the designed CSOPSSs work satisfactorily for most of the scenarios of severe disturbances of unseen operating cases of TAFM power system.

In addition to time-domain simulation results, the robustness and effectiveness of CSOPSS controllers is also noticed by calculating indices *IAE* and *ITAE* for observed scenarios 5-13 of unseen operating cases 4-12. The bar charts of both indices values obtained with CSOPSSs for defined scenarios are shown in Fig. 6.12 (a) and (b) respectively.

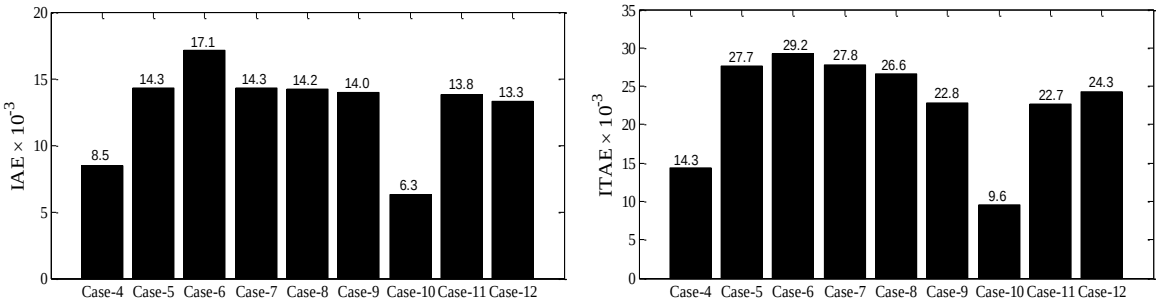

Fig. 6.12 Value of (a) *IAE* and (b) *ITAE* with CSOPSSs for scenarios 5-13 of unseen operating cases 4-12

Both indices values with CSOPSSs are minimum and maximum for 6-cycle operation of unseen cases 10 and 7 respectively. Therefore, it is concluded that Scenario-11 and 8 are least and most severe scenario of disturbance respectively. Hence, the CSOPSS controllers design provide the improved damping performance to damp out both local and inter-area modes of oscillations with improved overshoot and settling time than without PSS for unseen operating cases of TAFM power system.

6.2.3 Example 3: Ten-Machine, Thirty-Nine Bus New England Power System (NEPS)

The operating condition details and single-line diagram of NEPS is described in Section 3.4.3 and Appendix respectively.

A. Eigenvalue Analysis of NEPS without PSS and with CSOPSSs

Open-loop eigenvalues, damping ratio, frequency, participation modes and participation factor associated with electromechanical modes of the system are illustrated in Table 3.19 and discussed in Section 3.4.3 (A). An eigenvalue-based multi-objective function *J* (equation 3.1) presented in Section 3.2 is minimized using CSO for designing twenty-seven PSS parameters of nine generators. The CSO is applied with population size 100, maximum generation 100, probability index (p_a) = 0.25.

The CSO is able to find the desired solution for which fitness function *J* is zero. The final value of *J* equal to zero indicates that nine unstable and/or poorly damped eigenvalues are shifted to a specified D-shape zone in the left-half of the *s*-plane. The optimum designed parameters for CSOPSSs are shown in Table 6.7. The closed-loop eigenvalues and their damping ratio with CSOPSSs for loading cases 1-3 are determined using PSAT [215] and are shown in Table 6.8. Figure 6.13 (a)-(c) and (d)-(f) present the eigenvalue maps for without PSS and with CSOPSSs of NEPS for loading cases 1-3 respectively.

Table 6.7: Optimal designed parameters of CSOPSSs for NEPS

Optimized Parameters	**Generators**								
	G_2	G_3	G_4	G_5	G_6	G_7	G_8	G_9	G_{10}
K_1	6.044	21.838	72.428	58.056	5.398	19.712	26.025	80.382	24.625
T_1	0.300	0.011	0.175	0.497	0.470	0.046	0.023	0.214	0.327
T_3	0.583	0.305	0.024	0.037	0.262	0.408	0.393	0.124	0.634

Table 6.8: Eigenvalues and damping ratio with CSOPSSs for operating cases 1-3 of NEPS

Case-1	**Case-2**	**Case-3**
– 2.362 ± j 11.928, 0.194	– 2.396 ± j 11.573, 0.202	– 2.177 ± j 13.408, 0.160
– 1.611 ± j 7.386, 0.213	– 1.517 ± j 7.312, 0.203	– 1.534 ± j 7.387, 0.203
– 1.088 ± j 8.834, 0.122	– 0.927 ± j 8.787, 0.104	– 1.108 ± j 8.824, 0.124

The eigenvalue maps of without PSS for unstable and lightly damped modes of NEPS are discussed in Section 3.4.3 (A). Table 6.8 and Fig. 6.13 (d)-(f) show that the CSOPSSs shift the eigenvalues to a specified D-shape zone in the left half of the *s*-plane with desired damping factor and damping ratio as compared to without PSS for three loading cases. Hence, CSOPSS controllers provide improved stability and damping characteristics of the NEPS as compared to same obtained using without PSS.

B. Time-Domain Simulation Results and Discussions with CSOPSSs and without PSS of NEPS

The simulations of NEPS are performed with PSSs for five different scenarios of disturbances mentioned in Table 3.24 for three loadings cases. The speed deviations $\Delta w_1, \Delta w_2, \Delta w_3, \Delta w_4, \Delta w_5, \Delta w_6, \Delta w_7, \Delta w_8, \Delta w_9$ and Δw_{10} for without PSS and with CSOPSSs for scenarios 1-5 of severe Case-3 loading are shown in Fig. 6.14 (a)-(e) and (f)-(j) respectively.

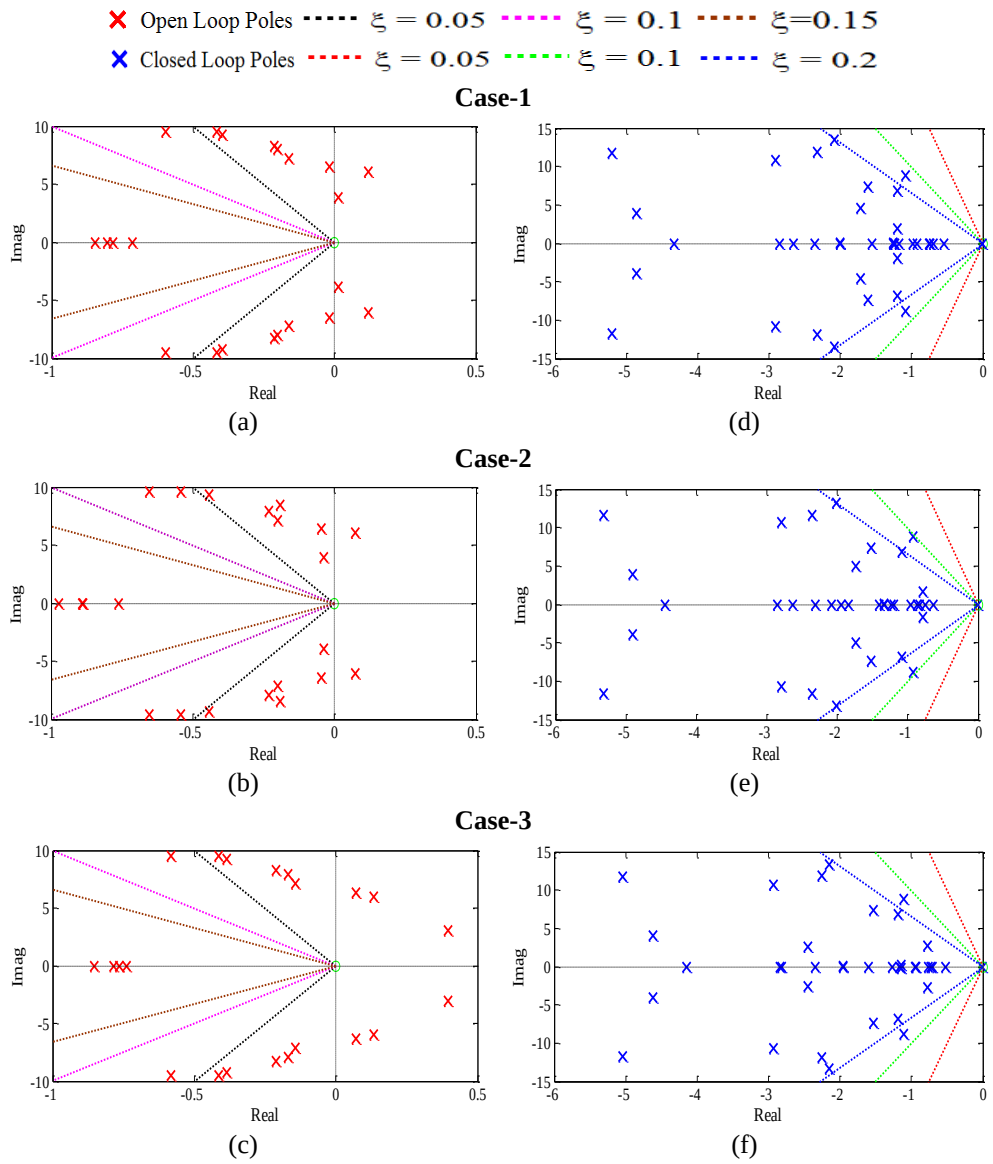

Fig. 6.13 Eigenvalue maps (a)-(c) without PSS and (d)-(f) with CSOPSSs for loading cases 1-3 of NEPS

The analysis of response plots without PSS already discussed in Section 3.4.3 (B). Figure 6.14 (f)-(j) reveals that the speed response with CSOPSSs for Scenario-1 of Case-3 loading have large peak overshoot and consumed more time to die out oscillations as compared to others. Therefore, it is concluded that with CSOPSSs Scenario-1 is most severe scenario than others. This demonstrates the potential of CSO technique to obtain the desired set of PSS parameters for NEPS and the designed CSOPSSs are capable to damp out LFO for wide range of loading cases under severe scenarios of disturbances.

C. Performance Indices Results and Discussions with CSOPSSs of NEPS

In addition to simulation results, the effectiveness of designed CSOPSS controllers is also observed by determining indices *IAE* and *ITAE* for earlier five observed scenarios of different disturbances. The bar charts of both indices values obtained by CSOPSS controllers for scenarios 1-5 of three loading cases are shown in Fig. 6.15 (a)-(e) and (f)-(j) respectively.

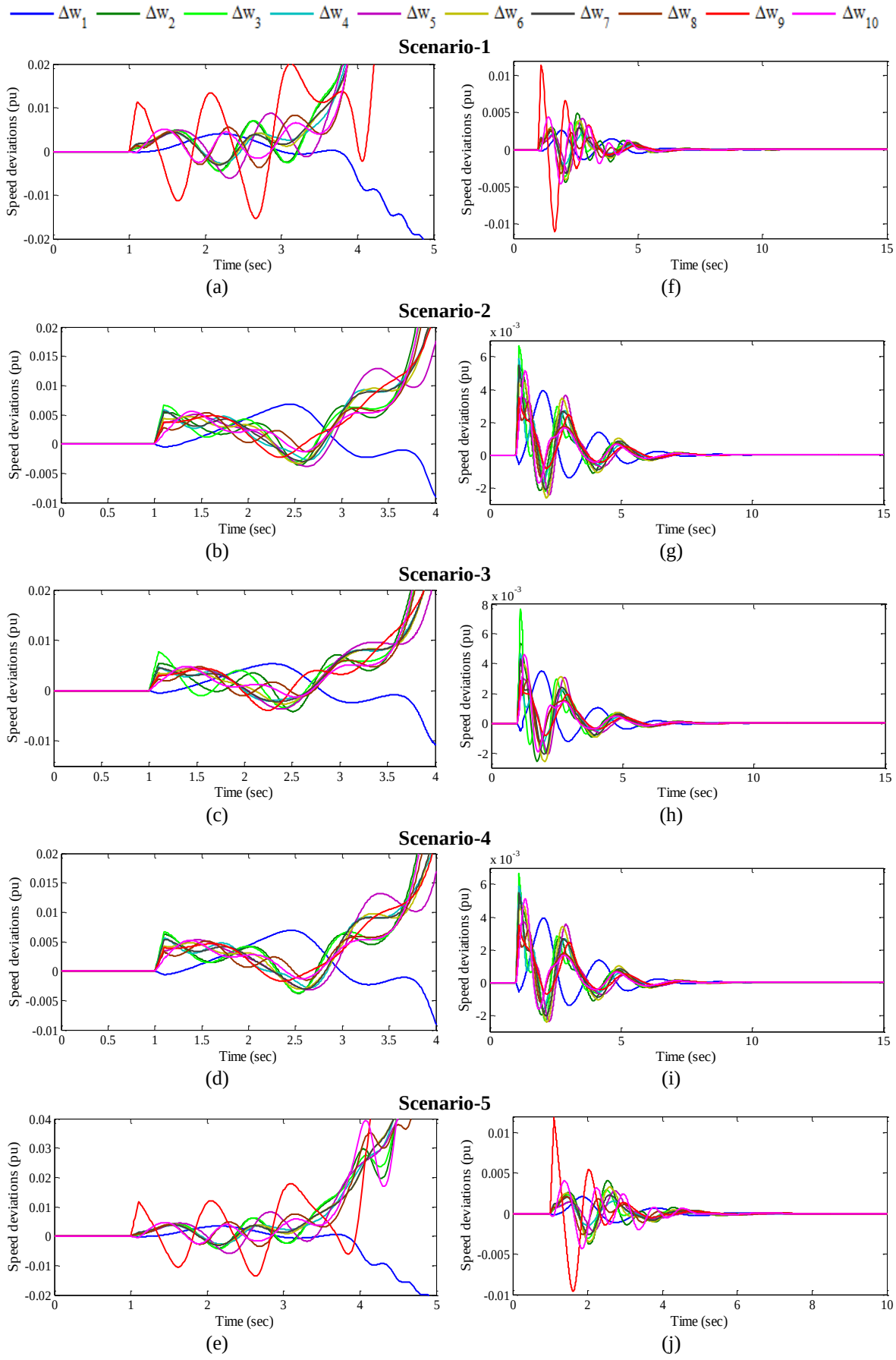

Fig. 6.14 Speed deviations (a)-(e) without PSS and (i)-(j) with CSOPSSs for scenarios 1-5 of loading case-3

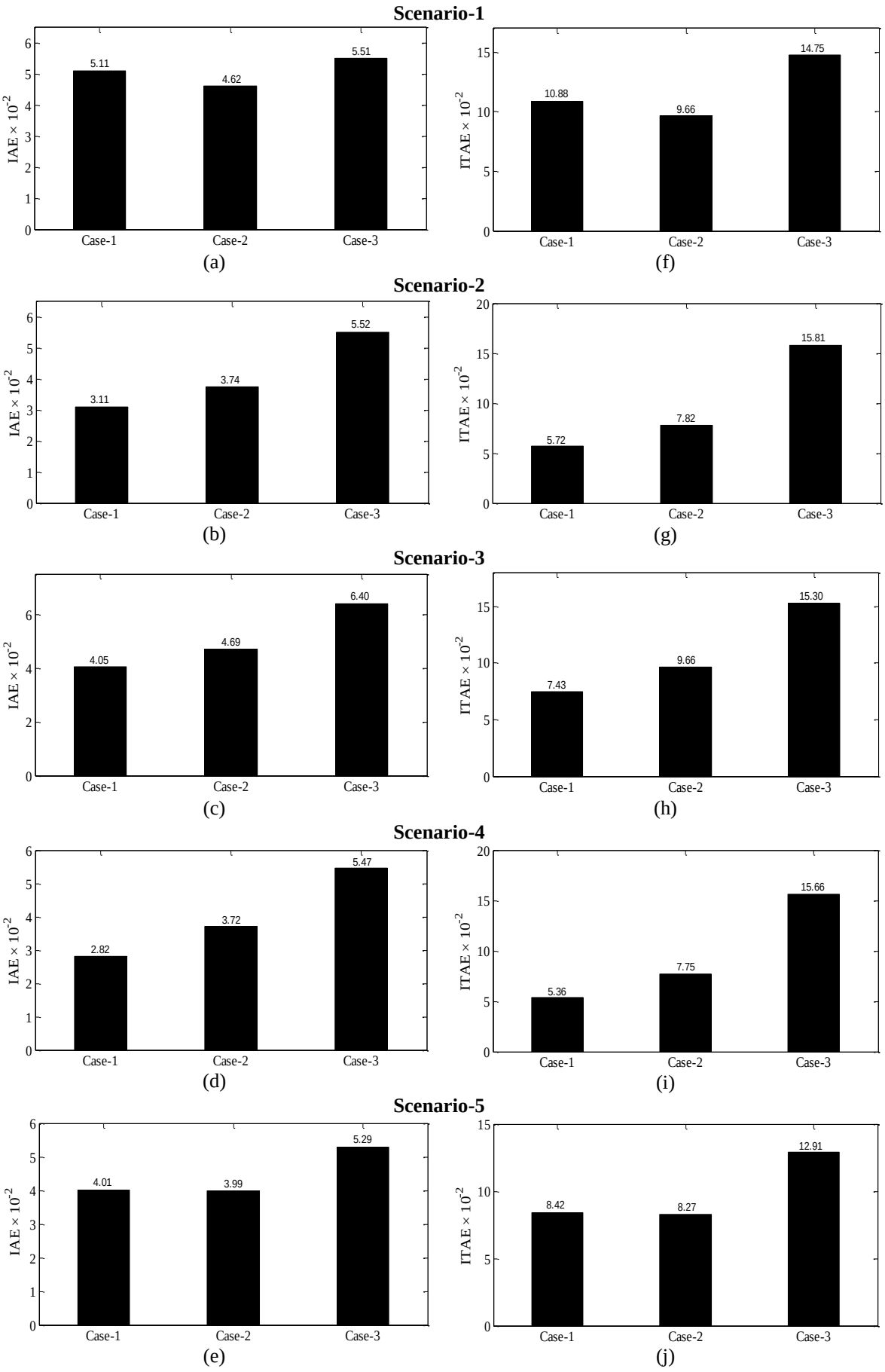

Fig. 6.15 Values of (a)-(e) *IAE* and (f)-(j) *ITAE* with CSOPSSs for scenarios 1-5 of loading cases 1-3

The values of both indices with CSOPSSs for Scenario-1 of loading Case-2 and Case-3 are minimum and maximum respectively whereas for scenarios 2-5 of loading Case-1 and Case-3 are minimum and maximum respectively. Moreover, the Scenario-2 and Scenario-5 for Case-3 loading is most and least severe scenario than others.

Comparing Fig. 6.15 with Figs. 3.18 and 3.19, it may be observed that the designed CSOPSSs controllers of NEPS provide sufficient damping to damp out low frequency local and inter-area modes of oscillations with less overshoot and settling time than that of without PSS.

D. Robustness Test of Designed CSOPSS Controllers of NEPS

To test the robustness of previously designed CSOPSS controllers, fifteen unseen operating cases 4-18 mentioned in Table 3.25 are considered. In this section, the effectiveness of CSOPSS controllers is checked by eigenvalue analysis, time-domain simulation results and performance indices for four observed scenarios of cases 4-18 and compared with to that of without PSS.

Open-loop eigenvalues, damping ratio, frequency, participation modes and participation factor for only unstable and critical poorly damped modes of unseen cases 4-18 of NEPS without PSS illustrated in Table 3.26 and discussed in Section 3.4.3 (D). Table 6.9 shows the closed-loop eigenvalues and damping ratio for unseen cases 4-18 of NEPS with CSOPSS controllers for only unstable and critical poorly damped modes respectively.

Table 6.9: Eigenvalues and damping ratio with CSOPSSs for unseen operating cases 4-18 of NEPS

Cases	**With CSOPSSs**		
Case-4	– 1.235 ± j 7.014, 0.173	– 1.492 ± j 4.971, 0.287	– 5.266 ± j 11.752, 0.408
Case-5	– 1.756 ± j 6.056, 0.278	– 2.350 ± j 11.909, 0.193	– 5.221 ± j 11.683, 0.408
Case-6	– 1.811 ± j 4.402, 0.380	– 1.156 ± j 1.991, 0.502	– 1.588 ± j 7.386, 0.210
Case-7	– 1.618 ± j 7.385, 0.214	– 1.711 ± j 4.684, 0.343	– 1.149 ± j 1.899 0.517
Case-8	– 1.893 ± j 4.248, 0.407	– 0.907 ± j 2.007, 0.411	– 1.510 ± j 6.032, 0.242
Case-9	– 0.510 ± j 1.762, 0.278	– 1.642 ± j 5.183, 0.302	– 2.155 ± j 3.695, 0.503
Case-10	– 1.106 ± j 6.124, 0.175	– 1.229 ± j 2.033, 0.517	– 1.507 ± j 7.153 0.205
Case-11	– 0.782 ± j 1.893, 0.381	– 1.598 ± j 7.169, 0.217	– 2.368 ± j 11.905, 0.195
Case-12	– 1.155 ± j 1.959, 0.507	– 2.384 ± j 11.843, 0.197	– 2.838 ± j 10.647, 0.257
Case-13	– 1.500 ± j 7.178, 0.204	– 2.362 ± j 11.862, 0.195	– 2.906 ± j 10.714, 0.261
Case-14	– 1.089 ± j 8.828, 0.123	– 1.674 ± j 7.233, 0.225	– 1.574 ± j 4.518, 0.329
Case-15	– 1.332 ± j 6.939, 0.188	– 1.562 ± j 6.364, 0.238	– 1.798 ± j 4.390, 0.379
Case-16	– 1.138 ± j 6.203, 0.180	– 1.301 ± j 8.152, 0.157	– 1.542 ± j 7.062, 0.213
Case-17	– 1.322 ± j 6.920, 0.187	– 1.557 ± j 6.359, 0.237	– 1.771 ± j 4.371, 0.375
Case-18	– 1.275 ± j 6.375, 0.196	– 2.300 ± j 8.788, 0.253	– 1.493 ± j 7.165, 0.203

The table reveals that with CSOPSSs eigenvalues are shifted in the left half of the *s*-plane with improved damping factor and damping ratio as compared to without PSS for all unseen operating cases. This ensures that the NEPS will be stable for all considered unseen cases also. It is also found that designed CSOPSS controllers satisfy the earlier selected criterion for the value of desired damping factor and damping ratio for all unseen operating cases except cases 9 where slightly more settling time may occur. Hence, the CSO provides robustness with improved stability and damping performance for unseen operating cases 4-18 of the NEPS as compared to that of without PSS.

In order to check the robustness performance of the designed CSOPSS controllers in terms of speed deviations, earlier four scenarios of disturbances mentioned in Table 3.24 are considered for unseen cases 4-18 of NEPS without PSS. The speed deviations Δw_1, Δw_2, Δw_3, Δw_4, Δw_5, Δw_6, Δw_7, Δw_8, Δw_9 and Δw_{10} for the system without PSS and with CSOPSSs for severe disturbances Scenario-1 of various unseen cases 4-12 of NEPS are shown in Fig. 6.16 (a)-(i) and (j)-(r) respectively.

The analysis of response plots without PSS already discussed in Section 3.4.3 (D). From Fig. 6.16 (j)-(r), it is observed that the speed deviations with CSOPSSs, the oscillations are well damped out. Moreover, it is observed that the Case-9 delivers more oscillations and consumed more time to reach in steady state as compared to others. In unseen cases 4-12, the Δw_9 is most severe speed deviations than others. Furthermore, peak overshoot of Δw_9 is almost similar in all considered operating cases.

To check the robustness of designed CSOPSS controllers on other unseen cases, the Scenario-4 is performed on other unseen operating cases 13-18. The speed deviations of NEPS without PSS and with CSOPSSs for Scenario-4 of cases 13-18 are shown in Fig. 6.17 (a)-(f) and (g)-(l) respectively.

The analysis of response plots without PSS already discussed in Section 3.4.3 (D). From Fig. 6.17 (g)-(l), it is noticed that LFO in speed response with CSOPSSs are well damped out. Moreover, it is observed that speed responses in unseen Case-16 have high peak overshoot and Case-18 consumed more time to die out oscillations as compared to others. It is clear that the system performance with CSOPSSs is improved to that of without PSS for severe disturbance scenarios 1 and 4 of unseen operating cases. This may be concluded that the designed CSOPSSs work satisfactorily for most of the scenarios of severe disturbances of unseen operating cases of NEPS.

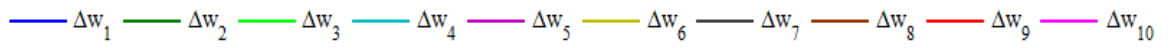

Case-4

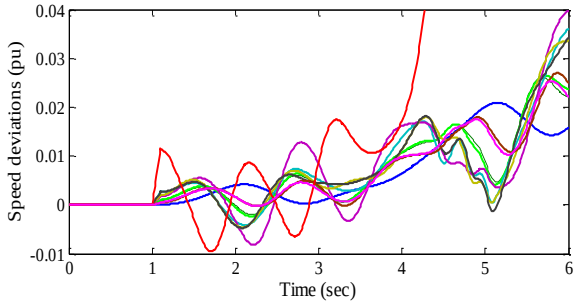

(a)

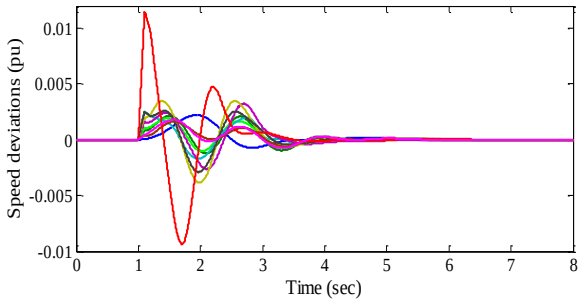

(j)

Case-5

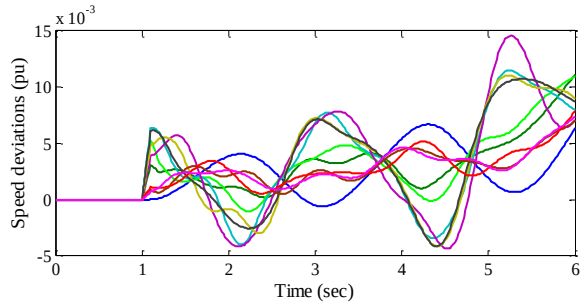

(b)

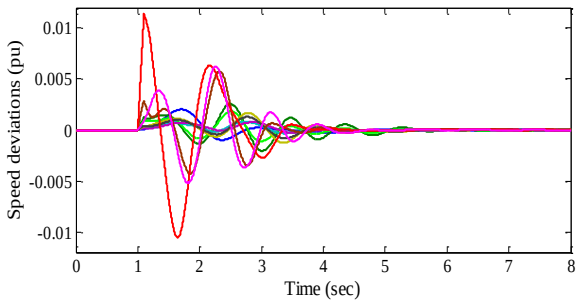

(k)

Case-6

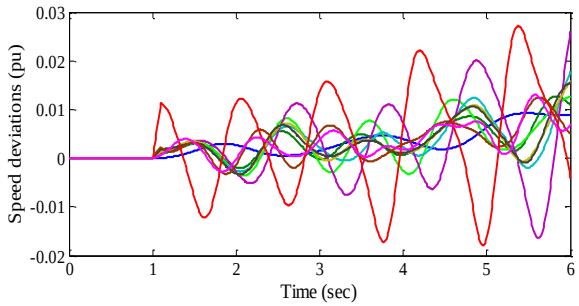

(c)

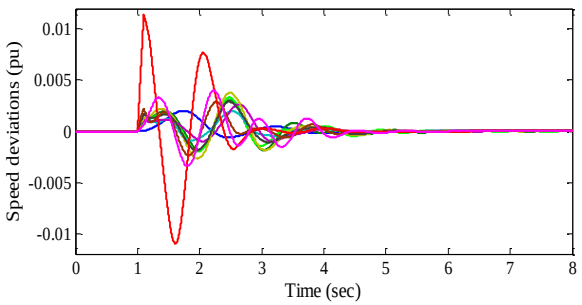

(l)

Case-7

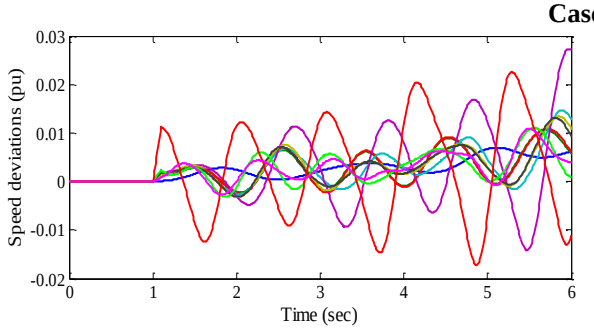

(d)

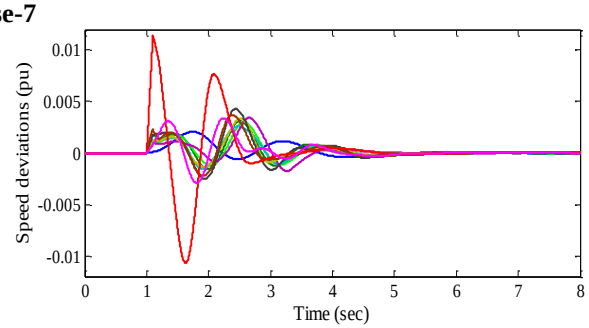

(m)

Case-8

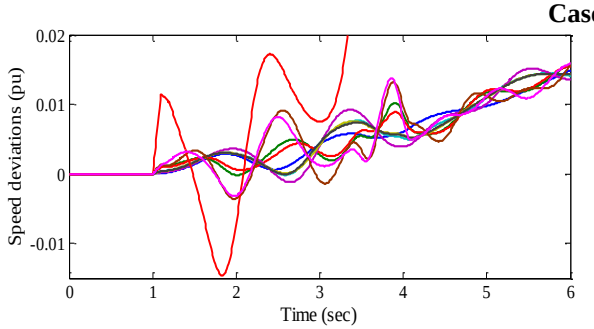

(e)

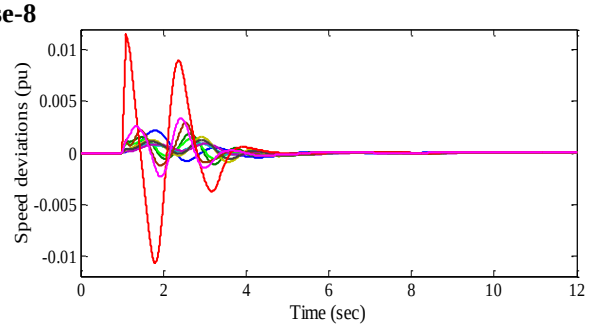

(n)

Cont.

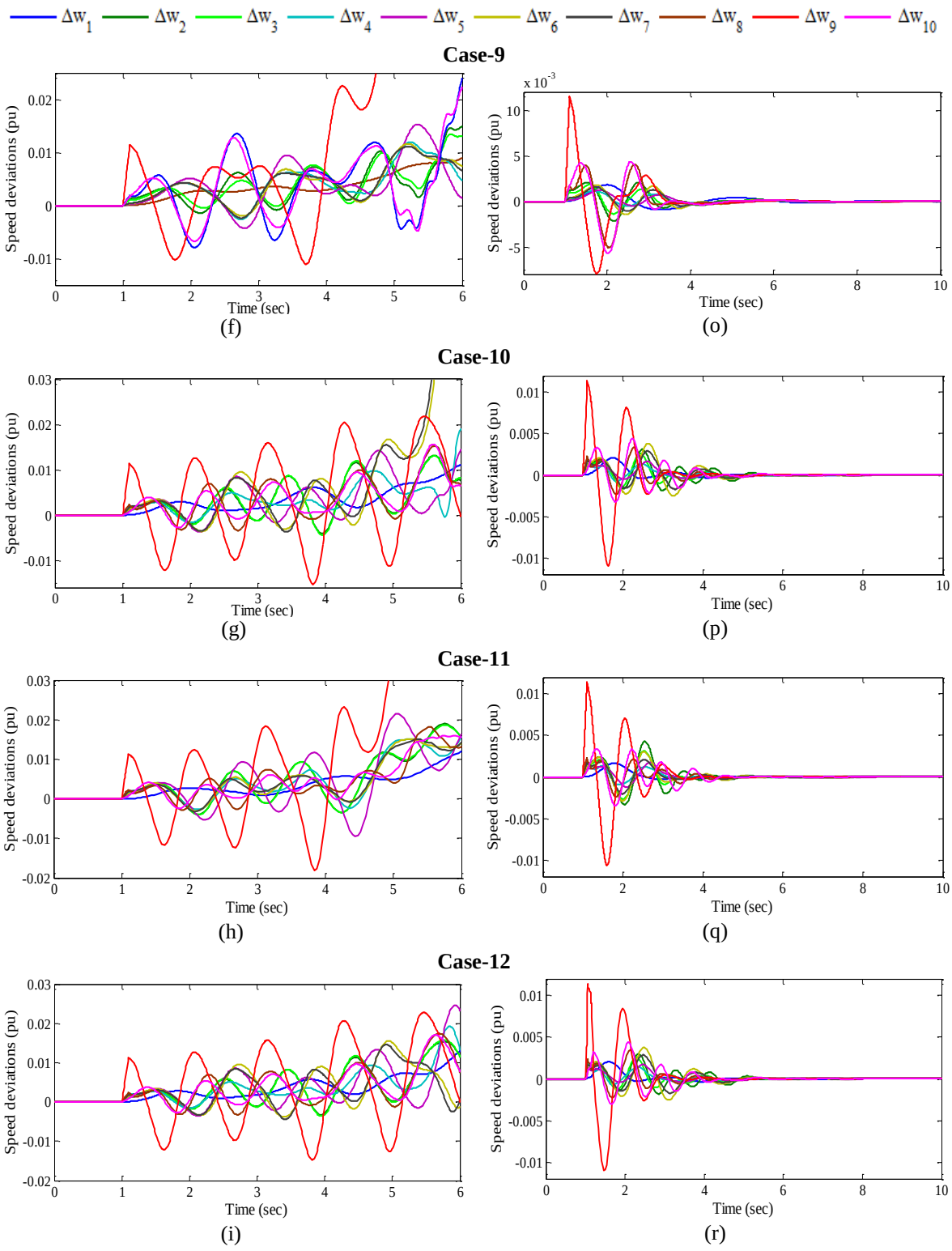

Fig. 6.16 Speed deviations (a)-(i) without PSS and (j)-(r) with CSOPSSs for scenario-1 of unseen operating cases 4-12

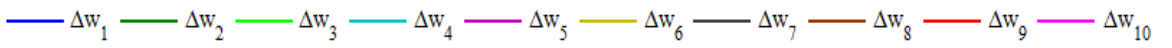

Case-13

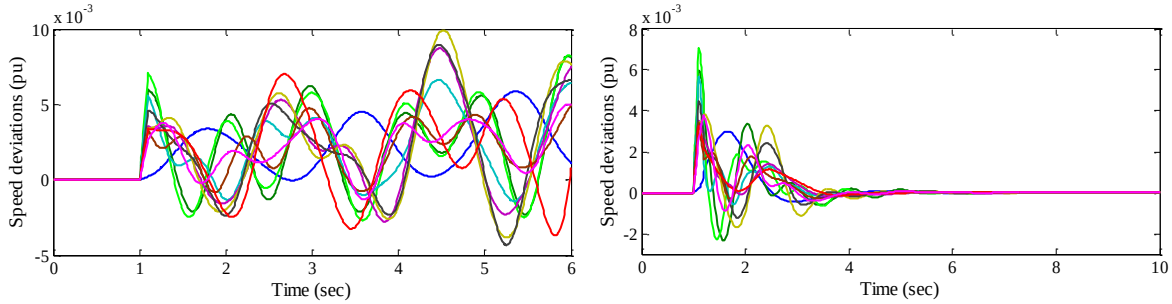

(a) (g)

Case-14

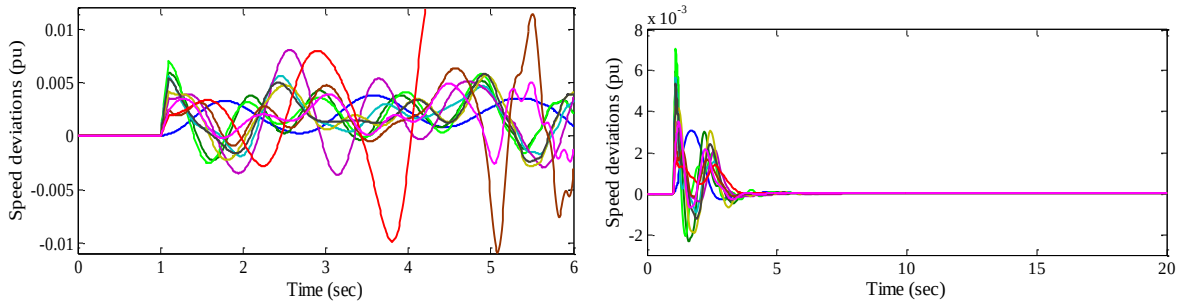

(b) (h)

Case-15

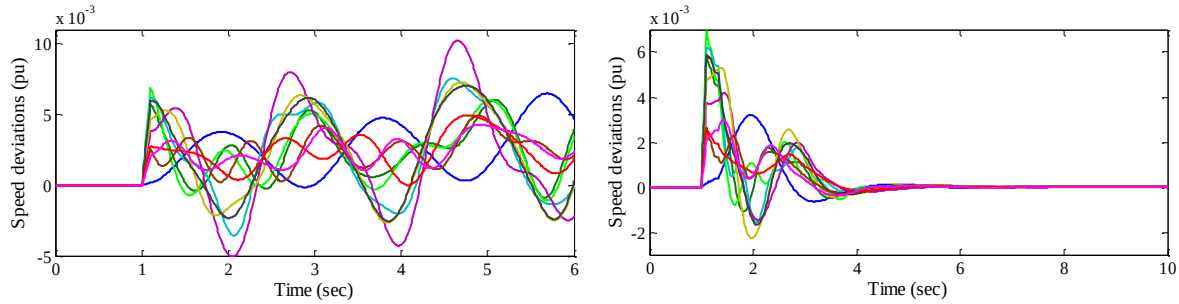

(c) (i)

Case-16

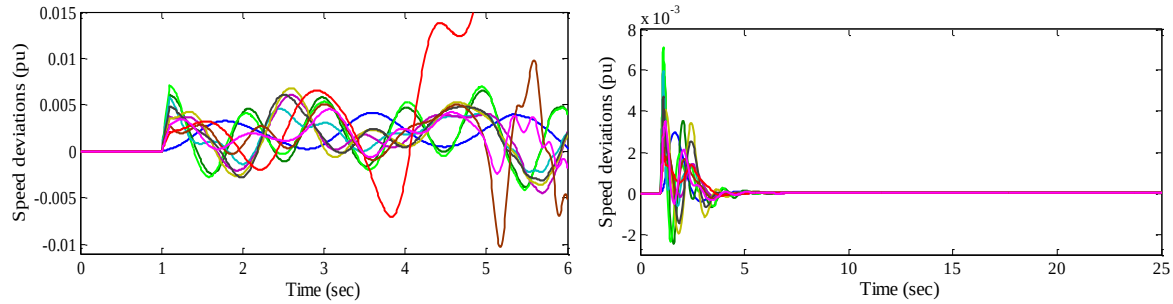

(d) (j)

Case-17

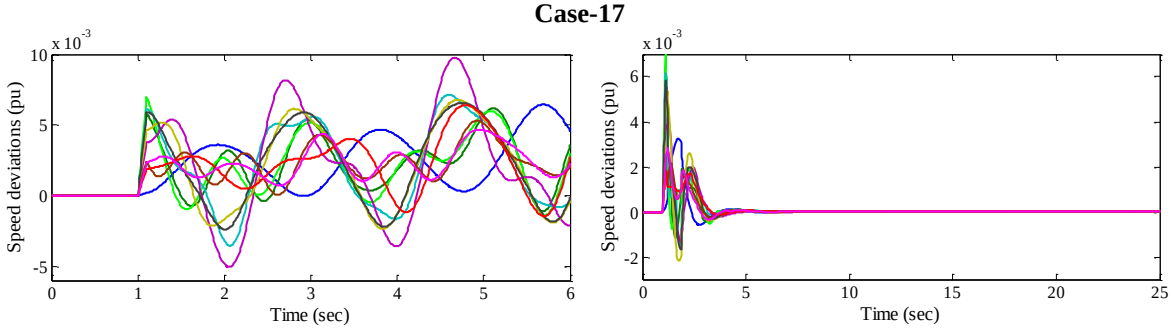

(e) (k)

Cont.

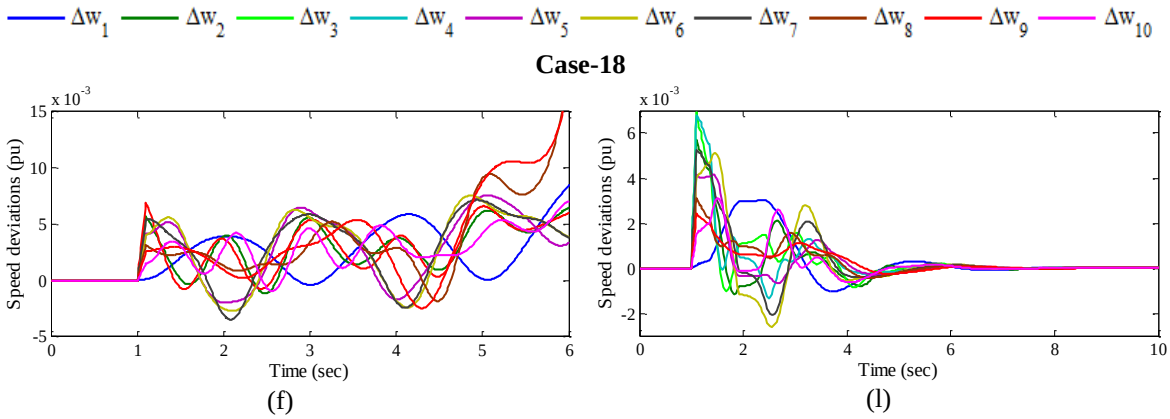

Fig. 6.17 Speed deviations (a)-(f) without PSS and (g)-(l) with CSOPSSs for scenario-4 of unseen operating cases 13-18

In addition to time-domain simulation results, the effectiveness of CSOPSS controllers is observed by evaluating two indices: *IAE* and *ITAE* for observed scenarios 1-4 of all unseen operating cases. The bar charts of both indices values for designed CSOPSS controllers for Scenario-1 of unseen cases 4-12 are shown in Fig. 6.18 (a) and (b) respectively. Similarly, both indices with designed CSOPSSs for Scenario-2 of unseen cases 4-18 except Case-6, for Scenario-3 of cases 4-18 except cases 6, 9 and for Scenario-4 of cases 4-18 are shown in Fig. 6.19 (a)-(c) and (d)-(f) respectively.

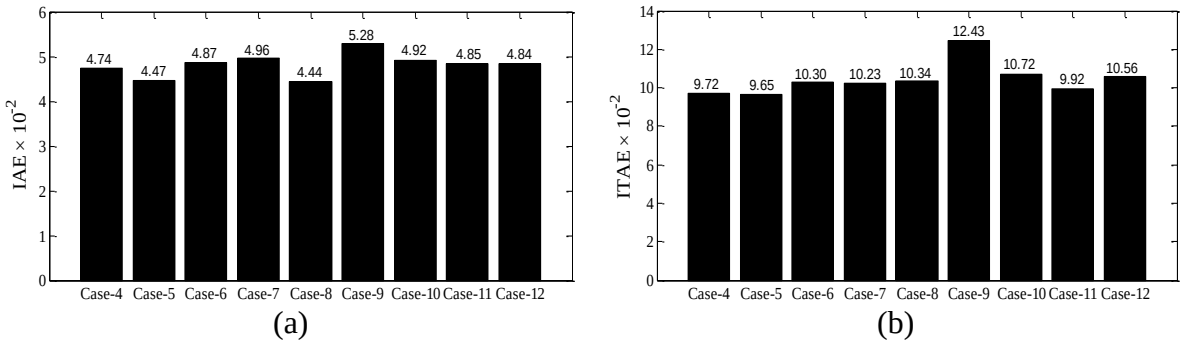

Fig. 6.18 Values of (a) *IAE* and (b) *ITAE* with CSOPSSs for scenario-1 of unseen operating cases 4-12

From Fig. 6.18 (a)-(b), it is observed that values of *IAE* with CSOPSSs for unseen cases 8 and 9 of Scenario-1 are minimum and maximum respectively whereas values of *ITAE* for cases 5 and 9 are minimum and maximum respectively. Therefore, it is concluded that Case-9 under Scenario-1 is severe than others.

From Fig. 6.19 (a)-(c) and (d)-(f), it is noticed that values of *IAE* with CSOPSSs for cases 8 and 11 of scenarios 2-3 are minimum and maximum respectively. Similarly, values of *IAE* with CSOPSSs for unseen cases 7 and 18 of Scenario-4 are minimum and maximum respectively. Moreover, values of *ITAE* with CSOPSSs for cases 14 and 9 of Scenario-2, for cases 14 and 11 of Scenario-3 and for cases 7 and 9 of Scenario-4, are minimum and maximum respectively. Moreover, the Scenario-4 of Case-9 is most severe than other scenarios 1, 3-4 of unseen cases.

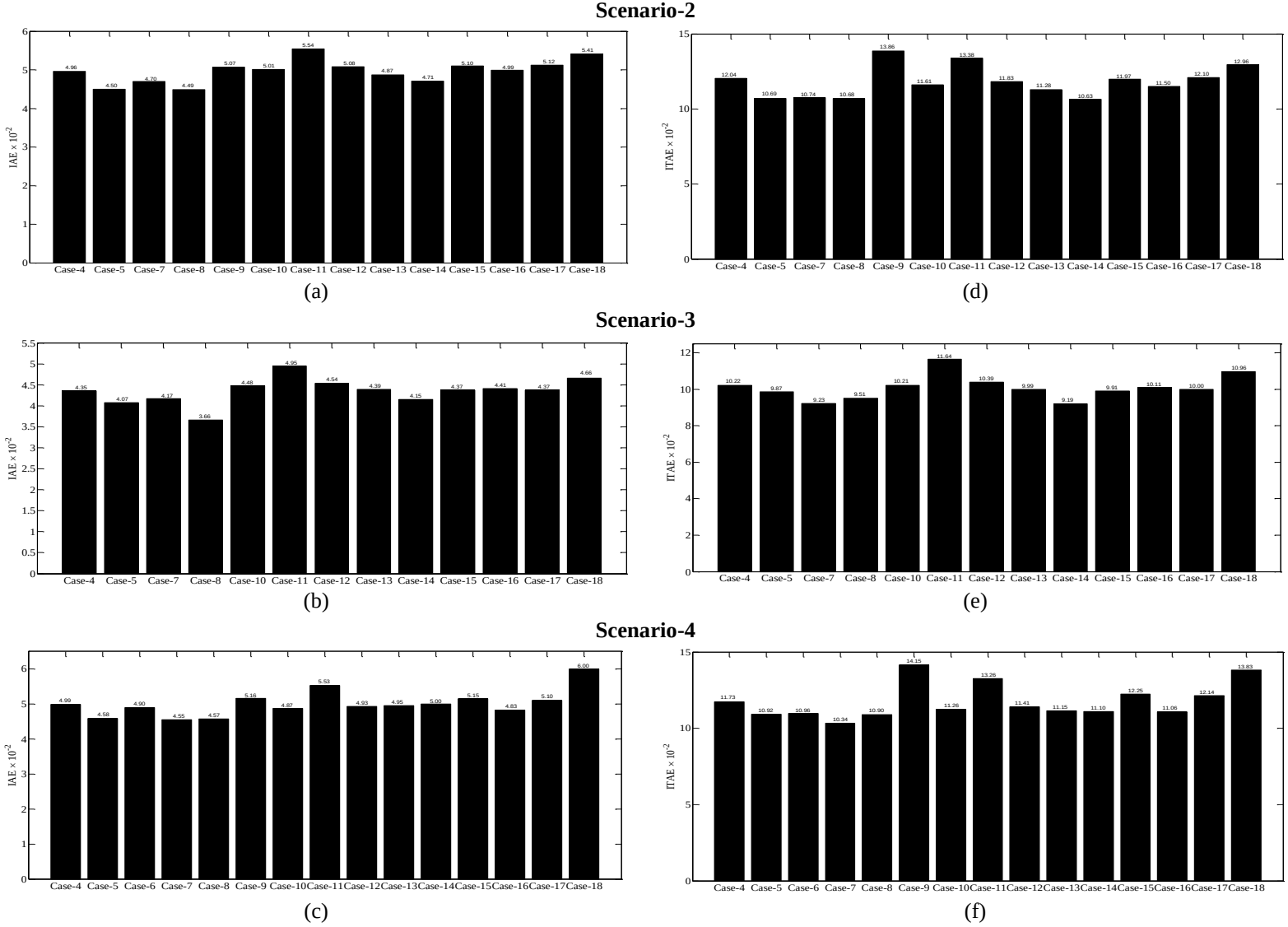

Fig. 6.19 Values of (a)-(c) *IAE* and (d)-(f) *ITAE* with CSOPSSs for scenarios 2-4 of unseen operating cases 4-18

Hence, the designed CSOPSS controllers for NEPS is capable to damp out low frequency local and inter-area modes of oscillations with improved stability and damping performances for wide range of loading cases under different scenarios of severe disturbances and also for unseen operating cases under severe scenarios of disturbances.

6.2.4 Example 4: Sixteen-Machine, Sixty-Eight Bus New England Extended Power System (NEEPS)

The operating condition details and single-line diagram of NEEPS is described in Section 3.4.4 and Appendix respectively.

A. Eigenvalue Analysis of NEEPS without PSS and with CSOPSSs

Open-loop eigenvalues, damping ratio, frequency, participation modes and participation factor associated with electromechanical modes of the system are illustrated in Table 3.28 and discussed in Section 3.4.4 (A). An eigenvalue-based multi-objective function J (equation 3.1) is used in Section 3.2 and minimized using CSO for tuning the forty-two parameters of PSSs. The CSO is applied with population size 100, maximum generation 100, probability index (p_a) = 0.25.

The CSO is able to find the desired solution for which fitness function J is zero. The final value of J equal to zero indicates that fourteen unstable and/or poorly damped eigenvalues are shifted to a specified D-shape zone in the left-half of the s-plane. The optimum designed forty-two parameters of CSOPSSs for fourteen generators are shown in Table 6.10.

Table 6.10: Optimal designed parameters of CSOPSSs for NEEPS

Generators	K_1	T_1	T_3
G_1	62.376	0.360	0.296
G_2	28.928	0.209	0.837
G_3	90.124	0.522	0.187
G_4	35.997	0.254	0.362
G_5	19.214	0.145	0.228
G_7	93.062	0.223	0.493
G_8	30.327	0.101	0.452
G_9	33.003	0.390	0.111
G_{10}	50.542	0.390	0.388
G_{11}	2.541	0.303	0.974
G_{12}	32.651	0.237	0.244
G_{13}	18.640	0.328	0.658
G_{15}	91.811	0.293	0.405
G_{16}	6.944	0.168	0.657

The closed-loop eigenvalues and their damping ratio with designed CSOPSSs for unstable modes of operating cases 1-6 are determined using PSAT [215] and are shown in Table 6.11.

Table 6.11: Eigenvalues and damping ratio with CSOPSSs for operating cases 1-6 of NEEPS

Cases	With CSOPSSs		
Case-1	– 0.924 ± j 1.340, 0.567	– 2.039 ± j 1.441, 0.816	– 1.943 ± j 2.030, 0.691
Case-2	– 1.989 ± j 2.050, 0.696	– 0.920 ± j 2.058, 0.408	– 0.915 ± j 1.150, 0.622
Case-3	– 2.506 ± j 5.797, 0.396	– 1.029 ± j 2.196, 0.424	– 1.045 ± j 7.097, 0.145
Case-4	– 1.969 ± j 2.043, 0.693	– 0.929 ± j 1.149, 0.628	– 0.878 ± j 1.954, 0.409
Case-5	– 0.926 ± j 1.343, 0.567	– 1.045 ± j 2.217, 0.426	– 1.940 ± j 2.031, 0.690
Case-6	– 0.888 ± j 1.108, 0.625	– 1.059 ± j 2.208, 0.432	– 2.041 ± j 1.442, 0.816

The eigenvalue maps of NEEPS without PSS for operating cases 1-3 and 4-6 are shown in Fig. 6.20 (a)-(c) and (g)-(i) whereas with CSOPSSs for same cases are shown in Fig. 6.20 (d)-(f) and (j)-(l) respectively.

The eigenvalue maps of without PSS for unstable and lightly damped modes of NEEPS system are discussed in Section 3.4.4 (A). Table 6.11 and 6.20 (d)-(f) & (j)-(l) show that the CSOPSSs shift the eigenvalues to a specified D-shape zone in the left half of the *s*-plane with desired damping factor and damping ratio as compared to without PSS for all operating cases. Hence, CSOPSS controllers provide improved stability and damping characteristics of the NEEPS as compared to same obtained using without PSS.

B. Time-Domain Simulation Results and Discussions with CSOPSSs and without PSS of NEEPS

In order to examine the performance of designed CSOPSS controllers in previous section in terms of speed deviations, the time-domain simulation of NEEPS is performed for without PSS and with CSOPSSs for observed four scenarios of severe operating Case-6 only. The speed deviations $\Delta w_1, \Delta w_2, \Delta w_3, \Delta w_4, \Delta w_5, \Delta w_6, \Delta w_7, \Delta w_8, \Delta w_9, \Delta w_{10}, \Delta w_{11}, \Delta w_{12}, \Delta w_{13}, \Delta w_{14}, \Delta w_{15}$ and Δw_{16} for without PSS and with CSOPSSs for scenarios 1-4 of operating Case-6 are shown in Fig. 6.21 (a)-(d) and (e)-(h) respectively.

The analysis of response plots without PSS already discussed in Section 3.4.4 (D). From Fig. 6.21 (e)-(h), it is noticed that that with CSOPSSs, LFO are well damped out for all scenarios. Moreover, the Δw_9 has larger peak overshoot and generates more oscillations in Scenario-1 than others. It is clear that the system performance with CSOPSSs is much improved to that of without PSS for all scenarios of operating Case-6.

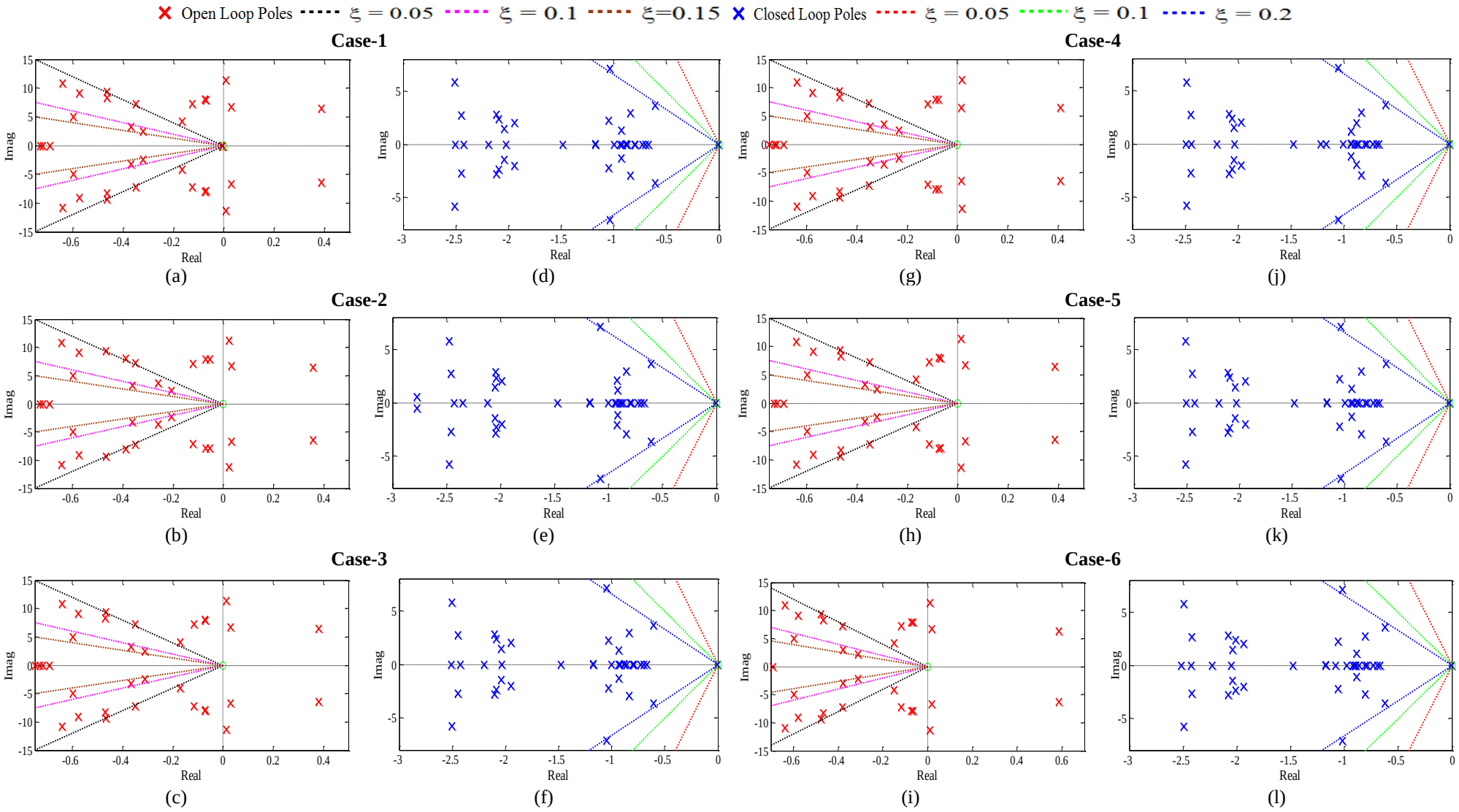

Fig. 6.20 Eigenvalue maps (a)-(c) & (g)-(i) without PSS and (d)-(f) & (j)-(l) with CSOPSSs for operating cases 1-6 of NEEPS

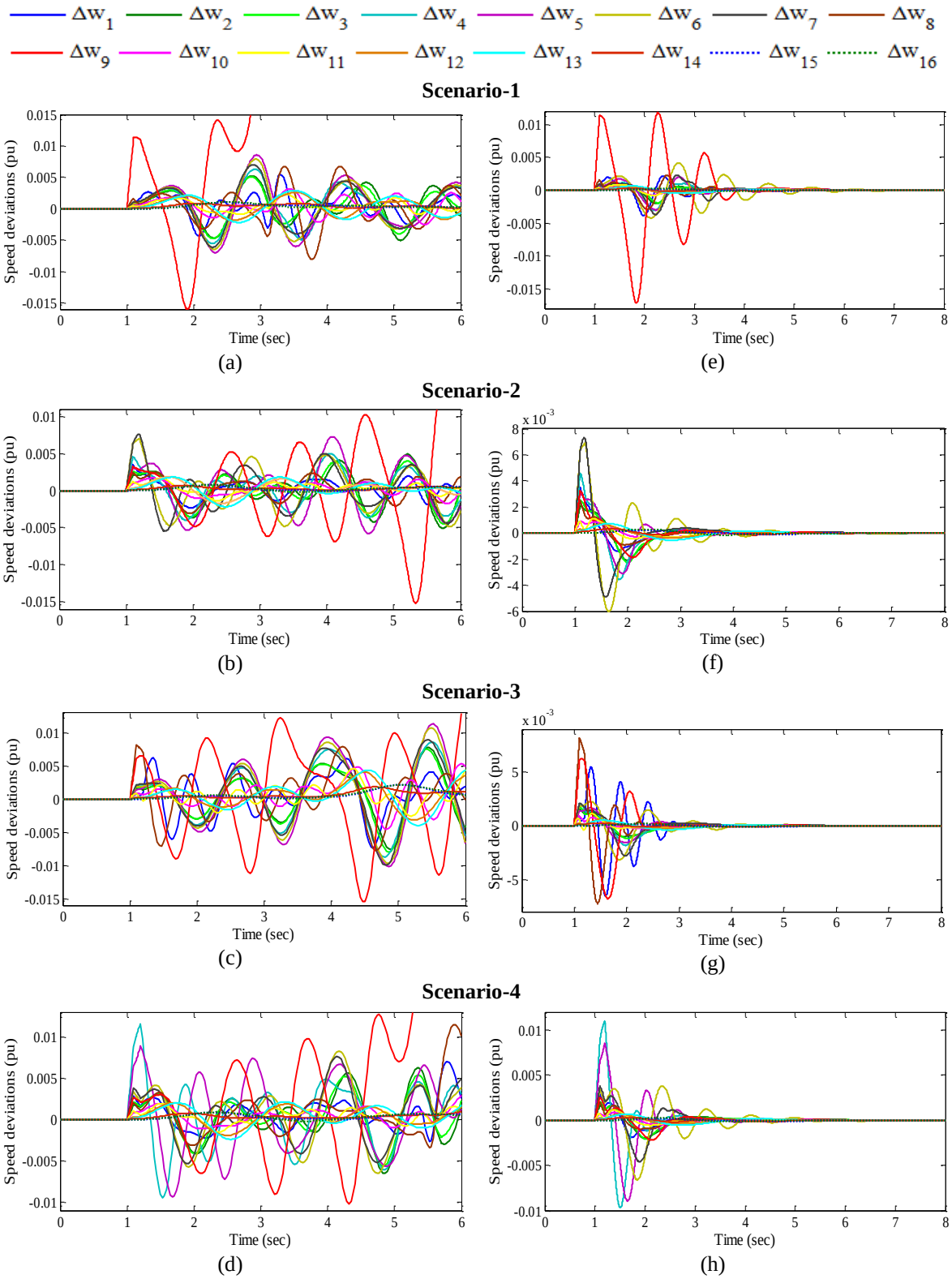

Fig. 6.21 Speed deviations (a)-(d) without PSS and (e)-(h) with CSOPSSs for scenarios 1-4 of operating case-6

This demonstrates the potential of CSO technique to obtain the desired set of PSS parameters for NEEPS and the designed CSOPSSs are capable to damp out LFO for wide range of operating cases under severe scenarios of disturbances.

C. Performance Indices Results and Discussions with CSOPSSs of NEEPS

In addition to time-domain simulation results, the effectiveness of designed CSOPSS controllers is noticed by evaluating *IAE* and *ITAE* for observed four scenarios of different disturbances. The bar charts of both indices values with CSOPSSs for scenarios 1-4 of cases 1-6 are shown in Fig. 6.22 (a)-(d) and (e)-(h) respectively.

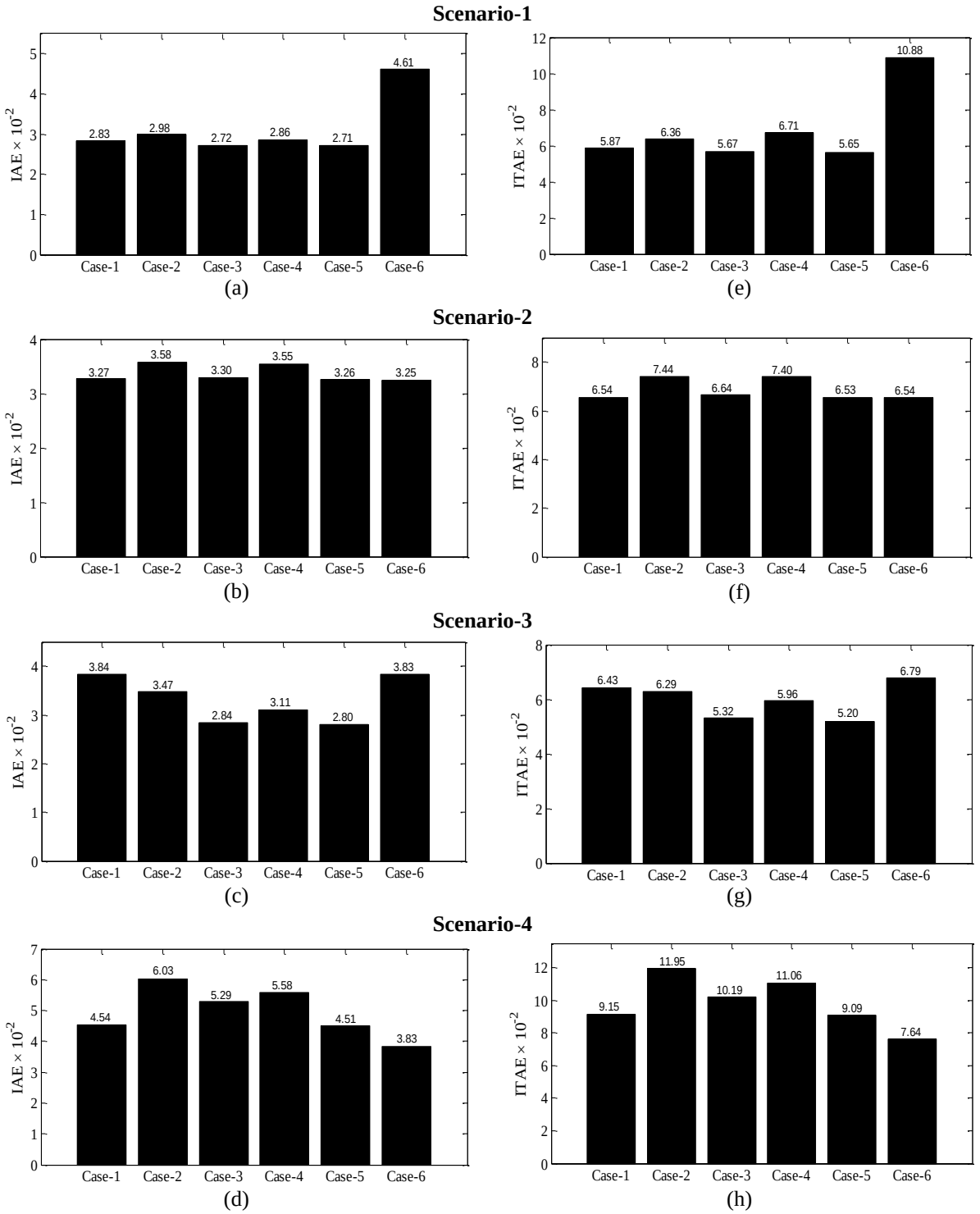

Fig. 6.22 Values of (a)-(d) *IAE* and (e)-(h) *ITAE* with CSOPSSs for scenarios 1-4 of operating cases 1-6

From the Fig. 6.22 (a)-(d), it is observed that both indices for Case-5 and Case-6 of Scenario-1, for Case-6 and Case-2 of Scenario-2, for Case-6 and Case-2 of Scenario-4 are lower and higher values respectively whereas for Scenario-3, the *ITAE* is higher for Case-5 and lower for Case-6 respectively. Moreover, it is concluded that for scenarios 1 & 4, operating Case-6 and for scenarios 2 & 4, Case-2 are most severe than others respectively. Furthermore, it is also noticed that for all cases the Scenario-4 is most severe other scenarios whereas for Case-6, the Scenario-1 is most severe than others.

Comparing Fig. 6.22 with Fig. 3.27, it may be observed that the designed CSOPSS controllers of NEEPS provide sufficient damping to damp out low frequency local and inter-area modes oscillation with less overshoot and settling time than that of without PSS.

D. Robustness Test of Designed CSOPSS Controllers of NEEPS

To test the robustness of earlier designed CSOPSS controllers for NEEPS, nine unseen operating cases 7-15 mentioned in Table 3.33 are considered. In this section, the effectiveness of designed CSOPSSs is evaluated by eigenvalue analysis, time-domain simulation results and performance indices for earlier observed four scenarios of all unseen operating cases and compared with that of without PSS.

Open-loop eigenvalues, damping ratio, frequency, participation modes and participation factor for only unstable modes of unseen operating cases 7-15 of NEEPS without PSS and closed-loop eigenvalues and damping ratio with designed CSOPSSs for the same unseen cases of system are obtained using PSAT [215] and shown in Table 6.12.

The table shows that the designed CSOPSSs shift the eigenvalues to the left half of the *s*-plane with improved damping factor and damping ratio as compared to without PSS for all unseen operating cases. This ensures that the NEEPS will be stable for all considered unseen cases also. It is also observed that designed CSOPSS controllers satisfy the earlier selected criterion for the value of desired damping factor and damping ratio for all unseen cases. Hence, the CSO provides robustness with enhanced stability and improved damping performance for unseen operating cases 7-15 of NEEPS as compared to that of without PSS.

In order to examine the robustness performance of the designed CSOPSSs in terms of speed deviations, the simulations are performed using PSAT [215] for four earlier observed scenarios on unseen cases 7-15 of NEEPS. The speed deviations Δw_1, Δw_2, Δw_3, Δw_4, Δw_5, Δw_6, Δw_7, Δw_8, Δw_9, Δw_{10}, Δw_{11}, Δw_{12}, Δw_{13}, Δw_{14}, Δw_{15} and Δw_{16} without PSS and with CSOPSSs for severe test Scenario-1 of cases 7-11 are shown in Fig. 6.23 (a)-(e) and (f)-(j) respectively whereas for Scenario-2 of cases 12-15 are shown in Fig. 6.24 (a)-(d) and (e)-(h) respectively.

Table 6.12: Eigenvalues and damping ratio with CSOPSSs for unseen operating cases 7-15 of NEEPS

Cases	With CSOPSSs
Case-7	– 0.958 ± j 1.809, 0.468
	– 0.795 ± j 2.985, 0.257
Case-8	– 1.048 ± j 7.098, 0.146
	– 0.626 ± j 3.604, 0.171
	– 1.777 ± j 3.024, 0.506
	– 0.732 ± j 2.788, 0.254
Case-9	– 1.057 ± j 7.093, 0.147
	– 0.626 ± j 3.603, 0.171
	– 1.773 ± j 3.027, 0.505
	– 0.732 ± j 2.786, 0.254
	– 0.913 ± j 1.236, 0.594
Case-10	– 1.054 ± j 7.091, 0.147
	– 0.620 ± j 3.631, 0.168
	– 1.010 ± j 2.124, 0.429
	– 0.738 ± j 2.808, 0.254
Case-11	– 1.074 ± j 7.072, 0.150
	– 0.683 ± j 3.418, 0.196
Case-12	– 1.049 ± j 7.086, 0.146
	– 0.614 ± j 3.645, 0.166
	– 0.742 ± j 2.839, 0.252
	– 1.001 ± j 2.119, 0.427
Case-13	– 1.070 ± j 7.036, 0.150
	– 0.609 ± j 3.652, 0.164
	– 1.034 ± j 2.208, 0.424
Case-14	– 0.614 ± j 3.651, 0.166
	– 0.741 ± j 2.856, 0.251
Case-15	– 0.634 ± j 2.354, 0.260
	– 0.702 ± j 3.383, 0.203
	– 1.207 ± j 6.932, 0.171

The analysis of response plots without PSS already discussed in Section 3.4.4 (D). From Figs. 6.23 (f)-(j) and 6.24 (e)-(h), it is observed that with CSOPSSs all oscillations of speed deviations are well damped out for Sceanrio-1 of cases 7-11 and Scenario-2 of cases 12-15. Moreover, the peak overshoot of speed responses in Scenario-1 and Scenario-2 are almost same in all considered operating cases. Furthermore, oscillations in response of cases 13-15 in Scenario-2 take more time to reach in steady state as compared to others. It is clear that the system performance with CSOPSSs is improved to that of without PSS for considered scenarios

of unseen operating cases. This may be concluded that the designed CSOPSSs work satisfactorily for observed scenarios of severe disturbances of unseen operating cases of NEEPS.

In addition to time-domain simulation results, the effectiveness of designed CSOPSS controllers is observed by evaluating *IAE* and *ITAE* for observed four scenarios of unseen cases 7-15. The bar charts of both indices with CSOPSSs for Scenario-1 of cases 7-11, Scenario-2 of cases 7-15, Scenario-3 of cases 7-12 and Scenario-4 of cases 7-14 are shown in Fig. 6.25 (a)-(d) and (e)-(h) respectively.

From the figure, it is noticed that the values of both indices with CSOPSSs for Case-11 of Scenario-1, Case-15 of Scenario-2, Case-11 of Scanerio-3 and Case-14 of Scenario-4 are higher than others. Moreover, it is concluded that the unseen Case-15 of Scenario-2 of and Case-7 of Scenario3 are most and least severe than others.

Hence, the designed CSOPSS controllers for NEEPS is capable to damp out low frequency local and inter-area modes of oscillations with enhanced stability and damping performances for wide range of loading cases under different scenarios of severe disturbances and also for unseen operating cases under severe scenarios of disturbances.

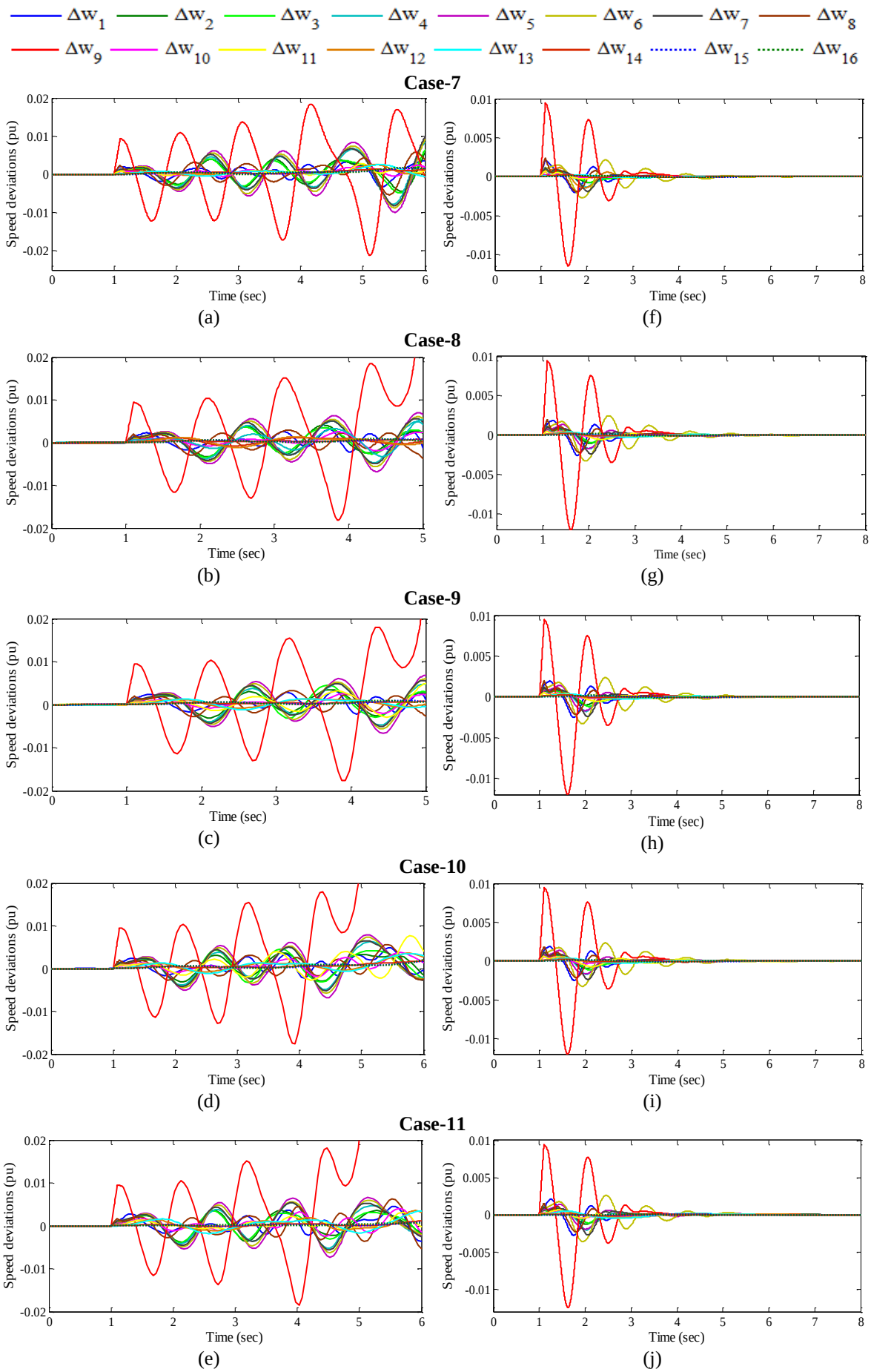

Fig. 6.23 Speed deviations (a)-(e) without PSS and (e)-(j) with CSOPSSs for scenario-1 of unseen operating cases 7-11

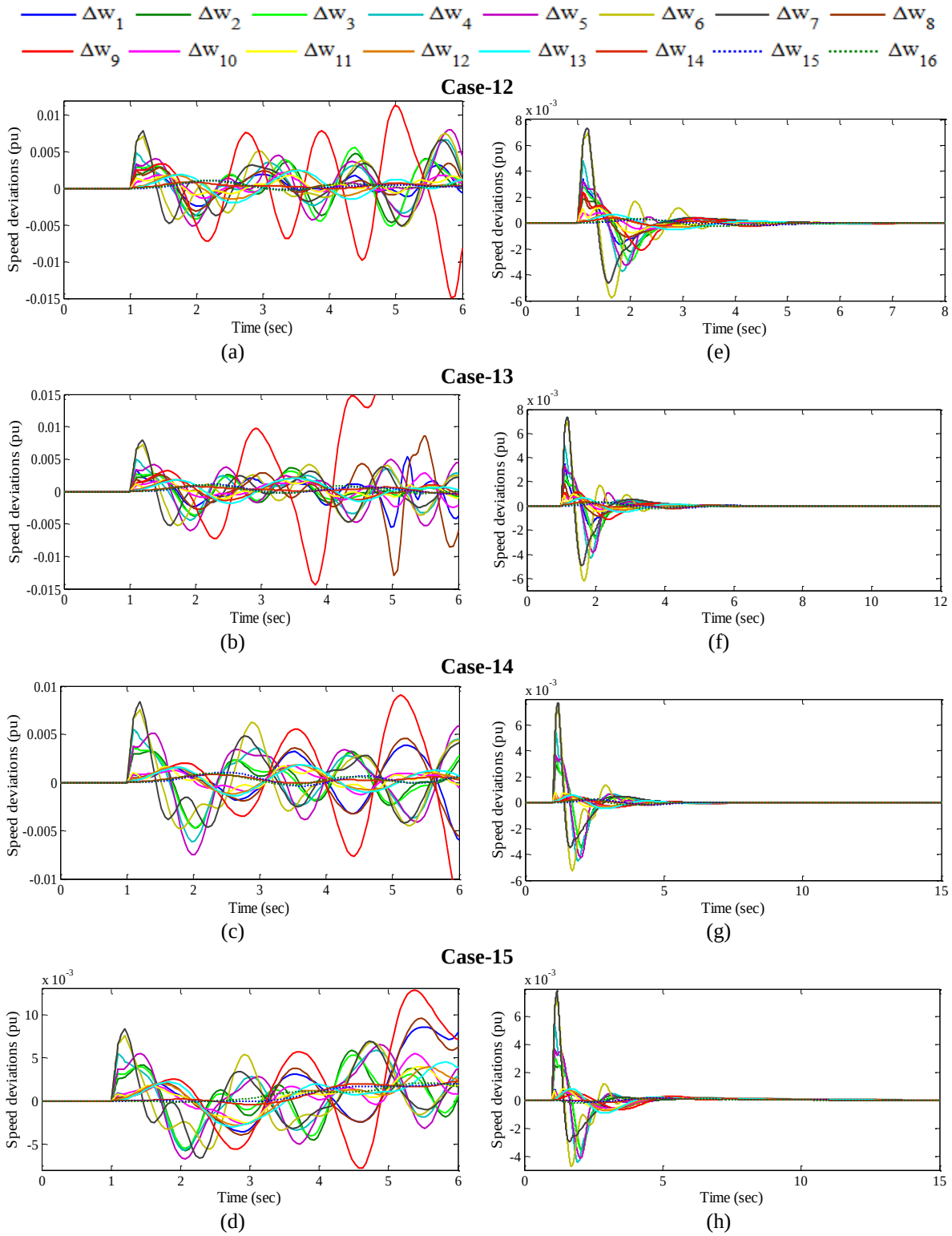

Fig. 6.24 Speed deviations (a)-(d) without PSS and (e)-(h) with CSOPSSs for scenario-2 of unseen operating cases 12-15

6.3 Summery

In this chapter, a meta-heuristic technique CSO is implemented for effectively designing of PSS under wide range of operating conditions of WSCC power system, TFAM power system, NEPS and NEEPS for SSS enhancement. The CSO is capable of shifting all unstable and/or poorly damped eigenvalues of MMPS to a specified D-shape zone in the left half of the *s*-plane.

Moreover, the effectiveness of designed CSOPSS controllers has been evaluated by eigenvalue analysis, eigenvalue maps, time-domain simulation results and performance indices namely *IAE* and *ITAE*. Furthermore, the robustness of designed CSOPSSs is observed by testing them on under wide range of unseen operating cases of MMPS. It is found that the design CSOPSSs have shifted unstable and/or poorly damped eigenvalues of all unseen cases of MMPS to the left half of the *s*-plane for mitigating low frequency local and inter-area modes of oscillations.

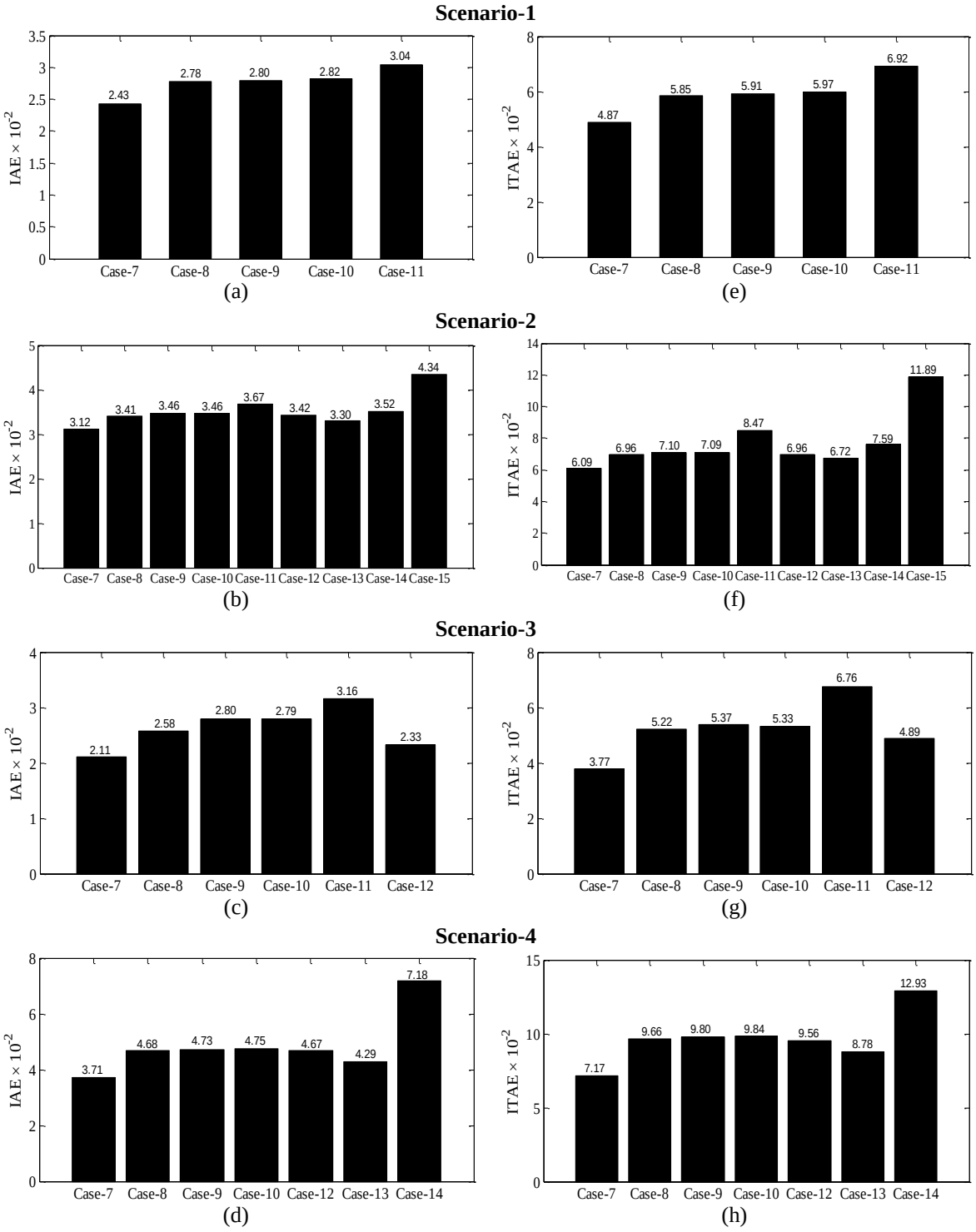

Fig. 6.25 Values of (a)-(d) *IAE* and (e)-(h) *ITAE* with CSOPSSs for scenarios 1-4 of unseen operating cases 7-15

CHAPTER-7
CONCLUSIONS AND FUTURE SCOPE

The present trends towards enhancement of damping performance and SSS are forcing the modern power system to operate under highly stressed operating conditions due to continuously growing energy consumptions. Therefore, stability of large interconnected modern power system is important key for its reliable and secure operation. Small amplitude low frequency power oscillations often sustained for long period of time. In some cases these oscillations have tendency to reduce the power transfer capabilities in transmission lines. Therefore, extensive research efforts are being carried to maintain SSS of power system under all operating conditions. The PSS is most important link between generator and excitation system to achieve suitable damping performance for wide range of operating conditions to mitigate LFO of SMIB system and MMPS. However, the power system operating conditions changes drastically due to disturbance like load changes, topology and short circuits changes in the power system. Therefore, the CPSS design structure is not suitable to overcome these disturbances. For guaranteed stability and assured the relative stability of the MMPS, an eigenvalue based multi-objective function is defined for simultaneous control of damping factor and damping ratio to transfer unstable and/or poorly damped mode eigenvalues to a specified D-shape zone in the left half of the *s*-plane. Four different meta-heuristic techniques namely GA, PSO, HSO and CSO have been used to optimize the considered objective function. GA and PSO are established techniques for parameter design of PSS. However, these techniques have been reinvestigated for the design of PSS parameters for wider and more stressed operating conditions on four different small to large multi-machine test systems and the application results are presented in chapter 3 and chapter 4 respectively. The HSO and CSO are relatively new optimization techniques which have not been explored for the design and tuning of PSS parameters. Therefore, applicability of these techniques has been also explored by applying them on same four multi-machine test systems in chapter 5 and chapter 6 respectively. It has been found that all investigated techniques are capable of tuning of PSS design parameters and designed PSSs work satisfactorily for most of the cases including unseen operating conditions. A comparative study of GAPSSs, PSOPSSs, HSOPSSs and CSOPSSs for the design of PSS is presented as follows.

7.1 Comparative Analysis and Conclusions

To obtain the optimal parameters of PS S for wide range of operating conditions of four standard test systems e.g., 3-machine, 9-bus WSCC power system, TAFM power system, 10-machine, 39-bus NEPS and 16-machine, 68-bus NEEPS, the GA, PSO, HSO and CSO are

applied on these systems. An eigenvalue-based multi-objective function is used for simultaneous control of damping factor and damping ratio to mitigate low frequency electromechanical oscillations of MMPS. The parameters of PSS are so designed that unstable and/or poorly damped open-loop eigenvalues are shifted to a specified D-shape zone in the left-half of the *s*-plane for wide range of operating conditions under different scenarios of severe disturbances. This is obtained by minimizing the objective function (3.1) using GA, PSO, HSO and CSO. The effectiveness of all designed PSS controllers are evaluated by eigenvalue analysis, eigenvalue maps, time-domain simulation results and performance indices *IAE* and *ITAE* and the system performance with GAPSSs, PSOPSSs, HSOPSSs and CSOPSSs is compared. The robustness of all designed PSS controllers is also checked by testing them on unseen operating conditions under different scenarios of severe disturbances and compared.

7.1.1 Example 1: Three-Machine, Nine-Bus WSCC Power System

A. Convergence and Eigenvalue Analysis of WSCC power system

An eigenvalue-based multi-objective function *J* presented in (3.1) is minimized using GA, PSO, HSO and CSO by tuning the six parameters of PSSs. Typical convergence of GAPSSs, PSOPSSs, HSOPSSs and CSOPSSs are shown in Fig. 7.1. Figure shows that all algorithms are able to find the solution for which fitness function *J* is zero.

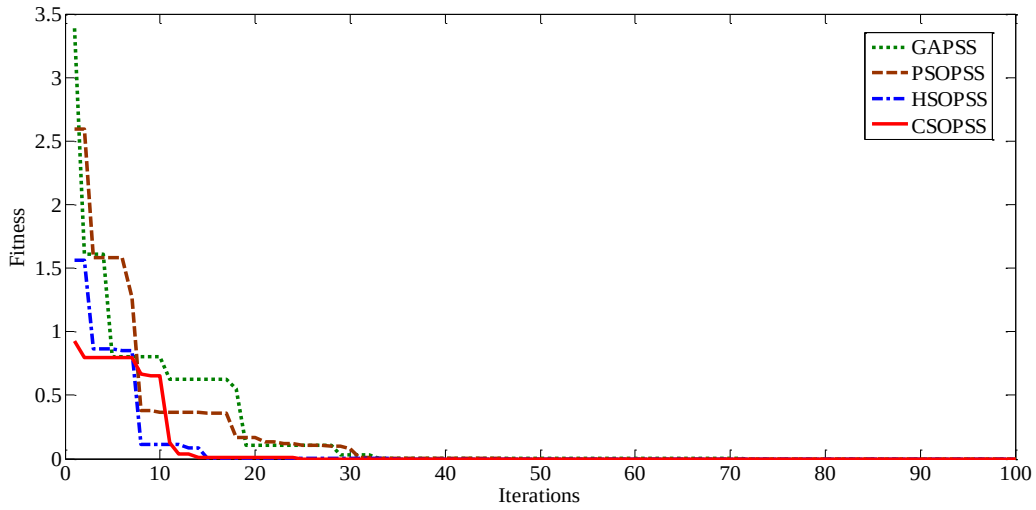

Fig. 7.1 Typical convergence characteristics of various optimization techniques

However, the CSO algorithm is able to find the best solution in comparative less number of iterations. Performance of HSO is very close to CSO whereas performance of GA and PSO is more or less similar but slower than CSO and HSO. The optimum designed parameters of GAPSSs, PSOPSSs, HSOPSSs and CSOPSSs for two generators are shown in chapters 3 to 6.

The comparison of eigenvalues and their damping ratio with GAPSSs, PSOPSSs, HSOPSSs and CSOPSSs for operating cases 1-3 are shown in Table 7.1. The Comparison of

eigenvalue maps of WSCC power system with designed GAPSSs, PSOPSSs, HSOPSSs and CSOPSSs for operating cases 1-3 are shown in Fig. 7.2 (a)-(c), (d)-(f), (g)-(i) and (j)-(l) respectively.

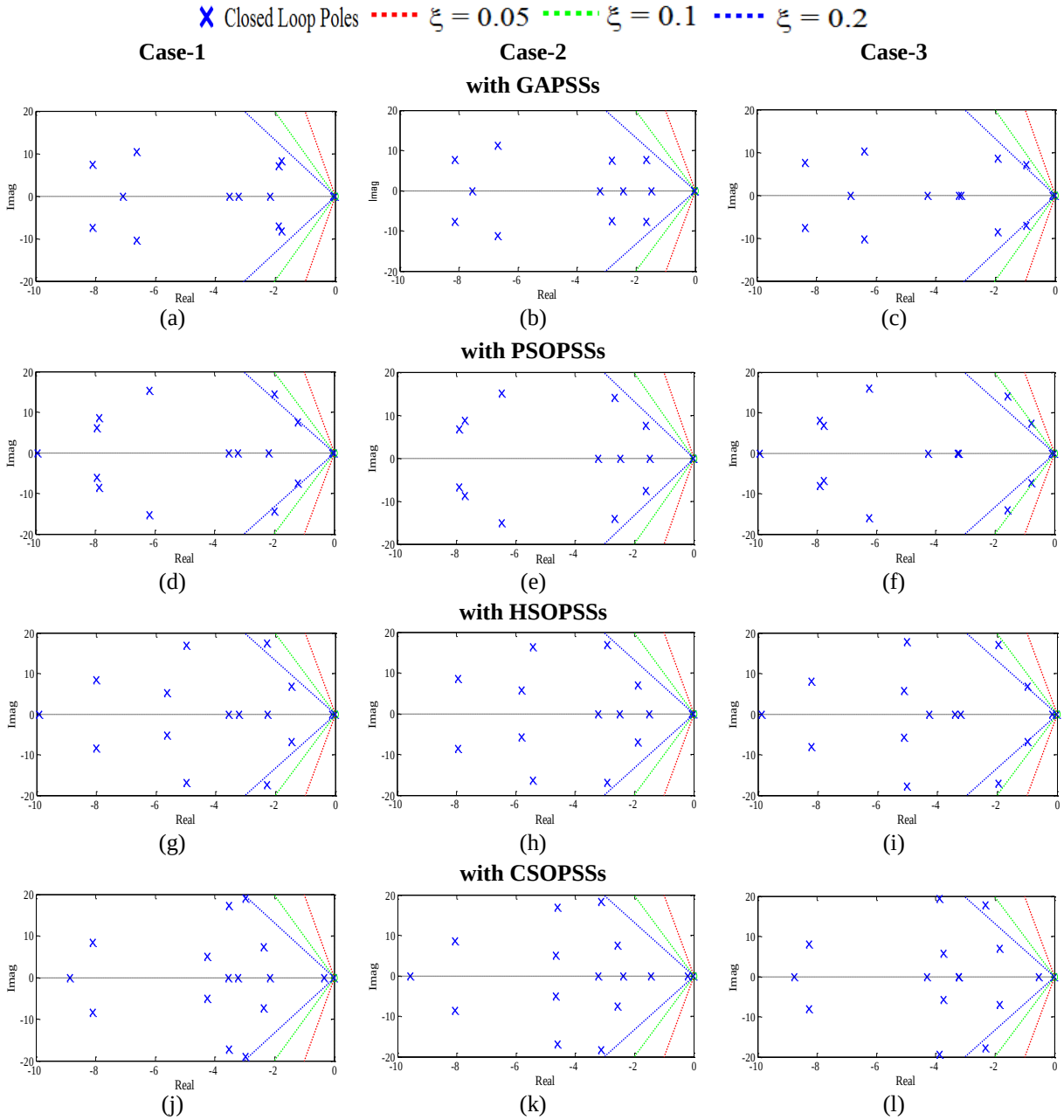

Fig. 7.2 Eigenvalue maps comparison (a)-(c) with GAPSSs (d)-(f) with PSOPSSs (g)-(i) with HSOPSSs (j)-(l) with CSOPSSs for operating cases 1-3 of WSCC power system

Table 7.1 and Fig. 7.2 show that the CSOPSSs shift the eigenvalues to a specified D-shape zone in the left half of the *s*-plane with superior damping factor and damping ratio as compared to GAPSSs, PSOPSSs and HSOPSSs for all operating cases. Hence, designed CSOPSS controllers provide better stability and damping performance of the WSCC power system as compared to same obtained using other designed PSS controllers.

Table 7.1: Eigenvalues and damping ratio comparison with designed PSSs for operating cases 1-3 of WSCC power system

With GAPSSs	With PSOPSSs	With HSOPSSs	With CSOPSSs
Case-1			
– 1.778 ± j 8.323, 0.209	– 1.212 ± j 7.549, 0.158	– 1.466 ± j 6.856, 0.209	– 2.982 ± j 19.103, 0.154
– 1.887 ± j 7.160, 0.254	– 2.007 ± j 14.393, 0.138	– 2.278 ± j 17.457, 0.129	– 3.526 ± j 17.245, 0.200
Case-2			
– 1.659 ± j 7.724, 0.210	– 1.614 ± j 7.563, 0.208	– 1.876 ± j 6.935, 0.261	– 2.563 ± j 7.596, 0.319
– 2.811 ± j 7.480, 0.351	– 2.669 ± j 14.041, 0.351	– 2.918 ± j 16.950, 0.169	– 3.133 ± j 18.265, 0.169
Case-3			
– 0.961 ± j 7.148, 0.133	– 0.768 ± j 7.381, 0.103	– 0.982 ± j 6.791, 0.143	– 1.852 ± j 7.060, 0.253
– 1.930 ± j 8.508, 0.221	– 1.570 ± j 14.157, 0.110	– 1.956 ± j 17.143, 0.113	– 2.332 ± j 17.774, 0.130

B. Time-Domain Simulation Results and Discussions of WSCC power system

The performance of previously designed GAPSS, PSOPSS, HSOPSS and CSOPSS controllers in terms of speed deviations, the comparison of severe speed deviations Δw_{12} and Δw_{23} for scenarios 1 and 2corresponding to 3-phase fault at bus 1 and 2 respectively of Case-3 (high loading condition) are shown in Fig. 7.3 (a)-(b) and (c)-(d) respectively.

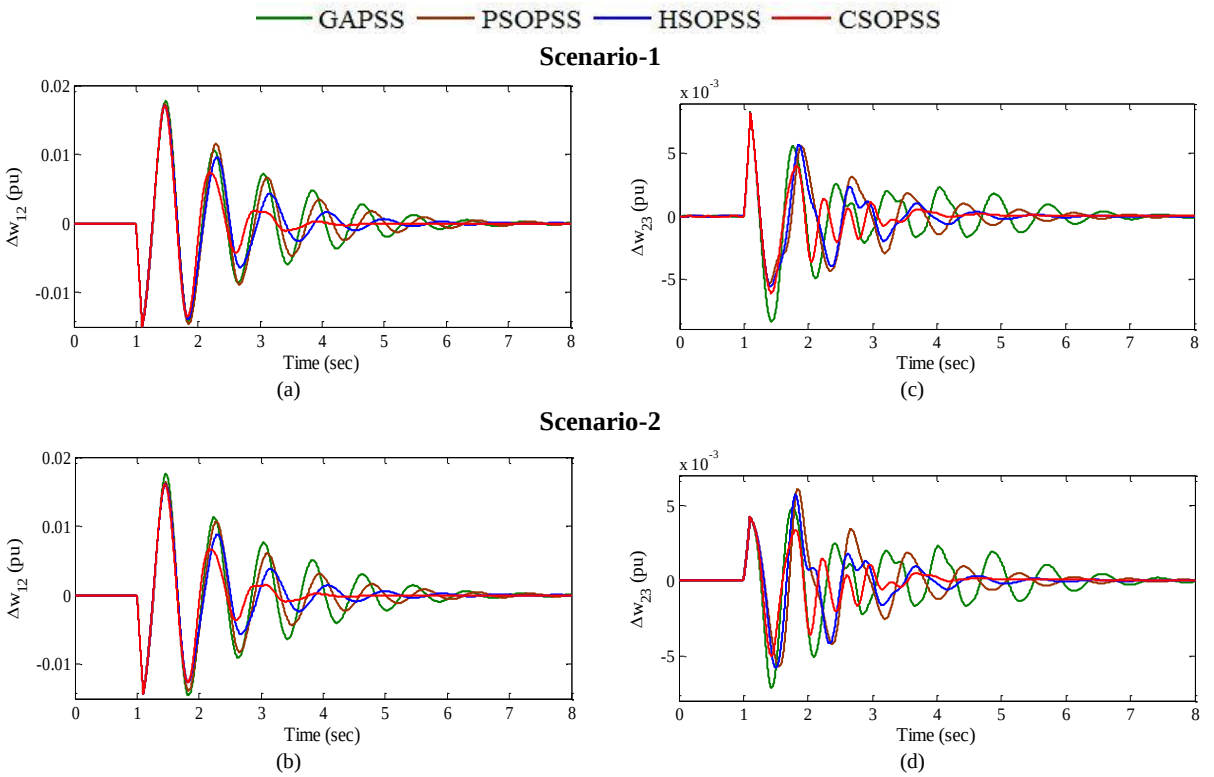

Fig. 7.3 (a)-(b) Δw_{12} and (c)-(d) $\Delta w_{23}$with GAPSSs, PSOPSSs, HSOPSSs, CSOPSSs for scenarios 1-2 of operating case-3 of WSCC power system

From Fig. 7.3, it is clear that the system performance with CSOPSSs is much better than that of GAPSSs, PSOPSSs and HSOPSSs for severe disturbance scenarios of operating Case-3.

The CSOPSSs seem to provide comparatively better damping performance. This illustrates the superiority of CSO technique to obtain desired set of PSS parameters.

C. Performance Indices Results and Discussions of WSCC power system

In addition to time-domain simulation results, the superior effectiveness of designed CSOPSS controllers are observed by comparing bar charts of *IAE* and *ITAE* with other designed PSSs for scenarios 1-2 of cases 1-3 and are shown in Fig. 7.4 (a), (c) and (b), (d) respectively.

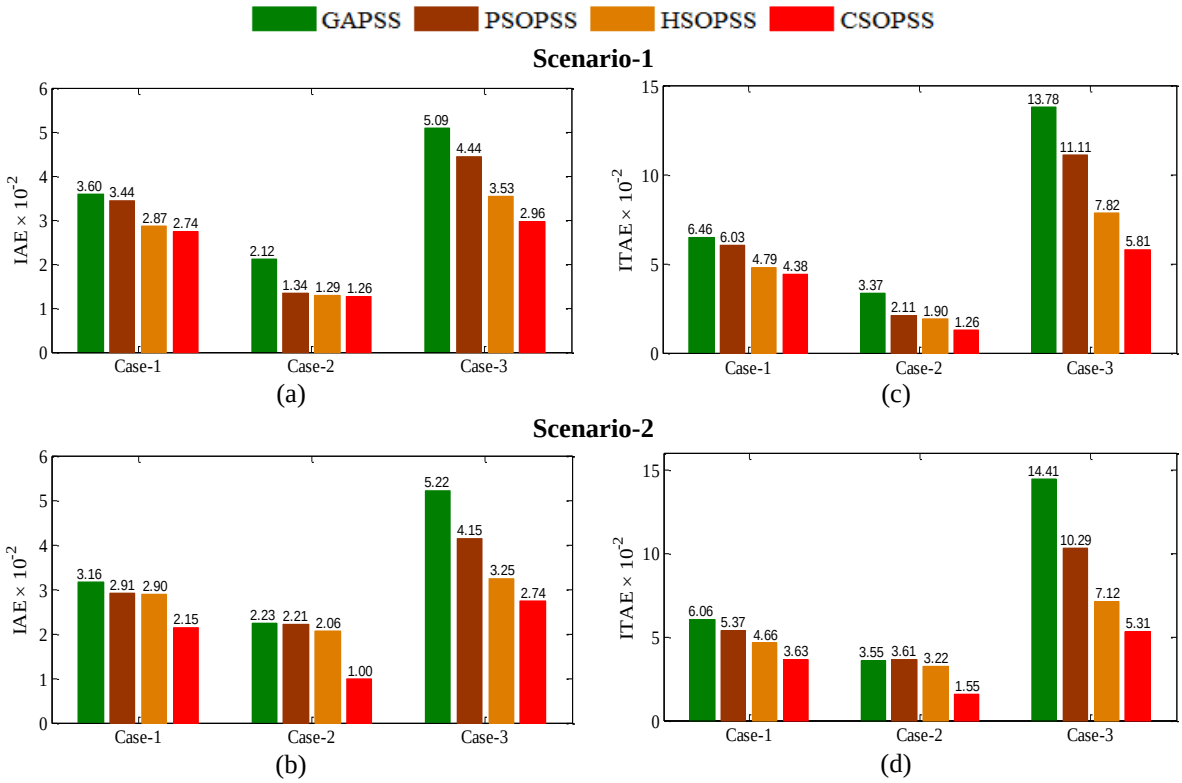

Fig. 7.4 Values of *IAE* and *ITAE* for (a), (c) Scenario-1 (b), (d) Scenario-2 of operating cases 1-3 of WSCC power system

The figure reveals that both indices values for the CSOPSSs are minimum for scenarios 1-2 of operating cases 1-3 as compared to the same obtained by GAPSSs, PSOPSSs and HSOPSSs to settle low frequency local modes of oscillations. These comparisons clearly show that CSOPSS controllers provide relatively superior damping to damp out low frequency local modes of oscillations with less overshoot and settling time than that of other designed PSS controllers.

D. Robustness Test of Designed PSS Controllers of WSCC power system

To investigate the robustness performance of designed PSS controllers, eigenvalue analysis, simulation results and performance indices are evaluated for the same scenarios under unseen cases 4-6.The comparison of eigenvalues and their damping ratio with GAPSSs, PSOPSSs, HSOPSSs and CSOPSSs for operating cases 1-3 are shown in Table 7.2.

Table 7.2: Eigenvalues and damping ratio comparison with designed PSSs for unseen operating cases 4-6 of WSCC power system

With GAPSSs	With PSOPSSs	With HSOPSSs	With CSOPSSs
Case-4			
– 0.766 ± j 7.225, 0.105	– 0.664 ± j 7.530, **0.087**	– 0.939 ± j 6.922, 0.134	– 1.619 ± j 7.332, 0.215
– 1.829 ± j 8.273, 0.215	– 1.565 ± j 13.977, 0.111	– 2.038 ± j 17.156, 0.118	– 3.119 ± j 18.920, 0.162
Case-5			
– 1.228 ± j 8.052, 0.150	– 0.557 ± j 7.442, **0.074**	– 0.828 ± j 6.835, 0.120	– 1.781 ± j 7.056, 0.244
– 1.327 ± j 7.440, 0.175	– 1.587 ± j 14.234, 0.110	– 1.974 ± j 17.283, 0.113	– 2.587 ± j 17.855, 0.143
Case-6			
– 0.746 ± j 8.283, **0.089**	**– 0.465** ± j 7.442, **0.062**	– 0.746 ± j 6.827, 0.108	– 1.761 ± j 6.908, 0.247
– 1.692 ± j 7.092, 0.232	– 1.495 ± j 14.387, 0.103	– 1.816 ± j 17.429, 0.103	– 2.390 ± j 17.777, 0.133

The table shows that the CSOPSSs shift the eigenvalues to a specified D-shape zone in the left half of the *s*-plane with better quality damping factor and damping ratio as compared to GAPSSs, PSOPSSs and HSOPSSs for all unseen cases. The PSOPSSs provide minimum value of damping ratio for all unseen cases. It is also observed that only HSOPSSs and CSOPSSs satisfy the selected criterion for the value of desired damping factor and damping ratio for PSS design. Hence, the designed CSOPSSs is robust as it works with superior damping performance even for unseen operating cases 4-6 as compared to that of other designed PSS controllers.

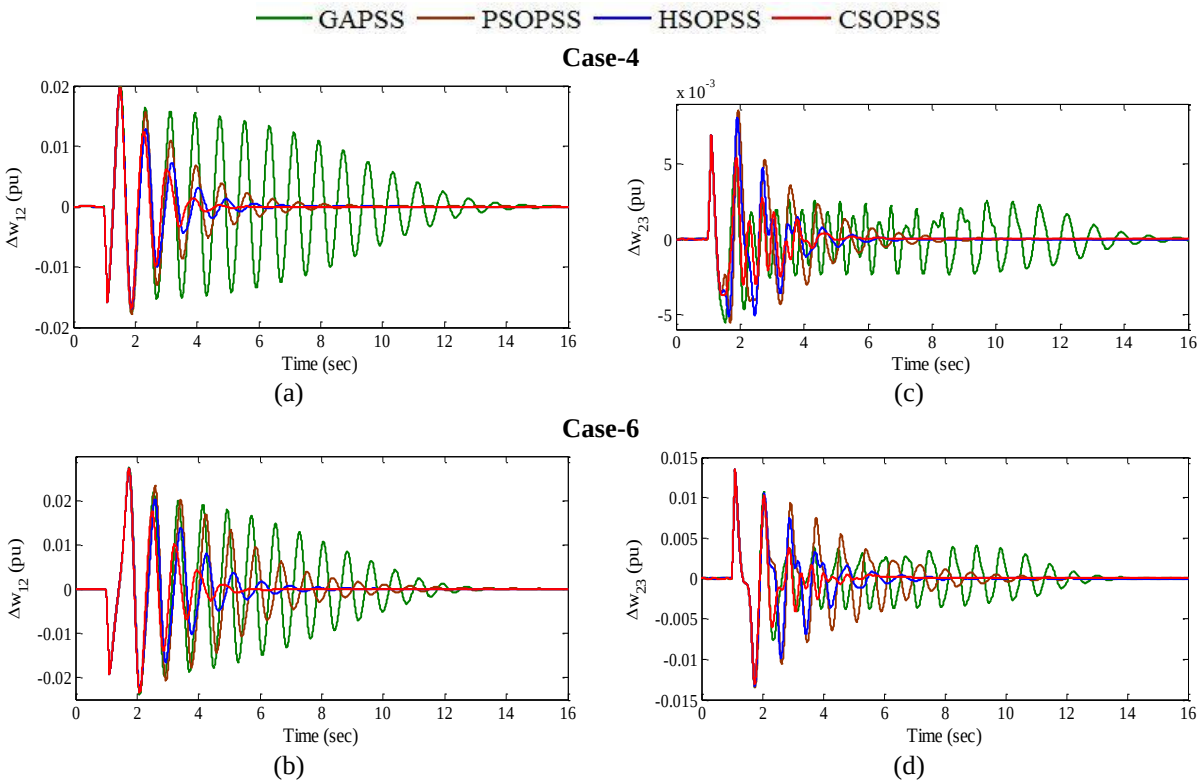

Fig. 7.5 (a)-(b) $\Delta w_{12}$and (c)-(d) $\Delta w_{23}$with GAPSSs, PSOPSSs, HSOPSSs, CSOPSSs for scenario-1 of unseen operating cases 4 and 6 of WSCC power system

In order to examine the robustness performance in terms of speed deviations, the comparison of severe speed deviations $\Delta w_{12}$with other designed PSS controllers for scenarios 1

and 2 of unseen specimen operating cases 4 and 6 are shown in Figs. 7.5 (a)-(b) and 7.6 (a)-(b) respectively and whereas Δw_{23} for same condition are shown in Figs. 7.5 (c)-(d) and 7.6 (c)-(d) respectively.

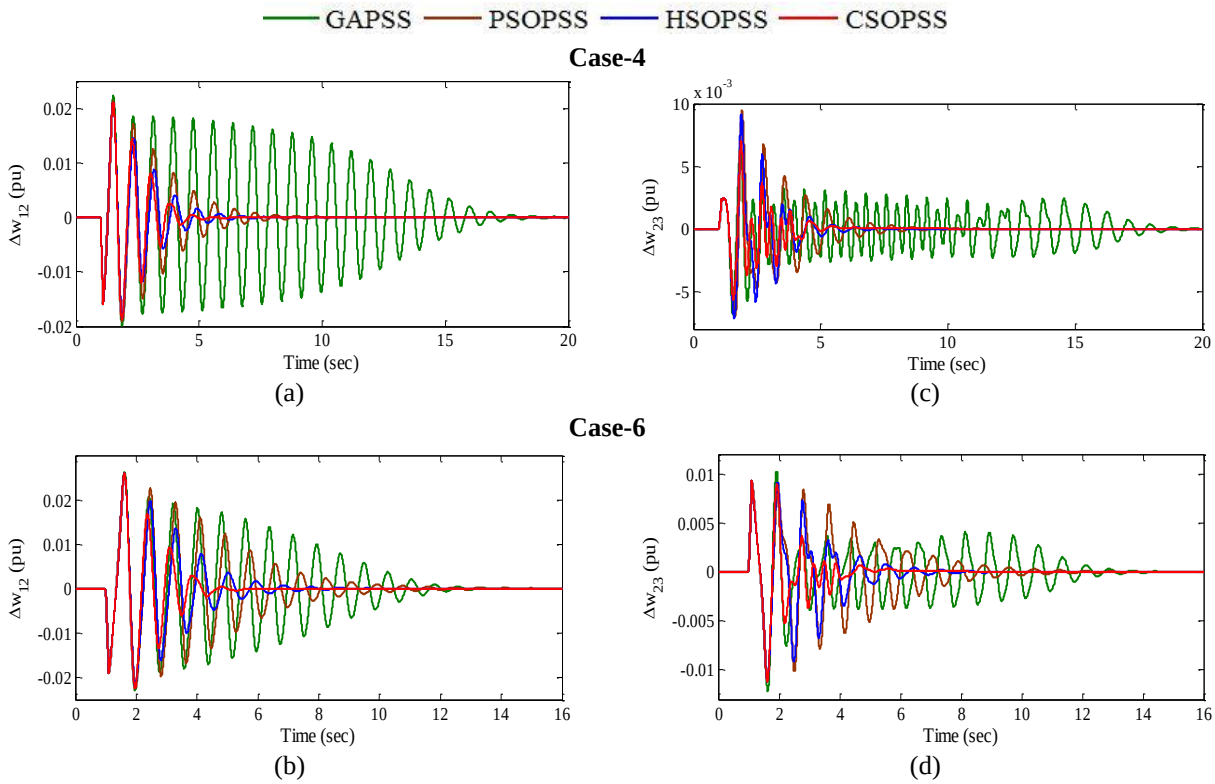

Fig. 7.6 (a)-(b) Δw_{12} and (c)-(d) Δw_{23} with GAPSSs, PSOPSSs, HSOPSSs, CSOPSSs for scenario-2 of unseen operating cases 4 and 6 of WSCC power system

From Figs. 7.5 (a)-(d) and 7.6 (a)-(d), it may be observed that the controllers designed using CSOPSSs for scenarios 1-2 of unseen cases 4-6 show much better damping because oscillations are damped out quickly as compared to that of other designed PSS controllers. Therefore, it may be concluded that with CSOPSSs, the system quickly settles down the LFO even for scenarios of unseen cases as compared to other designed PSS controllers. This shows that CSOPSS controllers are more robust than other designed PSS controllers. GAPSSs provide relatively poor results of speed deviation.

In addition to time-domain simulation results, the effectiveness and robustness performance of designed PSS controllers are also observed by comparing bar charts of *IAE* and *ITAE* for scenarios 1-2 of unseen operating cases 4-6 and are shown in Fig. 7.7 (a), (c) and (b), (d) respectively.

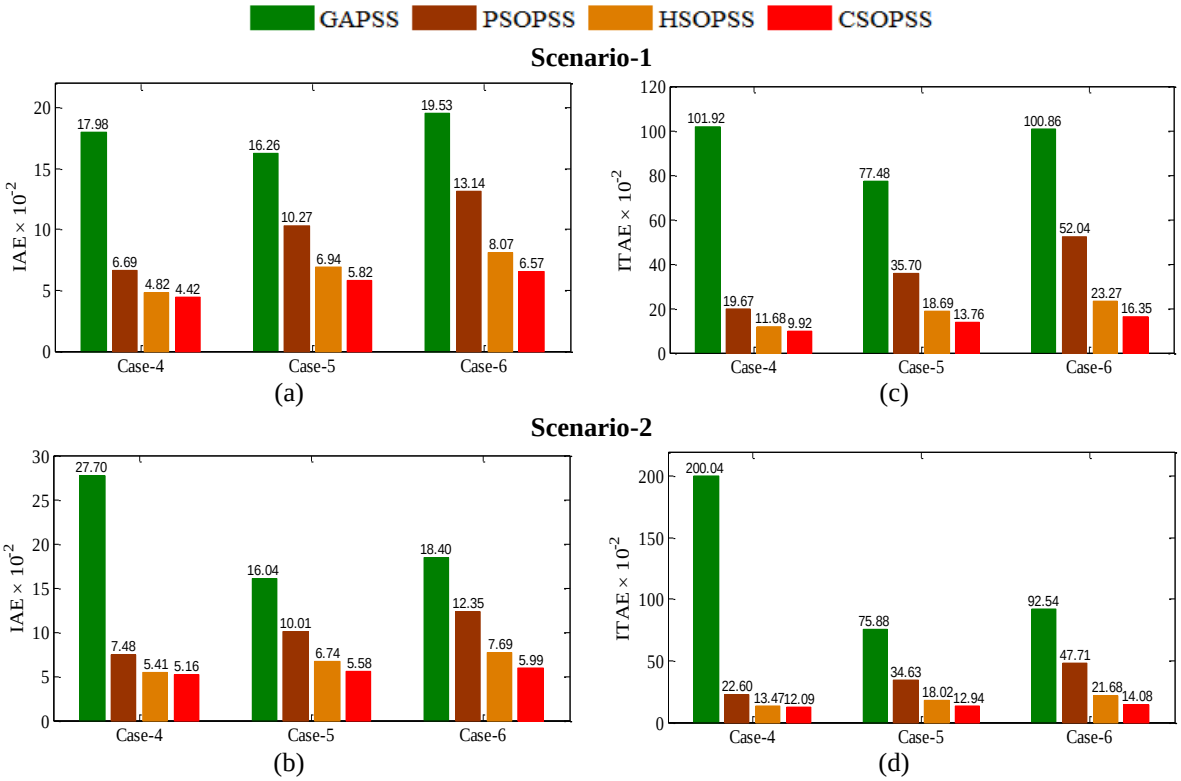

Fig. 7.7 Values of *IAE* and *ITAE* for (a), (c) scenario-1 (b), (d) scenario-2 of unseen operating cases 4-6 of WSCC power system

From the figures, it may be observed that the values of both indices for CSOPSSs are minimum and for GAPSSs are maximum for all scenarios of unseen operating cases 4-6. It highlights that the designed CSOPSS controllers is most suitable as compared to other designed PSS controllers to damp out LFO with improved stability and damping performances for wide range of operating cases under severe scenarios of disturbances and also for unseen operating cases under same scenarios of disturbances.

7.1.2 Example 2: Two-Area, Four-Machine Power System

A. Convergence and Eigenvalue Analysis of TAFM Power System

An eigenvalue-based multi-objective function J presented in (3.1) is minimized using GA, PSO, HSO and CSO by tuning the nine parameters of PSSs. Typical convergence of GAPSSs, PSOPSSs, HSOPSSs and CSOPSSs are shown in Fig. 7.8. Figure shows that all algorithms are able to find the desired solution for which fitness function J is zero. The figure depicts that the CSO algorithm is able to find the best solution before any other optimization techniques. Performance of HSO is close to CSO whereas performance of GA and PSO is slower than HSO and CSO. In fact performance of GA is worst. The optimum designed parameters of GAPSSs, PSOPSSs, HSOPSSs and CSOPSSs for three generators are shown in chapters 3 to 6.

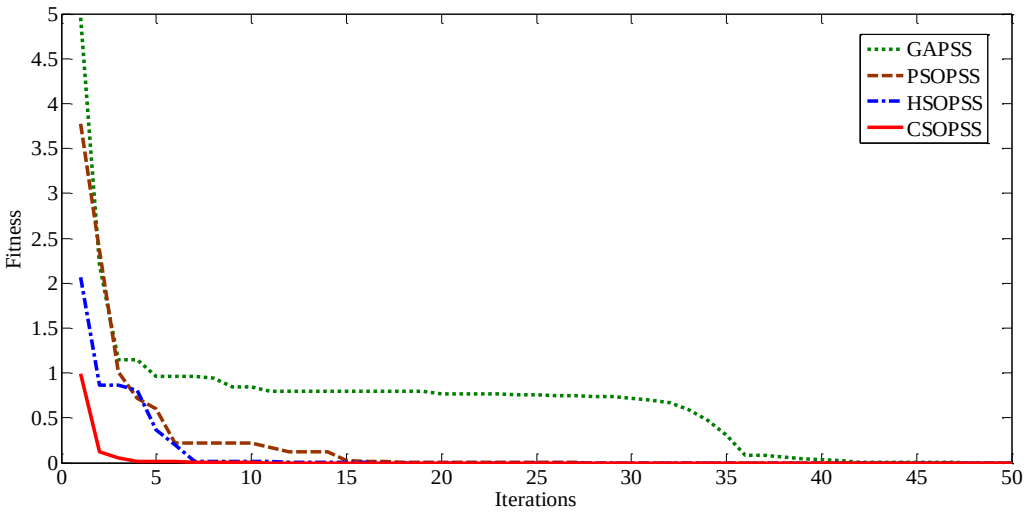

Fig. 7.8 Convergence characteristics of various optimization techniques

The comparison of eigenvalues and their damping ratio without PSS and with GAPSSs, PSOPSSs, HSOPSSs and CSOPSSs for loading cases 1-3 are shown in Table 7.3.

Table 7.3: Eigenvalues and damping ratio comparison with designed PSSs for operating cases 1-3 of TAFM power system

With GAPSSs	With PSOPSSs	With HSOPSSs	With CSOPSSs
	Case-1		
– 1.109 ± j 4.044, 0.26	– 1.188 ± j 4.045, 0.28	– 1.085 ± j 4.318, 0.24	– 1.157 ± j 4.275, 0.26
– 2.240 ± j 1.175, 0.88	– 3.707 ± j 4.290, 0.65	– 4.920 ± j 4.658, 0.72	– 6.742 ± j 4.788, 0.81
– 1.493 ± j 2.582, 0.50	– 2.378 ± j 0.945, 0.92	– 3.228 ± j 1.803, 0.87	– 7.733 ± j 2.332, 0.95
	Case-2		
– 1.098 ± j 3.354, 0.31	– 1.000 ± j 3.362, 0.28	– 1.000 ± j 3.602, 0.26	– 1.090 ± j 3.595, 0.29
– 2.058 ± j 0.841, 0.92	– 2.276 ± j 0.673, 0.95	– 2.996 ± j 1.555, 0.88	– 7.472 ± j 2.563, 0.94
– 1.426 ± j 2.758, 0.45	– 3.841 ± j 3.968, 0.69	– 4.741 ± j 4.268, 0.74	– 6.237 ± j 4.167, 0.83
	Case-3		
– 1.433 ± j 5.434, 0.25	– 1.174 ± j 5.643, 0.20	– 1.127 ± j 5.401, 0.20	– 1.119 ± j 5.322, 0.20
– 1.231 ± j 2.490, 0.44	– 1.637 ± j 3.019, 0.47	– 2.623 ± j 3.873, 0.56	– 4.343 ± j 2.917, 0.83
– 2.393 ± j 3.439, 0.57	–2.732 ± j 0.721, 0.96	– 4.964 ± j 1.080, 0.97	– 5.049 ± j 0.353, 0.99

The Comparison of eigenvalue maps of TAFM power system with GAPSSs, PSOPSSs, HSOPSSs, CSOPSSs for loading cases 1-3 are shown in Fig. 7.9 (a)-(c), (d)-(f), (g)-(i) and (j)-(l) respectively. The Table 7.3 and Fig. 7.9 show that the CSOPSSs shift the eigenvalues to a specified D-shape zone in the left half of the *s*-plane with superior damping factor and damping ratio as compared to GAPSSs, PSOPSSs and HSOPSSs for all loading cases. Hence, designed CSOPSS controllers provide much better stability and damping performance of the TAFM power system as compared to same obtained using other designed PSS controllers.

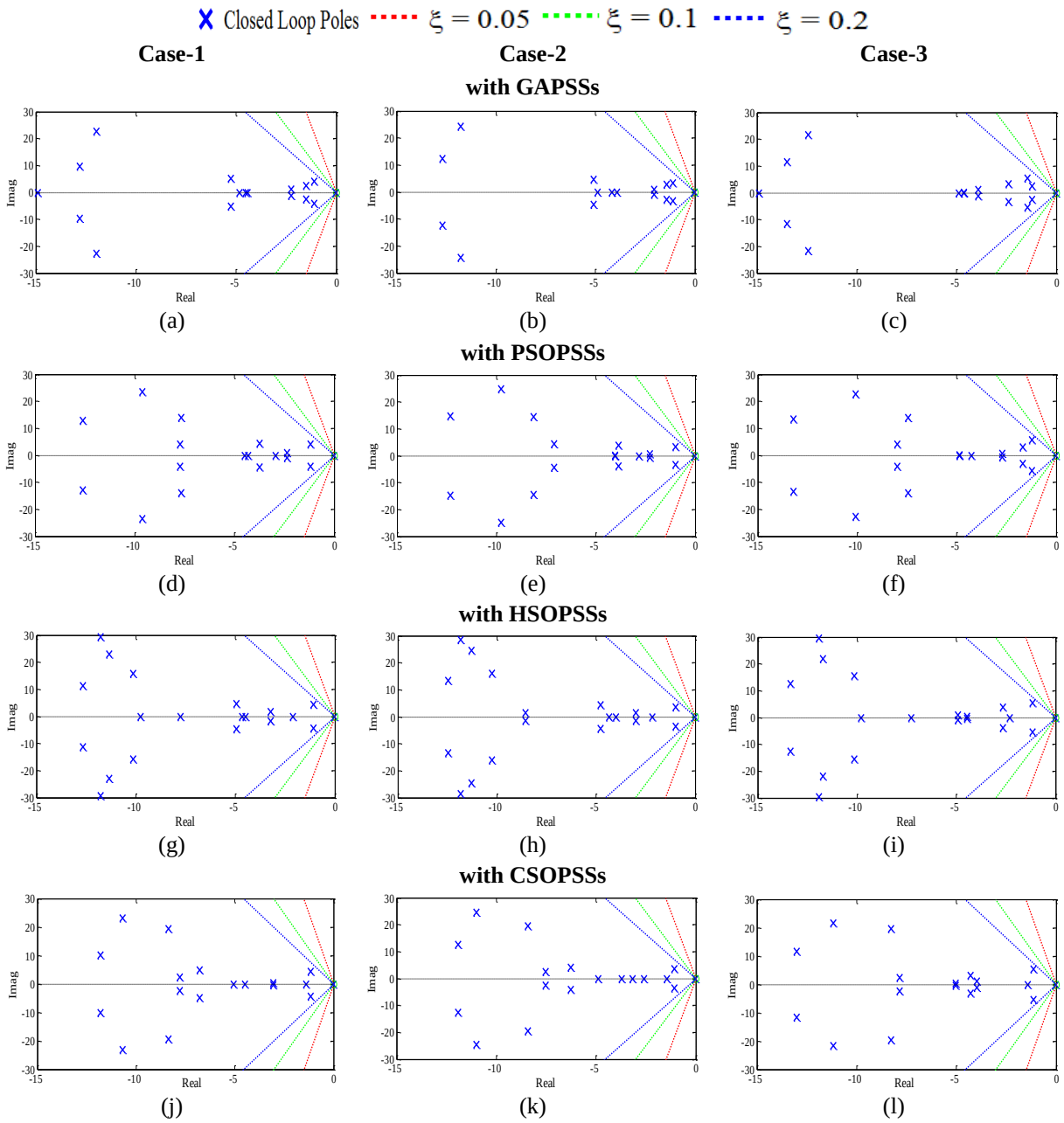

Fig. 7.9 Eigenvalue maps comparison (a)-(c) with GAPSSs (d)-(f) with PSOPSSs (g)-(i) with HSOPSSs (j)-(l) with CSOPSSs for loading cases 1-3 of TAFM power system

B. Time-Domain Simulation Results and Discussions of TAFM Power System

Due to space limitation, specimen results for the comparison of speed deviations Δw_1, Δw_3 for Scenario-1 of Case-2 and the Δw_2, Δw_4 for Scenario-2 of Case-3 with designed PSS controllers are shown in Fig. 7.10 (a)-(b) and (c)-(d) respectively.

From Fig. 7.10, it is clear that the system performance with CSOPSSs is much better than that of GAPSSs, PSOPSSs and HSOPSSs for all severe loading cases and oscillations are comparatively quickly damped out. This illustrates the superiority and potential of CSO technique to obtain desired set of PSS parameters for system over GA, PSO and HSO techniques and the designed CSOPSSs is capable to damp out the LFO rapidly for wide range of loading cases under severe scenarios of disturbances than other designed PSS controllers.

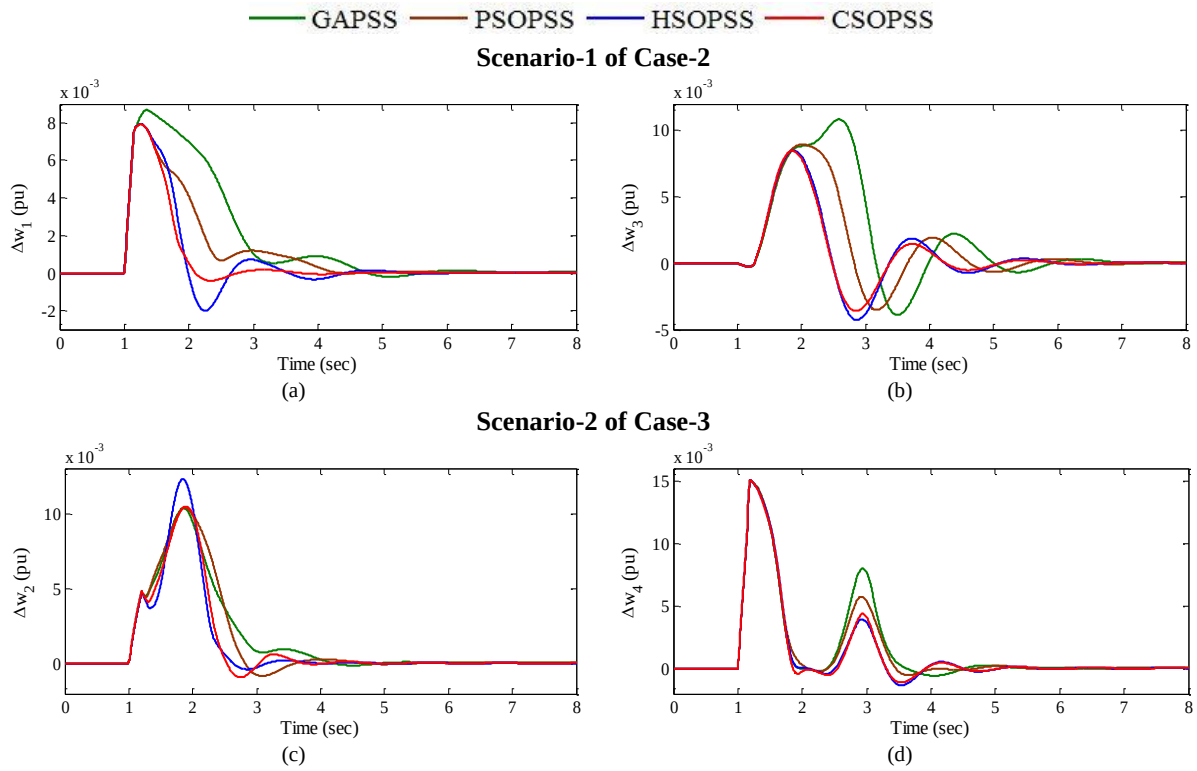

Fig. 7.10 (a)-(b) $\Delta w_1, \Delta w_3$ and (c)-(d) $\Delta w_2, \Delta w_4$ with GAPSSs, PSOPSSs, HSOPSSs, and CSOPSSs for scenario-1 of case-2 and scenario-2 of case-3 of TAFM power system

C. Performance Indices Results and Discussions of TAFM Power System

The comparison of time-domain simulation results in terms of *IAE* and *ITAE* values for scenarios 1-4 of loading cases 1-3 are shown in Fig. 7.11 (a)-(d) and (e)-(h) respectively. The figure reveals that both indices with CSOPSSs are minimum for scenarios 1-4 of loading case 1-3 as compared to the same obtained by GAPSSs, PSOPSSs and HSOPSSs to settle the LFO. Hence, it may be concluded that the designed CSOPSS controllers provide superior damping to damp out low frequency local and inter-area modes of oscillations with less overshoot and settling time than that of other designed PSS controllers.

D. Robustness Test of Designed PSS Controllers of TAFM Power System

The comparison of eigenvalues and damping ratio with only unstable and poorly damped modes for unseen operating cases 4-12 of system with GAPSSs, PSOPSSs, HSOPSSs and CSOPSSs are illustrated in Table 7.4. The table shows that the CSOPSSs shift the eigenvalues to a specified D-shape zone in the left half of the *s*-plane with superior damping factor and damping ratio as compared to other designed PSSs for all unseen cases. Hence, the designed CSOPSSs is robust as it works with superior damping performance for unseen operating cases 4-12 as compared to that of other designed PSS controllers.

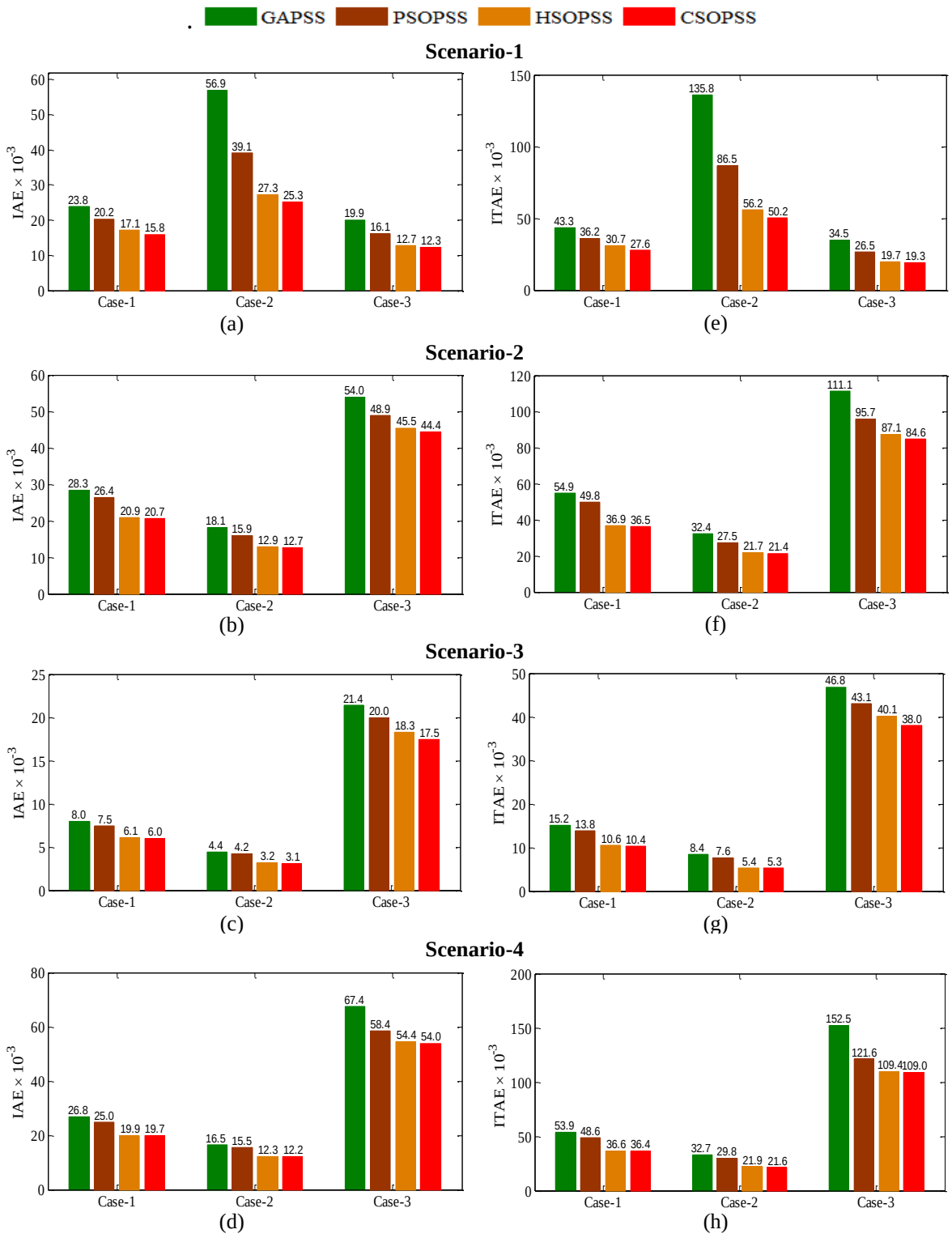

Fig. 7.11 Values of (a)-(d) *IAE* and (e)-(h) *ITAE* with GAPSSs, PSOPSSs, HSOPSSs and CSOPSSs for scenarios 1-4 of loading cases 1-3 of TAFM power system

Table 7.4: Eigenvalues and damping ratio comparison with designed PSSs for unseen operating cases 4-12 of TAFM power system

S. No.	With GAPSSs	With PSOPSSs	With HSOPSSs	With CSOPSSs
Case-4	– 1.528 ± j 2.511, 0.519 – 1.601 ± j 3.600, 0.406 – 4.460 ± j 5.011, 0.664	– 2.928 ± j 4.650, 0.532 – 1.667 ± j 3.064, 0.477 – 7.335 ± j 4.306, 0.862	– 4.249 ± j 4.479, 0.688 – 1.473 ± j 3.759, 0.365 – 3.323 ± j 1.819, 0.877	– 5.878 ± j 4.573, 0.789 – 1.454 ± j 3.902, 0.349 – 7.597 ± j 2.453, 0.951
Case-5	– 1.189 ± j 2.169, 0.480 – 1.469 ± j 5.736, 0.248 – 2.058 ± j 2.873, 0.582	– 1.438 ± j 2.435, 0.508 – 1.245 ± j 5.825, 0.209 – 7.560 ± j 14.156, 0.471	– 2.451 ± j 3.108, 0.619 – 1.311 ± j 5.617, 0.227 – 10.119 ± j 15.675, 0.542	– 4.720 ± j 1.945, 0.924 – 1.339 ± j 5.466, 0.237 – 13.058 ± j 11.902, 0.739
Case-6	– 1.522 ± j 2.495, 0.520 – 1.597 ± j 3.602, 0.405 – 4.443 ± j 5.013, 0.663	– 2.923± j 4.656, 0.531 – 1.655 ± j 3.076, 0.473 – 7.920 ± j 14.435, 0.481	– 4.237 ± j 4.485, 0.686 – 1.467 ± j 3.765, 0.363 – 12.806 ± j 11.598, 0.741	– 5.856 ± j 4.573, 0788 – 1.451 ± j 3.907, 0.348 – 12.198 ± j 10.415, 0.760
Case-7	– 1.181 ± j 2.172, 0.477 – 1.466 ± j 5.742, 0.247 – 2.068 ± j 2.868, 0.584	– 1.436 ± j 2.442, 0.506 – 1.242 ± j 5.829, 0.208 – 7.521 ± j 14.150, 0.469	– 2.440 ± j 3.111, 0.617 – 1.309 ± j 5.622, 0.226 – 10.095 ± j 15.663, 0.541	– 4.707 ± j 1.922, 0.925 – 1.337 ± j 5.471, 0.237 – 13.062 ± j 11.920, 0.738
Case-8	– 1.163 ± j 3.358, 0.327 – 1.370 ± j 2.743, 0.446 – 4.678 ± j 4.262, 0.739	– 1.026 ± j 3.305, 0.296 – 3.483 ± j 3.821, 0.673 – 6.918 ± j 4.464, 0.840	**– 0.961** ± j 3.568, 0.260 – 4.337 ± j 4.125, 0.724 – 8.387 ± j 1.778, 0.978	– 1.064 ± j 3.604, 0.283 – 5.796 ± j 3.977, 0.824 – 7.391 ± j 2.632, 0.942
Case-9	– 1.035 ± j 2.446, 0.389 – 1.066 ± j 5.864, **0.178** – 1.988 ± j 3.117, 0.537	– 1.315 ± j 2.822, 0.422 **– 0.889** ± j 5.908, **0.148** – 7.922 ± j 4.131, 0.886	– 2.228 ± j 3.571, 0.529 **– 0.938** ± j 5.745, **0.161** – 13.520 ± j 13.591, 0.705	– 2.988 ± j 2.547, 0.760 **– 0.968** ± j 5.650, **0.168** – 13.262 ± j 12.968, 0.715
Case-10	**– 0.993** ± j 2.042, 0.437 – 1.004 ± j 6.012, **0.164** – 1.876 ± j 2.840, 0.551	– 1.191 ± j 2.227, 0.471 **– 0.856** ± j 6.031, **0.140** – 7.542 ± j 14.138, 0.470	– 2.321 ± j 2.812, 0.636 **– 0.924** ± j 5.907, **0.154** – 10.143 ± j 15.653, 0.543	– 2.597 ± j 1.572, 0.855 **– 0.987** ± j 5.815, **0.167** – 13.273 ± j 13.125, 0.711
Case 11	**– 0.987** ± j 2.045, 0.434 – 1.000 ± j 6.015, **0.164** – 1.884 ± j 2.828, 0.554	– 1.188 ± j 2.230, 0.470 **– 0.853** ± j 6.033, **0.139** – 7.504 ± j 14.133, 0.468	– 2.308 ± j 2.812, 0.634 **– 0.921** ± j 5.910, **0.154** – 10.120 ± j 15.642, 0.543	– 2.587 ± j 1.583, 0.852 **– 0.984** ± j 5.818, **0.166** – 13.275 ± j 13.142, 0.710
Case 12	– 1.291 ± j 3.475, 0.348 – 1.319 ± j 2.645, 0.446 – 3.971 ± j 4.007, 0.703	– 1.173 ± j 3.219, 0.342 – 2.830 ± j 3.827, 0.594 – 6.691 ± j 4.518, 0.828	**– 0.955** ± j 3.583, 0.257 – 3.731 ± j 4.082, 0.674 – 8.301 ± j 1.978, 0.972	– 1.060 ± j 3.701, 0.275 – 5.161 ± j 3.783, 0.806 – 7.338 ± j 2.685, 0.939

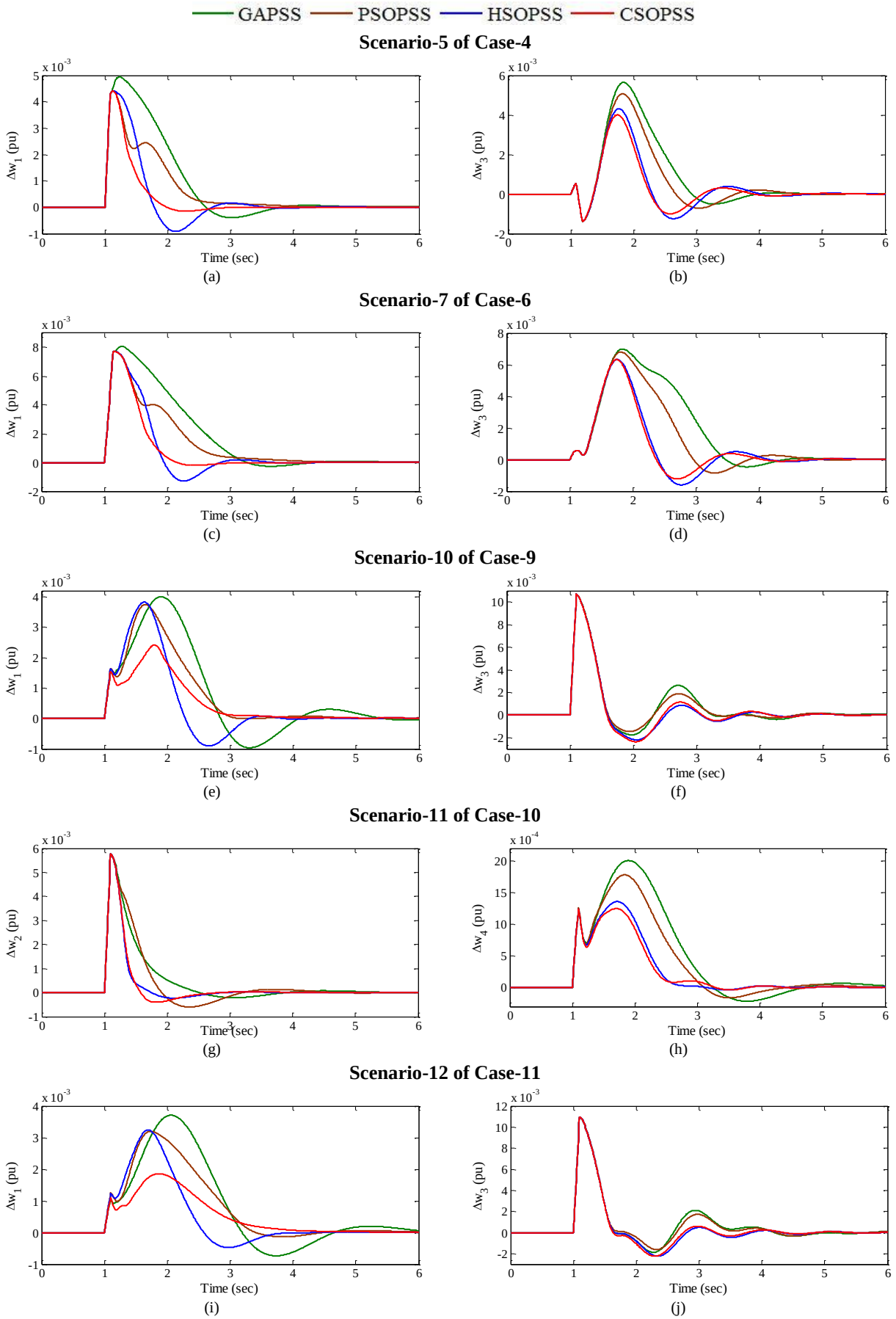

Fig. 7.12 (a)-(b), (c)-(d), (e)-(f), (i)-(j) $\Delta w_1, \Delta w_3$ and (g)-(h) $\Delta w_2, \Delta w_4$ with GAPSSs, PSOPSSs, HSOPSSs, CSOPSSs for scenarios 5, 7, 10, 12and 11 respectively

Due to space limitation, specimen results for the comparison of speed deviations Δw_1, Δw_3 with designed PSS controllers for scenarios 5, 7, 10, 12 of corresponding unseen cases are shown in Fig. 7.12 (a)-(b), (c)-(d), (e)-(f), and (i)-(j) respectively whereas the Δw_2, Δw_4 for Scenario-11 are shown in Fig. 7.12 (g)-(h) respectively.

From Fig. 7.12, it is clear that the system performance with CSOPSSs is much better than that of GAPSSs, PSOPSSs and HSOPSSs for all considered scenarios of severe operating cases and oscillations are rapidly damped out as compared to that of other designed PSS controllers. This may be concluded that the designed CSOPSSs work superiorly for most of the scenarios of severe disturbances of unseen operating cases of TAFM power system as compared to that of other designed PSS controllers.

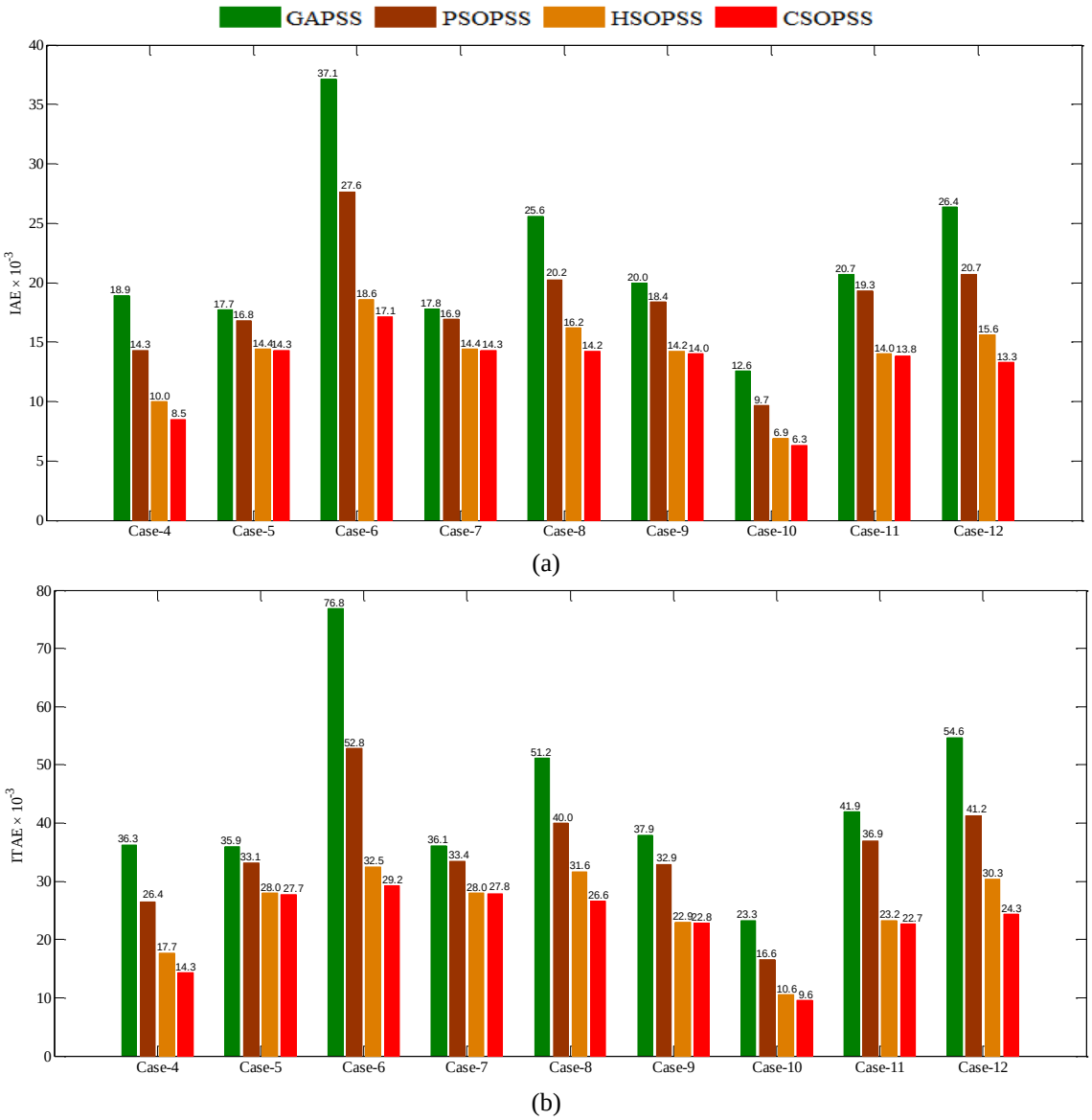

Fig. 7.13 Value of (a) *IAE* and (b) *ITAE* with GAPSSs, PSOPSSs, HSOPSSs and CSOPSSs for scenarios 5-13 of unseen cases 4-12 of TAFM power system

In addition to time-domain simulation results, the superior robustness and effectiveness performance of previously designed CSOPSS controllers is observed by comparing bar charts of *IAE* and *ITAE* with other designed PSSs for scenarios 5-13 of unseen operating cases 4-12 and are shown in Fig. 7.13 (a) and (b) respectively.

From the Fig. 7.13 (a)-(b), it may be noticed that the values of both indices for CSOPSSs are minimum and for GAPSSs are maximum for all scenarios of unseen operating cases 4-12. It highlights that the designed CSOPSS controllers is most competent as compared to other designed PSS controllers to damp out LFO with improved SSS and damping performances for wide range of operating cases under severe scenarios of disturbances and also for unseen operating cases under same scenarios of disturbances.

7.1.3 Example 3: Ten-Machine, Thirty-Nine Bus New England Power System

A. Convergence and Eigenvalue Analysis of NEPS

An eigenvalue-based multi-objective function J presented in (3.1) is minimized using GA, PSO, HSO and CSO by tuning the twenty-seven parameters of PSSs. Typical convergence of GAPSSs, PSOPSSs, HSOPSSs and CSOPSSs are shown in Fig. 7.14.

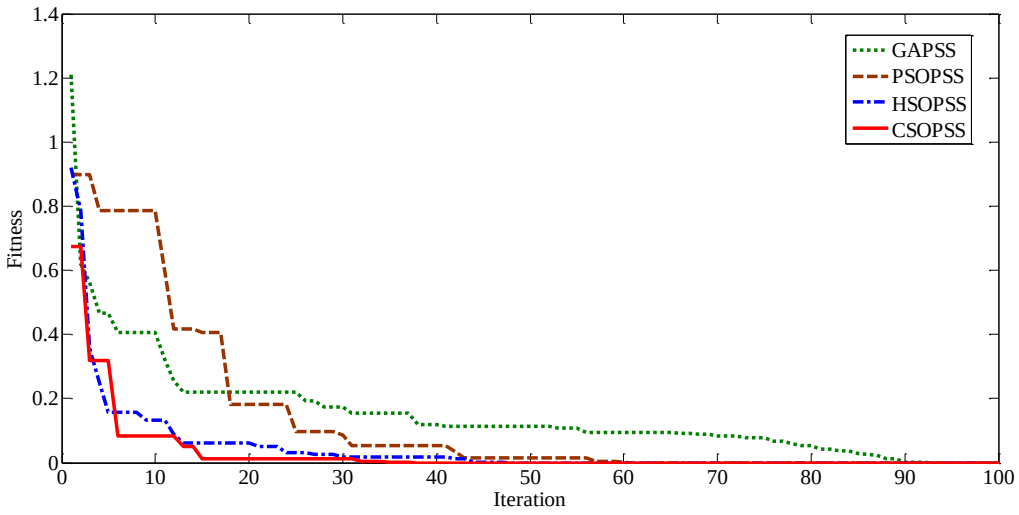

Fig. 7.14 Convergence characteristics of various optimization techniques

Figure shows that all algorithms are able to find the desired solution for which fitness function J is zero. The figure depicts that the CSO algorithm is able to find the best solution before any other optimization techniques. Performance of HSO is close to CSO whereas performance of GA and PSO is slower than HSO and CSO. The optimum designed parameters of GAPSSs, PSOPSSs, HSOPSSs and CSOPSSs for nine generators are shown in chapters 3 to 6. The comparison of eigenvalues and their damping ratio with GAPSSs, PSOPSSs, HSOPSSs and CSOPSSs for operating cases 1-3 are shown in Table 7.5. The comparison of eigenvalue

maps of NEPS with GAPSSs, PSOPSSs, HSOPSSs and CSOPSSs for loading cases 1-3 are shown in Fig. 7.15 (a)-(c), (d)-(f), (g)-(i) and (j)-(l)respectively.

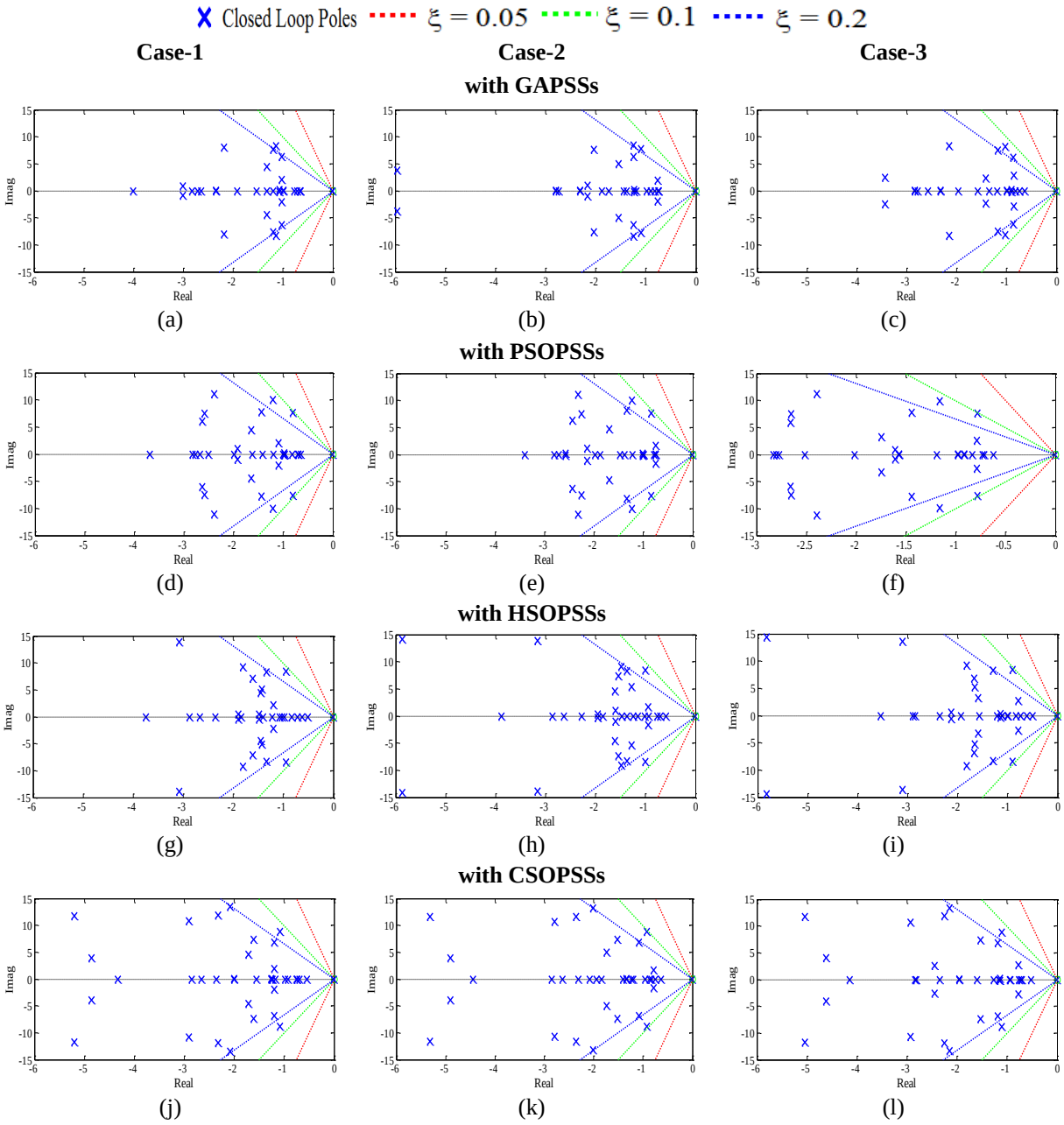

Fig. 7.15 Eigenvalue maps comparison (a)-(c) with GAPSSs (d)-(f) with PSOPSSs (g)-(i) with HSOPSSs (j)-(l) with CSOPSSs for cases 1-3 of NEPS

Table 7.5 and Fig. 7.15 show that the CSOPSSs shift the eigenvalues to a specified D-shape zone in the left half of the *s*-plane with superior damping factor and damping ratio as compared to GAPSSs, PSOPSSs and HSOPSSs for all loading cases. Hence, designed CSOPSS controllers provide best stability and damping performance as compared to same obtained using other designed PSS controllers.

Table 7.5: Eigenvalues and damping ratio comparison with designed PSSs for loading cases 1-3 of NEPS

With GAPSSs	With PSOPSSs	With HSOPSSs	With CSOPSSs
Case-1			
– 1.136 ± j 8.283, 0.135	– 1.439 ± j 7.822, 0.181	– 1.812 ± j 9.262, 0.192	– 2.362 ± j 11.928, 0.194
– 1.195 ± j 7.568, 0.155	– 1.231 ± j 9.971, 0.122	– 1.351 ± j 8.337, 0.160	– 1.611 ± j 7.386, 0.213
– 1.030 ± j 6.289, 0.161	– 0.818 ± j 7.691, 0.105	– 0.948 ± j 8.420, 0.111	– 1.088 ± j 8.834, 0.122
Case-2			
– 1.240 ± j 8.427, 0.145	– 1.248 ± j 9.976, 0.124	– 1.490 ± j 9.092, 0.161	– 2.396 ± j 11.573, 0.202
– 1.249 ± j 6.369, 0.192	– 1.329 ± j 8.106, 0.161	– 1.390 ± j 8.283, 0.165	– 1.517 ± j 7.312, 0.203
– 1.101 ± j 7.700, 0.141	– 0.848 ± j 7.619, 0.110	– 0.999 ± j 8.362, 0.118	– 0.927 ± j 8.787, 0.104
Case-3			
– 1.032 ± j 8.191, 0.125	– 1.180 ± j 9.910, 0.118	– 1.719 ± j 16.765, 0.102	– 2.177 ± j 13.408, 0.160
– 1.180 ± j 7.502, 0.155	– 1.442 ± j 7.800, 0.181	– 1.306 ± j 8.308, 0.155	– 1.534 ± j 7.387, 0.203
– 0.864 ± j 6.184, 0.138	– 0.789 ± j 7.644, 0.102	– 0.897 ± j 8.384, 0.106	– 1.108 ± j 8.824, 0.124

B. Time-Domain Simulation Results and Discussions of NEPS

The comparison of severe speed deviations Δw_1 and Δw_9 with other designed PSS controllers are considered for scenarios 1-5 of Case-3 and shown in Fig. 7.16 (a)-(e) and (f)-(j) respectively. From Fig. 7.16, it is clear that the system performance with CSOPSSs is much better than that of GAPSSs, PSOPSSs and HSOPSSs for all considered scenarios of Case-3 and oscillations are quickly damped out as compared to that of other designed PSSs. This illustrates the superiority and potential of CSO technique to obtain desired set of PSS parameters.

C. Performance Indices Results and Discussions of NEPS

The comparison of *IAE* and *ITAE* indices with other designed PSSs for scenarios 1-5 of loading cases 1-3 are shown in Fig. 7.17 (a)-(e) and (f)-(j) respectively. The figure reveals that both indices values with CSOPSSs are minimum for scenarios 1-5 of loading cases 1-3 as compared to the same obtained by GAPSSs, PSOPSSs and HSOPSSs to settle the LFO.

D. Robustness Test of Designed PSS Controllers of NEPS

The eigenvalue analysis, simulation results and performance indices for observed scenarios 1-2 of fifteen unseen cases 4-18 are considered. The comparison of only unstable modes eigenvalues and damping ratio for unseen operating cases 4-18 with all designed PSS controllers are illustrated in Table 7.6.

The table shows that the CSOPSSs shift the eigenvalues to a specified D-shape zone in the left half of the *s*-plane with better damping factor and damping ratio as compared to GAPSSs, PSOPSSs and HSOPSSs for all unseen cases. Hence, the designed CSOPSSs is robust as it works with superior damping performance for unseen operating cases 4-18 of the NEPS as compared to that of other designed PSS controllers.

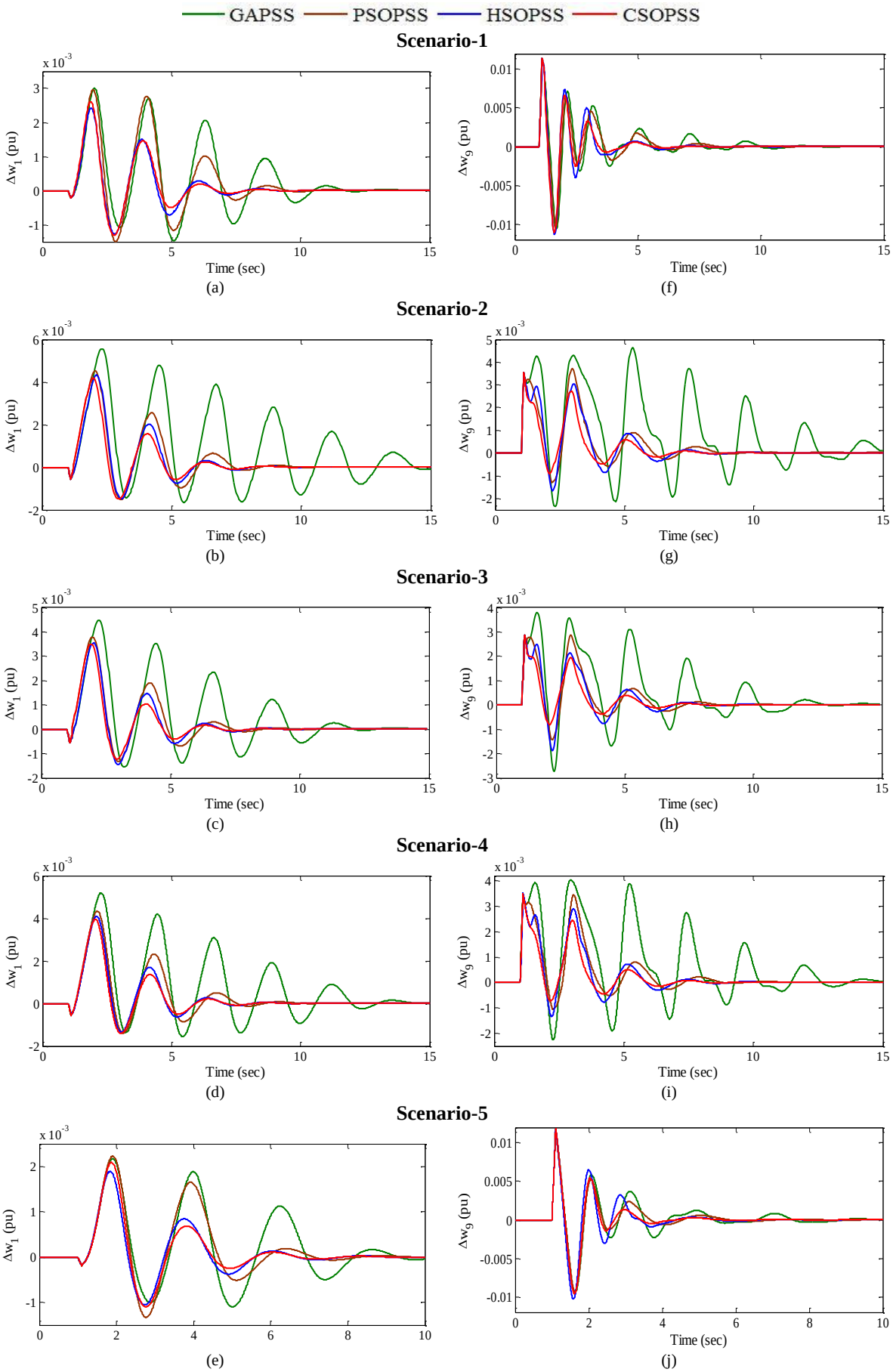

Fig. 7.16 (a)-(e) Δw_1 and (f)-(j) $\Delta w_9$with GAPSSs, PSOPSSs, HSOPSSs, CSOPSSs for scenarios 1-5 of loadingcase-3 of NEPS

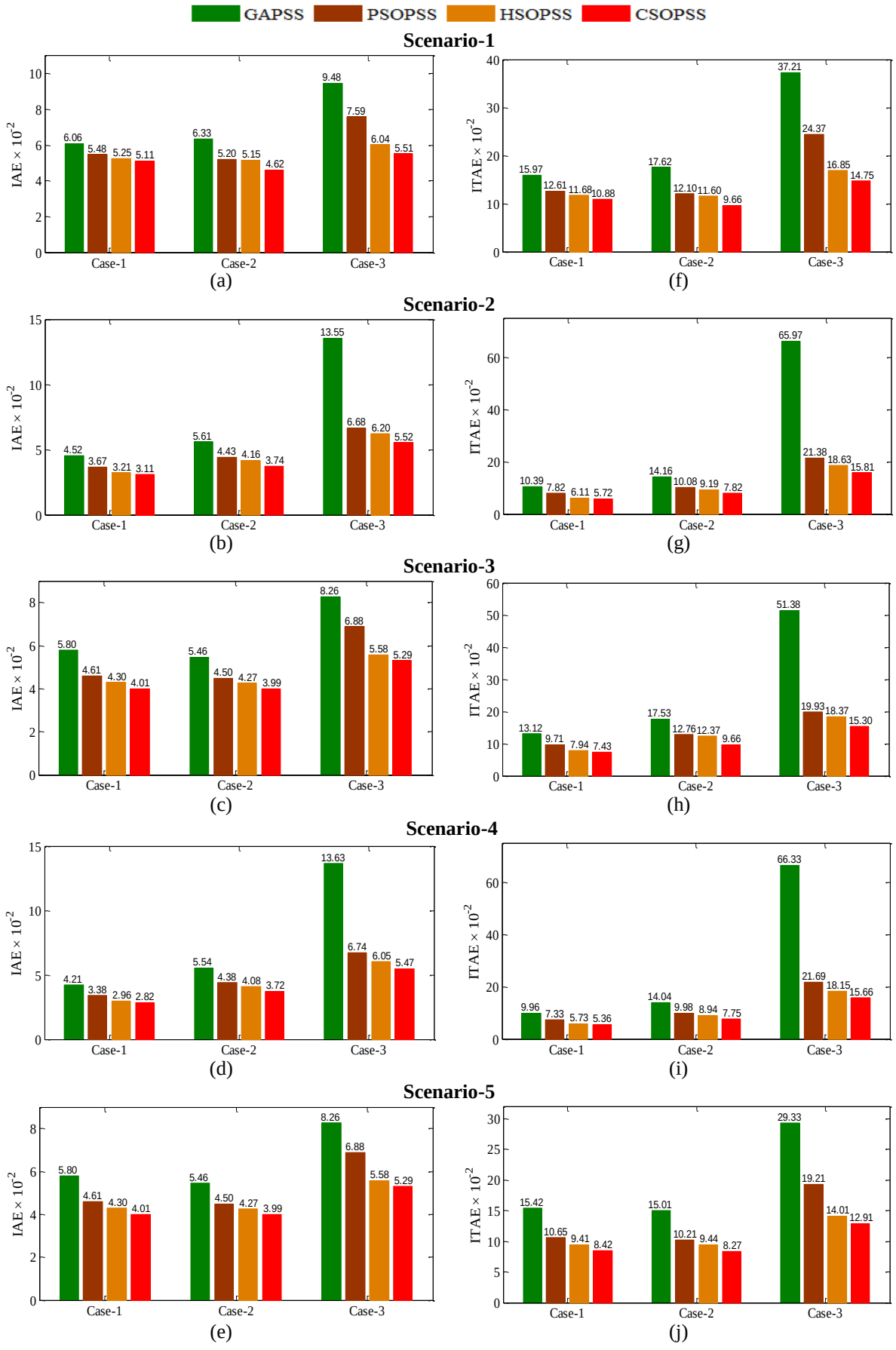

Fig. 7.17 Values of (a)-(e) *IAE* and (f)-(j) *ITAE* with GAPSSs, PSOPSSs, HSOPSSs and CSOPSSs for scenarios 1-5 of loading cases 1-3 of NEPS

Table 7.6: Eigenvalues and damping ratio comparison with designed PSSs for unseen operating cases 4-18 of NEPS

Cases	With GAPSSs	With PSOPSSs	With HSOPSSs	With CSOPSSs
	– 1.059 ± j 7.378, 0.142	– 1.189 ± j 7.153, 0.164	– 1.207 ± j 7.664, 0.155	– 1.235 ± j 7.014, 0.173
Case-4	– 1.132 ± j 5.861, 0.189	– 1.320 ± j 7.628, 0.170	– 1.411 ± j 5.125, 0.265	– 1.492 ± j 4.971, 0.287
	– 1.681 ± j 8.275, 0.199	– 2.398 ± j 11.136, 0.210	– 3.536 ± j 13.616, 0.251	– 5.266 ± j 11.752, 0.408
	– 0.747 ± j 4.840, 0.142	– 1.271 ± j 7.615, 0.164	– 1.292 ± j 8.389, 0.152	– 1.756 ± j 6.056, 0.278
Case-5	– 1.051 ± j 7.615, 0.136	– 1.157 ± j 9.781, 0.117	– 1.466 ± j 7.671, 0.187	– 2.350 ± j 11.909, 0.193
	– 1.254 ± j 7.135, 0.170	– 1.806 ± j 7.232, 0.242	– 3.128 ± j 13.735, 0.222	– 5.221 ± j 11.683, 0.408
	– 0.750 ± j 6.112, 0.121	– 1.167 ± j 7.607, 0.151	– 1.196 ± j 4.409, 0.261	– 1.811 ± j 4.402, 0.380
Case-6	– 1.017 ± j 2.034, 0.447	– 1.039 ± j 2.082, 0.448	– 1.152 ± j 2.216, 0.469	– 1.156 ± j 1.991, 0.502
	– 1.132 ± j 8.279, 0.135	– 1.232 ± j 9.969, 0.122	– 1.377 ± j 8.342, 0.162	– 1.588 ± j 7.386, 0.210
	– 1.147 ± j 8.295, 0.136	– 1.240 ± j 9.988, 0.123	– 1.359 ± j 8.342, 0.160	– 1.618 ± j 7.385, 0.214
Case-7	– 1.195 ± j 7.578, 0.155	– 1.435 ± j 7.821, 0.180	– 1.608 ± j 7.207, 0.217	– 1.711 ± j 4.684, 0.343
	– 1.005 ± j 1.992 0.450	– 1.063 ± j 1.997 0.470	– 1.176 ± j 2.093 0.489	– 1.149 ± j 1.899 0.517
	– 0.448 ± j 4.329, 0.102	– 1.157 ± j 9.781, 0.117	– 1.292 ± j 8.388, 0.152	– 1.893 ± j 4.248, 0.407
Case8	– 0.736 ± j 1.840, 0.371	– 0.800 ± j 1.951, 0.379	– 0.848 ± j 1.978, 0.394	– 0.907 ± j 2.007, 0.411
	– 1.074 ± j 7.388, 0.143	– 1.271 ± j 7.613, 0.164	– 1.354 ± j 7.641, 0.174	– 1.510 ± j 6.032, 0.242
	– 0.416 ± j 1.721, 0.235	– 0.469 ± j 1.764, 0.256	– 0.476 ± j 1.740, 0.264	– 0.510 ± j 1.762, 0.278
Case-9	– 1.067 ± j 6.290, 0.167	– 1.214 ± j 7.600, 0.157	– 1.577 ± j 6.848, 0.224	– 1.642 ± j 5.183, 0.302
	– 1.157 ± j 7.284, 0.156	– 1.555 ± j 5.203, 0.286	– 1.324 ± j 3.657, 0.340	– 2.155 ± j 3.695, 0.503
	– 0.996 ± j 8.389, 0.117	– 0.889 ± j 6.393, 0.137	– 1.091 ± j 6.478, 0.168	– 1.106 ± j 6.124, 0.175
Case-10	– 1.007 ± j 2.115, 0.429	– 1.066 ± j 2.138, 0.446	– 1.093 ± j 2.239, 0.438	– 1.229 ± j 2.033, 0.517
	– 1.097 ± j 7.747, 0.140	– 1.375 ± j 7.817, 0.173	– 1.506 ± j 7.854, 0.188	– 1.507 ± j 7.153 0.205

Cont.

Cases	With GAPSSs	With PSOPSSs	With HSOPSSs	With CSOPSSs
	– 0.617 ± j 1.867, 0.313	– 0.663 ± j 1.831, 0.340	– 0.737 ± j 1.814, 0.376	– 0.782 ± j 1.893, 0.381
Case-11	– 0.972 ± j 6.128, 0.156	– 1.501 ± j 7.908, 0.186	– 1.598 ± j 7.390, 0.211	– 1.598 ± j 7.169, 0.217
	– 1.139 ± j 8.290, 0.136	– 1.230 ± j 9.968, 0.122	– 1.723 ± j 9.076, 0.186	– 2.368 ± j 11.905, 0.195
	– 0.971 ± j 2.078, 0.423	– 1.045 ± j 2.065, 0.450	– 1.089 ± j 2.159, 0.451	– 1.155 ± j 1.959, 0.507
Case-12	– 0.997 ± j 8.406, 0.117	– 1.282 ± j 9.817, 0.129	– 1.773 ± j 9.227, 0.188	– 2.384 ± j 11.843, 0.197
	– 1.089 ± j 7.755, 0.139	– 1.374 ± j 7.829, 0.172	– 1.542 ± j 7.891, 0.191	– 2.838 ± j 10.647, 0.257
	– 0.604 ± j 4.498, 0.133	– 0.907 ± j 6.657, 0.135	– 1.236 ± j 8.220, 0.148	– 1.500 ± j 7.178, 0.204
Case-13	– 1.100 ± j 7.640, 0.142	– 1.374 ± j 7.805, 0.173	– 1.468 ± j 7.869, 0.173	– 2.362 ± j 11.862, 0.195
	– 0.998 ± j 8.369, 0.118	– 1.274 ± j 9.835, 0.128	– 1.792 ± j 9.236, 0.190	– 2.906 ± j 10.714, 0.261
	– 0.283 ± j 4.078, 0.069	– 0.876 ± j 7.581, 0.114	– 1.039 ± j 8.349, 0.122	– 1.089 ± j 8.828, 0.123
Case-14	– 1.174 ± j 7.501, 0.154	– 1.539 ± j 7.761, 0.194	– 1.583 ± j 7.089, 0.218	– 1.674 ± j 7.233, 0.225
	– 1.236 ± j 8.138, 0.150	– 1.215 ± j 9.910, 0.121	– 1.347 ± j 8.322, 0.159	– 1.574 ± j 4.518, 0.329
	– 0.320 ± j 4.280, 0.074	– 1.161 ± j 9.793, 0.117	– 1.288 ± j 8.377, 0.152	– 1.332 ± j 6.939, 0.188
Case-15	– 1.038 ± j 7.545, 0.136	– 1.295 ± j 7.636, 0.167	– 1.339 ± j 7.852, 0.168	– 1.562 ± j 6.364, 0.238
	– 1.308 ± j 6.999, 0.183	– 1.647 ± j 6.850, 0.233	– 1.615 ± j 6.837, 0.229	– 1.798 ± j 4.390, 0.379
	– 0.208 ± j 4.054, 0.051	– 1.000 ± j 6.561, 0.150	– 1.153 ± j 6.619, 0.171	– 1.138 ± j 6.203, 0.180
Case-16	– 1.016 ± j 8.302, 0.121	– 1.283 ± j 9.734, 0.130	– 1.081 ± j 8.805, 0.121	– 1.301 ± j 8.152, 0.157
	– 1.065 ± j 7.640, 0.138	– 1.420 ± j 7.811, 0.178	– 1.494 ± j 7.878, 0.186	– 1.542 ± j 7.062, 0.213
	– 0.179 ± j 3.996, 0.044	– 1.160 ± j 9.789, 0.117	– 1.291 ± j 8.373, 0.152	– 1.322 ± j 6.920, 0.187
Case-17	– 1.015 ± j 7.534, 0.133	– 1.318 ± j 7.847, 0.165	– 1.344 ± j 7.655, 0.172	– 1.557 ± j 6.359, 0.237
	– 1.309 ± j 6.975, 0.184	– 1.580 ± j 6.943, 0.222	– 1.610 ± j 6.836, 0.229	– 1.771 ± j 4.371, 0.375
	– 0.511 ± j 3.993, 0.127	– 1.216 ± j 6.313, 0.189	– 1.210 ± j 6.067, 0.195	– 1.275 ± j 6.375, 0.196
Case-18	– 0.928 ± j 7.471, 0.123	– 1.259 ± j 9.477, 0.131	– 1.778 ± j 9.227, 0.189	– 2.300 ± j 8.788, 0.253
	– 1.139 ± j 8.029, 0.140	– 1.301 ± j 7.805, 0.164	– 1.585 ± j 7.914, 0.196	– 1.493 ± j 7.165, 0.203

In order to compare the robustness performance of the designed PSS controllers in terms of simulation results, specimen results for the comparison of severe speed deviations Δw_5, Δw_9 for Scenario-1 of unseen Case-8 are shown in Fig. 7.18 (a)-(b) whereas Δw_1, Δw_9 for Scenario-1 of unseen cases 9-12 are shown in Fig. 7.18 (c)-(j) respectively. Moreover, to check the robustness performance of designed PSS controllers on other unseen cases, specimen results for the comparison of severe speed deviations Δw_1 and Δw_9 for Scenario-4 of unseen cases 14-18 are shown in Fig. 7.19 (a)-(b), (c)-(d), (e)-(f), (g)-(h) and (i)-(j) respectively.

From Figs. 7.18 and 7.19, it is clear that the system performance with CSOPSSs is much better than that of GAPSSs, PSOPSSs and HSOPSSs for all considered scenarios of unseen operating cases 8-12 & 14-18 and oscillations are quickly damped out as compared to that of other designed PSSs. This illustrates the superiority of CSO technique to obtain desired set of PSS parameters. The designed CSOPSSs are capable to damp out the LFO rapidly than other designed PSS controllers for wide range of unseen operating cases 4-18 under severe scenarios of disturbances.

The comparison of *IAE* and *ITAE* for Scenario-1 of unseen cases 4-12 are shown in Fig. 7.20 (a) and (c) respectively whereas for Scenario-2 of unseen cases 4-18 are shown in Fig. 7.20 (b) and (d) respectively. The figures reveal that both indices values with CSOPSSs are minimum for scenarios 1-2 of unseen operating cases 4-12 and 4-18 as compared to the same obtained by GAPSSs, PSOPSSs and HSOPSSs to settle the LFO. Hence, it may be observed that the designed CSOPSS controllers of NEPS provide superior damping to mitigate low frequency local and inter-area modes oscillation with less overshoot and settling time than that of other designed PSS controllers.

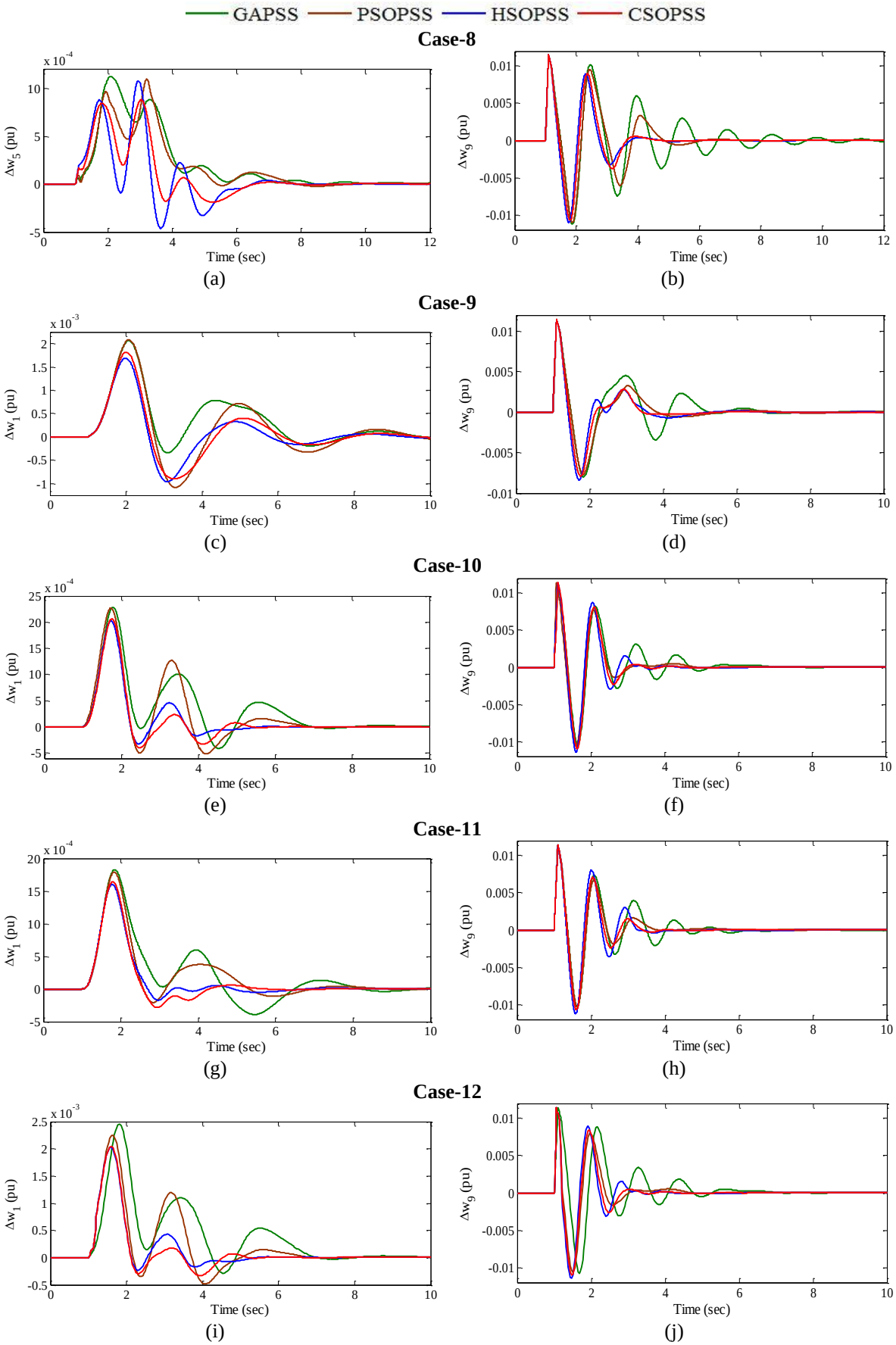

Fig. 7.18 (a)-(b) Δw_5, Δw_9 and (c)-(d), (e)-(f), (g)-(h) and (i)-(j) Δw_1, Δw_9 with GAPSSs, PSOPSSs, HSOPSSs, CSOPSSs for scenario-1 of unseen operating cases 8-12 of NEPS

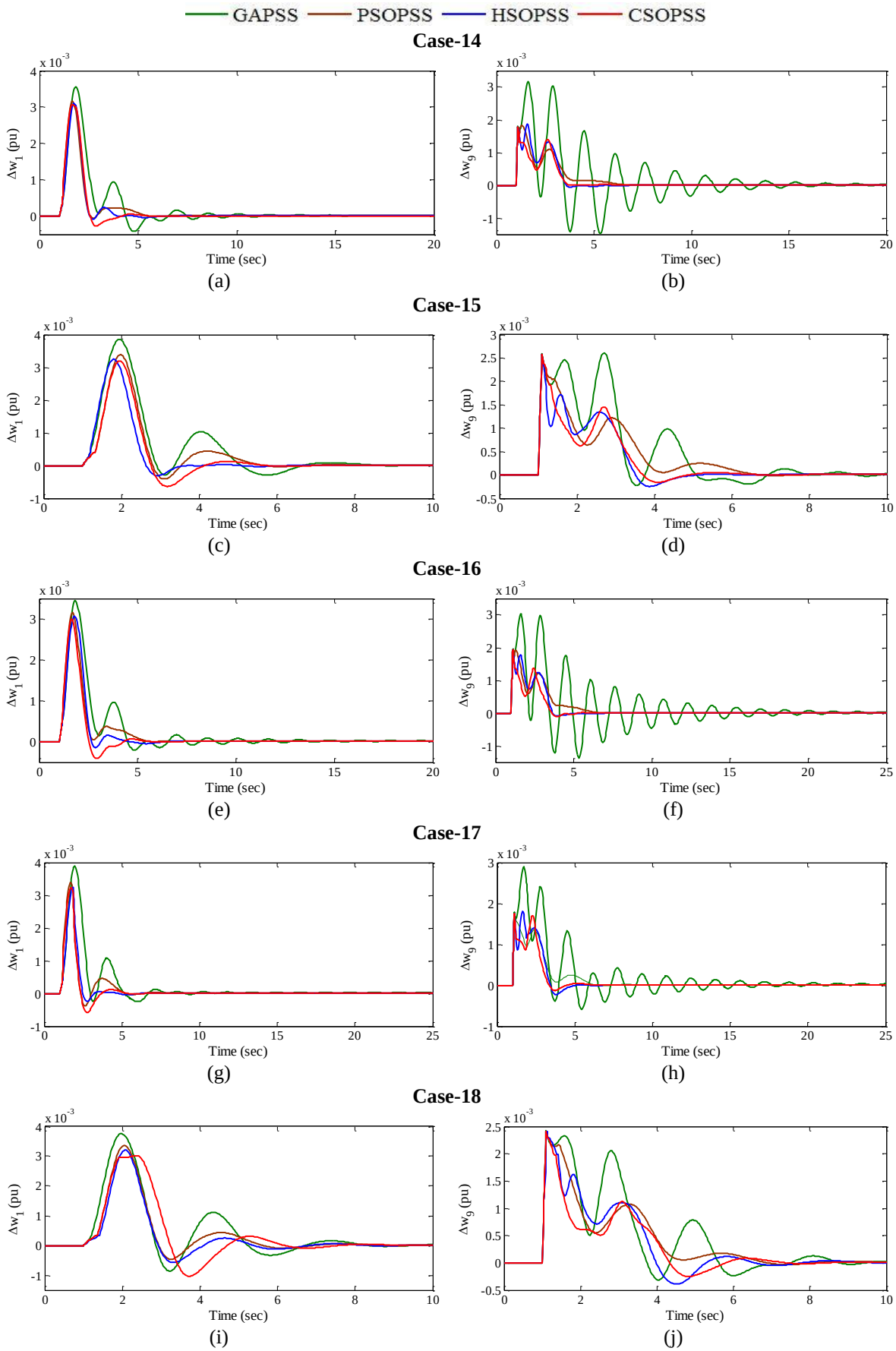

Fig. 7.19 (a)-(b), (c)-(d), (e)-(f), (g)-(h) and (i)-(j) Δw_1 and Δw_9 with GAPSSs, PSOPSSs, HSOPSSs, CSOPSSs for scenario-2 of unseen operating cases 14-18 of NEPS

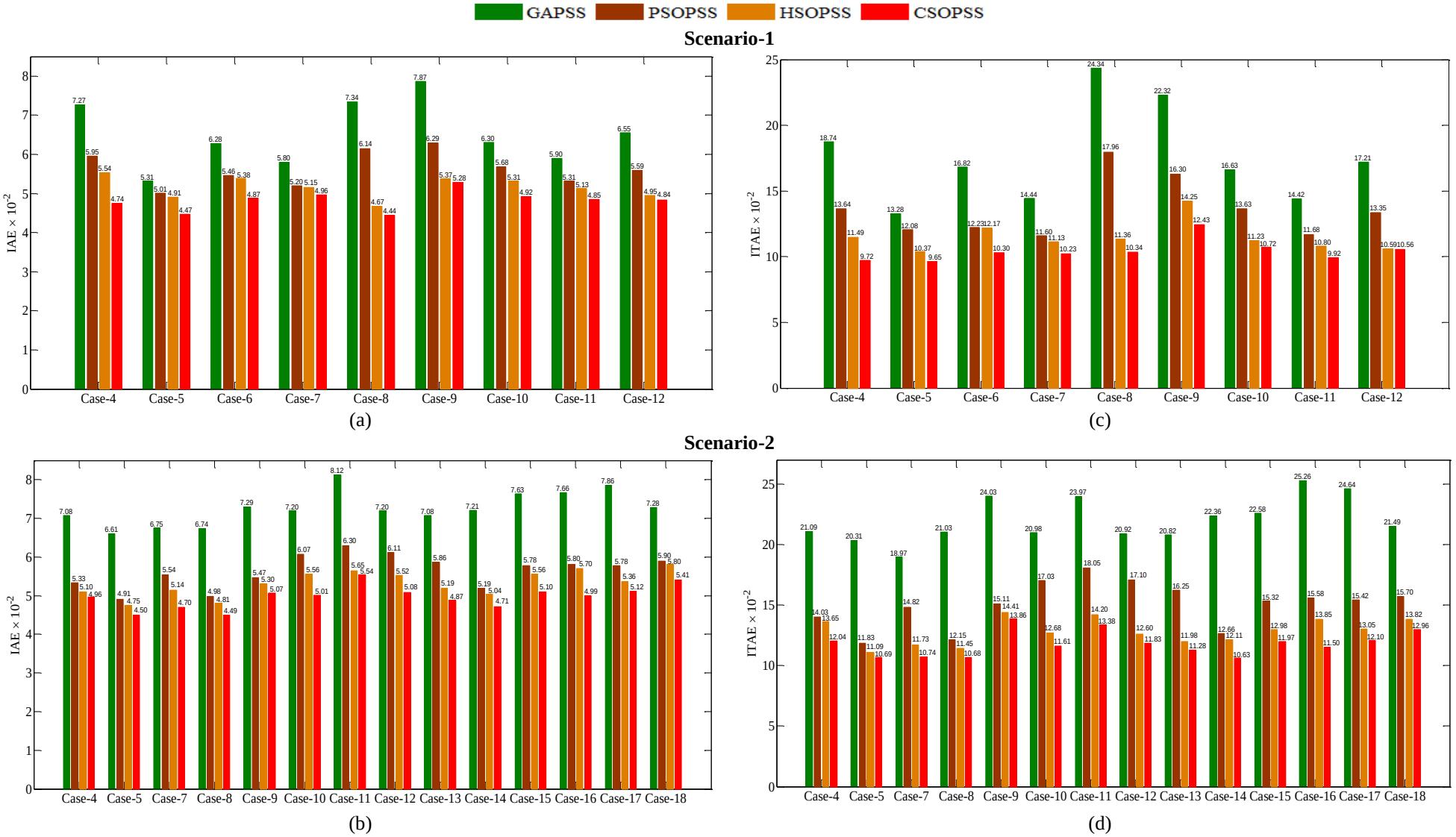

Fig. 7.20 Values of (a)-(b) *IAE* and (c)-(d) *ITAE*with GAPSSs, PSOPSSs, HSOPSSs, CSOPSSs for scenarios 1-2 of unseen operating cases 4-12 and 4-18 respectively

7.1.4 Example 4: Sixteen-Machine, Sixty-Eight Bus New England Extended Power System

A. Convergence and Eigenvalue Analysis of NEEPS

An eigenvalue-based multi-objective function J presented in (3.1) is minimized using GA, PSO, HSO and CSO by tuning the forty-two parameters of PSSs. Typical convergence of GAPSSs, PSOPSSs, HSOPSSs and CSOPSSs are shown in Fig. 7.21.

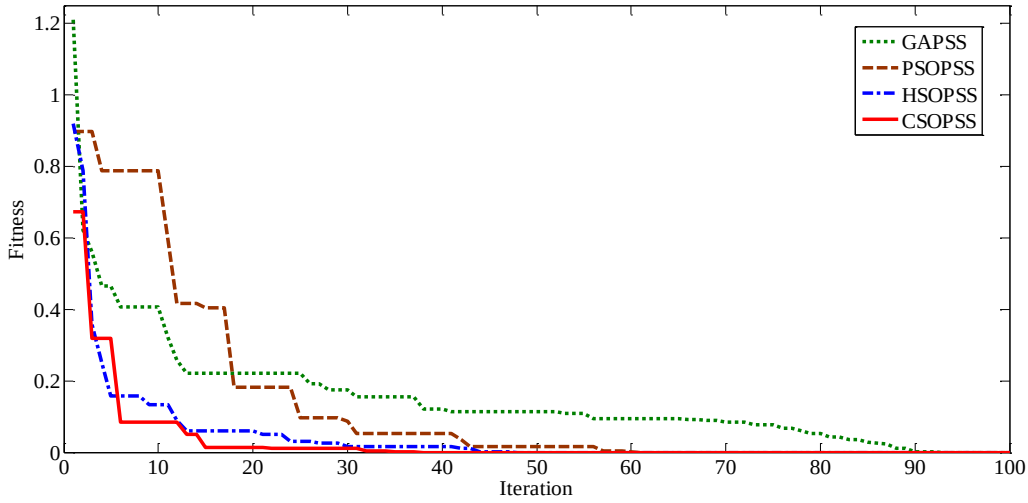

Fig. 7.21 Convergence characteristics of various optimization techniques

Figure shows that all algorithms are able to find the desired solution for which fitness function J is zero. The figure depicts that the CSO algorithm is able to find the best solution before any other optimization techniques. Performance of HSO is close to CSO whereas performance of GA and PSO is slower than HSO and CSO. The optimum designed parameters of GAPSSs, PSOPSSs, HSOPSSs and CSOPSSs for fourteen generators are shown in chapters 3 to 6 respectively.

The comparison of eigenvalues and their damping ratio with GAPSSs, PSOPSSs, HSOPSSs and CSOPSSs for operating cases 1-6 are shown in Table 7.7. The comparison of eigenvalue maps of NEEPS with GAPSSs, PSOPSSs, HSOPSSs and CSOPSSs for operating cases 1-3 and cases 4-6 are shown in Fig. 7.22 (a)-(c), (d)-(f), (g)-(i), (j)-(l) and 7.24 (a)-(c), (d)-(f), (g)-(i), (j)-(l)respectively.

Tables 7.7 and Figs. 7.22 & 7.23 show that the CSOPSSs shift the eigenvalues to a specified D-shape zone in the left half of the *s*-plane with superior damping factor and damping ratio as compared to GAPSSs, PSOPSSs and HSOPSSs for all operating cases.

Table 7.7: Eigenvalues and damping ratio comparison with designed PSSs for operating cases 1-6 of NEEPS

Cases	Case-1	Case-2	Case-3	Case-4	Case-5	Case-6
With GAPSSs	– 0.601 ± j 2.214, 0.262	– 0.643 ± j 1.138, 0.492	– 0.638 ± j 1.251, 0.454	– 0.633 ± j 1.181, 0.472	– 0.601 ± j 2.215, 0.262	– 0.623 ± j 2.186, 0.274
	– 0.609 ± j 1.265, 0.434	– 0.655 ± j 2.214, 0.283	– 0.645 ± j 2.218, 0.279	– 0.652 ± j 2.225, 0.281	– 0.608 ± j 1.269, 0.472	– 0.651 ± j 0.984, 0.552
	– 0.744 ± j 3.996, 0.183	– 0.750 ± j 3.987, 0.184	– 0.746 ± j 3.992, 0.183	– 0.743 ± j 2.436, 0.291	– 0.744 ± j 3.997, 0.183	– 0.688 ± j 2.391, 0.276
With PSOPSSs	– 0.755 ± j 2.426, 0.297	– 0.972 ± j 1.642, 0.509	– 0.945 ± j 1.616, 0.504	– 0.959 ± j 1.654, 0.501	– 0.676 ± j 2.806, 0.234	– 0.751 ± j 2.387, 0.300
	– 0.914 ± j 1.707, 0.472	– 0.698 ± j 2.776, 0.243	– 0.742 ± j 2.409, 0.294	– 0.683 ± j 2.266, 0.288	– 0.915 ± j 1.707, 0.473	– 0.688 ± j 2.799, 0.238
	– 0.847 ± j 1.341, 0.534	– 0.790 ± j 1.195, 0.551	– 0.883 ± j 1.350, 0.547	– 0.709 ± j 2.717, 0.252	– 0.755 ± j 2.423, 0.297	– 0.899 ± j 1.659, 0.476
With HSOPSSs	– 0.755 ± j 2.128, 0.334	– 0.955 ± j 1.717, 0.483	– 1.399 ± j 3.898, 0.337	– 1.290 ± j 1.383, 0.682	– 0.755 ± j 2.129, 0.334	– 0.773 ± j 2.085, 0.347
	– 0.959 ± j 1.772, 0.476	– 0.800 ± j 2.108, 0.354	– 0.797 ± j 2.113, 0.353	– 0.902 ± j 1.096, 0.635	– 0.962 ± j 1.777, 0.476	– 0.929 ± j 1.789, 0.460
	– 0.906 ± j 1.171, 0.611	– 0.901 ± j 1.069, 0.644	– 0.954 ± j 1.767, 0.475	– 0.799 ± j 2.117, 0.353	– 0.905 ± j 1.176, 0.609	– 0.913 ± j 0.856, 0.729
With CSOPSSs	– 0.924 ± j 1.340, 0.567	– 1.989 ± j 2.050, 0.696	– 2.506 ± j 5.797, 0.396	– 1.969 ± j 2.043, 0.693	– 0.926 ± j 1.343, 0.567	– 0.888 ± j 1.108, 0.625
	– 2.039 ± j 1.441, 0.816	– 0.920 ± j 2.058, 0.408	– 1.029 ± j 2.196, 0.424	– 0.929 ± j 1.149, 0.628	– 1.045 ± j 2.217, 0.426	– 1.059 ± j 2.208, 0.432
	– 1.943 ± j 2.030, 0.691	– 0.915 ± j 1.150, 0.622	– 1.045 ± j 7.097, 0.145	– 0.878 ± j 1.954, 0.409	– 1.940 ± j 2.031, 0.690	– 2.041 ± j 1.442, 0.816

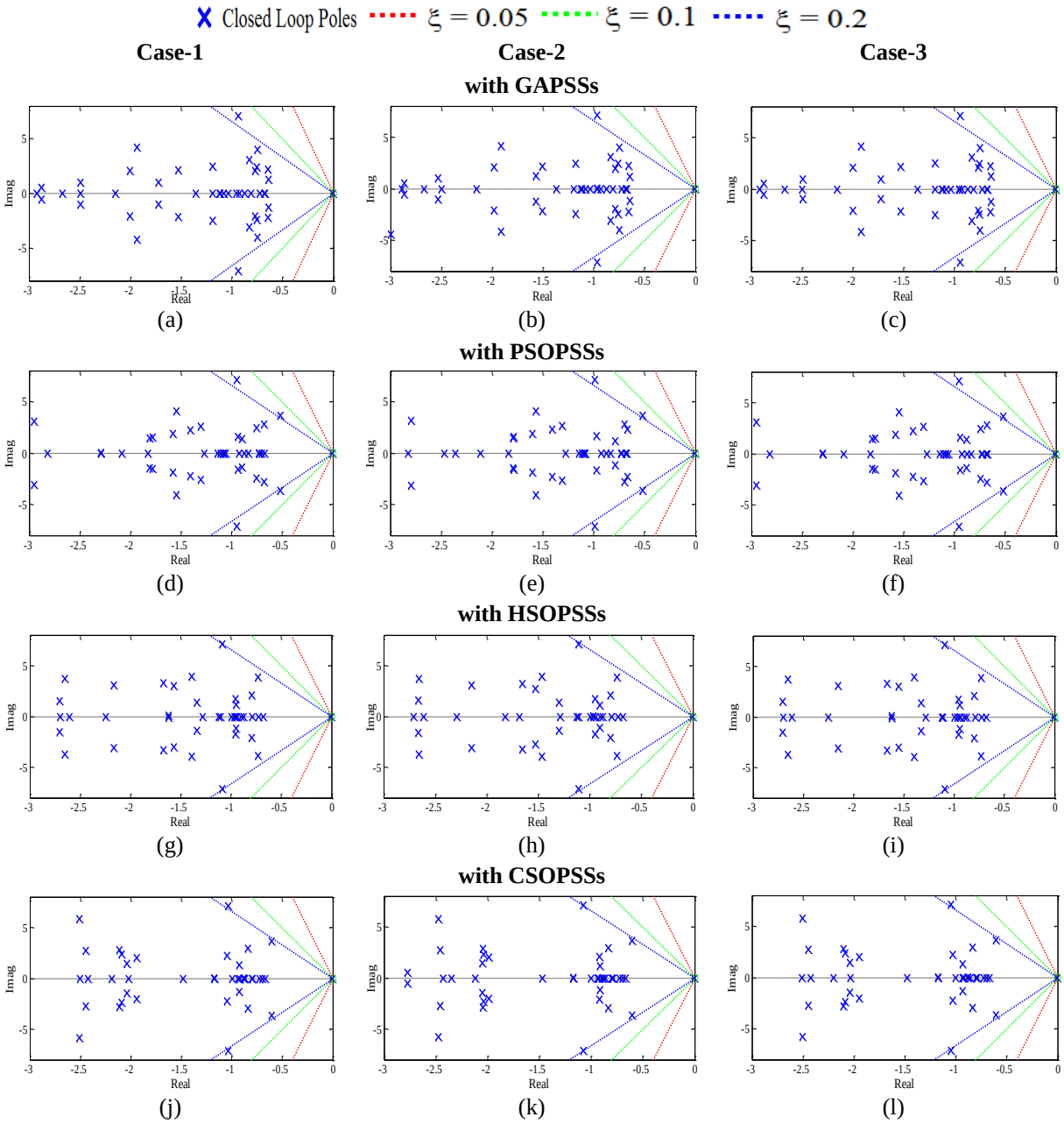

Fig. 7.22 Eigenvalue maps comparison (a)-(c) with GAPSSs (d)-(f) with PSOPSSs (g)-(i) with HSOPSSs (j)-(l) with CSOPSSs for operating cases 1-3 of NEEPS

Hence, designed CSOPSS controllers provide best stability and damping performance for NEEPS as compared to same obtained using other designed PSS controllers.

B. Time-Domain Simulation Results and Discussions of NEEPS

In order to examine the superior robustness performance of previously designed CSOPSS controllers in terms of simulation results, the comparison of severe speed deviations Δw_5 and Δw_9 with other designed PSS controllers are considered for scenarios 1-4 of Case-6 and shown in Fig. 7.24 (a)-(d) and (e)-(h) respectively.

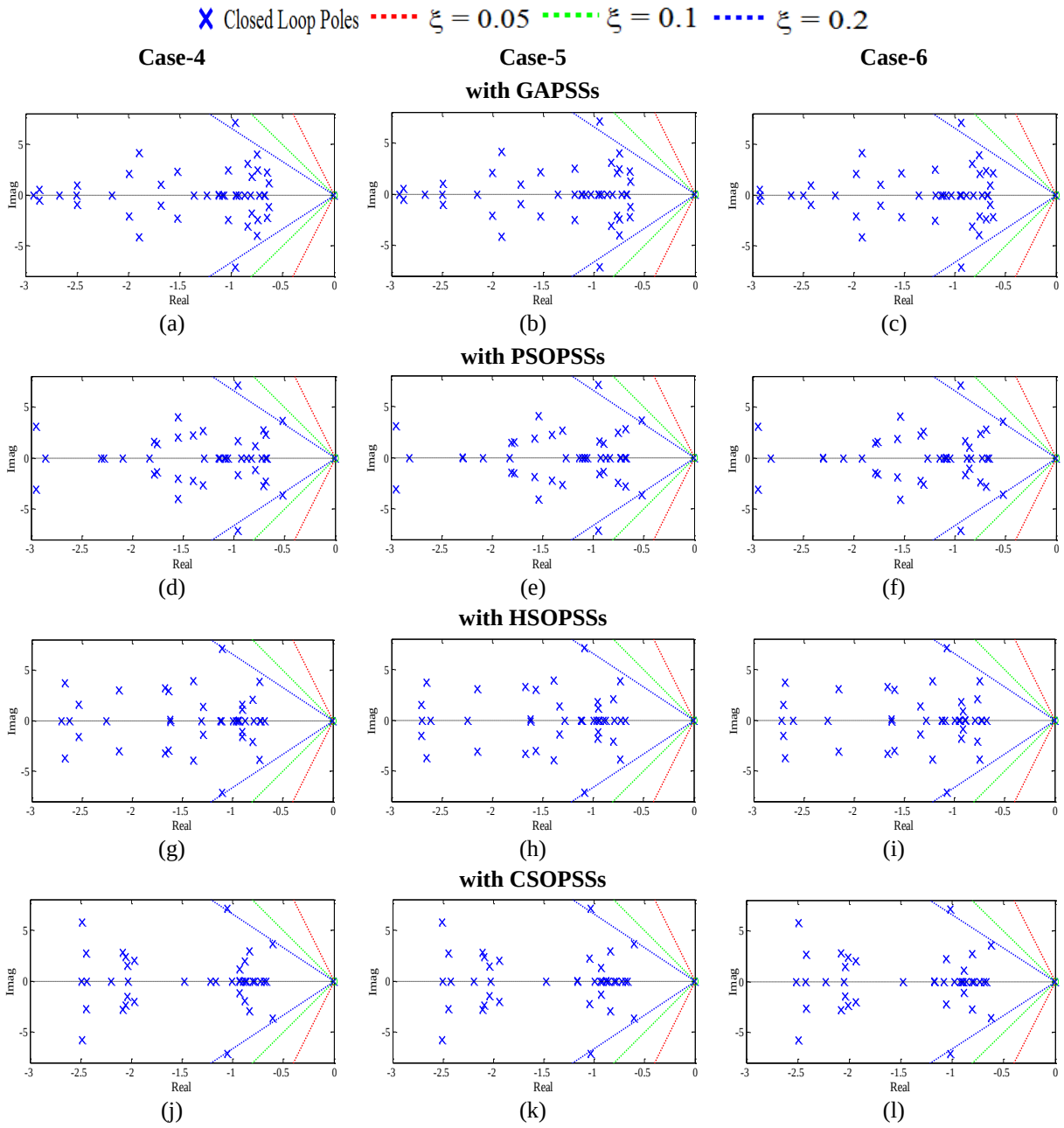

Fig. 7.23 Eigenvalue maps comparison (a)-(c) with GAPSSs (d)-(f) with PSOPSSs (g)-(i) with HSOPSSs (j)-(l) with CSOPSSs for operating cases 4-6 of NEEPS

From Fig. 7.24, it is clear that the system performance with CSOPSSs is much better than that of GAPSSs, PSOPSSs and HSOPSSs for all considered scenarios of Case-6 and oscillations are quickly damped out as compared to that of other designed PSSs. This illustrates the superiority and potential of CSO technique to obtain desired set of PSS parameters over GA, PSO and HSO techniques. The designed CSOPSSs are capable to damp out the LFO relatively faster than other designed PSS controllers over wide range of operating cases under severe scenarios of disturbances.

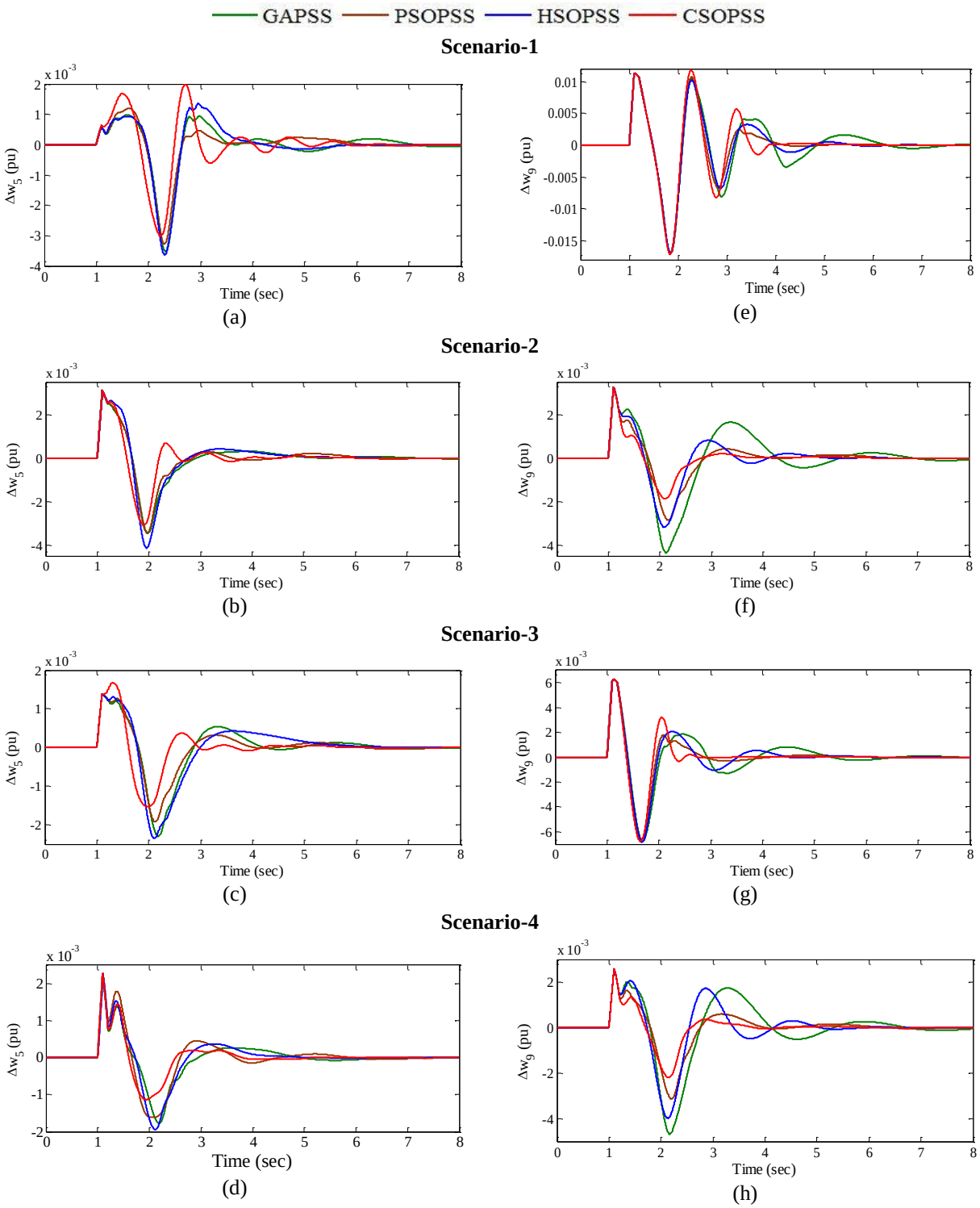

Fig. 7.24 (a)-(d) Δw_5 and (e)-(h) Δw_9 with GAPSSs, PSOPSSs, HSOPSSs, CSOPSSs for scenarios 1-4 of operating case-6 of NEEPS

C. Performance Indices Results and Discussions of NEEPS

The comparison of bar charts of *IAE* and *ITAE* with designed PSSs for Scenario-1 of operating cases 1-6 are shown in Fig. 7.25 (a), (c) whereas forScenario-4 of same cases are shown in Fig. 7.25 (b), (d) respectively. The figures reveal that both indices values with CSOPSSs are minimum for scenarios 1 and 4 of operating case 1-6 as compared to the same obtained by GAPSSs, PSOPSSs and HSOPSSs to settle LFO.

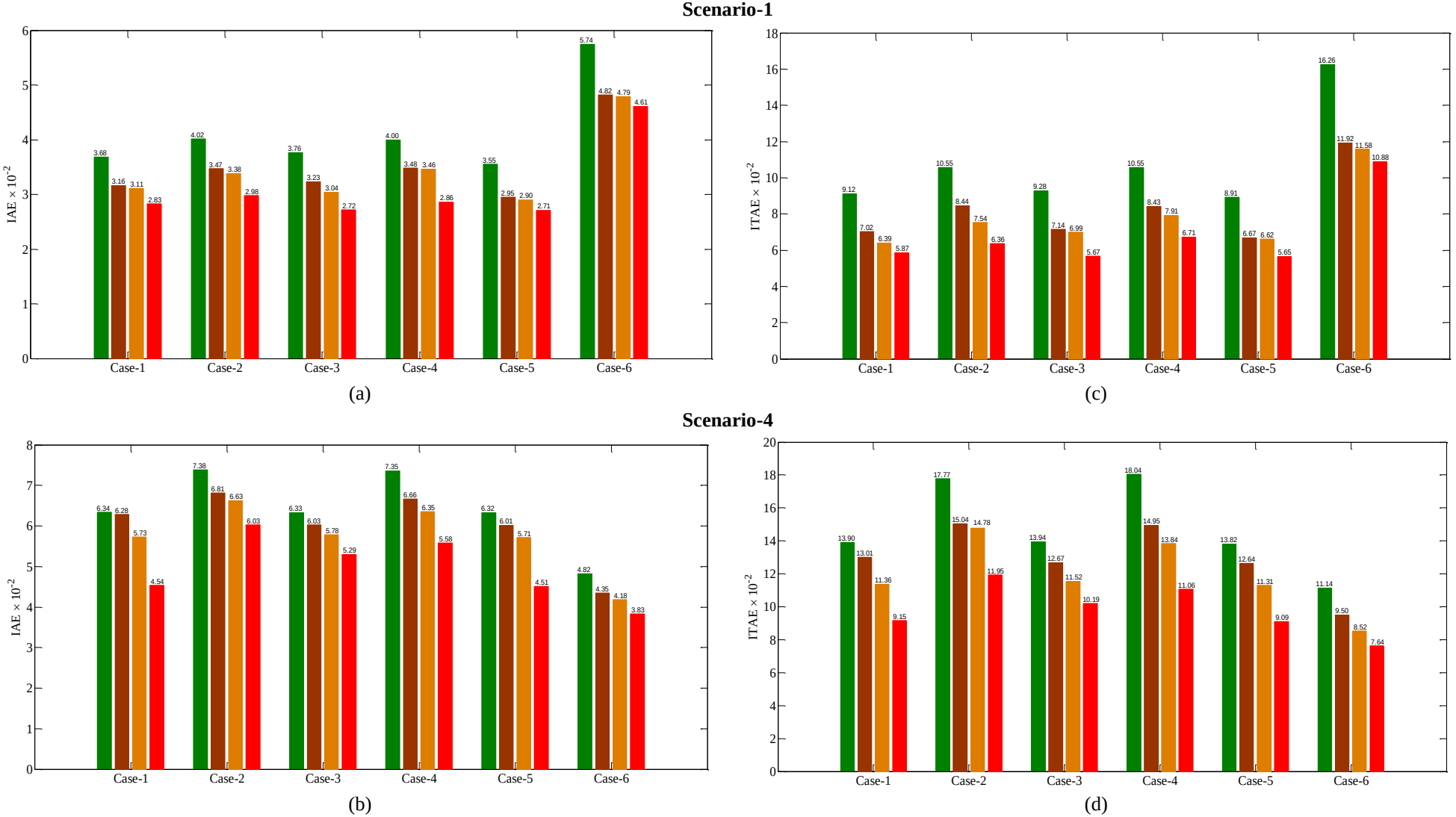

Fig. 7.25 Values of (a), (b) *IAE* and (b), (d) *ITAE* with GAPSSs, PSOPSSs, HSOPSSs, CSOPSSs for scenarios 1 and 4 of operating cases 1-6 of NEEPS

D. Robustness Test of Designed PSS Controllers of NEEPS

The comparison of eigenvalues and damping ratio for nine unseen operating cases 7-15 of NEEPS with all designed PSS controllers are illustrated in Table 7.8.

Table 7.8: Eigenvalues and damping ratio comparison with designed PSSs for unseen operating cases 7-15 of NEEPS

Cases	With GAPSSs	With PSOPSSs	With HSOPSSs	With CSOPSSs
Case-7	– 0.756 ± j 2.440, 0.295	– 0.765 ± j 2.238, 0.323	– 0.790 ± j 2.113, 0.350	– 0.958 ± j 1.809, 0.468
	– 0.705 ± j 4.039, 0.171	– 0.821 ± j 4.178, 0.192	– 0.689 ± j 3.942, 0.172	– 0.795 ± j 2.985, 0.257
Case-8	– 0.949 ± j 7.084, 0.132	– 0.781 ± j 7.420, 0.104	– 1.095 ± j 7.090, 0.152	– 1.048 ± j 7.098, 0.146
	– 0.754 ± j 3.966, 0.186	– 0.874 ± j 4.129, 0.207	– 0.744 ± j 3.844, 0.190	– 0.626 ± j 3.604, 0.171
	– 0.829 ± j 3.083, 0.259	– 0.979 ± j 3.429, 0.274	– 1.403 ± j 3.909, 0.337	– 1.777 ± j 3.024, 0.506
	– 0.584 ± j 2.184, 0.258	– 0.719 ± j 2.173, 0.314	– 0.737 ± j 2.728, 0.260	– 0.732 ± j 2.788, 0.254
Case-9	– 0.956 ± j 7.077, 0.133	– 0.784 ± j 7.417, 0.105	– 1.103 ± j 7.084, 0.153	– 1.057 ± j 7.093, 0.147
	– 0.754 ± j 7.084, 0.186	– 0.875 ± j 4.129, 0.207	– 0.744 ± j 3.843, 0.190	– 0.626 ± j 3.603, 0.171
	– 0.831 ± j 3.084, 0.260	– 0.979 ± j 3.397, 0.276	– 1.405 ± j 3.913, 0.338	– 1.773 ± j 3.027, 0.505
	– 0.750 ± j 2.434, 0.294	– 0.514 ± j 2.631, 0.192	– 0.735 ± j 2.724, 0.260	– 0.732 ± j 2.786, 0.254
	– 0.584 ± j 2.183, 0.258	– 0.720 ± j 2.172, 0.314	– 0.819 ± j 1.770, 0.420	– 0.913 ± j 1.236, 0.594
Case-10	– 0.953 ± j 7.078, 0.133	– 0.783 ± j 7.418, 0.105	– 1.104 ± j 7.084, 0.154	– 1.054 ± j 7.091, 0.147
	– 0.751 ± j 3.988, 0.185	– 0.867 ± j 4.146, 0.204	– 0.737 ± j 3.865, 0.187	– 0.620 ± j 3.631, 0.168
	– 0.832 ± j 3.084, 0.260	– 0.987 ± j 3.462, 0.274	– 1.403 ± j 3.913, 0.337	– 1.010 ± j 2.124, 0.429
	– 0.750 ± j 2.433, 0.294	– 0.723 ± j 2.184, 0.314	– 0.812 ± j 2.828, 0.276	– 0.738 ± j 2.808, 0.254
Case 11	– 0.953 ± j 7.048, 0.134	– 0.762 ± j 7.419, 0.102	– 1.118 ± j 7.055, 0.156	– 1.074 ± j 7.072, 0.150
	– 0.810 ± j 3.862, 0.205	– 0.929 ± j 4.052, 0.223	– 0.811 ± j 3.7133, 0.213	– 0.683 ± j 3.418, 0.196
Case-12	– 0.958 ± j 7.073, 0.134	– 0.785 ± j 7.417, 0.105	– 1.114 ± j 7.064, 0.155	– 1.049 ± j 7.086, 0.146
	– 0.748 ± j 3.990, 0.184	– 0.865 ± j 4.151, 0.204	– 0.735 ± j 3.877, 0.186	– 0.614 ± j 3.645, 0.166
	– 0.830 ± j 3.076, 0.260	– 1.005 ± j 3.414, 0.282	– 0.997 ± j 3.750, 0.256	– 0.742 ± j 2.839, 0.252
	– 0.636 ± j 2.385, 0.257	– 0.729 ± j 2.203, 0.314	– 0.750 ± j 2.113, 0.334	– 1.001 ± j 2.119, 0.427

Cont.

Cases	With GAPSSs	With PSOPSSs	With HSOPSSs	With CSOPSSs
Case-13	– 0.971 ± j 7.038, 0.133	– 0.787 ± j 7.409, 0.105	– 1.155 ± j 7.022, 0.162	– 1.070 ± j 7.036, 0.150
	– 0.745 ± j 3.995, 0.183	– 0.864 ± j 4.153, 0.203	– 0.732 ± j 3.876, 0.185	– 0.609 ± j 3.652, 0.164
	– 0.516 ± j 2.229, 0.225	– 0.729 ± j 2.220, 0.312	– 0.754 ± j 2.126, 0.334	– 1.034 ± j 2.208, 0.424
Case-14	– 0.596 ± j 2.196, 0.261	– 0.659 ± j 2.778, 0.231	– 0.603 ± j 3.076, 0.192	– 0.614 ± j 3.651, 0.166
	– 0.532 ± j 1.991, 0.258	– 0.726 ± j 2.208, 0.312	– 0.757 ± j 2.112, 0.337	– 0.741 ± j 2.856, 0.251
Case-15	– 0.488 ± j 2.018, 0.235	– 0.671 ± j 2.886, 0.226	– 0.550 ± j 2.986, 0.181	– 0.634 ± j 2.354, 0.260
	– 0.820 ± j 3.840, 0.208	– 0.939 ± j 4.037, 0.226	– 0.820 ± j 3.683, 0.217	– 0.702 ± j 3.383, 0.203
	– 1.045 ± j 6.920, 0.149	– 0.783 ± j 7.385, 0.105	– 1.280 ± j 6.932, 0.181	– 1.207 ± j 6.932, 0.171

The table shows that the CSOPSSs shift the eigenvalues to a specified D-shape zone in the left half of the *s*-plane with better damping factor and damping ratio as compared to GAPSSs, PSOPSSs and HSOPSSs for all unseen cases. Hence, the designed CSOPSSs are robust as it works with superior damping performance for unseen operating cases.

In order to check the superior robustness performance of the designed CSOPSS controllers in terms of simulations results, the comparison of severe speed deviations $\Delta w_3$and Δw_9 with other designed PSS controllers for Scenario-1 of unseen cases 7-11 are considered and shown in Fig. 7.26 (a)-(e) and (f)-(j) respectively. Moreover, to check the superior robustness performance of designed CSOPSSs on other unseen cases, the comparison of severe speed deviations Δw_8 and Δw_9 with other designed PSS controllers for Scenario-2 of unseen cases 12-15 are considered and shown in Fig. 7.27 (a)-(d) and (e)-(h) respectively.

From Figs. 7.26 and 7.27, it is clear that the system performance with CSOPSSs is much better than that of GAPSSs, PSOPSSs and HSOPSSs for all considered scenarios of unseen operating cases 7-11 & 12-15 and oscillations are quickly damped out as compared to that of other designed PSSs. This illustrates the superiority and potential of CSO technique to obtain desired set of PSS parameters for NEEPS than GA, PSO and HSO techniques. Hence, the designed CSOPSSs are competent to damp out the LFO rapidly than other designed PSS controllers for wide range of unseen operating cases 7-15 under severe scenarios of disturbances.

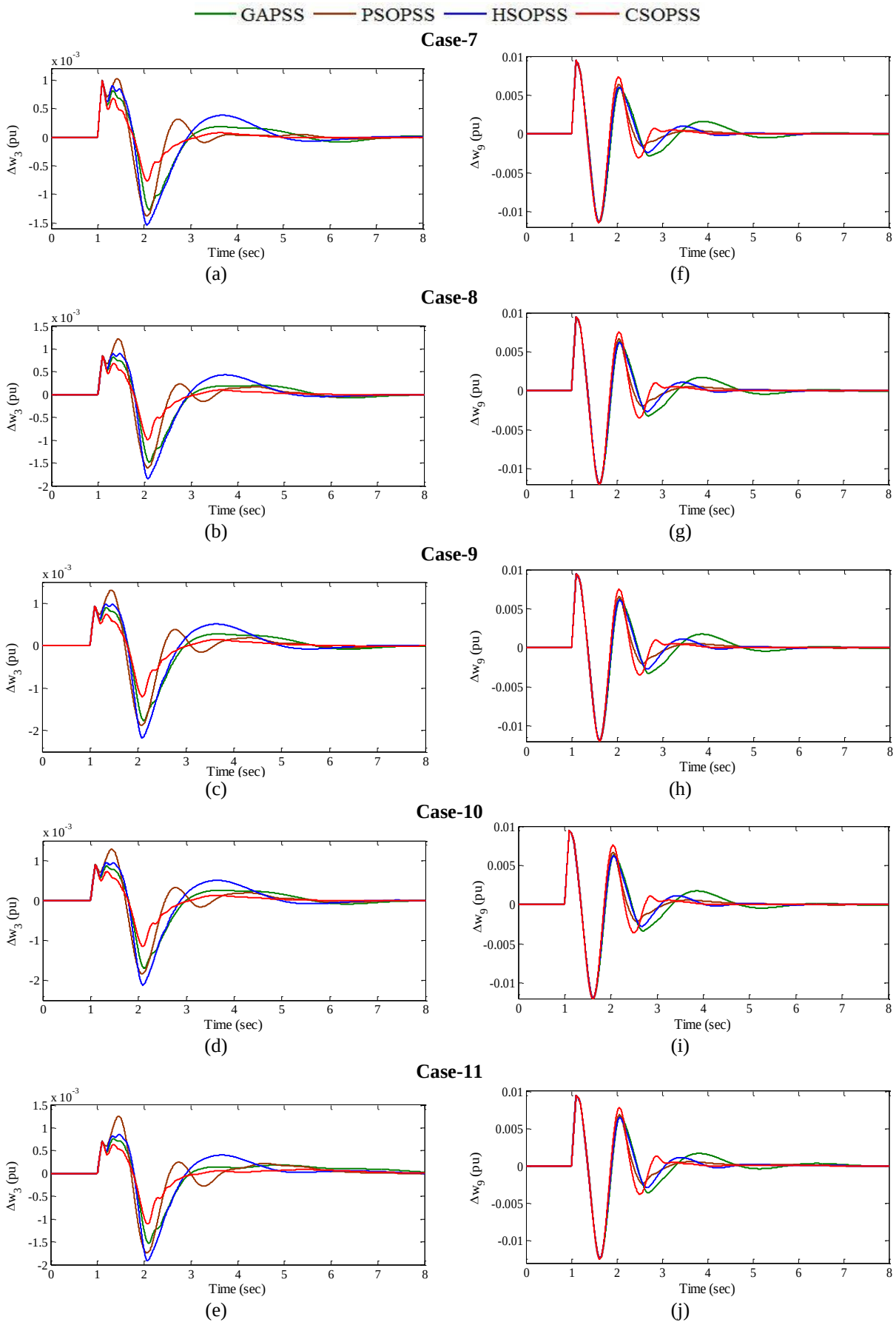

Fig. 7.26 (a)-(e) Δw_3 and (f)-(j) Δw_9 with GAPSSs, PSOPSSs, HSOPSSs, CSOPSSs for scenario-1 of unseen operating case 7-11 of NEEPS

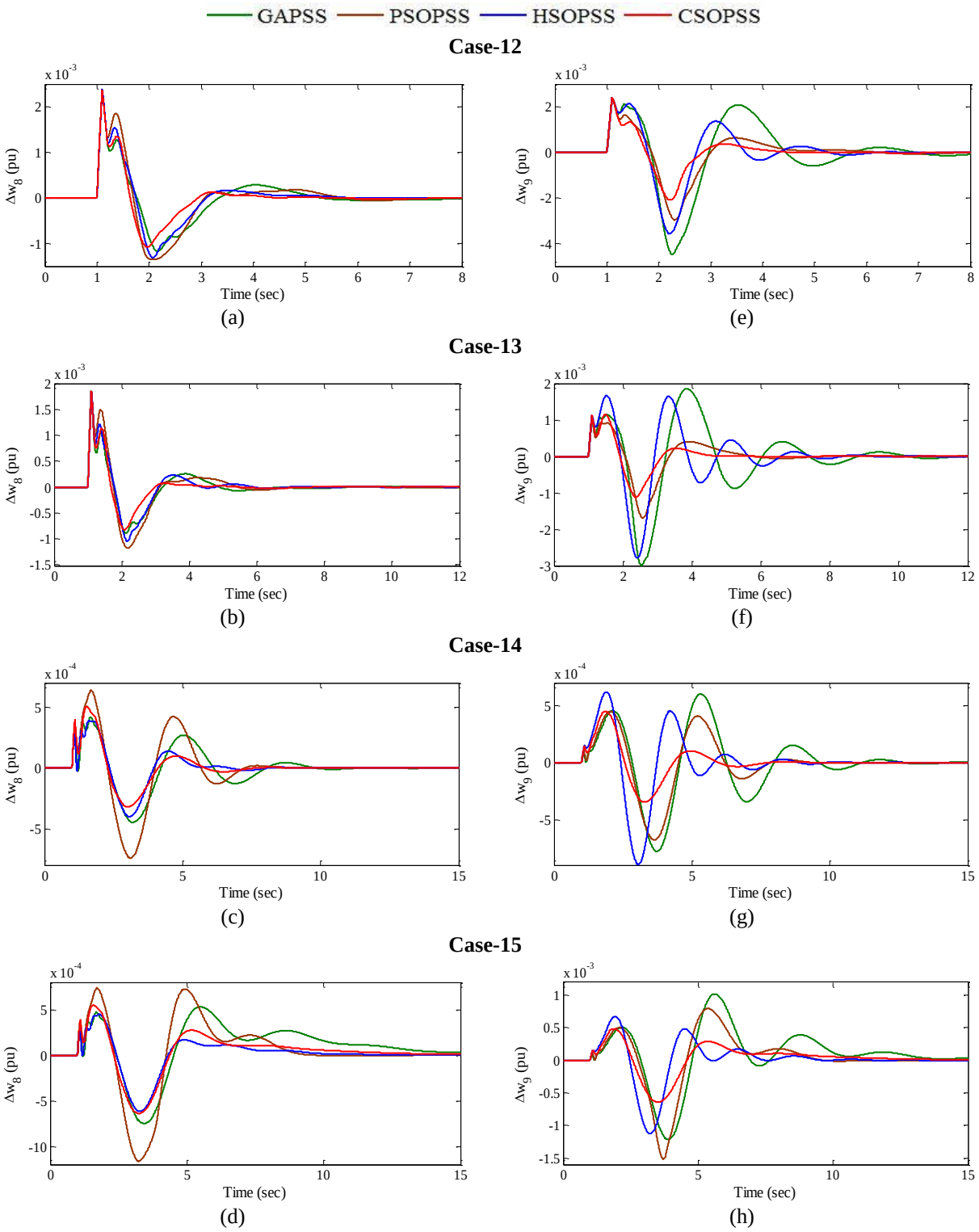

Fig. 7.27 (a)-(d) Δw_8 and (e)-(h) Δw_9 with GAPSSs, PSOPSSs, HSOPSSs, CSOPSSs for scenario-2 of unseen operating cases 12-15 of NEEPS

In addition to time-domain simulation results, the superior robustness and effectiveness of earlier designed CSOPSS controllers is observed by comparing bar charts of *IAE* and *ITAE* with other designed PSSs for Scenario-1 of unseen cases 7-11 and 7-15 are shown in Fig. 7.28 (a), (c) and (b), (d) respectively.

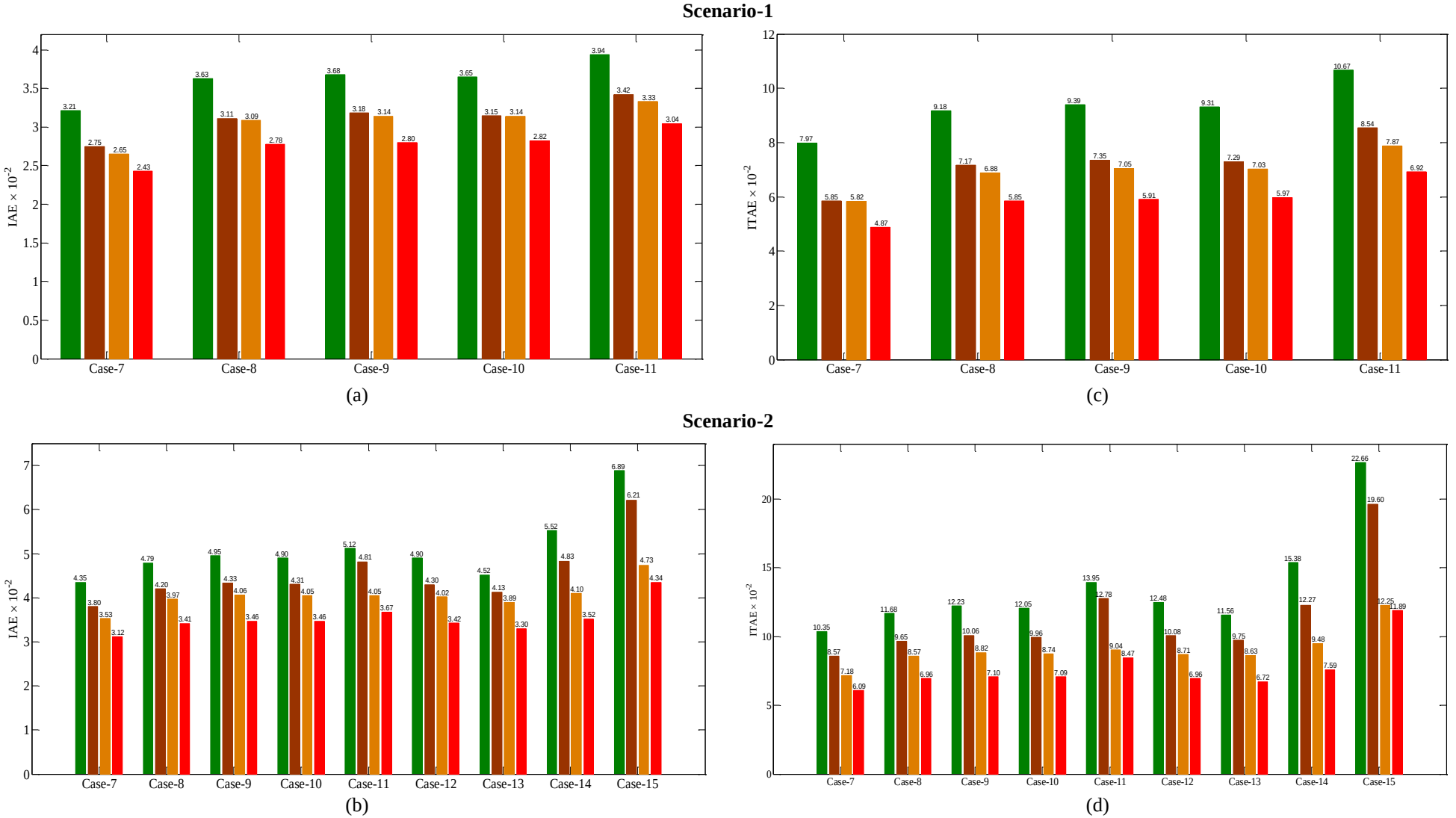

Fig. 7.28 Values of (a)-(b) *IAE* and (c)-(d) *ITAE* with GAPSSs, PSOPSSs, HSOPSSs, CSOPSSs for scenarios 1-2 of unseen operating cases 7-11 and 7-15 of NEEPS

Following are the salient conclusions drawn from the thesis work:

1. The newly explored HSO and CSO are capable of effectively designing PSS parameters for enhancement of damping performance and SSS of MMPS.
2. All the investigated meta-heuristic techniques namely, GA, PSO, HSO and CSO are capable of designing PSS parameters and are capable of shifting the eigenvalues of MMPS to a specified D-shape zone in the left half of the *s*-plane. The effectiveness of all designed PSS controllers has been evaluated by eigenvalue analysis, eigenvalue maps, time-domain simulation results and performance indices *IAE* and *ITAE*.All the design PSSs works satisfactorily under most of the operating conditions except certain unseen operating conditions.
3. The convergence characteristics, eigenvalue analysis, time-domain simulation results and performance indices results of designed PSSs of four different standard MMPS depict the superiority of CSOPSSs over GAPSSs, PSOPSSs and HSOPSSs. The performance of HSO in most of the cases is close to CSO whereas performance of GA and PSO is more or less similar but worse than CSO and HSO.
4. It is also observed that only HSOPSSs and CSOPSSs satisfy the selected criterion for the value of desired damping factor and damping ratio for PSS design in almost all cases.
5. The robustness of GAPSSs is minimum. However, the designed CSOPSSs are most robust as it works with superior damping performance even for unseen operating conditions as compared to that of other designed PSS controllers.

7.2 Major Contributions

The major contributions of the thesis may be summarized as follows:

1. To re-investigate the applicability of GA and PSO for designing PSS parameters under wide range of operating conditions and to evaluate their performance under wide range of unseen operating conditions also on different standard IEEE test systems
2. To explore the applicability of recently developed CSO algorithm for designing PSS parameters and thoroughly investigate the performance of developed CSOPSSs on four different MMPSs under wide range of operating conditions.
3. To explore the applicability of recently developed HSO algorithm for designing PSS parameters and thoroughly investigate the performance of developed HSOPSSs on four different MMPSs under wide range of operating conditions.
4. To carry out a detailed comparative analysis of the performances of GAPSSs, PSOPSSs, HSOPSSs and CSOPSSs on four standard IEEE MMPS:3-machine, 9-bus WSCC power

system, TAFM power system, 10-machine, 39-bus NEPS and 16-machine, 68-bus NEEPS.

7.3 Future Scope

This thesis investigated the applicability and performance of different meta-heuristic algorithm based PSS on different MMPS for enhancing small signal damping of power system oscillations. The following are the possible future extensions of present research work:

1 In this work, the parameter optimization of speed based lead-lag PSSs have been investigated using four different meta-heuristic optimization techniques for damping out power system LFO. This work can be extended to optimize the parameters of other PSSs design like PSS2B, PSS4B, etc.

2 The new optimization techniques such as, Collective Decision Optimization (CDO) algorithm, Grey Wolf Optimization (GWO), Differential Evolution (DE), Whale Optimization Algorithm (WOA) and Crow Search Algorithm (CSA), can also be explored for designing PSS parameters of SMIB system and MMPS under wide range of operating conditions.

3 In this work, participation factor method is used to identify the optimum locations of installing PSS. This work can be extended to consider a new technique such as Optimum PSS Location Index (OPLX) for selection of optimum site of a PSS to mitigate SSS problem in a MMPS.

4 In present work, CSOPSS designed controllers are compared with other designed GAPSS, PSOPSS and HAOPSS controllers for wide range of operating conditions of MMPS. This work can be extended to carry out a comparative analysis of mentioned techniques with PID and Thyristor Controlled Dynamic Brake (TCDB) through number of K-constants for wide range of operating conditions of SMIB system.

5 In this work, four standard IEEE test systems are used for SSS analysis. This work can be extended to investigate the voltage stability enhancement by PSS.

6 The present research work can also be extended to develop a coordinated design of PSS with FACTS damping controllers design using WAMS, hybrid AI techniques, for enhancement of damping performance of MMPS.

7 In the present work, optimal solutions for designing PSS parameters of MMPS have been investigated wherein it is assumed that all generators are synchronous machine. The future power system will have a large number of renewable energy sources which do not employ synchronous machine. Most of these renewable energy sources are non-inertial sources of power and it is not established how these non-inertial sources behave when there is the SSS

problem. Therefore the present work may be extended to investigate the behaviour of PSS in MMPS having fair amount non-inertial sources of energy.

8 In power system, FACTS controllers have gained great research interest due to their versatile capability in mitigating power system stability issues. FACTS controllers have been extensively used in enhancing power system stability and damping performance of the LFO. The present research work can be extended to tune FACTS based damping controllers such as SVC, TCSC, STATCOM etc. for enhancing the SSS of power systems

9 The present research work can also be extended to develop a coordinated design of PSS with different series and shunt FACTS damping controllers for enhancing the SSS of power systems.

PUBLICATIONS

Following papers have been published out of this thesis work.

International Journal Papers

1. Dhanraj Chitara, K. R. Niazi, Anil Swarnkar, Nikhil Gupta "Cuckoo Search Optimization Algorithm for Designing of Multi-machine Power System Stabilizer," is accepted in *IEEE Transactions on Industry Applications (TIA),* 2018.
2. Dhanraj Chitara, K. R. Niazi, Anil Swarnkar, Nikhil Gupta, R. C. Bansal "Optimal Tuning of Multi-machine Power System Stabilizer using Cuckoo Search Algorithm," *IFAC-papers on Line, Elsevier,* vol. 48, no. 30, pages 143-148, 2015.

International Conferences

1. Dhanraj Chitara, K. R. Niazi, Anil Swarnkar, Nikhil Gupta "Multi-machine Power System Stabilizer tuning using Harmony Search Algorithm," is presented in *IEEE International Conference on Electrical Power Energy systems (ICEPES-2016),* 14^{th}-16^{th} December 2016, MNAIT Bhopal, India.
2. Dhanraj Chitara, K. R. Niazi, Anil Swarnkar, Nikhil Gupta "Small Signal Stability Enhancement of Multimachine Power System Stabilizer using Cuckoo Search Algorithm," is presented in *7^{th} IEEE Power India International Conference (PIICON-2016),* 25^{th}-27^{th} November 2016, Government Engineering College Bikaner, Rajasthan, India.
3. Dhanraj Chitara, K. R. Niazi, Anil Swarnkar, Nikhil Gupta "Cuckoo Search Optimization Algorithm for Designing of Multi-machine Power System Stabilizer," presented in *IEEE International Conference on Power Electronics, Intelligent Control and Energy systems (ICPEICS 2016),* 4^{th}-6^{th} July 2016, Delhi Technical University (DTU), Delhi, India.
4. Dhanraj Chitara, K. R. Niazi, Anil Swarnkar, Nikhil Gupta "Robust Tuning of Multi-machine Power System Stabilizer via Cuckoo Search Optimization Algorithm," presented in *6^{th} IEEE International Conference on Power Systems (ICPS 2016),* 4^{th} -6^{th} March 2016, IIT Delhi, India.

National Conference

1. Dhanraj Chitara, K. R. Niazi, Anil Swarnkar, Nikhil Gupta "Small-Signal Stability Enhancement of Multi-machine Power System using Bio-inspired Algorithms," is presented in *National Power Systems Conference (NPSC-2016),* 19^{th}-21^{st} December 2016, IIT Bhubaneswar, Odisha, India.

REFERENCES

[1] P. Kundur, *Power System Stability and Control*, New York: Mc-Graw-Hill, 1994.

[2] P. M. Anderson and A. A. Fouad, *Power System Control and Stability*, Piscataway, NJ: *IEEE Press*, 2003.

[3] P. Kundur, J. Paserba, V. Ajjarapu, G. Andersson, A. Bose, C. Canizares, N. Hatziargyriou, D. Hill, A. Stankovic, C. Taylor, T. Van Cutsem, and V. Vittal, "Definition and classification of power system stability," *IEEE Transactions on Power Syst*em, vol. 19, no. 2, pp. 1387–1401, May 2004.

[4] F. P. de Mello and C. Concordia, "Concepts of synchronous machine stability as affected by excitation control," *IEEE Transactions on Power Apparatus and Systems*, vol. 88, pp. 316-329, April 1969.

[5] K. E. Bollinger, A. Laha, R. Hamilton, and T. Harras, "PSS design using root locus methods," *IEEE Transactions on Power Apparatus and Systems*, vol. PAS-94, no. 5, pp. 1484–1488, Oct. 1975.

[6] W. K. Marshall and W. J. Smolinski, "Dynamic stability determination by synchronizing and damping torque analysis," *IEEE Transactions on Power Apparatus and Systems*, vol. PAS-92, no. 4, pp. 1239-1246, July 1973.

[7] K. E. Bollinger, R. Winsor, and A. Campbell, "Frequency response methods for tuning stabilizers to damp out tie-line power oscillations: theory and field-test results," *IEEE Transactions on Power Apparatus and Systems*, vol. PAS-98, no. 5, pp. 1509-1515, September/October 1979.

[8] F. P. de Mello, L. N. Hannet, D. W. Parkinson, and J. S. Czuba, "A power system stabilizer design using digital control," *IEEE Transactions on Power Apparatus and Systems*, vol. PAS-101, no. 8, pp.2860-2868, August 1982.

[9] A. Ghandakly and P. Kronegger, "Digital controller designs method for synchronous generator excitation and stabilizer systems Part -I: methodology and computer simulation," *IEEE Transactions on Power Syst*em, vol. PWRS-2, no. 3, pp.633-637, August 1987.

[10] A. Ghandakly and P. Kronegger, "Digital controller designs method for synchronous generator excitation and stabilizer systems Part-II: hardware/software design and implementation results," *IEEE Transactions on Power Syst*em, vol. PWRS-2, no. 3, pp.638-643, August 1987.

[11] A. K. Laha and K. E. Bollinger, "Power-stabilizer design using pole-placement techniques on approximate power-system models," *Electrical Engineers, Proceedings of the Institution of*, vol. 122, no. 9, pp. 903-907, September 1975.

[12] K. R. Padiyar, et al., "Design of stabilizers by pole assignment with output feedback," *Electrical Power and Energy Systems*, vol. 2, pp. 140-146, July 1980.

[13] V. Arcidiacono, E. Ferrari, R. Marconato, J. Dosghali and D. Crandez, "Evaluation and improvement of electromechanical oscillation damping by means of eigenvalue-eigenvector analysis practical results in the Central Peru Power System," *IEEE Transactions on Power Apparatus and Systems*, vol. PAS-99, no. 1, pp. 769-778, March/April 1980.

[14] Y. Obata, S. Takeda, and H. Suzuki, "An efficient eigenvalue estimation technique for multi-machine power system dynamic stability analysis," *IEEE Transactions on Power Apparatus and Systems*, vol. PAS-100, pp. 259-263, 1981.

[15] F. W. Keay and W. H. South, "Design of a power system stabilizer sensing frequency deviation," *IEEE Transactions on Power Apparatus and Systems*, vol. PAS-90, no. 2, pp. 707–713, Mar./Apr. 1971.

[16] D. Lee, R. Beaulieu and J. Service, "A power system stabilizer using speed and electrical power inputs-design and field experience," *IEEE Transactions on Power Apparatus and Systems*, vol. PAS-100, no. 9, pp. 4151–4157, Sep. 1981.

[17] E. V. Larsen and D. A. Swann, "Applying power system stabilizers, part I: general concepts," *IEEE Transactions on Power Apparatus and Systems*, vol. PAS-100, no. 6, pp. 3017–3024, Jun. 1981.

[18] E. V. Larsen and D. A. Swann, "Applying power system stabilizers, part II: performance objectives and tuning concepts," *IEEE Transactions on Power Apparatus and Systems*, vol. PAS-100, no. 6, pp. 3025–3033, Jun. 1981.

[19] E. V. Larsen and D. A. Swann, "Applying power system stabilizers, part III: practical considerations," *IEEE Transactions on Power Apparatus and Systems*, vol. PAS-100, no. 6, pp. 3034–3046, Jun. 1981.

[20] F. P. deMello, P. J. Nolan, T. F. Loaskowoski, and J. M. Undrill, "Coordinate application of stabilizers in multi-machine power system," *IEEE Transactions on Power Apparatus and Systems*, vol. PAS-114, no. 3, pp. 892–901, May/Jun. 1980.

[21] R. J. Fleming, M. A. Mohan, and K. Parvatisam, "Selection of parameters of stabilizers in multi-machine power systems," *IEEE Transactions on Power Apparatus and Systems*, vol. PAS-100, no. 5, pp. 2329–2333, May 1981.

[22] S. Lefebvre, "Tuning of stabilizers in multi-machine power systems," *IEEE Transactions on Power Apparatus and Systems*, vol. PAS-102, no. 2, pp. 290–299, Feb. 1983.

[23] H. B. Gooi, E. F. Hill, M. A. Mobarak, D. H. Throne and T. H. Lee, "Coordinated multi-machine stabilizer settings without eigenvalue drift," *IEEE Transactions on Power Apparatus and Systems*, vol. PAS-100, no. 8, pp. 3879–3887, Aug. 1981.

[24] S. Abe and A. Doi, "A new power system stabilizer synthesis in multi-machine power systems," *IEEE Transactions on Power Apparatus and Systems*, vol. PAS-102, no. 12, pp. 3910–3918, Dec. 1983.

[25] A. Doi and S. Abe, "Coordinated synthesis of power system stabilizers in multi-machine power systems," *IEEE Transactions on Power Apparatus and Systems*, vol. PAS-103, no. 6, pp. 1473–1479, Jun. 1984.

[26] S. Sivakumar, A. M. Sharaf, and H. G. Hamed, "Coordinated tuning of power system stabilizers in multi-machine power systems," *International Journal of Electric Power Systems Research*, vol. 8, pp. 275-284, 1985.

[27] C. M. Lim and S. Elangovan, "Design of stabilizers in multi-machine power systems," *IEE Proceedings*, vol. 132, no. 3, pp. 146–153, 1985.

[28] C. L. Chen and Y. Y. Hsu, "Coordinated synthesis of multi-machine power system stabilizer using an efficient Decentralized Modal Control (DMC) algorithm," *IEEE Transactions on Power Syst*em, vol. PS–2, no. 3, pp. 543–551, Aug. 1987.

[29] Y. Y. Hsu and C. Y. Hsu, "Design of a proportional-integral power system stabilizer," *IEEE Transactions Power Systems*, vol. PWRS-1, no. 2, pp. 46-53, May 1986.

[30] Y. Y. Hsu and K. L. Liou, "Design of self-tuning PID power system stabilizers for synchronous generators," *IEEE Transaction on Energy Conversion*, vol. 2, no. 3, pp. 343-348, Sept. 1987.

[31] C. J. Wu and Y. Y. Hsu, "Design of self-tuning PID power system stabilizer for multi-machine power systems," *IEEE Transactions on Power Syst*em, vol. 3, no. 3, pp. 1059-1064, Aug. 1988.

[32] S. J. Cheng, O. P. MaliK and G. S. Hope, "Damping of multi-modal oscillations in power systems using a dual-rate adaptive stabilizer," *IEEE Transactions on Power Syst*em, vol. PWRS-3, no. 1, pp.101-108, February 1988.

[33] Y. Y. Hsu and C. L. Chen, "Identification of optimum location for stabilizer applications using participation factors," *IEE Proceedings C - Generation, Transmission and Distribution*, vol. 134, no. 3, pp. 238-244, May 1987.

[34] E. Z. Zhou, O. P. Malik and G. S. Hope, "Theory and method for selection of power system stabilizer location," *IEEE Transactions on Power Syst*em, vol. 6, no. 2, pp. 170–176, Mar. 1991.

[35] A. Ghosh, G. Ledwich, O. P. Malik and G. S. Hope, "Power system stabilizer based on adaptive control techniques," *IEEE Transactions on Power Apparatus and Systems*, vol. 103, pp. 1983-1989, 1984.

[36] A. Chandra, O. P. Malik and G. S. Hope, "A self-tuning controller for the control of multi-machine power systems," *IEEE Transactions on Power Syst*em, vol. 3, no. 3, pp. 1065-1071, Aug.1988.

[37] W. Gu and K. E. Bollinger, "A self-tuning power system stabilizer for wide range synchronous generation," *IEEE Transactions on Power Syst*em, vo1. 4, no. 3, pp. 1191-1199, Aug. 1989.

[38] N. C. Pahalawaththa, G. S. Hope and O. P. Malik, "Multivariable self-tuning power system stabilizer simulation and implementation studies," *IEEE Transactions on Energy Conversion*, vol. 6, no. 2, pp. 310-319, June 1991.

[39] G. P. Chen, O. P. Malik, G. S. Hope, Y. H. Qin and G. Y. Xu, "An adaptive power system stabilizer based on the self-optimizing pole shifting control strategy," *IEEE Transaction on Energy Conversion*, vol. EC-8, pp. 639–646, Dec. 1993.

[40] J. Y. Fan, T. H. Ortmeyer and R. Mukundan, "Power system stability improvement with multivariable self-tuning control," *IEEE Transactions on Power Syst*em, vol. 5, no. 1, pp. 227-234, Feb. 1990.

[41] D. J. Trudnowski, D. A. Pierre, J. R. Smith, and R. Adapa, "Coordination of multiple adaptive PSS units using a decentralized control scheme," *IEEE Transactions on Power Syst*em, vol. 7, no. 1, pp. 294–300, Feb. 1992.

[42] Shaoru Zhang and Fang Lin Luo, "An improved simple adaptive control applied to power system stabilizer," *IEEE Transactions of Power Electronics*, vol. 24, no. 2, pp. 369-375, Feb. 2009.

[43] P. Kundur, M. Klein, G. J. Rogers and M. S. Zywno, "Application of power system stabilizers for enhancement of overall system stability," *IEEE Transactions on Power Syst*em, vol. 4, no. 2, pp. 614–626, May 1989.

[44] Y. N. Yu and H. A. M. Moussa, "Optimal power system stabilization through excitation and/or governor control," *IEEE Transactions on Power Apparatus and Systems*, vol. PAS-90, pp. 1166-1173, 1971.

[45] C. X. Mao, K. S. Prakash, O. P. Malik, G. S. Hope and J. Fan, "Implementation and laboratory test results for an adaptive power system stabilizer based on linear optimal control," *IEEE Transactions on Energy Conversion*, vol. 5, no. 4, pp. 666-672, Dec. 1990.

[46] R. J. Fleming and Jun Suo, "An optimal multivariable stabilizer for a multi-machine plant," *IEEE Transactions on Energy Conversion*, vol. 5, no. 1, pp. 15-22, March 1990.

[47] V. A. F. De Campos, J. J. da Cruz, and L. C. Zanetta, "Robust and optimal adjustment of power system stabilizers through linear matrix inequalities," *International Journal of Electrical Power & Energy Systems*, vol. 42, no. 1, pp. 478-486, 2012.

[48] T. L. Huang, T. Y. Hwang and W. T. Yang, "Two level output feedback stabilizer design," *IEEE Transactions on Power Syst*em, vol. PWRS-6, no. 3, pp. 1042–1047, Aug. 1991.

[49] G. P. Chen, O. P. Malik, Y. H. Qin and G. Y. Xu, "Optimization technique for the design of a linear optimal power system stabilizer," *IEEE Transactions on Energy Conversion*, vol. 7, no. 3, pp. 453-459, Sep 1992.

[50] A. J. A. Simoes Costa et al., "Power system stabilizer design via structurally constrained optimal control," *Electrical Power System Research*, vol. 33, no. 1, pp. 33–40, Apr. 1995.

[51] K. T. Law, D. J. Hill and N. R. Godfrey, "Robust controller structure for coordinated power system voltage regulator and stabilizer design," *IEEE Transactions on Control System Technology*, vol. 2, no. 3, pp. 220–232, Sep. 1994.

[52] Q. Zhao and J. Jiang, "Robust control design for generator excitation system," *IEEE Transactions on Energy Conversion*, vol. 10, no. 2, pp. 201–209, June 1995.

[53] H. Bourlès, S. Peres, T. Margotin and M. P. Houry, "Analysis and design of a robust coordinated AVR/PSS," *IEEE Transactions on Power Syst*em, vol. 13, pp. 568–575, May 1998.

[54] H. Quinot, H. Bourles and T. Margotin, "Robust coordinated AVR + PSS for damping large scale power systems," *IEEE Transactions on Power Syst*em, vol. 14, no. 4, pp. 1446–1451, Nov. 1999.

[55] P. S. Rao and I. Sen, "Robust pole placement stabilizer design using linear matrix inequalities," *IEEE Transactions on Power Syst*em, vol. 15, no. 1, pp. 313–319, Feb. 2000.

[56] H. Bevrani, T. Hiyama and H. Bevrani, "Robust PID based power system stabilizer: design and real-time implementation," *International Journal on Electrical Power Energy System*, vol. 33, pp. 179-188, 2011.

[57] A. I. Konara and U. D. Annakkage, "Robust power system stabilizer design using Eigen-structure assignment," *IEEE Transactions on Power Systems*, vol. 31, no. 3, pp. 1845-1853, May 2016.

[58] R. Asgharian, "A robust H_∞ power system stabilizer with no adverse effect on shaft torsional modes," *IEEE Transactions on Energy Conversion*, vol. 9, pp. 475–481, Sept. 1994.

[59] S. Chen and O. P. Malik "H_∞ based power system stabilizer design," *IEE Proceedings on Generation Transmission Distribution*, vol. 142, no 2, pp 179- 184, March 1995.

[60] F. Komla A., N. Yorino and H. Sasaki, "Design of H_∞–PSS numerator-denominator uncertainty representation," *IEEE Transactions on Energy Conversion*, vol. 12, no. 1, pp. 45-50, March 1997.

[61] Antal Soos and O. P. Malik, "An H_2 optimal adaptive power system stabilizer," *IEEE Transactions on Energy Conversion*, vol. 17, no. 1, pp. 143-149, March 2002.

[62] C. M. d. S. Neto, F. B. Costa, R. L. d. A. Ribeiro, R. L. Barreto and T. d. O. A. Rocha, "Wavelet-based power system stabilizer," *IEEE Transactions on Industrial Electronics*, vol. 62, no. 12, pp. 7360-7369, Dec. 2015.

[63] D. J. Trudnowski, J. R. Smith, T. A. Short and D. A. Pierre, "An application of Prony methods in PSS design for multi-machine systems," *IEEE Transactions on Power Syst*em, vol. 1, no. 1, pp. 118–126, Feb. 1991.

[64] S. Chen and O. P. Malik, "Power system stabilizers design using μ-synthesis," *IEEE Transactions on Energy Conversion*, vol. 10, no. 1, pp. 175–181, March 1995.

[65] J. J. da Cruz and L. C. Zanetta Jr., "Stabilizer design for multi-machine power systems using mathematical programming," *International Journal of Electrical Power & Energy Systems*, vol. 19, no. 8, pp. 519–523, 1997.

[66] L. C. Zanetta and J. J. Da Cruz, "An incremental approach to the coordinated tuning of power system stabilizers using mathematical programming," *IEEE Transactions on Power Syst*em, vol. 20, no. 2, pp. 895–902, May 2005.

[67] C. Y. Chung, K. W. Wang, C. T. Tse and R. Niu, "Power-system stabilizer (PSS) design by probabilistic sensitivity indexes (PSIS)," *IEEE Transactions on Power Syst*em, vol. 17, no. 3, pp. 688–693, Aug. 2002.

[68] C. T. Tse, K. W. Wang, C. Y. Chung and K. M. Tsang, "Robust PSS design by probabilistic eigenvalue sensitivity analysis," *Electrical Power System Research*, vol. 59, pp. 47-54, 2001.

[69] C. Y. Chung, K. W. Wang, C. T. Tse, X. Y. Bian and A. K. David, "Probabilistic eigenvalue sensitivity analysis and PSS design in multi-machine systems," *IEEE Transactions on Power Syst*em, vol. 18, no. 4, pp. 1439–1445, Nov. 2003.

[70] R. A. Jabr, B. C. Pal and N. Martins, "A sequential conic programming approach for the coordinated and robust design of power system stabilizers," *IEEE Transactions on Power Syst*em, vol. 25, no. 3, pp. 1627–1637, Aug. 2010.

[71] Gurunath Gurrala and Indraneel Sen, "Power system stabilizers design for interconnected power systems," *IEEE Transactions on Power Syst*em, vol. 25, no. 2, pp. 1042–1051, May 2010.

[72] Gurunath Gurrala and Indraneel Sen, "Synchronizing and damping torques of non-linear voltage regulators," *IEEE Transactions on Power Syst*em, vol. 26, no. 3, pp. 1175–1185, Aug. 2011.

[73] Gurunath Gurrala and Indraneel Sen, "A non-linear voltage regulator with one tunable parameter for multi-machine power system," *IEEE Transactions on Power Syst*em, vol. 26, no. 3, pp. 1186–1195, Aug. 2011.

[74] M. L. Kothari, J. Nanda and K. Bhattacharya, "Design of variable structure power system stabilizers with desired eigenvalues in the sliding mode," *IEE Proceedings C - Generation, Transmission and Distribution*, vol. 140, no. 4, pp. 263-268, July 1993.

[75] Yijia Cao, Lin Jiang, Shijie Cheng, Deshu Chen, O. P. Malik and G. S. Hope, "A nonlinear variable structure stabilizer for power system stability," *IEEE Transactions on Energy Conversion*, vol. 9, no. 3, pp. 489-495, Sep 1994.

[76] V. G. D. C. Samarasinghe and N. C. Pahalawaththa, "Damping of multimodal oscillations in power systems using variable structure control techniques," *IEE Proceedings - Generation, Transmission and Distribution*, vol. 144, no. 3, pp. 323-331, May 1997.

[77] V. Bandal and B. Bandyopadhyay, "Robust decentralized output feedback sliding mode control technique-based power system stabilizer (PSS) for multi-machine power system," *IET Control Theory & Applications*, vol. 1, no. 5, pp. 1512-1522, Sept. 2007.

[78] Z. Jiang, "Design of power system stabilizers using synergetic control theory," *IEEE Power Engineering Society General Meeting*, Tampa, FL, pp. 1-8, 2007.

[79] E. Babaei, S. A. K. H. Mozaffari Niapour and M. M. Tabarraie, "Design of a non-linear power system stabiliser using the concept of the feedback linearization based on the back-stepping technique," *IET Generation, Transmission & Distribution*, vol. 5, no. 8, pp. 860-868, August 2011.

[80] T. K. Roy, M. A. Mahmud, W. Shen and A. M. T. Oo, "Nonlinear adaptive excitation controller design for multimachine power systems with unknown stability sensitive parameters," *IEEE Transactions on Control Systems Technology* , vol. 99, pp.1-13, 2017

[81] W. Yao, L. Jiang, J. Fang, J. Wen and S. Cheng, "Decentralized nonlinear optimal predictive excitation control for multi-machine power systems," *International Journal of Electrical Power & Energy Systems*, vol. 55, pp. 620-627, 2014.

[82] I. Kamwa, R. Grondin and G. Trudel, "IEEE PSS2B versus PSS4B: the limits of performance of modern power system stabilizers," *IEEE Transactions on Power Syst*em, vol. 20, no. 2, pp. 903–915, May 2005.

[83] D. Rimorov, I. Kamwa and G. Joós, "Model-based tuning approach for multi-band power system stabilisers PSS4B using an improved modal performance index," *IET Generation, Transmission & Distribution*, vol. 9, no. 15, pp. 2135-2143, Nov. 2015.

[84] H. Kang, Y. Liu, Q. H. Wu and X. Zhou, "Switching excitation controller for enhancement of transient stability of multi-machine power systems," *CSEE Journal of Power and Energy Systems*, vol. 1, no. 3, pp. 86-93, Sept. 2015.

[85] Y. Liu, Q. H. Wu, H. Kang and X. Zhou, "Switching power system stabilizer and its coordination for enhancement of multi-machine power system stability," *CSEE Journal of Power and Energy Systems*, vol. 2, no. 2, pp. 98-106, June 2016.

[86] N. Martins and T. H. S. Bossa, "A modal stabilizer for the independent damping control of aggregate generator and intra plant modes in multi-generator Power Plants," *IEEE Transactions on Power Systems*, vol. 29, no. 6, pp. 2646-2661, Nov. 2014.

[87] J. Ma, H. J. Wang and K. L. Lo, "Clarification on power system stabilizer design," *IET Generation, Transmission & Distribution*, vol. 7, no. 9, pp. 973-981, Sept. 2013.

[88] F. J. De Marco, N. Martins and J. C. R. Ferraz, "An automatic method for power system stabilizers phase compensation design," *IEEE Transactions on Power Systems*, vol. 28, no. 2, pp. 997-1007, May 2013.

[89] J. Zhang, C. Y. Chung and Y. Han, "A novel modal decomposition control and its application to pss design for damping interarea oscillations in power systems," *IEEE Transactions on Power Systems*, vol. 27, no. 4, pp. 2015-2025, Nov. 2012.

[90] I. Erceg, D. Sumina, S. Tusun, and M. Kutija, "Power system stabilizer based on point-wise min-norm control law," *Electric Power Systems Research*, vol. 143, pp. 215-224, 2017.

[91] Yuan-Yih Hsu and Chao-Rong Chen, "Synchronous machine steady state stability analysis using an artificial neural network," *IEEE Transactions on Energy Conversion*, vol. 6, no. 1, pp. 12-20, March 1991.

[92] Yuan-Yih Hsu and Chao-Rong Chen, "Tuning of power system stabilizer using an artificial neural network," *IEEE Transactions on Energy Conversion*, vol. 6, no. 4, pp. 612-618, Dec. 1991.

[93] D. M. Gillard and K. E. Bollinger, "Neural network identification of power system transfer function," *IEEE Transactions on Energy Conversion*, vol. 11, no. 1, pp. 104–109, Mar. 1996.

[94] Y. Zhang, G. P. Chen, O. P. Malik, and G. S. Hope, "An artificial neural network based adaptive power system stabilizer," *IEEE Transactions on Energy Conversion*, vol. 8, no. 1, pp. 71-77, March 1993.

[95] Y. Zhang, O. P. Malik, G. S. Hope and G. P. Chen, "Application of an inverse input/output mapped ANN as a power system stabilizer," *IEEE Transactions on Energy Conversion*, vol. 9, no. 3, pp. 433-441, Sept. 1994.

[96] Y. Zhang, O. P. Malik and G. P. Chen, "Artificial neural network power system stabilizers in multi-machine power system environment," *IEEE Transactions on Energy Conversion*, vol. 10, no. 1, pp. 147–155, March 1995.

[97] Young-Moon Park, Myeon-Song Choi and Kwang Y. Lee, "A neural network-based power system stabilizer using power flow characteristics," *IEEE Transactions on Energy Conversion*, vol. 11, no. 2, June 1996.

[98] P. Shamsollahi and O. P. Malik, "An adaptive power system stabilizer using on-line trained neural networks," *IEEE Transactions on Energy Conversion*, vol. 12, no. 4, pp. 382–387, Dec. 1997.

[99] P. Shamsollahi and O. P. Malik, "Application of neural adaptive power system stabilizer in a multi-machine power system," *IEEE Transaction on Energy Conversion*, vol. 14, no. 3, pp. 731–736, Sep. 1999.

[100] P. Shamsollahi and O. P. Malik, "Real-time implementation and experimental studies of a neural adaptive power system stabilizer," *IEEE Transaction on Energy Conversion*, vol. 14, pp. 737–742, Sept. 1999.

[101] R. Segal, M. L. Kothari and S. Madnani, "Radial Basis Function (RBF) network adaptive power system stabilizer," *IEEE Transactions on Power Syst*em, vol. 15, pp. 722–727, May 2000.

[102] B. Park, R. G. Harley and G. K. Venayagamoorthy, "Adaptive critic based optimal neuro control for synchronous generator in power system using MLP/RBF neural networks," *IEEE Transactions on Industry Applications*, vol. 39, no. 5, pp. 1529–1540, Sep./Oct. 2003.

[103] G. Ramakrishna and O. P. Malik, "Radial basis function identifier and pole-shifting controller for power system stabilizer applications," *IEEE Transactions on Energy Conversion,* vol. 19, no. 4, pp. 663-670, Dec. 2004.

[104] D. K. Chaturvedi, O. P. Malik and P. K. Kalra, "Experimental studies with a generalized neuron based power system stabilizer," *IEEE Transactions on Power Syst*em, vol. 19, no. 3, pp. 1445–1453, Aug. 2004.

[105] D. K. Chaturvedi, O. P. Malik and P. K. Kalra, "Performance of a generalized neuron-based PSS in a multi-machine power system," *IEEE Transactions on Energy Conversion*, vol. 19, no. 4, pp. 625-632, Sept. 2004.

[106] D. K. Chaturvedi and O. P. Malik, "A generalized neuron based adaptive power system stabilizer for multi-machine environment," *IEEE Transactions on Power Syst*em, vol. 20, no. 1, pp. 358–366, Feb. 2005.

[107] J. He and O. P. Malik, "An adaptive power system stabilizer based on recurrent neural networks," *IEEE Transactions on Energy Conversion*, vol. 12, pp. 413–418, Dec. 1997.

[108] Peng Zhao and O. P. Malik, "Design of adaptive PSS based on recurrent adaptive control theory," *IEEE Transactions on Energy Conversions*, vol. 24, no. 4, pp. 884-892, Dec. 2009.

[109] S. Kamalasadan and G. D. Swann, "A novel system-centric intelligent adaptive control architecture for damping inter-area mode oscillations in power system," *IEEE Transactions on Industry Applications*, vol. 47, no. 3, pp. 1487-1497, May-June 2011.

[110] S. Kamalasadan, G. D. Swann and R. Yousefian, "A novel system-centric intelligent adaptive control architecture for power system stabilizer based on adaptive neural networks," *IEEE Systems Journal*, vol. 8, no. 4, pp. 1074-1085, Dec. 2014.

[111] Y. Y. Hsu and C. H. Cheng, "Design of fuzzy power system stabilizers for multi-machine power systems," *IEE Proceedings on Generation, Transmission, Distribution*, vol. 137, no. 3, pp. 233–238, May 1990.

[112] M. A. M. Hassan, O. P. Malik and G. S. Hope, "A fuzzy logic based stabilizer for a synchronous machine," *IEEE Transactions on Energy Conversion*, vol. 6, no. 3, pp. 407-413, Sept. 1991.

[113] M. A. M. Hassan and O. P. Malik, "Implementation and laboratory test results for a fuzzy logic based self-tuned power system stabilizer," *IEEE Transactions on Energy Conversion*, vol. 8, no. 2, pp. 221–228, June 1993.

[114] T. Hiyama, "Robustness of fuzzy logic power system stabilizers applied to multi-machine power system," *IEEE Transactions on Energy Conversion*, vol. 9, pp. 451–459, Sept. 1994.

[115] T. H. Ortmeyer and T. Hiyama, "Frequency response characteristics of the fuzzy polar power system stabilizer," *IEEE Transactions on Energy Conversion*, vol. 10, no. 2, pp. 333–338, Jun. 1995.

[116] H. A. Toliyat, J. Sadeh, and R. Ghazi, "Design of augmented fuzzy logic power system stabilizers to enhance power system stability," *IEEE Transactions on Energy Conversion*, vol. 11, no. 1, pp. 97–103, March 1996.

[117] Y. M. Park and K. Y. Lee, "A self-organizing power system stabilizer using fuzzy auto-regressive moving average (FARMA) model," *IEEE Transactions on Energy Conversion*, vol. 11, no. 2, pp. 442–448, June 1996.

[118] P. Hong and K. Tomsovic, “Design and analysis of an adaptive fuzzy power system stabilizer,” *IEEE Transactions on Energy Conversion*, vol. 11, no. 2, pp. 455–461, Jun. 1996.

[119] J. Lu, M. H. Nehrir, and D. A. Pierre, “A fuzzy logic-based adaptive power system stabilizer for multi-machine systems,” *IEEE Power Engineering Society Summer Meeting*, Seattle, WA, July 15–19, 2000.

[120] J. Lu, M. H. Nahrir, D.A. Pierre, “A fuzzy logic-based adaptive power system stabilizer for multi-machine systems,” *Electric Power Systems Research*, vol. 60, no. 2, pp. 115–121, 2001.

[121] N. Hossein-Zodeh, A. Kalam, “An indirect adaptive fuzzy logic power system stabilizer,” *Electric Power & Energy Systems*, vol. 24, no. 10, pp. 837-842, 2002.

[122] T. Hussein, M. S. Saad, A. L. Elshafei and A. Bahgat, “Damping Inter-Area Modes Of Oscillation Using An Adaptive Fuzzy Power System Stabilizer,” *Electric Power Systems Research*, vol. 80, no. 12, pp. 1428–1436, 2010.

[123] E. Nechadi, M. N. Harmas, A. Hamzaoui, N. Essounbouli, “A new robust adaptive fuzzy sliding mode power system stabilizer,” *Electric Power & Energy Systems*, vol. 42, no. 1, pp. 1-7, 2012.

[124] K. Saoudi, M. N. Harmas, “Enhanced design of an indirect adaptive fuzzy sliding mode power system stabilizer for multi-machine power systems,” *Electric Power & Energy Systems*, vol. 54, pp. 425-431, 2014.

[125] E. Nechadi, M. N. Harmas, A. Hamzaoui, N. Essounbouli, “Type-2 fuzzy based adaptive synergetic power system control,” *Electric Power Systems Research*, vol. 88, pp. 9–15, 2012.

[126] Z. Bouchama, N. Essounbouli, M.N. Harmas, A. Hamzaoui, K. Saoudi, “Reaching phase free adaptive fuzzy synergetic power system stabilizer,” *Electric Power & Energy Systems*, vol. 77, pp. 43-49, 2016.

[127] M. A. Abido and Y. L. Abdel-Magid, “A hybrid neuro-fuzzy power system stabilizer for multi-machine power systems,” *IEEE Transactions on Power Syst*em, vol. 13, pp. 1323–1330, Nov. 1998.

[128] N. Hosseinzadeh and A. Kalam, “A rule-based fuzzy power system stabilizer tuned by neural network,” *IEEE Transactions on Energy Conversion*, vol. 14, pp. 773–779, Sept. 1999.

[129] R. You, H. J. Eghbali and M. H. Nehrir, “An online adaptive neuro-fuzzy power system stabilizer for multi-machine systems,” *IEEE Transactions on Power Syst*em, vol. 18, no. 1, pp. 128–135, Feb. 2003.

[130] Z. Barton, “Robust control in a multi-machine power system using adaptive neuro-fuzzy stabilizers,” *IEE Proceedings - Generation, Transmission and Distribution*, vol. 151, no. 2, pp. 261-267, 2 March 2004.

[131] D. K. Chaturvedi and O. P. Malik, “Neuro-fuzzy power system stabilizer,” *IEEE Transactions on Energy Conversions*, vol. 23, no. 3, pp. 887-894, Sept. 2008.

[132] M. R. Gonzalez and O. P. Malik, “Power system stabilizer design using an online adaptive neuro-fuzzy controller with adaptive input link weights,” *IEEE Transactions on Energy Conversions*, vol. 23, no. 3, pp. 914-922, Sept. 2008.

[133] S. M. Radaideh, I. M. Nejdawi, and M. H. Mushtaha, “Design of power system stabilizers using two level fuzzy and adaptive neuro-fuzzy inference systems,” *International Journal of Electrical Power & Energy Systems*, vol. 35, no. 1, pp. 47-56, 2012.

[134] Y. L. Abdel-Magid and M. M. Dawoud, “Tuning of power system stabilizers using genetic algorithms,” *Electric PowerSystems Research*, vol. 39, pp. 137-143, 1996.

[135] Y. L. Abdel-Magid, M. Bettayeb and M. M. Dawoud, “Simultaneous stabilization of power systems using genetic algorithms,” *IEE Proceedings - Generation, Transmission and Distribution*, vol. 144, no. 1, pp. 39-44, Jan 1997.

[136] M. A. Abido and Y. L. Abdel-Magid, "Hybridizing rule-based power system stabilizers with genetic algorithms," *IEEE Transactions on Power Syst*em, vol. 14, pp. 600–607, May 1999.

[137] Y. L. Abdel-Magid, M. A. Abido, S. Al-Baiyat, and A. H. Mantawy, "Simultaneous stabilization of multi-machine power systems via genetic algorithms," *IEEE Transactions on Power Syst*em, vol. 14, pp. 1428–1439, Nov. 1999.

[138] A. L. B. Do Bomfim, G. N. Taranto and D. M. Falcao, "Simultaneous tuning of power system damping controllers using genetic algorithms," *IEEE Transactions on Power Syst*em, vol. 15, no. 1, pp. 163–169, Feb. 2000.

[139] P. Zhang and A. H. Coonick, "Coordinated synthesis of PSS parameters in multi-machine power systems using the method of inequalities applied to genetic algorithms," *IEEE Transactions on Power Syst*em, vol. 15, no. 2, pp. 811–816, May 2000.

[140] M. A. Abido, "Parameter optimization of multi-machine power system stabilizers using genetic local search," *International Journal of Electrical Power & Energy Systems*, vol. 23, pp. 785-794, 2001.

[141] A. Andreoiu and K. Bhattacharya, "Robust tuning of power system stabilizers using a Lyapunov method based genetic algorithm," *IEE Proceedings - Generation, Transmission and Distribution*, vol. 149, no. 5, pp. 585-592, Sep 2002.

[142] Y. L. Abdel-Magid and M. A. Abido, "Optimal multi-objective design of robust power system stabilizers using genetic algorithms," *IEEE Transactions on Power Syst*em, vol. 18, no. 3, pp. 1125–1132, Aug. 2003.

[143] Hasan Alkhatib and Jean Duveau, "Dynamic genetic algorithms for robust design of multi-machine power system stabilizers," *International Journal of Electrical Power & Energy Systems*, vol. 45, pp. 242-251, 2013.

[144] H. Verdejo, D. Gonzalez, J. Delpiano and C. Becker, "Tuning of power system stabilizers using multiobjective optimization NSGA-II," *IEEE Latin America Transactions*, vol. 13, no. 8, pp. 2653-2660, Aug. 2015.

[145] M. Mary Linda and N. Kesavan Nair, "A new-fangled adaptive mutation breeder genetic optimization of global multi-machine power system stabilizer," *International Journal of Electrical Power & Energy Systems*, vol. 44, pp. 249-258, 2013.

[146] Lokman H. Hassan, et al, "Optimization of power system stabilizers using participation factor and genetic algorithm," *International Journal of Electrical Power & Energy Systems*, vol. 55, pp. 668-679, 2014.

[147] Karim Sebaa and Mohamed Boudour, "Optimal locations and tuning of robust power system stabilizer using genetic algorithms," *Electric Power Systems Research*, vol. 79, pp. 406-416, 2009.

[148] M. A. Abido, "A novel approach to conventional power system stabilizer design using tabu search," *International Journal of Electrical Power & Energy Systems*, vol. 21, pp. 443-454, 1999

[149] Y. L. Abdel-Magid, M. A. Abido and A. H. Mantaway, "Robust tuning of power system stabilizers in multimachine power systems," *IEEE Transactions on Power Syst*em, vol. 15, no. 2, pp. 735–740, May 2000.

[150] M. A. Abido, "Robust design of multi-machine power system stabilizers using simulated annealing," *IEEE Transactions on Energy Conversions*, vol. 15, no. 3, pp. 297–304, Sep. 2000.

[151] M. A. Abido, "An efficient heuristic optimization technique for robust power system stabilizer design," *Electric Power Systems Research*, vol. 58, pp. 53-62, 2001.

[152] M. A. Abido and Y. L. Abdel-Magid, "Optimal design of power system stabilizer using evolutionary programming," *IEEE Transactions Energy Conversions*, vol. 17, no. 4, pp. 429–436, Sep. 2002.

[153] M. A. Abido, "Optimal design of power system stabilizers using particle swarm optimization," *IEEE Transactions on Energy Conversions*, vol. 17, no. 3, pp. 406–413, Sep. 2002.

[154] Hossam E. Mostafa, et al, "Design and allocation of power system stabilizers using the particle swarm optimization technique for an interconnected power system," *International Journal of Electrical Power & Energy Systems,* vol. 34, pp. 57-65, 2012.

[155] Mahdiyeh Eslami, et al, "An efficient particle swarm optimization technique with chaotic sequence for optimal tuning and placement of PSS in power systems," *International Journal of Electrical Power & Energy Systems,* vol. 43, pp. 1467-1478, 2012.

[156] S. Mishra, M. Tripathy and J. Nanda, "Multi-machine power system stabilizer design by rule based bacteria foraging," *Electric Power Systems Research,* vol. 77, pp. 1595-1607, 2007.

[157] E. S. Ali, "Optimization of power system stabilizers using bat search algorithm," *International Journal of Electrical Power & Energy Systems*, vol. 61, pp. 683-690, May 2014.

[158] D. K. Sambariya and R. Prasad, "Robust tuning of power system stabilizer for small signal stability enhancement using meta-heuristic bat algorithm," *International Journal of Electrical Power & Energy Systems,* vol. 61, pp. 229-238, April 2014.

[159] H. Yassami, A. Darabi, S. M. R. Rafiei, "Power system stabilizer design using Strength Pareto multi-objective optimization approach," *Electric Power System Research,* vol. 80, pp. 838-846, 2010.

[160] H. Shayeghi, H. A. Shayanfar, S. Jalilzadeh and A. Safari, "Multi-Machine Power System Stabilizers Design Using Chaotic Optimization Algorithm," *Energy Conversion and Management*, vol. 51, pp. 1572-1580, March 2010.

[161] Amin Khodabakhshian and Reza Hemmati, "Multi-machine power system stabilizers design by using cultural algorithms," *International Journal of Electrical Power & Energy Systems*, vol. 44, pp. 571-580, September 2013.

[162] Amin Khodabakhshian, Reza Hemmati and Majid Moazzami, "Multi-band power system stabilizer design by using CPCE algorithm for multi-machine power system," *Electric Power Systems Research,* vol. 101, pp. 36-48, 2013.

[163] H. Shayeghi, A. Ghasemi, "A multi objective vector evaluated improved honey bee mating optimization for optimal and robust design of power system stabilizers," *International Journal of Electrical Power & Energy Systems*, vol. 62, pp. 630-645, May 2014.

[164] Wesley Peres, Edimar Jose de Oliveira, Joao Alberto Passos Filho, Ivo Chaves da Silva Junior, "Coordinated tuning of power system stabilizers using bio-inspired algorithms," *International Journal of Electrical Power & Energy Systems*, vol. 64, pp. 419-428, 2015.

[165] Anouar Farah, Tawfik Guesmi, Hsan Hadj Abdallah, Abderrazak Ouali, "A novel chaotic teaching–learning-based optimization algorithm for multi-machine power system stabilizers design problem," *International Journal of Electrical Power & Energy Systems*, vol. 75, pp. 197-209, 2016.

[166] K. A. Hameed and S. Palani, "Robust design of power system stabilizer using harmony search algorithm," *Journal for Control, Measurement, Electronics, Computing and Communications,* vol. 55 (2) , pp. 162-169 , 2014.

[167] S. M. Abd-Elazim and E. S. Ali, "Optimization of power system stabilizer design via cuckoo search algorithm," *International Journal of Electrical Power & Energy Systems*, vol. 75, pp. 99-107, 2016.

[168] Dhanraj Chitara, Anil Swarnkar, Nikhil Gupta, K. R. Niazi, R. C. Bansal, "Optimal tuning of multi-machine power system stabilizer using cuckoo search algorithm", *IFAC Papers On-Line*, vol. 48, no. 30, pp. 143-148, 2015.

[169] Dhanraj Chitara, K. R. Niazi, Anil Swarnkar, Nikhil Gupta "Cuckoo Search Optimization Algorithm for Designing of Multi-machine Power System Stabilizer," is accepted in *IEEE Transactions on Industry Applications (TIA)*, 2018.

[170] Naz Niamul Islam, M. A. Hannan, Hussain Shareef, Azah Mohamed, "An application of backtracking search algorithm in designing power system stabilizers for large multi-machine system," Neurocomputing, vol. 237, pp. 175-184, 2017.

[171] Wesley Peres, Ivo Chaves Silva Júnior, João Alberto Passos Filho, "Gradient based hybrid meta-heuristics for robust tuning of power system stabilizers," *International Journal of Electrical Power & Energy Systems*, vol. 95, pp. 47-72, 2018.

[172] M. Kashki, Y. L. Abdel-Magid, and M. A. Abido, "Parameter optimization of multi-machine power system conventional stabilizers using CDCARLA method," *International Journal on Electrical Power Energy & Systems*, vol. 32, pp. 498-506, 2010.

[173] Tridib Kumar Das, G. K. Venayagamoorthy and U. O. Aliyu, "Bio-inspired algorithm for the design of multiple optimal power system stabilizers: SPPSO And BFA," *IEEE Transactions on Industry Applications*, vol. 44, no. 5, pp. 1445–1457, Sept./Oct. 2008.

[174] S. K. Wang, J. P. Chiou, and C. W. Liu, "Parameters tuning of power system stabilizers using improved ant direction hybrid differential evolution," *International Journal on Electrical Power Energy Systems*, vol. 31, pp. 34-42, 2009.

[175] S. M. Abd-Elazim and E. S. Ali, "A hybrid particle swarm optimization and bacterial foraging for optimal power system stabilizers design," *International Journal of Electrical Power & Energy System*s, vol. 46, pp. 334-341, 2013.

[176] I. Eke, M. C. Taplamacioglu, "Robust tuning of power system stabilizer by using orthogonal learning artificial bee colony," *IFAC Papers On-Line*, vol. 48, no. 30, pp. 149-154, 2015.

[177] J. Wen, S. Cheng and O. P. Malik, "A synchronous generator fuzzy excitation controller optimally designed with a genetic algorithm," *IEEE Transactions on Power Syst*em, vol. 13, pp. 884–889, Aug. 1998.

[178] P. Lakshmi and M. Abdullah Khan, "Stability enhancement of a multi-machine power system using fuzzy logic based power system stabilizer tuned through genetic algorithm," *International Journal of Electrical Power & Energy Systems*, vol. 22, pp. 137-145, 2000.

[179] J. Lu, M. H. Nehrir and D. A. Pierre, "A fuzzy logic-based self-tuning power system stabilizer optimized with a genetic algorithm," *Electric Power Systems Research*, vol. 60, pp. 77-83, 2001.

[180] P. S. Bhati and Rajeev Gupta, "Robust fuzzy logic power system stabilizer based on evolution and learning," *International Journal of Electrical Power & Energy Systems*, vol. 53, pp. 357-366, 2013.

[181] F. Mayouf Adjeroud et al, "A coordinated genetic based type-2 fuzzy stabilizer for conventional and superconducting generators," *Electric Power Systems Research*, vol. 129, pp. 51-61, 2015.

[182] V. S. Vakula and K. R. Sudha, "Design of differential evolution algorithm-based robust fuzzy logic power system stabilizer using minimum rule Base", *IET Generation Transmission Distribution*, vol. 6, Iss. 2, pp. 121–132, 2012.

[183] D. E. Kvasov et al, "Tuning fuzzy power-system stabilizers in multi-machine systems by global optimization algorithms based on efficient domain partitions," *Electric Power Systems Research,* vol. 78, pp. 1217-1229, 2008.

[184] A. M. El-Zonkoly, A. A. Khalil and N. M. Ahmied, "Optimal tuning of lead–lag and fuzzy logic power system stabilizers using particle swarm optimization," *Expert System Applications*, vol. 36, no. 2, pp. 2097–106, 2009.

[185] Vahid Keumarsi, Mohsen Simab and Ghazanfar Shahgholian, "An integrated approach for optimal placement and tuning of power system stabilizer in multi-machine systems," *International Journal of Electrical Power & Energy Systems,* vol. 63, pp. 132-139, 2014.

[186] Binod Shaw et al, "Comparative seeker and bio-inspired fuzzy logic controllers for power system stabilizers," *International Journal of Electrical Power & Energy Systems,* vol. 33, pp. 1728-1738, 2011.

[187] A. Chatterjee, S. P. Ghoshal and V. Mukherjee, "Chaotic ant swarm optimization for fuzzy-based tuning of power system stabilizer," *International Journal of Electrical Power & Energy Systems,* vol. 33, pp. 657-672, 2011.

[188] Ali Ghasemi, Hossein Shayeghi and Hasan Alkhatib, "Robust design of multi-machine power system stabilizers using fuzzy gravitational search algorithm," *International Journal of Electrical Power & Energy Systems,* vol. 51, pp. 190-200, 2013.

[189] A. Afzalian and D. A. Linkens, "Training of neuro-fuzzy power system stabilizers using genetic algorithms," *International Journal of Electrical Power & Energy Systems,* vol. 22, pp. 93-102, 2000.

[190] H. E. A. Talaat, A. Abdennour and A. A. Al-Sulaiman, "Design and experimental investigation of a decentralized GA-optimized neuro-fuzzy power system stabilizer," *International Journal on Electrical Power Energy System*, vol. 32, pp. 751-759, 2010.

[191] Sheng-Kuan Wang, "Coordinated parameter design of power system stabilizers and static synchronous compensator using gradual hybrid differential evaluation," *International Journal of Electrical Power & Energy Systems,* vol. 81, pp. 165-174, 2016.

[192] Elenilson de Vargas Fortes, Leonardo H. Macedo, Percival Bueno de Araujo, Rubén Romero, "A VNS algorithm for the design of supplementary damping controllers for small-signal stability analysis," *International Journal of Electrical Power & Energy Systems,* vol. 94, pp. 41-56, 2018.

[193] Tamer Fetouh, Mohamed S. Zaky, "New approach to design SVC-based stabilizer using genetic algorithm and rough set theory," *IET Generation, Transmission & Distribution*, vol. 11, no. 2, pp. 372-382, 2017.

[194] Deping Ke, Feifan Shen, C. Y. Chung, Chen Zhang, Jian Xu, Yuanzhang Sun, "Application of information gap decision theory to the design of robust wide-area power system stabilizers considering uncertainties of wind power," *IEEE Transactions on Sustainable Energy*, vol. 9, no. 2, pp. 805-817, 2018.

[195] Jingsen Zhou, Deping Ke, C. Y. Chung, Yuanzhang Sun, "A computationally efficient method to design probabilistically robust wide-area PSSs for damping inter-area oscillations in wind integrated power systems," *IEEE Transactions on Power Systems*, 2018.

[196] BhinalMehta, PraghneshBhatt, VivekPandya, "Small signal stability analysis of power systems with DFIG based wind power penetration," *International Journal of Electrical Power & Energy Systems,* vol. 58, pp. 64-74, 2014.

[197] Tossaporn Surinkaew, Issarachai Ngamroo, "Coordinated robust control of DFIG wind turbine and PSS for stabilization of power oscillations considering system uncertainties," *IEEE Transactions on Sustainable Energy*, vol. 5, no. 3, pp. 823-833, 2014.

[198] RahmatKhezri, HassanBevrani, "Voltage performance enhancement of DFIG-based wind farms integrated in large-scale power systems: Coordinated AVR and PSS," *International Journal of Electrical Power & Energy Systems*, vol. 73, pp. 400-410, 2015.

[199] Chen Zhang, Deping Ke, Yuanzhang Sun, C. Y. Chung; Jian Xu, Feifan Shen, "Coordinated supplementary damping control of DFIG and PSS to suppress inter-area oscillations with optimally controlled plant dynamics," *IEEE Transactions on Sustainable Energy*, vol. 9, no. 2, pp. 780-791, 2018.

[200] X. Y. Bian, X. X. Huang, K. C. Wong, K. L. Lo, Yang Fu, S. H. Xuan, "Improvement on probabilistic small-signal stability of power system with large-scale wind farm integration," *International Journal of Electrical Power & Energy Systems*, vol. 61, pp. 482-488, 2014.

[201] Shamik Chatterjee, Abishek Naithani, V. Mukherjee, "Small-signal stability analysis of DFIG based wind power system using teaching learning based optimization," *International Journal of Electrical Power & Energy Systems*, vol. 78, pp. 672-689, 2016.

[202] Z. W. Geem, J. H. Kim, G.V. Loganathan, "A new heuristic optimization algorithm: harmony search, simulation," *SAGE Journals*, vol. 76, no. 2, pp. 60–68, 2001.

[203] Z. W. Geem et. al, *Harmony Search Algorithms for Structural Design Optimization*, Springer, 2010.

[204] X. S. Yang and S. Deb, "Cuckoo search via Lévy flights. In: Proceedings of world congress on nature & biologically inspired computing," NABIC, pp. 210–214, 2009.

[205] X. S. Yang, *Engineering optimization: an introduction with meta-heuristic applications*, John Wiley and Sons; 2010.

[206] X. S. Yang and S. Deb, "Engineering optimization by cuckoo search. International Journal of Mathematical Modelling & Numerical Optimization," vol. 1, no. 4, pp. 330–43, 2010.

[207] J. H. Holland, *Adaptation in Natural and Artificial Systems*, University of Michigan Press, Michigan, 1975.

[208] D. E. Goldberg, *Genetic algorithms in search, optimization and machine learning*, Addison-Wesley; 1989.

[209] P. Martín and A. Sierra, "Improving power system static security margins by means of a real coded genetic algorithm," *IEEE Transactions on Power Systems*, vol. 31, no. 3, pp. 1915-1924, May 2016.

[210] H. H. Müller and C. A. Castro, "Genetic algorithm-based phasor measurement unit placement method considering observability and security criteria," *IET Generation, Transmission & Distribution*, vol. 10, no. 1, pp. 270-280, 1 7 2016.

[211] W. Sheng, K. Y. Liu, Y. Liu, X. Meng and Y. Li, "Optimal placement and sizing of distributed generation via an improved non-dominated sorting genetic algorithm II," *IEEE Transactions on Power Delivery*, vol. 30, no. 2, pp. 569-578, April 2015.

[212] H. D. de Macedo Braz and B. A. de Souza, "Distribution network reconfiguration using genetic algorithms with sequential encoding: subtractive and additive approaches," *IEEE Transactions on Power Systems*, vol. 26, no. 2, pp. 582-593, May 2011.

[213] M. A. Pai, *Energy Function Analysis for Power System Stability*, Kluwer Academic Publishers, 1989.

[214] G. Rogers, *Power system oscillations, Springer*; 1999.

[215] F. Milano, *Power System Analysis Toolbox. Version 2.1.6*, 2010.

[216] S. Ganguly, "Multi-objective planning for reactive power compensation of radial distribution networks with unified power quality conditioner allocation using particle swarm optimization," *IEEE Transactions on Power Systems*, vol. 29, no. 4, pp. 1801-1810, July 2014.

[217] P. Siano and G. Mokryani, "Assessing wind turbines placement in a distribution market environment by using particle swarm optimization," *IEEE Transactions on Power Systems*, vol. 28, no. 4, pp. 3852-3864, Nov. 2013.

[218] W. C. Wu and M. S. Tsai, "Application of enhanced integer coded particle swarm optimization for distribution system feeder reconfiguration," *IEEE Transactions on Power Systems*, vol. 26, no. 3, pp. 1591-1599, Aug. 2011.

[219] M. Ramezani, M. R. Haghifam, C. Singh, H. Seifi and M. P. Moghaddam, "Determination of capacity benefit margin in multi-area power systems using particle swarm optimization," *IEEE Transactions on Power Systems*, vol. 24, no. 2, pp. 631-641, May 2009.

[220] J. Kennedy and R. C. Eberhart, "Particle swarm optimization", *Proc. IEEE international conference on neural networks*, Piscataway, NJ, vol. IV, pp. 1942-1948, 1995.

[221] Y. Shi and R. C. Eberhart, "A modified particle swarm optimizer," *Proc. IEEE Computation Intelligence World Congress*, pp. 69–73, May 1998.

[222] W. Sheng, K. y. Liu, Y. Liu, X. Ye and K. He, "Reactive power coordinated optimization method with renewable distributed generation based on improved harmony search," *IET Generation, Transmission & Distribution*, vol. 10, no. 13, pp. 3152-3162, 10 6 2016.

[223] C. K. Shiva and V. Mukherjee, "Automatic generation control of multi-unit multi-area deregulated power system using a novel quasi-oppositional harmony search algorithm," *IET Generation, Transmission & Distribution*, vol. 9, no. 15, pp. 2398-2408, 11 19 2015.

[224] M. N. Ambia, H. M. Hasanien, A. Al-Durra and S. M. Muyeen, "Harmony search algorithm-based controller parameters optimization for a distributed-generation system," *IEEE Transactions on Power Delivery*, vol. 30, no. 1, pp. 246-255, Feb. 2015.

[225] L. Wei, W. Guo, F. Wen, G. Ledwich, Z. Liao and J. Xin, "Waveform matching approach for fault diagnosis of a high-voltage transmission line employing harmony search algorithm," *IET Generation, Transmission & Distribution*, vol. 4, no. 7, pp. 801-809, July 2010.

[226] M. K. Kim, "Short-term price forecasting of Nordic power market by combination Levenberg–Marquardt and Cuckoo search algorithms," *IET Generation, Transmission & Distribution*, vol. 9, no. 13, pp. 1553-1563, 10 1 2015.

[227] A. A. El-fergany and A. Y. Abdelaziz, "Capacitor allocations in radial distribution networks using cuckoo search algorithm," *IET Generation, Transmission & Distribution*," vol. 8, no. 2, pp. 223-232, February 2014.

APPENDIX

The single-line diagrams, generator, line and bus data and other relevant data of standard IEEE dynamic systems are considered for simulation using different meta-heuristic techniques throughout this thesis are given in this appendix.

1. Three-Machine, Nine-Bus WSCC Power System

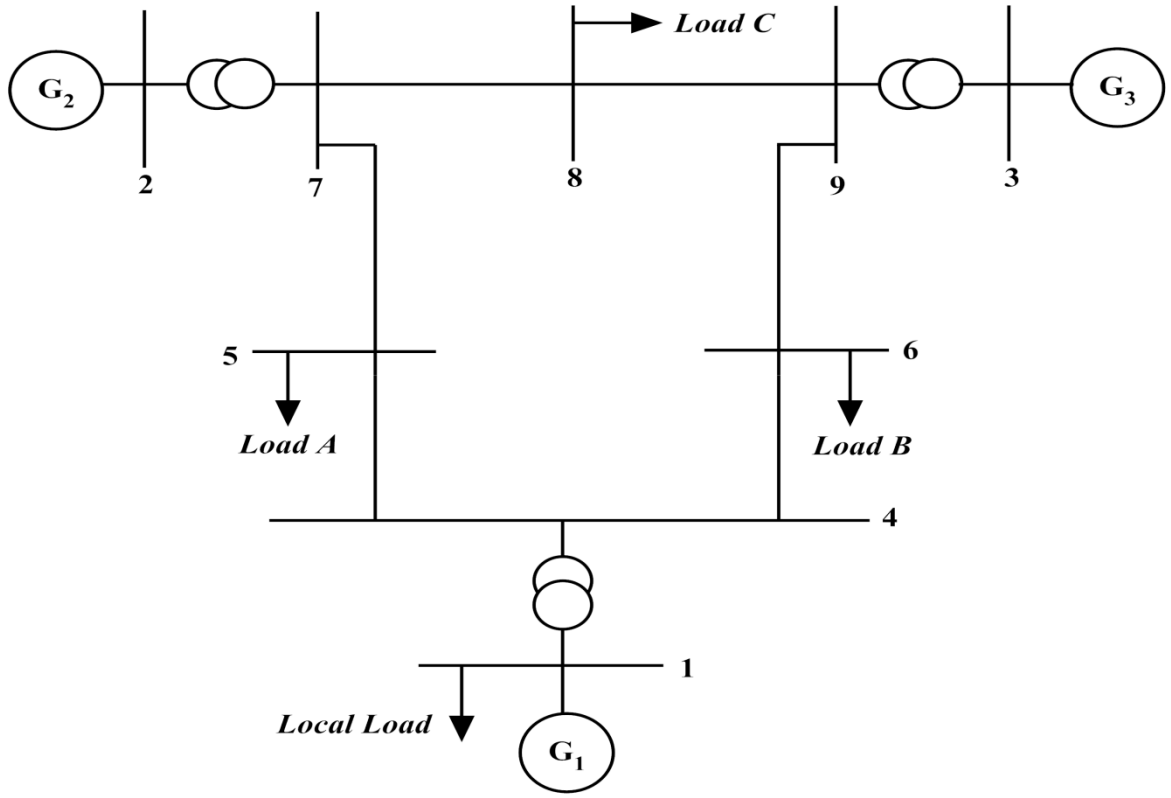

Fig. 1 Single-line diagram of three-machine, nine-bus WSCC power system

Table 1: Generator data of 3-machine, 9-bus WSCC power system

Unit No	x_l	R_a	x_d	$x_d^{'}$	$T_{d0}^{'}$	x_q	$x_q^{'}$	$T_{q0}^{'}$	M
1	0	0	0.1460	0.0608	8.96	0.0969	0.0969	0.310	47.28
2	0	0	0.8958	0.1198	6.00	0.8645	0.1969	0.535	12.8
3	0	0	1.3125	0.1813	5.89	1.2578	0.2500	0.600	6.02

Table 2: Line data of 3-machine, 9-bus WSCC power system

Line Number	Line Data					Transformer Tap	
	From Bus	To Bus	R	X	B	Magnitude	Angle
1	9	8	0.0119	0.1008	0.2090	1.0000	0
2	7	8	0.0085	0.0720	0.1490	1.0000	0
3	9	6	0.0390	0.1700	0.3580	1.0000	0
4	7	5	0.0320	0.1610	0.3060	1.0000	0
5	5	4	0.0100	0.0850	0.1760	1.0000	0
6	6	4	0.0170	0.0920	0.1580	1.0000	0

Cont.

Line Number	Line Data					Transformer Tap	
	From Bus	To Bus	R	X	B	Magnitude	Angle
7	2	7	0	0.0625	0	1.0000	0
8	3	9	0	0.0586	0	1.0000	0
9	1	4	0	0.0576	0	1.0000	0

Table 3: Bus data of 3-machine, 9-bus WSCC power system

Bus	Type	Voltage (KV)	Load		Generator		
			P_L (p.u.)	Q_L (p.u.)	P_G (p.u.)	Q_G (p.u.)	Unit No.
1	SW	16.5	1.00	0.35	-	-	G_1
2	PV	18.0	-	-	1.63	0.06	G_2
3	PV	13.8	-	-	0.85	− 0.10	G_3
4	-	230	-	-	-	-	-
5	PQ	230	1.25	0.50	-	-	-
6	PQ	230	0.90	0.30	-	-	-
7	-	230	-	-	-	-	-
8	PQ	230	1.00	0.35	-	-	-
9	-	230	-	-	-	-	-

2. Two-Area, Four-Machine (TAFM) Power System

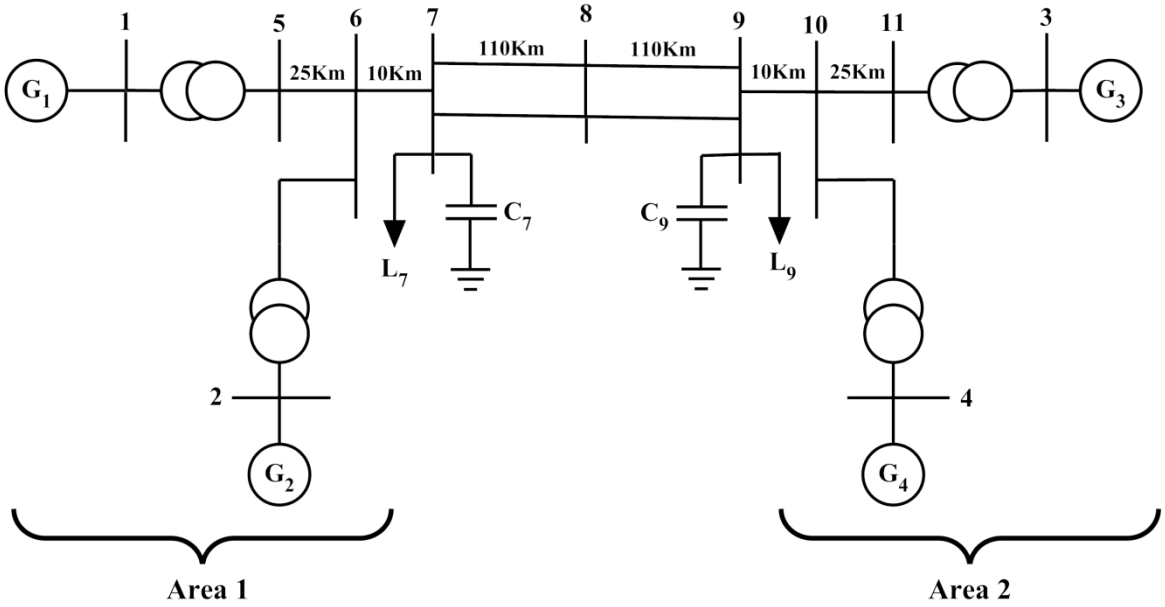

Fig. 2 Single-line diagram of two-area, four-machine (TAFM) power system

Table 4: Generator data of 2-area, 4-machine (TAFM) power system

Unit No	x_l	R_a	x_d	$x_d^{'}$	$x_d^{''}$	$T_{d0}^{'}$	$T_{d0}^{''}$	x_q	$x_q^{'}$	$x_q^{''}$	$T_{q0}^{'}$	$T_{q0}^{''}$	M
1	0.2	0.0025	1.8	0.3	0.25	8	0.03	1.7	0.55	0.25	0.40	0.05	13
2	0.2	0.0025	1.8	0.3	0.25	8	0.03	1.7	0.55	0.25	0.40	0.05	13
3	0.2	0.0025	1.8	0.3	0.25	8	0.03	1.7	0.55	0.25	0.40	0.05	12.35
4	0.2	0.0025	1.8	0.3	0.25	8	0.03	1.7	0.55	0.25	0.40	0.05	12.35

Table 5: Line data of 2-area, 4-machine (TAFM) power system

Line Number	Line Data					Transformer Tap	
	From Bus	To Bus	R	X	B	Magnitude	Angle
1	5	6	0.0025	0.0250	0.0437	1.00	0
2	6	7	0.0010	0.0100	0.0175	1.00	0
3	7	8	0.0110	0.1100	0.1925	1.00	0
4	8	9	0.0110	0.1100	0.0963	1.00	0
5	8	9	0.0110	0.1100	0.1925	1.00	0
6	11	10	0.0025	0.0250	0.0437	1.00	0
7	9	10	0.0010	0.0100	0.0175	1.00	0
8	7	8	0.0110	0.1100	0.0963	1.00	0
9	1	5	0	0.0167	0	1.00	0
10	2	6	0	0.0167	0	1.00	0
11	4	10	0	0.0167	0	1.00	0
12	3	11	0	0.0167	0	1.00	0

Table 6: Bus data of 2-area, 4-machine (TAFM) power system

Bus	Type	Voltage (KV)	Load		Generator		
			P_L (p.u.)	Q_L (p.u)	P_G (p.u.)	Q_G (p.u.)	Unit No.
1	PV	20	-	-	7.00	1.8245	G_1
2	PV	20	-	-	7.00	2.2843	G_2
3	SW	20	-	-	-	-	G_3
4	PV	20	-	-	7.00	1.9356	G_4
5	-	230	-	-	-	-	-
6	-	230	-	-	-	-	-
7	PQ	230	9.67	- 1.00	-	-	-
8	-	230	-	-	-	-	-
9	PQ	230	17.67	- 2.50	-	-	-
10	-	230	-	-	-	-	-
11	-	230	-	-	-	-	-

3. Ten-Machine, Thirty-Nine Bus New England Power System (NEPS)

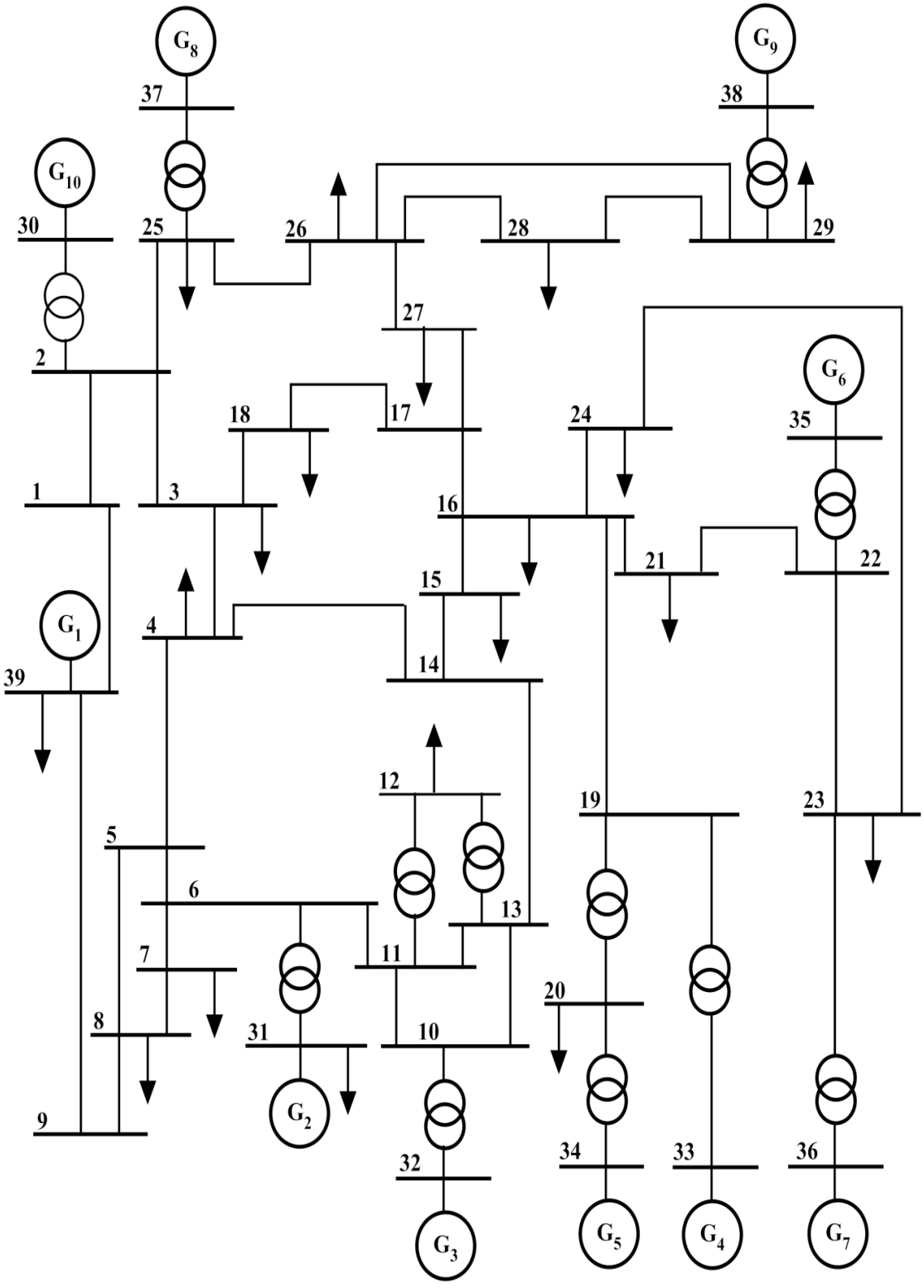

Fig. 3: Single-line diagram of ten-machine, thirty-nine bus New England Power System (NEPS)

Table 7: Generator data of 10-machine, 39-bus New England power system

Unit No	x_l	R_a	x_d	$x_d^{'}$	$T_{d0}^{'}$	x_q	$x_q^{'}$	$T_{q0}^{'}$	M
1	0.0030	0.0001	0.0200	0.0060	7.00	0.019	0.0060	0.70	1000
2	0.0350	0.0027	0.2950	0.0697	6.56	0.282	0.0697	1.50	60.6
3	0.0304	0.0004	0.2495	0.0531	5.70	0.237	0.0531	1.50	71.6
4	0.0295	0.0002	0.2620	0.0436	5.69	0.258	0.0436	1.50	57.2
5	0.0540	0.0001	0.6700	0.1320	5.40	0.620	0.1320	0.44	52
6	0.0224	0.0062	0.2540	0.0500	7.30	0.241	0.0500	0.40	69.6
7	0.0322	0.0003	0.2950	0.0490	5.66	0.292	0.0490	1.50	52.8
8	0.0280	0.0007	0.2900	0.0570	6.70	0.280	0.0570	0.41	48.6
9	0.0298	0.0003	0.2106	0.0570	4.79	0.205	0.0570	1.96	69
10	0.0125	0.0001	0.1000	0.0310	10.20	0.069	0.0310	1.50	84

Table 8: Line data of10-machine, 39-bus New England power system

Line Number	Line Data					Transformer Tap	
	From Bus	To Bus	R	X	B	Magnitude	Angle
1	1	2	0.0035	0.0411	0.6987	1.000	0
2	1	39	0.0010	0.0250	0.7500	1.000	0
3	2	3	0.0013	0.0151	0.2572	1.000	0
4	2	25	0.0070	0.0086	0.1460	1.000	0
5	2	30	0	0.0181	0	1.025	0
6	3	4	0.0013	0.0213	0.2214	1.000	0
7	3	18	0.0011	0.0133	0.2138	1.000	0
8	4	5	0.0008	0.0128	0.1342	1.000	0
9	4	14	0.0008	0.0129	0.1382	1.000	0
10	5	8	0.0008	0.0112	0.1476	1.000	0
11	6	5	0.0002	0.0026	0.0434	1.000	0
12	6	7	0.0006	0.0092	0.1130	1.000	0
13	6	11	0.0007	0.0082	0.1389	1.000	0
14	6	31	0	0.0250	0	1.070	0
15	7	8	0.0004	0.0046	0.0780	1.000	0
16	8	9	0.0023	0.0363	0.3804	1.000	0
17	9	39	0.0010	0.0250	1.2000	1.000	0
18	10	11	0.0004	0.0043	0.0729	1.000	0
19	10	13	0.0004	0.0043	0.0729	1.000	0
20	10	32	0	0.0200	0	1.070	0
21	12	11	0.0016	0.0435	0	1.006	0
22	12	13	0.0016	0.0435	0	1.006	0
23	13	14	0.0009	0.0101	0.1723	1.000	0
24	14	15	0.0018	0.0217	0.3660	1.000	0
25	15	16	0.0009	0.0094	0.1710	1.000	0
26	16	17	0.0007	0.0089	0.1342	1.000	0
27	16	19	0.0016	0.0195	0.3040	1.000	0
28	16	21	0.0008	0.0135	0.2548	1.000	0
29	16	24	0.0003	0.0059	0.0680	1.000	0
30	17	18	0.0007	0.0082	0.1319	1.000	0
31	17	27	0.0013	0.0173	0.3216	1.000	0

Cont.

Line Number	Line Data					Transformer Tap	
	From Bus	To Bus	R	X	B	Magnitude	Angle
32	19	33	0.0007	0.0142	0	1.070	0
33	19	20	0.0007	0.0138	0	1.060	0
34	20	34	0.0009	0.0180	0	1.009	0
35	21	22	0.0008	0.0140	0.2565	1.000	0
36	22	23	0.0006	0.0096	0.1846	1.000	0
37	22	35	0	0.0143	0	1.025	0
38	23	24	0.0022	0.0350	0.3610	1.000	0
39	23	36	0.0005	0.0272	0	1.000	0
40	25	26	0.0032	0.0323	0.5130	1.000	0
41	25	37	0.0006	0.0232	0	1.025	0
42	26	27	0.0014	0.0147	0.2396	1.000	0
43	26	28	0.0043	0.0474	0.7802	1.000	0
44	26	29	0.0057	0.0625	1.0290	1.000	0
45	28	29	0.0014	0.0151	0.2490	1.000	0
46	29	38	0.0008	0.0156	0	1.025	0

Table 9: Bus data of 10-machine, 39-bus New England power system

Bus	Type	Voltage (p.u.)	Load		Generator		
			P_L (p.u.)	Q_L (p.u.)	P_G (p.u.)	Q_G (p.u.)	Unit No.
3	PQ	-	3.22	0.024	-	-	-
4	PQ	-	5	1.84	-	-	-
7	PQ	-	2.338	8.4	-	-	-
8	PQ	-	5.22	1.76	-	-	-
12	PQ	-	0.075	0.88	-	-	-
15	PQ	-	3.2	1.53	-	-	-
16	PQ	-	3.294	0.323	-	-	-
18	PQ	-	1.58	0.3	-	-	-
20	PQ	-	6.8	1.03	-	-	-
21	PQ	-	2.74	1.15	-	-	-
23	PQ	-	2.475	0.846	-	-	-
24	PQ	-	3.086	-0.6454	-	-	-
25	PQ	-	2.24	0.472	-	-	-
26	PQ	-	1.39	0.17	-	-	-
27	PQ	-	2.81	0.755	-	-	-
28	PQ	-	2.06	0.276	-	-	-
29	PQ	-	2.835	0.269	-	-	-
30	PV	1	-	-	2.5	-	G_{10}
31	PV	1	0.092	0.046	5.729	-	G_2
32	PV	1	-	-	6.5	-	G_3
33	PV	1	-	-	6.32	-	G_4
34	PV	1	-	-	5.08	-	G_5
35	PV	1	-	-	6.5	-	G_6
36	PV	1	-	-	5.6	-	G_7
37	PV	1	-	-	5.4	-	G_8
38	PV	1	-	-	8.3	-	G_9
39	SW	1	11.04	2.5	-	-	G_1

4: Sixteen-Machine, Sixty-Eight Bus New England Extended Power System (NEEPS)

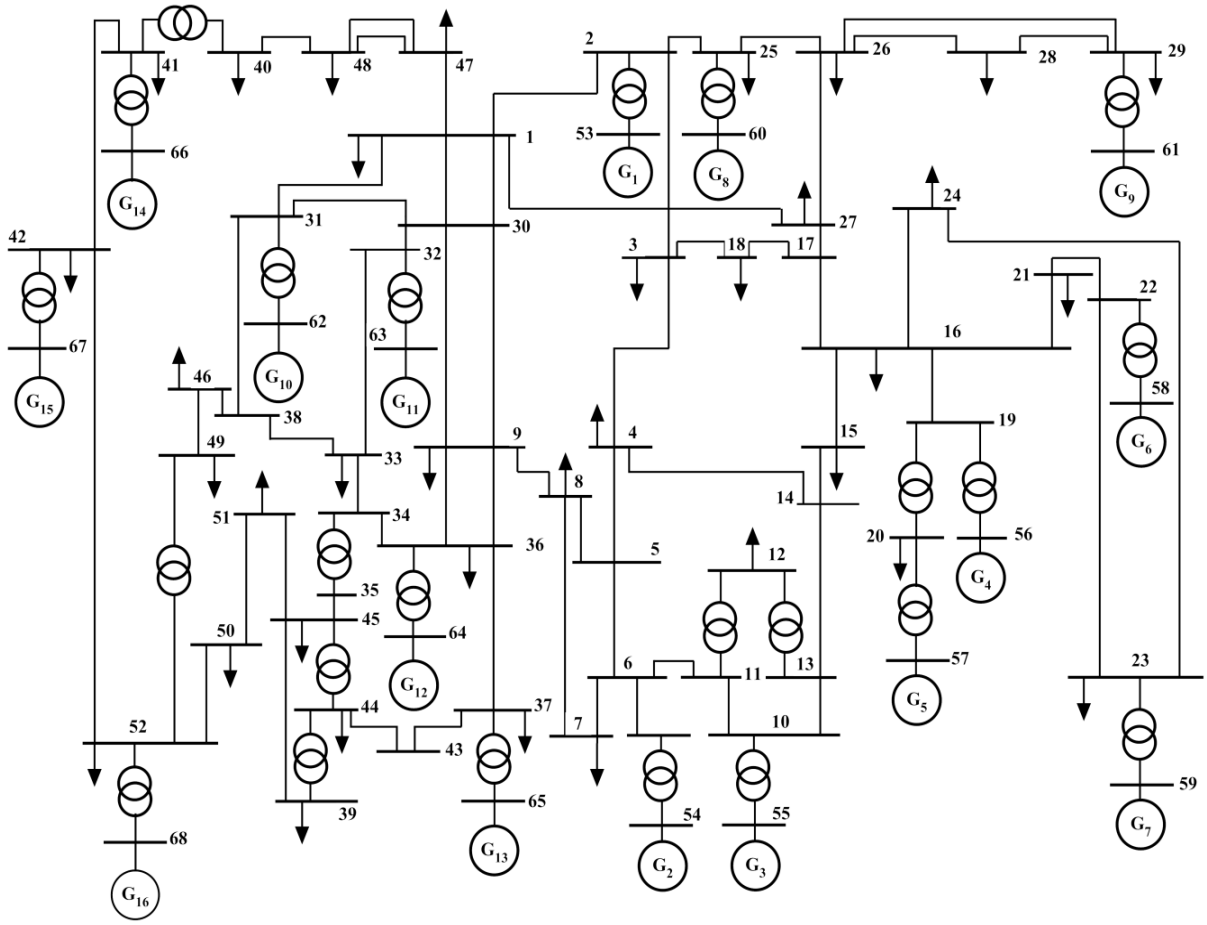

Fig. 4 Single-line diagram of sixteen-machine, sixty-bus New England Extended Power System (NEEPS)

Table 10: Generator data of 16-machine, 68-bus New England extended power system

Unit No	x_l	R_a	x_d	$x_d^{'}$	$x_d^{''}$	$T_{d0}^{'}$	$T_{d0}^{''}$	x_q	$x_q^{'}$	$x_q^{''}$	$T_{q0}^{'}$	$T_{q0}^{''}$	M
1	0.0125	0	0.10	0.031	0.025	10.2	0.05	0.069	0.0417	0.025	1.5	0.035	84.0
2	0.035	0	0.295	0.0697	0.050	6.56	0.05	0.282	0.0933	0.050	1.5	0.035	60.4
3	0.0304	0	0.2495	0.0531	0.045	5.7	0.05	0.237	0.0714	0.045	1.5	0.035	71.6
4	0.0295	0	0.262	0.0436	0.035	5.69	0.05	0.258	0.0586	0.035	1.5	0.035	57.2
5	0.027	0	0.330	0.066	0.050	5.4	0.05	0.310	0.0883	0.050	0.44	0.035	52.0
6	0.0224	0	0.254	0.050	0.040	7.3	0.05	0.241	0.0675	0.040	0.4	0.035	69.6
7	0.0322	0	0.295	0.049	0.040	5.66	0.05	0.292	0.0667	0.040	1.5	0.035	52.8
8	0.028	0	0.290	0.057	0.045	6.7	0.05	0.280	0.0767	0.045	0.41	0.035	48.6
9	0.0298	0	0.2106	0.057	0.045	4.79	0.05	0.205	0.0767	0.045	1.96	0.035	69.0
10	0.0199	0	0.169	0.0457	0.040	9.37	0.05	0.115	0.0615	0.040	1.5	0.035	62.0
11	0.0103	0	0.128	0.018	0.012	4.1	0.05	0.123	0.0241	0.012	1.5	0.035	56.4
12	0.022	0	0.101	0.031	0.025	7.4	0.05	0.095	0.0420	0.025	1.5	0.035	184.6
13	0.003	0	0.0296	0.0055	0.004	5.9	0.05	0.0286	0.0074	0.004	1.5	0.035	496.0
14	0.0017	0	0.018	0.0029	0.0023	4.1	0.05	0.0173	0.0038	0.0023	1.5	0.035	600.0
15	0.0017	0	0.018	0.0029	0.0023	4.1	0.05	0.0173	0.0038	0.0023	1.5	0.035	600.0
16	0.0041	0	0.0356	0.0071	0.0055	7.8	0.05	0.0334	0.0095	0.0055	1.5	0.035	450.0

Table 11: Line data of 16-machine, 68-bus New England extended power system

Line Number	Line Data					Transformer Tap	
	From Bus	To Bus	R	X	B	Magnitude	Angle
1	1	2	0.0035	0.0411	0.6987	1.0000	0
2	1	30	0.0008	0.0074	0.4800	1.0000	0
3	2	3	0.0013	0.0151	0.2572	1.0000	0
4	2	25	0.0070	0.0086	0.1460	1.0000	0
5	2	53	0	0.0181	0	1.0250	0
6	3	4	0.0013	0.0213	0.2214	1.0000	0
7	3	18	0.0011	0.0133	0.2138	1.0000	0
8	4	5	0.0008	0.0128	0.1342	1.0000	0
9	4	14	0.0008	0.0129	0.1382	1.0000	0
10	5	6	0.0002	0.0026	0.0434	1.0000	0
11	5	8	0.0008	0.0112	0.1476	1.0000	0
12	6	7	0.0006	0.0092	0.1130	1.0000	0
13	6	11	0.0007	0.0082	0.1389	1.0000	0
14	6	54	0	0.0250	0	1.0700	0
15	7	8	0.0004	0.0046	0.0780	1.0000	0
16	8	9	0.0023	0.0363	0.3804	1.0000	0
17	9	30	0.0019	0.0183	0.2900	1.0000	0
18	10	11	0.0004	0.0043	0.0729	1.0000	0
19	10	13	0.0004	0.0043	0.0729	1.0000	0
20	10	55	0	0.0200	0	1.0700	0
21	12	11	0.0016	0.0435	0	1.0600	0
22	12	13	0.0016	0.0435	0	1.0600	0
23	13	14	0.0009	0.0101	0.1723	1.0000	0
24	14	15	0.0018	0.0217	0.3660	1.0000	0
25	15	16	0.0009	0.0094	0.1710	1.0000	0
26	16	17	0.0007	0.0089	0.1342	1.0000	0
27	16	19	0.0016	0.0195	0.3040	1.0000	0
28	16	21	0.0008	0.0135	0.2548	1.0000	0
29	16	24	0.0003	0.0059	0.0680	1.0000	0
30	17	18	0.0007	0.0082	0.1319	1.0000	0
31	17	27	0.0013	0.0173	0.3216	1.0000	0
32	19	20	0.0007	0.0138	0	1.0600	0
33	19	56	0.0007	0.0142	0	1.0700	0
34	20	57	0.0009	0.0180	0	1.0090	0
35	21	22	0.0008	0.0140	0.2565	1.0000	0
36	22	23	0.0006	0.0096	0.1846	1.0000	0
37	22	58	0	0.0143	0	1.0250	0
38	23	24	0.0022	0.0350	0.3610	1.0000	0
39	23	59	0.0005	0.0272	0	1.0000	0
40	25	26	0.0032	0.0323	0.5310	1.0000	0
41	25	60	0.0006	0.0232	0	1.0250	0
42	26	27	0.0014	0.0147	0.2396	1.0000	0
43	26	28	0.0043	0.0474	0.7802	1.0000	0
44	26	29	0.0057	0.0625	1.0290	1.0000	0
45	28	29	0.0014	0.0151	0.2490	1.0000	0
46	29	61	0.0008	0.0156	0	1.0250	0

Cont.

Line Number	Line Data					Transformer Tap	
	From Bus	To Bus	R	X	B	Magnitude	Angle
47	9	30	0.0019	0.0183	0.2900	1.0000	0
48	9	36	0.0022	0.0196	0.3400	1.0000	0
49	9	36	0.0022	0.0196	0.3400	1.0000	0
50	36	37	0.0005	0.0045	0.3200	1.0000	0
51	34	36	0.0033	0.0111	1.4500	1.0000	0
52	35	34	0.0001	0.0074	0	0.9460	0
53	33	34	0.0011	0.0157	0.2020	1.0000	0
54	32	33	0.0008	0.0099	0.1680	1.0000	0
55	30	31	0.0013	0.0187	0.3330	1.0000	0
56	30	32	0.0024	0.0288	0.4880	1.0000	0
57	1	31	0.0016	0.0163	0.2500	1.0000	0
58	31	38	0.0011	0.0147	0.2470	1.0000	0
59	33	38	0.0036	0.0444	0.6930	1.0000	0
60	38	46	0.0022	0.0284	0.4300	1.0000	0
61	46	49	0.0018	0.0274	0.2700	1.0000	0
62	1	47	0.0013	0.0188	1.3100	1.0000	0
63	47	48	0.0025	0.0268	0.4000	1.0000	0
64	47	48	0.0025	0.0268	0.4000	1.0000	0
65	48	40	0.0020	0.0220	1.2800	1.0000	0
66	35	45	0.0007	0.0175	1.3900	1.0000	0
67	37	43	0.0005	0.0276	0	1.0000	0
68	43	44	0.0001	0.0011	0	1.0000	0
69	44	45	0.0025	0.0730	0	1.0000	0
70	39	44	0	0.0411	0	1.0000	0
71	39	45	0	0.0839	0	1.0000	0
72	45	51	0.0004	0.0105	0.7200	1.0000	0
73	50	52	0.0012	0.0288	2.0600	1.0000	0
74	50	51	0.0009	0.0221	1.6200	1.0000	0
75	49	52	0.0076	0.1141	1.1600	1.0000	0
76	52	42	0.0040	0.0600	2.2500	1.0000	0
77	42	41	0.0040	0.0600	2.2500	1.0000	0
78	41	40	0.0060	0.0840	3.1500	1.0000	0
79	31	62	0	0.0260	0	1.0400	0
80	32	63	0	0.0130	0	1.0400	0
81	36	64	0	0.0075	0	1.0400	0
82	37	65	0	0.0033	0	1.0400	0
83	41	66	0	0.0015	0	1.0000	0
84	42	67	0	0.0015	0	1.0000	0
85	52	68	0	0.0030	0	1.0000	0
86	1	27	0.0320	0.3200	0.4100	1.0000	0

Table 12: Bus data of16-machine, 68- bus New England extended power system

Bus	Type	Voltage (p. u.)	Load		Generator		
			P_L (p.u.)	Q_L (p.u.)	P_G (p.u.)	Q_G (p.u.)	Unit No.
1	PQ	-	2.527	1.186	-	-	-
3	PQ	-	3.22	0.02	-	-	-

Cont.

Bus	Type	Voltage (p. u.)	Load		Generator		
			P_L (p.u.)	Q_L (p.u.)	P_G (p.u.)	Q_G (p.u.)	Unit No.
4	PQ	-	5.00	1.84	-	-	-
7	PQ	-	2.34	0.84	-	-	-
8	PQ	-	5.22	1.77	-	-	-
9	PQ	-	1.04	1.25	-	-	-
12	PQ	-	0.09	0.88	-	-	-
15	PQ	-	3.2	1.53	-	-	-
16	PQ	-	3.29	0.32	-	-	-
18	PQ	-	1.58	0.3	-	-	-
20	PQ	-	6.8	1.03	-	-	-
21	PQ	-	2.74	1.15	-	-	-
23	PQ	-	2.48	0.85	-	-	-
24	PQ	-	3.09	- 0.92	-	-	-
25	PQ	-	2.24	0.47	-	-	-
26	PQ	-	1.39	0.17	-	-	-
27	PQ	-	2.81	0.76	-	-	-
28	PQ	-	2.06	0.28	-	-	-
29	PQ	-	2.84	0.27	-	-	-
33	PQ	-	1.12	0	-	-	-
36	PQ	-	1.02	-0.1946	-	-	-
37	PQ	-	60	3	-	-	-
39	PQ	-	2.67	0.126	-	-	-
40	PQ	-	0.6563	0.2353	-	-	-
41	PQ	-	10	2.5	-	-	-
42	PQ	-	11.5	2.5	-	-	-
44	PQ	-	2.676	0.0484	-	-	-
45	PQ	-	2.08	0.21	-	-	-
46	PQ	-	1.507	0.285	-	-	-
47	PQ	-	2.031	0.3259	-	-	-
48	PQ	-	2.412	0.022	-	-	-
49	PQ	-	1.64	0.29	-	-	-
50	PQ	-	1	- 1.47	-	-	-
51	PQ	-	3.37	- 1.22	-	-	-
52	PQ	-	24.7	1.23	-	-	-
53	PV	1	-	-	2.5	-	G_1
54	PV	1	-	-	5.45	-	G_2
55	PV	1	-	-	6.5	-	G_3
56	PV	1	-	-	6.32	-	G_4
57	PV	1	-	-	5.052	-	G_5
58	PV	1	-	-	7.0	-	G_6
59	PV	1	-	-	5.6	-	G_7
60	PV	1	-	-	5.4	-	G_8
61	PV	1	-	-	8.0	-	G_9
62	PV	1	-	-	5.0	-	G_{10}
63	PV	1	-	-	10.0	-	G_{11}
64	PV	1	-	-	13.5	-	G_{12}
65	SW	1	-	-	-	-	G_{13}
66	PV	1	-	-	17.85	-	G_{14}
67	PV	1	-	-	10	-	G_{15}
68	PV	1	-	-	40	-	G_{16}

Brief Bio-Data of Author

Dhanraj Chitara received his B.E. (Electrical Engineering) and M.E. (Control Systems) in Honors from M. B. M. Engineering College, JNV University, Jodhpur, India in 2002 and 2006 respectively. Currently, he is pursuing his Ph.D. degree in Department of Electrical Engineering, Malaviya National Institute of Technology (MNIT), Jaipur, India. His research interest includes power system operation and control. Mr. Chitara is a student member of IEEE.